Department of Civil, Environmental and Safety Engineering
University of Messina

Critical state approach and equivalent granular state theory for predicting the undrained cyclic and monotonic behaviour of non-plastic silty sands

Giuseppe Tomasello

This dissertion is submitted for the degree of
Doctor of Philosophy in Civil, Environmental and Safety Engineering (XXXIV Cycle)
Curriculum: Geotechnical Engineering (ICAR/07)
A.A. 2020/2021

Tutors:
Prof.ssa Ing. Daniela Dominica Porcino
Prof. Ing. Nicola Moraci

Head of doctoral school:
Prof. Ing. Gaetano Bosurgi

December, 2021

Table of content

List of tables

List of figure

Notations

α	Initial static shear stress ratio
α_{thre}	Threshold initial static shear stress ratio
a, b	Empirical constants of the new pore water pressure model
β	Empirical constant of Seed's model
β^{1}	Fines influence factor defined by Lashkari
$\beta_{(0)}$	Roundness parameter to calculate the fines influence factor
b	Fines influence factor
b_{CRR}	Fines influence factor obtained from cyclic tests
b_{CSL}	Fines influence factor obtained from critical state lines
CSR	Cyclic stress ratio
$CSRs$	Cyclic stress ratios
CRR	Cyclic resistance ratio
CRR_N	Cyclic resistance ratio for N cycles
$CRR_{N=10}$	Cyclic resistance ratio for 10 cycles
$CRR_{N=15}$	Cyclic resistance ratio for 15 cycles
$CRR_{N=20}$	Cyclic resistance ratio for 20 cycles
$CRR_{fc=0}$	Cyclic resistance for clean sand
CRR_{fc}	Cyclic resistance for silty sand
CRR_{Mw}	Cyclic resistance for a given M_w
$CRR_{Mw=7,5}$	Cyclic resistance for M_w=7,5
C_U	Coefficient of uniformity
$C_{U,S}$	Coefficient of uniformity of sand
$C_{U,f}$	Coefficient of uniformity of fines
D	Sieve diameter of the host sand
D_{10}	Sieve diameter of the host sand correspond to 10% of passing
D_{30}	Sieve diameter of the host sand correspond to 30% of passing
D_{50}	Sieve diameter of the host sand correspond to 50% of passing
D_{60}	Sieve diameter of the host sand correspond to 60% of passing
d	Sieve diameter of the fines
d_{10}	Sieve diameter of the fines correspond to 10% of passing
d_{50}	Sieve diameter of the fines correspond to 50% of passing
d_{60}	Sieve diameter of the fines correspond to 60% of passing

D_R	Relative density
$\Delta p'$	Difference in mean effective stress at current and critical state
$\Delta \sigma'_v$	Applied vertical effective stress
Δu	Excess pore water pressure
$\delta \varepsilon^p_v$	Incremental plastic volumetric strain
$\delta \varepsilon^p_q$	Incremental plastic deviatoric strain
ε_a	Axial strain
ε_q	Deviatoric strain
e	Global void ratio
e_0	Initial global void ratio
e^*	Equivalent granular void ratio
e_{CS}	Critical state void ratio
e_g	Skeleton void ratio
e_{lim}	Intercept of the critical state lines
e_{max}	Maximum void ratio
e_{min}	Minimum void ratio
e_s	Void ratio of the sand
e_f	Void ratio of the fines
e_{UR}	Void ratio at upper reference line
e_{QSS}	Void ratio at quasy steady state
E, F	Fitting parameter for CRR-N_f relationship
φ'_{CS}	Friction angle at critical state
F, p, s	Fitting parameter of Vucetic and Dobry correlation
f_c	Fines content
F_h	Cyclic horizontal load
f_{thre}	Threshold fines content
g, h	Fitting parameter for K_{fc}
G_S	Specific gravity
G_s	Specific gravity of the sand
G_f	Specific gravity of the fines
γ	Shear strain
γ_{SA}	Shear strain in single amplitude
h_0	Initial eight of the specimen
H_{ref}	Reference value of the height

I_p	Pressure index
$I_{p(0)}$	Initial pressure index
I_p^*	Equivalent pressure index
$I_p^*{}_{(0)}$	Initial equivalent pressure index
I_S	State index
k	Empirical constant to calculate b factor
K_α	Correction factor of initial static shear stress
K_{fc}	Correction factor of fines content
K_0	Coefficient of lateral earth pressure
λ_{CS}	Slope of the critical state line
m	Fitting parameter to calculate e^* for high percentage of fines
μ	Empirical constant to calculate b factor
M	Critical state line slopes
M_c	Compressional critical state line slopes
M_e	Extensional critical state line slopes
M_w	Moment magnitude
MSF	Magnitude scaling factor
η_{IS}	Instability stress ratio
η_{PT}	Phase transformation stress ratio
N	Number of cycles
N_f	Number of cycles to liquefaction
N_{SPT}	Number of blows of standard penetration test
p'	Mean affective stress
p'_0	Initial mean effective stress
p'_{CR}	Mean affective stress at upper reference line
p'_{CS}	Critical state mean effective stress
P_a	Atmospheric pressure
PI	Plasticity index
q	Deviatoric stress
q_{c1}	Normalized cone tip resistance
q_{CS}	Critical state deviator stress
q_{IS}	Normalized instability deviator stress
q_{min}	Minimum deviator stress
q_{peak}	Peak deviator stress

r	Empirical constant to calculate b factor
$RMSD$	Root mean standard deviation
R_d	Ratio between mean diameter of host sand and fines
R_u	Excess pore water pressure ratio
$R_{u,lim}$	Limiting excess pore water pressure ratio
$R_{u,res}$	Residual excess pore water pressure ratio
S_r	Degree of saturation
σ	Vertical stress
σ'_v	Vertical effective stress
σ'_h	Horizontal effective stress
σ'_1	Major principal stress
σ'_3	Minor principal stress
σ'_{v0}	Initial vertical effective stress
θ	Empirical parameter of Baziar's model
τ	Shear stress
τ_{stat}	Initial static shear stress
V_S	Shear wave velocity
V_{S1}	Normalized shear wave velocity
V_s	Volume of solids
V_v	Voilume of voids
w	Water content
W_{fines}	Fines solid weight
W_{sand}	Sand solid weight
χ	Size disparity ratio
ξ	Empirical parameter of critical state line
ξ_R	Relative state parameter
ψ	State parameter
$\psi_{(0)}$	Initial state parameter
ψ_{PT}	Transformation phase state parameter
ψ^*	Equivalent granular state parameter
$\psi^*_{(0)}$	Initial equivalent granular state parameter
ψ_g	Skeleton state parameter
ψ_m	Modified state parameter

$\Psi_{m(0)}$	Initial modified state parameter
Ψ^*_m	Equivalent modified state parameter
$\Psi^*_{m(0)}$	Equivalent initial modified state parameter
$\Psi_m{}^*$	Equivalent state parameter
z	Empirical paramater to calculate β^1 factor

Abbreviations

A	Angular
A-SA	Angular to sub-angular
A-SR	Angular to sub-rounded
BSS	Buzzard silty sand
CPT	Cone penetration test
CPTU	Cone penetration test with piezocone
CM	Cyclic mobility
CS	Critical state
CSL	Critical state line
CSLs	Critical state lines
CSS	Cyclic simple shear
CSSM	Critical state soil mechanics
DEM	Discrete element method
DICEAM	Department of Civil, Energy, Environmental and Materials Engineering
DSS	Direct simple shear
EG-CSL	Equivalent granular critical state line
F	Flow
FL	Flow liquefaction
GMP	Green-Mitchell-Polito model
INT	Intermediate
ICL	Isotropically consolidation line
LF	Limited flow
LFL	Limited flow liquefaction
LVDT	Linear variable differential transducer
MI	Majura silt
MII	2/3 Majura silt + 1/3 of commercial kaolin
MSS	Manufactures silica sand+crushed silica silt
MT	Moist tamping
MTX	Monotonic triaxial
NF	Non flow
NCEER	National Center for Earthquake Engineering Research

NGI	Norwegian Geotechnical Institute
NR	Non reversal
OSS	Ottawa sand
OSS(20-30)	Ottawa sand (20-30)
OSS(50-70)	Ottawa sand (50-70)
PWP	Pore water pressure
PWPs	Pore water pressures
PSA	Plastic strain accumulation
QSS	Quasi steady state
QSSL	Quasi critical state line
R	Reversal
R-SR	Rounded to sub-rounded
R^2	Coefficient of determination
R-SR	Rounded to sub-rounded
SA-SR	Sub-angular to sub-rounded
SEM	Scanning electron microscope
SL	Slurry deposition
SPT	Standard penetration test
SS	Simple shear
SI	Sydney silt
SII	2/3 of Sydney silt + 1/3 of commercial kaolin
SANISAND	Simple anisotropic sand plasticity model
TS	Ticino clean sand
TSS	Toyoura sand+crushed silica silt
TSS(5)	Toyoura sand with 5% of fines
TX	Triaxial
USCS	Unified critical state compatible
WP	Water pluviation

Acknowledgements

From beginning to end, my university career, first as a student and now as doctoral candidate, has spanned just over ten years. To fully thank everyone involved in making this project possible and for helping to make me the person and engineer that I have become would require a second volume, at least as large as the following document. If I have left anyone off this list, please realize that you are only missing from this page, not from my heart.

When I started my university career in 2011, I didn't even know there was a conclusion that involved a graduation. I was not good at writing in Italian, let alone in English. During the second year of my course of study I had the pleasure of following the course of geotechnic with my current supervisor, Professor Daniela Dominica Porcino, her way of transmitting notions, even complex, to the class made me decide to follow this path which first led me to obtain a master's degree and now a doctorate. My sincerest gratitude is expressed to my supervisor, Professor Daniela Dominica Porcino, for her illuminating guidance, insightful advice and unfailing encouragement throughout my study. The accomplishment of this challenging doctoral study would have been be possible without the brilliant supervision offered thanks to her experience and invaluable suggestions.

I would like to thank you my doctoral colleagues with whom, before the advent of the pandemic, I spent a good time at the university bar for our breaks, without which it would not have been easy to continue the research with the same strength and passion, and for the good moments that we spent in mission, in Italy and abroad. The trips made with the university will always remain in my heart.

I would really like to thank you Ph.D. Eng. Vincenzo Marciano', who taught me to use the simple shear apparatus and with whom we had several constructive discussions on the obtained results. Thanks to him I developed my tendency to solve problems and to use experimental results for solving practical problems.

And a very special and heartfelt thanks to my family for its patience and support throughout my extended period of study.

Abstract

Recent earthquake events revealed that liquefaction of silty sands remains an unsolved issue, even after decades of investigations. Difficulties in the prediction of the undrained cyclic response of silty sands arise from combined effects of various factors affecting the behaviour such as fines content, gradation, particle shape, plasticity of fines, initial static shear stress, and so on. This study attempts mainly to quantify the effect of an initial static shear stress through undrained cyclic simple shear tests on sand mixed with non-plastic fines dug up from Ticino river, Italy.

The cyclic behaviours and the liquefaction resistance of silty sands were investigated in the framework of critical state soil mechanics. A cyclic simple shear tests programme was accomplished, covering different fines content f_c, initial void ratios e_0, initial vertical effective stresses σ'_{v0} and initial static shear stress ratios (factor α). In the present study undrained monotonic triaxial tests conducted in a previous study on the same materials were also reinterpreted to enable further characterisation and analysis.

Four typical cyclic failure patterns were identified and discussed. They were found dependent on the initial state of the specimens and cyclic loading characteristics. The undrained cyclic test results were interpreted using different measures of the initial state density. When a constant void ratio e was considered, the addition of fines to the Ticino sand caused more contractive behaviour and lower liquefaction resistance up to a threshold fines content f_{thre}. When the equivalent granular void ratio e^* was used instead, similar cyclic resistances ratios for the Ticino sand-silt mixtures were found, regardless of fines content and global void ratio. This aim was reached by introducing in the relationship defining e^*, a parameter b termed the fines influence factor which quantifies the fraction of fines particles that participates actively in the force transmission chains between grains within the mixture. The value of b was determined to be different according to whether it is evaluated by back analysis conducted on the undrained cyclic resistance of the mixtures (b_{CRR}) or on their critical state lines in e-log(p') plane (b_{CSL}). Correlations between the fines influence factor b with material properties were proposed to simplify the use of the equivalent granular void ratio approach in practical applications. To take into account the combined effect of void ratio, initial vertical stress and fines content, different initial state indices, defined in the frame of the critical state theory, were used and unique correlations were obtained between the undrained monotonic and cyclic behaviours of the investigated mixtures

and the aforementioned state indexes. Unique correlations continued to be found even in tests in which an initial static shear stress was applied. Among these state indexes the state parameter Ψ and the equivalent granular state parameter Ψ^* provided the more reliable correlations with the undrained response of silty sands. This allowed the conclusion that they can be used effectively for describing the main features of the undrained monotonic and cyclic behaviour of the non-plastic silty sands regardless of fines content (lower than the threshold value), stress level and density. However the equivalent granular state parameter Ψ^* has the advantage that it can be assessed referring to an unique critical state line (*EG-CSL*) without the need to perform several sets of triaxial tests, each one for a given value of f_c. A further advantage resides in the fact that this unique *EG-CSL* can be legitimately assumed to coincide with the *CSL* of the clean sand.

Finally, the pore pressure generated in the cyclic tests was investigated and it was found to be significantly influenced by the initial static shear stress. For this reason, a cyclic pore pressure generation model was proposed capable to predict the residual excess pore pressure rise of non-plastic silty sands under various initial static shear stress conditions.

Chapter 1

Introduction

1.1 Background of the Research

The research topic is part of the study of the behaviour of numerous materials defined as "transition" (or "intermediate") which include silty sands, sandy silts, clayey sands, etc. and, more generally, mixtures of coarse-grained and fine-grained materials, which therefore cannot fit into the classic behaviour exhibited by sands and gravels, on the one hand, and fine soils, on the other.

The "intermediate" soils are very common in natural and artificial deposits: for this reason, the knowledge of their behaviour is of fundamental importance in many practical applications.

The characterization and modeling of "intermediate" soils (such as silty sands) turns out to be problematic in engineering practice (Carraro and Sagado 2004; Huang 2016); this difficulty is related to some peculiarities that distinguish the behaviour of these materials, in particular:

1) Their behaviour appears to be different depending on the percentages of fines content (f_c) as well as on its mineralogical nature, which conditions their plasticity (plastic or non-plastic fines) (Boulanger and Idriss 2004; Boulanger and Idriss 2006);
2) There are uncertainties about the choice of the most appropriate state variable that characterizes the densification state for the analysis of the exhibited behaviour (Yang at al. 2015; Huang 2016), for example the use of the state variable “relative density” D_R, commonly used in the characterization of granular soils, can be misleading and therefore should be avoided;
3) The mechanical response is significantly influenced by the microstructure (Yang and Wei 2012; Fuggle et al. 2014); in fact, as well as the presence of the fines, the shape of the constituent particles also plays an important role. For example Yang and Wei (2012), for fine percentages lower than 15%, have found that the addition of non-plastic fines with a rounded shape to a host sand results in a reduction of the friction angle in the critical state, while angular shaped fines cause an increase;

4) Intermediate values of hydraulic conductivity: it turns out that the drainage conditions, that hinder the rise of the excess pore water pressures induced by static and cyclic loads, are partial (Huang 2016; Karim and Alam 2017). This aspect is of fundamental importance in the interpretation of the results of in situ tests carried out on these materials. In fact, in the static penetration tests with measurement of excess pore water pressures (*CPTU* tests) performed in silty sands, the resistance at the tip will be significantly lower than that of clean sand characterized by the same relative density and therefore the existing correlations, generally obtained for the clean sands, are no longer valid;
5) Intermediate materials appear to be very variable and heterogeneous in nature. In the presence of low plasticity fines, the collection of high-quality undisturbed samples, at sustainable costs, is not easy (Huang 2016). Attempts to take undisturbed samples in low-plastic silty sands have been conducted over the years but the results, although of great interest, have not yet received an adequate number of confirmations. In this regard, the experiences carried out by Huang and Huang (2007) with Laval type sampler (La Rochelle et al. 1981) and by Tani and Kaneko (2006) using the Gel-Push sampler (Lee et al. 2006) can be mentioned.

The study and understanding of the undrained behaviour of low-plastic silty sands is of fundamental importance in order to avoid catastrophic events that have affected them in the past. Recent seismic events have shown how significant deformation levels and resistance losses can affect these materials (Lee et al. 2012; Tonni et al. 2015; Sharma et al. 2019; Cubrinovski et al. 2019) and that the simplified approaches currently available in the literature for assessment of the risks associated with them can fall into defect, underestimating the liquefaction potential, especially in the case of the presence of low-plastic or non-plastic fines.

Two very interesting cases involving silty sands with a non-plastic nature are reported by the Sapporo City Office (2018) and by Tsukamoto et al. (2009): in the two case histories, subsidence phenomena due to settlements, caused by the dissipation of the excess pore water pressures generated during the seismic event, were observed. A factor that played an important role was the presence of an initial static shear stress. The cases under consideration are:

- The 2018 Hokkaido Iburi-East earthquake in the residential area of Sapporo;
- The Tokachi-oki earthquake of 2003 in the Kitami agricultural area.

Some images are reported below (**Figure 1** and **Figure 2**), representing the pre and post earthquake situation following the 2018 Hokkaido Iburi-East earthquake and the post-earthquake situation of the Tokachi-oki earthquake, from which we can observe the importance of being able to predict and therefore prevent such phenomena from occurring following a seismic event.

Figure 1 – Deformations induced by the phenomenon of liquefaction following the Hokkaido Iburi-East earthquake (2018) (Sapporo City Office 2018).

Figure 2 – Deformations induced by the phenomenon of liquefaction following the Tokachi-oki earthquake (2013) (Tsukamoto et al. 2009).

The two cases, which had very similar manifestations, involved materials with comparable characteristics, average grain diameter (D_{50}) between 0.13 and 0.20 mm, coefficient of uniformity (C_U) between 25 and 35 and fines content (f_c) of a non-plastic nature between 33% and 36%. Both deposits were located on slopes with an average gradient of about 3%.

Another very interesting case history that confirms the importance of studying and fully understanding the behaviour of sandy-silt soils with low plasticity fines is that which took place in Italy following the 2012 seismic sequence (M_w = 6.1) (Sinatra and Foti 2015; Tonni et al. 2015; Porcino et al. 2019a). In this case, a river embankment where several civil and industrial settlements were located was seriously damaged by the phenomenon of cyclic liquefaction of the soil (**Figure 3**).

Figure 3 – Effects of the liquefaction phenomenon following the 2012 Emilia Romagna earthquake (Tonni et al. 2015).

The deposits were constituted by silty sands and sandy silts with low plasticity fines varying, in content, between 40% and 70%. The greatest damage occurred along the banks of the embankment, which suggests that an important role was also played by the presence of an initial static shear stress (Porcino 2019).

Recently, manifestations of the phenomenon of liquefaction have also been observed in deposits consisting of mixtures of gravel, sand and low plasticity silt, emphasizing the importance of also taking into account the presence of a coarser fraction in the

mixture. The case study in question is that of the port of Wellington (Cubrinowski et al. 2019) which, following the 2016 Kaikoura earthquake, suffered various damages caused by the phenomenon of liquefaction, such as: cracks in the ground, gravel volcanoes and permanent deformations of the soil that caused the phenomenon of "lateral spreading". Some images of the damage observed are shown in the following figure (**Figure 4**).

Figure 4 – Manifestations of the phenomenon of liquefaction in the Wellington harbor area following the 2016 Kaikoira earthquake (Cubrinovski et al. 2019).

Over the years these materials have also suffered damage related to static liquefaction of the ground and therefore loss of resistance associated with loads of static origin. A particularly relevant aspect from a practical point of view in these cases is that of the design and construction of dams and fillings (Jamiolkowski 2014; Gens 2019).
Gens (2019) reports two interesting case histories that involved materials such as silty sands and silts of a low plastic nature and in particular the collapse of the Aznalcollar dam in 1998 (**Figure 5**) and that of the harbor of Prat Quay in 2007 (**Figure 6**), in both cases the phenomenon of static liquefaction was the cause of the main damage observed.

1.2 Objective and Purpose of the Present Research

The present study mainly investigates the combined effects of fines and initial static shear stress on the liquefaction behaviours of silty sands. A systematic laboratory testing programme involving cyclic simple shear tests has been accomplished,

covering a relatively wide range of initial void ratio, initial static shear stress ratio and fines content.

(a) (b)

Figure 5 – View of the Aznalcollar dam following the collapse (a) and evidence of the phenomenon of static liquefaction (b) (Gens 2019).

Figure 6 – View of the harbor section of Prat Quay following the collapse (Gens 2019).

Recent literature studies (Murthy et al. 2007; Huang and Chuang 2011; Yang and Sze 2010a, b; Yang and Luo 2015; Wei and Yang 2019a; Rahman and Sitharam 2020) on sandy soils revealed that the critical soil mechanics can be a promising mechanical framework to study the cyclic behaviours of silty sands, but limited studies were conducted considering the effect of an initial static shear stress (Wei 2017; Wei and Yang 2019b). Some interesting and innovative results regarding cyclic behaviours of silty sands are presented in this thesis based on cyclic simple shear tests under the framework of the critical state soil mechanics.

Firstly, the failure patterns of non-plastic silty sands under undrained cyclic loading, taking also into account the presence of an initial static shear stress, have been presented and categorised basing on the conventional initial state variables (e_0 and p') of the specimens. Secondly, the liquefaction resistance of silty sands specimens has been determined and the effects of fines are analysed both in absence and in presence of various initial static shear stresses. New state indexes defined in the framework of the critical state soil mechanics theory, namely state parameter Ψ, pressure index I_p and modified state parameter Ψ_m, have been considered to further reduce the influencing factors by unifying the effects of void ratio and effective stresses. To this purpose the undrained monotonic triaxial tests results obtained in a previous research conducted at the University Mediterranea of Reggio Calabria (Diano 2017) have been reinterpreted to define the critical state lines of each sand–fine mixture. Starting from the knowledge of the critical state lines of each mixture, unified correlations between the undrained cyclic resistance of non-plastic silty sands have been proposed for a given initial static shear stress using the critical state indexes mentioned above. Characteristics features of the undrained monotonic behaviour of silty sands have been considered and unified correlations have also been established between them and the afore mentioned critical state indexes.

Later, the concept of equivalent granular void ratio e^* (Thevanayagam et al. 2002) has been applied with the aim to unify the cyclic undrained responses of non-plastic silty sands mixed with various fines content. The reliability of the fines influence factor (b) evaluated by two approaches, one based on static tests and the other on cyclic tests, has been analysed and correlations have been established between the cyclic liquefaction resistance and the equivalent granular void ratio. Going ahead the previously defined critical state parameters have been rewritten obtaining similar ones but expressed in terms of e^*, such as: the equivalent granular state parameter Ψ^* (Hsiao and Phan 2016; Rahman and Sitharam 2020; Porcino et al. 2019b), the equivalent pressure index I^*_p (Qadimi and Mohammadi 2014) and the equivalent modified state parameter Ψ^*_m (Qadimi and Mohammadi 2014). The main advantage of using these parameters instead of the traditional ones resides in the fact that they are based on the confirmed evidence of a unique equivalent critical state line (*EG-CSL*) for all fines content (from 0 to the threshold fines contents f_{thre}) and this keeps one from determining the critical state lines of all mixtures, that would be a very time consuming process.

As a final point, the development of the excess pore water pressures of the investigated non-plastic silty sand mixtures during cyclic loading has been analysed taking also into account the effect of an initial static shear stress. An empirical model defined in terms of stress has been proposed and empirical relationships have been presented to derive the parameters of the model from the main factors influencing the undrained behaviour of the mixtures including the initial static shear stresses. The model may be usefully adopted in numerical codes for analyses of local non-linear seismic soil response.

1.3 Thesis Organization

This thesis is organized in nine chapters whose contents are briefly summarized below:

- Chapter 1 gives an introduction to the backgrounds of the present study, and briefly
  illustrates objectives and development of the present research.
- Chapter 2 presents a critical review of the literature concerning the specific topics treated in the thesis. It is focused on 1) key factors affecting undrained behaviour of low plasticity silty sands under monotonic and cyclic loads; 2) theoretical framework of the mechanical behaviour of low plasticity silty sands under monotonic and cyclic loads; 3) design procedures for determining in situ cyclic liquefaction resistance in silty sands.
- Chapter 3 describes the experimental activity performed. The basic properties of the tested non-plastic silty sands materials are presented and an approximate estimation of the threshold fines content based on their density indexes is made. A detailed description of the testing apparatus and the experimental procedures is reported. An exhaustive description of the testing programme is provided and example plots illustrating the typical behaviours exhibited by the specimens under different test conditions are presented.
- Chapter 4 illustrates the failure patterns observed in the undrained cyclic tests carried out on the investigated specimens under different test conditions. The factors affecting the failure patterns are identified and their influence on the observed failure modes is discussed.
- Chapter 5 focuses on the undrained cyclic resistance of the tested specimens. Factors affecting the undrained cyclic resistance of silty sands are also discussed. Besides, the cyclic liquefaction resistance vs. number of cycles relationships exhibited by specimens with different fines contents, initial state

conditions and cyclic loading amplitudes are also discussed. An empirical magnitude scaling factor is proposed for the materials been tested. Finally, an approach to determine the threshold fines content from the values of the cyclic resistance is applied and the result obtained is critically discussed.

- Chapter 6 analyses the undrained monotonic and cyclic behaviour of the tested materials in the framework of the critical state soil mechanics. In this chapter the undrained monotonic triaxial tests from a previous research (Diano 2017) are reinterpreted to define the critical state lines for each mixture. Different state variables in the framework of the critical state theory are considered and their relationships with the undrained monotonic and cyclic behaviour of the tested mixtures are presented and analysed.
- Chapter 7 is focused on the concept of the equivalent granular void ratio e^* and its application to the tested mixtures with the aim to describe in a unified way the undrained monotonic and cyclic behaviour exhibited by the sand-fines mixtures regardless of their fines content. An in depth analysis is reported on the reliability of the methods followed to determine the fines influence factor, which is a fundamental parameter of the equivalent granular void ratio approach. The capability of the equivalent granular void ratio concept to predict in a unified way the undrained monotonic and cyclic behaviour of silty sands with different fines content taking also into account the presence of initial static shear stresses is examined and commented. Introducing the equivalent granular void ratio in lieu of the traditional one in the critical state theory new “equivalent” critical state variables are obtained. Correlations are presented between these variables and the undrained cyclic behaviour of the tested mixtures taking also into account the presence of initial static shear stresses.
- Chapter 8 presents the findings of the study on the effect of fines on the excess pore water pressure generation under undrained cyclic loading. The effect of different initial static shear stresses on the excess pore water pressure generation is showed and commented. Moreover, the applicability of some cyclic pore water pressure generation models proposed for clean and silty sands is discussed, and the accuracy of their prediction to silty sands, with the intention of developing, if necessary, a new revised model based cyclic simple shear tests is proposed.

- Chapter 9 reports general conclusions on the results obtained and provides recommendations for future works.

Chapter 2

Literary review

2.1 Key factors affecting undrained behaviour of low plasticity silty sands under monotonic and cyclic loads

2.1.1 Influence of fines content

The definition of fines as meant in this thesis is the material passing through the sieve n° 200 (mesh opening 0.074 mm) and it can include two particle size fractions: silt (particles with a grain diameter between 0.06 mm and 0.002 mm) and clay (particles with a grain diameter smaller than 0.002 mm).

The effect of fines on the response of sands to monotonic and cyclic loadings has been one of the most challenging topics in geotechnical engineering. The behaviour of sands containing non-plastic silt is mainly controlled by three variables: fines content, f_c, void ratio, e, and stress level, p'. At a constant void ratio and stress level, as the content of non-plastic silt increases up to a threshold fines content, the undrained monotonic and cyclic strengths of the mixture decrease, but further increase in the non-plastic silt content beyond the threshold value would increase the undrained strength (Dash and Sitharam 2009; Dash and Sitharam 2011; Koester 1994; Papadopoulou and Tika 2008; Phan et al. 2016; Polito and Martin 2003; Porcino et al. 2019b; Thevanayagam and Martin 2002; Thevanayagam et al. 2002; Yang et al. 2006a). As to the sands mixed with clay, the behaviour and the strength are affected by further factors such as mineralogy, plasticity properties and stress history of the fines, in addition to f_c, e and p' (Georgiannou et al. 1990; Ni et al. 2004a; Polito 1999; Yasuda et al. 1994).

Figure 7a shows the effective stress paths and stress–strain curves of two non-plastic silty sands (*TSS*, Toyoura silty sand) specimens along with those of the base sand (*TS*, Toyoura sand) at a similar post-consolidation void ratio (e_0) obtained by Yang et al. (2015). All specimens were sheared starting at the mean effective stress of p'_0=500 kPa. The clean sand specimen exhibited a highly dilative, strain-hardening response, whereas mixed soil specimen *TSS(5)* with 5% fines content displayed a contractive response with a significant reduction in strength. When the percentage of fines was increased to 15% (material *TSS(15)*), the reduction in strength became more remarkable and the mixed soil specimen underwent complete liquefaction with zero residual strength at large strains.

Similar observations were also obtained for another non-plastic silt sand mixtures in the same study for Leighton Buzzard silty sand (*BSS*) specimens (**Figure 7b**). In addition, by comparing **Figure 7a** and **Figure 7b**, the increase in contractiveness, due to the presence of fines, appears to be more significant for *BSS* mixture than for *TSS* mixture.

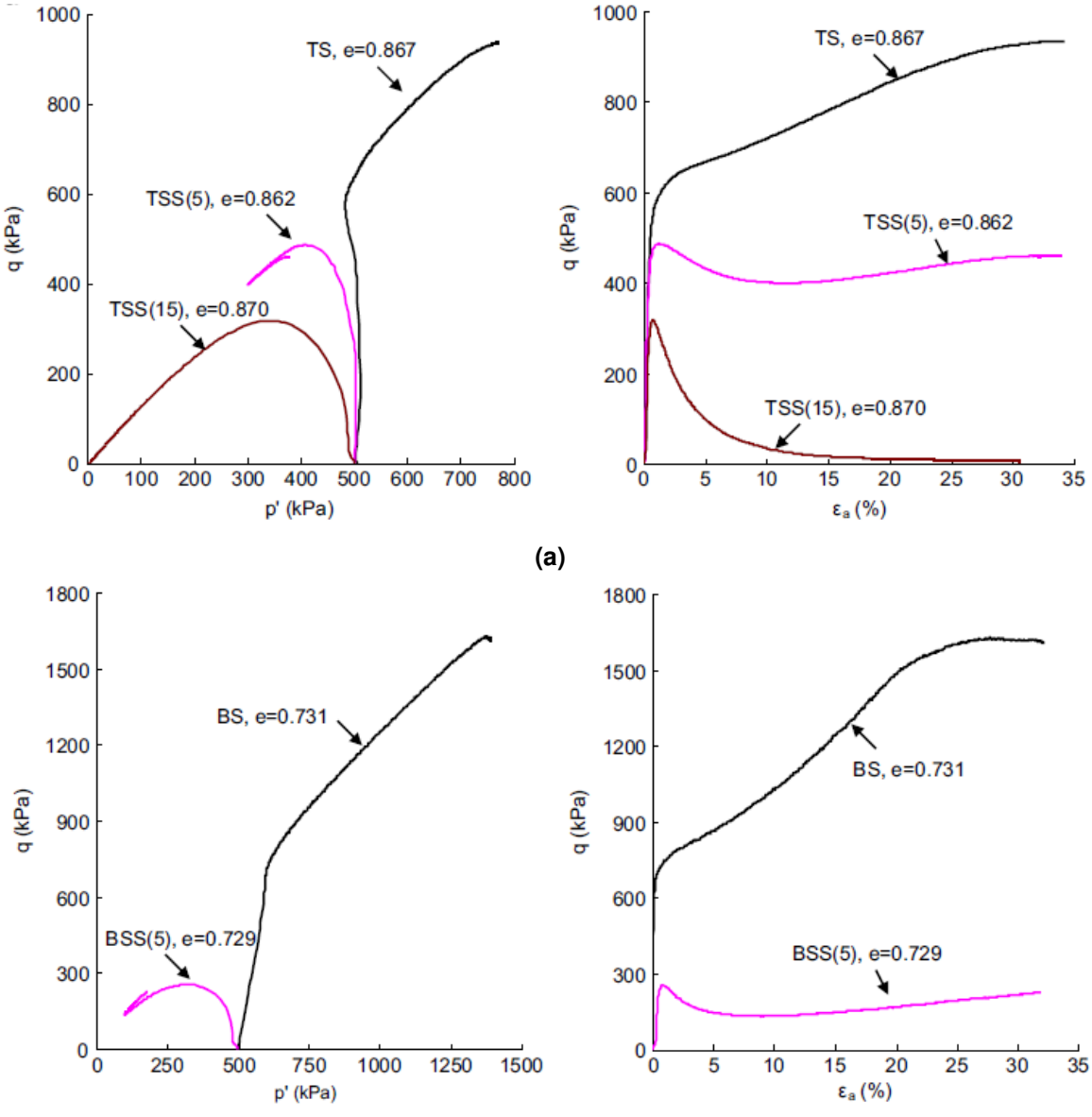

Figure 7 – Undrained monotonic shear responses of clean sand and mixtures with crushed silica fines at a similar global void ratio: (a) *TS* and *TSS* and (b) *BS* and *BSS*, in terms of effective stress path and shear stress-strain behaviour (Yang et al. 2015).

This difference is considered to be associated mainly with the difference in the size disparity between the coarse and fine particles (factor χ =3.1 for Toyoura silty sand,

TSS, and factor χ =11.8 for Leighton buzzard silty sand, *BSS*) of the two mixtures. Compared with *TSS*, *BSS* has a markedly large-size disparity, which may facilitate the movement of fines into the void spaces, thus leading to the soil structure being more unstable. A similar behaviour, i.e. a reduction in the small-strain stiffness of the material, was obtained in resonant column tests by Liu and Yang (2018), and this reduction was found to be all the more evident as the ratio χ increases, while an opposite behaviour was observed in monotonic undrained triaxial tests by Monkul and Yamamuro (2011) for non-plastic sand-fines mixtures specimens reconstituted with the slurry deposition method and at an initial mean effective pressure of 30 kPa, which suggests that further studies on the effects of non-plastic fines characterized by several χ need to be conducted to clarify this effect. Further discussion on this point will be given in a later section. It can be therefore affirmed that, as the percentages of non-plastic fines increased, at the same initial state (e_0, p'_0), a reduction in the undrained peak shear stress resistance as well as in the shear stress resistance at critical state was observed in undrained monotonic tests along with a more contractive behaviour of the material. Such evidences have been found in several studies in literature (Lade and Yamamuro 1997; Murthy et al. 2007; Nguyen et al. 2017; Rees 2010; Porcino et al. 2019b). This type of behaviour was observed for percentages of non-plastic fines lower than the limiting ("threshold") fines content, f_{thre}, beyond which the behaviour became opposite. There are not many literature studies in which the effect of non-plastic fines has been studied in materials characterized by a percentage of fines above the threshold fines content in undrained monotonic triaxial tests. In **Figure 8** some experimental results for sands with fines contents between 0% and 60% as well as the pure silt obtained by Thevanayagam et al. (2002) are shown. It is possible to observe an increase in shear stress resistance and a more hardening behaviour with increasing the percentage of fines from 60% to 100% (pure silt), for soils characterized by the same initial state.

Numerous studies that have investigated the effects of fines on the undrained monotonic behaviour of sand have discussed the soil response using the critical state line. In particular, the location of the critical state line of clean sand in the e-log(p') plane has been compared with the location of the critical state line of silty sands. Theoretically, critical state data points in the e-log(p') plane should follow a single trend that is called the critical state line (*CSL*). Recently, the change of the shape and the position of the *CSL* in the e-log(p') space of sands with increasing fines content has

received increasing attention. However, there is still much debate over the trend of *CSLs* with fines content. There is few data on the critical state lines for non-plastic sand-silt mixtures covering a wide range of fines content. The research results of different authors seem to be contradictory. Interpretations of the shape and position of *CSLs* can be divided into two groups.

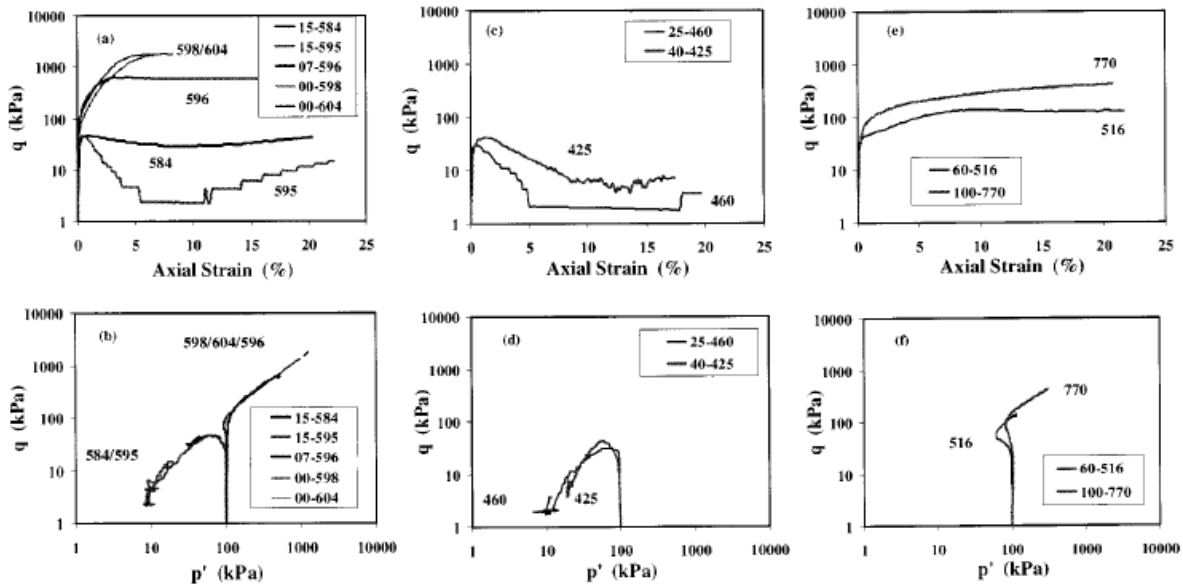

Figure 8 – Effects of fines content on the undrained monotonic behaviour of non-plastic silty sands (Thevanayagam et al. 2002). The first number in the legend corresponds to the fines content.

The first group reported that *CSLs* are linear and that the slope of *CSL* changes with changing fines content (Been and Jefferies 1985; Bouckovalas et al. 2003), whereas the second group showed that *CSLs* are curved and more or less parallel for different fines content (Zlatovic and Ishihara 1995; Thevanayagam et al. 2002; Rahman et al. 2008; Rahman and Sitharam 2020). It has been also reported that an increase in non-plastic fines content within the range $f_c<f_{thre}$ gradually leads to a downward movement of the *CSL* in the *e*-log(*p*') space, while beyond the threshold value with increasing fines content it moves upward again (Pitman et al. 1994; Zlatovic and Ishihara 1995; Thevanayagam and Mohan 2000; Thevanayagam et al. 2002; Yang et al. 2006b; Murthy et al. 2007; Papadopoulou and Tika 2008; Rahman et al. 2008; Bobei et al. 2009; Carrera et al. 2011; Porcino et al. 2019b). In the following paragraphs, the effect of fines content on the location of *CSL* is discussed in detail.

Been and Jefferies (1985) argued that the slope of the *CSLs* increases with increasing fines content in *e*-log(*p'*) plane, see **Figure 9a**. The experimental data clearly show that there is a tendency of the *CSL* to rotate clockwise around a pivot corresponding roughly to mean effective stresses between 20 and 80 kPa and void ratios between 0.73 and 0.78. This effect of f_c implies that increasing the fines content would decrease the tendency to dilate for mean effective stresses greater than that of the pivot and increase this tendency for lower mean stresses. Similarly, Bouckovalas et al. (2003), interpreting 42 tests from various studies and researchers, observed that the *CSL* rotates clockwise around a pivot point in *e*-log(*p'*) space with increasing fines content, see **Figure 9b**.

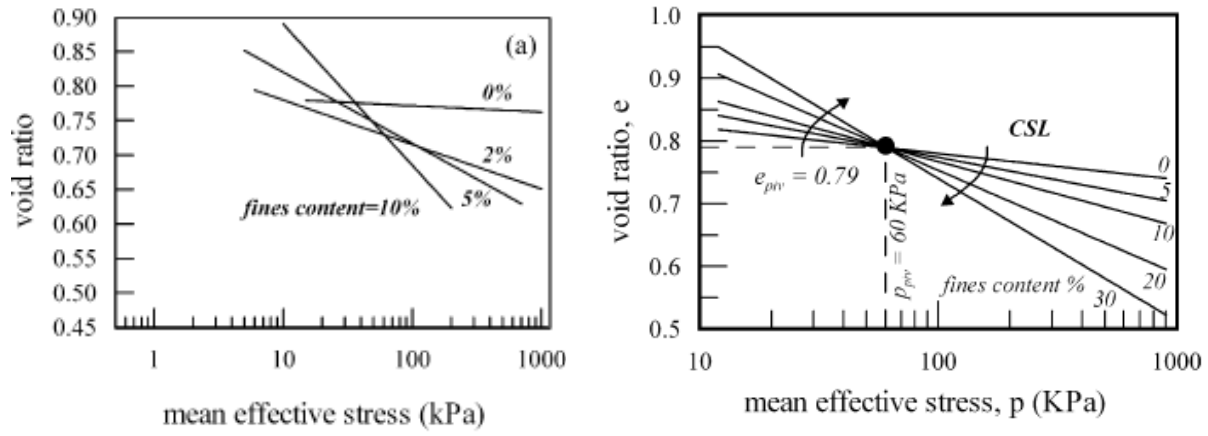

(a) **(b)**

Figure 9 – Effect of fines content on *CSL* location reported by: (a) Been and Jefferies (1985) and (b) Bouckovalas et al. (2003).

Poulos et al. (1985) and Cho et al. (2006) indicated that a small change in soil gradation and grain angularity resulted in significant changes in the location and the slope of the *CSLs*. They also showed that increasing grain angularity results in steeper *CSLs*. Castro and Poulos (1977) reported results from tests on four sands, where the steepest *CSL* belongs to the sand with the most angular grains. Similar results were reported by Olson (2001), who showed that grain angularity may affect the slope of the *CSL* more significantly than the fines content.

Yamamuro and Lade (1998) performed drained and undrained triaxial tests on Nevada sand containing 7% of non-plastic silt. They showed that the *CSLs* of clean sand and sand with fines from drained tests met each other at confining pressures higher than 200 kPa, but the two lines diverged at low pressures. Murthy et al. (2007) conducted

several drained and undrained triaxial tests with different sample preparation methods, namely moist tamping (*MT*), water pluviation (*WP*) and slurry deposition (*SD*), on Ottawa sand mixed with non-plastic fines varying from 0 to 15%. They stated that the position of the *CSL* moves downwards in *e*-log(*p'*) space with increasing fines content. Rahman and Lo (2014) reported a similar tendency for Sydney sand mixed with different percentages of non-plastic fines from 0% to 30%. The results of his study are presented in **Figure 10**.

Chiu and Fu (2008) performed tests on poorly graded sand mixed with 0% to 30% fines with low plasticity (*PI* = 9%). The samples were prepared with the moist tamping method. They reported downward movement of *CSLs* in the *e*-log(*p'*) space with increasing fines content from 0% to 20%. At higher fines content, the shifting direction was reversed.

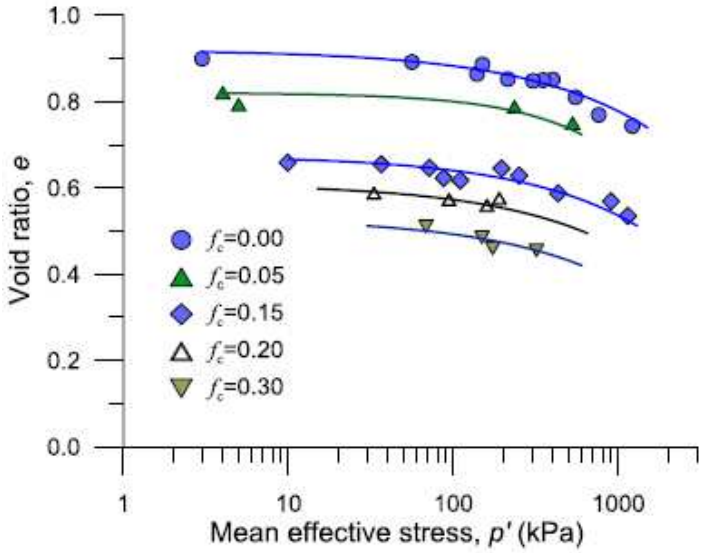

Figure 10 – Critical state lines of Sidney sand with fines content of 0% to 30% (Rahman and Lo 2014).

Furthermore, Papadopoulou and Tika (2008) tested quartz sand mixed with non-plastic fines from 0 to 100% fines content. Their results, depicted in **Figure 11a**, show that *CSLs* shift downwards with increasing fines content up to 35% (known as threshold fines content, f_{thre}) and thereafter the trend is reversed up to f_c = 100%. Thevanayagam and Martin (2002) obtained similar results for the location of the *CSLs* of sand-silt mixtures with fines content ranging from 0% to 100%. Their results indicated that the *CSL* moved downwards from pure sand to sand with 40% fines content (f_{thre}) and then, moved upwards with increasing amounts of fines content right up to pure silt, see

Figure 11b. Naeini and Baziar (2004) observed the same *CSL* tendency for Ardebil sand mixed with non-plastic fines, where the samples were prepared using moist tamping with the under-compaction method. In their work, the f_{thre} was around 35%. In summary, the importance of fines content in shifting the location of *CSLs* in *e*-log(*p'*) framework is indicated. This resulted in difficulties in applying the framework of *CSSM* to analyse the mechanical behaviour of sand-fines mixtures.

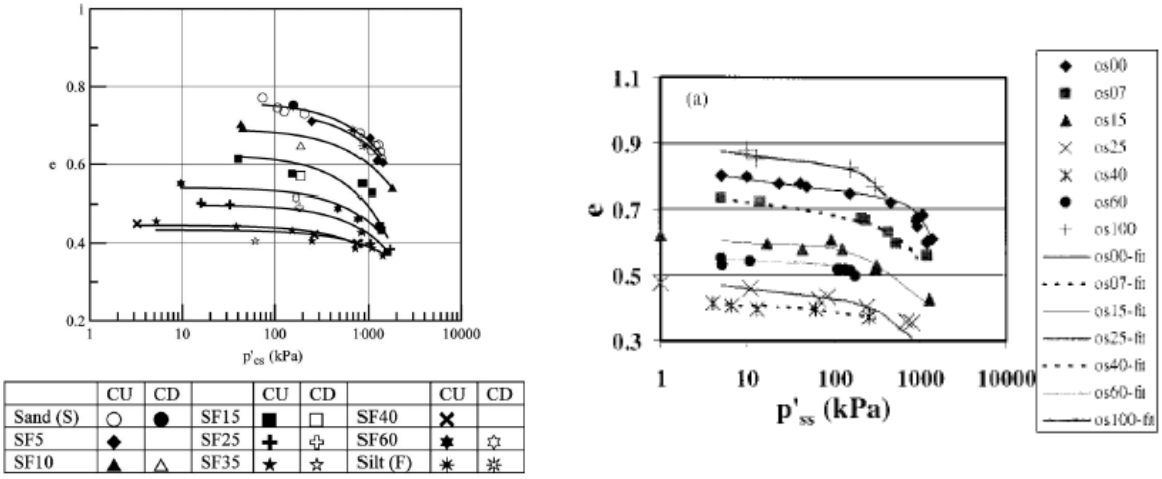

	CU	CD		CU	CD		CU	CD
Sand (S)	○	●	SF15	■	□	SF40	✕	
SF5	◆		SF25	✚	✣	SF60	✸	✡
SF10	▲	△	SF35	★	☆	Silt (F)	✳	✵

Figure 11 – Critical state lines of sand silt-mixtures obtained by: (a) Papadopoulou and Tika (2008) and (b) Thevanayagam and Martin (2002).

Another important research topic is the effect of fines on the cyclic liquefaction resistance of sand-fines mixtures. The cyclic resistance ratio at a given number of cycles (CRR_N) is defined as the ratio of the cyclic shear stress to the effective vertical normal stress required to cause liquefaction in a specified number of loading cycles (*N*). Early studies on cyclic liquefaction were mainly concentrated on clean sand although the occurrence of loose sand with fines is not uncommon.

Since the 1960's, it has been understood that the presence of fines in some manner affects the resistance to liquefaction, but systematic studies on sand with fines are relatively limited. Previous researchers worked on the effect of the presence of non-plastic fines on the cyclic resistance of the soil at a constant relative density. There are many uncertainties in the literature regarding this effect. Some researchers (Chang et al. 1982; Vaid 1994; Singh 1995; Finn et al. 1994; Chien et al. 2002) reported that cyclic resistance decreased with an increase in non-plastic fines content (**Figure 12**). On the other hand, some studies (Amini and Qi 2000; Kaufman and Change 1982; Chang 1987) indicated opposite results (**Figure 13**).

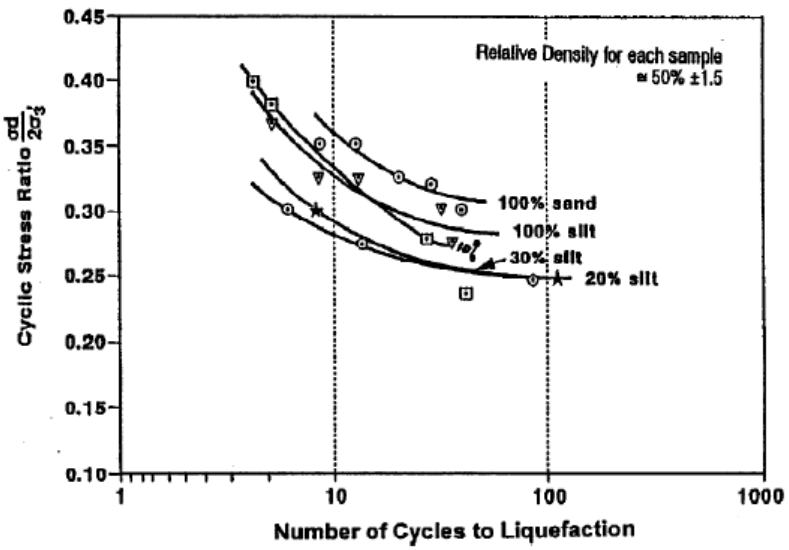

Figure 12 – Influence of non-plastic fines content on the cyclic liquefaction resistance (Singh 1995).

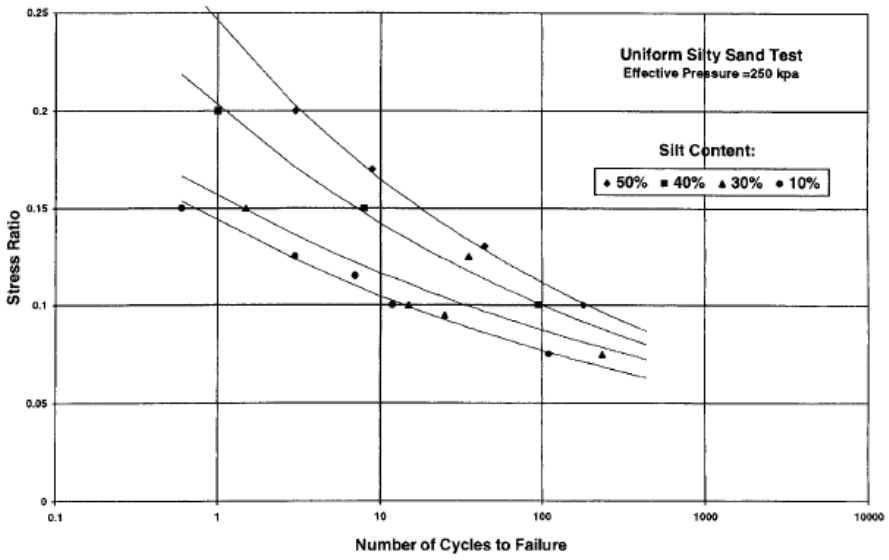

Figure 13 – Influence of non-plastic fines content on the cyclic liquefaction resistance (Amini and Qi 2000).

Other researchers (Polito 1999; Polito and Martin 2001; Xenaki and Athanasopoulos 2003; Ghahremani et al. 2006; Sadek and Saleh 2007; Athanasopoulos and Xenaki 2008; Papadopoulou and Tika 2008; Porcino and Diano 2017) reported that cyclic strength increases with an increase in non-plastic fines content up to a significant amount of f_c and, beyond this point, the trend reversed with an increase in f_c, see **Figure 14**.

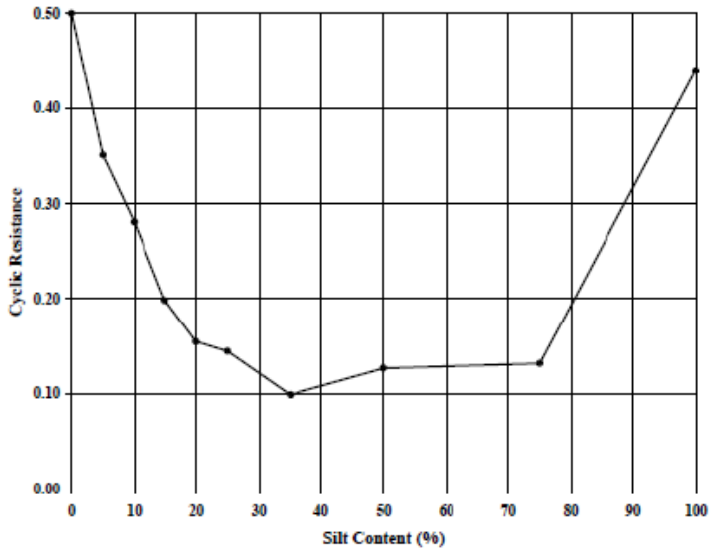

Figure 14 – Influence of non-plastic fines content on the cyclic liquefaction resistance (Polito 1999).

For this reason, some research efforts have also been directed to explain the contradictory evidences mentioned before. Those studies revealed that these apparently contradictory outcomes were due to the inconsistency of the variables assumed as comparison basis (Polito and Martin 2001; Sadek and Saleh 2007; Xenaki and Athanasopoulos 2003). When the conventional void ratio is used as a common comparison basis, many researchers reported a consistent outcome. However, they also reported that the conventional void ratio may not be a good parameter for sands with fines.

2.1.2 Influence of fines plasticity

The effect of fines plasticity on the overall undrained response of sand-fines mixtures has been the object of many studies (Chang 1990; Ghahremani and Ghalandarzadeh 2006; Koester 1994; Guo and Prakash, 1999; Thevanayagam and Mohan, 2000; Sadek and Saleh 2007; Tsai et al. 2010; Papadopoulou and Tika 2016). Nevertheless more research is necessary to have a better understanding on the effect that the nature and the content of the plastic fines can exert on the cyclic liquefaction behaviour of the sand-fines mixtures (Sadek and Saleh 2007). The influence of fines plasticity on cyclic liquefaction resistance and pore water pressure generation was analysed by Koester (1994), using the data from Chang (1990) on reconstituted samples of sand-fines mixtures. The sand-fines mixtures were prepared from a uniform fine sand and pre-selected proportions of uniform low plasticity silt (Vicksburg) and plastic clay

(Vicksburg, Mississippi "buckshot"). The plasticity of fines was controlled by the amount of added plastic clay. It was reported that for the same void ratio, the plasticity of fines has less influence on cyclic strength than the content of fines. A systematic study has been done by Ghahremani and co-workers (Ghahremani and Ghalandarzadeh 2006; Ghahremani et al. 2006). The sand used in the testing program was Firouzkooh sand, which is a medium fine sand with sub-angular particles. The fines were kaolin and bentonite. The plasticity of fines was varied by adjusting the relative amount of these two fines. As reported by Ghahremani and Ghalandarzadeh (2006), in sand-fines mixtures with 16% of fines tested at the same void ratio after consolidation, the undrained cyclic resistance increased with the increase in plasticity of fines (plasticity index varying from *PI*=20 to *PI*=40). The same trend was observed as far as the undrained monotonic resistance is concerned in sand-fines mixtures with 30% fines as shown in **Figure 15**. Differently from the other studies carried out with a triaxial (*TX*) apparatus, Wijewickreme and Sanin (2007) studied the mechanical response of four fine-grained soils having different plasticity using laboratory data from constant volume cyclic direct simple shear (*DSS*) tests. Comparison of the observed cyclic resistance ratio (*CRR*) for the different materials revealed that the value of $CRR_{N=15}$ increased with increasing the plasticity index of the soils. This supported previous experimental findings based mainly on data from triaxial tests conducted on re-constituted samples (**Figure 16**).

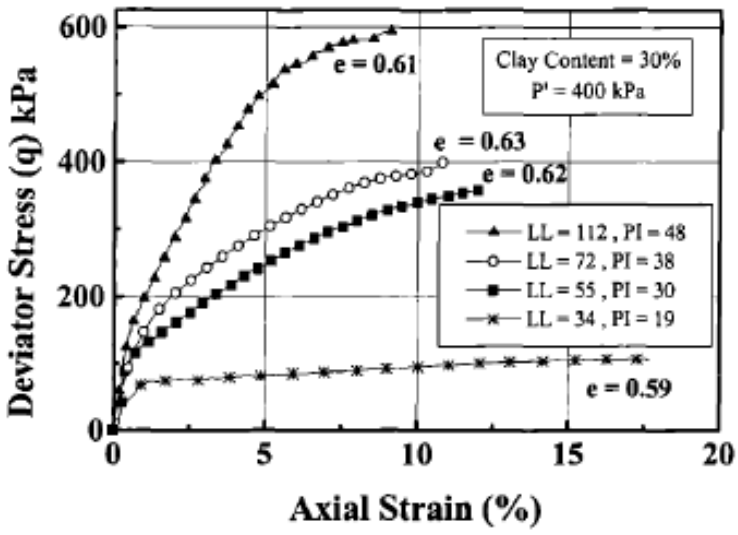

Figure 15 – Increase of undrained monotonic resistance with increasing the plasticity of fines (Ghahremani et al. 2006).

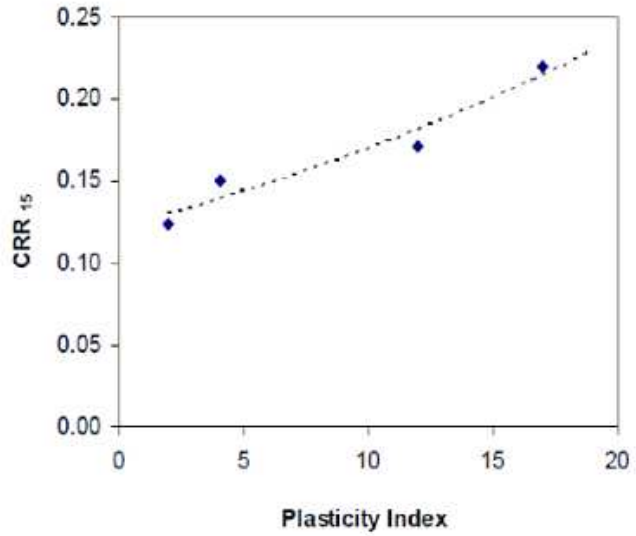

Figure 16 – Undrained cyclic resistance ratio to reach γ=3.75% in 15 cycles ($CRR_{N=15}$) versus plasticity index for tested fine-grained materials (Wijewickreme and Sanin 2007).

Recently, Park and Kim (2013) performed a series of undrained cyclic triaxial tests on specimens having a constant (10%) fines content but different plasticity indexes (*PI*) of the fines, to evaluate the effect of the nature of the plastic fines on cyclic liquefaction. The results showed that liquefaction resistance tended to decrease as the *PI* of fines increased. In contrast to dense and medium dense samples, the liquefaction resistance of loose specimens was marginally influenced by the plasticity of fines (**Figure 17**).

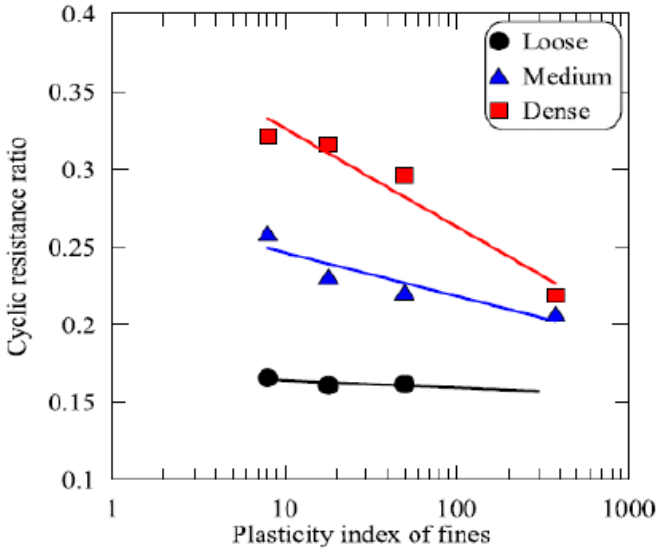

Figure 17 – Cyclic resistance ratio versus plasticity index of fines (Park and Kim 2013).

Recently Papadopolou and Tika (2016) presented interesting results; in fact on the basis of cyclic undrained triaxial tests performed on two silty sands (f_c = 5% and f_c = 15%) and in a range of plasticity index (*PI*) variable between 0% and 30%, the authors pointed out that, as the plasticity increases, the undrained cyclic shear strength of the materials exhibits a different trend depending on whether the plasticity index is lower or higher than a threshold value. In particular in the range below the threshold *PI* the cyclic liquefaction resistance tends to decrease with increasing *PI* while in the range above it the cyclic resistance tends to increase. The threshold *PI* identified by the authors seems to depend on the percentage of fines in the mixture. Some results obtained by the aforementioned authors are shown in **Figure 18**.

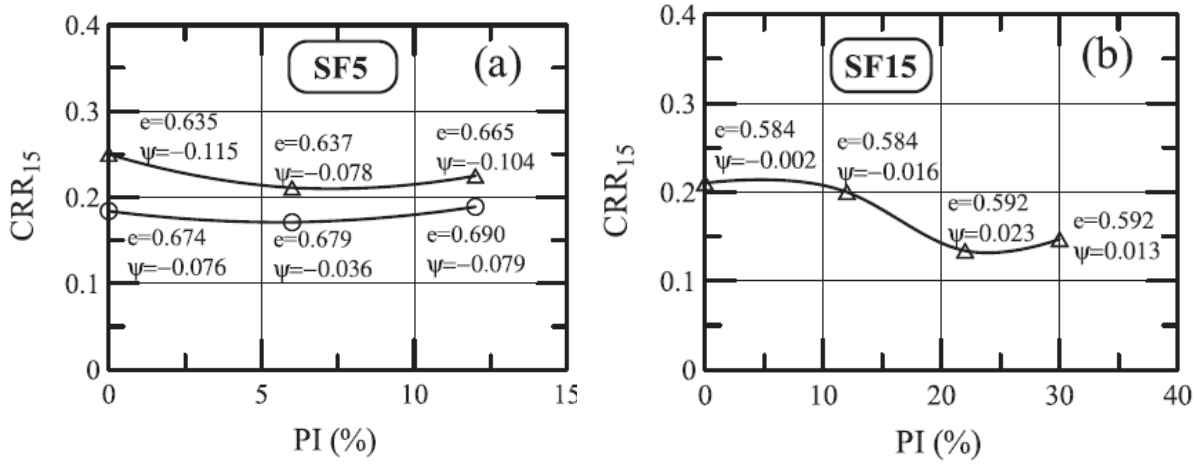

Figure 18 – Variation of the undrained cyclic resistance versus plasticity index for two silty sands with (a) f_c=5% and (b) f_c=15%, at the same initial mean effective stress p'_0=100 kPa (Papadopoulou and Tika 2016).

2.1.3 Influence of particle size disparity and particle shape

The controversial or even contradictory views and results in the literature indicate that the influence of fines on the undrained behaviour of sand-fines mixtures remains an area of great difficulty and uncertainty. The problem is complex, because the mixtures of sand and fines are granular materials in nature, comprising discrete particles that interact with each other during shearing. Most previous work has tended to focus on the effect of fines content by testing specimens of sand mixed with a specific type of fines of varying quantities. From a more fundamental point of view, the characteristics of both fine and coarse particles, such as shape and size, can significantly affect the packing patterns and interactions of the particles, and hence their mechanical

behaviour. Therefore, it is essential to explore how particle characteristics play a role in the overall response of mixed soils.

Wei et al. (2020), by comparing the correction factor for the presence of fines on cyclic resistance ($K_{fc} = CRR_{fc}/CRR_{fc=0}$), observed that *OSS (20-30)* (Ottawa sand (20–30) with fines, χ=11.7), exhibited a more intense decrease of K_{fc} than *OSS(50-70)* (Ottawa sand (50–70) with fines, χ=4.1) with increasing fines content (**Figure 19**). The major difference between the two series of materials may be the particle size disparity between the sandy particles (coarse particles) and the silty particles (fine particles). Particle size disparity has been found to be one of the major factors that control the packing structure and density of a mixture containing grains with two different particle sizes. For example, Lade et al. (1998) reported a particle size disparity ratio (D/d, where D is the sieve diameter of the host sand and d is the sieve diameter of the fines) of 7 for spherical binary mixtures to be a possible threshold value beyond which added fines may be more likely to reside in the voids. Ni et al. (2004b) reported that the active fraction of fines (factor b) participating to the force transmission in the structure could be affected by size disparity ratio (D_{10}/d_{50}). A similar finding was also reported by Rahman and Lo (2008) in a more sophisticated way. Luo (2016) reported simulations by discrete element method (*DEM*) which might support the observation that the larger is the particle size disparity (D_{50}/d_{50}), the more downward shift of the critical state line in e-log(p') plane is observed for the same additional amount of fines.

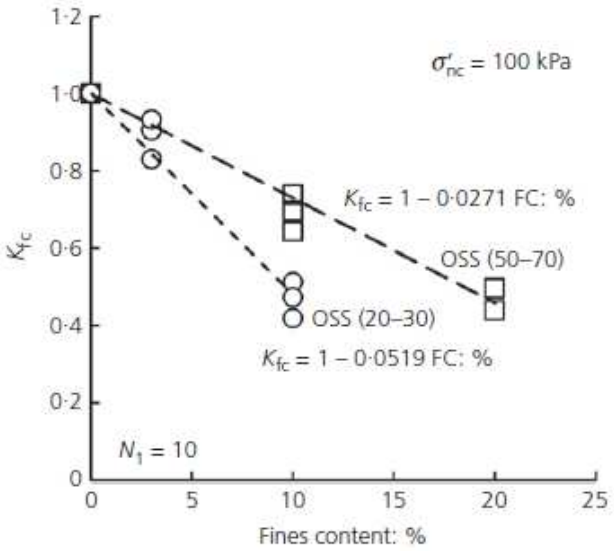

Figure 19 – Effect of fines content f_c on the correction factor K_{fc} for sand-fines mixtures with different particle disparity (Wei et al. 2020).

When compared at the same void ratio, a higher particle size disparity may also lead to a more significant reduction of the undrained cyclic resistance. Polito (1999) performed cyclic triaxial tests on two base sands with the addition of the same non-plastic silt. The test results were replotted by Wei (2017) together with data of *OS* (Ottawa sand) silt mixtures in **Figure 20**.

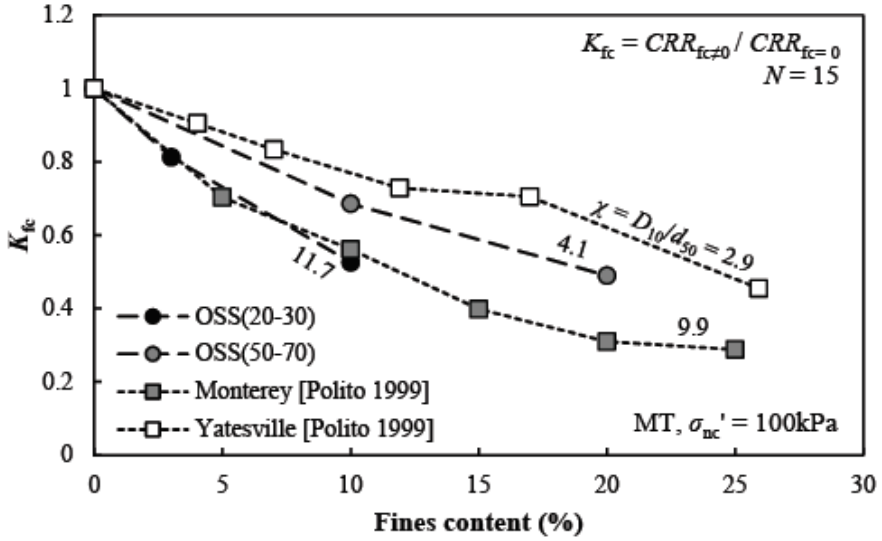

Figure 20 – Effects of particle size disparity on the reduction factor K_{fc} (Wei 2017).

It is clear that for a higher size disparity there is more reduction of cyclic resistance. However, it should be noted that the investigated materials have different particle shapes and this may have potential effects on the cyclic resistance.

Particle shape has long been recognised to affect packing density, small-strain stiffness, strength, compressibility and other mechanical properties (e.g. Miura et al. 1997; Cho et al. 2006; Cavarretta et al. 2010; Yang and Wei 2012; Yang and Luo 2015). Wei (2017) performed undrained cyclic triaxial tests on two different fines-sand mixtures with "sub-angular to sub-rounded sand" (*TSS*) and a more "angular sand" (*MSS*). The results in terms of cyclic resistance ratio and K_{fc} factor are depicted in **Figure 21**. The undrained cyclic resistance decreased with increasing fines content when compared at the same void ratio (**Figure 21**). The cyclic resistance ratios ($CRR_{N=10}$) of *MSS* series were all higher than in *TSS* series, even though the specimens of the *TSS* series had a lower void ratio. However, the reduction factor K_{fc} decreased with increasing the fines content with an approximately parallel trend (**Figure 21**). The experimental results evidence that the particle shape of base sand may have effects on both the packing density and the cyclic resistance of the sand-silt

mixtures; however the shape of sand grains has only a marginal impact on the reduction of the cyclic resistance caused by an increasing amount of fines, provided that the base sands have the same particle size distribution.

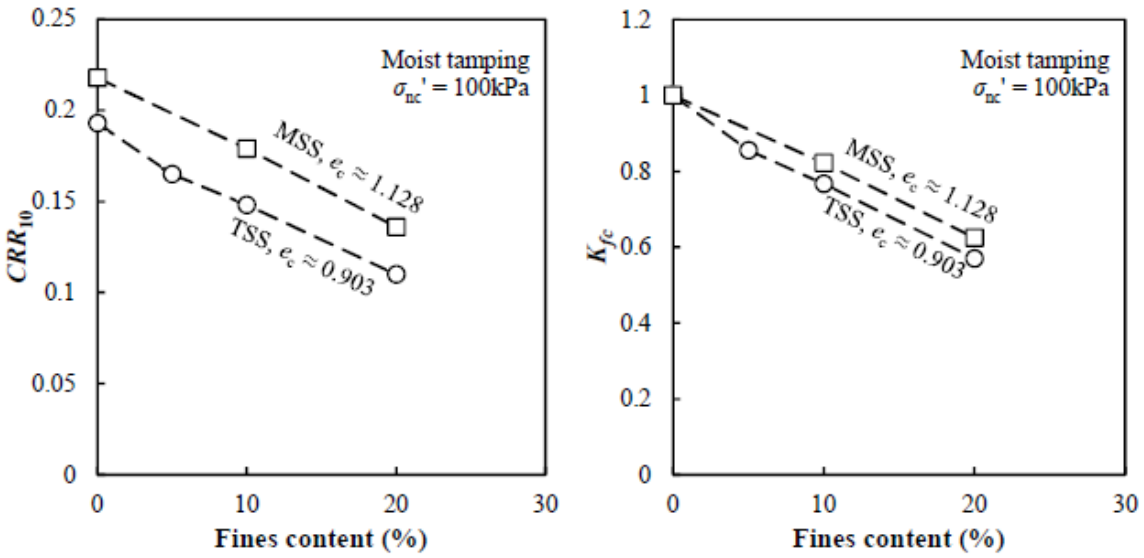

Figure 21 – Effects of base sands grain shape on the undrained cyclic resistance of silty sands (Wei 2017).

To examine the effect of particle shapes of fines Rahman (2009) compared two sets of tests conducted on the same base sand but with fines having different shapes namely *SI* and *MI* fines, with *SI* being a highly angular fine and *MI* a nearly rounded one. Each set consists of three pairs of tests at initial confining pressure of 350 kPa, 600 kPa and 850 kPa. Thus, the comparison of the effective stress paths in (q-p') plane and the stress-strain plots in (q-ε_q) plane of the sand with *SI* and *MI* fines should manifest the effect of angularity of fines in a sand-fines mixture. This comparison is presented in **Figure 22**. As it can be seen both materials manifested contractive response and flow-type behaviour. However sand with *SI* fines manifested higher q_{peak} compared to *MI* fines for all values of the "equivalent granular state parameter" $\Psi^*_{(0)}$ used to represent the initial state conditions of the mixtures. Furthermore the overall effective stress paths for sand with *SI* fines are located above of those for sand with *MI* fines. The reason of such behaviour is the presence of highly angular particles in *SI* fines (crushed Sydney sand) that enhance inter-locking effects between sand grains. On the other hand, sand with *MI* fines exhibited lower initial q_{peak} due to their rounded smooth shape.

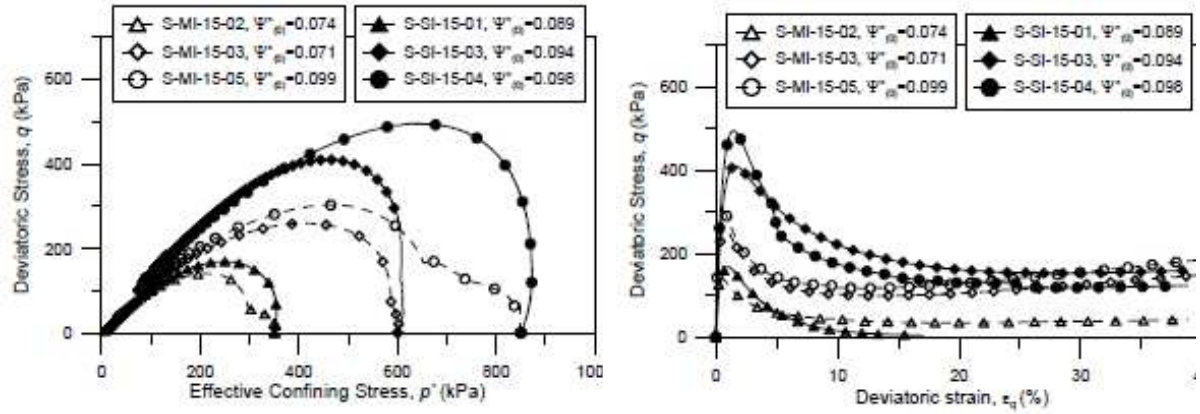

Figure 22 – Effects of fines shape on (a) effective stress-path and (b) stress strain behaviour (Rahman 2009).

The shape of fines was found to affect the monotonic mechanical behaviour of silty sands by other authors (Yang and Wei 2012; Wei and Yang 2014). Yang and Wei (2012) found that adding rounded shape fines into clean sand can result in a marked increase of collapsibility or liquefaction susceptibility compared with adding fines of more angular shape into the same base sand. They proposed an interesting grain scale conceptual model to explain the diverse patterns of overall response associated with particle shape (**Figure 23**).

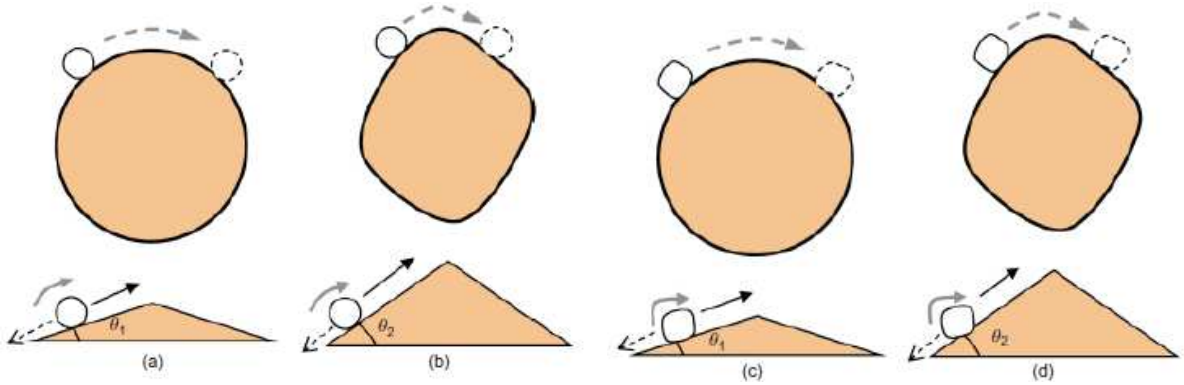

Figure 23 – Conceptual models explaining particle shape effects in mixed soils: (a) Type I, round-to-round; (b) Type II, round-to-angular; (c) Type III, angular-to-round; (d) Type IV, angular-to-angular (Yang and Wei 2012).

The conceptual models describing intergranular contacts and movements in a binary mixture provide a useful framework for explaining the variation in the overall material response. The round-to-round model represents the most unstable structures, where rounded fine particles favour rolling, as manifested by the drastic fluctuations in the

stress–strain behaviour of the specimens tested by the authors Yang and Wei (2012). The angular-to-angular model represents the most stable structures, where angular particles favour sliding rather than rolling.

2.1.6 Influence of an initial static shear stress

In seismic liquefaction analyses the initial static shear stress is the shear stress on the horizontal plane of a soil element under static loading conditions before the cyclic loading occurs. Typically, it occurs in soils that are near a shallow foundation of a structure, in soils below natural or artificial slopes, etc.. Its magnitude can be conventionally represented by the initial static shear stress ratio (α), which is defined as follows:

$$\alpha = \frac{\tau_{stat}}{\sigma'_{v0}} \tag{1}$$

where τ_{stat} is the static shear stress on the horizontal plane of a soil element, and σ'_{v0} is the effective vertical stress on the soil element. The effects of the initial static shear stress on the cyclic resistance of soils can be either beneficial or detrimental, depending on the initial state of the soils (e.g. Boulanger 2003; Yang and Sze 2011a, b). Seed (1981) proposed the correction factor, K_α, to take into account such effects under the same density and confining pressure. The correction factor is defined as follows:

$$K_\alpha = \frac{CRR_{\alpha \neq 0}}{CRR_{\alpha = 0}} \tag{2}$$

Seed and Harder (1990) provided a K_α chart accounting for different relative densities and initial effective stress levels lower than 300 kPa (**Figure 24**). Another K_α chart was proposed by Boulanger et al. (1991) and slightly modified by Harder and Boulanger (1997) (**Figure 25**). This chart adopted 3% of shear strain as failure criterion instead of 7.5% since 3% of shear strain was found to better capture the onset of large excess pore water pressure generation. Moreover, it also assigned a higher rank to simple shear tests and torsional shear tests than to triaxial tests because the former ones better reproduce the stress state in a soil deposit under earthquake loading. However, various editions of K_α charts have been proposed with poor convergence, and as a result the *NCEER* committee suggested the importance of further investigations (Youd et al. 2001).

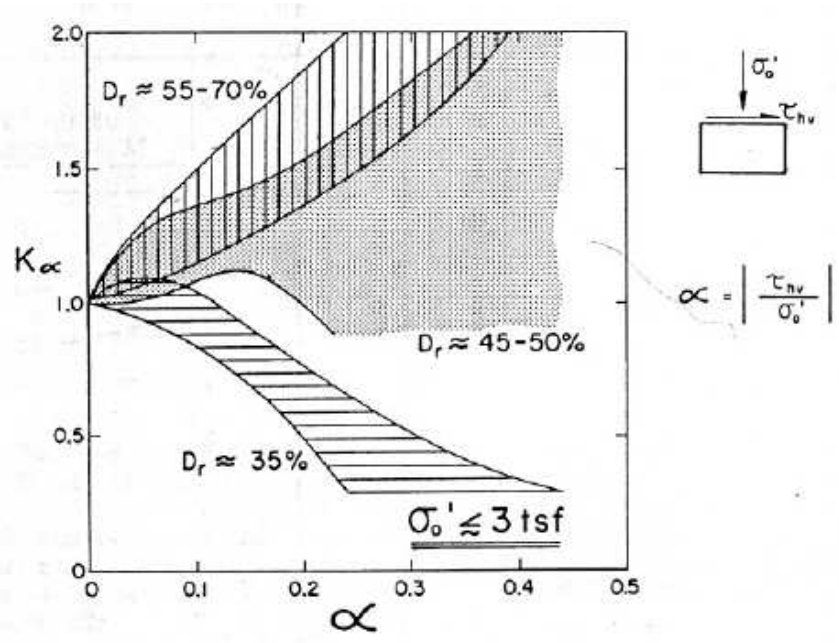

Figure 24 – Relationship between initial static shear stress ratio α and correction factor K_α (Seed and Harder 1990).

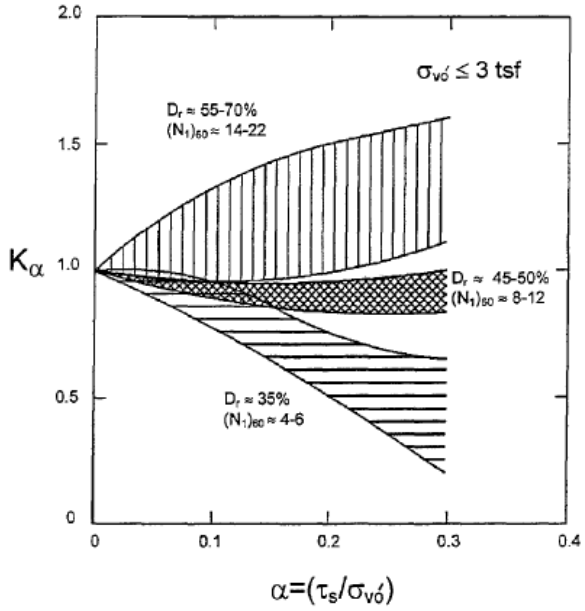

Figure 25 – Recommended K_α values for effective confining pressures less than 3 tsf = 300 kPa (Harder and Boulanger 1997).

A set of experimental data from Sivathayalan and Ha (2011) is also plotted in **Figure 26**. Clearly, the experimental results reported by Sivathayalan and Ha (2011) (**Figure 26**) overestimated the correction factor for sub-rounded sands and underestimated the correction factor for angular sands with respect to the two charts proposed by Seed and Harder (1990) (**Figure 24**) and Harder and Boulanger (1997) (**Figure 25**). These

evidences indicate that the role played by static shear stresses on cyclic resistance is dependent on the material itself, in addition to density and confining stress levels. The results suggest that K_α could be much smaller than 1 in contractive strain-softening sands but is often greater than 1 in dilative strain-hardening sands. Differences in the level of dilatancy, occurring on account of different soil fabric, control excess pore-pressure generation, and thus the cyclic resistance. The fabric of the material is dependent on the particle gradations and shapes for a given deposition mechanism.

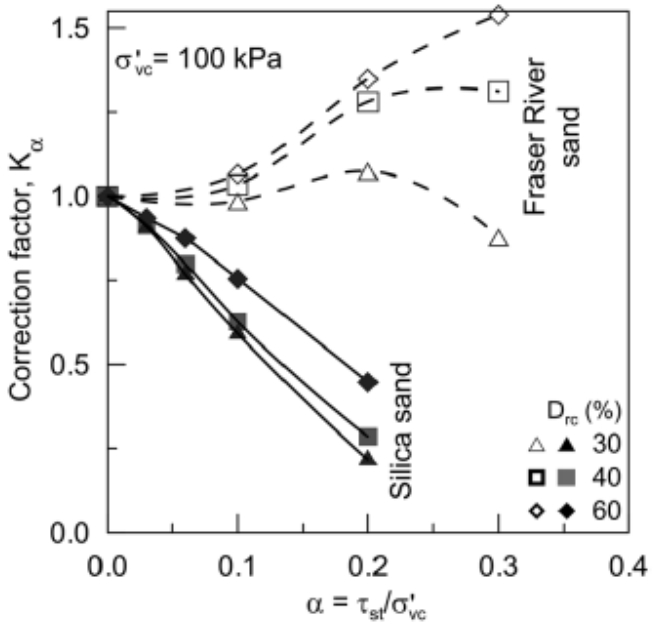

Figure 26 – Variation of K_α with α for two different sands in simple shear tests (Sivathayalan and Ha 2011).

As angular sands are often much more dilative, it can be argued that increasing static shear would decrease the cyclic resistance of sub-rounded to rounded sands; instead it will increase the cyclic resistance of angular sands.

More recently, the framework of critical state soil mechanics has been introduced to investigate the effects of initial static shear stress, such as in Boulanger (2003), Yang and Sze (2011a, b). Sze (2010) derived a semi-empirical equation for the K_α factor from the state dependent threshold α, showing a strong state dependence of the K_α - α relationships. Threshold α is the value of α below which the cyclic resistance increases with increasing α, whereas beyond which the cyclic resistance decreases with further increase of α. This application of critical state soil mechanics seems to provide a new perspective to investigate the effects of initial static shear stress. Wei

and Yang (2019b) extended the state dependent threshold α to silty sands, implying the applicability of the framework proposed by Sze (2010). However, contributions regarding low plasticity silty sand are still limited (Wei and Yang 2015; Porcino et al. 2018; Wei and Yang 2019b; Kokusho 2020).

The actual experimental evidence related to these materials show that the effect of a static shear stress can be positive or negative depending on the initial global void ratio, the initial mean effective stress and the percentage of fines. In this regard, the results obtained by Wei and Yang (2019b) are reported (**Figure 27**). This figure shows the trends of the cyclic resistance against liquefaction evaluated for a number of cycles equal to 10 ($CRR_{N=10}$) obtained in anisotropically consolidated undrained cyclic triaxial tests on specimens characterized by different values of initial global void ratio and mean effective stress with different α. From **Figure 27a** it is possible to observe how, for loose materials (e_0=0.903), the cyclic resistance against liquefaction tends to initially increase with the value of α and then decrease beyond a threshold value of the latter (α_{thre}). However, this didn't happen in case of a denser material (e_0=0.847 and e_0=0.791); this effect is also different depending on the normal effective confining pressure (**Figure 27b**).

In **Figure 28** the authors showed the trend of the threshold ratio α_{thre} with the normal effective confining pressure for specimens characterized by different fines content. It can be observed how α_{thre} tends to decrease with the normal effective confining pressure, while it tends to increase with the decrease in the percentage of fines (**Figure 28**). Further studies should be conducted to confirm the results obtained by Wei and Yang (2019b) with different percentages of fines taking into account other factors such as the shape and mineralogy of the particles, the induced stress-path, etc.

2.1.8 Influence of fines content on excess pore water pressures induced by cyclic loading

Dynamic and impulsive loading cause development of excess pore water pressure (Δu), which leads to degradation of strength, additional settlement, and deformation of soil. Excessive increase in excess pore pressure can lead to liquefaction (Kramer 1996). The response of saturated soil and structure under dynamic loading predominantly depends on the magnitude of development of excess pore pressure. It is very important to determine an accurate value of pore pressure to analyse in a reliable way soil behaviour under dynamic loading.

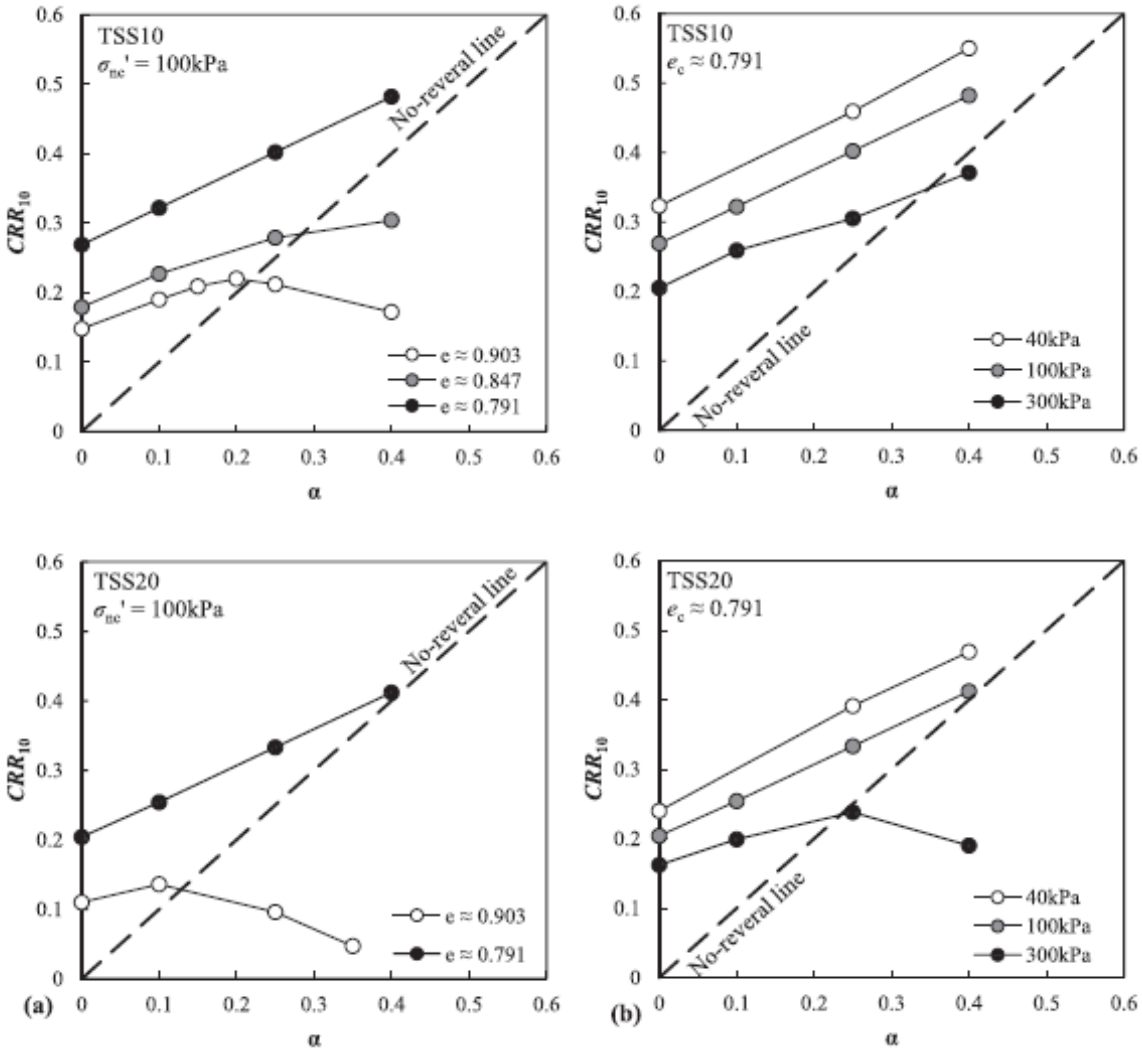

Figure 27 – Effects of *α* on $CRR_{N=10}$ for various (a) packing density and (b) confining pressure (Wei and Yang 2019b).

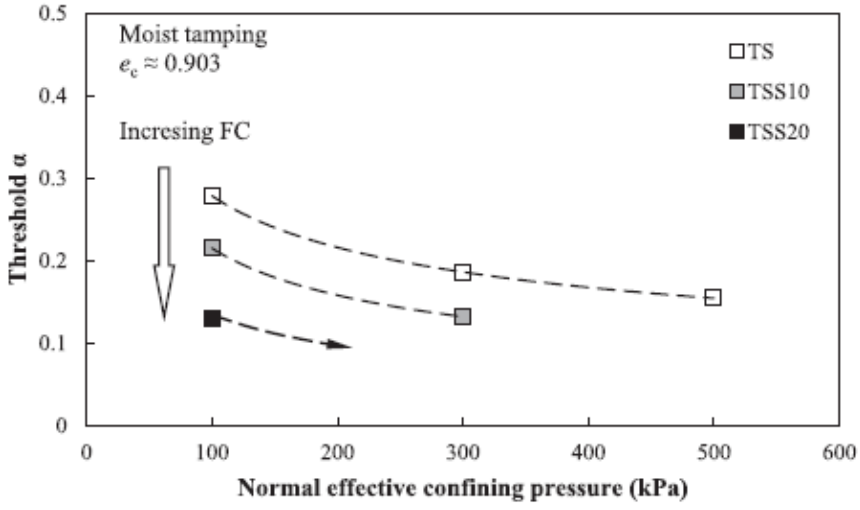

Figure 28 – Threshold *α* determined for clean and silty sands (Wei and Yang 2019b).

In the last decades, various attempts have been made to model the excess pore water pressure through various techniques in order to solve the stability problem, some foundation problems and, especially, to determine the liquefaction potential of a soil. The modelling of pore pressure response in non-linear site response analysis has seen extensive development based on the results of field measurements (Matasovic and Vucetic 1993) and laboratory tests (Ishihara et al. 1976), including the effects of multidirectional shaking (Seed et al. 1978). Pore pressure can be predicted by various methods. Cetin and Bilge (2012) have described a total of four types of models to estimate excess pore pressure generated during cyclic loading. These methods are stress-based methods (e.g. Seed et al. 1975; Booker et al. 1976), strain-based methods (e.g. Martin et al. 1975; Dobry et al. 1985), energy-based methods (e.g. Davis and Berrill 1982; Green et al. 2000), and plasticity-based methods (e.g. Prevost 1985; Elgamal et al. 2003).

In the stress-based models, reference is made to the residual pore pressures that are defined as the pore pressure values picked up at the instants when the applied deviatoric stresses become equal to zero. Methods based on total stress concept do not consider the progressive degradation of stiffness due to the increase in pore pressure. On the basis of stress-controlled cyclic triaxial tests results on Monterey and Sacramento River sands, Lee and Albaisa (1974) proposed an empirical relationship between the excess pore-water pressure ratio (R_u) defined as: $R_u=\Delta u/\sigma'_{v0}$ and the cycles number ratio (N/N_f), which was claimed to be insensitive to soil type, relative density (D_R), initial effective confining stress (p'), and number of cycles to liquefaction (N_f). On the basis of experimental data of De Alba et al. (1975), Seed et al. (1975) developed an empirical, closed-form solution that is given in Eq. (3):

$$R_u = \left\{\frac{1}{2} + \frac{1}{\pi}\cdot \sin^{-1}\left[2\cdot\left(\frac{N}{N_f}\right)^{1/\beta} - 1\right]\right\} \tag{3}$$

where β is a constant that is assumed to be a function of soil properties and test conditions with an average value of 0.7. The proposed expression was subsequently simplified by Booker et al. (1976):

$$R_u = \frac{2}{\pi}\cdot \sin^{-1}\left(\frac{N}{N_f}\right)^{1/2\beta} \tag{4}$$

Each of the above equations makes use of two calibration parameters (i.e. N_f and β) that can be determined from stress controlled cyclic triaxial tests, as well as from other types of undrained cyclic tests. For a given soil, N_f increases as relative density

increases and decreases as the amplitude of the cyclic loading increases, with the amplitude of the cyclic loading typically expressed in terms of cyclic stress ratio *CSR* being $CSR=\tau_{cycl}/\sigma'_{v0}$. Due to the presence of N_f, the use of relationships (3) and (4) has its drawback in that they can only be applied to liquefiable soils. However, "non-liquefiable" soils, such as dense sands and soils with plastic fines, can still undergo significant pore pressure increases and deformations as a result of cyclic softening (Boulanger and Idriss 2006). The second parameter β is an empirical constant. Both equations (3) and (4) have been found to produce results that are in good agreement with the results from cyclic triaxial tests (Lee and Albaisa 1974) and cyclic simple shear tests (De Alba et al. 1975) on clean sands. Lee and Albaisa's recommended upper and lower bounds of residual pore pressure ratio for Monterey No.0 sand are shown in **Figure 29**. Also shown in this figure is the trend curve of the predicted residual excess pore pressure ratio generated using Eq. (4) with β=0.7, an average value recommended for clean sands by Booker et al. (1976).

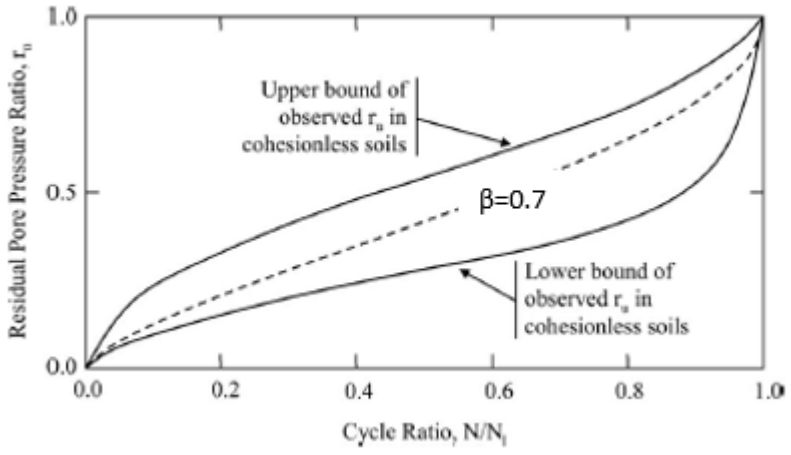

Figure 29 – Observed bounds of residual excess pore water pressure ratio as a function of cycle ratio and approximate average trendline given by Eq. (4) with β=0.7 (adapted from Seed et al. 1975).

In practical applications, besides the need to get reliable values of the two aforementioned parameters, a disadvantage of the stress based models resides in the fact that they require to convert the irregular time histories of real earthquakes into regular (constant amplitude) ones characterized by an equivalent number of cycles. Furthermore this equivalent number of cycles depends on the reference amplitude conventionally assumed to better represent the seismic hazard of the real earthquake.

The numbers of cycles N and N_f appearing in equations (3) and (4) should be considered as "equivalent number of cycles". Polito et al. (2008), in order to take into account the effect of non-plastic fines content, re-evaluated on statistical basis, the method proposed by Seed et al. (1975) and concluded that the model coefficient β needs to be estimated as a function of fines content (f_c), relative density (D_R), and cyclic stress ratio (CSR) as well:

$$\beta = 0.01166 \cdot f_c + 0.007397 \cdot D_R + 0.01034 \cdot CSR + 0.5058 \quad (5)$$

Eq. (5) is suggested to be used for soils with $f_c < 35\%$. Seed et al. (1975) model is able to effectively capture the measured build-up of pore pressure for clean sand, however it has some limitations when applied to sands with a silt content higher than 35%, consistent with the limiting fines content concept (Polito 1999; Polito and Martin 2001; Green et al. 2006). More recently, Porcino (2019) confirmed this observation interpreting cyclic simple shear test results performed on reconstituted samples of Ticino sand mixed with different percentage of non-plastic fines. In the research, the following key features for silty sands with $f_c \leq 35\%$ (**Figure 30**) were observed: 1) the specimens experienced zero, or near zero, vertical effective stress conditions during cyclic loading; 2) the soils with a higher fines content are more contractive, causing a faster rate of excess pore water pressure generation; 3) the shape of Seed's model for clean sands agrees well with experimental data but only data points for $f_c \leq 20\%$ fall inside the band suggested for clean sands ($0.6 \leq \beta \leq 1$) (see **Figure 30**) while for higher f_c values a proposed expansion of the upper bound is necessary (i.e. β=1.50 for the tested soils). Instead, for low-plastic fines percentages greater than 35% Porcino (2019), interpreting the results of cyclic simple shear tests performed on undisturbed samples recovered from a site shaken by the catastrophic 2012 Emilia Romagna (Italy) earthquake, showed that these soils exhibit a development of residual R_u during loading cycles generally less than 0.95 (in the range 0.82-0.94) and a different response in terms of shape of plots R_u vs. N/N_f compared to sands with a fines percentage less than 35% (**Figure 30**). Accordingly it was concluded that the model of Seed et al. (1975) is no longer appropriate for the prediction of the R_u (**Figure 31**) and a new relationship was proposed that is defined by the following expression (Porcino and Diano 2016):

$$R_u = A \cdot \left(\frac{N}{N_f}\right)^B \quad (6)$$

where A and B are two empirical parameters controlling the shape of the curve.

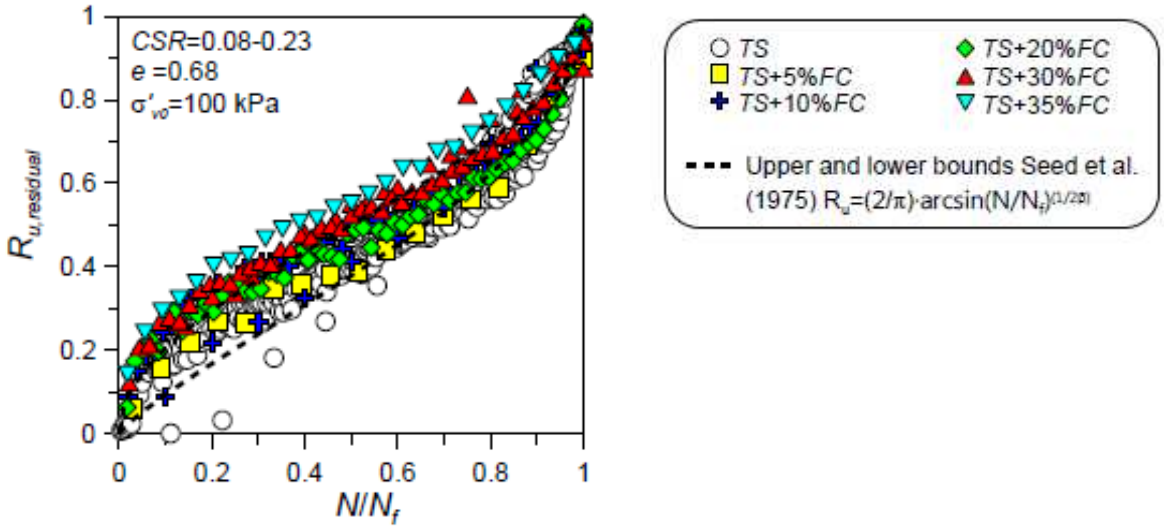

Figure 30 – Residual pore water pressure build up for Ticino sand-non-plastic fines mixtures ($f_c \leq 35\%$) and comparison with upper and lower bounds proposed for clean sands (adapted from Porcino 2019).

It may be argued that Eq. (6) fits the data points with greater overall accuracy, even in the last part of the tests; therefore, it is suitable for the application to sandy silts and silty sands with $f_c > 35\%$.

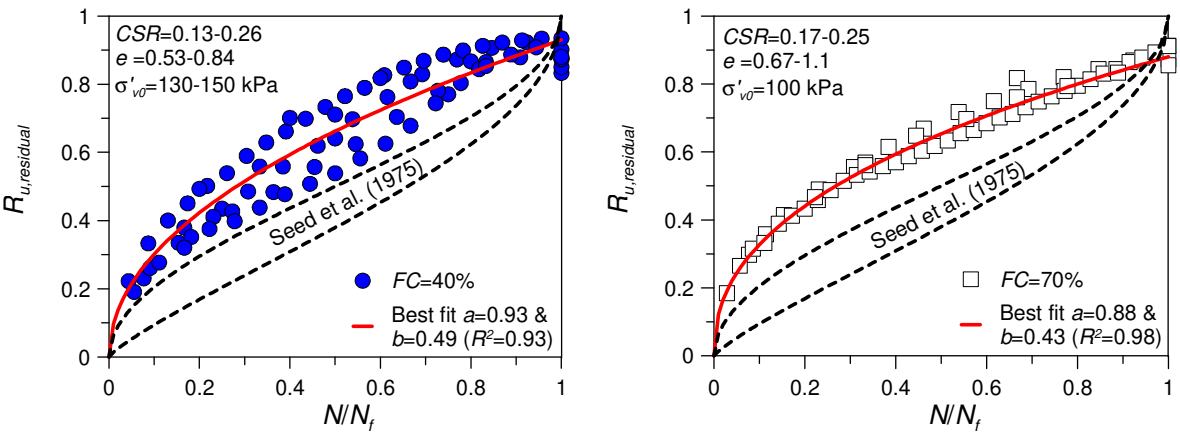

Figure 31 – Residual pore water pressure versus normalized number of cycles for undisturbed samples of low plasticity silty sands (f_c=40-70%) and prediction of the *PWP* generation model (adapted from Porcino 2019).

With a different approach, Baziar et al. (2011) proposed a modified model based on undrained cyclic hollow cylinder torsional tests carried out on Firouzkooh sand and non-plastic silt mixtures to take into account the effect of fines content:

$$R_u = \frac{2}{\pi} \cdot \sin^{-1}\left(\frac{N}{N_f}\right)^{1/2\beta} + \theta \cdot \sqrt{\left[1 - \left(2 \cdot \frac{N}{N_f} - 1\right)^2\right]} \quad (5)$$

where ϑ and β are two parameters defined for different types of soils based on their silt content. This model always predics $R_u = 1$ when the normalized number of cycles N/N_f is equal to 1 in contrast to the model of Porcino and Diano (2016) that capture in most realable way the experimental data in the last part of the test (in proximity of liquefaction N/N_f >0.8).

Comparison of the two aforementioned pore pressure build up models with Seed's model indicates that they reproduce quite satisfactorily the trend of the curves for soils with large amounts of non-plastic silt (**Figure 31** e **Figure 32**).

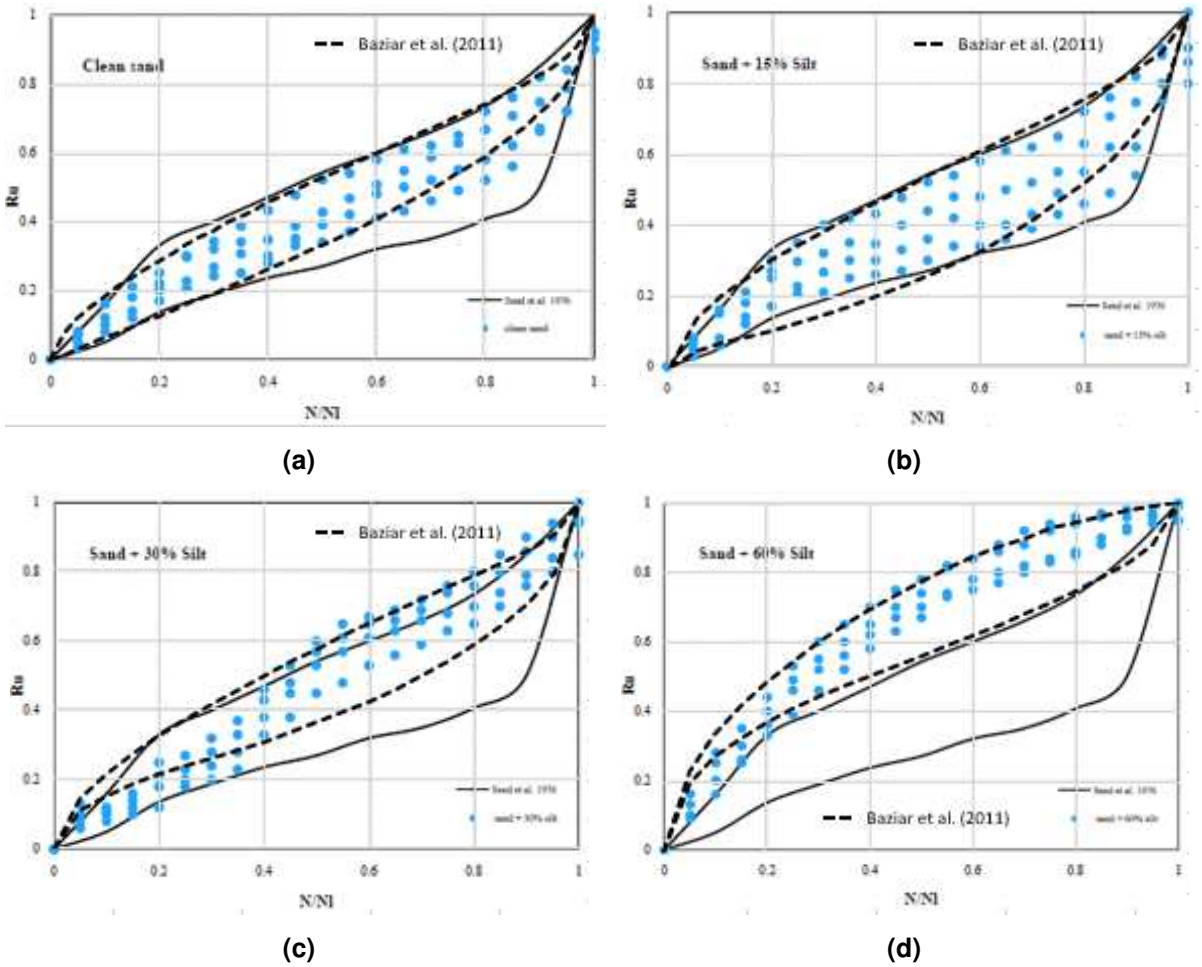

Figure 32 – Excess pore water pressure versus normalized number of cycles for sand-silt mixtures and comparison with model of Seed et al. (1975) (adapted from Baziar et al. 2011).

Recently, there has been a development of the stress-based models that has been pursued by considering a damage parameter defined as accumulated shear stress

during cyclic loading. The proposal has been developed basing on undrained cyclic stress-controlled tests carried out in triaxial and simple shear devices on sandy soils (Park and Ahn 2013; Park et al. 2015). The model expresses the onset of liquefaction in terms of accumulated shear stress irrespective on the real features of the shear stress time history induced by an earthquake. Accordingly the cycle ratio N/N_f appearing in the empirical equations defining the stress-based pore pressure models, becomes a function of the accumulated shear stress. Since the damage parameter is an incremental quantity that increases with time, the model can be incorporated in a time domain program to perform dynamic coupled effective stress analyses in soils subjected to transient motions. Furthermore, the model is very easy to be applied since all the input parameters can be derived from undrained cyclic stress-controlled tests performed to assess the liquefaction resistance.

Another one of the most commonly used pore pressure generation models is the strain-based model, first proposed by Martin et al. (1975). As it is well known shear deformation is strongly associated with pore pressure generation in saturated soils, and it provides a good assessment of excess pore pressure modelling using strain-controlled tests (Derakhshandi et al. 2008). Ladd et al. (1989) found that the sample preparation has a small influence on the response of soil under strain-controlled tests compared to stress-controlled tests and suggested that the threshold strain to generate excess pore pressure can be easily investigated under strain-controlled testing. Although strain-controlled models have numerous advantages over stress-based methods, there are difficulties in testing shear strain levels higher than of 0.01 (i.e. 1%). This brought the researchers to opt for the stress based methods when a more reliable assessment of the pore pressure response after 0.01 shear strain was required (Cetin and Bilge 2012). Erten and Maher (1995) showed that there is little pore water pressure generation in silty soils if the strain level is less than a threshold value of the order of 0.01%, that is similar to that observed for sand. The pore pressure generation increased with the increase of silt content up to 30%, if the comparison was made at the same void ratio (**Figure 33**). Derakhshandi et al. (2008) investigated the effect of plastic fines on the pore pressure generation in saturated sand-fines mixtures by strain-controlled tests. They stated that the pore pressure response of sand-clay mixtures can be explained by the relative values of the sand-skeleton void ratio (considering the presence of fines, $e_s=(e+f_c)/(1-f_c)$) compared to the maximum void ratio of the clean sand. For sand-skeleton void ratios smaller than the maximum void ratio of the clean

sand, the sand matrix dominates, and the soil response is sand-like. When the sand-skeleton void ratio is larger than the maximum void ratio of the clean sand, the fines matrix dominates the soil structure, and the soil responds like clay does.

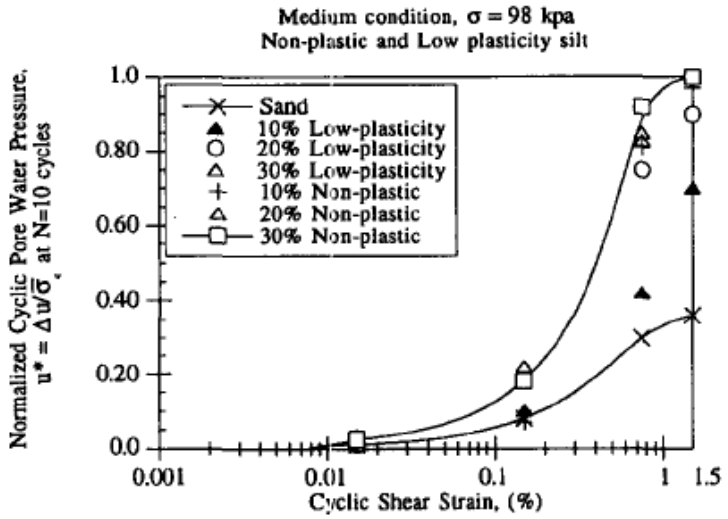

Figure 33 – Normalized pore pressure change vs cyclic shear strain at *N*=10 cycles (Erten and Maher 1995).

Hazirbaba and Rahtje (2009) studied the effect of fines content on excess pore water pressure generation in sands and silty sands. They showed that the effects of fines content were observed in the form of a decrease in excess pore water pressure and an increase in the threshold strain. However, pore water pressure appears to increase when enough fines are present to create a sand skeleton void ratio greater than the maximum void ratio of the clean sand.

Energy-based models gained particular relevance from the practical-applicative point of view. In fact they require, as an input parameter for the prediction of excess pore water pressures, the stress-strain curves of the material; for this reason they can be easily implemented in calculation codes for dynamic analysis. An energy-based model, *GMP*, was developed by Green et al. (2000), which relates the excess pore pressure to the unit energy dissipated (energy dissipated per unit volume) within the soil mass normalised to the corresponding one dissipated at the onset of liquefaction. This model can be considered as a special case of a model proposed by Berrill and Davis (1985) and it can be also applied to non-plastic silt-sand mixtures with various amount of fines. Some authors demonstrated that for soils having a percentage of fines equal to seven both models, (Seed et al.1975) and (Green et al. 2000) give approximately the same

results (**Figure 34**). *GMP* model is unable to precisely simulate the pore pressure development in dense sand, compared to Seed et al. (1975) model and it leads to great differences in the R^2 values.

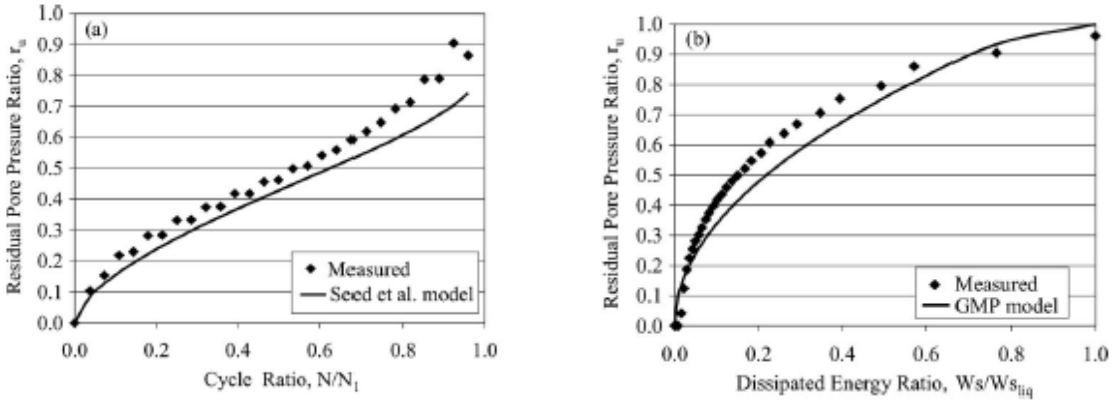

Figure 34 – Plots of measured and predicted pore water pressure ratios for 7% fines: (a) Seed et al. model and (b) *GMP* model (Polito et al. 2008).

Polito et al. (2013) examined whether the energy required to cause liquefaction is dependent on or independent of the load shape applied. With this aim, a series of 28 cyclic undrained triaxial tests were performed using five different load shapes (i.e. sinusoidal, square, triangular, irregular symmetric, and irregular asymmetric) (e.g. **Figure 35**), having a range of cyclic stress ratios.

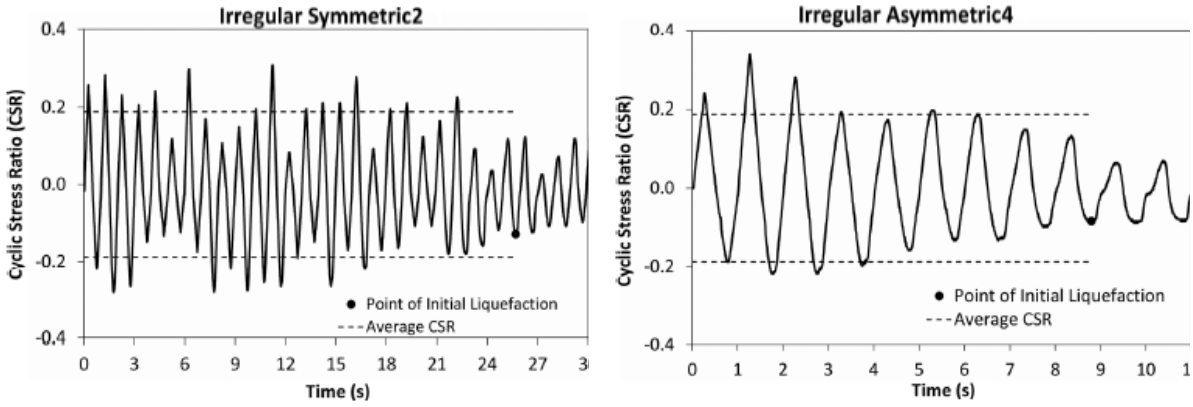

Figure 35 – Example of (a) irregular symmetric loading and (b) irregular asymmetric loading (Polito et al. 2013).

It was found that the dissipated energy to cause initial liquefaction was normally distributed and independent of the load shape, although it was somewhat dependent on duration of loading. A corollary to this finding is that laboratory data from specimens

tested using sinusoidal loadings can be used to calibrate the Green, Mitchell, and Polito (*GMP*) energy-based pore pressure generation models even in soils subjected to non-sinusoidal loadings (e.g. earthquake loadings).

2.2 Theoretical framework of the mechanical behaviour of low plasticity silty sands under monotonic and cyclic loads

2.2.1 Application of critical state approach for the prediction of the mechanical behaviour of low plasticity silty sands

Following the concept of critical void ratio by Casagrande (1936), critical state soil mechanics was originated by Roscoe et al. (1958), Schofield and Wroth (1968) basing on experimental study on reconstituted clay. Its early application on sands was not successful (Been et al. 1991), and it has long been debated whether the steady state (Castro 1969) and the critical state were the same (e.g. Casagrande 1975). Been et al. (1991) claimed that the steady state is, in fact, the same as the critical state. Recently, critical state soil mechanics has received increasing attention in characterising the cyclic behaviours and resistance of silty sands (Bouckovalas et al. 2003; Huang et al. 2004; Jefferies and Been 2006; Papadopoulou and Tika 2008; Stamatopoulos 2010; Yang and Sze 2011a, b; Huang and Chuang 2011; Wei and Yang 2019a; Hsiao and Phan 2016; Rahman and Sitharam 2020).

The loci of critical states form a curve in the *e* - *p′* - *q* space with *q* being the deviatoric stress and *p′* the mean effective stress. Its projections in the *q*-*p′* plane (stress plane) and in the *e*-*p′* plane (compression plane) represent different characteristics of the soil (**Figure 36**). The critical state line of sand in the stress plane is a straight line with slope *M* passing through the origin, indicating no cohesion at the critical state. It can be formulated by the following equation using conventional triaxial notations:

$$q_{CS} = \pm M \cdot p'_{CS} \tag{6}$$

where the subscript *CS* represents that the stresses are at critical state; positive for triaxial compression and negative for triaxial extension. The slope *M* can be converted equivalently to critical state friction angle using the following equations

$$\sin \varphi'_{CS} = \frac{3 \cdot M_e}{6 + M_e} \tag{7a}$$

$$\sin \varphi'_{CS} = \frac{3 \cdot M_c}{6 - M_c} \tag{7b}$$

where the subscript *c* and *e* represents compression and extension, respectively; φ'_{CS} and *M* are positively valued. The critical state friction angle depends on mineralogy, grading characteristics, shape and roughness of particles (Yang and Wei 2012; Yang and Luo 2015).

For sands the critical state line in the compression plane (*CSL*) is a curve when it is plotted in the *e*-log(*p'*) plane. The commonly used equation to formulate the critical state line in the compression plane for sands adopts a power law as follows (Li et al. 1999):

$$e_{CS} = e_{lim} - \lambda_{CS} \cdot \left(\frac{p'}{P_a}\right)^{\xi} \tag{8}$$

where e_{lim} is the intercept and λ_{CS} is the slope of the critical state line in the $e - (p'/P_a)^{\xi}$ plane; P_a is a reference pressure which is equal to the atmospheric pressure; ξ is a positive value.

A different equation is adopted when a linear trend in the *e*-log(*p'*) plane can be considered sufficiently approximate:

$$e_{CS} = e_{lim} - \lambda_{CS} \cdot log\left(\frac{p'}{P_a}\right) \tag{9}$$

where e_{lim} is now the void ratio evaluated for $p'=P_a$ and λ_{CS} the slope of the curve in the *e*-log(*p'*) plane.

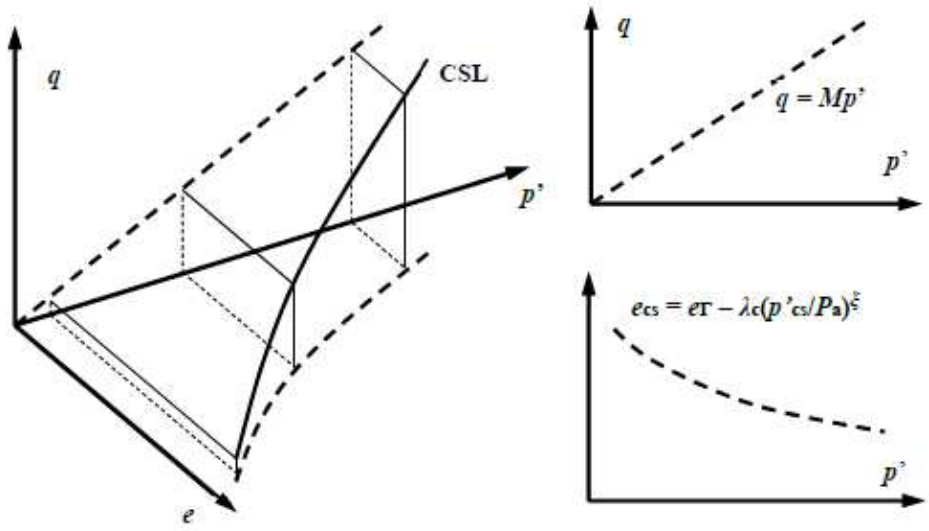

Figure 36 – Schematics of the critical state lines in different space or planes (Wei 2017).

The analyses based on critical state soil mechanics rely on the assumption that a unique critical state line (*CSL*) exists for a given material. However, several

researchers argued that the critical state line in the compression plane may depend on several factors such as stress history (Finno and Rechenmacher 2003), initial fabric (Vaid et al. 1990), and loading conditions (Vaid et al. 1990; Riemer and Seed 1997). However, some recent studies revealed that the critical state line seemed to be unique regardless of initial fabric and drainage conditions (Murthy et al. 2007). Jefferies and Been (2006) discussed the uniqueness of critical state line by compiling published data and claimed that the discrepancy observed in the published data between drained and undrained tests (Alarcon-Guzman et al. 1988; Casagrande 1975; Hird and Hassona 1990) and the non-uniqueness caused by different initial fabric (Vaid et al. 1990) could be ascribed to the mistakes in the determination of critical state in the tests. For example, some errors in the definition of the critical state could be due to the consideration of a quasi-critical state instead of a critical one, which depends on both the test conditions and the method of preparation of the specimen. Besides, some mistakes are due to the determination of the critical state at an insufficient (not sufficiently extended) strain level or from picked data of dense samples that might not reach the critical state. It is believed that a unique critical state line can be defined with proper testing technique and rigorous interpretation. Li and Dafalias (2012) proposed anisotropic critical state theory and explained the role of initial fabric on the non-unique critical state lines. They numerically demonstrated that different initial fabric and loading conditions may result in a unique critical state line at extremely high strain level, which may be not possible under laboratory conditions. Moreover, initial density and initial effective confining pressure seemed to be widely accepted as non-influential to the critical state lines (e.g. Sze 2010; Yang and Wei 2012), but material properties, such as gradation, particle shape, fines content, etc., may have certain effects on the critical state line (e.g. Yang and Wei 2012; Yang and Luo 2015).

Starting from the critical state line it is possible to define different state parameters to interpret the behaviour of silty sands that are the subject of this thesis. These variables are defined as follows: state parameter, Ψ proposed by Been and Jefferies (1985); state index proposed by Ishihara (1993); state pressure index, I_p proposed by Wang et al. (2002); modified state parameter, Ψ_m proposed by Bobei et al. (2009); equivalent granular state parameter Ψ^* proposed by Rahman (2012); equivalent pressure index I^*_p and equivalent modified parameter Ψ^*_m proposed by Qadimi and Mohammadi (2014). Among all of these parameters, the state parameter is the most frequently

applied. It is defined as the difference between the current void ratio and the void ratio at the same mean effective stress on the critical state line (**Figure 37**):

$$\Psi = e - e_{CS} \tag{10}$$

where e and e_{CS} are the initial void ratio and the critical void ratio at the same mean effective stress, respectively. For sands, it is widely observed that dilation tends to decrease by increasing void ratio or effective confining pressure before shearing. The increased void ratio or mean effective stress can be quantified by the state parameter that is capable to unify the effects separately exerted by the void ratio and the mean effective pressure; i.e. with increasing the state parameter, a decreased dilatancy can be anticipated. The application of the state parameter was seemed to be successful in characterising the behaviours of sands, such as Li and Dafalias (2000), Yang (2002), Murthy et al. (2007).

Jefferies and Been (2006) also collected cyclic test data from literature and critical state line information to facilitate cyclic resistance evaluation via initial state parameter. Generally, the cyclic resistance decreased with increasing state parameter. However, the database contained very limited data sets from silty sands. Boulanger (2003a, b) also developed an empirical critical state-based cyclic resistance evaluation procedure for clean sands. However, the empirical equations for the critical state line involve a parameter (relative state parameter ξ_R (Konrad 1988)) depending on soil minerals, whose effectiveness is not proved by experimental data and may not be rational.

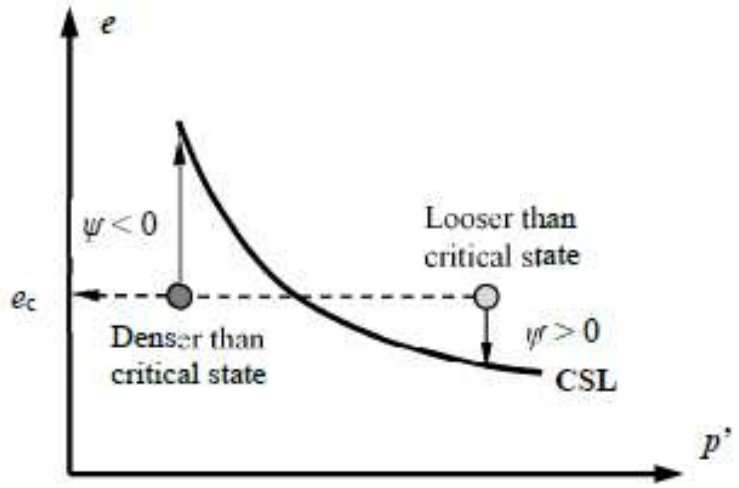

Figure 37 – Definition of state parameter according to Been and Jefferies (1985) (Wei 2017).

Yang and Sze (2011a, b) used the state parameter to characterise the cyclic resistance of clean sands with consideration of initial static shear stress. An interesting result obtained by these latter authors was the evidence that the threshold static shear stress (ratio α) decreases almost uniquely with increasing the state parameter. Application of critical state approach to clean sand seemed to be successful. Hence the state parameter was considered a promising state variable for characterising the undrained cyclic behaviour even of sand-silt mixtures (e.g. Papadoupoulou and Tika 2008; Stamatopoulos 2010; Yang and Sze 2011a, b; Huang and Chuang 2011). However, it should be reminded that nearly all of these investigations on the effects of fines do not take into account the presence of an initial static shear stress. In this regard more recently Wei and Yang (2019b) presented laboratory test results showing that the critical state soil mechanics may be applied to silty sands under various initial static shear stress level.

After analysing numerous test data, Ishihara (1993) concluded that if samples are sheared at low mean effective stresses with void ratios greater than a threshold one, then all samples will come up with zero residual strength, though their state parameters are not identical. To solve this problem he proposed a quasi critical state line *QSSL* as a reference base to capture the soil behaviours at low stress level and defined a new state index, I_s as:

$$\mathrm{I}_S = \frac{e_{UR} - e}{e_{UR} - e_{QSS}} \tag{11}$$

where the symbols have the meaning shown in **Figure 38**.

Recently, the state index I_S has been used to characterise the monotonic behaviour of Yellow silty sands (PI=9.3) (Rabbi et al. 2019). The results showed good correlations between some fundamental aspects of the undrained monotonic behaviour of the investigated silty sand with I_S, i.e.: static liquefaction potential and instability stress ratio for specimens that exhibited limited flow or flow behaviour.

Moving along a similar line, Wang et al. (2002) reported that the ratio of current mean effective stress, p' to the mean effective stress at critical state/steady state, p'_{CS} is an appropriate state variable for the constitutive modelling of sand. Thus, they introduced the concept of state pressure index, I_p as:

$$\mathrm{I}_P = \frac{p'}{p'_{CS}} \tag{12}$$

where, p' = current mean effective stress and p'_{CS} = mean effective stress at critical state at current void ratio, e. The definition of the state index is shown in **Figure 39**.

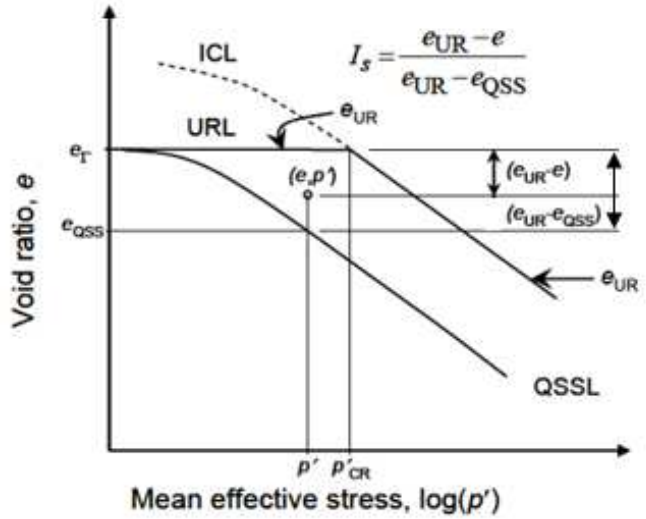

Figure 38 – Definition of state index I_S according to Ishihara (1993) (Rahman 2009).

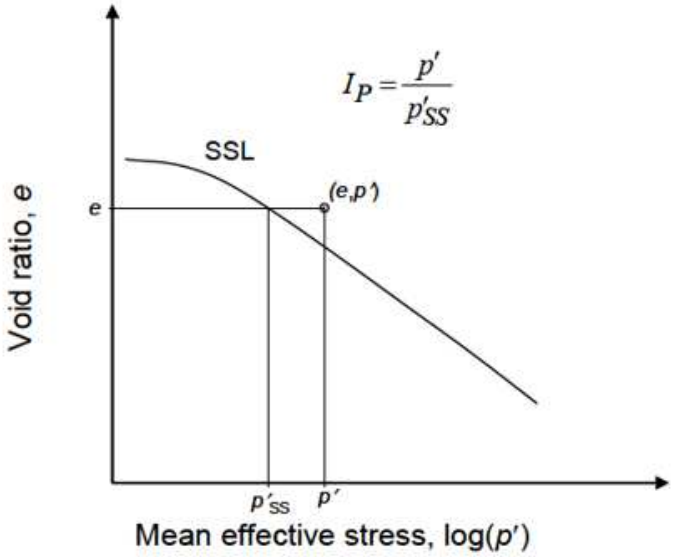

Figure 39 – Definition of state pressure index I_p according to Wang et al. (2002) (Rahman 2009).

Qadimi and Mohammadi (2014) and Rabbi et al. (2019) used the state pressure index I_p to characterise the undrained cyclic and monotonic behaviours of non-plastic and low-plastic silty sands. Quite good results were obtained for the prediction of the several aspects characterising the monotonic and cyclic behaviours of the investigated materials i.e.: static liquefaction potential, instability stress ratio, deviator stress at critical state and cyclic liquefaction resistance.

As already mentioned, the critical state line, *CSL* is not necessarily linear in *e*-log(*p'*) space. Recent literature data showed that *CSL* of non-plastic or low-plastic silty sands is curved (Bobei and Lo 2005; Li et al. 1999; Verdugo and Ishihara 1996). Bobei and Lo (2005) and Bobei et al. (2009) realized that due to the curve shape of *CSL*, state

parameters defined only in terms of void ratio or effective stress cannot capture in an exhaustive way the behaviour of sand-fines mixtures observed in undrained monotonic and cyclic shear tests.

Thus, they proposed a modified state parameter, Ψ_m, expressed as:

$$\Psi_m = \Psi \cdot \left|\frac{\Delta p'}{p'}\right| \cdot e \tag{13}$$

where: Ψ is the original state parameter, $\Delta p'$ is the difference between the mean effective stress at the current state and the corresponding one taken on *CSL* for the same value of void ratio (**Figure 40**). By combining the original "state parameter" (Been and Jefferies 1985) and the "state pressure index" (Wang et al. 2002), the modified state parameter Ψ_m can be rewritten as:

$$\Psi_m = \Psi \cdot \left|1 - \frac{1}{I_P}\right| \cdot e \tag{14}$$

Bobei et al. (2009) reported that Ψ_m has better prediction capability for sand with fines under the *CSSM* framework. Other researchers analyzed cyclic and monotonic behaviour of non-plastic or low-plastic silty sands with this state parameter (Qadimi and Mohammadi 2014; Rabbi et al. 2019) obtaining satisfactory results and a quite good correlation with some characteristics of undrained behaviour of these materials can be found.

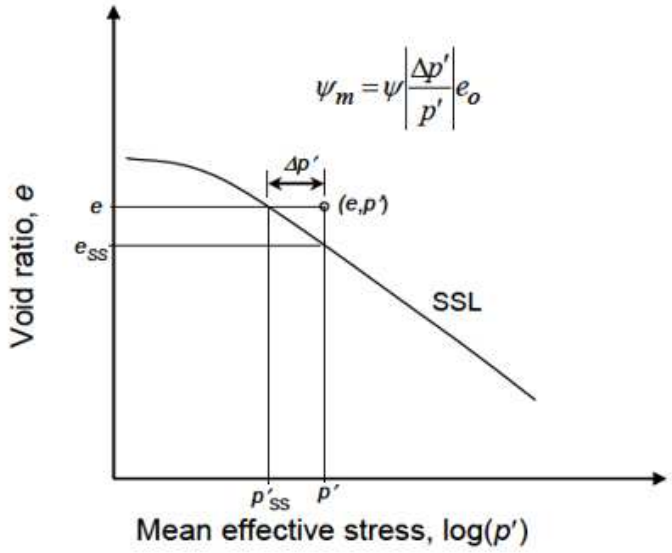

Figure 40 – Definition of modified state parameter according to Bobei et al. (2009) (Rahman 2009).

Analysis of literature studies shows that the capability of the state indices defined in terms of the conventional void ratio (*e)*, particularly Ψ, I_p and Ψ_m, to predict the undrained behaviour of non-plastic sandy soils is not general in the sense that they can only be applied for single values of fines content. This is mainly the result of the shift in the location of *CSL* in the compression plane by changing the fines content. Samples having the same initial state represented by a point in the *e*-log(*p'*) plane, but with different f_c values, have different values of the state parameters. Consequently, the application of the state indices defined in term of the conventional void ratio (*e*), requires that a specific *CLS* be determined for any given fines content. Recently, using the concept of equivalent granular void ratio e^* (Thevanayagam et al. 2002), the state indices previously defined have been rewritten obtaining similar state parameters, i.e. equivalent granular state parameter Ψ^* (Hsiao and Phan 2016; Rahman and Sitharam 2020; Porcino et al. 2019), equivalent pressure index I^*_p (Qadimi and Mohammadi 2014) and equivalent modified state parameters Ψ^*_m (Qadimi and Mohammadi 2014). The reason for using these modified state indices instead of the original ones is not in the quality of the predictions (that remains approximately unchanged) but in a practical convenience since they require the knowledge of a unique critical state line (*EG-CSL*) for all fines contents varying in the range from 0 to the limiting fines content f_{thre}. The critical state line (*CSL*) of the clean sand could then be used as unique *EG-CSL* resulting in a significant reduction in the necessary experimental activity.

2.2.2 State variables for the analysis of the behaviour of non-plastic silty sands: the equivalent granular state concept

Laboratory investigations can provide a better control of variables, and thus isolate each influential factor, leading to more insightful observations and conclusions than field tests. In laboratories, various amounts of fines can be added into clean sands to form sand-fines mixtures. Before fines are added into the sandy particles, only coarse grains may transfer normal stress and shear stress in the soil skeleton (**Figure 41a**). After some fines are added, these fines particles may, ideally, all fall into the voids formed by coarse sandy particles (**Figure 41b**). But, in fact, fines particles may either fall into the voids, or reside in between the sandy particles and thus become active in the force chains (**Figure 41c**), e.g. Lade and Yamamuro (1997), Luo and Yang (2013), and Yang et al. (2015). So far, the soil behaviour may still be controlled by the skeleton constituted by coarse sand particles. With further increase of fines content, more and

more fines may become active and the soil behaviour may gradually become dominated by skeleton constituted by fines, when the fines content is so high that the fines surround the coarse sandy particles and the sandy particles float in the matrix formed by fines (**Figure 41d**).

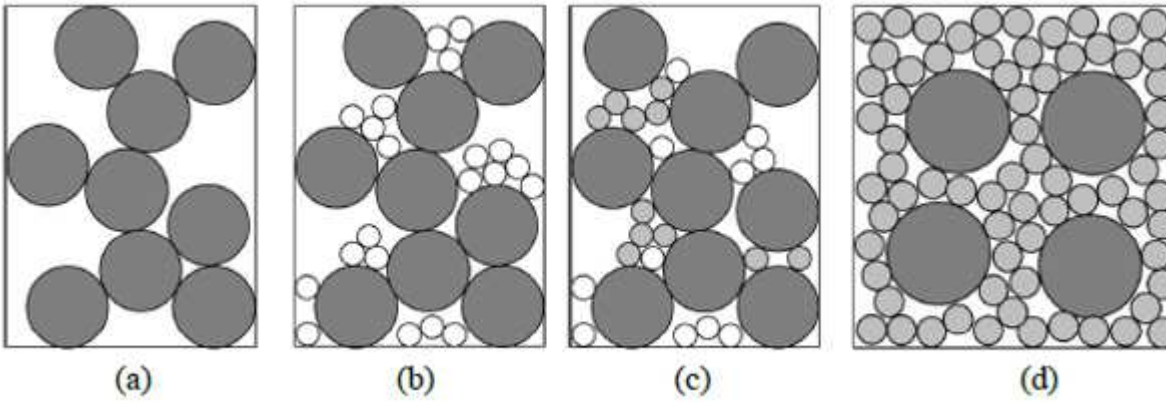

Figure 41 – Schematics of possible sand-fines interaction for different fines content: (a) clean sand; (b) sand-fines mixture with $f_c<f_{thre}$, fines all in the voids not participating in the force transfer; (c) sand-fines mixture with $f_c<f_{thre}$, part of the fines reside between coarser particles and are active in force chains; (d) sand-fines mixture with $f_c>f_{thre}$, coarse particles floating in fines (Wei 2017).

There seems to be a threshold fines content f_{thre} that may separate sand-dominant and fines-dominant soil skeleton. Threshold fines content (f_{thre}), also termed ‘‘limiting fines content’’ (Polito 1999; Hazirbaba 2005) or ‘‘transitional fines content’’ (Yang et al. 2006a) in the literature, is the specific value of the fines content at which the behavioral properties of the mixture is reversed (Mohammadi and Qadimi 2015). The threshold value serves as an indicator for the nature of mixed soils varying from being sand-dominant to fines-dominant (Thevanayagam et al. 2002; Yang et al. 2006a). Zuo and Baudet (2015) summarised several methods determine the threshold fines content including experimental methods and analytical methods. The analytical methods suggested that the threshold fines content might depend on various factors. Moreover, they also observed a discrepancy between the analytically determined values and the experimentally determined ones, indicating sophisticated behaviours of sand-fines mixtures. Nevertheless, the threshold fines content may range from approximately 30% to 50% (such as Polito and Martin 2001; Papadoupoulou and Tika 2008; Yang and Wei 2012).

For sand-fines mixtures there are several commonly used density parameters to characterise the soil behaviour and quantify the monotonic and cyclic resistance, namely relative density D_R, void ratio e, skeleton void ratio e_g, and equivalent granular void ratio e^*.

Relative density describes how dense the soil specimen is with reference to the maximum and minimum densities (minimum and maximum void ratios, respectively). Lee and Singh (1971) discussed drawbacks of relative compaction, which is another density index that may be popular in engineering practice and specifications and suggested relative density to be used especially for liquefaction analysis on granular soils. Relative density is defined as follows:

$$D_R = \frac{e_{max} - e_0}{e_{max} - e_{min}} \tag{15}$$

where e_{max} and e_{min} are the maximum and minimum void ratios, respectively. Many researchers compared the undrained cyclic resistance of sands with different fines contents at the same relative density. Singh (1994) found that undrained cyclic resistance decreased with increasing fines content (f_c=0, 10%, 20%, and 30%) when compared at the same relative density. The undrained cyclic resistance of pure silt was measured higher than for silty sands with fines contents of 10%, 20%, and 30%, but lower than that of pure sand. Chien et al. (2002) also observed a similar trend that the undrained cyclic resistance decreased with increasing fines content and the reduction of resistance was greater when the fines content was higher than 10%. Polito (1999) concluded that for specimens at the same relative density, increasing silt content seemed to have limited influence of undrained cyclic resistance when the fines content was lower than a certain value (**Figure 42**). Karim and Alam (2015) observed an intermediate behaviour in cyclic and static undrained monotonic tests, before limiting fines content the resistance decreases with increasing fines content, while for fines contents higher than limiting fines content the resistance is not influenced by the fines (**Figure 43**). Carraro et al. (2003) compared the cyclic resistance at the same relative density (40% to 70%) and found that it first increased slightly when the fines content increased from 0% to 5%, and then decreased with increasing fines content. Contrarily, Dash and Sitharam (2009) showed that the rate of pore water pressure generation increased with increasing fines content when fines content was below 5% and then decreased with further increasing fines content until the threshold fines content was reached. After this threshold, this rate is more or less a constant. Amini and Qi (2000)

reported that at the same void ratio or relative density the cyclic resistance would increase with increasing fines content.

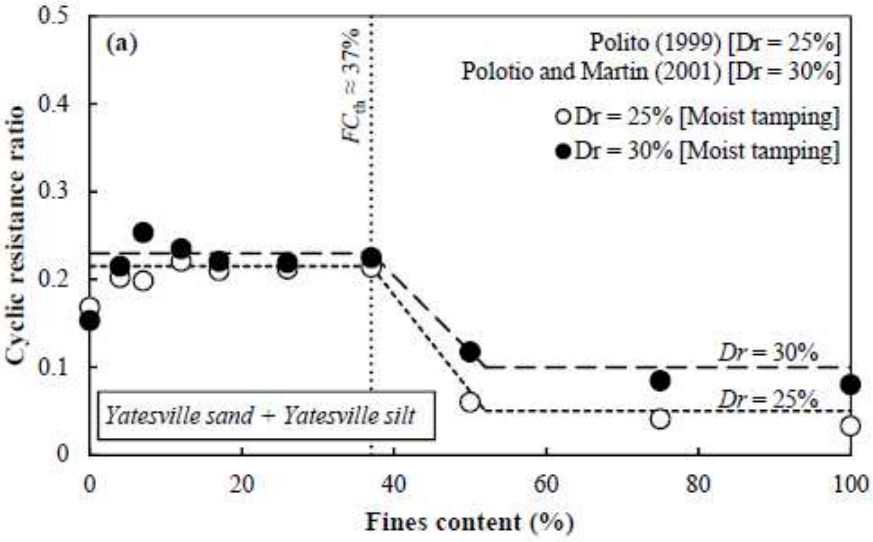

Figure 42 – Effect of fines compared at the same relative density obtained by Polito (1999) and Polito and Martin (2001) (Wei 2017).

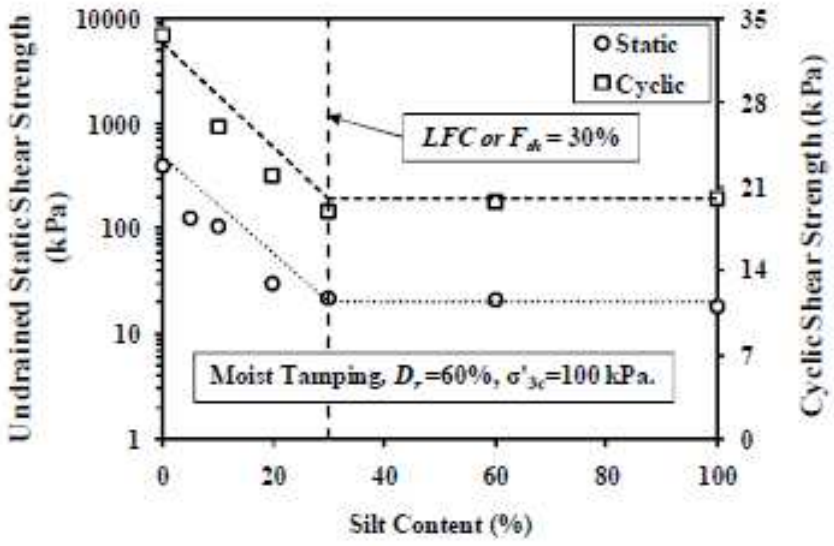

Figure 43 – Effect of fines compared at the same relative density obtained by Karim and Alam (2015).

This conclusion seems to be contradictory to many others studies reviewed previously; this might be because slurry deposition was adopted to reconstitute the specimens, through which the relative density or void ratio could be hardly controlled. Thus the conclusions may be inaccurate. The results based on the same relative density seem

to have a large discrepancy. The reasons behind may be as follows. First of all, calculating relative density requires determination of extreme void ratios, e_{max} and e_{min}. However, determination of e_{max} and e_{min} of silty sand may be inaccurate, especially when the fines content is relatively high. Secondly, when compared at the same relative density, the void ratio usually decreases with increasing fines content ($f_c<f_{thre}$) because both e_{max} and e_{min} would decrease. The decreased void ratio may cause increased cyclic resistance. Thus the detrimental effects of additional fines may be compromised to some extent by such decreased void ratio when compared at the same relative density. For these two reasons, controversial conclusions may be anticipated.

Void ratio is simply defined as the ratio between the volume of voids (V_v) and the volume of solids (V_s) as follows:

$$e = \frac{V_v}{V_S} \tag{16}$$

The void ratio thus defined for sand-silt mixtures is called “global void ratio”.

In a laboratory study performed on specimens prepared to a constant global void ratio, Chang et al. (1982) found that specimens with about 10% fines content displayed cyclic resistances approximately 10% smaller than clean sand specimens. However, specimens with high fines content (up to about 60% fines) exhibited as much as 50% higher cyclic resistance than a clean sand specimen. Troncoso and Verdugo (1985) used tailing materials to investigate the influence of fines content. They first separated the sandy and silty particles, then mixed the two types of particles at different ratios. They prepared samples to the same initial void ratio and found that silty fines reduce the cyclic resistance with increasing fines content. They attributed it to the larger compressibility and smaller permeability of specimens with higher fines content. Also comparing at the same void ratio, Erten and Maher (1995) used strain-controlled cyclic tests to study the effect of fines content. Addition of fine particles (both non-plastic and low plastic) could increase the excess pore water pressure reached after a given number of cycles. The pore pressure generation in sand containing non-plastic fines increased until the fines content reached 30%. The increase in low-plasticity fines content did not affect the pore pressure generation until 60% fines content was reached. Afterwards, the pore pressure generation reduced with further increase of fines content. Their data may indicate the existence of a threshold fines content. Later on, Polito (1999) performed a comprehensive study on how fines content influenced

the undrained cyclic resistance of silty sands. In this study, the cyclic resistance of sands with different fines content was compared using different state variables. Their results confirmed the observation made by Koester (1994) that, when mixtures are compared at the same void ratio, a threshold fines content exists below which the cyclic resistance may decrease with increasing fines content, while beyond it the cyclic resistance may increase (**Figure 44**). Similar observations were also reported by Xenaki and Athanasopoulos (2003) and Dash and Sitharam (2009), showing that a threshold fines content exists when compared at the same void ratio.

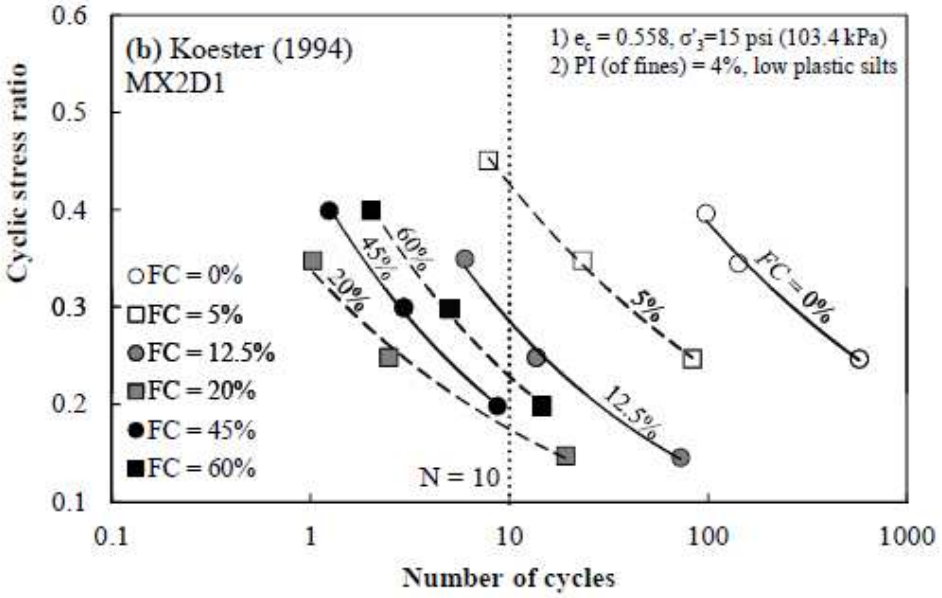

Figure 44 – Effect of fines compared at the same global void ratio obtained by Koester (1994) (Wei 2017).

When a small amount of fines is added into the base sand, especially when the particle size disparity is significantly large, most of the fine particles may reside in the voids formed by the base sands. Note that the fines residing in the voids may not participate in the force transfer chain, therefore the voids they fill, and not those formed by the overall (global) structure of the mixture, may be considered more representative of the mechanical behaviour of the mixture. This consideration led to the concept of skeleton void ratio or intergranular void ratio (Kuerbis et al. 1988). Assuming the same specific gravity for the sands and the fines, the skeleton void ratio may be defined as follows:

$$e_g = \frac{e + f_c}{1 - f_c} \tag{17}$$

where f_c is the fines content in decimal. Kuerbis et al. (1988) reported that the undrained cyclic resistance increased slightly with increasing fines content if compared at the same e_g, but Singh (1994) reported that the cyclic resistance decreased with increasing fines content when compared at the same skeleton void ratio, which was similar to the results obtained when the comparison was made at the same relative density. Unlike the previous two studies, Polito (1999) found that the cyclic resistance appeared to be a relative constant with various fines contents when the specimen was prepared at the same skeleton void ratio if the fines content would not exceed the limiting fines content. He argued that it might be explained by the combined relation existing between fines content, void ratio and extreme void ratios at the same skeleton void ratio. When specimens were prepared at the same skeleton void ratio, increasing fines content decreased the void ratio of the specimen. Meanwhile, the maximum and minimum void ratios decreased with increasing fines content. Such decrease in void ratio and index void ratios would lead to a nearly constant relative density and thus a nearly constant cyclic resistance. However, not every reported data showed the same conclusion. Carraro et al. (2003) presented data showing similar conclusion that fines content do not influence the undrained cyclic resistance when the samples are compared at the same skeleton void ratio, but the cyclic resistance of silty sand was found to be higher than that of clean sand. Dash and Sitharam (2009) reported that the relative density increased almost linearly with increasing fines content if compared at the same skeleton void ratio. They also observed that the cyclic resistance could increase with increasing fines content when compared at the same skeleton void ratio. Such increase of cyclic resistance could be very gentle unless the increased fines content resulted in a relative density approximately equal to 70%. Laboratory investigations based on the skeleton void ratio also showed discrepancy to some extent. The concept of skeleton void ratio assumes that all the fines fall into the voids formed by the sandy particles and take no participation in the force chains. However, many investigations showed that the addition of fines led to higher cyclic resistance than the one of clean sand, which may imply that this assumption may be incorrect. In real cases, not all of the fines are free from force transfer, but some may serve as a part of the force chains (e.g. Thevanayagam 2000; Luo and Yang 2013). These particles in force chains may be regarded as active fines and need be considered as part of the soil skeleton. For this reason, the equivalent granular void ratio was proposed (Thevanayagam et al. 2002) for silty sands with fines content smaller than

the threshold fines content. It is defined as follows, assuming the same specific gravity for the fine and sandy particles:

$$e^* = \frac{e + (1-b)\cdot f_c}{1-(1-b)\cdot f_c} \tag{18}$$

where *b* is the fraction of fines taking part in the force chains. When compared at the same equivalent granular void ratio, the undrained cyclic resistance of sand-silt mixtures with different fines content seemed to be the same (Rees 2010) (**Figure 45**).

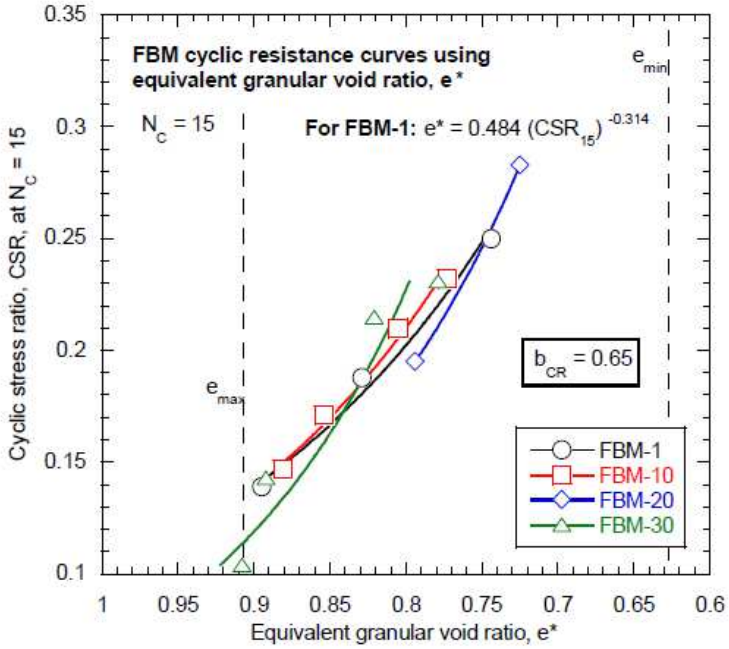

Figure 45 – Effect of fines content (numbers after *FBM* in the internal captures) in sand-silt mixtures compared at the same equivalent granular void ratio (Rees 2010).

By increasing fines content beyond the threshold value, fine grains can intrude among the coarser grains till the sand grains are floating in the fines, leading to a reduction in intergranular contact. Then, the force structure of the soil is dominated by the fines skeleton (sand-in-fine). For that case, Thevanayagam et al. (2002) suggested the following expression for the determination of the *e** value:

$$e^* = \frac{e}{f_c + (1-f_c)/(R_d)^m} \tag{19}$$

where, $R_d = D_{50}/d_{50}$ and *m* is a fitting parameter obtained by back analysis. D_{50} and d_{50} are the size of sand at 50% finer and the size of fines at 50% finer, respectively. Qadimi and Mohammadi (2015) for sand M31 with Assyros silt (for $f_c > f_{thre}$) obtained a unique critical state lines in the e^*-log(p') plane (**Figure 46**).

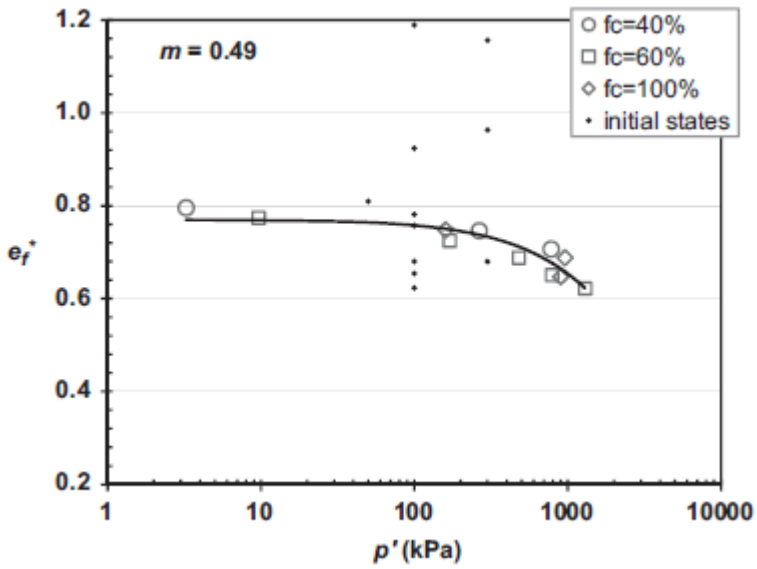

Figure 46 – Equivalent critical state line for Sand M31 with Assyros silt based on the best *m* value (Qadimi and Mohammadi 2015).

The same observation for $f_c<f_{thre}$ was obtained by many researchers (Rahman and Lo 2008; Porcino et al. 2019b; Rahman and Sitharam 2020) (e.g. **Figure 47**). In fact, the critical state line for a sand-fines mixture with fines content less than f_{thre} should follow a unique trend in the e^*-log(p') space (Thevanayagam et al. 2002). This unique relationship is achieved by choosing an appropriate b value for mixtures with fines content $f_c<f_{thre}$ and an appropriate value of m for $f_c>f_{thre}$.

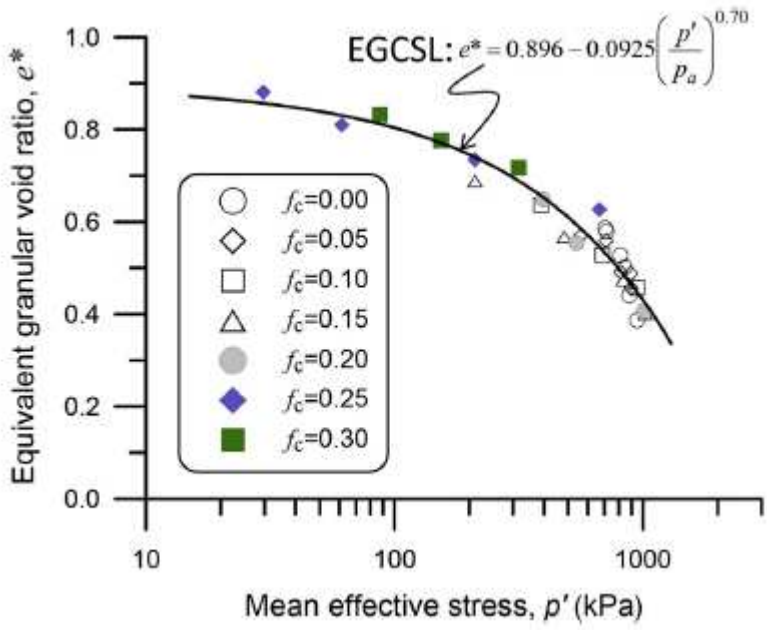

Figure 47 – Equivalent granular critical state line *EG-CSL* for Ahmedabad sand with fines (Rahman and Sitharam 2020).

Thevanayagam et al. (2002) used the back analysis method to obtain the *b* value for their results. They assumed *b* to be constant with a value $b = 0.25$ for a whole range of fines content below the threshold fines content. Later, other researchers reported the same value for the soil that Thevanayagam et al. (2002) used, applying back analysis (Yang et al. 2006b; Baki 2011). Note that Yang et al. (2006b) determined a constant *b* value of 0.25 for mixtures with fines contents less than the threshold, $b = 0.4$ for $f_c = f_{thre}$, and $m = 0.65$ for mixtures with fines contents higher than the threshold, to achieve a good fit for their own data. Thereafter, Rees (2010) found a *b* value of 0.35 for Toyoura sand, while Ni et al. (2004) considered a *b* value of 0.25 for the same soil. Carrera et al. (2011) found $b = 0.8$ to be the optimal value for the Stava tailings soils with $f_c < f_{thre}$. Moreover, previous researchers stated that the *b* value may vary between 0 to 1 (Chu and Leong 2002; Thevanayagam et al. 2002; Rahman and Lo 2008; Rahman 2009; Rahman et al. 2011; Lashkari 2014). A *b* value of 0 means that fines are not contributing to force transmission in the soil structure. This assumption leads to an e^* value being equal to the skeleton void ratio e_g. Kanagalingam and Thevanayagam (2005) reported that the *b* value, which they obtained from back analysis, may depend on soil grading parameters. These grading parameters are: (1) particle size ratio, defined as $R_d=(D_{50}/d_{50})$, (2) uniformity coefficient of sand, defined as $C_{U,S}=(D_{60}/D_{10})$, and (3) uniformity coefficient of fines, defined as $C_{U,f}=(d_{60}/d_{10})$, where *D* and *d* are the grain sizes of sand and fines, respectively. They proposed a correlation between *b* and $C_{U,S}\cdot C_{U,f}{}^2/R_d$ for $R_d > 6$, which is shown in **Figure 48**.

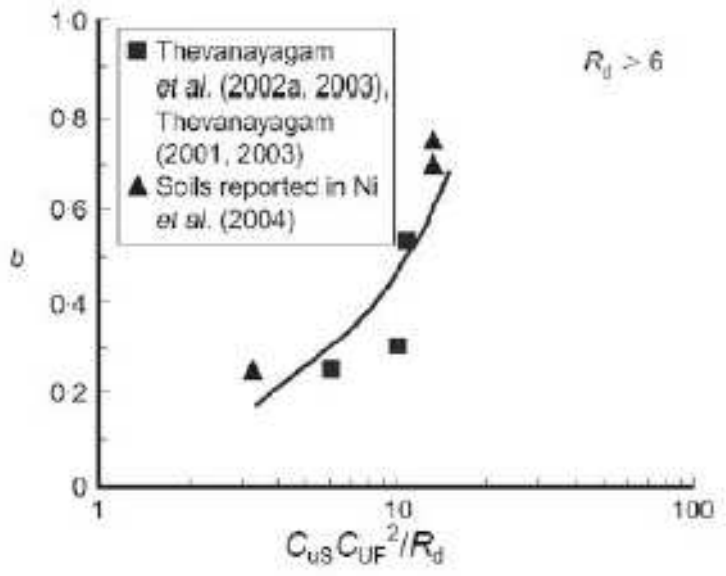

Figure 48 – Correlation of *b* with soil grading parameters (Kanagalingam and Thevanayagam 2005).

Furthermore, Ni et al. (2004) suggested a linear relationship between m and $C_{U,S} \cdot C_{U,f}^2/R_d$ for mixtures with high fines content. Recently, Goudarzy et al. (2016) performed a series of resonant column tests on Hostun sand mixed with quartz powder, and their results were in agreement with the function as suggested by Ni et al. (2004), see **Figure 49**.

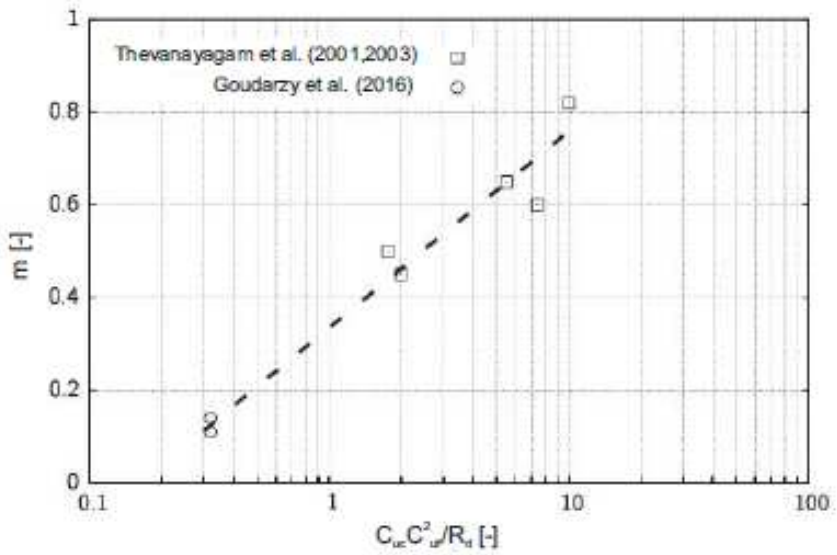

Figure 49 – Correlation of *m* with soil grading parameters (Goundazy et al. 2016).

It should be noted that the data of aforementioned studies was not sufficient to take a final decision regarding suitable functions for b and m parameters considering grain characteristics of the fine and coarse particles. Thevanayagam et al. (2002) and Rahman and Lo (2012) discussed the effect of fines content on the b value. Rees (2010) suggested different correlations to obtain the b value as a function of particle size ratio, $\chi = D_{10}/d_{50}$ and maximum void ratio of the sand. Recently, the so-called prediction method has been suggested to obtain the b value by Rahman and his co-workers (Rahman and Lo 2008; Rahman 2009; Rahman et al. 2011; Rahman and Lo 2012). The prediction method of Rahman and his co-workers is used in many recent studies. They suggested an empirical equation based on re-analysis of the McGeary (1961) study on the void ratio of binary packings. They indicated that the b value can be represented by a functional relationship of particle diameter ratio, χ and fines content, i.e. $b = F(\chi, f_c)$. A number of empirical constants are also used in this equation, which are defined according to the soil characteristics. This semi-empirical equation is used to get the b value for sand-fines mixtures with $f_c < f_{thre}$:

$$b = \left\{1 - exp\left[-\mu \cdot \frac{(f_c/f_{thre})^n}{k}\right]\right\} \cdot \left(\frac{r \cdot f_c}{f_{thre}}\right)^r \quad (20)$$

where, $r = \chi^{-1} = d_{50}/D_{10}$, $k = (1 - r^{0.25})$, and μ is a fitting parameter. Rahman and his co-workers used eight different published data sets to develop Eq. (20). Recently, Lashkari (2014) recommended a new definition of the *b* parameter, renamed as β^1 and formulated as a function of fines content and grain shape. The empirical relationship in Eq. (21) is proposed to obtain the β^1 parameter.

$$\beta^1 = \beta_0(r, f_c) \cdot f_c \cdot \chi^z \quad (21)$$

where the term $\beta_0(r, f_c)$ considers the combined infuence of the roundness of coarse and fine constituents. *z* is a material parameter, with $z \approx -0.2$ being a reasonable estimate for various silty sands, and χ is the particle diameter ratio, D_{10}/d_{50}. Based on available data in the literature, the parameter $\beta_0(r, f_c)$ is formulated, according to the following equation:

$$\beta_0(r, f_c) = [1.93 + 0.04 \cdot (r-1)^2] \cdot [1 + 3.2 \cdot (r-1)^2 \cdot exp(-22 \cdot f_c)] \quad (22)$$

where, $r = R_c/R_f$ is the roundness ratio in which R_c and R_f are the average roundness of the coarse and the fines fraction, respectively. Lashkari (2014) stated that, when the mixtures have well-rounded to sub-rounded coarse particles, then the divergence between calculated *b* and calculated β^1 parameter will be significant, see **Figure 50**. The linear curve is the equation for *b*, while the black solid curve with data points shows β^1. It can be implied that when the roundness ratio *r* between the coarse grains and the fines grains are almost the same then the value of *b* and β^1 would be the same.
Rahman et al. (2008) found an effect of fines content on the *b* value as shown in **Figure 51**. At lower fines content the influence of the ratio f_c/f_{thre} on parameter *b* is very small, but at higher fines content this influence begins to be more significant. This means that chosing a suitable *b* value presumes that a reliable value of f_c/f_{thre} is assumed.

2.2.3 Use of theoretical models for the prediction of the undrained behaviour of silty sands

Constitutive modeling of soil behaviour under static and cyclic loading has experienced rapid development in the past several decades (Pastor et al. 1990; Li and Dafalias 2000; Zhang and Wang 2012; Wang and Xie 2014; Jefferies 1993; Manzari and Dafalias 1997; Dafalias and Manzari 2004; Dafalias and Taiebat 2016; Yang et al. 2019). How to simulate the state-dependent behaviour of a granular material has been

a critical issue. One of the options is to adopt a state variable in the critical state soil mechanics (*CSSM*) framework.

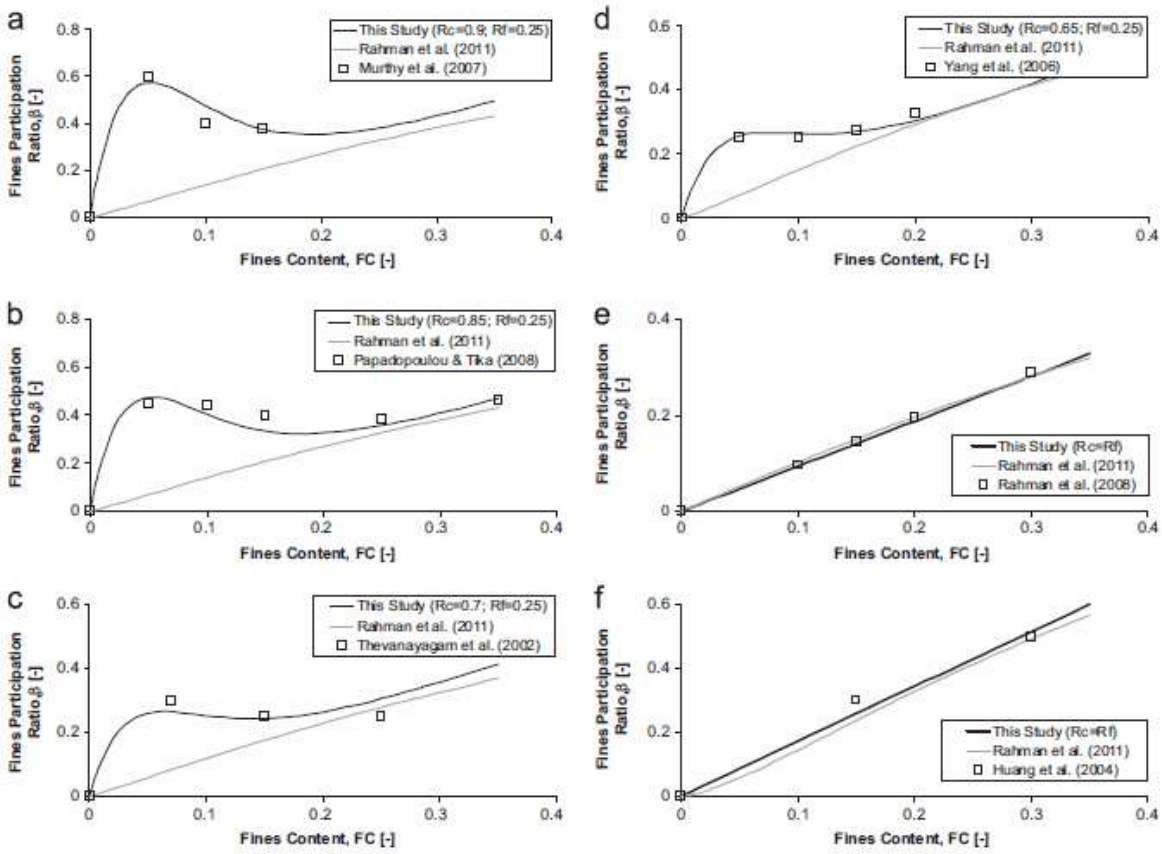

Figure 50 – Effect of angularity on the β^1 parameter (Lashkari 2014).

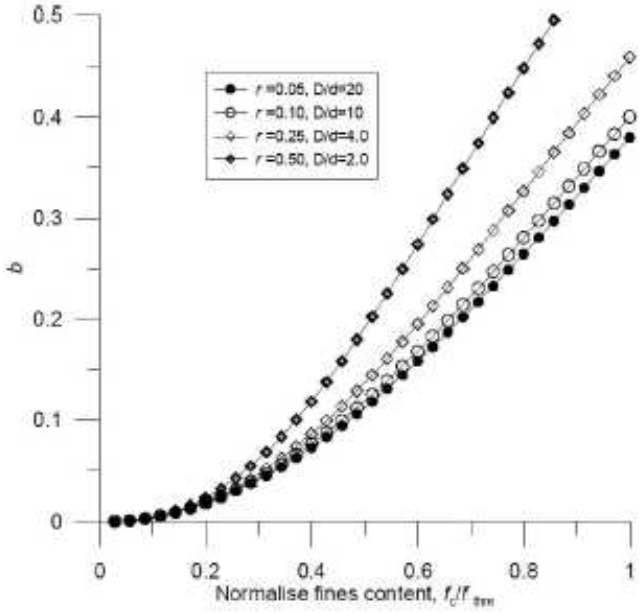

Figure 51 – Influence of fines content on *b* for f_{thre}=0.35 (Rahman and Lo 2008).

The state parameter Ψ (Been and Jefferies 1985) appears to be the most widely used state variable for characterizing the mechanical behaviour of sands and other granular materials. The relationships between Ψ and other parameters related to material behaviour (e.g. instability stress ratio, cyclic resistance ratio, etc.) have also been widely investigated in liquefaction studies (Nguyen et al. 2017; Rahman et al. 2008).

Among the critical state based models, there is a family of models now known as *SANISAND* (Manzari and Dafalias 1997; Li and Dafalias 2012; Dafalias and Manzari 2004; Dafalias and Taiebat 2016), which is featured by the state-dependent bounding surface and flow rule. Although the capability of these models in simulating the mechanical behaviour of sand has been well acknowledged, the calibration and validation are mainly based on experimental data on clean sand. When the models are applied to silty sand, f_c-specific parameters are generally required, implying that a clean sand mixed with different amounts of fines needs to be treated as a different material. This brings significant difficulty since the quantity of fines may vary appreciably even within a single deposit of sand. Yamamuro and Lade (1999) was the first who suggested a constitutive model for silty sands. However, the need for recalibration of yield function and model parameters for different fines contents, densities, and stress levels limit the model applicability in practice.

To model sand with fines behaviour, Thevanayagam and Mohan (2000) modified an existing model in terms of skeleton void ratio, e_g and skeleton state parameter, Ψ_g in order to predict flow rule $d\varepsilon^p_v/d\varepsilon^p_q$. However, the modified flow rule has some limitations; in particular, it assumed a unique isotropic consolidation line, which is not true for sand with fines. In recent years, some unified critical state compatible (*UCSC*) frameworks have been proposed for the constitutive modeling of both clean sand and mixed soils for $f_c < f_{thre}$, as reported by Chang and Yin (2011), Rahman et al. (2014) and Lashkari (2014). Chang and Yin (2011) and Lashkari (2014) proposed valuable models to describe the stress-strain behaviours of sand-fines mixtures taking into account the evolution of the *CSL* in the *e-p'* plane. Rahman et al. (2014) suggested a modified version of the model originally proposed by Li and Dafalias (2000) for clean-sand by using the equivalent granular state parameter Ψ^*. The *UCSC* framework of Rahman et al. (2014) model was established by merely substituting e^* and Ψ^* for e and Ψ into the equations of the state-dependent plasticity model proposed by Li and Dafalias (2000). This model could predict the flow, limited flow, and non-flow behaviours of sand-fines mixtures (**Figure 52**).

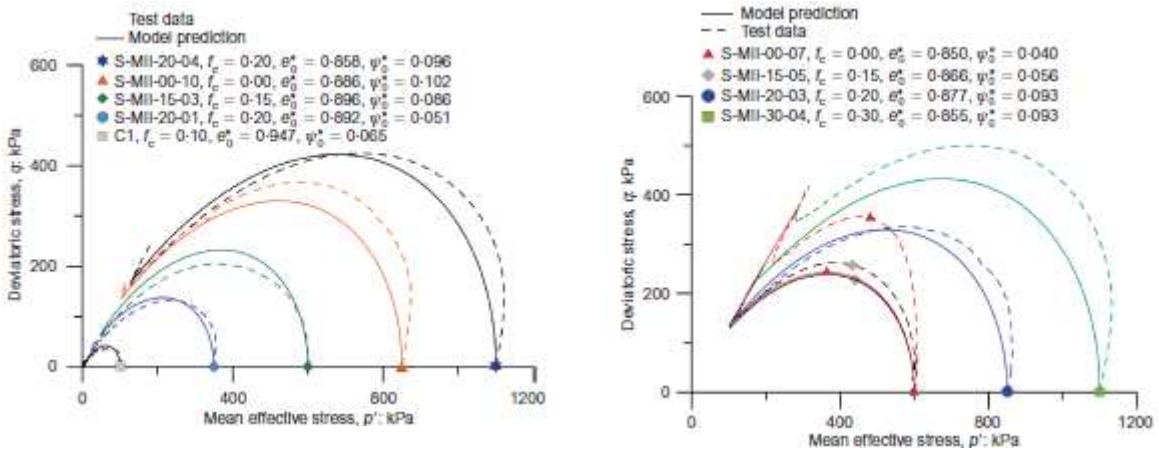

(a) **(b)**

Figure 52 – Comparison between tests results and model prediction for: (a) flow behaviour and (b) limited flow behaviour (Rahman et al. 2014).

However, as observed by Yang et al. (2006b), Murthy et al. (2007), and Papadopoulou and Tika (2008), this model doesn't consider the effect of fines content on the critical-state friction angle of sand-fines mixtures. Lashkari (2014) used a similar approach consisting in substituting e^* and Ψ^* for e and Ψ, respectively, for a fabric-related model developed by Dafalias et al. (2004). The aforementioned *UCSC* frameworks permit to perform the constitutive modeling of sands with various quantities of non-plastic or low-plasticity fines under monotonic loading using a unique set of model parameters. However, they cannot be applied to cyclic loading. Subsequently, using the concept of e^* and Ψ^* Lashkari (2016) and Xu et al. (2019) proposed a bounding surface plasticity model and a state-dependent plasticity model, respectively, for simulating the mechanical behaviour of clean and silty sands under monotonic and cyclic loadings (**Figure 53**).

The models presented in literature to describe the behaviour of silty sand considering in their formulation the state parameter Ψ or the equivalent granular state parameter Ψ^* are more interesting, but further verification must be performed to confirm the advantages. Moreover, these existing models have also some limitations. The samples used in the different studies for development constitutive models for silty sand were prepared by moist tamping that is known to give a soil fabric more representative of sandy deposits placed on land, such as embankment fill or colluviums. Consequentially the models, have not been validated for sandy soil formed by any other process. The concept of Ψ^* is only applicable for a fines-in-sand matrix, so that the proposed model considering this state parameter only works well for f_c below f_{thre}. Thus, mixtures with

higher f_c could not be studied by these models. The proposed models should be considered valid for sand with non-plastic and low plasticity fines. In fact, previous studies on applicability of the concept of e^*, single *EG-CSL* and Ψ^* were largely based on non-plastic, and, to a lesser extent, low-plasticity fines. More studies should then be conducted to extend the applicability of these models to sand-fines mixtures with plastic fines.

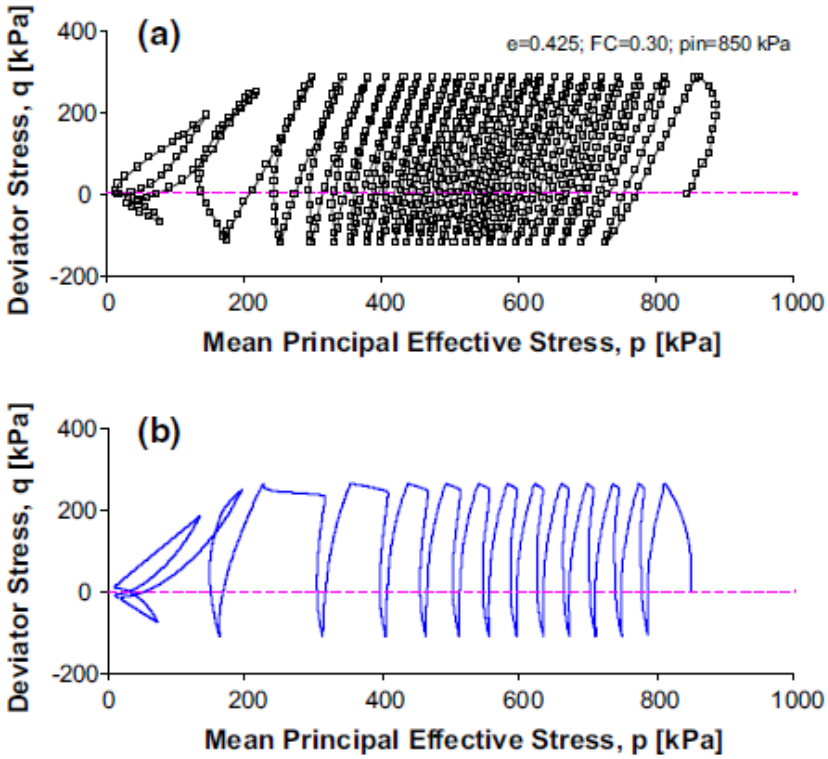

Figure 53 – Simulation of a test on Sydney sand-Majura river silt mixture with e = 0.425 and f_c = 0.30 subjected to cyclic loading: (a) measured stress path, (b) predicted stress path (Lashkari 2016).

2.3 Design procedures for determining in situ cyclic liquefaction resistance in silty sands

Liquefaction of fines containing soils was widely observed during past earthquake events. Okashi (1970) reported that the liquefied soils in the 1964 Niigata earthquake mainly contained fines with fines contents lower than 10%. Data compiled by Tokimatsu and Yoshimi (1983) from 17 earthquakes around the world implied a higher possibility of liquefaction for soils with fines contents lower than 5%. However, some other investigators also reported liquefaction of soils with higher fines content,

such as Trocoso and Verdugo (1985). For example, a study which presented data for 20 historic cases of liquefaction (Baziar and Dobry 1995) showed that sand with up to 80% fines was liquefiable: this corresponded to flow failure of Mochi-koshi tailings dams during the 1978 Izu-Oshima earthquake (M_w = 7.0). Another example included 1.6 m of lateral spreading occurring in sand with f_c = 65% at San Fernando Juvenile Hall during the 1971 San Fernando earthquake, M_w ≈ 6.5. Such case histories have confirmed that liquefaction in sand with fines is a reality in the field, and is not purely confined to laboratory tests. Recent reconnaissance on the liquefaction of soils during earthquakes revealed that liquefaction may occur in soils with fines content ranging from 0% to nearly 100% (e.g. Tokimatsu et al. 2012). Moreover, the recommended liquefaction evaluation charts, such as the *SPT*-based (e.g. Seed et al. 1985), *CPT*-based (e.g. Robertson and Wride 1998) and *Vs*-based (e.g. Andrus and Stokoe 2000) charts all suggest that the liquefaction resistance increases with increasing fines content as long as the cyclic resistance is compared at the same index value. In contradiction, the majority of laboratory test data showed a decreasing liquefaction resistance with fines content (f_c) (Thevanayagam and Martin 2002; Rahman et al. 2008), whereas a typical screening chart, for example *SPT* chart (**Figure 54**), shows increasing liquefaction resistance with f_c for the same standard penetration test, N_{SPT} value (Youd et al. 2001). It may be interesting to note that the explanation of these empirical observations are different according to different researchers. For example, Kokusho et al. (2012) claimed that ageing effects may lead to an increased cyclic resistance with the increase of fines content in the *CPT*-based liquefaction resistance evaluations. However, Thevanayagam and Ecemis (2008) claimed that higher fines content lead to lower permeability and consolidation property and such effects should lead to a reduction of the *CPT* tip resistance because of the inhibited drainage conditions. Besides these two articles, Carraro et al. (2003) investigated the effects of fines content on the *CPT*-based liquefaction resistance curves. They combined the (q_{c1}/P_a)-D_R correlations from numerical simulation and the *CRR*-D_R correlations from laboratory tests. They proposed a series of *CRR*–(q_{c1}/P_a) correlations for fines content ranging from 0% to 15%, showing that a higher fines content would correspond to a lower *CRR*. It should be noted that their simulations on the cone penetration test allowed fully drained conditions around the tip.

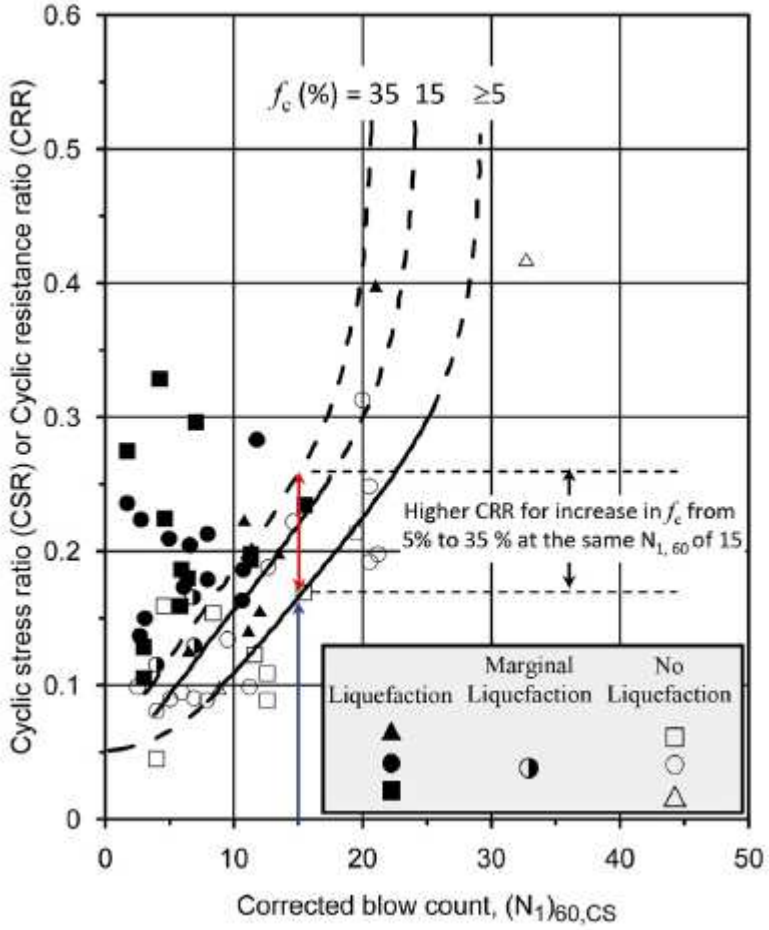

Figure 54 – Liquefaction screening chart for *SPT* based liquefaction evaluation (data collected from Youd et al. 2001)

Moreover, Dobry et al. (2015) reevaluated the *CRR-V_{S1}* database by Andrus and Stokoe (2000) and highlighted that the Andrus and Stokoe's (2000) curves for different fines content are located so close to each other that these differences may be covered by the data scatter and don't necessarily reflect a possible effect of fines content. All these discrepancies imply the complexity of the undrained cyclic behaviours in soils with fines. It should be noted that, even though the field observation may provide the engineers and the researchers with first-hand data and straightforward understanding of liquefaction phenomenon, field condition may be so complex that it is impossible to isolate every influential factor. Therefore, significant research efforts are going on worldwide to better understand the complexity of the problem, yet waiting for a well-accepted "final" screening protocol. Recently, critical state soil mechanics (*CSSM*) is emerging in the literature as a promising pathway for liquefaction analysis (Bouckovalas et al. 2003; Huang and Chuang 2011; Baki et al. 2014); among them Jefferies and Been (2006) provided the most comprehensive contribution. These

studies used state parameter Ψ as a key parameter for correlating liquefaction resistance for soil (**Figure 55**).

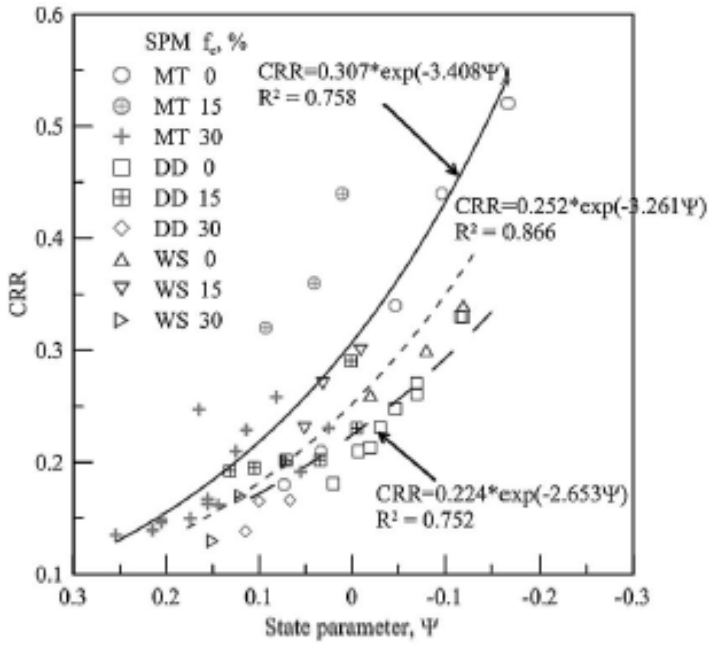

Figure 55 – Correlation between undrained cyclic strength and state parameter for silty sand reconstituted with different methods (Huang and Chuang 2011).

The predicted resistance from such relationships can be compared with expected stresses ratio (*CSR*) induced by the earthquake to assess liquefaction risk. The state parameter Ψ at the field condition can also be estimated from field tests e.g. cone penetration test (*CPT*), standard penetration test (*SPT*) or shear wave velocity (V_S) (Jefferies and Been 2006; Shuttle and Cunning 2007). However, the *CSSM* has other challenges for the effect of fines. Recently, the equivalent granular state parameter Ψ^* was correlated to the undrained cyclic resistance of sand-silt mixtures (Mohammadi and Qadimi 2015; Rahman and Sitharam 2020). Rahman and Sitharam (2020) used the $CRR_{N=20}$ - Ψ^* correlation to estimate the liquefaction resistance for sands with various fines content f_c. The $CRR_{N=20}$ and Ψ^* relation are presented as liquefaction screening chart in Youd et al. (2001). Any data points (Ψ^*, *CSR*) lying on the right side of $CRR_{N=20}$ and Ψ^* relationship represent non-liquefaction and vice-versa. The Ψ^* may be estimated from field tests. An *SPT* based case study of a site near Sabarmati river was used by Rahman and Sitharam (2020) to assess the liquefaction potential by the *CS* approach; the results obtained were compared with those provided by Youd et al. (2001) correlation (**Figure 56**). Both approaches predict no liquefaction which is

consistent with the field observation. The proposed approach needs further verifications, yet it is an interesting method to perform liquefaction analysis in silty sand with different percentages of fines.

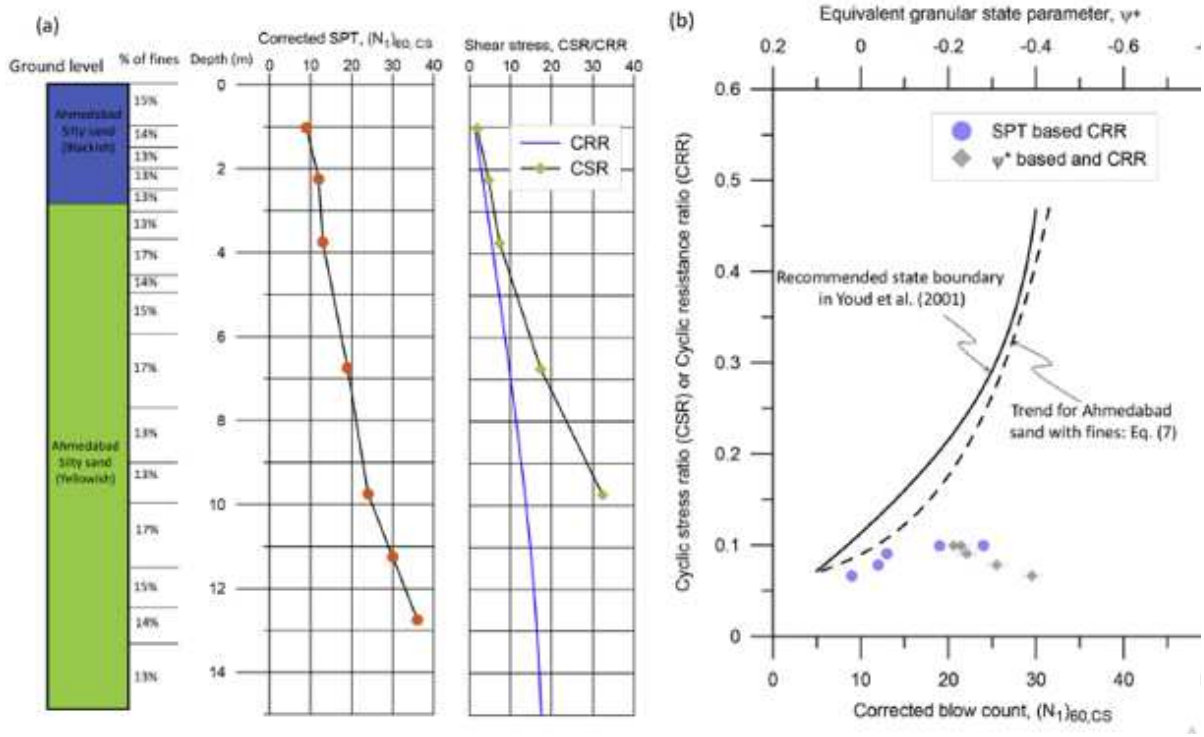

Figure 56 – A case study of Sabarmati river site: (a) soil profile and comparison between the estimated *CSR* and *CRR* (Youd et al. 2001); (b) liquefaction assessment from Youd et al. (2001) and comparison with Rahman and Sitharam (2020).

Chapter 3

Tested materials and experimental program

3.1 Tested Materials

Two types of materials were used in this research: 1) Ticino clean sand, an Italian silica sand from a fluvial (Ticino river) deposit; and 2) a non-plastic silt obtained by sieving and collecting the particles smaller than 75 μm of a natural silty sand dug out from the same deposit and provided by "Sabbie Sataf s.r.l company". They were adopted as host material and fines of the tested mixtures, respectively.

The physical properties of these materials are presented in the following sections. Scanning Electron Microscope (*SEM*) was used for the grain shape analysis.

3.1.1 Ticino clean sand

Ticino clean sand (*TS*) has been used in many previous studies (Fioravante 2000; Jamiolkowski et al. 2003; Jefferies and Been 2016) and has become a standard sand in soil mechanics research. Ticino sand is a silica sand from a fluvial deposit originated in northern Italy. It is a uniform (uniformity coefficient C_U =1.48) coarse to medium sand with a mean grain size (D_{50}) equal to 0.57 mm and a specific gravity (G_S) equal to 2.68. The grain size distribution is shown in **Figure 57a**. A *SEM* image of Ticino sand particles is presented in **Figure 57b**. The roundness chart after Cho et al. (2006) was used to determine the roundness of the particles. The sand particles resulted to have rounded to sub-rounded (*R – SR*) shape.

The values of the minimum and maximum void ratios, e_{min} and e_{max}, of Ticino sand were determined according to ASTM D4253 and ASTM D4254, respectively. The specific gravity was measured according to ASTM D854. The physical properties of Ticino sand are summarized in **Table 1**.

3.2.2 Fines (Non-Plastic Silt)

The grain size distribution curve of the silt obtained using the hydrometer test is shown in **Figure 58a**. The physical properties are presented in **Table 2**, and a *SEM* image is shown in **Figure 58b**. The shape of the silt grains was found to be angular (Cho et al.

2006). The silt resulted to be non-plastic (liquid limit = determination not possible and plastic limit = 32.2%).

Table 1 – Physical properties of Ticino sand.

Material	D_{50} (mm)	D_{30} (mm)	D_{10} (mm)	G_S	C_U	e_{max}	e_{min}	Shape of grains
TS	0.57	0.49	0.42	2.68	1.48	0.93	0.58	Rounded to sub-rounded

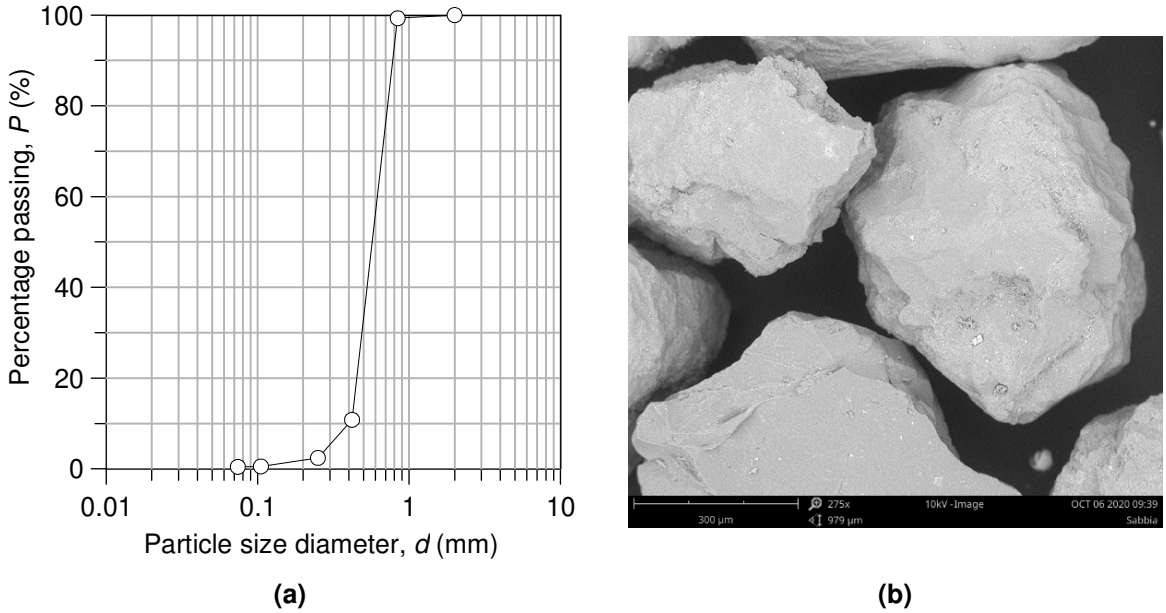

(a) **(b)**

Figure 57 – Particle characteristics of Ticino sand: (a) grain size distribution curve and (b) shape of particles (*SEM* image).

Table 2 – Physical properties of silt.

Material	D_{50} (mm)	D_{30} (mm)	D_{10} (mm)	G_S	C_U	e_{max}	e_{min}	Shape of grains
Fines	0.024	0.012	0.004	2.72	8.54	2.15	-	Angular

3.2.3 Sand-Silt Mixtures

Various amounts of non-plastic silt were mixed with clean Ticino sand to obtain target fines contents varying from 5% to 40% by dry weight of solids. The resulting grain size distribution curves are shown in **Figure 59** together with those of the pure Ticino sand and the pure non-plastic silt.

The maximum and minimum void ratios of the mixtures have been determined according to ASTM procedures. The minimum void ratio was determined using the vibratory table (ASTM D4253), while the maximum void ratio was determined with

method B according to ASTM D4254. It should be noted that the standard procedure for the determination of e_{max} and e_{min} is usually only applicable for sand with fines content up to 15%, because, with higher fines content, segregation during pouring of the mixed soil may occur. However, despite this limitation, repeatable values of maximum and minimum void ratios have been documented in the literature following the ASTM procedures with an extreme caution (Tao et al. 2004).

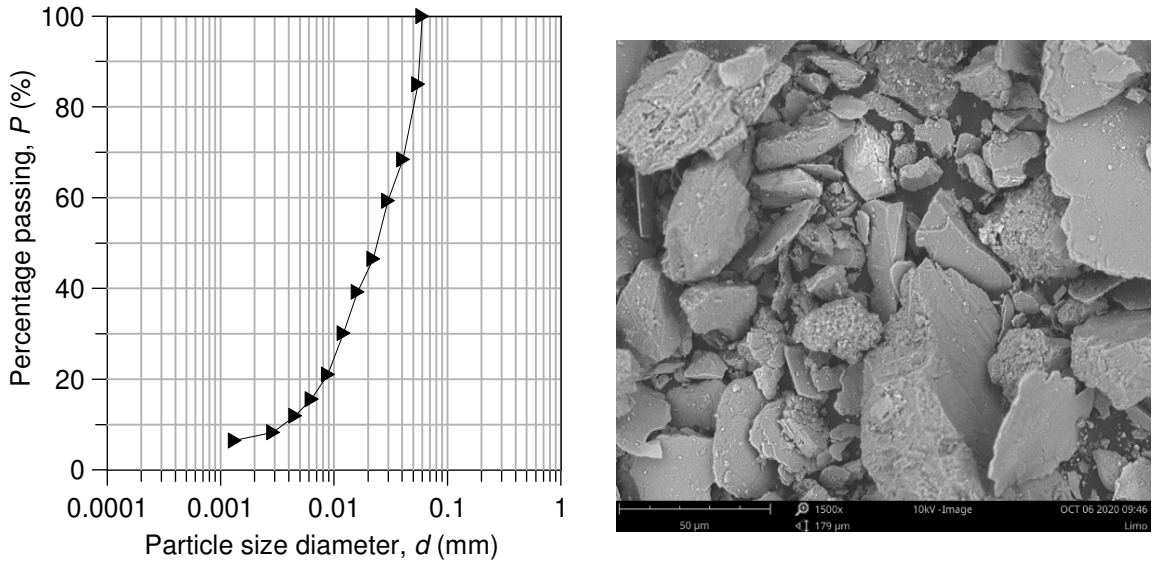

(a) **(b)**

Figure 58 – Particle characteristics of silt: (a) grain size distribution curve and (b) shape of particles (*SEM* image).

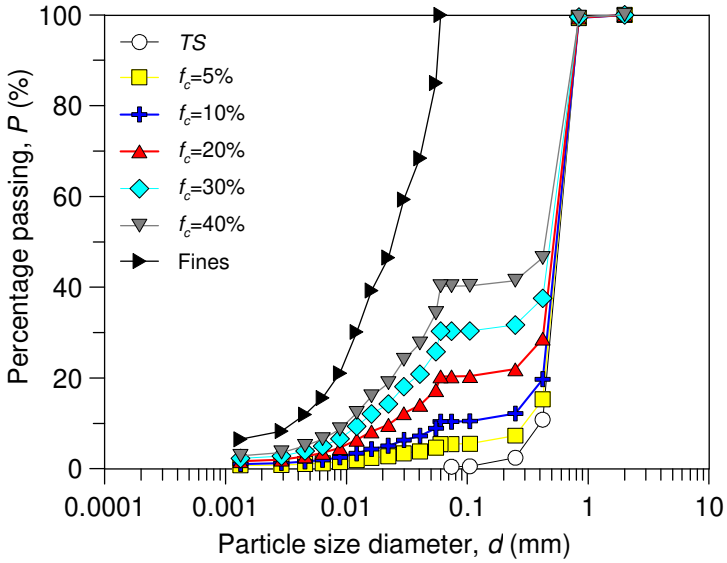

Figure 59 – Grain size distribution curves of Ticino sand-silt mixtures.

As for the minimum void ratio, some authors still use the ASTM procedure, like Thevanayagam (1998), Amini and Qi (2000), Xenaki and Athanasopoulos (2003), Huang et al. (2004), Stamatopoulos (2010), whereas others combine the ASTM procedure with the Proctor test to obtain consistent values, like Polito and Martin (2001), Yang et al. (2006a) or Papadopoulou and Tika (2008). In order to determine the maximum void ratio, the ASTM procedure (Amini and Qi 2000; Thevanayagam 1998) but also alternative methods such as simply pouring material into the mould with a funnel (Yang et al. 2006a) or a combination of the two (Papadopoulou and Tika 2008) are applied. In the ASTM D4253 procedure, the minimum void ratio is achieved by densifying dry soil in a standard mold with a volume of 2830 cm^3 using a vertically vibrating table. The vibratory table test was found to give more reproducible results. The method B of ASTM D4254, instead, consists of filling a tube whose base is sitting within a mold of known weight and volume, with dry soil and then slowly lifting the tube so that the soil flows out and fills the mold. The variation of e_{max} and e_{min} for Ticino sand mixed with different percentages of fines (f_c) and other physical properties of the mixtures are summarized in **Table 3**.

Table 3 – Physical properties of Ticino sand-silt mixtures.

Material	D_{50} (mm)	D_{30} (mm)	D_{10} (mm)	G_S	C_U	e_{max}	e_{min}
TS+5%·f_c	0.559	0.474	0.298	2.66	2.04	0.84	0.53
TS+10%·f_c	0.547	0.459	0.059	2.67	10.16	0.81	0.47
TS+20%·f_c	0.518	0.426	0.023	2.68	24.69	0.79	0.37
TS+30%·f_c	0.483	0.060	0.013	2.69	41.55	0.80	0.37
TS+40%·f_c	0.440	0.045	0.010	2.70	50.51	0.95	0.48

The graphic representation of test results for e_{min} and e_{max} in **Figure 60** shows that e_{min} and e_{max} decreased up to a fines content of around 30% and then increased with further increasing f_c. This result is in agreement with previously reported results on silty sands (Polito and Martin 2001; Hazirbaba 2005; Sadek and Saleh 2007; Dash et al. 2010; Belkhatir et al. 2011; Benahmed et al. 2015). The fines content at which the minimum and maximum void ratios change from a decreasing to an increasing tendency is defined as the threshold fines content, f_{thre} (Naeini and Baziar 2004; Zuo and Baudet 2015). Based on **Figure 60**, the threshold fines content for the given mixtures results to be around 20% to 30%. The determination of f_{thre} from solely void ratio involves uncertainties, in fact the method based on density index data of sand-fines mixtures

can give only an indication of the possible range in which the real value of f_{thre} may lie (Zuo and Baudet 2015). It is judged preferable to determine f_{thre} by laboratory tests with monotonic or cyclic loading. These other methods for estimating the limiting fines content will be discussed in chapter 5.

Table 3 presents the uniformity coefficients (C_U) of the sand-silt mixtures. An abrupt jump from 2.04 to 50.51 can be observed as silt content increases from 10 to 40 while it decreases to about 8.54 for pure silt (**Table 2**). This shows that the uniformity coefficient of silty sands, compared to other grading characteristics, gives a rather poor basis for classifying their behaviour (Kuerbis 1985).

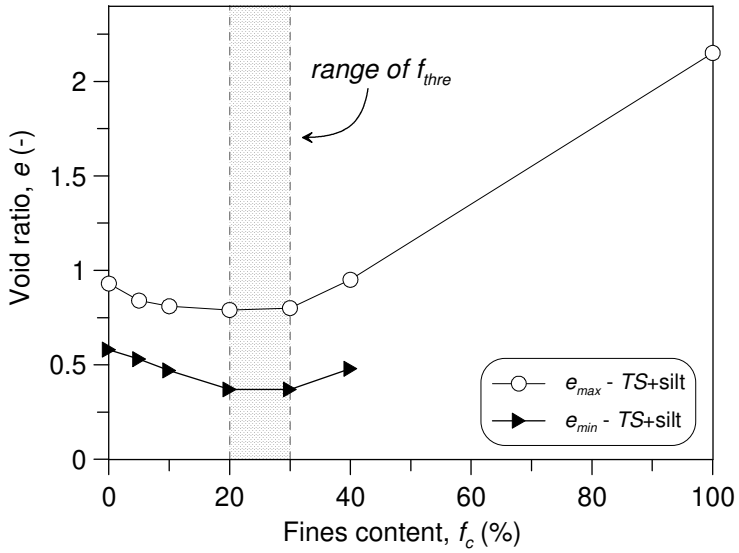

Figure 60 – Variation in index void ratios with silt content.

3.3 Testing Program

The main objective of the work presented in this thesis is to reach a better understanding of the undrained behaviour of silty sand mixtures under cyclic loading. The testing program includes a large number of undrained cyclic simple shear tests conducted both in the absence and in the presence of an initial static shear stress to better understand this aspect. It is worthwhile to mention that, in the literature, experimental investigations concerning the effects of the initial static shear stresses on the cyclic liquefaction resistance of silty sands, conducted with a simple shear apparatus, are still scarse. With this objective, the testing program (**Table 4** and **Table 5**) has been organized in the following series of tests that are briefly summarized below:

- 140 stress-controlled undrained cyclic simple shear tests performed on Ticino sand-silt mixtures samples (f_c = 0%, 5%, 10%, 20%, 30%; 40%), at different initial static shear stress (static stress ratio α=0, 0.05, 0.10, 0.20, 0.30), cyclic stress ratio (CSR=0.03-0.28) and initial (post-consolidation) void ratio (e_0=0.49-0.78), but at the same initial vertical effective stress σ'_{v0}=100 kPa.
- 20 stress-controlled undrained cyclic simple shear tests performed on Ticino sand-silt mixtures samples (f_c =0, 10, 20 and 30%), at different initial static shear stress (static stress ratio α=0, 0.10, 0.20 and 0.30), cyclic stress ratio (CSR=0.08-0.18), initial (post-consolidation) void ratio (e_0=0.58-0.82), and initial vertical effective stress σ'_{v0}=50 kPa.
- 3 undrained monotonic simple shear tests on Ticino sand with f_c =20% at an initial (post-consolidation) void ratio e_0=0.68 and different initial vertical effective stresses (25 kPa, 50 kPa, 100 kPa).

Some cyclic undrained simple shear tests (static stress ratio α = 0) performed on Ticino sand-silt mixtures, used in the present research, were conducted as a part of a previous research carried out at the Mediterranean University of Reggio Calabria (Diano 2017). Laboratory tests were carried out by the Norwegian Geotechnical Institute (*NGI*) type simple shear (*SS*) apparatus whose features are described in paragraph 3.4. Moist tamping method was used for the preparation of all test specimens. The fines content was varied throughout testing by adding different amounts of non-plastic silt to Ticino clean sand.

Table 4 - Summary of cyclic tests under simple shear loading.

Material	e_0	f_c (%)	σ'_{v0} (kPa)	α	CSR	N_f	α/CSR	Load Condition	Observed Behaviour
TS	0.82	0	50	0.00	0.15	15	0.00	*R*	*CM*
TS	0.78	0	100	0.00	0.12	47	0.00	*R*	*CM*
TS	0.78	0	100	0.00	0.14	12	0.00	*R*	*CM*
TS	0.78	0	100	0.00	0.16	5	0.00	*R*	*CM*
TS	0.78	0	100	0.00	0.20	2	0.00	*R*	*CM*
TS	0.74	0	100	0.00	0.12	126	0.00	*R*	*CM*
TS	0.74	0	100	0.00	0.14	21	0.00	*R*	*CM*
TS	0.74	0	100	0.00	0.16	12	0.00	*R*	*CM*
TS	0.74	0	100	0.00	0.18	7	0.00	*R*	*CM*
TS	0.68	0	100	0.00	0.14	76	0.00	*R*	*CM*
TS	0.68	0	100	0.00	0.16	19	0.00	*R*	*CM*

Material	e_0	f_c (%)	σ'_{v0} (kPa)	α	*CSR*	N_f	α/CSR	Load Condition	Observed Behaviour
TS	0.68	0	100	0.00	0.18	12	0.00	*R*	*CM*
TS	0.68	0	100	0.00	0.20	9	0.00	*R*	*CM*
TS	0.68	0	100	0.00	0.23	3	0.00	*R*	*CM*
TS	0.63	0	100	0.00	0.20	22	0.00	*R*	*CM*
TS	0.63	0	100	0.00	0.23	8	0.00	*R*	*CM*
TS	0.63	0	100	0.00	0.25	6	0.00	*R*	*CM*
TS	0.60	0	100	0.00	0.23	13	0.00	*R*	*CM*
TS	0.60	0	100	0.00	0.26	5	0.00	*R*	*CM*
TS	0.78	0	100	0.10	0.08	222	1.25	*NR*	*PSA*
TS	0.78	0	100	0.10	0.10	101	1.00	*NR*	*PSA*
TS	0.78	0	100	0.10	0.12	23	0.83	*R*	*PSA*
TS	0.78	0	100	0.10	0.14	5	0.71	*R*	*INT*
TS	0.68	0	100	0.10	0.16	23	0.62	*R*	*INT*
TS	0.68	0	100	0.10	0.20	8	0.50	*R*	*INT*
TS	0.68	0	100	0.10	0.22	3	0.45	*R*	*INT*
TS	0.60	0	100	0.10	0.23	16	0.43	*R*	*INT*
TS	0.60	0	100	0.10	0.25	8	0.40	*R*	*INT*
TS	0.60	0	100	0.10	0.28	4	0.36	*R*	*INT*
TS	0.78	0	100	0.20	0.10	60	2.00	*NR*	*PSA*
TS	0.78	0	100	0.20	0.12	8	1.67	*NR*	*PSA*
TS	0.68	0	100	0.20	0.16	18	1.25	*NR*	*PSA*
TS	0.68	0	100	0.20	0.20	7	1.00	*NR*	*PSA*
TS	0.60	0	100	0.20	0.20	59	1.00	*NR*	*PSA*
TS	0.60	0	100	0.20	0.26	10	0.77	*R*	*PSA*
TS	0.60	0	100	0.20	0.28	6	0.71	*R*	*PSA*
TS	0.78	0	100	0.30	0.10	25	3.00	*NR*	*PSA*
TS	0.78	0	100	0.30	0.12	1	2.50	*NR*	*PSA*
TS	0.68	0	100	0.30	0.16	14	1.87	*NR*	*PSA*
TS	0.68	0	100	0.30	0.18	7	1.67	*NR*	*PSA*
TS	0.60	0	100	0.30	0.22	59	1.36	*NR*	*PSA*
TS	0.60	0	100	0.30	0.28	8	1.07	*NR*	*PSA*
TS+5%·f_c	0.73	5	100	0.00	0.10	235	0.00	*R*	*CM*
TS+5%·f_c	0.73	5	100	0.00	0.12	15	0.00	*R*	*CM*
TS+5%·f_c	0.73	5	100	0.00	0.16	4	0.00	*R*	*CM*
TS+5%·f_c	0.68	5	100	0.00	0.14	22	0.00	*R*	*CM*
TS+5%·f_c	0.68	5	100	0.00	0.16	13	0.00	*R*	*CM*
TS+5%·f_c	0.61	5	100	0.00	0.14	34	0.00	*R*	*CM*

Material	e_0	f_c (%)	σ'_{v0} (kPa)	α	CSR	N_f	α/CSR	Load Condition	Observed Behaviour
TS+5%·f_c	0.61	5	100	0.00	0.20	8	0.00	*R*	*CM*
TS+5%·f_c	0.61	5	100	0.00	0.22	6	0.00	*R*	*CM*
TS+10%·f_c	0.68	10	50	0.00	0.14	16	0.00	*R*	*CM*
TS+10%·f_c	0.68	10	50	0.00	0.15	10	0.00	*R*	*CM*
TS+10%·f_c	0.68	10	50	0.00	0.18	7	0.00	*R*	*CM*
TS+10%·f_c	0.60	10	50	0.00	0.16	32	0.00	*R*	*CM*
TS+10%·f_c	0.60	10	50	0.00	0.18	13	0.00	*R*	*CM*
TS+10%·f_c	0.68	10	50	0.10	0.10	135	1.00	*NR*	*PSA*
TS+10%·f_c	0.68	10	50	0.10	0.14	28	0.71	*R*	*PSA*
TS+10%·f_c	0.68	10	50	0.10	0.18	10	0.55	*R*	*INT*
TS+10%·f_c	0.68	10	50	0.20	0.14	24	1.42	*NR*	*PSA*
TS+10%·f_c	0.68	10	50	0.20	0.16	13	1.25	*NR*	*PSA*
TS+10%·f_c	0.68	10	50	0.30	0.10	30	3.00	*NR*	*PSA*
TS+10%·f_c	0.68	10	50	0.30	0.14	4	2.14	*NR*	*PSA*
TS+10%·f_c	0.68	10	100	0.00	0.10	52	0.00	*R*	*CM*
TS+10%·f_c	0.68	10	100	0.00	0.12	25	0.00	*R*	*CM*
TS+10%·f_c	0.68	10	100	0.00	0.14	10	0.00	*R*	*CM*
TS+10%·f_c	0.68	10	100	0.00	0.16	5	0.00	*R*	*CM*
TS+10%·f_c	0.60	10	100	0.00	0.14	42	0.00	*R*	*CM*
TS+10%·f_c	0.60	10	100	0.00	0.16	12	0.00	*R*	*CM*
TS+10%·f_c	0.60	10	100	0.00	0.20	4	0.00	*R*	*CM*
TS+10%·f_c	0.55	10	100	0.00	0.14	88	0.00	*R*	*CM*
TS+10%·f_c	0.55	10	100	0.00	0.18	15	0.00	*R*	*CM*
TS+10%·f_c	0.55	10	100	0.00	0.20	8	0.00	*R*	*CM*
TS+10%·f_c	0.53	10	100	0.00	0.16	46	0.00	*R*	*CM*
TS+10%·f_c	0.53	10	100	0.00	0.19	20	0.00	*R*	*CM*
TS+10%·f_c	0.68	10	100	0.05	0.14	13	0.36	*R*	*CM*
TS+10%·f_c	0.68	10	100	0.05	0.16	7	0.31	*R*	*CM*
TS+10%·f_c	0.60	10	100	0.05	0.16	12	0.31	*R*	*CM*
TS+10%·f_c	0.68	10	100	0.10	0.08	102	1.25	*NR*	*PSA*
TS+10%·f_c	0.68	10	100	0.10	0.10	40	1.00	*NR*	*PSA*
TS+10%·f_c	0.68	10	100	0.10	0.12	6	0.83	*R*	*PSA*
TS+10%·f_c	0.60	10	100	0.10	0.14	37	0.71	*R*	*PSA*
TS+10%·f_c	0.60	10	100	0.10	0.16	12	0.63	*R*	*INT*
TS+10%·f_c	0.60	10	100	0.10	0.19	4	0.53	*R*	*INT*
TS+10%·f_c	0.55	10	100	0.10	0.17	22	0.59	*R*	*INT*
TS+10%·f_c	0.55	10	100	0.10	0.22	5	0.45	*R*	*INT*

Material	e_0	f_c (%)	σ'_{v0} (kPa)	α	*CSR*	N_f	α/CSR	Load Condition	Observed Behaviour
TS+10%·f_c	0.68	10	100	0.20	0.08	20	2.50	*NR*	*PSA*
TS+10%·f_c	0.68	10	100	0.20	0.10	10	2.00	*NR*	*PSA*
TS+10%·f_c	0.60	10	100	0.20	0.12	128	1.67	*NR*	*PSA*
TS+10%·f_c	0.60	10	100	0.20	0.14	10	1.43	*NR*	*PSA*
TS+10%·f_c	0.60	10	100	0.20	0.16	4	1.25	*NR*	*PSA*
TS+10%·f_c	0.55	10	100	0.20	0.18	29	1.11	*NR*	*PSA*
TS+10%·f_c	0.55	10	100	0.20	0.23	2	0.87	*R*	*PSA*
TS+10%·f_c	0.68	10	100	0.30	0.03	55	10.00	*NR*	*PSA*
TS+10%·f_c	0.68	10	100	0.30	0.06	11	5.00	*NR*	*PSA*
TS+10%·f_c	0.60	10	100	0.30	0.08	88	3.75	*NR*	*PSA*
TS+10%·f_c	0.60	10	100	0.30	0.10	4	3.00	*NR*	*PSA*
TS+10%·f_c	0.60	10	100	0.30	0.12	2	2.50	*NR*	*PSA*
TS+10%·f_c	0.55	10	100	0.30	0.16	47	1.86	*NR*	*PSA*
TS+10%·f_c	0.55	10	100	0.30	0.18	22	1.67	*NR*	*PSA*
TS+20%·f_c	0.58	20	50	0.00	0.14	27	0.00	*R*	*CM*
TS+20%·f_c	0.58	20	50	0.00	0.15	11	0.00	*R*	*CM*
TS+20%·f_c	0.68	20	100	0.00	0.08	59	0.00	*R*	*LFL*
TS+20%·f_c	0.68	20	100	0.00	0.10	21	0.00	*R*	*LFL*
TS+20%·f_c	0.68	20	100	0.00	0.12	8	0.00	*R*	*LFL*
TS+20%·f_c	0.58	20	100	0.00	0.12	16	0.00	*R*	*CM*
TS+20%·f_c	0.58	20	100	0.00	0.14	12	0.00	*R*	*CM*
TS+20%·f_c	0.58	20	100	0.00	0.16	5	0.00	*R*	*CM*
TS+20%·f_c	0.55	20	100	0.00	0.14	17	0.00	*R*	*CM*
TS+20%·f_c	0.55	20	100	0.00	0.16	12	0.00	*R*	*CM*
TS+20%·f_c	0.55	20	100	0.00	0.20	4	0.00	*R*	*CM*
TS+20%·f_c	0.51	20	100	0.00	0.14	34	0.00	*R*	*CM*
TS+20%·f_c	0.51	20	100	0.00	0.16	19	0.00	*R*	*CM*
TS+20%·f_c	0.51	20	100	0.00	0.18	14	0.00	*R*	*CM*
TS+20%·f_c	0.51	20	100	0.00	0.19	7	0.00	*R*	*CM*
TS+20%·f_c	0.68	20	100	0.10	0.04	50	2.50	*NR*	*FL*
TS+20%·f_c	0.68	20	100	0.10	0.07	7	1.43	*NR*	*FL*
TS+20%·f_c	0.68	20	100	0.10	0.10	4	1.00	*NR*	*FL*
TS+20%·f_c	0.59	20	100	0.10	0.10	22	1.00	*NR*	*PSA*
TS+20%·f_c	0.59	20	100	0.10	0.12	9	0.83	*R*	*PSA*
TS+20%·f_c	0.55	20	100	0.10	0.14	19	0.71	*R*	*INT*
TS+20%·f_c	0.55	20	100	0.10	0.16	10	0.63	*R*	*INT*
TS+20%·f_c	0.55	20	100	0.10	0.20	3	0.50	*R*	*INT*

Material	e_0	f_c (%)	σ'_{v0} (kPa)	α	CSR	N_f	α/CSR	Load Condition	Observed Behaviour
TS+20%·f_c	0.59	20	100	0.20	0.08	25	2.50	*NR*	*PSA*
TS+20%·f_c	0.59	20	100	0.20	0.10	10	2.00	*NR*	*PSA*
TS+20%·f_c	0.55	20	100	0.20	0.13	35	1.54	*NR*	*PSA*
TS+20%·f_c	0.55	20	100	0.20	0.16	6	1.25	*NR*	*PSA*
TS+20%·f_c	0.55	20	100	0.30	0.14	25	2.14	*NR*	*PSA*
TS+20%·f_c	0.55	20	100	0.30	0.16	2	1.88	*NR*	*PSA*
TS+30%·f_c	0.68	30	50	0.00	0.12	58	0.00	*R*	*CM*
TS+30%·f_c	0.68	30	50	0.00	0.14	12	0.00	*R*	*CM*
TS+30%·f_c	0.68	30	50	0.00	0.18	4	0.00	*R*	*CM*
TS+30%·f_c	0.68	30	50	0.10	0.08	27	1.25	*NR*	*FL*
TS+30%·f_c	0.68	30	50	0.10	0.12	3	0.83	*R*	*FL*
TS+30%·f_c	0.68	30	100	0.00	0.08	46	0.00	*R*	*LFL*
TS+30%·f_c	0.68	30	100	0.00	0.10	15	0.00	*R*	*LFL*
TS+30%·f_c	0.68	30	100	0.00	0.12	7	0.00	*R*	*LFL*
TS+30%·f_c	0.68	30	100	0.00	0.14	4	0.00	*R*	*LFL*
TS+30%·f_c	0.58	30	100	0.00	0.12	17	0.00	*R*	*CM*
TS+30%·f_c	0.58	30	100	0.00	0.14	10	0.00	*R*	*CM*
TS+30%·f_c	0.58	30	100	0.00	0.18	3	0.00	*R*	*LFL*
TS+30%·f_c	0.55	30	100	0.00	0.16	34	0.00	*R*	*CM*
TS+30%·f_c	0.55	30	100	0.00	0.20	9	0.00	*R*	*CM*
TS+30%·f_c	0.49	30	100	0.00	0.20	33	0.00	*R*	*CM*
TS+30%·f_c	0.49	30	100	0.00	0.22	12	0.00	*R*	*CM*
TS+30%·f_c	0.49	30	100	0.00	0.24	3	0.00	*R*	*CM*
TS+30%·f_c	0.68	30	100	0.10	0.06	22	1.67	*NR*	*FL*
TS+30%·f_c	0.68	30	100	0.10	0.10	4	1.00	*NR*	*FL*
TS+30%·f_c	0.59	30	100	0.10	0.10	63	1.00	*NR*	*INT*
TS+30%·f_c	0.59	30	100	0.10	0.12	11	0.83	*R*	*INT*
TS+30%·f_c	0.55	30	100	0.10	0.16	23	0.63	*R*	*INT*
TS+30%·f_c	0.55	30	100	0.10	0.19	11	0.53	*R*	*INT*
TS+30%·f_c	0.59	30	100	0.20	0.08	61	2.50	*NR*	*PSA*
TS+30%·f_c	0.59	30	100	0.20	0.10	3	2.00	*NR*	*PSA*
TS+30%·f_c	0.55	30	100	0.20	0.14	21	1.43	*NR*	*PSA*
TS+30%·f_c	0.55	30	100	0.20	0.16	9	1.25	*NR*	*PSA*
TS+30%·f_c	0.55	30	100	0.30	0.12	91	2.50	*NR*	*PSA*
TS+30%·f_c	0.55	30	100	0.30	0.14	3	2.14	*NR*	*PSA*
TS+40%·f_c	0.68	40	100	0.00	0.12	50	0.00	*R*	*CM*
TS+40%·f_c	0.68	40	100	0.00	0.14	10	0.00	*R*	*CM*

Material	e_0	f_c (%)	σ'_{v0} (kPa)	α	CSR	N_f	α/CSR	Load Condition	Observed Behaviour
TS+40%·f_c	0.68	40	100	0.00	0.16	5	0.00	*R*	*CM*

Note:

R= stress reversal

NR=non stress reversal

FL=flow liquefaction

LFL=limited flow liquefaction

CM=cyclic mobility

PSA=plastic strain accumulation

INT=intermediate

Table 5 - Summary of monotonic tests under simple shear loading.

Material	e_0	f_c (%)	σ'_{v0} (kPa)	α	Observed Behaviour
TS+20%·f_c	0.68	20	25	0.00	*FL*
TS+20%·f_c	0.68	20	50	0.00	*FL*
TS+20%·f_c	0.68	20	100	0.00	*FL*

3.4 Simple Shear Device (*DSS*)

3.4.1 General description of the apparatus

The undrained cyclic tests were performed on moist tamped samples of sand-silt mixtures, by the Norwegian Geotechnical Institute (*NGI*) type simple shear (*SS*) apparatus (Bjerrum and Landva 1966) operated at Department of Civil, Energy, Environmental and Materials Engineering (*DICEAM*), of the Mediterranean University of Reggio Calabria (Italy).

The original *NGI* type simple shear apparatus (**Figure 61**) has been modified in the geotechnical laboratory of *DICEAM* to enable the application of uni-directional monotonic and cyclic simple shear loading through an automated electro-mechanical control system (Porcino et al. 2006).

The apparatus is designed to perform cyclic tests through the application of a cyclic horizontal load (stress-controlled test) or displacement (strain-controlled tests) of prefixed amplitude and frequency. All the cyclic tests described here were performed in stress-controlled conditions at a frequency of 0.10 Hz, while the monotonic tests were performed with a constant speed of 0.10 mm/min.

The advantages of using this apparatus for carrying out undrained tests, compared to the triaxial one, are related to the following aspects:

- sample doesn't need to be saturated (constant volume testing);

- problems associated with the generation of pore pressure (membrane penetration) do not exist.

To generate and transmit the horizontal loads, the apparatus is provided with:

- a connection fork (**Figure 62a**);
- a sliding box (**Figure 62a**);
- a horizontal load piston (**Figure 62b**);
- a gear-box (**Figure 62b**).

The system for the application of vertical loads is composed of:

- a tower (**Figure 63**);
- a lever arm (**Figure 63**);
- a disk for positioning weights (**Figure 63**);
- a counterweight (**Figure 63**);
- a vertical load piston (**Figure 63**);
- a mechanism for the manual adjustment of the load.

Figure 61 – The modified *NGI* simple shear apparatus used in the present research.

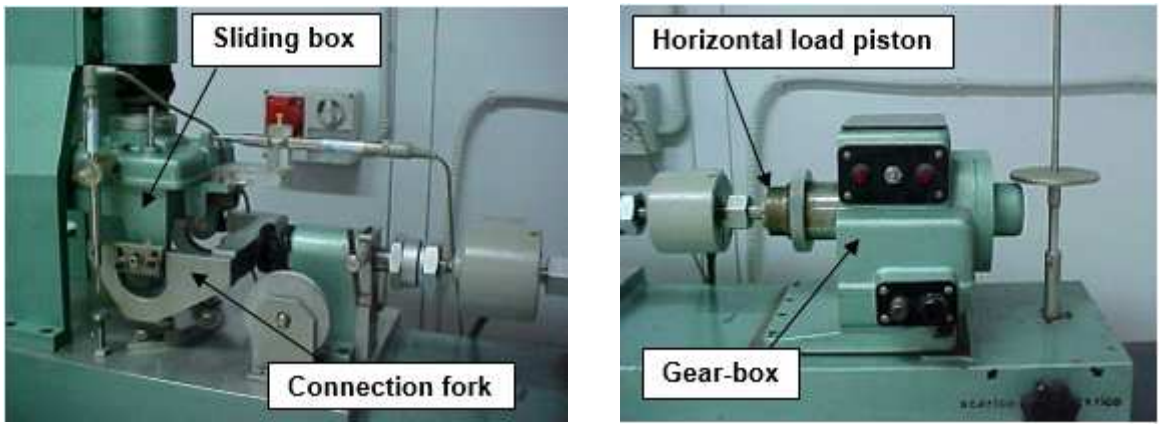

(a) (b)

Figure 62 – System for generating and transmitting horizontal loads: (a) connection fork and sliding box and (b) gear-box and horizontal load piston.

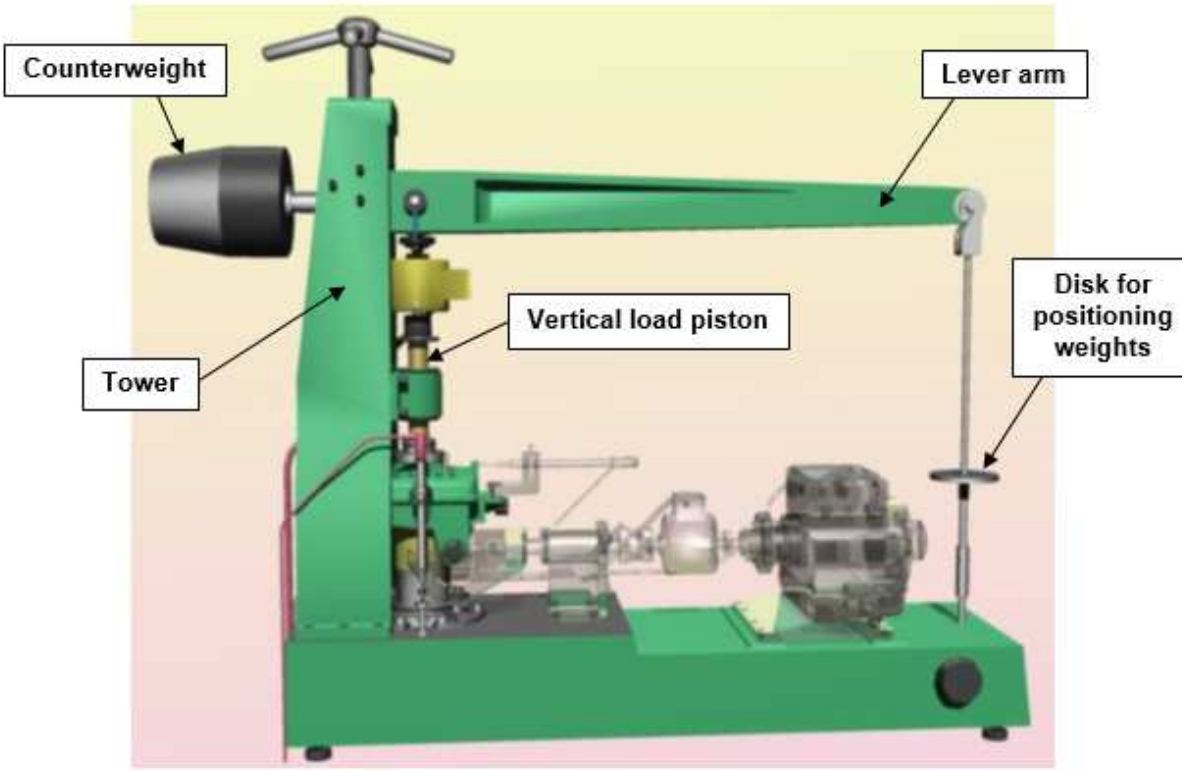

Figure 63 – System for the application of vertical loads.

The tower has the function of supporting the lever arm. Both the tower and the lever arm are made of aluminium alloy. The lever arm has a ratio of 1:10 and is dimensioned to withstand a vertical load equal to twice the maximum statically applicable load (800 kg). The height level of the lever arm can be adjusted by using a screw with four handles arranged above the tower. The plate for the positioning of the weights is superiorly connected to the lever arm by means of a metal rod, and at the bottom with

a hook to the mechanical system for the manual adjustment of the load. The latter is constituted by a worm gear and the gear wheel on which it is possible to act by using the control knob. The counterweight is designed to balance the weight of the vertical load cell, of the vertical sliding box and of the vertical piston. The measurement of the horizontal and the vertical loads is performed using two load cells built by H.B.M. (Hottinger Baldwin Messtechnik, Darmstadt, Germany), U1 type with full scale (F.S.) 200 kg, accuracy class ± 0.02% F.S. and nominal sensitivity 2 mV/V.

The measurements of the horizontal and vertical displacements are carried out through two transducers of the *LVDT* (Linear Variable Differential Transducer) W10TK model, built by H.B.M. and having a 20 mm measuring range (±10 mm), sensitivity of 1 digit/microns and a nominal sensitivity of 80 mV/V. It is important to underline that, in this type of apparatus, since the specimens are laterally constrained (zero lateral strain condition; see paragraph 3.4.2), the undrained tests are performed as constant volume tests (Dyvik et al. 1987; Finn 1985) by automatically adjusting the vertical load in order to keep the height of the specimen constant. Therefore, during simple shear tests, pore pressures are not directly measured during shearing, but they are inferred from the changes in the vertical stresses that are needed to maintain a constant specimen height. In simple shear tests, normal and shear stresses on the upper horizontal plane are the only measured stress quantities, and they are not enough to describe the complete state of stress of the samples. The approach followed in the analysis of undrained *SS* tests is based on the assumption that the horizontal plane is the plane of maximum shear stress. This assumption is considered to be sufficiently accurate in undrained tests whatever the void ratio, in agreement with other authors (Roscoe 1970; Sivathayalan 1994, Porcino et al. 2005a). The theoretical framework validation of this approach was the subject of a previous research carried out at the Mediterranean University of Reggio Calabria (Porcino et al. 2005a; Porcino et al. 2005b).

3.4.2 Samples features and assembly

The *NGI* version of the *SS* apparatus is characterized by a cylindrical sample (80 mm in diameter and approximately 20 mm in height), laterally confined by a rubber membrane reinforced by steel wires (**Figure 64**). Accordingly, the lateral restraint provided by the reinforced membrane ensures a zero-lateral strain condition that can be considered, in a first approximation, as a K_0 condition. This condition applies both during the consolidation phase and in the shearing phase.

The reinforced membranes must be carefully preserved in the absence of light and at low temperatures. The metal wire used as reinforcing element has a diameter of 0.15 mm, modulus of elasticity of $1.55 \cdot 10^{-6}$ kg/cm^2, and tensile strength of 5800 kg/cm^2; the metal windings have a pitch of 20 turns per centimetre of height and are tested to horizontal tensions of 1.8 kg/cm^2. Specimens superiorly and inferiorly are confined by a porous stone mounted to the bottom and the top cap.

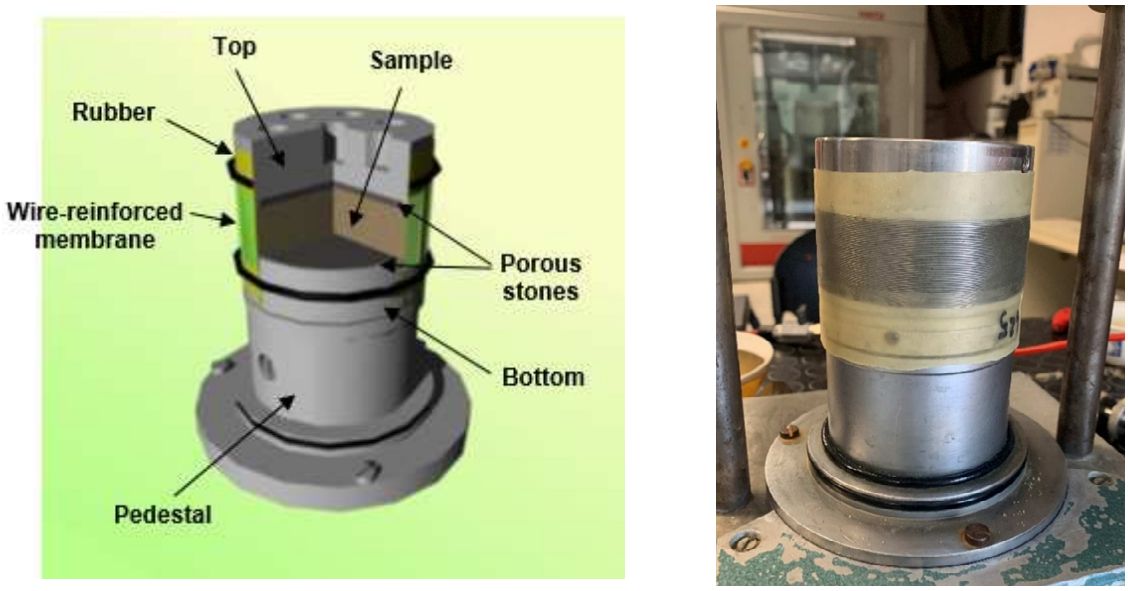

(a) (b)

Figure 64 – Specimen components and assembly: (a) scheme and (b) picture before a simple shear test.

3.5 Test procedure and presentation of results

The following paragraphs report the procedure for the execution of cyclic undrained simple shear tests and a description of the sample preparation method chosen for the reconstitution of samples. In particular, for the last aspect, a lot of precautions, modifications and checks have been adopted in order to adapt the standard procedure of the moist tamping method to the simple shear apparatus and they will be presented in detail in the following sections. Moreover, typical test results, obtained by simple shear apparatus, are briefly discussed.

3.5.1 Test procedure and specimen preparation

The steel wires reinforced rubber membrane is placed into an aluminium mold (**Figure 65a**) and a vacuum pressure of about - 40 kPa is applied to make the membrane to

adhere to the internal wall of the mold. Subsequently, the lower part of the membrane is folded on the bottom sealing it with o-rings, and the sample reconstitution is started. In this research for the preparation of the specimens, the moist tamping method has been specifically adapted for the simple shear apparatus. For this purpose, some additional components have been designed and realized (**Figure 65b**), such as:

- an aluminium plate with a circular hole that has a diameter of 43 mm;
- a steel graduated rod of 39 cm in height;
- a circular hammer in stainless steel which has a diameter of 50 mm;
- a steel cylinder that slides along the rod and leans on the aluminium plate;
- a steel ring with an inner (internal) diameter of 12 mm and outer diameter of 35 mm.

(a) **(b)**

Figure 65 – (a) Set-rubber and application of vacuum and (b) components for the reconstitution of sample with moist tamping in *SS* apparatus.

The reference height (H_{ref}) for the realization of the layers is carried out by fixing the plate at a specified height and placing the pestle on the porous stone of the bottom, as illustrated in **Figure 66a**. Due to the small size of the specimen (only about 2 cm in height), the effects of inhomogeneity along its height can be neglected: for this reason, the specimen has been made of two layers of equal thickness having a height equal to about 1 cm. After, the desired void ratio and the density for the test had been determined, the soil was prepared by weighing the proper weight of dry soil (sand and silt) for each layer in separate containers.

(a) (b)

Figure 66 – (a) Reference height for the realization of layers and (b) realization of moist tamping samples in two layers.

Then dry sand and fines were mixed in the selected weight ratio, and an amount of deaired water was added to the mixture, corresponding to a water content of $w = 12.5\% \pm 2.5\%$ for all tested fines contents. The values of w were selected to obtain a prefixed degree of saturation $S_r = 50\%$. At this point, the material necessary for the realization of the first layer was poured with a spoon in small quantities and then distributed inside the membrane. The surface of the layer was then compacted with a manual hammer that is connected to a guide on the setup frame to ensure a precise falling height. The height of the last compacted layer (**Figure 66b**) was kept slightly greater (generally 1-2 mm) than the target one in order to take into account the weight of the top cap.

The density distribution within the reconstituted specimens was investigated in preliminary tests by means of a two-part mold section along the height of the sample. A homogeneous distribution of density was verified by comparing the densities of the upper and lower layers. In all *CSS* tests, the specimens were tested in the moist state, without reaching a full water-saturation. The saturation degree of the samples should not be of real concern in constant volume *SS* tests carried out on clean medium to coarse sands; however it could have an impact on silty sands with high fines content due to possible suction effects. Verifications carried out in a previous research on the same materials (Diano 2017) demonstrated that suction effects associated with the chosen degree of saturation were practically irrelevant.

After the realization of the last layer, the top cap was released gently on the upper surface of the specimen using an automatic mechanism that allows to lay it, without causing any disturbance to the specimen (**Figure 67a**). The rubber membrane was then folded inferiorly and superiorly on the bottom and top cap, and another o-ring was inserted in the lower part, allowing a greater tightness of the specimen during the test. **Figure 67b** shows a sample ready to be disposed within the simple shear apparatus for performing the test.

3.5.2 Consolidation phase

The consolidation phase was conducted by applying vertical load steps in successive increments of 10 kPa or 20 kPa. Each load step was maintained for about 15 minutes during which the height of the sample was continuously monitored and automatically recorded. At the end of the stage the post-consolidation void ratio was determined. The accuracy of the *LVDT* sensor led to an accuracy of about ±0.0015 in terms of the void ratio.

After the consolidation phase, it was necessary to make the specimen tightly fastened to the apparatus, for the transmission of the loads. Details of the clamping system are shown in **Figure 68**.

(a) **(b)**

Figure 67 – (a) Positioning of the top cap on the surface of the last layer and (b) specimen ready for the execution of the simple shear test.

Figure 68 – Detail of the specimen clamping system.

3.5.3 Static shear stress application phase

After the end of the consolidation phase, if required, the specimens were subjected to a static shear stress (τ_{stat}) on the horizontal plane to meet the desired value of shear stress ratio $\alpha=\tau_{stat}/\sigma'_{v0}$. The prefixed static shear stress was applied in loading steps under drained conditions; each step was maintained until both the vertical and the horizontal strains were stable with time prior to the application of a subsequent step.

3.5.4 Shear loading phase

After the end of the consolidation phase, plus (in case) the static shear stress application, the specimens were subjected to either constant-volume monotonic or cyclic shear loading.

In monotonic shear loading tests, the shearing was applied in strain-controlled mode with a rate of approximately 0.10 mm/min. Tests were stopped at shear strains of approximately 20% - 30%.

The undrained cyclic tests were carried out in stress-controlled mode at 0.10 Hz frequency, by applying constant amplitude shear stress time histories sinusoidally varying around the initial value. The amplitude of the applied cyclic horizontal load F_h was calculated with the following relation:

$$F_h = \sigma'_{v0} \cdot CSR \cdot A \qquad (23)$$

where: A is the cross-sectional area of the specimen, σ'_{v0} is the initial vertical effective stress and CSR represents the prefixed cyclic stress ratio defined as $CSR=\tau_{cycl}/\sigma'_{v0}$ with τ_{cycl} being one-half of the peak to peak cyclic shear stress amplitude (single amplitude). The cyclic loading was continued until liquefaction failure (defined as the attainment of a 3.75% single amplitude shear strain (γ_{SA}) (NRC 1985)) was achieved.
The undrained conditions were obtained by shearing the samples under a constant volume condition. Since the samples are laterally constrained by the steel wires reinforced membrane this condition is simply reached by maintaining the sample height constant. The vertical constraint imposed to the sample makes the total vertical stress ($\Delta\sigma_v$) change all along the shearing phase. In this way the change in total vertical stress equals the excess pore water pressure generated in an equivalent undrained test (Dyvik et al.1987; Finn 1985). The adopted system consists of a closed-loop control software written in Visual Basic version 7.1, where two algorithms are implemented, one for maintaining the specimen height constant and another one for generating and controlling the cyclic horizontal load (stress-controlled tests) or displacement (strain-controlled tests) of a given amplitude and frequency (Porcino et al. 2006).
As already mentioned in paragraph 3.4.1 the interpretation of the undrained cyclic simple shear tests was based on the simplified assumption that the principal stress and strain increment direction coincide (Roscoe 1970). In this case, the horizontal plane can be assumed as the plane of maximum shear stress. According to previous authors (Roscoe et al. 1967; Sivathayalan 1994; Vaid and Sivathayalan 2000; Porcino et al. 2005a), this assumption can be considered reasonable in undrained tests irrespective of the initial void ratio.

3.5.5 Results presentation

A continuous record of all measured data was realized by means of a data acquisition system connected to a computer. The development of the shear stress (τ), vertical stress (σ_v; its change $\Delta\sigma_v$ is equivalent to the change in pore water pressure, Δu, in a truly undrained test), and shear strain (γ) with time was recorded. All tests were conducted until a single amplitude shear strain (γ_{SA}) of approximately 3.75% was reached (NRC 1985), and this strain-based criterion was selected for identifying the onset of liquefaction or other patterns of failure, respectively.
In **Figure 69**, are presented typical results of a cyclic simple shear test carried out on Ticino sand with 10% of silt in presence of an initial static shear stress τ_{stat}, while in

Figure 70 are presented typical results of a monotonic shear test carried out on Ticino sand with 20% of silt.

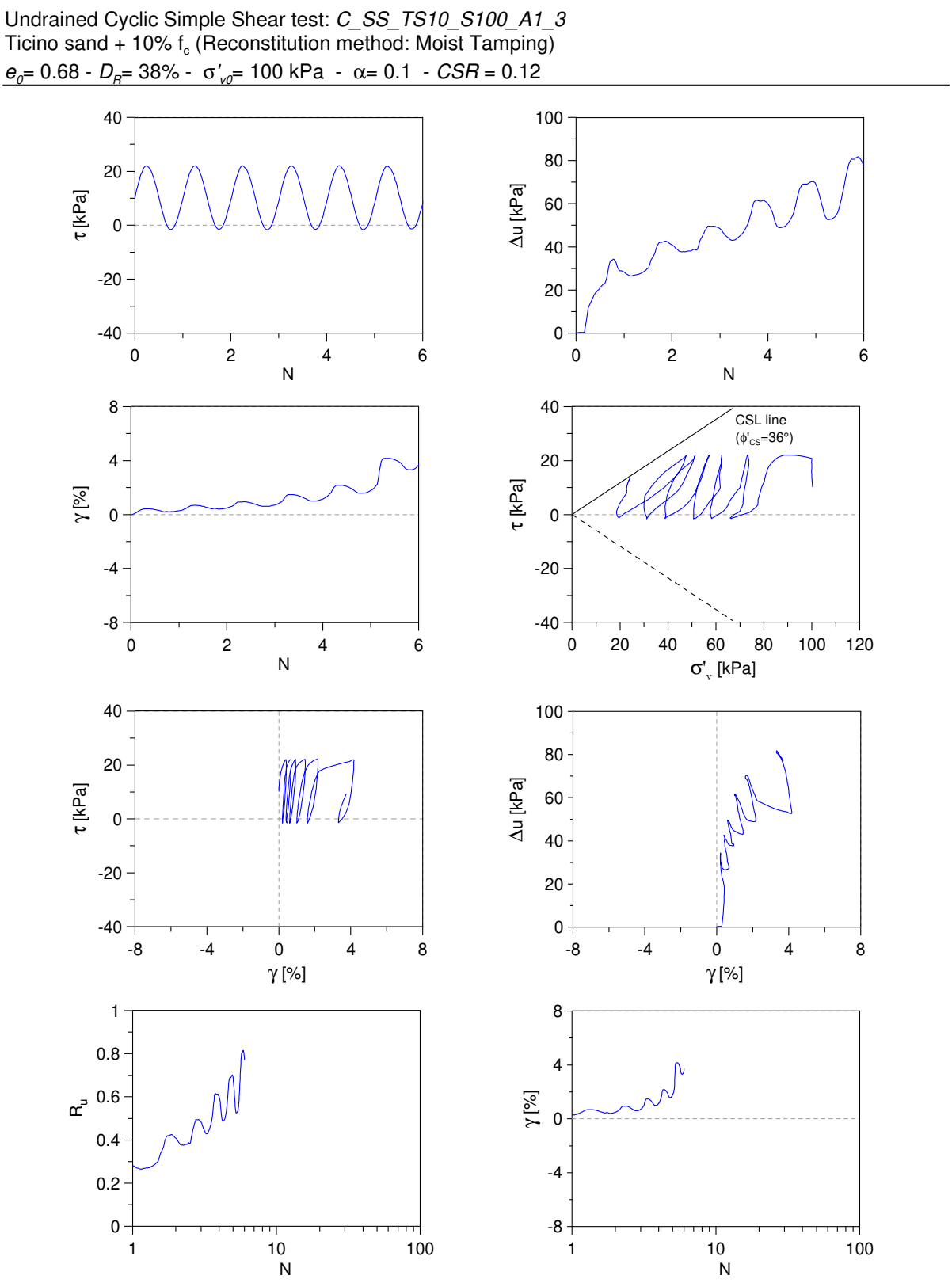

Figure 69 – Example of cyclic simple shear tests results on Ticino sand-silt mixtures (f_c=10%) with an initial static shear stress of 10 kPa.

In the cyclic test the shear stress varies with a sinusoidal law around an initial static shear stress of 10 kPa. The pore pressure data are expressed both in terms of excess pore water pressure Δu and normalized pore pressure ratio R_u. As it can be seen R_u reaches a limiting value (approximately 0.8) that is below the range of values usually associated to liquefaction. In the stress-strain (τ-γ) plane a progressive reduction of the stiffness of the material with the number of cycles can be observed. In (γ, N) plane the shear strains exhibit a quite regular trend in the first cycles undergoing an abrupt increase in the final part of the test until liquefaction occurs in correspondence to the value of 3.75% in single amplitude shear strain (**Figure 69**).

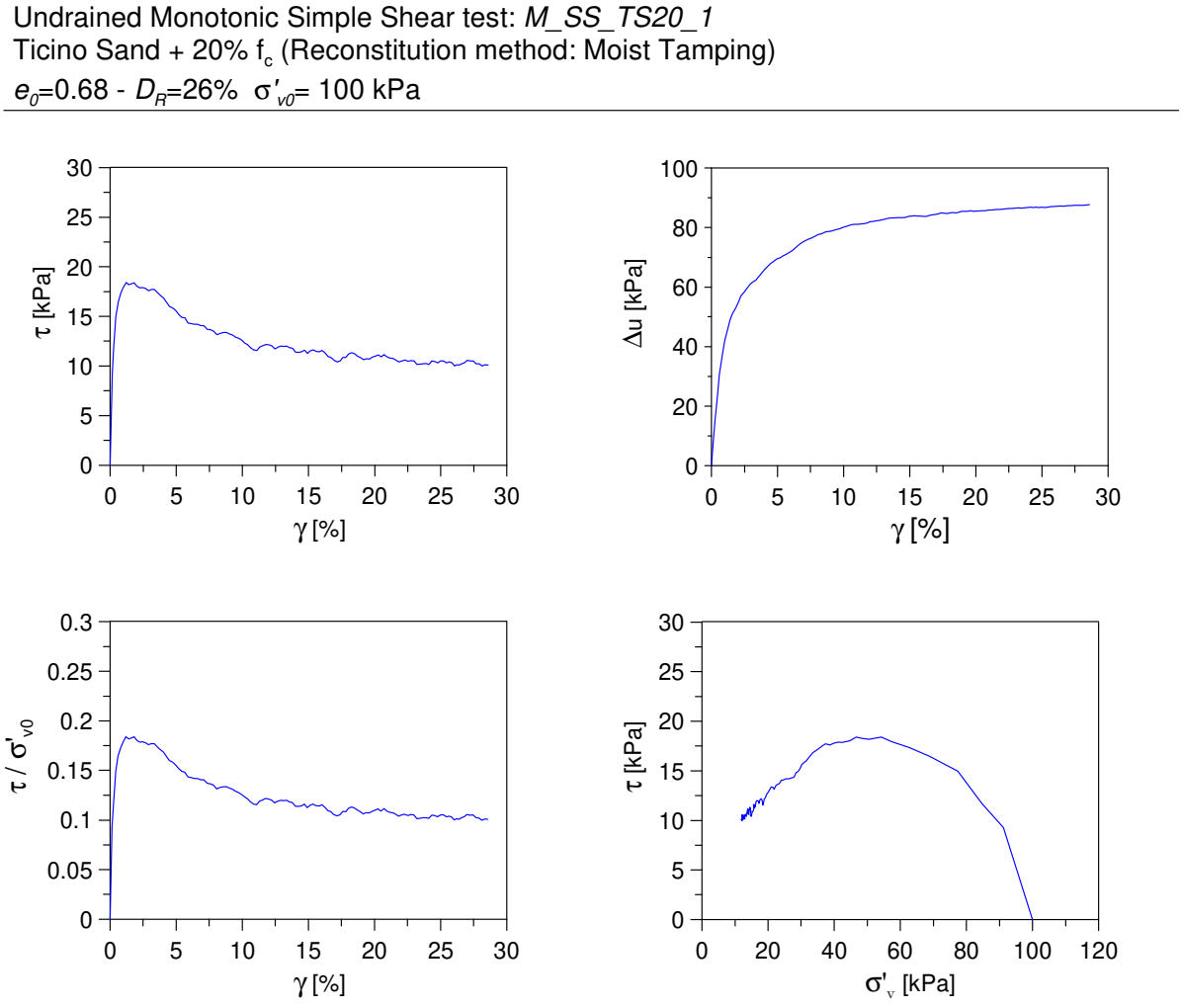

Figure 70 – Example of monotonic simple shear tests results on Ticino sand-silt mixtures (f_c=20%).

In monotonic test the behaviour exhibited is reported in terms of: a) stress-strain response in (τ-γ) plane, b) development of excess pore water pressures in (Δu–γ) plane

and effective stress-path in (τ-σ'_v) plane. In **Figure 70** a typical flow failure behaviour was observed.

Chapter 4

Analysis of tests results – undrained cyclic behaviour of Ticino silty sand

4.1 Typical failure patterns of silty sand

Failure pattern is one of the fundamental behaviours of soils subjected to cyclic loading, which may imply the response of the site to seismic waves. Previous authors (Yang and Sze 2011a, b; Sze and Yang 2014; Wei and Yang 2019a, b) reported different failure patterns of specimens of clean sands and silty sands reconstituted with different sample preparation methods in cyclic triaxial tests. The reported failure patterns were flow liquefaction, limited flow liquefaction, cyclic mobility and plastic strain accumulation. Going into more details failure patterns can be divided into two major categories, i.e. flow type failure and non-flow type failure. Furthermore, there are two sub-categories for flow type failure, namely flow liquefaction (*LF*) and limited flow liquefaction (*LFL*). There are also two sub-categories for non-flow type failure, namely cyclic mobility (*CM*) and plastic strain accumulation (*PSA*). This kind of failure patterns was observed in cyclic simple shear tests performed in the present study and detailed descriptions of these failure patterns are presented in the following sub-section.

4.2 Flow type failure

Two types of flow failure were identified through the experimental observations of several research: flow liquefaction (*FL*) and limited flow liquefaction (*LFL*). Both failure patterns are characterised by a sudden and rapid increase of shear strain once failure is triggered. If flow failure does not cease with a complete loss or resistance, it belongs to flow liquefaction. If flow failure ceases with a control of the load, it then belongs to limited flow liquefaction.

4.2.1 Flow liquefaction

Figure 71 presents test results from a loose *TS*+20%f_c specimen (e_0=0.68; σ'_{v0}=100 kPa) with an initial static shear stress equal to 10 kPa ($\alpha \neq 0$). The stress-strain relationship shows that the increase in shear strain was negligible before its sudden

and rapid increase. After flow failure, the excess pore water pressure became equal to that developed at the critical state on the critical state strength envelope, indicating that a completely liquefied failure state had been reached. This type of failure is referred as cyclic flow liquefaction. For exhibiting cyclic flow liquefaction (*FL*), the initial state of the specimen should be highly contractive for complete liquefaction to take place. The term *complete liquefaction failure* is here used for the reason that the specimen would not regain its stiffness and strength after liquefaction, and thus to avoid confusion with the term *initial liquefaction* or *transient liquefaction* which are also used for intermediate states within a phase with *cyclic mobility*.

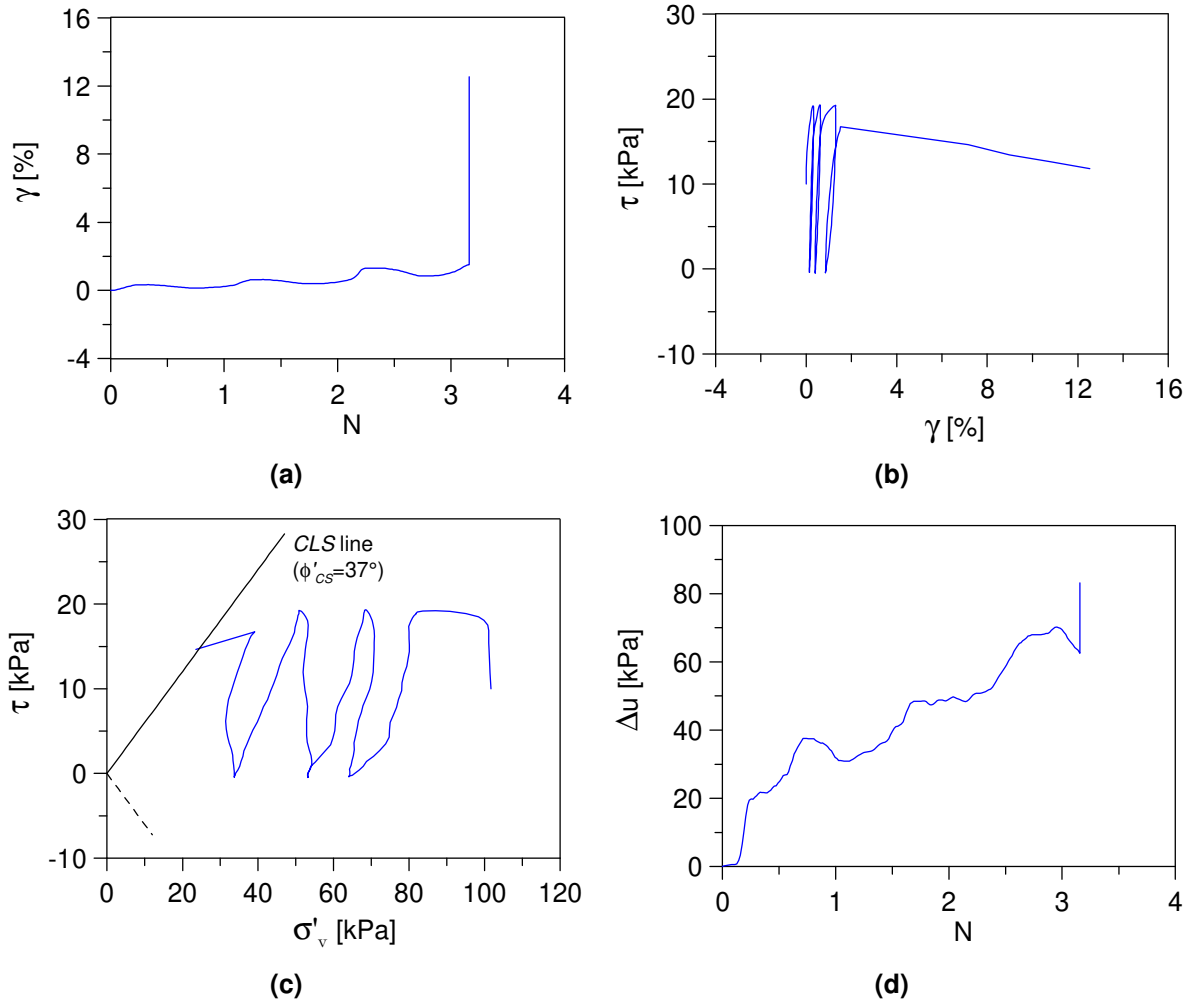

Figure 71 – Typical cyclic flow liquefaction response (moist tamped *TS*+20%·f_c, e_0=0.68, σ'_{v0}=100 kPa, α=0.10) in terms of: (a) shear strain vs number of cycles, (b) shear stress-strain response, (c) stress-path and (d) development of excess pore water pressure.

A similar behaviour was observed on silty sand with a fines content equal to 30% at a void ratio e_0 and an effective vertical stress σ'_{v0} equal to 0.68 and 100 kPa, respectively.

Therefore, the phenomenon of cyclic flow-liquefaction, from the analyses carried out in the present study, occurs in the case of loose materials in presence of fines; in particular, it has been observed for fines content of 20% and 30% and it occurs in materials with e_0 greater than 0.68. These indications are valid for an effective vertical stress of 100 kPa for TS+20%·f_c and from 50 to 100 kPa for TS+30%·f_c.

In order to verify the correspondence between the observed behaviour in undrained cyclic and monotonic simple shear tests for the silty sand reported in **Figure 71**, some additional monotonic tests were performed on the same material (**Figure 72**). As can be seen in **Figure 72a**, the material, even in undrained monotonic conditions, exhibits a "flow" failure type behaviour with a peak resistance after which there is a rapid loss of the shear resistance until an ultimate state condition is reached.

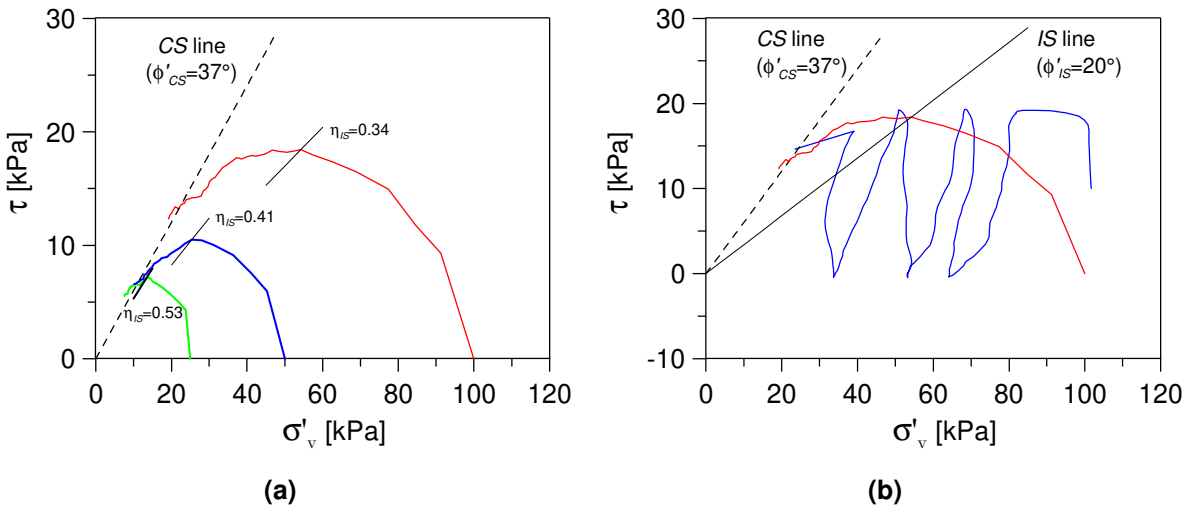

Figure 72 – Undrained monotonic and cyclic (α=0.10) response of Ticino silty sand with a flow type behaviour (TS+20%·f_c; e_0=0.68): (a) effective stress paths from monotonic triaxial tests evidencing *CSL* and *ISL*; (b) effective stress path from cyclic simple shear test.

Reduction of resistance was triggered at the stress ratio, η_{IS} of the peak point on the effective stress path (**Figure 72a**). This stress ratio is called *instability stress ratio*; it represents the slope of a line drawn from the peak point of the effective stress path to the origin of (τ-σ'_v) plane (Chu and Leong 2002; Lade 1992). As it is shown in **Figure 72a**, η_{IS} is not unique so that it would not be appropriate to assume that a single instability line exists. In fact the instability stress ratio η_{IS} decreased as the initial vertical effective stress increases, according to previous studies (Chu and Leong 2002; Sladen et al. 1985; Rahman and Lo 2012). In the same figure (**Figure 72a**) the critical state line of the material in the stress (τ-σ'_v) plane was also presented. In each test the

samples were considered to have attained the critical state when the shear strain reached a value $\gamma = 25\%$. The critical state angle of shearing resistance φ'_{CS} obtained was near to the value obtained from *TX* tests carried out on the same material in a previous research (Porcino et al. 2019).

In **Figure 72b** a direct comparison between the undrained cyclic and monotonic behaviours is shown. In the fist two cycles, cyclic effective stress path was always below the instability state line (*ISL*) of the corresponding monotonic test carried out at the same σ'_{v0}. In the third cycle, τ crossed the *ISL* line as shown in **Figure 72b**. It is to be noted that after this cycle, the effective stress path curved downward with rapid loss of shear resistance and afterward neither τ_{max} nor τ_{min} imposed (stress-controlled test) could be achieved. Thus, it can be said that observed behaviour was a form of instability. There is therefore a good correspondence of behaviour observed in undrained conditions in the cyclic and monotonic tests with the evidence of a strongly contracting tendency of the material.

4.2.1 Limited flow liquefaction

Figure 73 presents test results of a moist-tamped $TS+30\%\cdot f_c$ specimen exhibiting limited cyclic flow liquefaction (*LFL*). Similar to flow liquefaction, the shear strain did not accumulate significantly before the triggering of the flow. Once the flow was triggered, the shear strain abruptly increased accompanied by an increase of excess pore water pressure.

In accordance with Robertson's (1994) behavioural chart, the phenomenon of flow liquefaction in the presence of an initial static shear stress occurs when τ_{stat} is greater than the residual shear strength (τ_{CS}) of the material (**Figure 72**) evaluated in the monotonic test carried out at the same effective vertical stress; τ_{CS} is assessed in the (τ-σ'_v) plane from the point in which the effective stress path reaches the *CSL*. Conversely when the initial static shear stress is equal to zero the flow liquefaction doesn't happen (**Figure 73**) unless the material in monotonic conditions exhibits a behaviour of complete static flow liquefaction. Unlike what is reported in the Robertson's paper, materials with a contracting behaviour that do not exhibit a complete static flow liquefaction do not necessarily fit into the non flow failure patterns exhibited by dilating soils, but rather they manifest failure mechanisms that can be classified as limited flow liquefaction (**Figure 73**); this is in accordance with a recent study (Wei and Yang 2019a).

The phenomenon of limited flow liquefaction (**Figure 73**), from the analyses carried out in the present study, occurs in the case of loose sands with fines; in particular, it has been observed for fines content of 20% (*TS*+20%·f_c) with e_0 greater than 0.68 and for fines content of 30% (*TS*+30%·f_c) with e_0 greater than 0.58. These indications are valid for an effective vertical stress of 100 kPa.

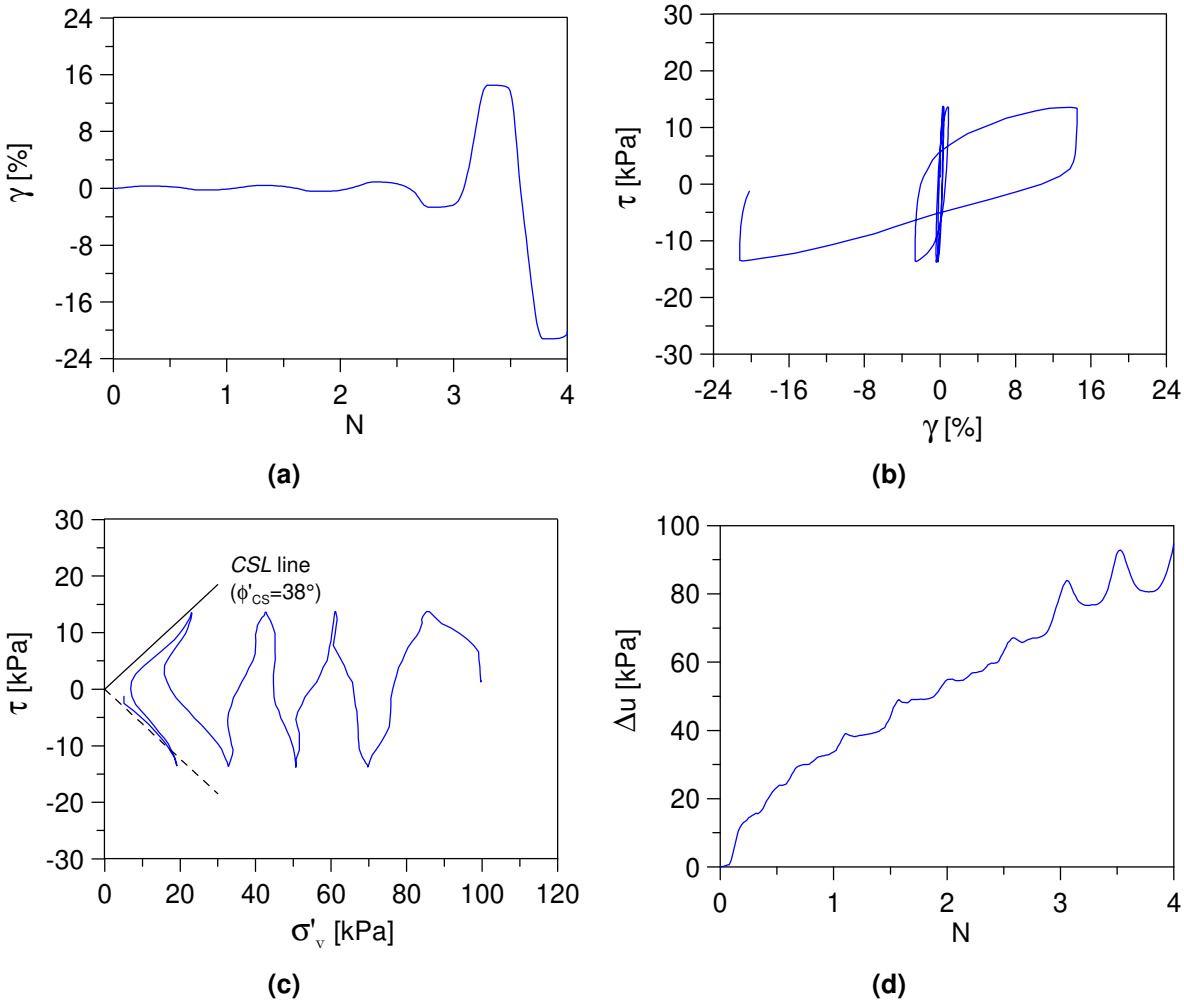

Figure 73 – Typical limited flow liquefaction response (moist tamped *TS*+30%·f_c, e_0=0.68, σ'_{v0}=100 kPa, α=0) in terms of: (a) shear strain vs number of cycles, (b) shear stress-strain response, (c) stress-path and (d) development of excess pore water pressure.

4.3 Non-flow type failure

This category can be observed in medium dense to dense specimens, which are generally considered to be dilative. Two are the main types of failure that have been identified for these soils: *cyclic mobility* (*CM*) and *plastic strain accumulation* (*PSA*). The definition of cyclic mobility follows from that given by Castro (1975); it is described in detail in the subsequent paragraphs and consistently used in the present study.

Conversely the term plastic strain accumulation is referred to a failure pattern characterised by a gradually increased residual plastic strain, which predominantly occurs when the shear stress does not reverse. It should be noted that Robertson and Fear (1995) used the term cyclic liquefaction for the behaviour that in the present study is termed cyclic mobility, and the term cyclic mobility for plastic strain accumulation.

4.3.1 Cyclic mobility

The undrained cyclic response of a silty sand specimen exhibiting a *cyclic mobility* (*CM*) failure mechanism is presented in **Figure 74**. The excess pore water pressure increased progressively and finally reached a transient liquefied state ($\Delta u = 0.95 \cdot \sigma'_{v0}$, $\sigma'_v \approx 0$).

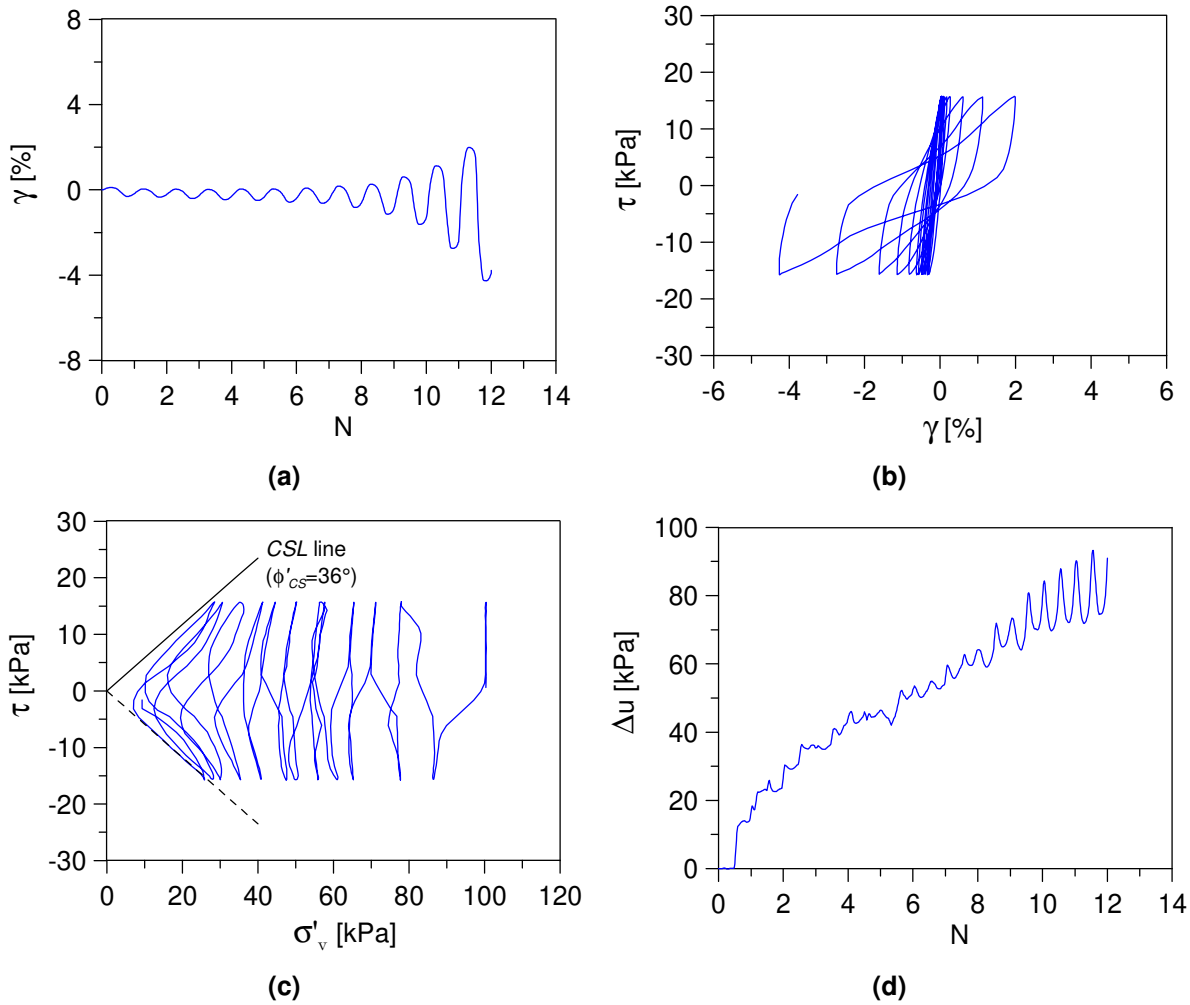

Figure 74 – Typical cyclic mobility response (moist tamped *TS*+10%·f_c, e_0=0.60, σ'_{v0}=100 kPa, α=0) in terms of: (a) shear strain vs number of cycles, (b) shear stress-strain response, (c) stress-path and (d) development of excess pore water pressure.

When this state was attained for the first time, initial liquefaction is said to occur. Since then, significant shear strain development took place during subsequent cycles. These transient liquefied states correspond to the reversal of cyclic stress. Rapid shear strain development took place when the load was about to reverse because the specimen exhibited very low stiffness due to the lowered vertical effective stress. After the loading reversed, the specimen regained its stiffness and strength, due to the decrease in pore water pressure and the corresponding increase in the vertical effective stress. These transient liquefied states and subsequently regained stiffness and strength led to sharp peaks in the pore pressure graph and elbow-like stress path. Besides other conditions, that will be discussed in more detail in the next paragraph, a necessary condition for this type of failure to occur is that a stress reversal exists.

Figure 75 presents the results of an undrained cyclic *SS* test conducted on a specimen with α=0.05 that also failed in the pattern of cyclic mobility. Upon cyclic loading, the transient liquefied state could be reached accompanied by large shear strain development. As mentioned before, stress reversal is one of the necessary conditions for cyclic mobility. As it can be seen from plots in (τ-σ'_v) or (τ-γ) planes this condition is fulfilled in the analysed test. However, there are cases in which, despite the presence of a stress reversal condition, the behaviour exhibited by the material is *intermediate* (*INT*) between *cyclic mobility* and *plastic strain accumulation*. Evidences gained in this resarch allowed to identify the ratio α/*CSR* as a controlling factor for the occurrence of the intermediate failure pattern. A list of α/*CSR* ratios adopted in the undrained cyclic *SS* tests carried out on samples exhibiting the intermediate behaviour is reported in **Table 6**. α/*CSR* ranges evidenced in this table can be used for predicting the occurrence of the intermediate behaviour in preliminary analyses. More information on the plastic strain accumulation will be given in the next paragraph.

4.3.2 Plastic strain accumulation

Figure 76 presents the results of an undrained cyclic *SS* test conducted on a specimen tested with α=0.20 that exhibited plastic strain accumulation. Irrecoverable residual shear strains (measured at the neutral points of cycles) accumulated with increasing number of loading cycles, and gradually increased to a large strain level. This is the reason behind the adoption of the term *plastic strain accumulation*. The excess pore water pressure gradually increased and eventually became stable. No liquefaction was observed in this case.

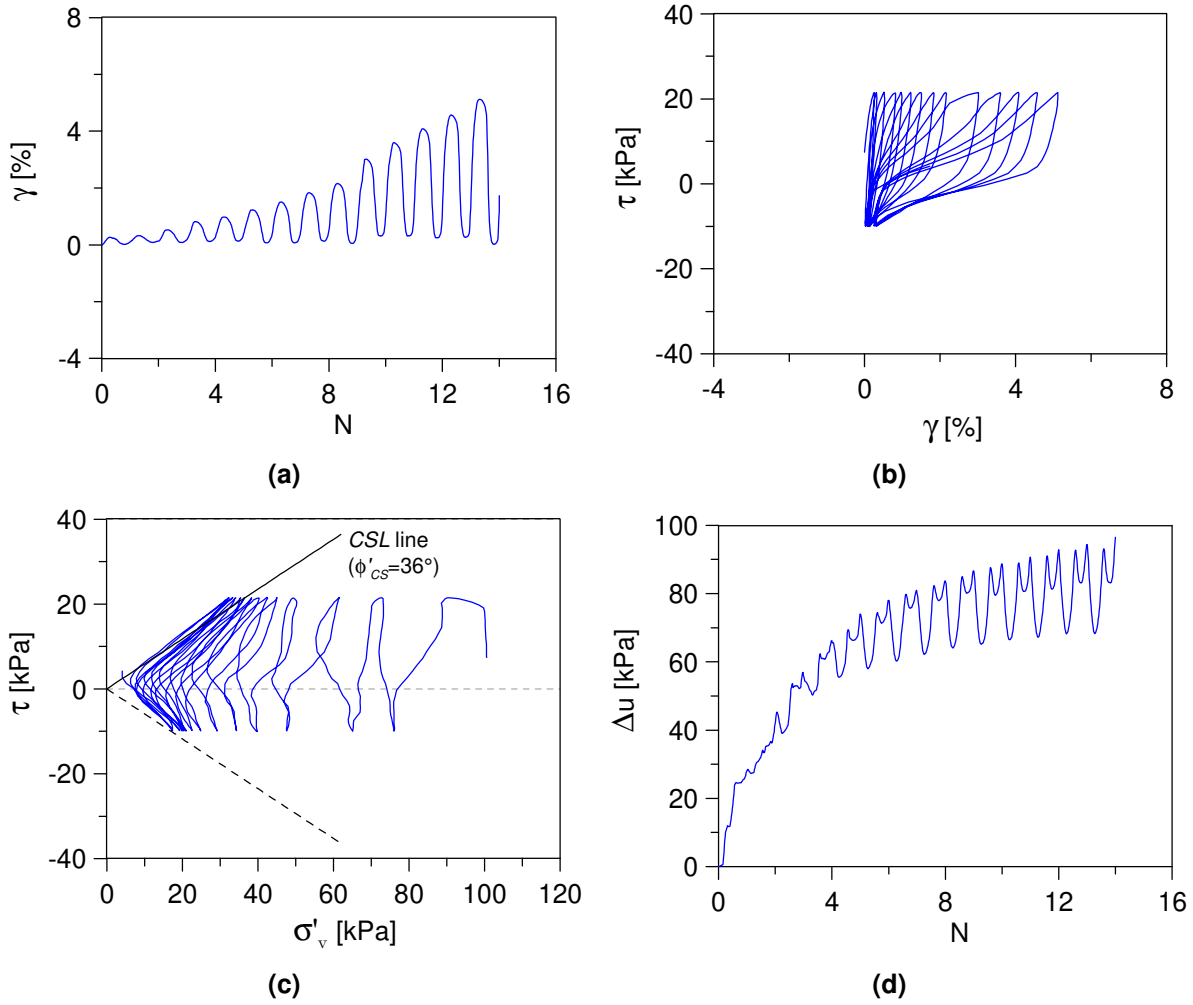

Figure 75 – Typical cyclic mobility response (moist tamped *TS*+10%·f_c, e_0=0.60, σ'_{v0}=100 kPa, α=0.05) in terms of: (a) shear strain vs number of cycles, (b) shear stress-strain response, (c) stress-path and (d) development of excess pore water pressure.

Table 6 – α/*CSR* ratios for mixtures exhibiting intermediate behaviour.

Material	e_0	σ'_{v0} (kPa)	α/*CSR*
TS	0.60-0.78	100	0.36-0.71
TS+10%·f_c	0.55-0.68	50-100	0.45-0.63
TS+20%·f_c	0.55	100	0.50-0.71
TS+30%·f_c	0.55-0.59	100	0.53-1.00

This type of failure may occur when the specimens are loaded without stress reversal and satisfy the requirements of an initial state capable of inducing a hardening behaviour. However, in some cases, even with a limited shear stress reversal condition, this kind of behaviour can be observed. As already stated in the previous paragraph, a useful indicator to evaluate when this phenomenon occurs in presence of a limited shear stress reversal is the α/*CSR* ratio (**Table 7**).

4.4 Factors affecting failure patterns

The cyclic failure patterns described in the previous section can be affected by several factors, the most relevant of which are the initial state (post-consolidation void ratio e_0 and initial mean effective stress p'_0 or initial vertical effective stress σ'_{v0}), the applied initial static shear stress and the stress reversal conditions. This sub-section discusses how these factors influence the failure patterns.

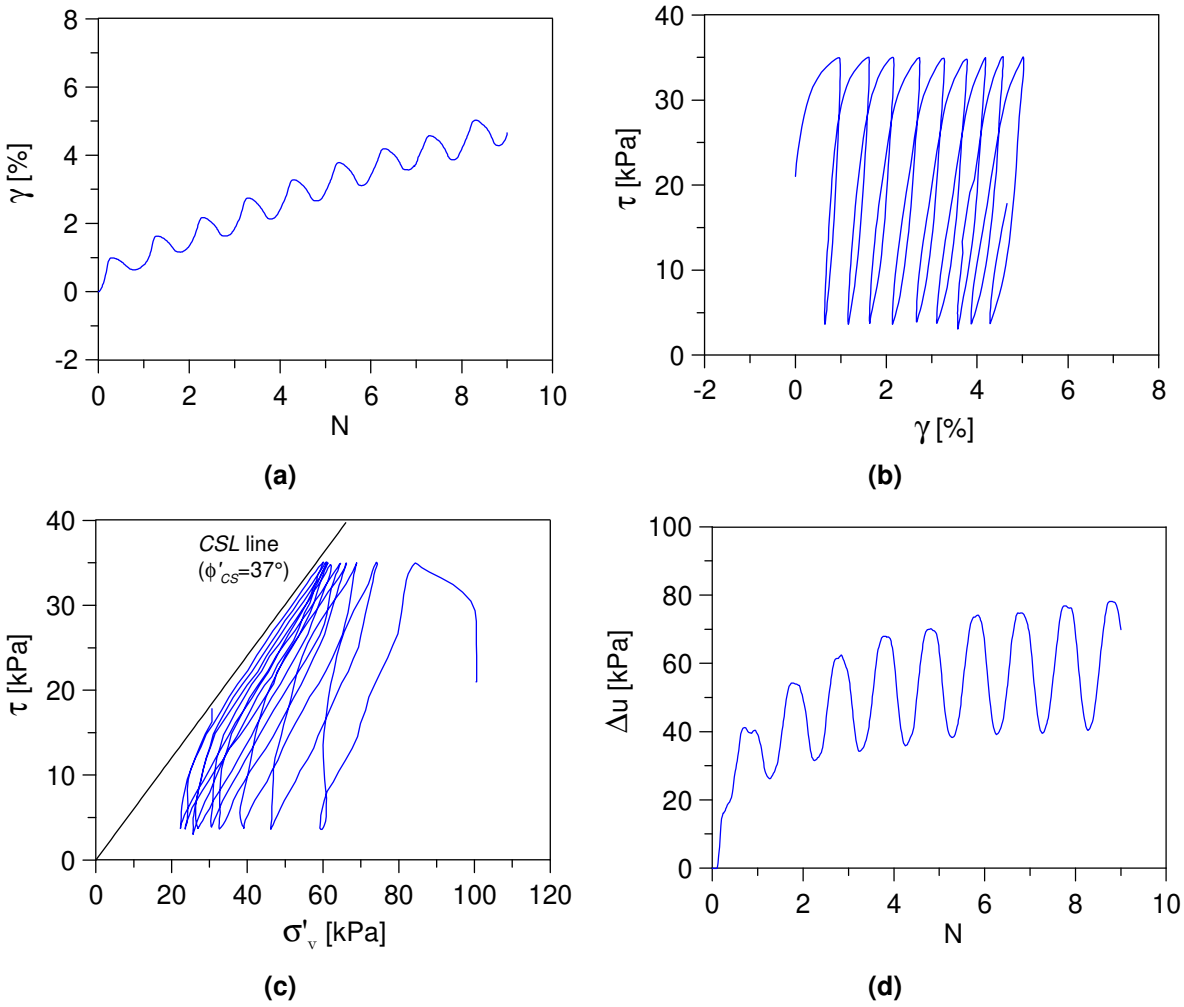

Figure 76 – Typical plastic strain accumulation response (moist tamped *TS*+20%·f_c, e_0=0.55, σ'_{v0}=100 kPa, α=0.20) in terms of: (a) shear strain vs number of cycles, (b) shear stress-strain response, (c) stress-path and (d) development of excess pore water pressure.

Table 7 – α/*CSR* ratios for mixtures exhibiting plastic strain accumulation behaviour with limited shear stress reversal.

Material	e_0	σ'_{v0} (kPa)	α/*CSR*
TS	0.60-0.78	100	0.71-0.83
TS+10%·f_c	0.55-0.68	50-100	0.71-0.83

Material	e_0	σ'_{v0} (kPa)	α/CSR
TS+20%·f_c	0.59	100	0.83

From a theoretical point of view the effects of void ratio on the failure pattern can be described by observing that with decreasing void ratio, specimens become more dilative under otherwise similar conditions. The failure pattern of a specimen would gradually change from flow-type failure to non-flow type failure. Such trend is presented in **Figure 77a** for moist-tamped specimens without initial static shear stress.

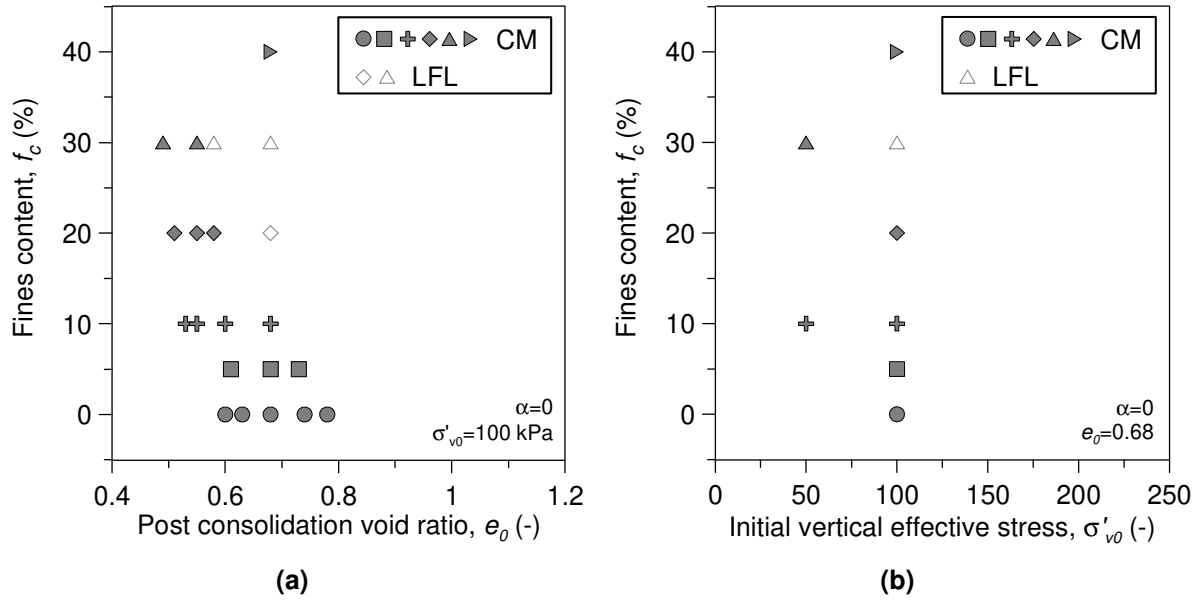

Figure 77 – Effects of (a) void ratio and (b) initial vertical effective stress on failure patterns (*CM*=cyclic mobility, *LFL*=limited flow liquefaction).

In **Figure 77a** two types of behaviour changing from limited flow liquefaction (*LFL)* to cyclic mobility (*CM)* were observed with decreasing (e_0). According to **Figure 74** *CM* behaviour was characterized by a typical "butterfly" shape of cycles in τ–γ plane with a loss of stiffness and a progressive accumulation of the shear strain amplitude with cycling, associated with the development of high excess pore water pressures. On the other hand the failure pattern of *LFL* type (**Figure 73**) included some features of the cyclic mobility but, once the failure is triggered, the shear strains may develop rapidly without a complete loss of resistance. Therefore the effects of increasing void ratio on the undrained cyclic response of *TS*–silt mixtures can be summarized as a more strain-softening behaviour with a tendency to limited flow type response (**Figure 77a**). The above mentioned effects of void ratio are consistent with previous studies (e.g. Wei and Yang 2019) irrespective of sample preparation methods, initial static shear stress

and types of materials. Besides void ratio, initial effective confining pressure can also affect the failure pattern. With increasing confining pressure, dilation of the specimen can be suppressed whereas contraction can be enhanced. With increasing confining pressure, failure patterns of the specimens with a given void ratio may turn from non-flow type failure to flow type failure. One example is shown in **Figure 77b** for f_c=30 % e_0=0.68 and α=0.

Furthermore, different cyclic loading amplitudes may cause different failure patterns of a specimen with a given initial state (equal initial void ratio and vertical effective stress). The two moist-tamped *TS*+30%·f_c specimens in **Figure 78** have similar initial states but are loaded under different *CSRs*. The specimen in **Figure 78a** was loaded under the lower *CSR* (=0.12) whereas the one in **Figure 78b** was loaded under the higher *CSR* (=0.18).

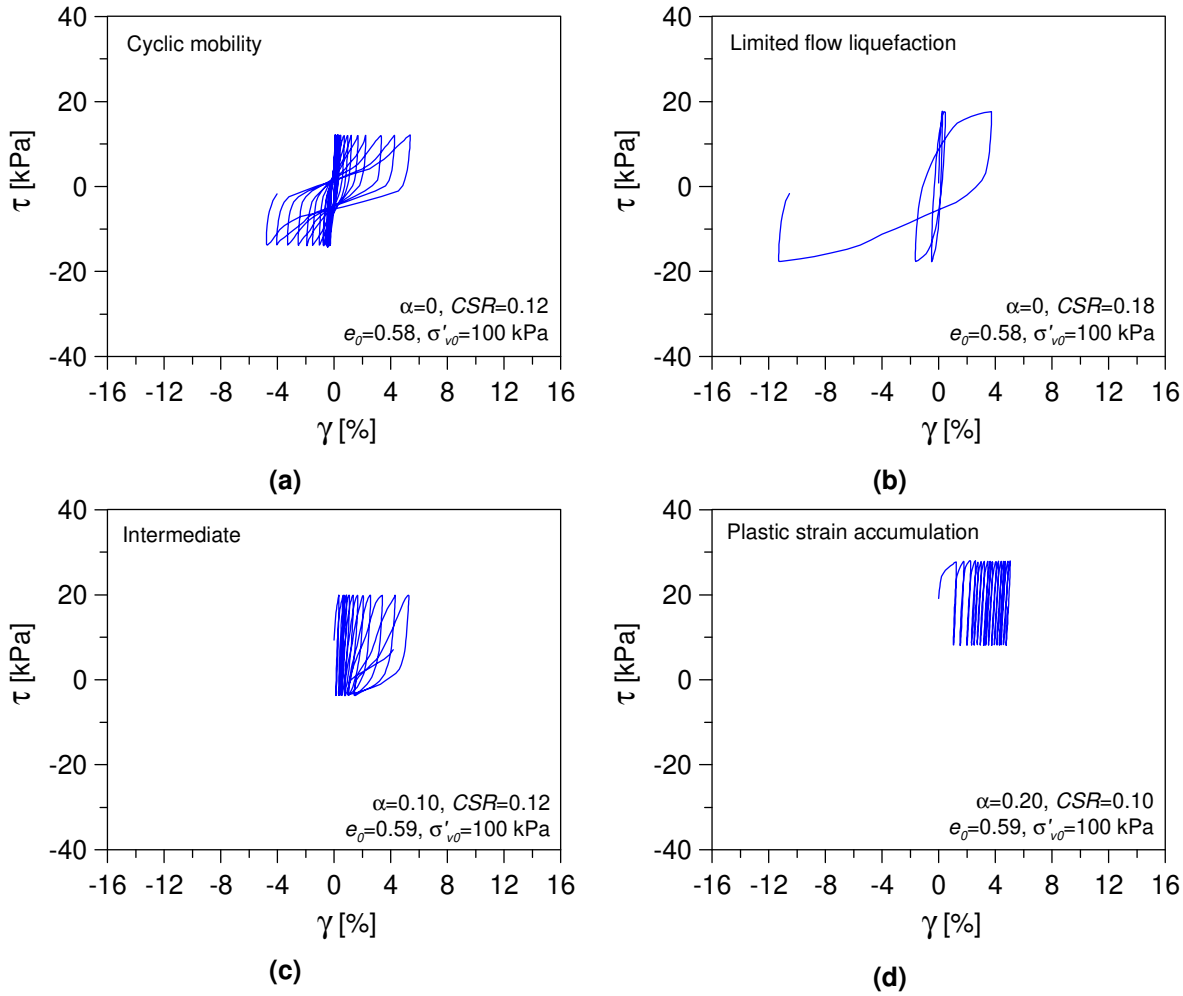

Figure 78 – Effect of *CSR* and *α* on failure patterns for *TS*+30%·f_c sand silt mixtures at the same initial state (e_0=0.58-59, σ'_{v0}=100 kPa): (a) *CSR*=0.12 and *α*=0; (b) *CSR*=0.18 and *α*=0; (b) *CSR*=0.12 and *α*=0.10; (b) *CSR*=0.10 and *α*=0.20.

It is clear that the specimen loaded with lower *CSR* exhibited cyclic mobility (*CM*) but the other loaded with higher *CSR* showed limited flow liquefaction (*LFL*). The existence of an initial static shear stress may also affect the failure patterns. This is because its presence results in unsymmetrical loading cycles, leading to different stress reversal conditions. Taking **Figure 78a, c,** and **d** for example, increased initial static shear stress causes stress reversal to disappear and this turns failure pattern from cyclic mobility to intermediate and plastic strain accumulation. For relatively loose specimens, limited flow liquefaction may be observed for low initial static shear stress and high cyclic stress ratio, whereas limited flow liquefaction was not observed for high initial static shear stress. In fact, the effects of the cyclic loading amplitude and the initial static shear stress should be studied together because both of them affect simultaneously the characteristics of the cyclic loading.

Chapter 5

Characterization of cyclic resistance of silty sand

In the previous chapter, the basic behaviours and failure patterns of non-plastic silty sands under undrained cyclic loading have been discussed from a qualitative point of view for different fines content, initial void ratio and vertical effective stress (initial states) and various initial static shear stresses. These behaviours may correlate with ground response to cyclic loading for different site conditions. However, estimation of cyclic resistance against liquefaction, which is a crucial step in engineering practice (Seed 1981), has not yet been discussed. This chapter discusses the cyclic liquefaction resistance of non-plastic silty sands as well as factors that affect this characteristic through the results of the present research.

5.1 Evaluation of cyclic resistance of non-plastic silty sands

5.1.1 Failure criterion

As discussed in the previous chapter, there are mainly four distinguished failure patterns, namely flow liquefaction, limited flow liquefaction, cyclic mobility, and plastic strain accumulation. Different failure patterns, corresponding to different characteristics of strain development and excess pore water pressure generation, are the results of different combinations of initial state, initial static shear stress and loading amplitude. The failure criteria for cyclically loaded specimens are commonly defined through the development of excess pore water pressure or, alternatively, the development of shear strain. In the present study both of them were considered but the criterion based on development of shear strain turned out to have a more general validity irrespective of the failure pattern analysed.

Figure 79 presents the strain development observed in tests exhibiting each type of failure pattern. **Figure 79a** to **79c** represent the typical trends featuring flow liquefaction, cyclic mobility and plastic strain accumulation, respectively. Since the strain level before flow liquefaction is rather small, its abrupt and unlimited nature makes the onset point of flow failure to correspond to the point that define failure. In fact after the flow is initiated, the shear strain increases so rapidly, reaching a very

large level, that the process cannot be captured. Accordingly this failure criterion can be treated as a strain-based one. A criterion based on excess pore water pressure may not be suggested for this failure type because the excess pore water pressure may not reach pore pressure ratio R_u = 1 even after flow failure.

Cyclic mobility usually occurs for dilative specimens. Stress reversal is one of the essential conditions, although in some cases we can also observe an intermediate behaviour with plastic strain accumulation. In these tests the shear strain changes cyclically between positive and negative side, and for this reason a strain criterion based on single amplitude deformation seems to be useful to define the onset of liquefaction. For cyclic mobility in literature, excess pore water pressure is also widely used as an indicator that determines failure, usually in the form of pore pressure ratio, R_u. Nevertheless in these tests the number of cycles causing R_u = 1 is very close to that causing S.A. of shear strain = 3.75% (NCR 1985). Hence, 3.75% of S.A. of shear strain can be consistently chosen as the failure criterion for cyclic mobility and intermediate behaviours (**Figure 79b**).

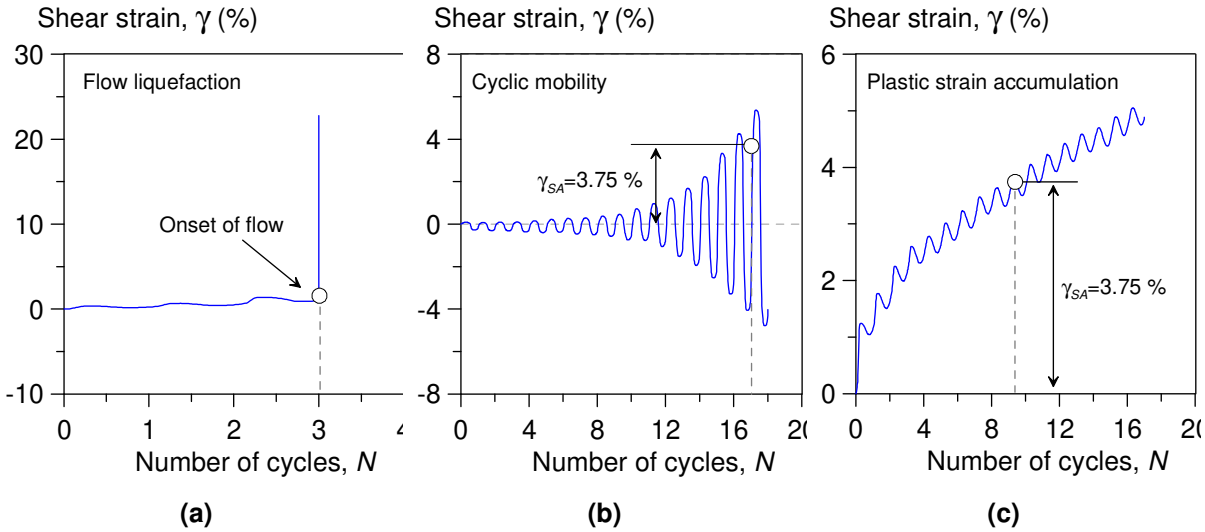

Figure 79 – Strain development of different cyclic failure patterns: (a) flow liquefaction, (b) cyclic mobility and (c) plastic strain accumulation.

Plastic strain accumulation occurs when there is no stress reversal in general or when a little reversal is present, leading to strain accumulation. The shear strain oscillates cyclically around a median curve (**Figure 79c**). In this case the accumulated peak shear strain of 3.75% was used as the indicator to define failure, which may give a relatively conservative estimation. A criterion based on excess pore water pressure

may not be suggested because the excess pore water pressure is a complex result of the interaction between initial state, initial static shear stress and loading amplitude, and may remain significantly lower than the initial effective confining pressure or the initial effective vertical stress (R_u < 1) for some cases (e.g. **Figure 80**).

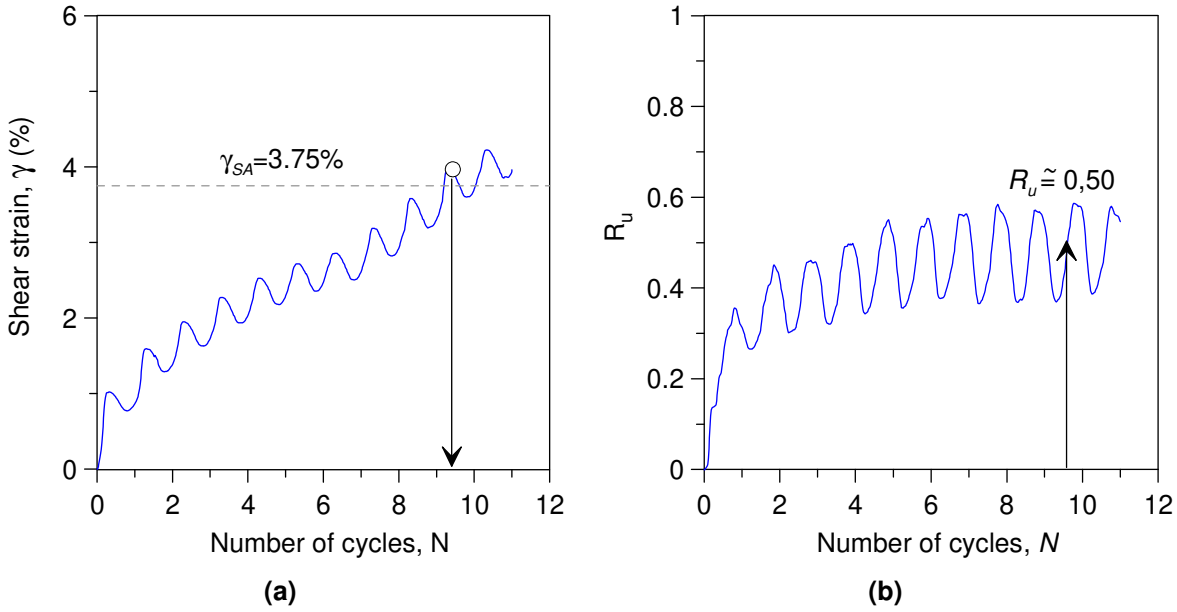

Figure 80 – Typical plastic strain accumulation response (moist tamped *TS*+10%·f_c, e_0=0.60, σ'_{v0}=100 kPa, α=0.20) in terms of: (a) shear strain vs number of cycles, (b) development of excess pore water pressure.

5.1.2 CSR – N_f relationship and cyclic resistance of non-plastic silty sands at a given number of cycles

The cyclic resistance, in terms of cyclic resistance ratio (*CRR*), is defined as the *CSR* causing failure at a given number of stress cycles. It is commonly determined using the relationship between *CSR* and the number of cycles that the soil can sustain until failure/liquefaction (N_f). **Figure 81** presents selected *CSR*-N_f relationships, showing that N_f increases with decreasing *CSR*. The following equation is commonly adopted in engineering practice:

$$CSR = E \cdot N_f^{-F} \quad (24)$$

where *E* and *F* are positive fitting parameters. By measuring several N_f values corresponding to different *CSRs*, it is possible to best-fit the test data and finally calculate the cyclic resistance at a given number of uniform cycles to failure, CRR_N.

In the engineering practice, the typical number of equivalent uniform cycles of an earthquake is related to the moment magnitude (M_w) of the earthquake (e.g. Seed and

Idriss 1982; Idriss 1999; Idriss and Boulanger 2008). Approximately, $N_f = 10$ represents an earthquake with M_w=7, and N_f = 15 represents M_w = 7.5. Considering the fact that in liquefaction analyses a reference earthquake of magnitude M_w=7.5 corresponding to 15 cycles of uniform cyclic loading is usually adopted (Youd et al. 2001; Idriss and Boulanger 2006), in the present study N_f = 15 has been considered. Moreover, CRR_{10} and CRR_{20} are also estimated in order to compare them with literature data.

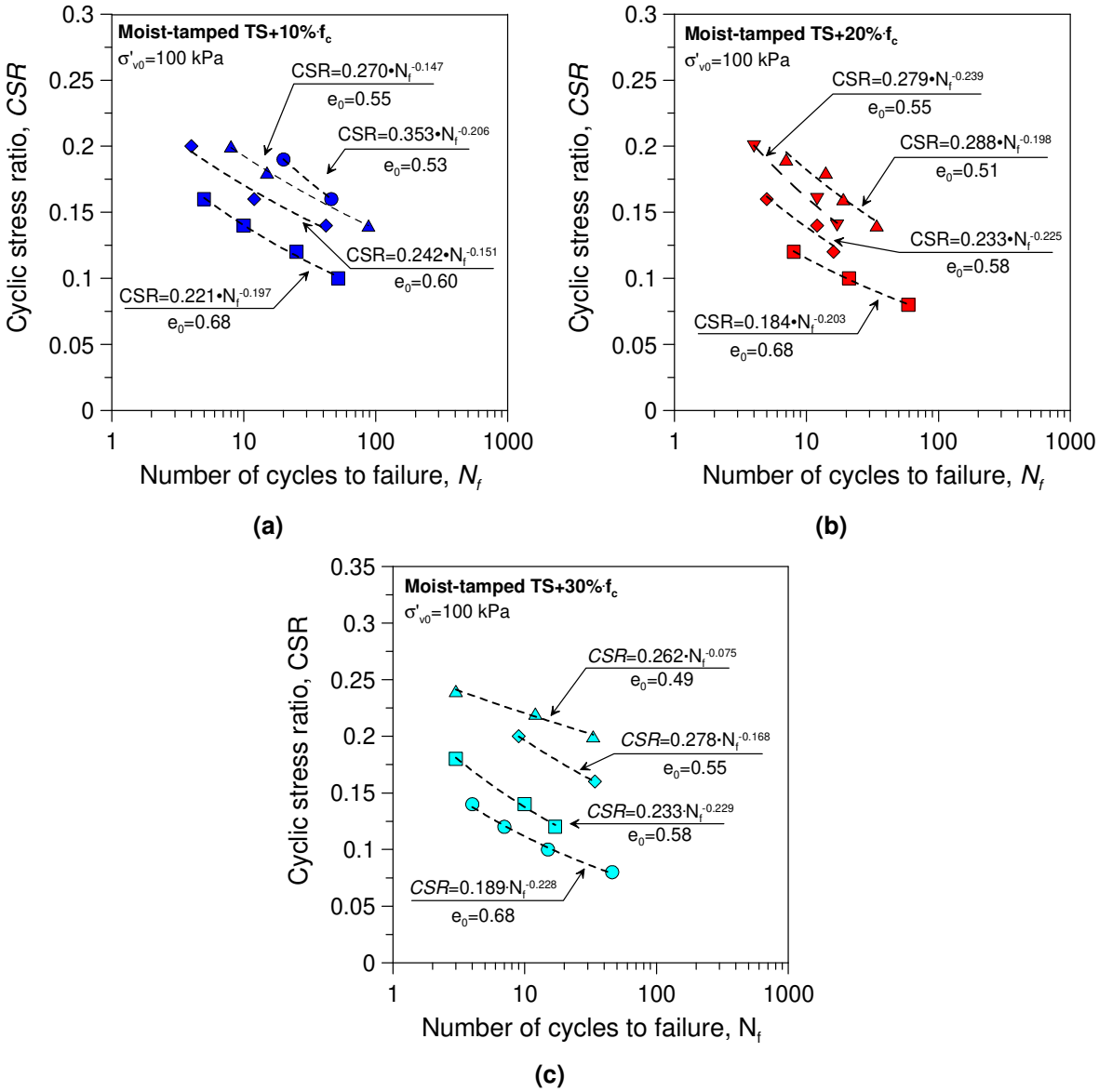

Figure 81 – Typical *CSR-N*$_f$ relationship for moist-tamped Ticino sand silt mixtures: (a) *TS*+10%· f_c, (b) *TS*+20%· f_c.

5.1.3 Determination of magnitude scaling factor

Besides to determine the cyclic resistance for seismic risk analyses, the *CRR–N*$_f$ relationship may play an important role to determine the magnitude scaling factor

(*MSF*). Laboratory measurements may serve as one of the methods to estimate *MSF* for a given sand (Seed and Idriss 1982). The magnitude scaling factor *MSF* can be defined as follows:

$$MSF = \frac{CRR_{M_w}}{CRR_{M_w=7.5}} \tag{25}$$

where CRR_{Mw} and $CRR_{Mw=7.5}$ are the cyclic resistance at a given M_w and at an M_w equal to 7.5, respectively.

The cyclic stress ratio causing failure at a given M_w can be regarded as the cyclic resistance for a specific number of cycles CRR_N; then this cyclic resistance is normalised by $CRR_{N=15}$ to obtain *MSF.* In **Figure 82** the experimental results in terms of *MSF* are plotted against the number of cycles. It is clear that the *MSF – N* relationship seems to be poorly affected by initial state (**Figure 82a**), fines content (**Figure 82b**) and initial static shear stress ratio (**Figure 82c**). An almost unique trend line may be found for each series with the only exception of the relationship expressing the influence of the initial static shear stress whose data points are a little more scattered. The procedure illustrated by Idriss (1999) was followed to obtain the *MSF-M_w* correlation. To this purpose, using the *N-M_w* relationship proposed by Idriss (1999), the *MSF – N* relationship in **Figure 82c** has been converted into *MSF-M_w* correlation. This correlation is plotted in **Figure 83** to compare with other *MSF-M_w* correlations proposed in literature. The series of magnitude scaling factors derived from Ticino sand-silt mixtures series are very close to those suggested by Wei and Yang (2019a), noting that their proposal is also based on laboratory investigation on sand mixed with non-plastic silt. However, other researchers have suggested different *MSF-M_w* relationships, showing poor consistency, excepted Seed and Idriss (1982). Youd et al. (2001) recommended the shaded area to be used for engineering practice when $M_w < 7.5$ and the values suggested by Idriss (1999) to be applied for $M_w > 7.5$. It seems that the discrepancy between these proposals has not been fully understood.

The present study suggests that the original *MSF* vs. M_w relationship suggested by Seed and Idriss (1982) may be applied to non-plastic reconstituted specimens, regardless of packing density, confining pressure, fines content and initial static shear stress. However in cases where these materials are found on site, the correlation defined by (Eq. 26) can used as an alternative approach:

$$MSF = 2.581 \cdot exp\left(-\frac{M_w}{7.931}\right) \tag{26}$$

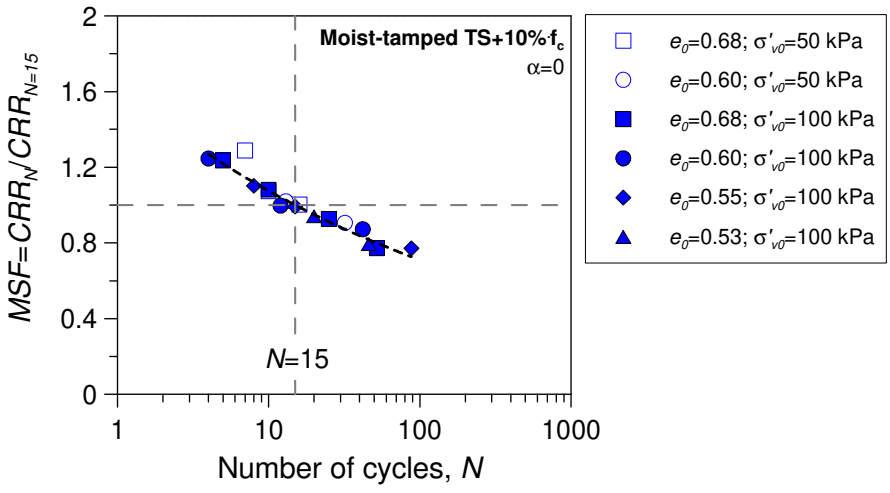

(a)

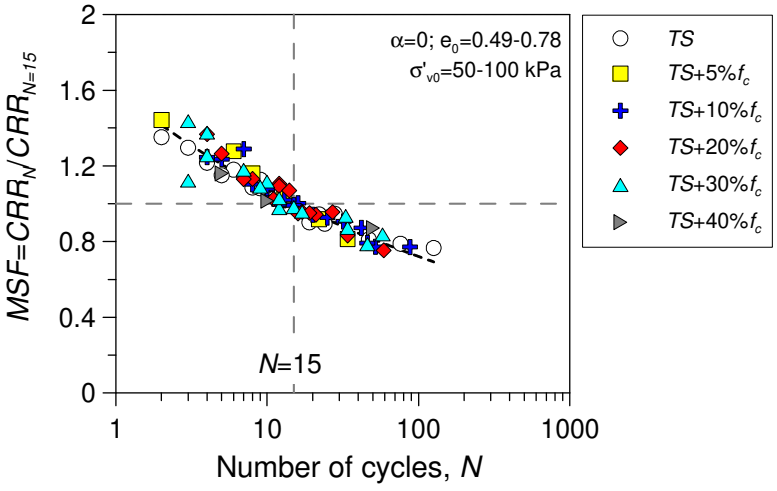

(b)

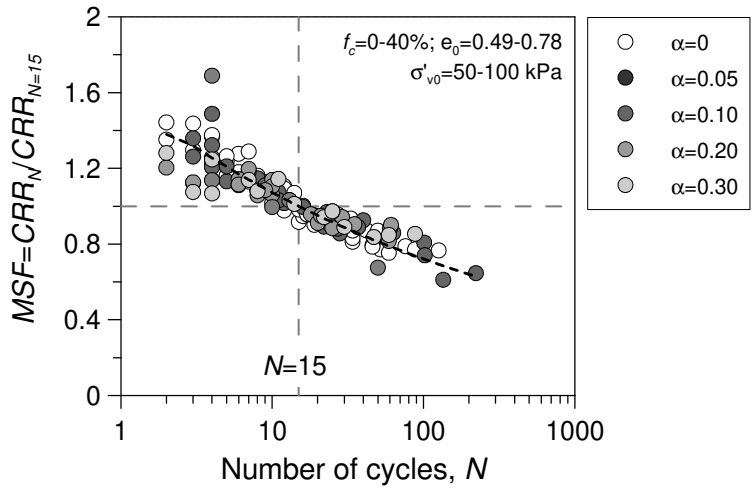

(c)

Figure 82 – Relationship between magnitude scaling factor and number of uniform stress cycles for moist-tamped Ticino silty sand: (a) *TS*+10%·f_c and without initial static shear stress, (b) all mixtures without initial static shear stress, (c) all mixtures and with different initial static shear stress.

This correlation, calibrated on the experimental data of the present study (**Figure 82c**) closely approximates the correlation proposed by Wei and Yang (2019a) for silty sands; it is characterized by a coefficient of determination R^2 equal to 0.83.

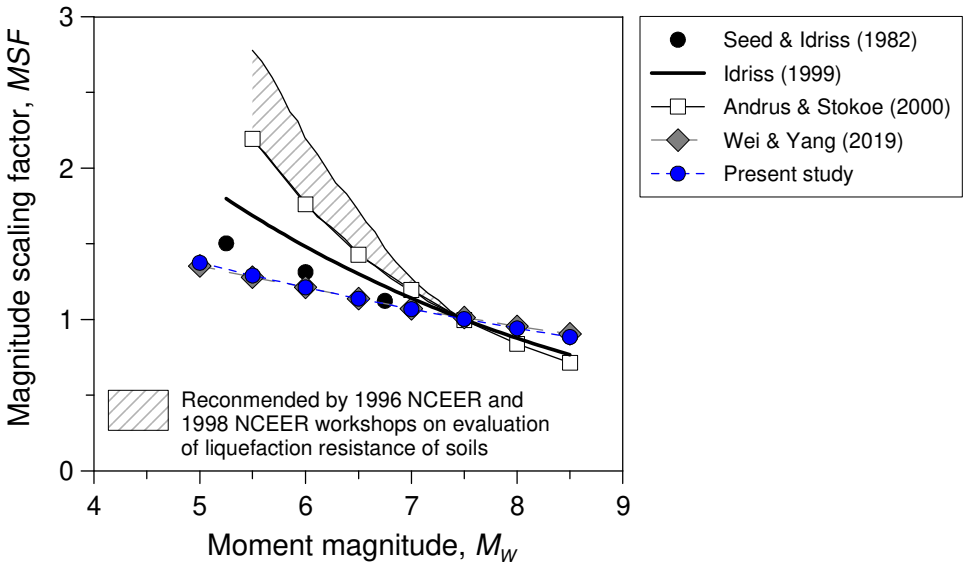

Figure 83 – Comparison between the *MSF* – M_w correlation calibrated by data of Ticino sand-silt mixtures and the existing correlations proposed in literature.

5.2 Factors affecting cyclic resistance of non-plastic silty sands

The effects of fines content can be controversial if the state variables used for comparison are different. Yang et al. (2015) discussed the effects of fines content using several density state variables and suggested that the conventional (global) void ratio (*e*) should be adopted; the relative density may be a good state variable, however it requires the determination of maximum and minimum void ratios which may exhibit relatively large scatter and some uncertainties due to the addition of fines and different methods adopted for their measurement (Lo Presti et al. 1992; Riemer et al. 1990; Polito and Martin 2003), in fact standardized procedures for percentages of fines higher than 15% do not exist. For these reasons, relative density was not considered as the state variable in this study and the void ratio was retained instead of it.

5.2.1 Effect of global void ratio

When the specimens of *TS*-fines mixtures were tested in undrained cyclic condition at the same (global) void ratio, the effect of an increase in non-plastic fines content was a faster increase in the cyclic shear strains and a more contractive response, thus

leading to liquefaction in a lower number of cycles. These results are consistent with the findings from numerous previous studies in the literature.

Relationships between the post-consolidation void ratio (e_0) and the cyclic resistance ratio ($CRR_{N=15}$) for different soil mixtures tested in this study are presented in **Figure 84**. All samples were consolidated at the same vertical effective stress (σ'_{v0}=100 kPa). It is evident in **Figure 84** that the cyclic resistance ratio causing liquefaction in 15 cycles (N=15) decreases with increasing fines content up to about f_c=20%-30%, while an increase is observed at larger fines contents.

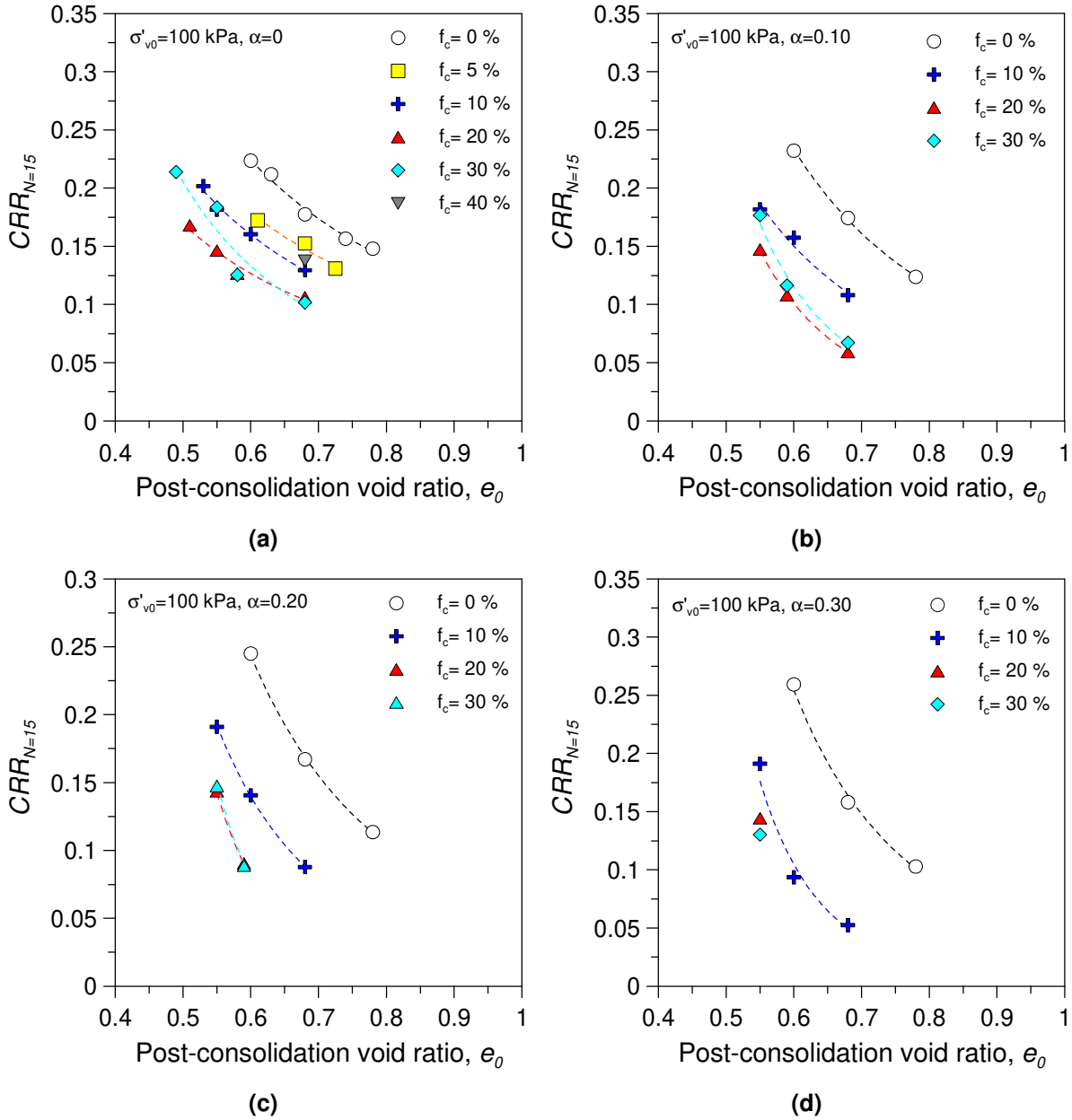

Figure 84 – Effects of post-consolidation void ratio on undrained cyclic resistance of silty sands for various f_c and α: (a) α=0, (b) α=0.10, (c) α=0.20 and (d) α=0.30.

This behaviour was similarly observed in undrained cyclic triaxial tests with $\alpha \neq 0$ in previous research (Rees 2010; Wei and Yang 2019b; Rahman and Sitharam 2020). However it should be noted that, in the present study, this pattern has been observed, for the first time, in cyclic simple shear tests carried out in presence of an initial static shear stress. As it can be argued from data on sand-silt mixtures reported in **Figure 84**, $CRR_{N=15}$ decreases the more with the void ratio the higher the value of α is (for example α=0.30 compared to α=0.10) (**Figure 84d** and **Figure 84b**). A similar observation was found by Wei and Yang (2019b) in cyclic triaxial tests on Toyoura sand mixed with non-plastic silt.

5.2.2 Effect of vertical effective stress

Another factor that may have an influence on the cyclic liquefaction resistance of silty sands is the initial effective vertical stress (σ'_{v0}). For that purpose, selected *CSS* tests on the *TS*-fines mixtures were performed at a lower vertical effective consolidation stress, σ'_{v0}=50 kPa disregarding, in a first phase, the presence of an initial static shear stress.

Figure 85 shows the curves of the cyclic stress ratio versus the number of cycles to failure for *TS* with 10% and 30% fines contents, respectively.

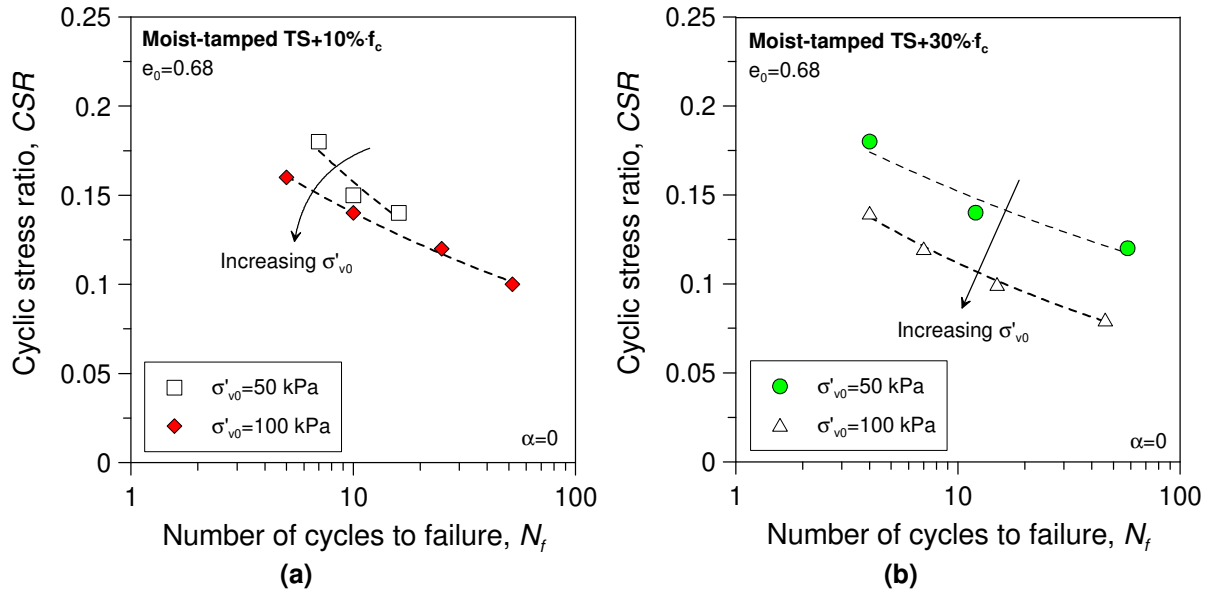

Figure 85 – Effects of initial vertical effective stress on cyclic resistance of silty sands for two different percentage of fines: (a) f_c =10% and (b) f_c =30%, without the presence of an initial static shear stress.

Specimens were prepared at the same global void ratio e_0=0.68. Consistently with previous studies (Amini and Qi 2000; Stamatopoulos 2010; Baziar et al. 2011; Montgomery et al. 2014), the undrained cyclic resistance decreased with an increase in the initial stress from 50 kPa to 100 kPa. The differences are more pronounced for 30% fines content, thereby suggesting that the effect of σ'_{v0} may additionally depend on the fines content (Stamatopoulos 2010), increasing as f_c increases, at least in the considered f_c range.

In order to investigate the effect of the initial effective vertical stress, taking also into account the presence of an initial static shear stress, selected tests have been carried out at the same initial state and percentage of fines but with an initial static shear stress characterized by α=0.10; the results are reported in **Figure 86**.

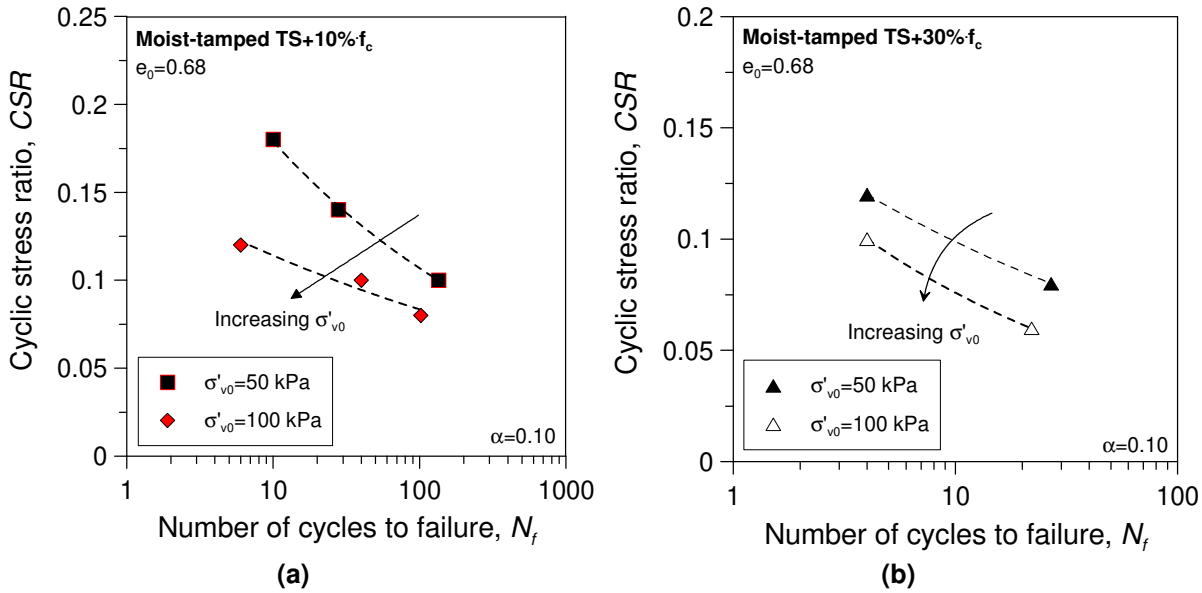

Figure 86 – Effects of vertical effective stress on undrained cyclic resistance of silty sands for two different percentages of fines: (a) f_c =10% and (b) f_c =30%, with the presence of an initial static shear stress (α=0.10).

Figure 86 shows that even when an initial static shear stress is applied, the cyclic resistance against liquefaction decreases as the effective vertical stress increases; furthermore, although the two materials had the same initial state, the trend line of the cyclic resistance was different depending on the percentage of fines. This reduction of the cyclic resistance that at first, in the absence of an initial static shear stress (**Figure 85**), seemed to be more pronounced for the mixture characterized by a higher percentage of fines, is now more pronounced for the mixture with less fines content. The mutual dependence of the cyclic resistance on both the initial vertical effective

stress and the initial static shear stress was already highlighted in previous studies carried out on clean sands (Vaid et al. 2001; Sivathayalan and Ha 2011; Park et al. 2020).

5.2.3 Effect of fines content

Experimental evidence for sand-silt mixtures suggests that if the initial global void ratio (e_0) is used as basis for comparison, as the content of silt increases up to the threshold f_c value the undrained cyclic strength of the mixture decreases (Polito and Martin 2001; Thevanayagam and Martin 2002; Ueng et al. 2004). Beyond the threshold value of f_c, the tendency is reversed, and the liquefaction resistance increases again as the fines content increases. In the present study the variation in cyclic resistance with increasing silt content for the Ticino sand-silt mixtures follows the pattern shown in **Figure 87** for different initial static shear stresses. The cyclic resistance initially decreases as the silt content increases until a minimum resistance value is reached, which occurs at a silt content ranging between 20% and 30%. As the silt content continues to increase, the cyclic resistance begins to increase again.

In the literature the effects of the fines were rarely reported for cases in which the presence of an initial static shear stress was also taken into account (Wei and Yang 2019b; Kokusho 2020); in the present study those effects were investigated and the results are presented in **Figure 87b**, **87c** and **87d**. As it can be seen, *CRR* tends to decrease with the addition of Ticino silica silts up to the threshold fines content. For specimens subjected to initial static shear stresses ($\alpha \neq 0$), this trend is more pronounced compared to that observed in companion tests with $\alpha = 0$. Conversely a small tendency to increase is observed for higher fines content. These figures only present test results under σ'_{v0}=100 kPa.

As suggested by Bouckovalas et al. (2003) and Polito and Martin (2003), the effect of fines on liquefaction resistance can be well described through a scaling factor K_{fc}, defined by the following expression:

$$K_{fc} = \frac{CRR_{fc}}{CRR_{fc=0}} \tag{27}$$

where CRR_{fc} and $CRR_{fc=0}$ are the cyclic resistance ratios corresponding to the same number of cycles evaluated for a silty sand and a clean sand, respectively having the same value of the (global) void ratio and subjected to the same initial effective vertical

stress. In both studies, the authors proposed a linear relationship between K_{fc} (evaluated for $CRR_{N=15}$) and f_c of silty sands.

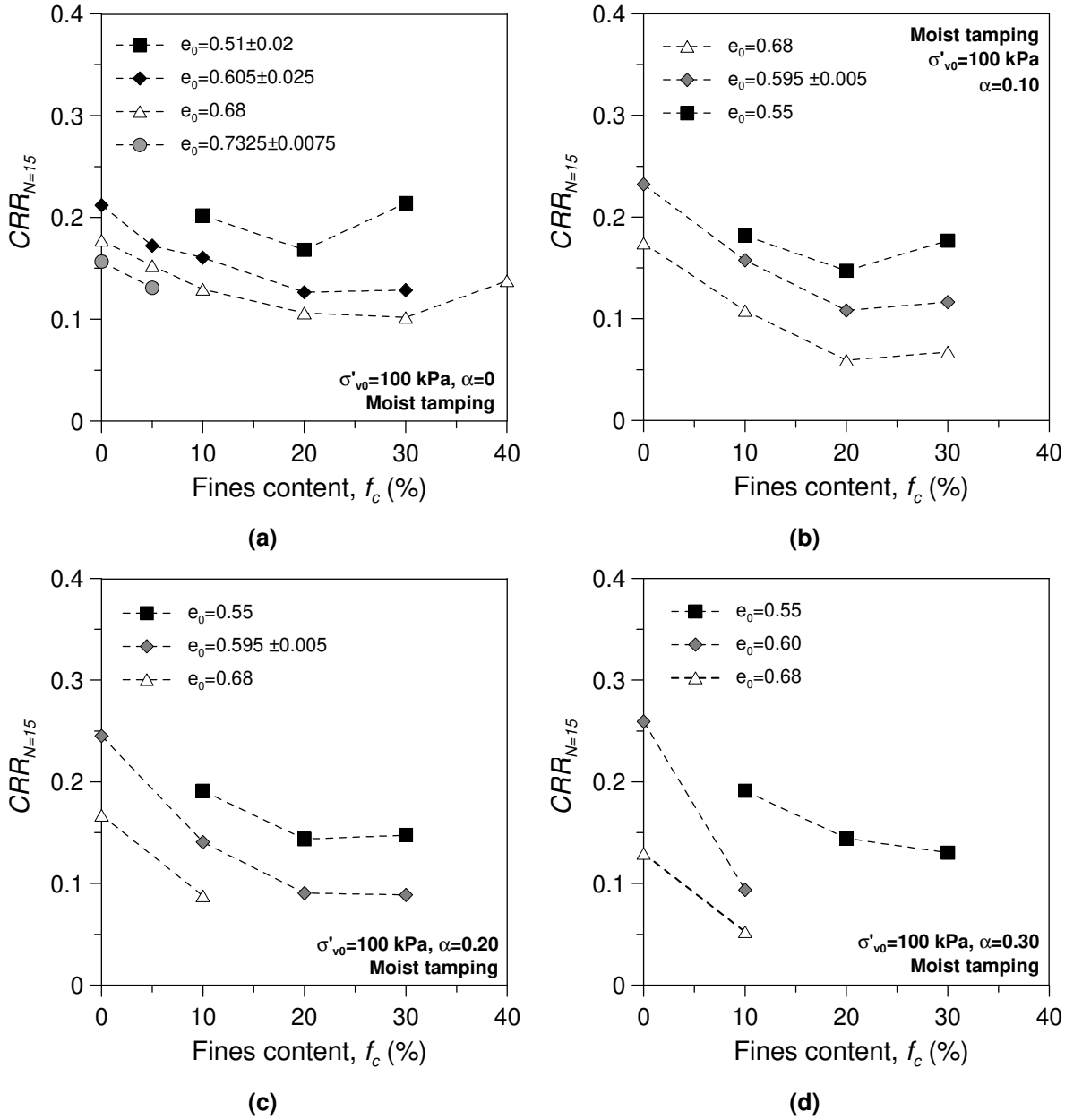

Figure 87 – Effects of fines content on the undrained cyclic resistance of silty sands for: (a) *α*=0, (b) *α*=0.10, (c) *α*=0.20 and (d) *α*=0.30.

Figure 88 presents the measured $K_{fc} - f_c$ relationship. Generally, the $K_{fc} - f_c$ data points lie in a relatively narrow band; the small scatter observed in some curves is mainly due to experimental errors rather than to the effects of void ratio because no consistent dependence of K_{fc} on void ratio was found (Wei et al. 2020). A linear function was proposed in the literature to well depict the trend of K_{fc} versus f_c (Bouckovalas et al. 2003). However, it should be noted that for the Ticino sand-silt mixtures studied in the

present research a linear relationship is inadequate because the $K_{fc} - f_c$ relationship is markedly non-linear (**Figure 88a**, **88b** and **88c**). This holds true for all initial static shear stresses with the sole exception of the highest one (α=0.30) (**Figure 88d**).

In the present study a parabolic expression was proposed to characterise the trend of the $K_{fc} - f_c$ relationship exhibited by theTicino sand-silt mixtures, namely:

$$K_{fc} = 1 - g \cdot f_c + h \cdot (f_c)^2 \qquad (28)$$

where g and h are empirical coefficients depending on the magnitude of the initial static shear stress ratio applied.

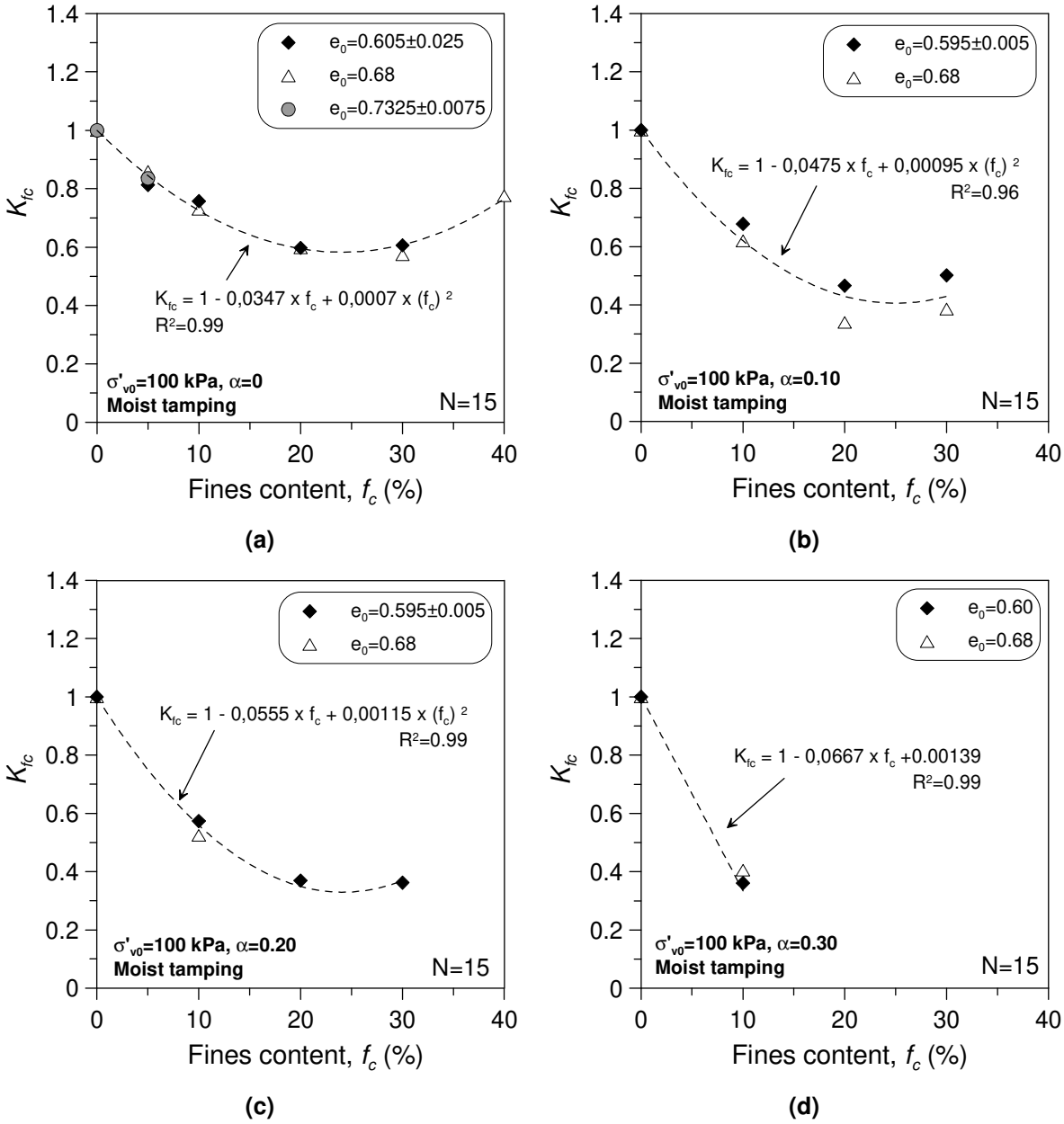

Figure 88 – Scaling factor for fines content of cyclic liquefaction resistance K_{fc} for Ticino sand-silt mixtures for: (a) α=0, (b) α=0.10, (c) α=0.20 and (d) α=0.30.

However it cannot be excluded that in general *g* and *h* could also be influenced by other factors such as mean effective stress, grading characteristics, grains shape, etc.. Notwithstanding this circumstance, for the silty sands studied in the present research (f_c=0–40%; σ'_{v0}=100 kPa; α=0−0.30; χ=17) the following linear relationships were found appropriate (**Figure 89**):

$$g = 0.0355 + 0.104 \cdot \alpha \tag{29}$$

$$h = 0.0007 + 0.0023 \cdot \alpha \tag{30}$$

The two equations reported above are, in fact, characterized by a coefficient of determination R^2 equal to 0.99.

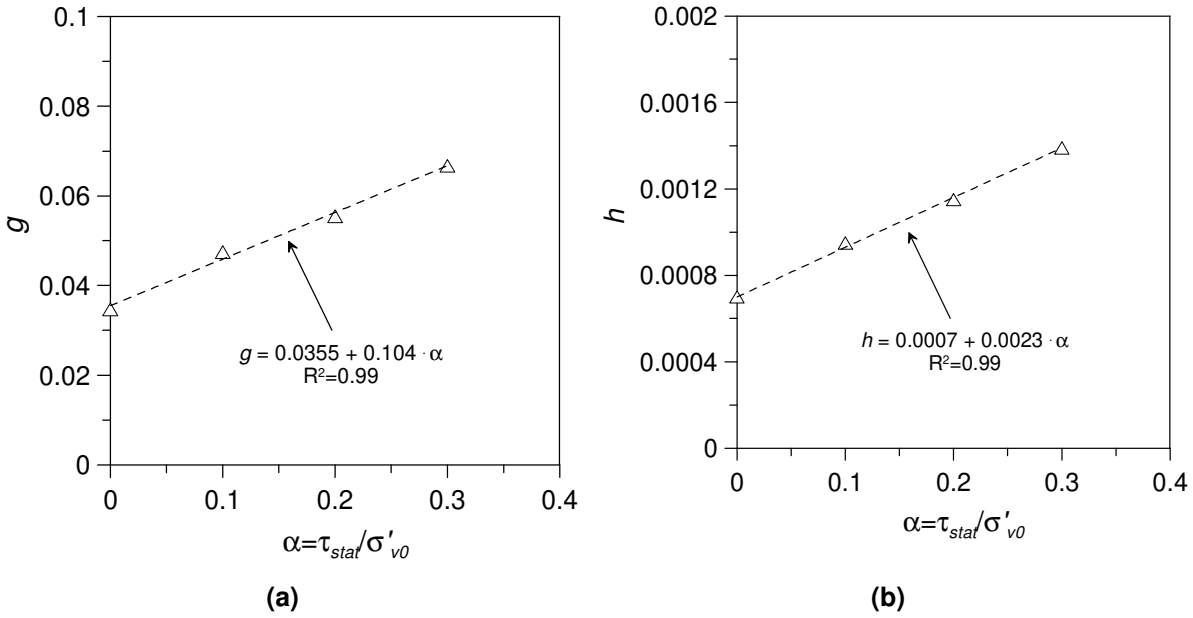

Figure 89 – Variation of parameter (a) *g* of Eq. (29) and (b) *h* of Eq. (30) with *α*.

Finally, consistently with the trend of the curves $CRR_{N=15}$ vs. f_c reported in **Figure 87,** it can be observed (**Figure 88**) that also K_{fc} tends to initially decrease with f_c and this reduction is more pronounced when the stress ratio α becomes higher. This trend continues up to the threshold fines content f_{thre}; when f_c becomes higher than f_{thre} the trend reverses. In **Figure 88** it is possible to observe that f_{thre} lies between 20% and 30%, consistently with the range estimated from the variation of the maximum and minimum void ratio with fines content in chapter 3. A more precise evaluation of the threshold fines content based on the experimental results reported in **Figure 88** will be discussed in the following paragraph and a comparison with other approaches presented in the literature will be made.

5.2.4 Determination of the threshold fines content f_{thre}

Threshold fines content (f_{thre}), also referred to as limiting fines content (Hazirbaba 2005; Polito 1999) and transitional fines content (Yang et al. 2006a) in the literature, is the specific value of the fines content at which the way the fines influence the behavioural properties of the mixture is reversed. The type of behaviour considered for the determination of the threshold fines content can be the critical state line or the undrained cyclic strength of the soil. Based on this definition, the value of f_{thre} or a range of the fines contents that probably include the f_{thre} was determined here for the Ticino sand silt mixtures from experimental data of cyclic simple shear tests. Besides the method based on the trend of the maximum and minimum void ratios with fines content (paragraph 3.2.3), the other types of behaviour that have been considered in the present study for the determination of the threshold fines content of non-plastic Ticino silty sands are: the location of the critical state line (*CSL*s) in the compression plane and the trend of the undrained cyclic strength (expressed in terms of scaling factor K_{fc}) against fines content. **Figure 90** provides the relationship between K_{fc} and fines content derived from the experimental data presented in **Figure 88** for a number of cycles to failure equal to 15. K_{fc} values are observed to decrease with fines content up to a minimum value that is reached when f_{thre} is around 24.5%. At higher fines contents, the trend is reversed, which means that K_{fc} increases again.

Conceptually, when the fines content is relatively small (f_c < 21% in **Figure 90**), the microstructure of the granular mix is defined (and the deformational behaviour is controlled) by the sand matrix, as illustrated schematically for an idealized binary packing of spherical particles in **Figure 90b**. On the other hand, at high fine percentages (f_c > 28% in **Figure 90a**), the microstructure is controlled by the fine matrix, i.e. by the smaller grains (silt particles), as shown in **Figure 90c**. As indicated in **Figure 90a**, there is a transition in the microstructure from a sand-controlled-matrix to a fines-controlled-matrix as the fines content increases from 21 to 28% approximately. There are a number of variations in the possible arrangements (and hence on the role) of the fines grains even for an idealized binary mixture (e.g. Thevanayagam et al. 2002). However, **Figure 90** evidences that the link between the threshold fines content of granular mixes, and the undrained cyclic resistance determined in simple shear tests is conceptually sound since the threshold fines content f_{thre} desumed from these tests is the same irrespective of the initial static shear stress applied.

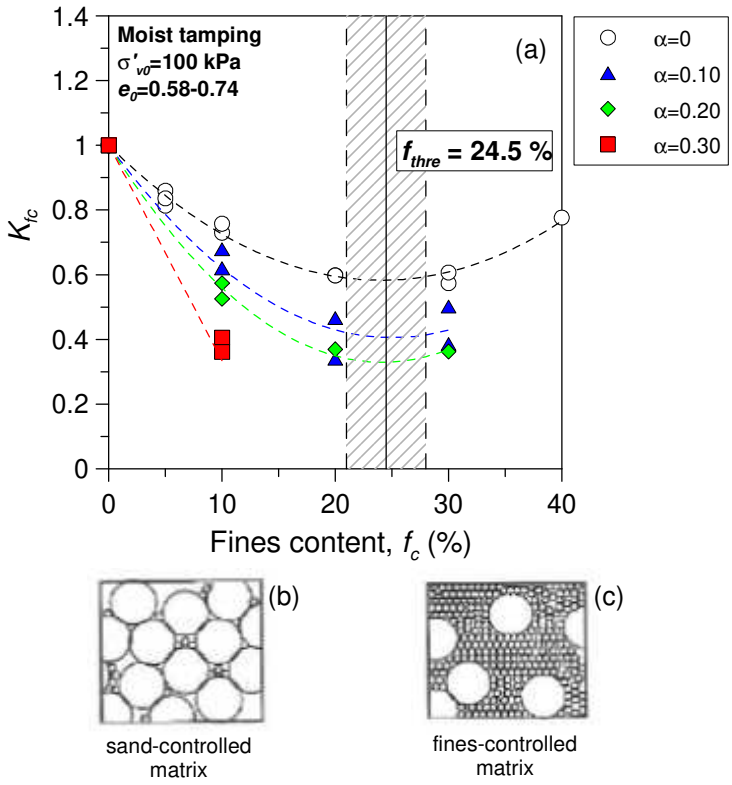

Figure 90 – Identification of f_{thre} by undrained cyclic simple shear tests.

The approach based on the location of *CSLs* in *e*-log(*p'*) plane for determining f_{thre} of non-plastic *TS* sand-silt mixtures is described in Porcino et al. (2019c). The concept of a threshold fines content, f_{thre}, which demarcates a fines-in-sand from a sand-in-fines matrix, is an idealization of a transition zone. This transition zone may be narrow, approximately 2% on either side of a distinct f_{thre} (Rahman and Lo 2008) or may be flat and wide with a less f_{thre}. In the present research, a transition zone of approximately 3.5% of f_{thre} was observed as in **Figure 90**. Similar transition zones for the same sand-silt mixtures were also obtained in the two other approaches mentioned before, such as the location of *CSLs* in the e-log(*p'*) plane (Porcino et al. 2019b) (**Figure 91a**) and the trend of the relationships e_{max} - f_c and e_{min} - f_c (Porcino et al. 2019c) (**Figure 91a**). Regarding the determination of the threshold fines content, alternative calculation methods have been proposed in the literature by several authors that are based on the simple knowledge of some physical and grading features of sand-silt mixtures, which are discussed in the following.

Polito (1999) proposed the following expression where the transitional fines content is calculated as the ratio of fines solid weight, W_{fines}, to sand solid weight, W_{sand}:

$$f_{thre} = \frac{W_{fines}}{W_{sand}} = \frac{G_f \cdot e_s}{G_S \cdot (1 + e_f)} \quad (31)$$

where *G* and *e* are the specific gravity and the maximum void ratio , while the subscripts of *f* and *s* denote fines and sand, respectively.

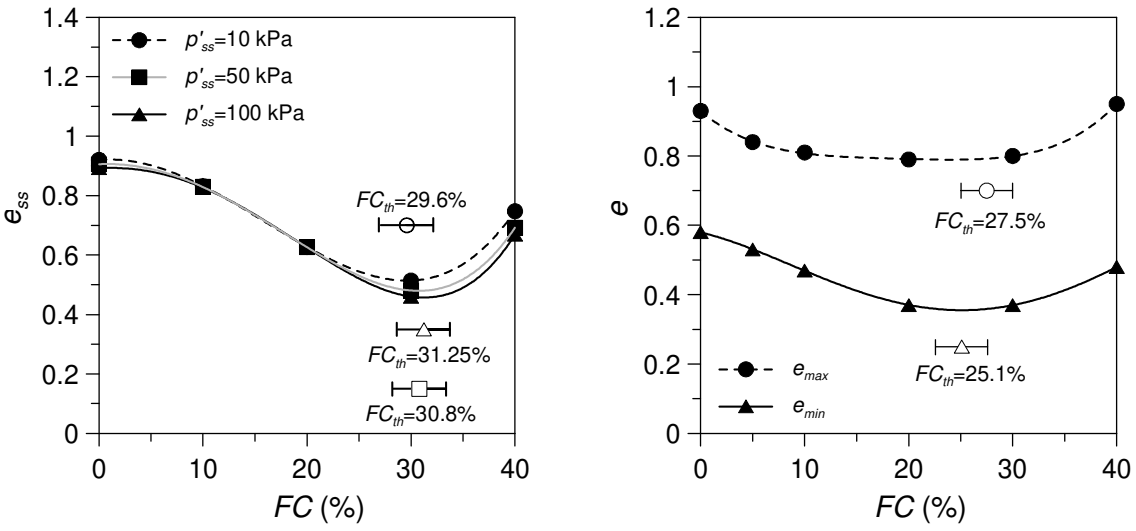

Figure 91 – Identification of f_{thre} by (a) the location of *CSLs* in *e*-log(*p'*) plane and (b) from index data (Porcino et al. 2019c).

Considering the traditional definition of the fines content as a fraction of the total amount of soil, Hazirbaba (2005) modified Eq. (31) and proposed a relation of f_{thre} based on the ratio of the weight of the fines, W_{fines}, to the total weight of the sand and fines, W_{sand} + W_{fines}, expressed as:

$$f_{thre} = \frac{W_{fines}}{W_{sand} + W_{fines}} = \frac{G_f \cdot e_s}{G_f \cdot e_S + G_S \cdot (1 + e_f)} \tag{32}$$

A semi-analytical approach was proposed by Rahman and Lo (2008) who carried out back analyses on nine sets of data to predict the value of f_{thre}. They proposed the following expression:

$$f_{thre} = A \cdot \left(\frac{1}{1 + e^{\rho - \omega \cdot \chi}} + \frac{1}{\chi} \right) \tag{33}$$

where the coefficient *A* is an asymptotic value equal to 0.40, while ρ and ω are fitting parameters equal to 0.50 and 0.13, respectively.

In this study the reliability of equations (31), (32) and (33) was evaluated by comparing the predicted f_{thre} values with the corresponding ones inferred from the trend of the undrained cyclic resistance observed in numerous research reported in the literature. In the following these latter are labeled as “experimental” while those derived from the equations above are labeled as “theoretical”. This comparison is presented in **Figure**

92 and **Table 8** for various sand-fines mixtures investigated in the literature, including that studied in the present research.

Figure 92a shows how the experimental threshold fines content varies with the particle diameter ratio χ, together with the predicted trend suggested by Rahman and Lo (2008) (Eq. 33). This relationship reveals a distinct pattern with two important features (Rahman 2009): i) f_{thre} is at minimum value when the particle diameter ratio χ is at $(D/d)_{crit}$ equal to 7, consistently with binary packing considerations (McGeary 1961); ii) an increase of χ beyond the reversal point leads to a gradual increase of f_{thre} up to an asymptotic value, since more particles can fit in the same void space between the large particles, thus providing a higher f_{thre}. Given the empirical nature of this formulation, it is expected that the calculated f_{thre} using Eq. (33) is close to the values determined from the experimental data, as it can be observed in **Figure 92a**.

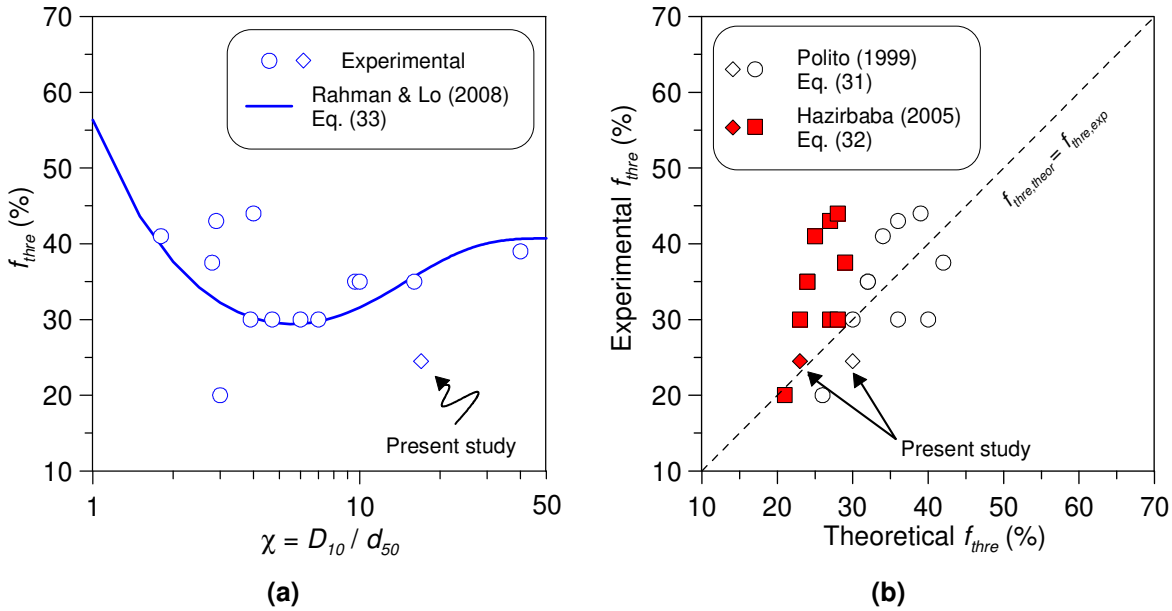

Figure 92 – Comparison of the theoretical and experimental threshold fines content of silty sands (data of Table 8).

Additionally, it can be noted from **Figure 92b** that the values predicted by Eq. (32) are significantly lower than the experimental values, in agreement with other authors (Mohammadi and Qadimi 2015). The predictions made by Eqs. (31) and (33) appear to be more consistent with the experimental results, providing acceptable predictions of f_{thre} in most of the cases (**Figure 92**). It is worth noting that the application of the equations (31) and (32) requires the knowledge of physical and index properties of the

fines and the host sand. For this reason, some data points of **Figure 92a** are not shown in **Figure 92b**.

Table 8 – Comparison of the theoretical and experimental threshold fines content of silty sands data revised in the present study.

Source work	χ	*PI* (%)	Particle shape	Threshold fines content			
				Theoretical results			Experimental results
				Eq. (31)	Eq. (32)	Eq. (33)	
Huang et al. (2004)	1.8	< 8	*N.R.*	34	25	39	41[(a)]
Naeini & Baziar (2004)	2.8	N.R.	*SR*	42	29	33	37.5[(b)]
Polito (1999)	2.9	N.P.	*SA* to *SR*	36	27	33	43[(c)]
Dash & Sitharam (2011)	3	1.57	*N.R.*	26	21	32	20[(a)]
Rahman & Sitharam (2020)	3.9	1.57	*SA* to *SR*	-	-	31	30[(a)]
Xenaki & Atanasopoulos (2003)	4	*N.P.*	*N.R.*	39	28	30	44[(c)]
Karim & Alam (2017)	4.7	*N.P.*	*A*	36	27	30	30[(b)]
Baziar & Sharafi (2011)	6	0.5-1	*SA* to *SR*	30	23	29	30[(d)]
Yang et al. (2006a)	7	*N.P.*	*A*	40	28	30	30[(a)]
Papadopoulou & Tika (2008)	9.6	*N.P.*	*R*	32	24	31	35[(a)]
Polito & Martin (2001)	10	*N.P.*	*SA* to *SR*	32	24	32	35[(c)]
Thevanayagam et al. (2002)	16	*N.P.*	*N.R.*	-	-	36	35[(b)]
Present study	17	*N.P.*	*R* to *SR*	30	23	36	24.5[(e)]
Rahman et al. (2009)	40	27	*N.R.*	-	-	41	39[(b)]

(a) obtained from undrained monotonic and cyclic triaxial test

(b) obtained from undrained monotonic triaxial test

(c) obtained from undrained cyclic triaxial test

(d) obtained from undrained cyclic torsional test

(e) obtained from undrained cyclic simple shear test

N.R. = not reported

N.P. = non-plastic

SR = sub-rounded

SA = sub-angular

A = angular

R = rounded

Figure 92b shows that the value of f_{thre} calculated from the relationship by Hazirbaba (2005) (f_{thre} = 23%) is in good agreement with the experimental average value obtained

in the present study, while f_{thre} derived from Polito's relation (f_{thre} = 30%) tends to overestimate the experimental value. Eq. (33) proposed by Rahman and Lo (2008) provides a value of f_{thre} = 36% being substantially higher than the experimental value. Finally, the threshold fines content obtained from Eqs. (31–33) for *TS*-fines mixtures were in a wide range from 23% to 36%. Other soil characteristics not considered in these equations, such as particle shape and mineralogy, may play a significant role in the behaviour of the sand-fines mixtures, especially for mixtures with intermediate values of the particle size ratio $10 < \chi < 25$ (Zuo and Baudet 2015), such as that tested in the present study.

5.2.5 Effects of initial static shear stress on undrained cyclic resistance

The initial static shear stress, as one factor of the initial state, can affect the undrained cyclic behaviour of sands and silty sands. The undrained cyclic resistance may either increase or decrease with increasing initial static shear stress. In clean sands such effects may depend on initial void ratio and initial vertical effective stress (e.g. Harder and Boulanger 1997; Seed and Harder 1990; Yang and Sze 2011a, b). It seems to be the same for non-plastic silty sands (Wei and Yang 2019b; Kokusho 2020). **Figure 93** presents the cyclic resistance evaluated at 15 cycles of *TS*-fines mixtures with initial effective vertical stress σ'_{v0} = 100kPa. The effects of α are positive (*CRR* increase) only for clean sand when the void ratio is relatively low (i.e. e_0 = 0.60); a small increase of cyclic resistance is also observed in sand–silt mixtures with a fines content of 10% and e_0 = 0.55. Conversely for larger fines contents and higher void ratios the effects of α can be neglected (f_c = 20%, e_0 = 0.55) or they are negative (*CRR* decrease with increasing α). The results obtained for f_c = 10% and e_0 = 0.68 are interesting since the effect of α is initially positive and then becomes negative after a certain value of α (α = 0.05); this would support the existence of an α threshold as proposed by Yang and Sze (2011b).

Figure 94 presents the cyclic resistance at 15 cycles of *TS*+10%·f_c mixtures with an initial void ratio e_0 = 0.68. The cyclic resistance decreases with increasing initial vertical effective stress. Regarding the effect of the initial static shear stress, it is possible to observe that, for an initial vertical effective stress of 50 kPa, the effect is positive for values of α up to 0.10, while it becomes negative once this value of α is exceeded; if tests with an initial vertical effective stress of 100 kPa are considered α threshold sets around α=0.05.

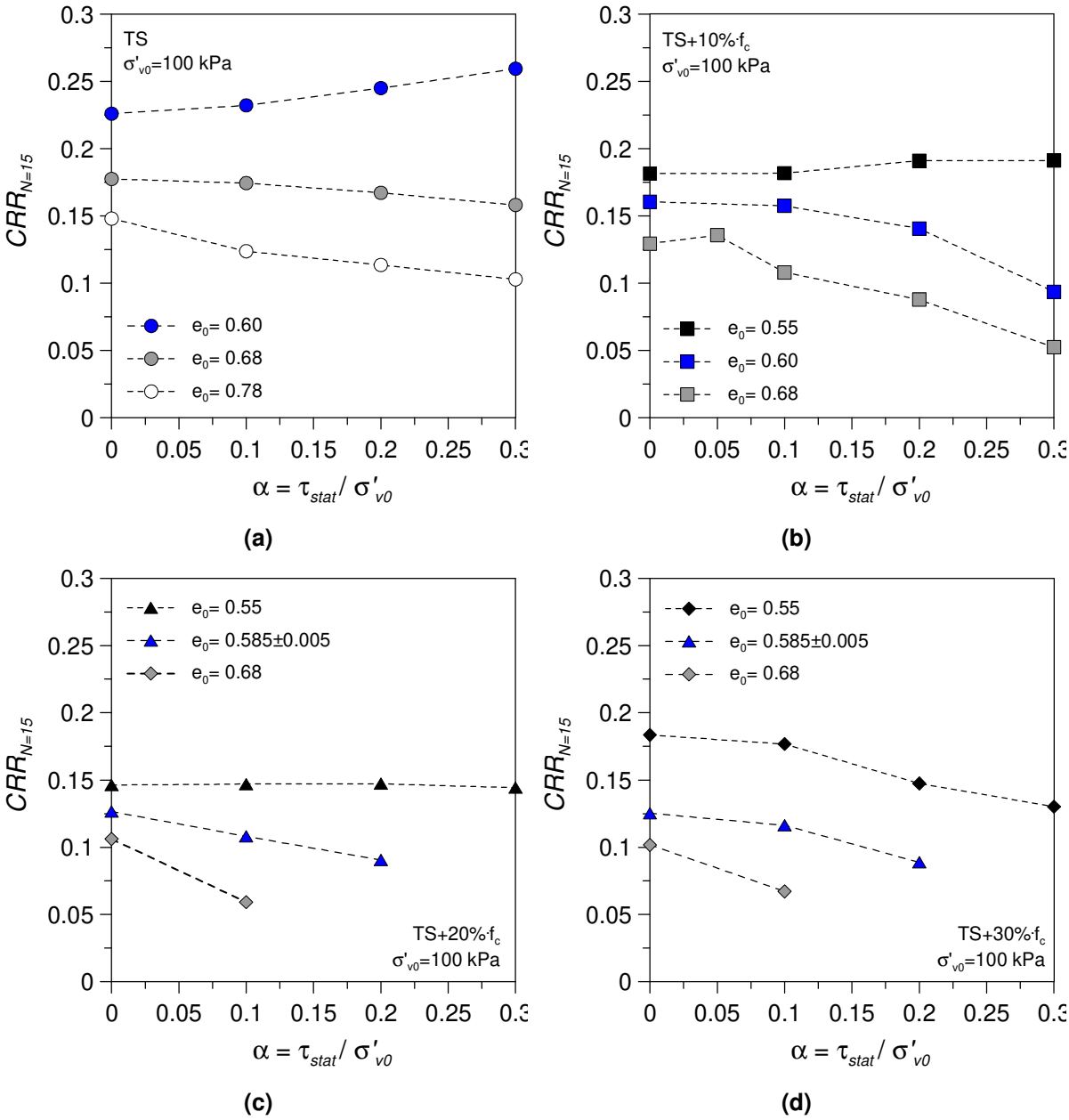

Figure 93 – Effects of initial static shear stress on the undrained cyclic resistance of silty sands (σ'_{v0}=100 kPa): (a) *TS*; (b) *TS*+10%·f_c; (c) *TS*+20%·f_c and (d) *TS*+30%·f_c.

This aspect demonstrates how the α threshold turns out to be influenced by the initial effective vertical stress and in particular it decreases as the initial vertical stress grows, coherently with what is reported in the literature (Wei and Yang 2019b). Apparently, the effects of initial static shear stress depend on the initial state of the specimens, as observed for clean sands. The state-dependence of the effects exerted by the initial static shear stress will be further discussed in chapter 6.

To characterize the effect of α, an initial static stress shear correction factor, K_α, was introduced by Seed (1981). It is defined as reported in Chapter 2 (Eq. 2). The impact

of the initial void ratio in terms of K_α is presented in **Figure 95** for various mixtures, whereas the effect of the initial vertical effective stress is presented in **Figure 96**, for only *TS*+10%·f_c.

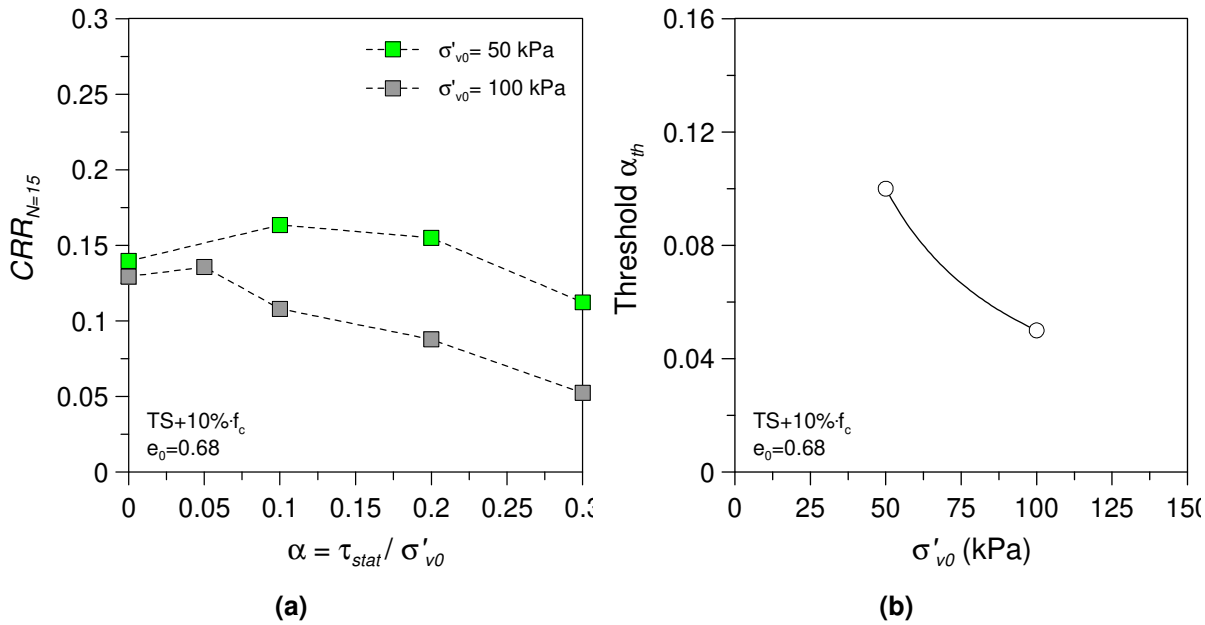

Figure 94 – (a) Effects of initial static shear stress on the undrained cyclic resistance of *TS*+10%·f_c (e_0=0.68) and (b) variation of threshold α with initial vertical effective stress.

The curves K_α - α drawn in **Figure 95a** show that for clean sand the specimens in a dense state (e_0 = 0.60, D_R = 94%) exhibit an increase in the undrained cyclic resistance as α increases, while specimens in a medium-dense state (e_0 = 0.68, D_R = 71%) and in a loose state (e_0 = 0.78, D_R = 43%) show a reduction in the undrained cyclic resistance as α increases. When compared with the correlations proposed by Harder and Boulanger (1997) for clean sands (**Figure 25**), the results obtained in the present study lie on the conservative side and, therefore, particular caution should be adopted in the use of the existing correlations, even in the case of clean sands. The differences found can be explained by considering some factors not taken into account in the various research, such as, according to Sivathayalan and Ha (2011), the shape of the grains constituting the sand and the type of apparatus used to obtain the results.

Of particular concern are the results obtained for Ticino silty sand mixtures with a percentage of fines equal to 10% that are shown in **Figure 95c**: in this case the effect of an initial static shear stress can be a limited increase (K_α > 1) or a significant reduction (K_α < 1) in the cyclic undrained resistance as α increases depending on the value of the initial global void ratio of the material. In particular, passing from a relatively

dense material (e_0 = 0.55), to a relatively loose material (e_0 = 0.68), a significant loss of the undrained cyclic resistance is observed with increasing α.

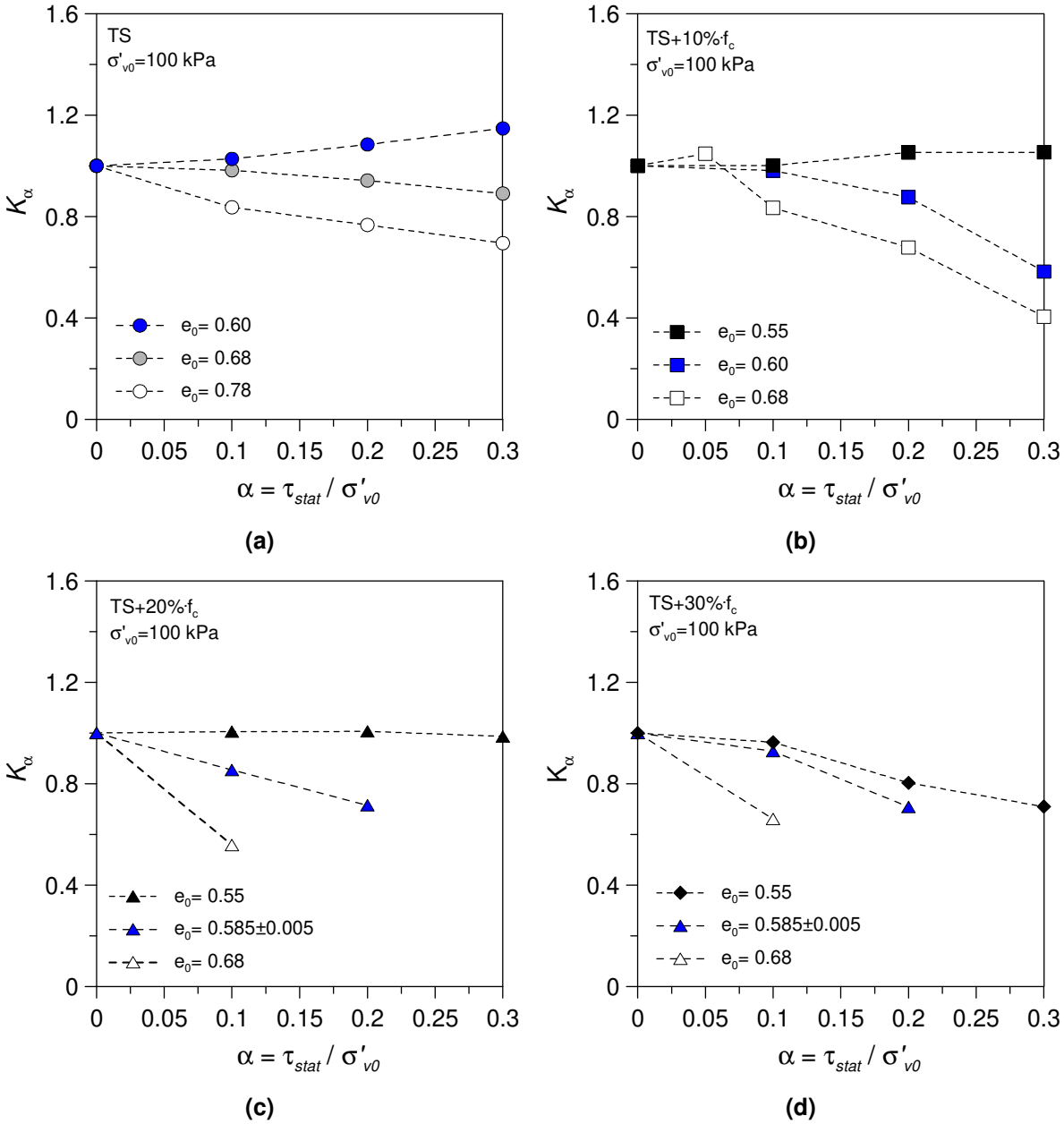

Figure 95 – Correlations K_α-α for Ticino silty sand showing void ratio effect: (a) *TS*; (b) *TS*+10%·f_c; (c) *TS*+20%·f_c and (d) *TS*+30%·f_c.

The results for silty sand with fine percentages of 20% and 30% at the same initial global void ratio e_0 = 0.55 show that the cyclic undrained resistances of the material don't significantly vary ($K_\alpha \approx 1$) (f_c = 20%) or slightly vary (f_c = 30%) with the parameter α. For the other initial global void ratios analysed a reduction of the cyclic resistance factor was observed that it is more pronounced for f_c = 20%, consistently with the

concept of limiting fines content f_{thre}. Infact the reduction in the undrained cyclic resistance decreases because after f_c increasing over the f_{thre} a changover is observed in the response of the sand-silt mixture (**Figure 90**).

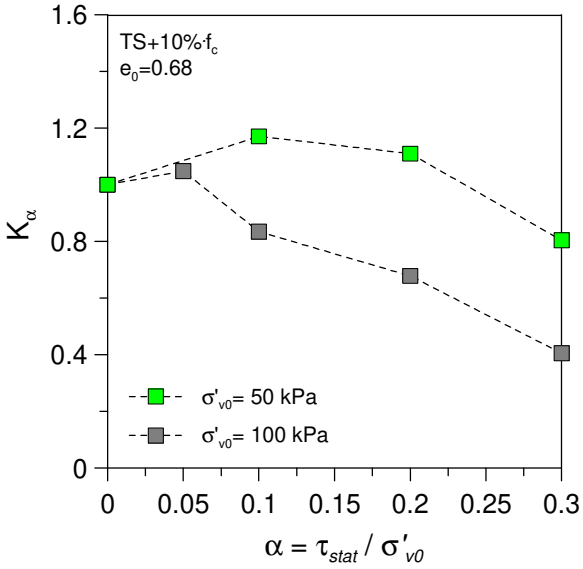

Figure 96 – Correlations K_α-α for Ticino silty sand showing initial vertical effective stress effect (*TS*+10%·f_c).

5.2.6 Effects of sample preparation methods

In laboratories, different sample preparation methods were used to simulate different deposition processes of soils (e.g. Oda 1972; Kuerbis and Vaid 1988; Sze and Yang 2014). Different inherent fabric in terms of particle assembly can be observed among specimens reconstituted by different sample preparation methods, because there could be a preferential orientation of particles under various reconstitution conditions (Arthur and Menzies 1972; Oda 1972). Different fabric may lead to different monotonic response (Kuerbis and Vaid 1988; Murthy et al. 2007) and cyclic response (Tatsuoka et al. 1986a; Huang and Chuang 2011; Sze and Yang 2014). In this context, limited to the clean Ticino sand, some results of previous research (Diano 2017; Caridi 2006; Marcianò 2011) are shown to highlight the effect of the fabric on the undrained cyclic resistance of the material. **Figure 97** presents the undrained cyclic resistance $CRR_{N=15}$ vs the initial global void ratio e_0 from cyclic simple shear tests on Ticino clean sand samples, prepared at σ'_{v0} = 100 kPa and reconstituted with three different reconstitution methods (air pluviation *AP*, moist tamping *MT* and water sedimentation *WS* methods).

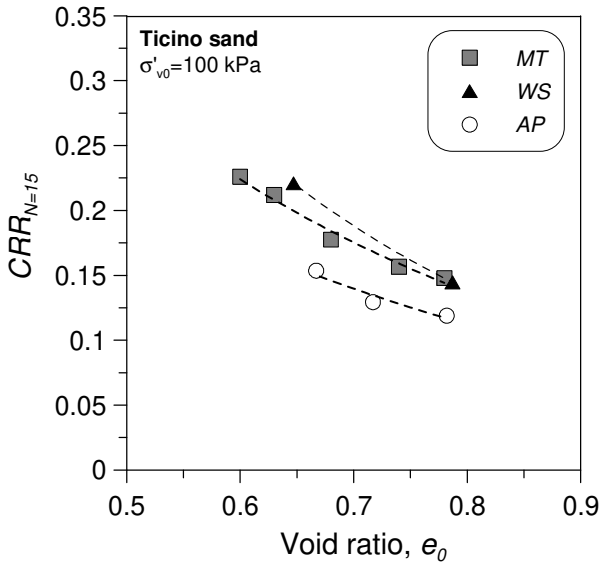

Figure 97 – Undrained cyclic resistance of clean Ticino sand for three different reconstitution methods.

The specimens prepared by the moist tamping method show a stronger liquefaction resistance and a more dilative response than those prepared with the air pluviation method. Similar findings are also reported by previous research performed on clean and silty sands (Ishihara 1993; Mulisis et al. 1977; Huang et al. 2004; Sze and Yang 2014; Tatsuoka et al. 1986). Moreover, the moist tamping resistance curve is very close to the water sedimentation one and this means that moist tamping method may better reflect the behaviour of in situ deposits of sands formed in a marine water environment, or by fluvial sedimentation (Porcino and Marcianò 2008).

However, in the lack of further evidences, the results obtained in the present study must be considered valid only for mixtures of Ticino sand with non-plastic local silt and specimens reconstituted by moist tamping method. The applicability of the results to other host or fine materials and other reconstitution methods needs further investigations.

Chapter 6

Predicting cyclic and monotonic response of sands with different fines contents using different state indices

The results of the present study and numerous previous investigations in the literature (Huang and Chuang 2011; Papadopoulou and Tika 2008; Rahman and Sitharam 2020; Stamatopoulos 2010; Wei and Yang 2019a, b) indicate that the undrained cyclic strength *CRR*, as well as the undrained monotonic resistance (Bobei et al. 2009; Mohammadi and Qadimi 2015; Rabbi et al. 2019; Rahman et al. 2011) of a silty sand are functions of several factors, including fines content, fabric, packing density, effective confining pressure, initial static shear stress, etc.. Furthermore the characterization of the effects of these parameters on *CRR* is not straightforward because the impact of a certain factor can be affected by the other ones. An example is provided by the contractive and dilative behaviour of a material that depend on both the void ratio and the mean effective stress. Critical state based theories can be useful to overcome this issue, as discussed in the next sections.

6.1 Critical state of silty sands from undrained monotonic triaxial tests

The effect of fines content on the features of the critical state line (*CSL*) for *TS*-fines mixtures was investigated through reinterpretation of undrained triaxial compression tests performed in previous research (Diano 2017; Porcino et al. 2019a). The specimens were reconstituted by moist tamping in eight layers. Mixtures with 0%, 10%, 20%, 30%, and 40% fines content were studied. The specimens were prepared with different initial void ratios and consolidated under different initial mean effective stresses p'_0 = 100 kPa, 300 kPa, and 500 kPa.

All tests were performed until the axial strain reached a value ε_a=25% at which samples were considered to have reached a condition equal or very near the critical state. The test procedure and results are described in detail by Porcino et al. (2019b). As an example, the stress-strain relationships and the effective stress paths measured for

specimens of *TS* with 10% fines for different values of the global void ratio (e_0), initial mean effective stress (p'_0), and, hence, state parameter Ψ_0, are compared in **Figure 98**.

The soil response became more contractive as the state parameter increased; this is visible from the larger reduction of the normalized mean effective stress p'/p'_0 in **Figure 98b**. For higher values of the state parameter, a strain softening occurred, i.e. after passing a local maximum, the normalized deviator stress q/p'_0, with $q = \sigma_v - \sigma_h$ decreased up to the steady-state (*SS*) value (**Figure 98a**). According to the literature (Been et al. 1991), it is assumed that the critical state and the steady-state (*CS*=*SS*) are equivalent.

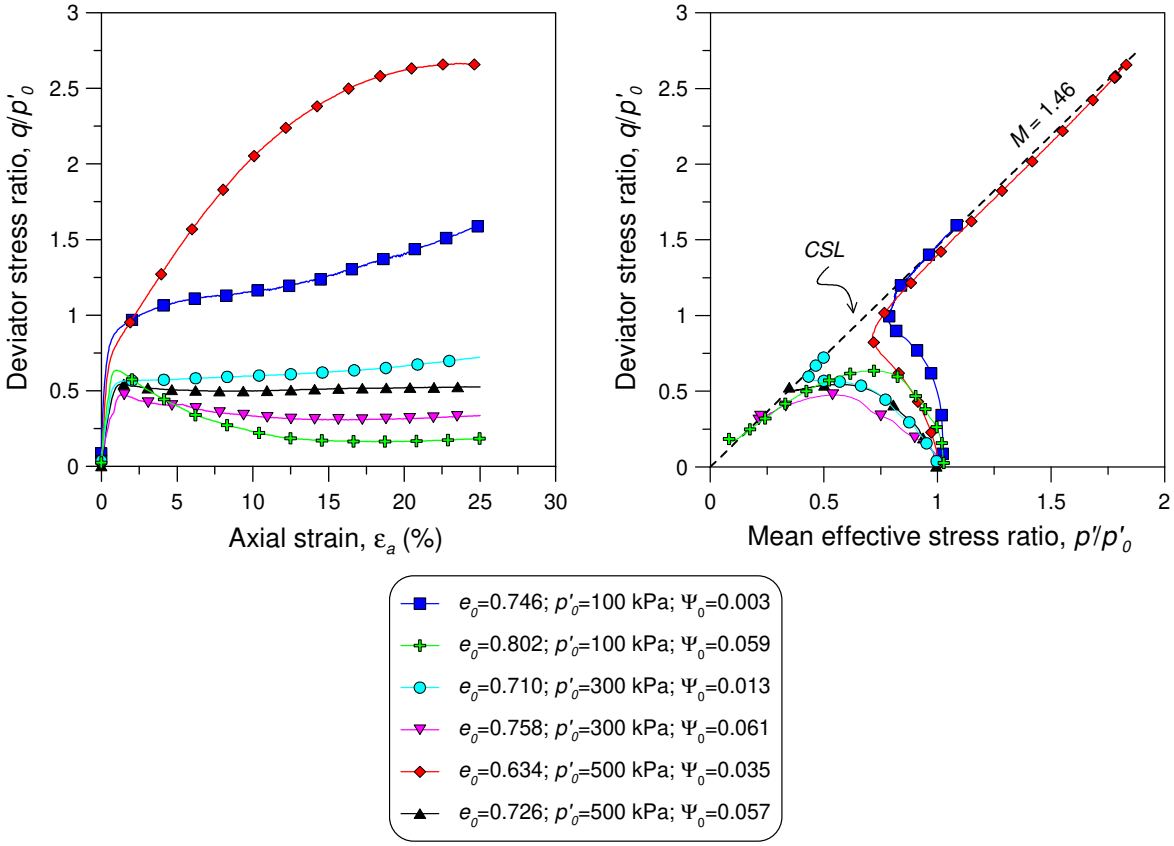

Figure 98 – Results of undrained monotonic triaxial tests performed on *TS*+10%-f_c: (a) stress-strain relationships; and (b) effective stress-paths (normalized by initial mean effective stress p'_0).

Figure 98b shows the *CSL* in the normalized *q*-*p'* plane for *TS* with 10% fines content. The critical state friction angle φ'_c, which is an intrinsic parameter for sand (Been et al. 1991), can be derived from the inclination $M_c = (q/p')_{CS}$ of the *CSL* in the *q*-*p'* plane. For

clean Ticino sand φ'_c was found to be 35° (M_c = 1.43). When non-plastic fines were added to the clean sand, the critical state friction angle of the mixture tended to increase, as shown by the values in **Table 9**. These findings are consistent with the observations of other researchers (Salgado et al. 2000; Carraro et al. 2009). A comparison of the *CSL* parameters of clean Ticino sand with the corresponding ones obtained in previous research on the same sand (amongst others, Jamiolkowski et al. 2003; Jefferies and Been 2016) reveals small differences, which might be due to slight variations in the grading features of the tested Ticino sand and different ultimate strain levels reached in the tests.

Table 9 – Friction angle at critical state for Ticino sand-fines mixtures obtained from undrained monotonic triaxial compression tests.

Material	φ'_c (°)	M_c
TS	35	1.43
f_c = 10%	36	1.46
f_c = 20%	37	1.49
f_c = 30%	38	1.57

Figure 99 presents the critical state lines (*CSLs*) (curved trends) for each *TS*-fines mixture gathered from the undrained monotonic triaxial tests in the *e*-log(*p'*) plane.

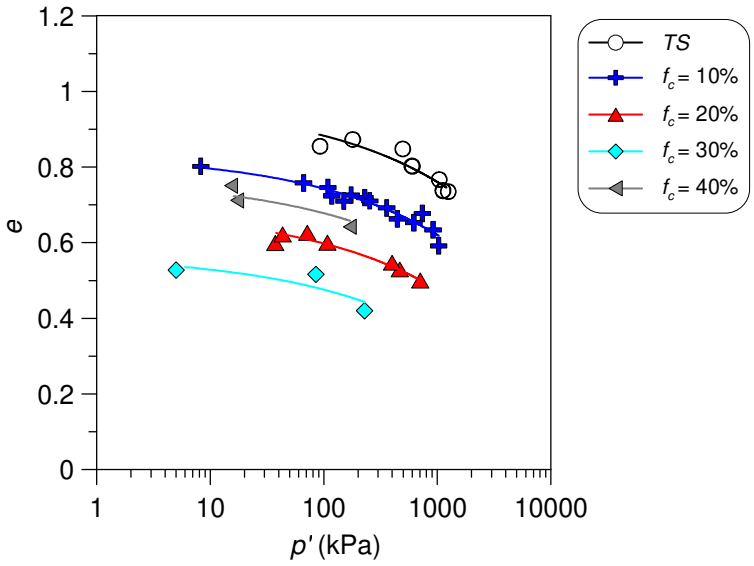

Figure 99 – Effects of fines content on critical state lines for *TS*-fines mixtures in *e-p'* plane (data from undrained monotonic triaxial compression tests).

As it is evident in **Figure 99**, the common shape *CSLs* are shifted downwards with increasing f_c up to the threshold fines content of 30% before the trend is reversed, and the *CSL* moves upwards again at higher fines contents. This tendency is quite consistent with the trend in the *CRR* - f_c relationships from the *DSS* tests. **Figure 99** also reveals that a small variation in f_c can significantly affect the position of the *CSL* (see also Thevanayagam et al. 2002; Yang et al. 2006b; Rahman et al. 2008). If the soil behaviour of silty sands, in particular the undrained shear behaviour under monotonic loading or the liquefaction resistance under cyclic loading, is analyzed in a critical state framework, a separate *CSL* in the *e*-log(*p'*) plane is needed for each f_c. The experimental effort may be reduced by incorporating the equivalent granular void ratio e^* in the critical state concept, as outlined in the next section (chapter 7).

6.1.1 Critical state and different state indices for silty sands

The critical state line (*CSL*) is an important reference state for analyzing the behaviour of sandy soil within critical state soil mechanics (*CSSM*) framework (Been and Jefferies 1985). The critical or steady state line is defined as the locus of points in the void ratio versus mean effective normal stress (*e*-log*p'*) space corresponding to the achievement of a critical state condition, where *e* is void ratio, and $p'=(\sigma'_1+2\cdot\sigma'_3)/3$ is mean effective stresses, σ'_1 and σ'_3 are major and minor principal effective stresses, respectively. It is hypothesized that critical state (*CS*) and steady state (*SS*) lines in the triaxial compression plane for the tested sand-silt mixtures are equivalent such as demonstrated by numerous experimental evidences (Been and Jefferies 1985; Been et al. 1991; Bobei and Lo 2005; Casagrande 1975; Sladen et al. 1985; Sladen et al. 1986; Verdugo and Ishihara 1996; Yamamuro and Lade 1998; Yoshimine and Ishihara 1998).

The state parameter Ψ is simply defined as the measure of that distance or deviation (**Figure 100**): $\Psi = e - e_{CS}$, where *e* is the current void ratio of the soil and e_{CS} is the void ratio of the critical state at the current mean effective stress. It is expected that soils having the same initial state parameter, $\Psi_{(0)}$, would have similar shearing behaviour under both monotonic and cyclic loadings. A positive or negative $\Psi_{(0)}$ value denotes that the state of a sand is located above or below the critical state line (*CSL*), respectively. In the first case, the soils exhibits a tendency to contract upon shearing, whereas the state point located below the *CSL* corresponds to a tendency of the sand to dilate during shearing. At low *p'* levels, the value of Ψ is strongly dependent on the

curvature of the *CSL*: therefore, an alternative state index, defined state pressure index, I_p, has been introduced. I_p is defined (**Figure 100**) as the ratio of the current mean effective pressure to the mean effective pressure at the critical state that corresponds to the current void ratio (Wang et al. 2002): $I_p=p'/p'_{CS}$. As outlined by several authors (Coop et al. 2005; Xiao et al. 2014), the value of I_p will be less influenced by the curvature of *CSL* with a clear advantage of using it even in constitutive modeling of sand behaviour. **Figure 100** shows that p'_{CS} can be determined from the critical-state line at the same global void ratio e_0. Under undrained conditions an initial value of $I_p > 1$ is associated with flow type (*F*) behaviour. Conversely $I_p < 1$ is associated with non-flow (*NF*) type behaviour. Limited flow (*LF*) behaviour is associated with I_p close to 1. A relevant issue of I_p is that, for the points located above the horizontal line (asymptote) of *CSL*, the values of p'_{CS} on the original *CSL* curve are not defined. For these cases the procedure based on the extension of the straight *CSL* (final portion) can be adopted for defining the initial values of I_p (i.e. $I_{p(0)}$) of the monotonic and cyclic tests in the present study. Such a procedure was successfully applied by several authors in previous research (e.g. Klotz and Coop 2001; Qadimi and Mohammadi 2014). In the current research, for these cases, the authors followed the procedure based on the extension of the straight portion of *CSL* suggested by Klotz and Coop (2001).

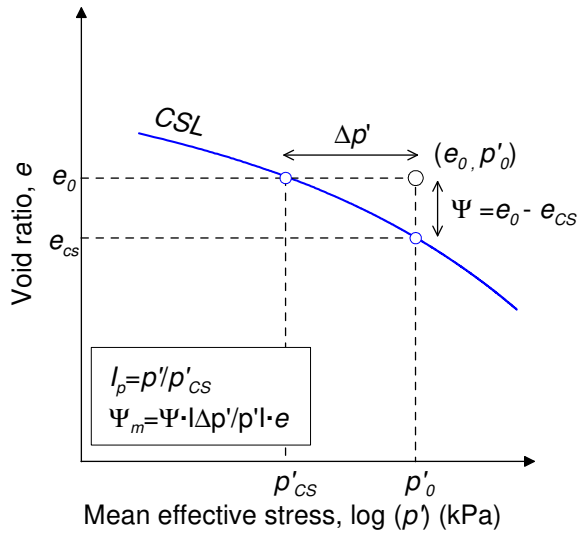

Figure 100 – Definition of state parameter, state pressure index and modified state parameter in terms of global void ratio *e*.

Combining Ψ and I_p, an alternative modified state parameter Ψ_m (**Figure 100**) was proposed by Bobei et al. (2009). They proposed the following expression to define the

modified state parameter: $\Psi_m = \Psi \cdot (\Delta p'/p') \cdot e = \Psi \cdot (1\text{-}1/I_p) \cdot e$, where $\Delta p'$ denotes the difference between the mean effective stress and the mean effective stress of the critical state at the current void ratio. The value of such parameter at the beginning of the shearing phase, denoted as $\Psi_{m(0)}$, can be used as a predictor of behaviour in shearing. Ψ_m is obtained by applying two factors: (i) a factor $|1\text{-}1/I_p|$ that considers the change in p' during shearing (horizontal direction in e-log(p') plane) and (ii) void ratio, which considers the state difference in the vertical direction of the e-log(p') plane. This improves the prediction of liquefaction tendency, particularly in case of specimens at high void ratios (Bobei et al. 2009).

The test data for each *TS*-fines mixture gathered from undrained triaxial compression tests are reported in e-log(p') space in **Figure 99**. It has been observed that the critical-state lines are not straight lines in e-log(p') space, consistently with previous laboratory studies for many different types of sandy soils (Papadopoulou and Tika 2008; Rahman and Lo 2014; Rabbi et al. 2019; Rahman and Sitharam 2020). The fitted *CS* curves are well represented by the Eq. (8) which is re-written below for readers' convenience:

$$e_{CS} = e_{lim} - \lambda_{CS} \cdot \left(\frac{p'}{P_a}\right)^{\xi}$$

where P_a is atmospheric pressure and e_{lim}, λ_{CS}, ξ are constants. The values of the empirical constants of Eq. (8), corresponding to the curves presented in **Figure 99**, are shown in **Table 10**.

Table 10 – Empirical constants that characterize the critical state lines for Ticino sand-fines mixtures of Figure 99.

Material	e_{lim}	λ_{CS}	ξ
TS	0.976	0.093	0.365
f_c = 10%	0.836	0.093	0.365
f_c = 20%	0.691	0.093	0.365
f_c = 30%	0.569	0.093	0.365
f_c = 40%	0.771	0.093	0.365

The capability of the above-defined state indices to predict the undrained monotonic and cyclic behaviour will be evaluated and discussed in the following paragraphs for different moist-tamped specimens of Ticino sand-fines mixtures with different initial states but taking into account only samples with fines contents below the threshold fines content (f_{thre} =24.5%, see chapter 5). Test data were processed here to evaluate

the state indices. For undrained monotonic triaxial test results, important characteristics of the deviator stress-strain curves and the effective stress paths were reported in terms of relevant parameters such as:

- Instability stress ratio, η_{IS}
- Normalized liquefaction potential, $(q_{min} / p'_0) / q_{IS}$
- Phase transformation stress ratio, η_{PT}
- Normalized critical state resistance, q_{CS} / p'_0

The parameters η_{IS}, q_{min}, q_{IS}, η_{PT},q_{CS} are defined in the next paragraph in **Figure 101**.

For undrained *DSS* tests, data were reported in terms of:

- Cyclic liquefaction resistance, $CRR_{N=15.}$

Since the initial state is defined in terms of global void ratio (e_0) and initial mean effective stress (p'_0), in *DSS* tests p'_0 was derived with the assumption $K_0 = 1 - \sin(\phi')$ for the coefficient of lateral earth pressure at rest and the friction angle at critical state was determined for each mixture from undrained monotonic triaxial compression tests. The assumption of a K_0 condition is considered sufficiently accurate for the consolidation stage of *SS* tests leading to K_0 values ranging from 0.38 to 0.43. Furthermore, in the current study it is implicitly assumed that the *CSL* for a given sand is independent of the applied stress path, and thus the *CSL* derived from undrained monotonic triaxial tests is applicable in the analysis of simple shear test data too.

6.2 Critical state-based interpretation of the undrained monotonic behaviour of silty sands

6.2.1 Categories of monotonic behaviours

Some qualitative information on this topic has been provided in the paragraph 6.1 with particular emphasis on the failure patterns. In this paragraph the analysis includes also other aspects that allow to define in a more exhaustive way and from a quantitative point of view the undrained monotonic behaviour of the tested materials. The deviatoric stress–strain and effective stress path response of a sandy soil in undrained shearing can be classified into three types of behaviour: i) flow (*F*), ii) non flow (*NF*), and iii) limited flow (*LF*), as illustrated in **Figure 101**.

For flow behaviour, the deviator stress, *q*, after attaining the initial peak, reduces with shearing until a minimum value is attained at the critical state (*CS*) value. When the

CS strength is zero, it is referred to as complete liquefaction (Yamamuro and Lade 1997).

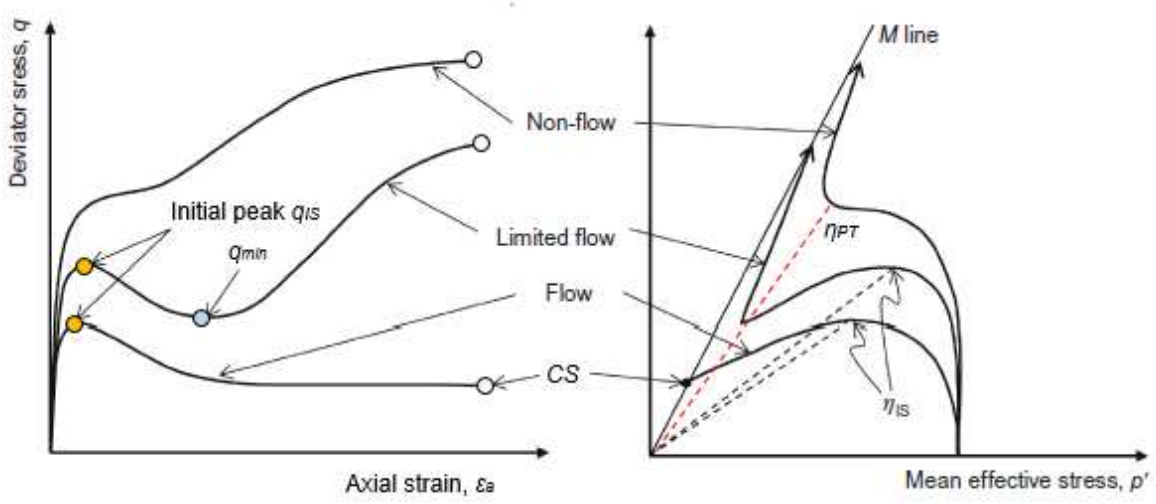

Figure 101 – Undrained behaviour of a sandy soils.

For *LF* behaviour, the deviator stress, after attaining the initial peak, also reduces with shearing, but to a transient minimum value referred to as the quasi critical state *CS* (q_{min}). Further shearing beyond q_{min} yields a gradual strain hardening to the *CS*. In case of *NF* behaviour, strain hardening occurs throughout shearing. A dense specimen showing *NF* behaviour often approaches but does not reach *CS* at the end of a test. In such a case, many researchers estimated the *CS* by extrapolation (Murthy et al. 2007; Carrera et al. 2011). As already mentioned, in the present study the critical state was generally considered to be reached at an axial strain equal to 25%.

6.2.2 Characterization of monotonic behaviours

A qualitative description of the monotonic behaviours has been previously presented. Some characteristic parameters of the undrained monotonic behaviour are analyzed in this paragraph as they are particularly relevant allowing to identify characteristic states of the investigated materials. The aim of the study was to establish a link between the characteristic states of the investigated materials (defined above) and their state parameters defined in the frame of the critical state soil mechanics (*CSSM*). In the present research the attention will be focused on the use of the above parameter (Ψ) even for silty sands and the applicability of other index parameters for the

characterization of the undrained monotonic behaviour of sand-silt mixtures will be verified.

Instability stress ratio η_{IS}

In the literature, the undrained instability state was also called critical effective stress ratio state (Vaid and Chern 1983); it was also associated with the collapse surface (Sladen et al. 1985) and the flow liquefaction line (Yang 2002). It is a characteristic state for triggering flow type failure (or strain softening). Lade (1993) defined the undrained instability line (*ISL*) to connect the undrained instability points in *q-p'* plane with the origin of the stress plane and stated that it was unique for a given relative density regardless of initial effective confining pressure. The slope of this line is the instability stress ratio η_{IS}. Afterwards Yang (2002) collected literature data and demonstrated that the instability stress ratio η_{IS} is affected by both density and initial confining pressure, and consequently suggested to use the initial state parameter to characterise its slope. Rabbi et al. (2019) proposed different state indices to characterise the instability stress ratio for a silty sand with a percentage of fines equal to 10%, such as state parameter, state index, pressure index, and modified state parameter. The authors proved that the relationships of η_{IS} with the different state indices are dependent on the type of soil. The data reported by Liang (2016) shows that adding crushed silica fines can affect the relationship between instability stress ratio and state parameter. Moreover, the stress ratio at undrained instability can be also affected by stress histories (Rabbi et al 2019).

In the present study the instability stress ratio η_{IS}, evaluated for all the percentaces of fines below the threshold fines content, was plotted against different state indices: $\Psi_{(0)}$, $I_{p(0)}$ and $\Psi_{m(0)}$ as shown in **Figure 102a**, **102b**, and **102c**, respectively. In **Figure 102b**, as well as in any other figure that reports correlations between the behavioural parameters of the investigated materials and $I_{p(0)}$, the curves are drawn in semi-logaritmic scale due to the large range of the values of $I_{p(0)}$ (from 0.01 to 10). The correlations adopted to fit the experimental points are shown in the same figures. The **Figure 102** shown how the data for all three fines contents approximately falls together in a unique curve, for all three studied state parameters. The coefficient of determination R^2 of the correlations η_{IS}-$\Psi_{(0)}$, η_{IS}-$I_{p(0)}$, and η_{IS}-$\Psi_{m(0)}$ with respect to the best fit trendline were 0.88, 0.77, and 0.88, respectively. These results confirmed that the intial state parameter $\Psi_{(0)}$ turns out to be a state index capable of interpreting, in a

univocal way, the undrained instability state for sand-fines mixtures ($f_c < f_{thre}$). The modified state parameter $\Psi_{m(0)}$ also worked quite well, while the pressure index $I_{p(0)}$ was less satisfactory.

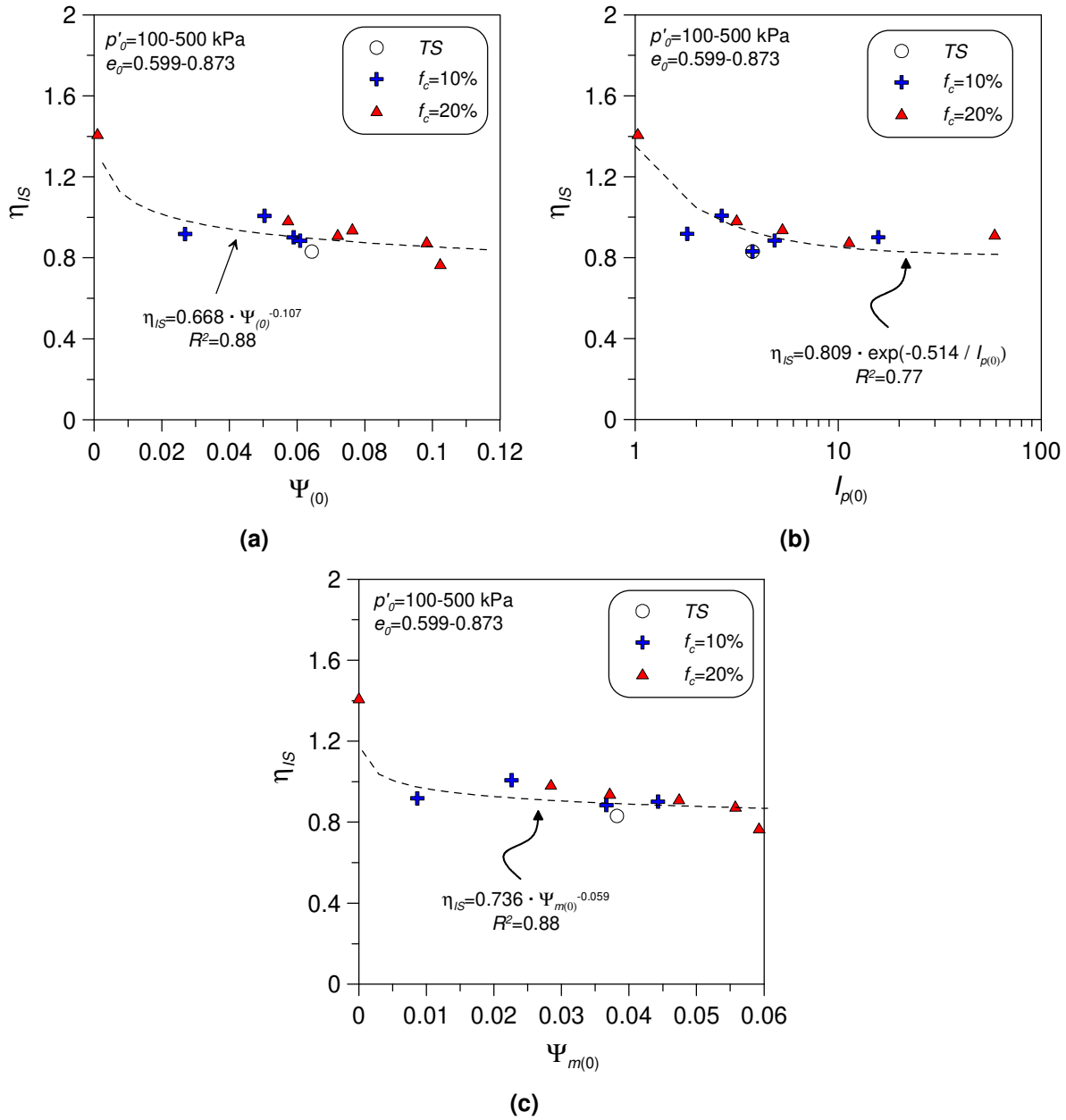

Figure 102 – Variation of undrained instability stress ratio η_{IS} with: (a) state parameter $\Psi_{(0)}$, (b) pressure index $I_{p(0)}$, and (c) modified state parameter $\Psi_{m(0)}$ for Ticino silty sand ($f_c<f_{thre}$).

Normalized liquefaction potential (q_{min} / p'_0) / q_{IS}

Yamamuro and Lade (1997) introduced the parameter q_{min}/q_{IS} to examine the liquefaction potential where, q_{IS} is the deviator stress at the instability state (i.e., peak q) and q_{min} is the minimum deviator stress attained during post peak deviator strain

softening. For complete liquefaction, $q_{min}/q_{IS} = 0$. Furthermore $q_{min}/q_{IS} \rightarrow 1$ holds for increasing resistance to liquefaction, with a maximum value of 1 for *NF* behaviour. This measure of liquefaction potential has been used in many liquefaction studies (Ishihara 1993; Lade and Yamamuro 2011; Rahman and Lo 2014) although a slightly different form of the liquefaction potential, namely the brittleness index, defined as $(q_{IS}-q_{min})/q_{IS} = (1-q_{min}/q_{IS})$, has been used in other studies (Chiu and Fu 2008; Sadrekarimi 2014; Sadrekarimi and Olson 2011). In the present research the liquefaction potential q_{min}/q_{IS} was divided to the initial mean effective stress p'_0 according to Rahman and Lo (2014) to take into account in a better way the effect of the confining stresses. The normalized liquefaction potential $(q_{min}/p'_0)/q_{IS}$ was investigated against the three state indices, to gain a deeper insight into the dependence of the liquefaction phenomena on the initial state. The relationship between $(q_{min}/p'_0)/q_{IS}$ and all three state indices: $\Psi_{(0)}$, $I_{p(0)}$ and $\Psi_{m(0)}$ for *F* and *LF* behaviour in undrained monotonic triaxial tests are shown in **Figure 103a**, **103b**, and **103c**, respectively. Regardless of the percentage of fines ($f_c < f_{thre}$), a unique exponential relationship can be used to describe the variation of $(q_{min}/p'_0)/q_{IS}$ with the state indices. The relationships $(q_{min}/p'_0)/q_{IS}$ - $\Psi_{(0)}$, $(q_{min}/p'_0)/q_{IS}$ - $I_{p(0)}$, and $(q_{min}/p'_0)/q_{IS}$ - $\Psi_{m(0)}$ have an R^2 of 0.93, 0.87, and 0.78, respectively. In this case the conventional state parameter $\Psi_{(0)}$ was also found to be the one capable of capturing in the most accurate way the behaviour of the sand-fines mixtures analyzed ($f_c < f_{thre}$) while the greatest dispersion was found for $\Psi_{m(0)}$.

Phase transformation stress ratio η_{PT}

Phase transformation is the state in which the response of a given specimen turns from contractive to dilative. In the present study, the terms contractive and dilative are used only referring to the excess pore water pressure generation in a given specimen. The excess pore pressure increases up to the phase transformation, and then starts to decrease with further straining. This state may occur in specimens that exhibit *NF* behaviour. The stress ratio at phase transformation may be characterised by the following equation (Li and Dafalias 2000): $\eta_{PT}=M\cdot\exp(A\cdot\Psi_{PT})$, where M is the critical state stress ratio, Ψ_{PT} is the state parameter at phase transformation and A is a positive fitting parameter. Furthermore, the initial state parameter $\Psi_{(0)}$ may also be used for correlation with η_{PT}. Experimental results (Sze 2010; Liang 2016; Murthy et al. 2007) showed that the stress ratio at phase transformation decreased with decreasing the initial state parameter (i.e. more dilative behaviour).

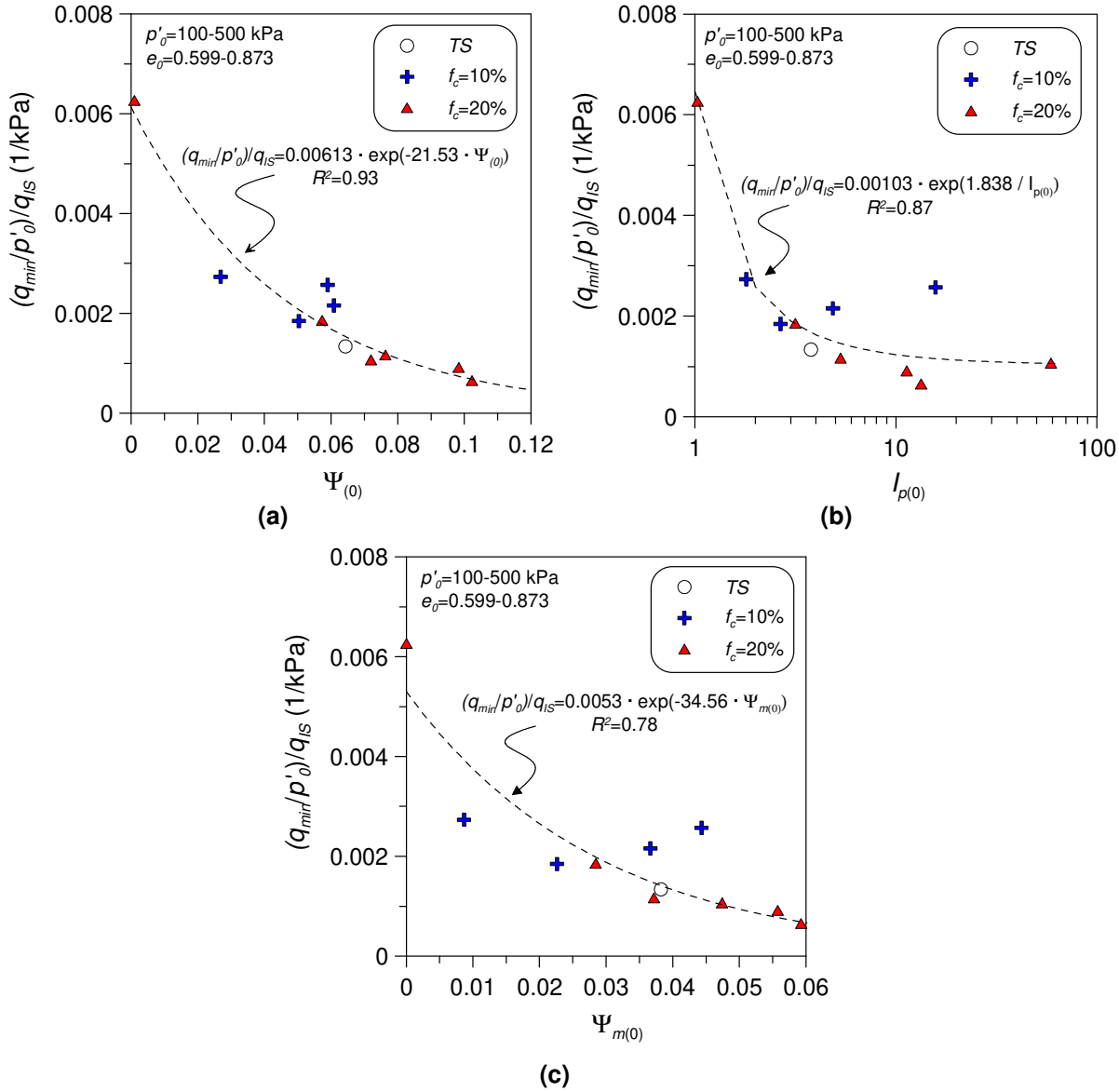

Figure 103 – Variation of normalized liquefaction potential ($q_{min}/p'_0)/q_{IS}$ with: (a) state parameter $\Psi_{(0)}$, (b) pressure index $I_{p(0)}$, and (c) modified state parameter $\Psi_{m(0)}$ for Ticino silty sand ($f_c<f_{thre}$).

In the present study, besides the initial state parameter, to characterize the phase transformation state (η_{PT}), also other initial state indexes such as the initial pressure index and the initial modified state parameter were used. In **Figure 104a**, **104b**, and **104c** η_{PT} was plotted against the aforementioned state indices: $\Psi_{(0)}$, $I_{p(0)}$ and $\Psi_{m(0)}$, respectively. The **Figure 104** shown how the data for all three fines contents approximately falls together in a unique curve, for all three studied state parameters. An exponential relationship was adopted to describe the variation of η_{PT} with all the three initial state indexes. The coefficients of determination R^2 of the correlations η_{PT}-$\Psi_{(0)}$, η_{PT}-$I_{p(0)}$, and η_{PT}-$\Psi_{m(0)}$ with respect to the best fit trendline were 0.80, 0.77, and 0.67, respectively. **Figure 104** confirms that, also in this case, for sand-fine mixtures

($f_c < f_{thre}$), the initial state parameter $\Psi_{(0)}$ is able to better capture the undrained monotonic behaviour.

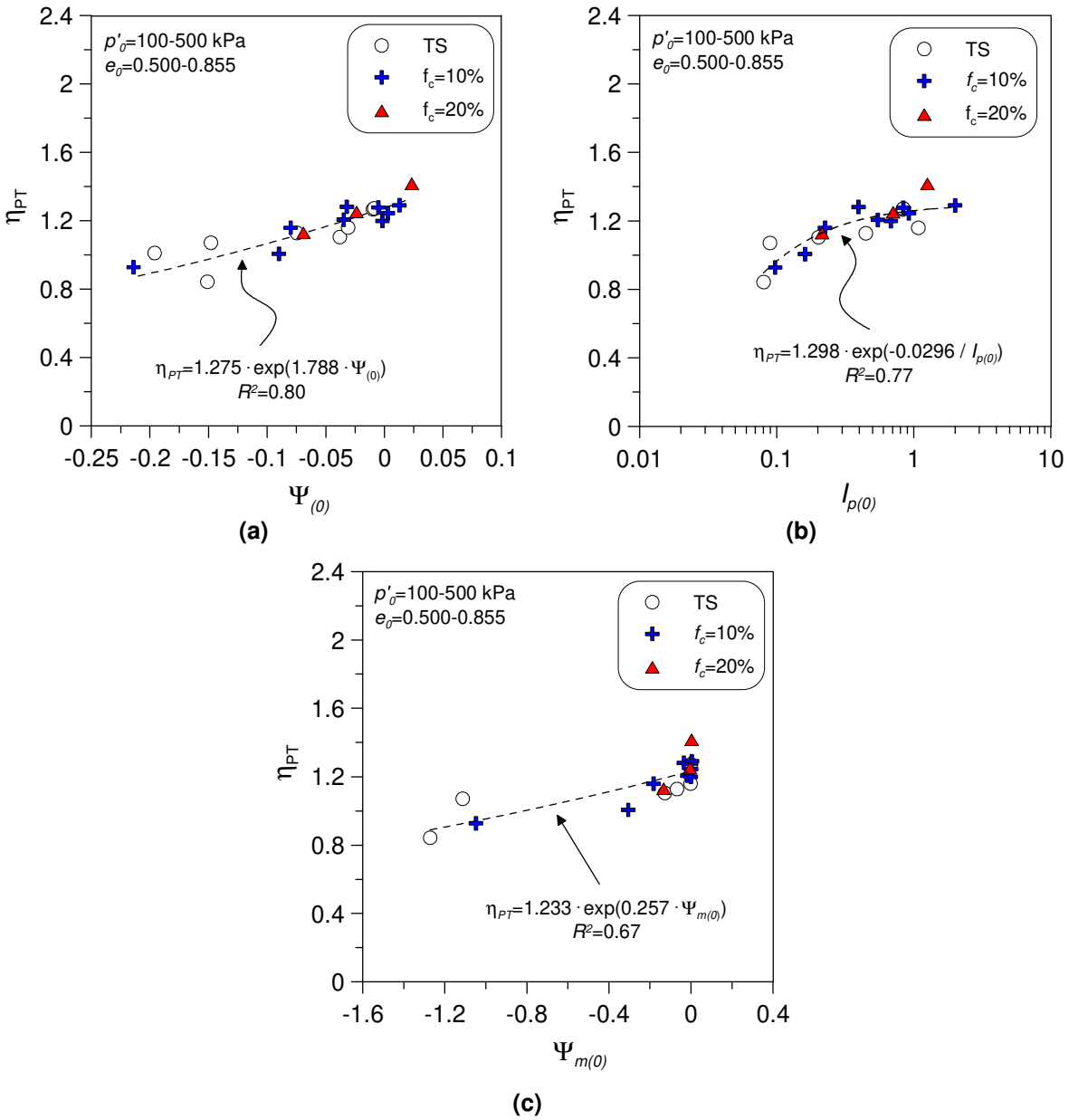

Figure 104 – Variation of phase transformation stress ratio η_{PT} with: (a) state parameter $\Psi_{(0)}$, (b) pressure index $I_{p(0)}$, and (c) modified state parameter $\Psi_{m(0)}$ for Ticino silty sand ($f_c<f_{thre}$).

Normalized critical state resistance q_{CS}/p'_0

The definition of critical state has been introduced abundantly in the previous paragraph; hence in the present subparagraph only the variation of the normalized critical state resistance is presented. Previous studies (Qadimi and Mohammadi 2014; Rahman and Lo 2014) showed that an empirical correlation can be established between the normalised critical state strength and the initial state parameter defined

by the following equation: $q_{CS}/p'_0=A\cdot\exp(B\cdot\Psi)$, where A and B are fitting parameters. This relationship generally showed good predictive ability; this has been confirmed by the results obtained in this study, see **Figure 105a**. If the initial pressure index or the initial modified state parameter are used (in lieu of $\Psi_{(0)}$) in correlations with q_{CS}/p'_0 (**Figure 105b**, **c**), the relationship varies from a power relationship to a linear relationship while maintaining a high degree of approximation for all the three initial state indexes, as can be observed in **Figure 105**.

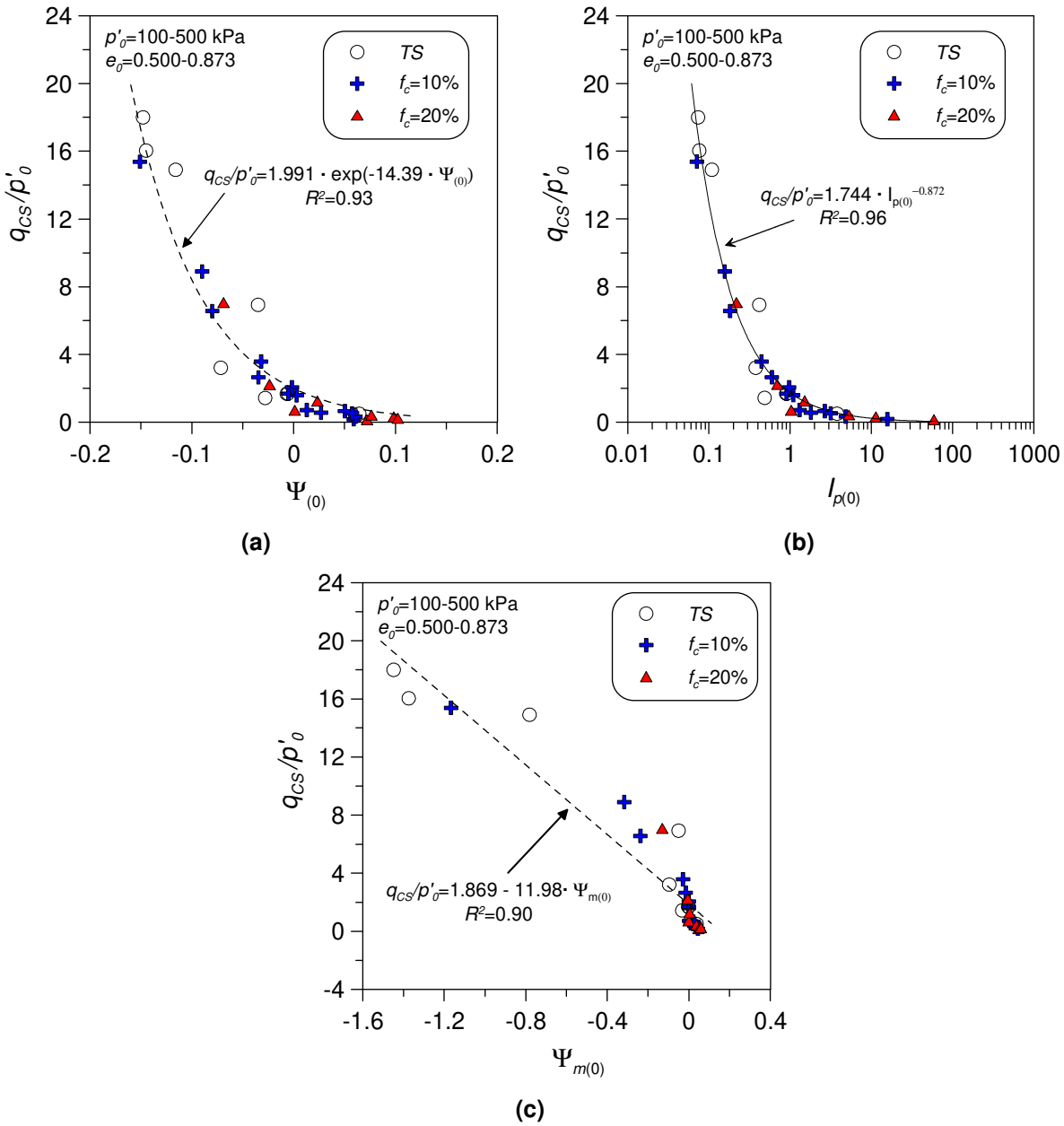

Figure 105 – Variation of normalized critical state resistance q_{CS}/p'_0 with: (a) state parameter $\Psi_{(0)}$, (b) pressure index $I_{p(0)}$, and (c) modified state parameter $\Psi_{m(0)}$ for Ticino silty sand ($f_c<f_{thre}$).

6.3 Critical state-based interpretation of the undrained cyclic resistance of silty sands

The critical state theory has been found useful to characterize the liquefaction resistance of sands (e.g. Yang and Sze 2011a, b; Jefferies and Been 2016).

The concept of state parameter, Ψ, proposed by Been and Jefferies (1985), was found useful to characterize the undrained cyclic behaviour and cyclic liquefaction resistance of sands. If it is assumed that the initial state in terms of void ratio and mean effective stress is the same for sands with different f_c, then, because of the different positions of the *CSLs* in *e*-log(*p'*) plane due to the different f_c, the initial state parameter of the sand-silt mixtures are different. To be more specific, the mixture $TS{+}30{\cdot}f_c$ has the highest state parameter whereas the clean *TS* has the lowest one. The higher is the initial state parameter, the more contractive is the behaviour. This results in a faster build-up of excess pore water pressure for $TS{+}30{\cdot}f_c$ compared to the clean sand and thus a lower cyclic resistance should be expected. Similarly, decreasing e_0 and decreasing p'_0 will lead to lower state parameters and thus more dilative response with higher cyclic resistance. It is interesting to inspect whether the cyclic resistance ratio of *TS,* both alone and in mixture with non-plastic silt, can be analyzed in terms of the traditional state parameter with different initial static shear stress applied. For this purpose, initially, the cyclic resistance ratio $CRR_{N=15}$ of clean *TS* specimens having different void ratios (e_0=0.60-0.82), initial vertical effective stresses (σ'_{v0}=50-100 kPa), and initial static shear stresses (α=0-0.30) has been plotted as a function of $\Psi_{(0)}$ in **Figure 106**.

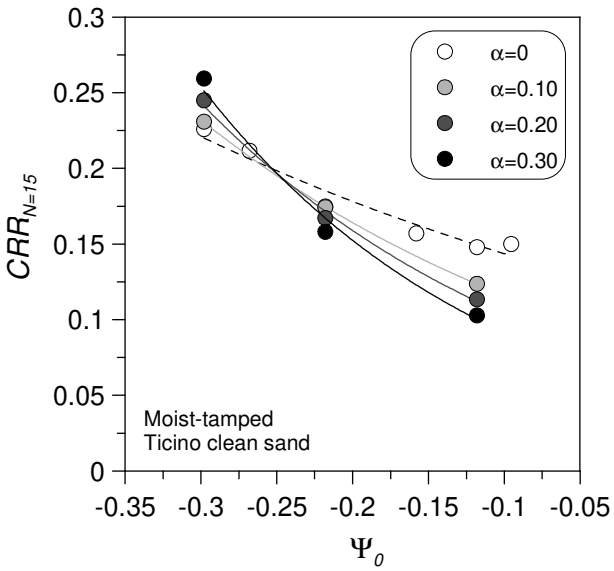

Figure 106 – Clockwise rotation of the $CRR_{N=15}$-$\Psi_{(0)}$ correlation of Ticino clean sand with increasing initial static shear stresses ratios.

In that plot the effects of packing density and confining pressure are unified by $\Psi_{(0)}$ and the effect of the initial static stress is evidenced by the several curves. The correlation between $CRR_{N=15}$ *and* $\Psi_{(0)}$ can be characterized fairly well by an exponential trend line for a given α level. These trend lines rotate clockwise with increasing α, as shown in **Figure 106**; the same behaviour was observed for Toyoura sand in a previous work of Yang and Sze (2011a, b) using undrained cyclic triaxial tests.

The $CRR_{N=15}$-$\Psi_{(0)}$ data of silty sands with $f_c < f_{thre}$ are plotted in **Figure 107** to compare with the trend lines fitting the clean sand data in **Figure 106**.

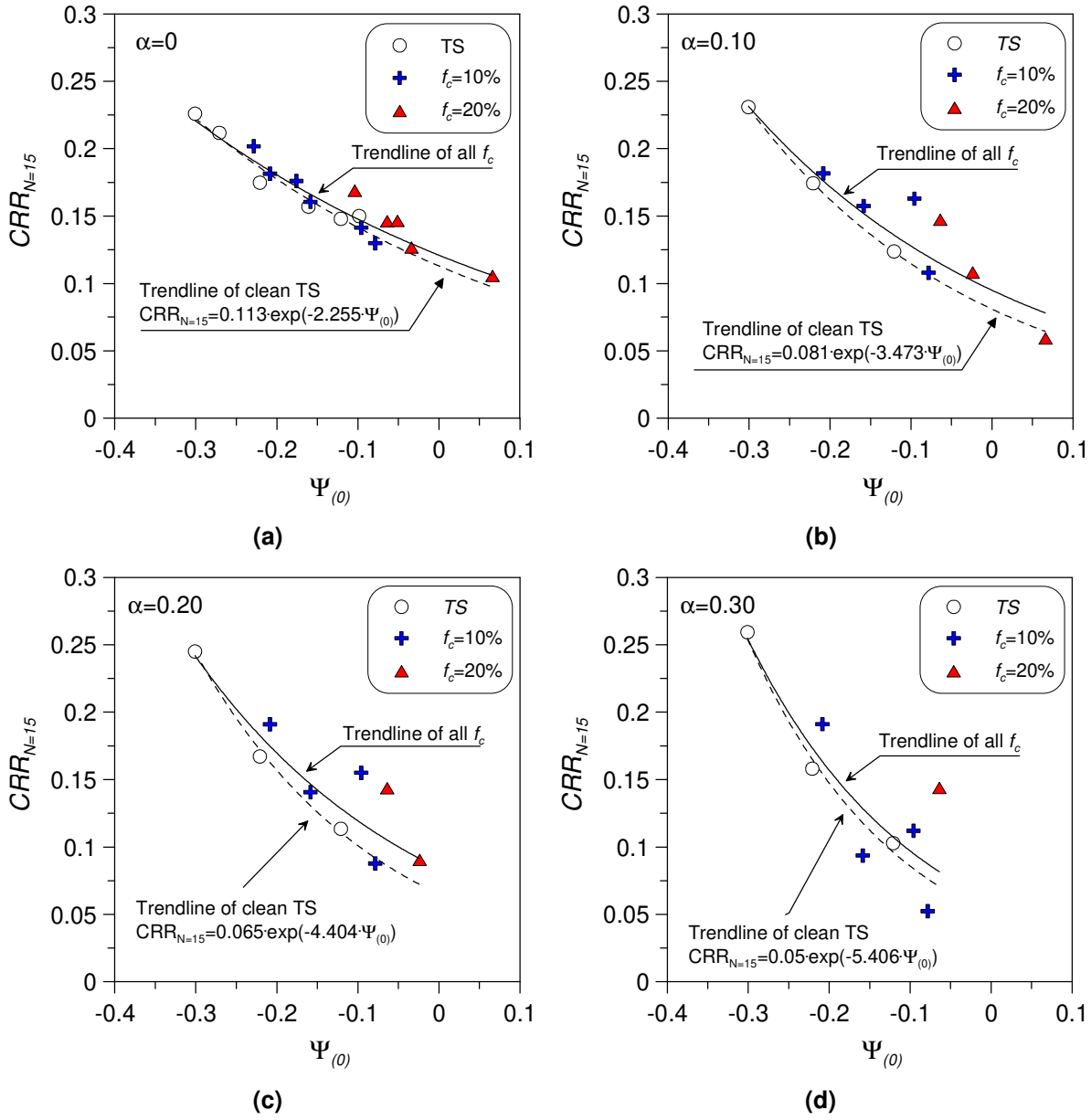

Figure 107 – $CRR_{N=15}$-$\Psi_{(0)}$ correlations of Ticino sand with fines (< f_{thre}) under different α levels: (a) α=0; (b) α=0.10; (c) α=0.20; and (d) α=0.30.

The new data of silty sands fall in the near vicinity of the trend lines, implying that, for a given value of α, the correlation between $CRR_{N=15}$ and $\Psi_{(0)}$ is almost f_c-independent. In addition, it is found that the α-induced clockwise rotation of the CRR-$\Psi_{(0)}$ curves is also applicable to silty sands, which is accordance with Wei and Yang (2019b).

In the present study, the critical state framework was also used considering other state indices, as previously done for the interpretation of the undrained monotonic behaviour. In particular, **Figure 108** and **Figure 109** show the correlations obtained considering the initial pressure index $I_{p(0)}$ and the initial modified state parameter $\Psi_{m(0)}$, respectively.

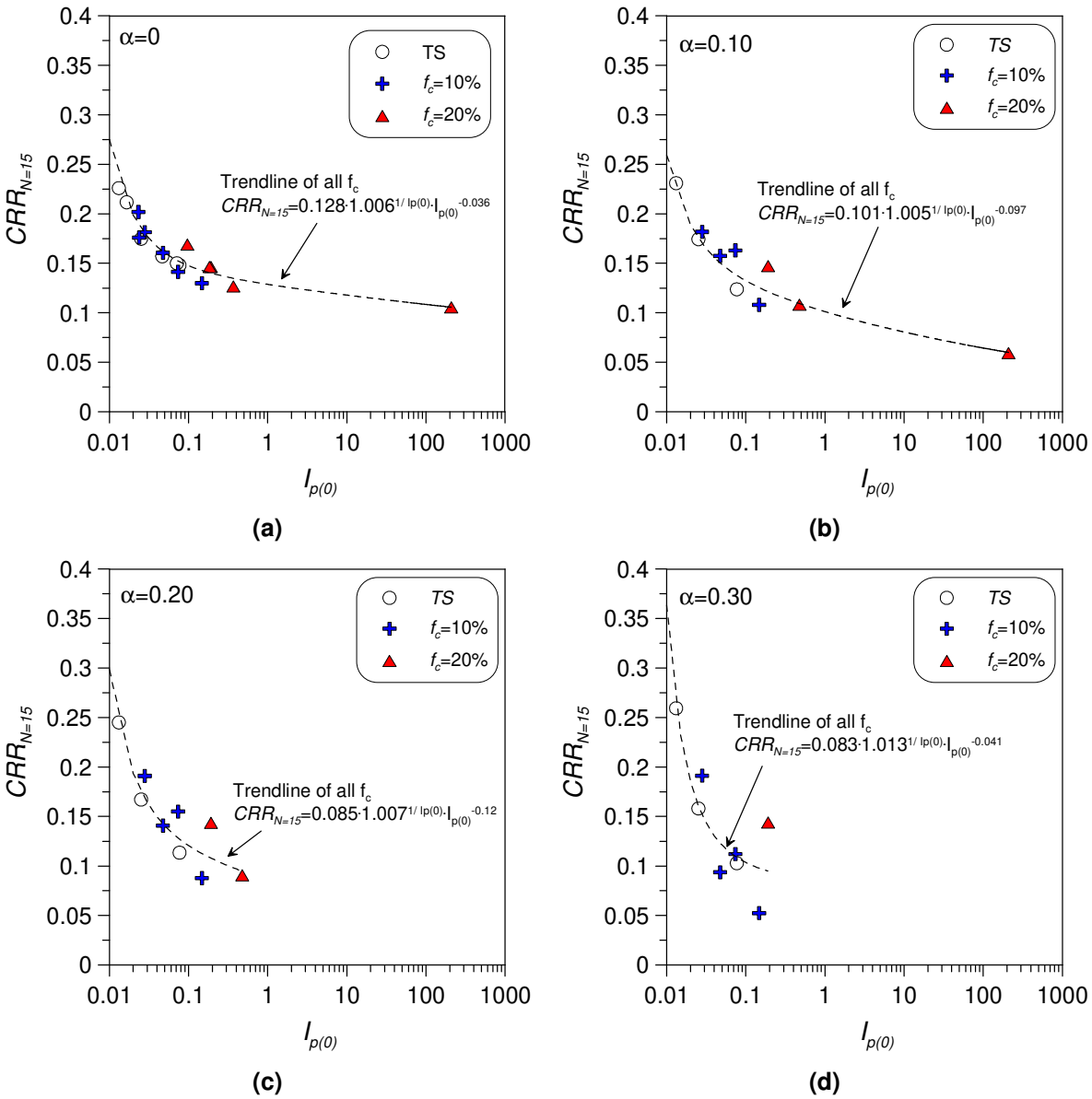

Figure 108 – $CRR_{N=15}$-$I_{p(0)}$ correlation of Ticino sand with fines (< f_{thre}) under different α levels: (a) α =0; (b) α =0.10; (c) α =0.20; and (d) α =0.30.

As can be concluded from **Figure 108**, the variation of the undrained cyclic simple shear strength with $I_{p(0)}$, for given values of initial static shear stress applied, can be defined by a unique correlation irrespective of the fines content of the mixtures with a scatter slightly greater than in case of the usual state parameter $\Psi_{(0)}$.

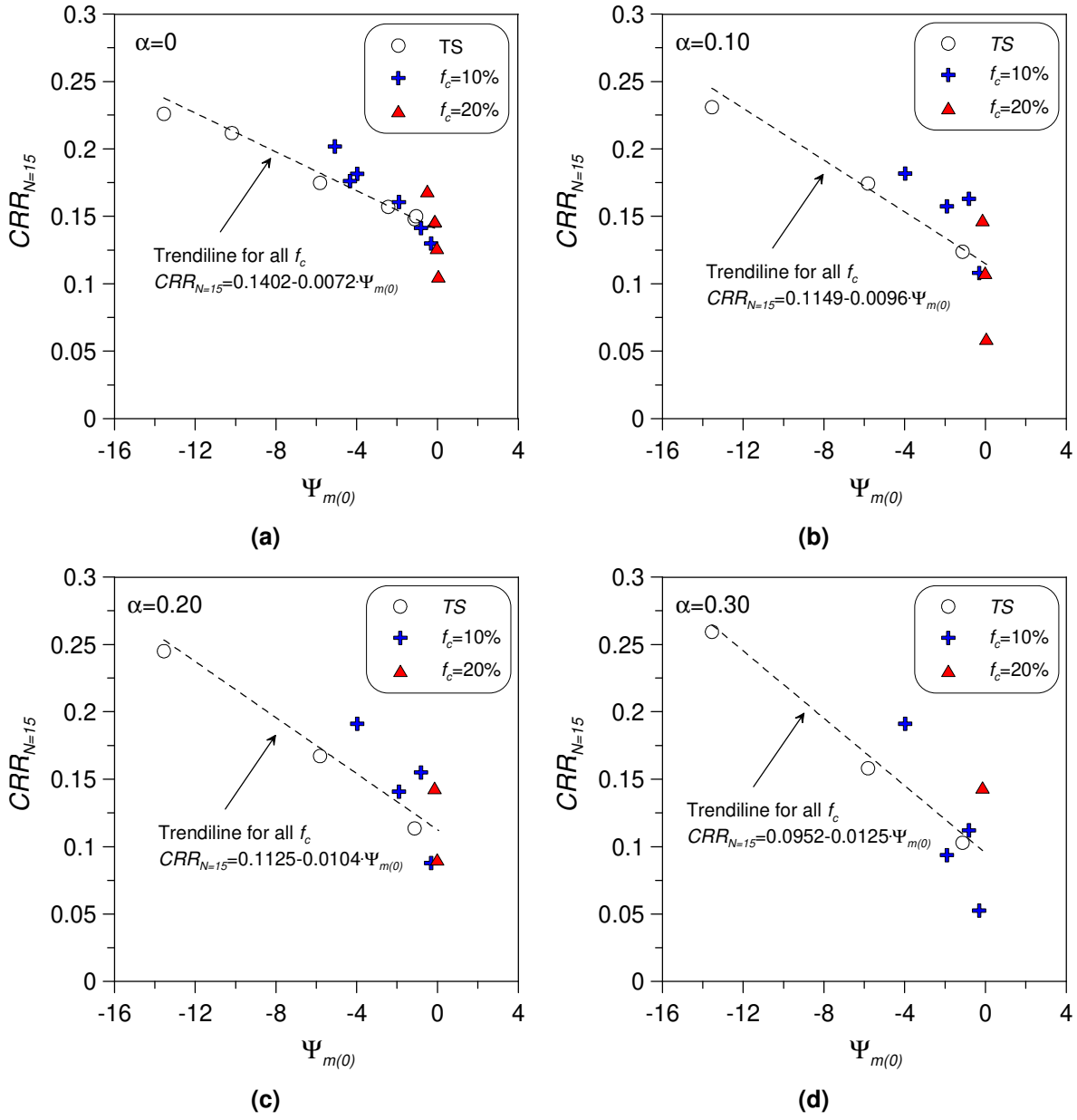

Figure 109 – $CRR_{N=15}$ - $\Psi_{m(0)}$ correlation of Ticino sand with fines (< f_{thre}) under different α levels: (a) α =0; (b) α =0.10; (c) α =0.20; and (d) α =0.30.

A linear regression analysis was adopted to fit the data points in **Figure 109**; the best fit lines obtained show the variation of $CRR_{N=15}$ of the investigated mixtures with $\Psi_{m(0)}$ for given values of α. For all fines contents below f_{thre}, the use of $\Psi_{m(0)}$ led again to unique correlations with the undrained cyclic resistance; nevertheless, the comparison

with the corresponding correlations in terms of $\Psi_{(0)}$ (**Figure 107**) reveals that the latter one worked better in nearly all of the four cases.

Analysis of results presented in **Figure 107**, **Figure 108**, and **Figure 109** showed that the state indices defined in terms of void index e, particularly Ψ, I_p and Ψ_m, were more or less capable of predicting the undrained cyclic resistance of the sandy soils with different fines contents (below the threshold fines content) and subjected to different initial static shear stress. The traditional state parameter Ψ turned out to be the more reliable one compared to the others.

Chapter 7

Application of equivalent granular void ratio to interpret the experimental results

7.1 Interpretation using equivalent granular void ratio

In the previous chapters, the void ratio (e) was considered to be a fundamental parameter capable to represent in a reliable way the effects that the density state of non-plastic sand-fines mixtures exert on the undrained monotonic and cyclic responses of these materials. The state parameter (Ψ), the pressure index (I_p) and the modified state parameter (Ψ_m) used to analyse the undrained response of such soils were all based on the void ratio (e). However the interpretation of the test data showed that as the fines content increased, similar values of initial global void ratio (e_0) did not correspond to similar soil response. Undrained soil strength appeared to decrease at higher soil fines contents, for $f_c < f_{thre}$, when using void ratio. The difference in response of non-plastic silty sands at similar values of (e_0) can be explained by the fact that the global void ratio doesn't provide a differentiation between the sand and the fines-sized particles within the soils (Rees 2010). All particle sizes are assumed to contribute to the overall force-chain of the soil when using this parameter (Thevanayagam and Mohan 2000), but this assumption may not be true from the standpoint of physics, especially when silty soils are mixed with sand. With the aim to differentiate the contribution of the sand particles from that of the non-plastic silt particles Thevanayagam et al. (2002) introduced the concept of the equivalent granular void ratio e^*. The equation defining the equivalent granular void ratio is Eq. (18); it includes a parameter, b, which can be thought of as an influencing factor that quantifies the fraction of the silt-sized particles participating in the soil force-chains during the undrained loading. The usefulness of the equivalent granular void ratio for interpretating the undrained monotonic and cyclic responses of the Ticino sand-silt mixtures is discussed in the following sections.

7.1.1 The equivalent granular void ratio concept

The equivalent granular void ratio e^* was proposed (Thevanayagam et al. 2002) as an improvement to the intergranular/skeleton void ratio (Mitchell 1976), e_g, by allowing for

some fines to participate in the soil force-chains. This concept is based on the consideration of a binary mixture, in which one component is constituted by the sand-sized particles and the other one by the silt-sized particles that interact with the former ones. The sand is still considered the dominant particle size, but the fines are considered to sit in between sand grains, as well as within the sand void space. This creates a soil structure whereby some fines participate in load transfer, and others do not, remaining inactive. **Figure 110** illustrates this concept using a schematic of 9 sand particles and 32 fines particles. In this schematic, 12 fines particles actively participate in the soil force-chains, while 20 fines particles are shown as being inactive, or sitting in the sand void space.

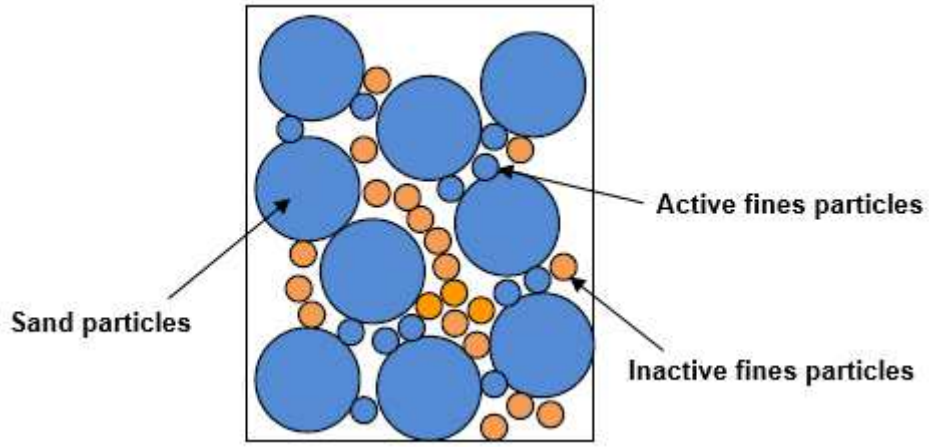

Figure 110 – Explanatory image of the equivalent granular void ratio concept. Sand particles are represented by higher solid blue circles, inactive fines are represented by smaller solid yellow circles, and active fines are represented by smaller solid blue circles (Rahemi 2017).

The equivalent granular void ratio, *e**, allows the active fines particles to be included in the density state measure through the introduction of the fines influence factor, *b*. As it can be seen in Eq. (18) this factor adjusts the fines content f_c of a binary mixture to take into account that a portion of the total fines is considered to be active in the soil force-chains. In the case of **Figure 110**, this portion would be $b = 12 / 32 = 0.375$ (the fraction of active grains). The Eq. (18) defining the equivalent granular void ratio e* has been re-written below for readers' convenience:

$$e^* = \frac{e + (1 - b) \cdot f_c}{1 - (1 - b) \cdot f_c}$$

According to the definition suggested by Rees (2010) the fines influencing factor *b* is a "*factor accounting for all the combined effects of different parameters on the undrained*

response of sand due to the addition of fines below threshold fines content". Then, it is evident that the mechanisms in which the presence of fines plays a role are quite complex and depend on many factors. Earlier studies claimed that the factor *b* is influenced by several factors such as: grading features of sand-silt mixtures represented by the particle size ratio $\chi=D_{10}/d_{50}$ (Ni et al. 2004b; Mohammadi and Qadimi 2015), fines content (generally normalized to the threshold value, f_c/f_{thre}) (Rahman and Lo 2008; Lashkari 2014) or angularity and mineralogy of particles (Rees 2010; Lahkari 2014). Only a few authors have considered the influence of the loading type (monotonic vs. cyclic) on *b* as a result of the different pattern of the force chains (Reese 2010).

It should be noted that the equivalent granular void ratio concept is only relevant for mixtures of sand and fines below the threshold fines content f_{thre}. As discussed in section 5.2.4, the soil structure fundamentally changes from being sand-dominated to fines-dominated as the threshold fines content is exceeded. There is however another density state parameter, the equivalent interfine void ratio (Thevanayagam et al. 2002), that can be used to describe the soil state when $f_c > f_{thre}$, but soils with high fines content soils are outside the scope of this study.

In the present study the fines influence factor (*b*) has been assumed firstly to be constant for a given mixture of sand and non-plastic fines, regardless of fines content. At a later stage, the fines influence factor values have been assumed to vary with the fines content. The validity of one assumption against the other is discussed. The notation b_{CSL} refers to the fines influence factor derived through an approach based on back analysis of experimental data concerning the critical state line (*CSL*) while b_{CRR} refers to the fines influence factor derived through an approach based on back analysis of experimental data concerning the undrained cyclic resistance (*CRR*).

7.1.2 Determination of fines influence factor b

The prediction of *b* factor is a critical aspect for the application of the e^*-based approach for sand-fines mixtures with $f_c < f_{thre}$. Some methods have been proposed to estimate the value of *b* for non-plastic binary mixtures basing on material properties (Thevanayagam et al. 2003; Rahman et al. 2008), but the most accurate way to determine *b* is to back-calculate it based on the observed soil response. As such, a back-calculation procedure for determining *b* is detailed below for a given mixture of sand and fines. It should be noted that the fines influence factor values b_{CSL} and b_{CRR}

are calculated separately: this is due to the difference in fines activity between monotonic and cyclic soil response observed in previous studies in literature (Rees 2010; Cubrinovski et al. 2010).

The back analysed *b* value reported in the literature for practical purposes is generally a constant value irrespective of fines contents. This is because a back analysis process of a large amount of data for different fines contents was adopted to increase the reliability of the averaging process. In this study a back-analysis considering the variation of fines content has been also considered.

The objective of the back-calculation procedure is to determine a value of *b* that makes the soil response similar for constant e^* values, regardless of the fines content of the soil. The procedure that is based on the consideration of Eq. (18) is reported in the following:

1) The first step in the back-calculation procedure is to define the clean sand benchmark response curve. For monotonic tests, the benchmark curve is the clean sand critical state line *CSL* whereas for cyclic tests, it is the curve showing the variation of the undrained cyclic resistance ratio $CRR_{N=15}$ of clean sand with the initial global void ratio. A preliminary choise of the mathematical equation is needed to fit the experimental data points using a method of least squares to generate the response curves. Eq. (8) is used for the critical state line and a power function of the type shown in **Figure 84** is used for the undrained cyclic resistance curve. The power function was chosen based on observation of the cyclic resistance data presented in **Figure 84**. The procedure described below is valid for b_{CSL} but it can be easily extended to b_{CRR}; more details about the method adopted for determining b_{CRR} and the results obtained are given in paragraph 7.1.4.
2) Tentative values of the equivalent granular void ratio $e^* = f(b)$ are calculated for each specimen by introducing in Eq. (18) *b* values ranging from 0 to 1 in increments of 0.001, given that *e* and f_c are known. This covers the fines activity range from fully active to fully inactive, meaning that all potential values of e^* for the soils are calculated.
3) For all points in the plane e^*- log(p') obtained by introducing in Eq. (18) and Eq. (8) a given tentative value of *b* and the f_c values of any specimen the distance *d* of these points from the benchmark response curve (corresponding to *CSL* of clean sand) as illustrated in **Figure 111a**, is measured. Note that the equivalent

granular void ratio values of the benchmark curve are defined as e^*_b. Therefore, to calculate d, e^* is subtracted from e^*_b, or $d = e^*_b - e^*$. The obtained values of d are then squared → $d^2 = (e^*_b - e^*)^2$.

4) The squared distances d^2 are summed up for all points corresponding to a given value of b, and divided by the total number of test specimens, N_S, and after that a root square is applied. This calculation gives the root mean squared deviation value, *RMSD* obtained from the e^* data of all specimens evaluated with the considered tentative value of b. Since in the procedure the same value of b is adopted for all specimens, it turns out that the approach is implicitly based on the assumption that b has a constant value irrespective of the fines contents. The procedure is repeated for other values of b and a curve *RMSD* vs. b is drawn as shown **Figure 111b.** The lowest *RMSD* is identified, and the corresponding b is chosen as the best fit for the fines influence factor. This final step is graphically shown for the b_{CSL} associated to Ticino silty sand with f_c = 20% in **Figure 111b**.

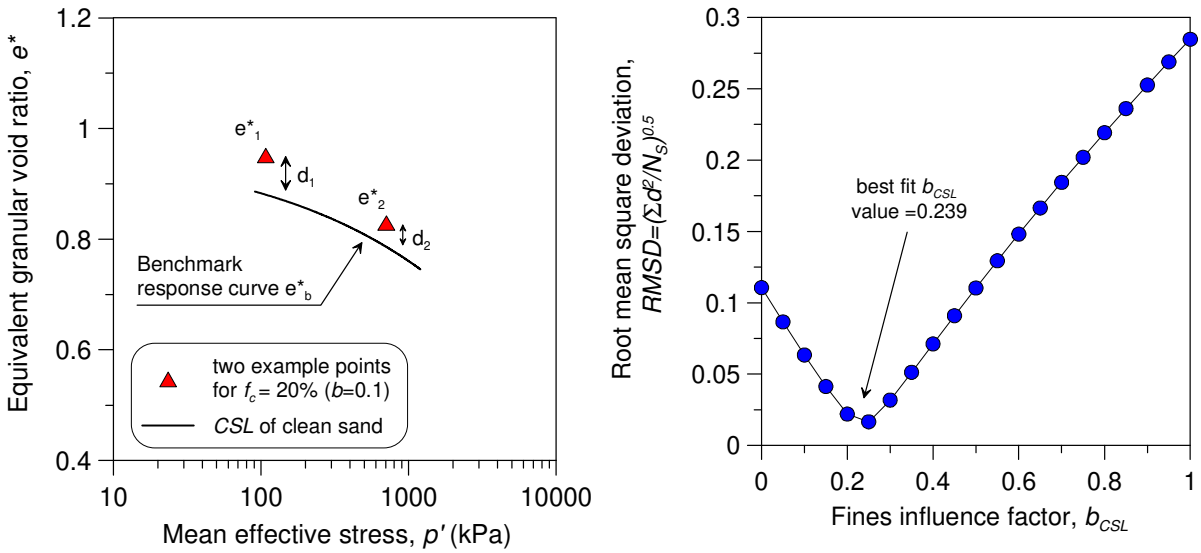

Figure 111 – (a) Definition of distance *d*, from the clean sand benchmark response curve and (b) determination of the best fit b_{CSL} for *TS*+20%·f_c.

The aforementioned procedure was repeated identifying a value of b for each f_c, instead of assuming a constant b for all f_c. This was performed by considering different series of specimens each one being characterised by a single mixture (i.e. the same value of f_c) prepared at different global void ratios. Once the best fit b has been

determined, other response curves (e.g. the undrained cyclic resistance curves or other) of all mixtures can be plotted together using, as density state measures, the equivalent granular void ratio values that correspond to the best fit *b* obtained with the previously described procedure. These response curves should, in principle, be located in close proximity to one another, indicating that similar values of e^* give similar soil response, regardless of the fines content.

The aforementioned back-calculation procedure was performed for all mixtures of sand and fines presented in this chapter. Specimens with fines contents equal to or above 24.5% were not included in the back-calculations, as f_c=24.5% is retained to be or to closely approximate the threshold fines content of Ticino silty sands.

7.1.3 Interpretation of the effects of fines content on the critical state line using the equivalent granular void ratio

Section 6.1 presented and discussed the effects of fines on the critical state line using the global void ratio as density state measure. In that case, increasing the fines content of sand appeared to make the soil response more contractive up to the threshold fines content, and, after that, more dilative. This section instead uses the equivalent granular void ratio e^* as density state measure, with the fines influence factor values, b_{CSL}, being derived using the procedure outlined in Section 7.1.2, and the equivalent granular void ratio values being calculated using Eq. (18). The equivalent critical state line *EG-CSL* of the Ticino sand-silt mixtures drawn as best fit curve of all points shown in **Figure 109** is presented in the same figure together with the critical state line *CSL* of the Ticino clean sand for comparison. In **Figure 112a** the b_{CSL} value was considered constant with the fines content, while in **Figure 112b** the b_{CSL} value was considered variable with the fines content. Both approximations lead to a very similar coefficient of determination R^2, i.e. a similar quality of approximation, since the b_{CSL} values derived for the different fines contents are quite similar.

Figure 112 firstly shows that the critical state points, when using the equivalent granular void ratio allowed to obtain a unique critical state line denominated equivalent critical state line *EG-CSL* regardless of the fines content. This is not surprising given that the values of a constant b_{CSL} = 0.237 (**Figure 112a**) or a variable b_{CSL}=0.236-0.241 (**Figure 112b**) were purposely back-calculated just to fit the experimental *CSL* data. The back-calculated value of the fines influence factor, that in the two approaches is about b_{CSL}=0.24, also provides insight into the actual effect of increasing the soil fines

content on the soil response. It suggests that approximately 24% of the fines added to the Ticino clean sand actually participate in the soil force-chains, and 76% of the fines simply sit in the soil without contributing to load resistance. The inactive fines however do decrease the global void ratio; this is the reason why the critical state lines are found to be characterized by a smaller global void ratio as the fines content increases, for $f_c < f_{thre}$. The information that 24% of the fines are participating in the soil force-chains is important as it means that the fines are having a significant effect on the overall soil response, and that the effect needs to be accounted for if the fines content of the soils is altered.

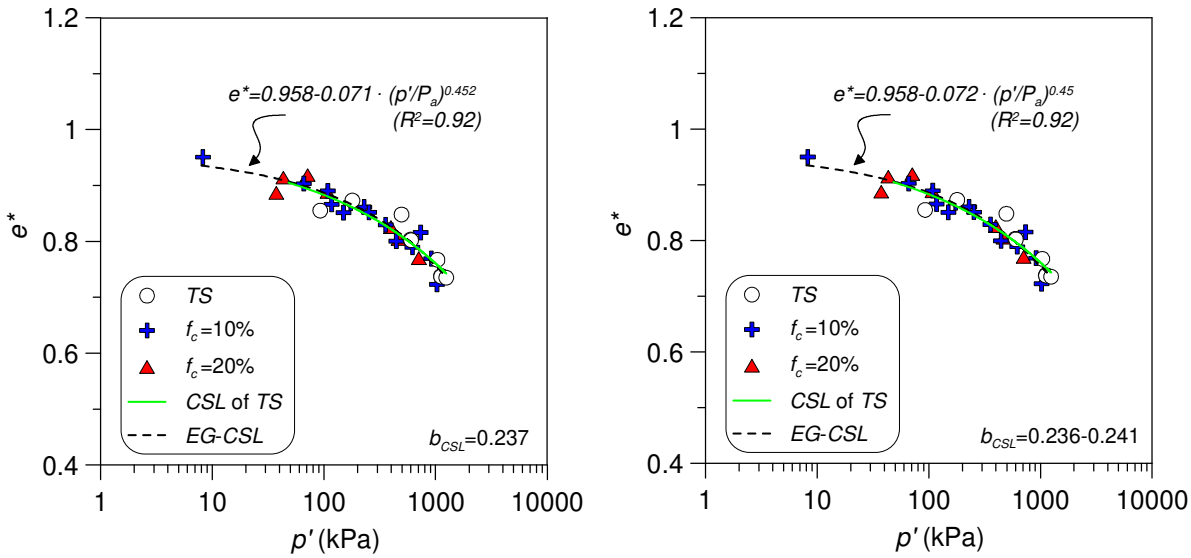

Figure 112 – Critical state line of *TS*-fines mixtures using the equivalent granular void ratio as the state measure: (a) interpretation based on a constant b_{CSL}=0.237 and (b) interpretation based on b_{CSL} variable with fines content (=0.236-0.241).

The central challenge in adopting the presented approach is how to determine the values of b_{CSL} in a simple and straightforward manner. Minimizing the amount of experimental data required to predict the behaviour of sand–fines mixtures through the presented approach would hinge upon determination of b using a minimum amount of experimental data. In the following section, the possibility of predicting or easily determining it in terms of some factors affecting this parameter will be investigated. Ni et al. (2004b) suggested that the b value could be a function of the particle size ratio $\chi = D_{10}/d_{50}$. The possibility of relating the b factor to the grading characteristics of the mixture is examined in **Figure 113a**. In **Figure 113a** literature data regarding b_{CSL}

processed by Rees (2010), as well as the values derived in the present study of Ticino sand-fines mixtures and data on Toyoura and Fujian sand-fines mixtures reported in Yang and Wei (2012), were plotted together versus the ratio of the particle size diameters. For the case of Yang and Wei (2012), in default of b_{CSL} back-analyzed value, critical state data were processed in the present study. **Figure 113a** suggests that the value of b_{CSL} can be well predicted for any sand–silt mixture as a linear function of χ, and two distinct relationships can be found for mixtures with angular to sub-angular particles of sand and for mixtures with rounded to sub-rounded particles of sand. The $b_{CSL} - \chi$ relationship could be improved and generalized by adding other b_{CSL} data determined experimentally for different types of sand–fines mixtures and different χ ratios.

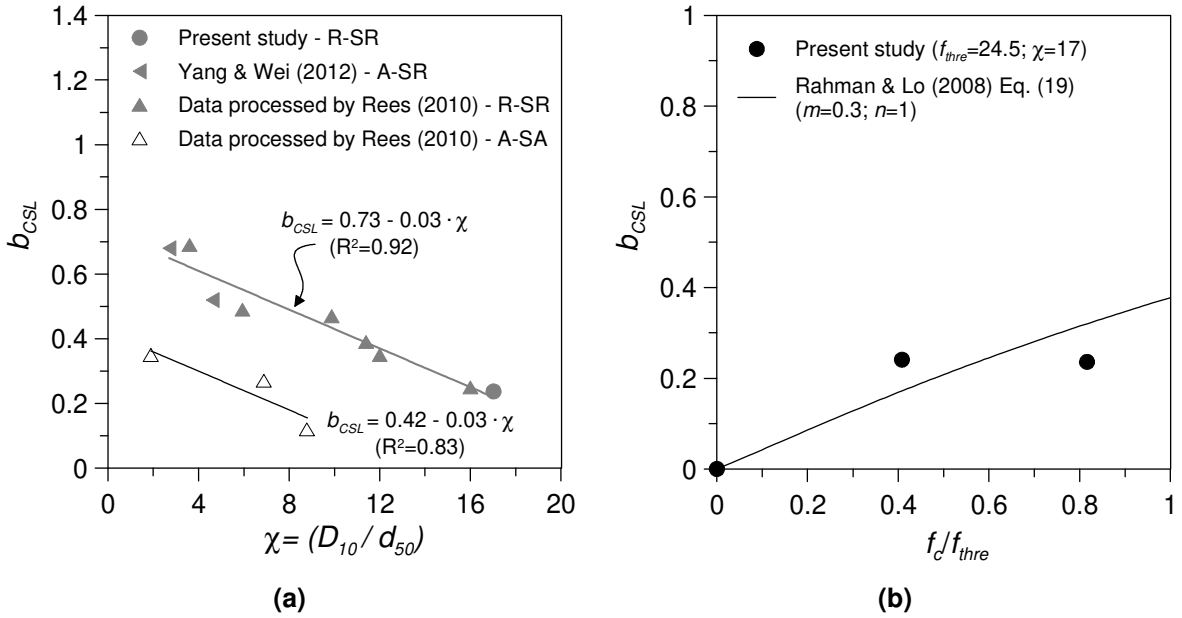

Figure 113 – Correlation of the fines influence factor values b_{CSL} with: (a) particle size disparity ratio χ and the angularity of the sand particles (i.e. *R-SR*=rounded to sub-rounded, *A-SR*=angular to sub-rounded, *A-SA*= angular to sub-angular), and (b) with fines content ratio f_c/f_{thre}, and comparison with Rahman and Lo (2008) correlation.

In addition to the particle size ratio and the shape of grains, the percentage of fines in the mixture is another factor that could affect the *b* value (Rahman and Lo 2008; Rahman et al. 2008). The determination of a reliable value for b_{CSL} based on a back-analysis of the data by trial and error, as employed in paragraph 7.1.2, considering the effect of fines content, seems to require a large number of experimental data at different percentages of fines. To solve this problem Rahman and Lo (2008), basing

on the binary packing studies of McGeary (1961), and considering the factor *b* as a function of f_c, f_{thre} and particle size ratio (χ), proposed a semi-empirical equation to predict the *b* value from simple input parameters, see Eq. (20). Based on calibrations with published datasets, values of the empirical parameters of the equation were suggested by Rahman and Lo (2008). The origins, justifications and physical meanings of this methodology and its details can be found in their work.

To clarify the influence of f_c on the value of *b*, the values obtained by back-analysing the raw data of the present study at different fines contents were plotted in **Figure 113b**. The b_{CSL} value reported for each f_c is the value giving the best coincidence between the clean sand data and the data for the available f_c. **Figure 113b** clearly shows that the values of b_{CSL} in the present study are almost independent of the fines content of the mixtures (f_c > 0). In other words, the fraction of the fines actively participating in the force structure of the mixture is quite equal for different values of fines content.

Rahman and Lo (2008) highlighted that, at low χ ratios (below 7), the *b* value should change rapidly with f_c. Nevertheless, in the case of the present study the use of a single *b* value for each mixture with different fines contents was found sufficient, probably because the value of χ is higher than 7 for the studied mixtures (χ =17). Furthermore, the capability of Eq. (20) to predict the b_{CSL} value is evaluated here and despite the different tendency the agreement in the absolute values is good, with a difference between the calculated and back-analyzed values not exceeding 0.08. In spite of the interesting findings derived from this evaluation, its generalization to other non-plastic sand-fines mixtures would still require more verification.

Basing on **Figure 112**, the critical state line of any Ticino sand-silt mixtures with f_c < f_{thre} could be estimated using the *EG-CSL* as a benchmark response curve, that is very similar to the *CSL* of the clean sand. This is an important advantage since the *CSL* of the clean sand can be used as *EG-CSL* of any non-plastic sand–silt mixture with fines content f_c < f_{thre}. Their corresponding *CSL* in *e*-log(*p'*) plane will then be determined by simply converting the equivalent granular void ratios (*e**) of the unique *EG-CSL* into the global void ratios (*e*) of the specific mixture using Eq. (18). This will allow one to avoid the execution of an extensive number of triaxial tests (namely a set for each fines content) that are needed if the traditional approach based on the consideration of the global void ratio (*e*) as density state index is followed.

Using the concept of a unique *EG-CSL*, the *CSL* for one f_c can also be used to infer the *CSL* at another f_c as demonstrated in Rahman et al. (2010) and briefly summarized here for the sake of completeness. As illustrated in **Figure 114**, the *CSL* at a particular f_c can be transformed into the *EG-CSL* by using Eq. (18) to convert e to e^*. Since the conversion between e and e^* is dependent on both b and f_c, the *EG-CSL* thus obtained can then be used to infer the *CSL*s at a different f_c. The above figure highlights an excellent opportunity to estimate the *CSL* for sand with a particular fines content from a known *CSL* either for clean sand or for a sand with another fines content.

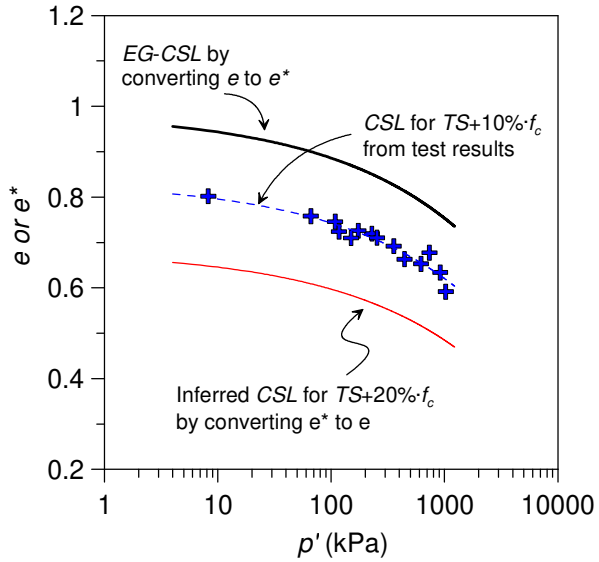

Figure 114 – Inferred *CSL* for unknown f_c using a *CSL* of known f_c.

7.1.4 Interpretation of the effects of fines content on the undrained cyclic resistance using the equivalent granular void ratio

The effects of fines on the liquefaction resistance ($CRR_{N=15}$) of sandy soils were also interpreted using the equivalent granular void ratio concept as the density state measure. As a first approximation, a constant value of b_{CRR}, i.e., b independent of fines content, was determined for the *TS*-fines mixtures considering a given consolidation vertical effective stress (σ'_{v0}=100 kPa) and different magnitudes of initial static shear stress ratio (α varying from 0 to 0.30).

According to the description made in paragraph 7.1.2, the values of b_{CRR} were inferred through a best fit procedure in which a power relationship was assumed to hold between $CRR_{N=15}$ and e^*; then b was varied iteratively up to minimizing the root mean squared deviation *RMSD* of the distance between the calculated values of $CRR_{N=15}$ =

f(*e**) and the reference $CRR_{N=15}$ vs. *e* curve of the clean sand. The best-fit $CRR_{N=15}$ - *e** curves for the different *α* values are shown in **Figure 115** (dashed lines).

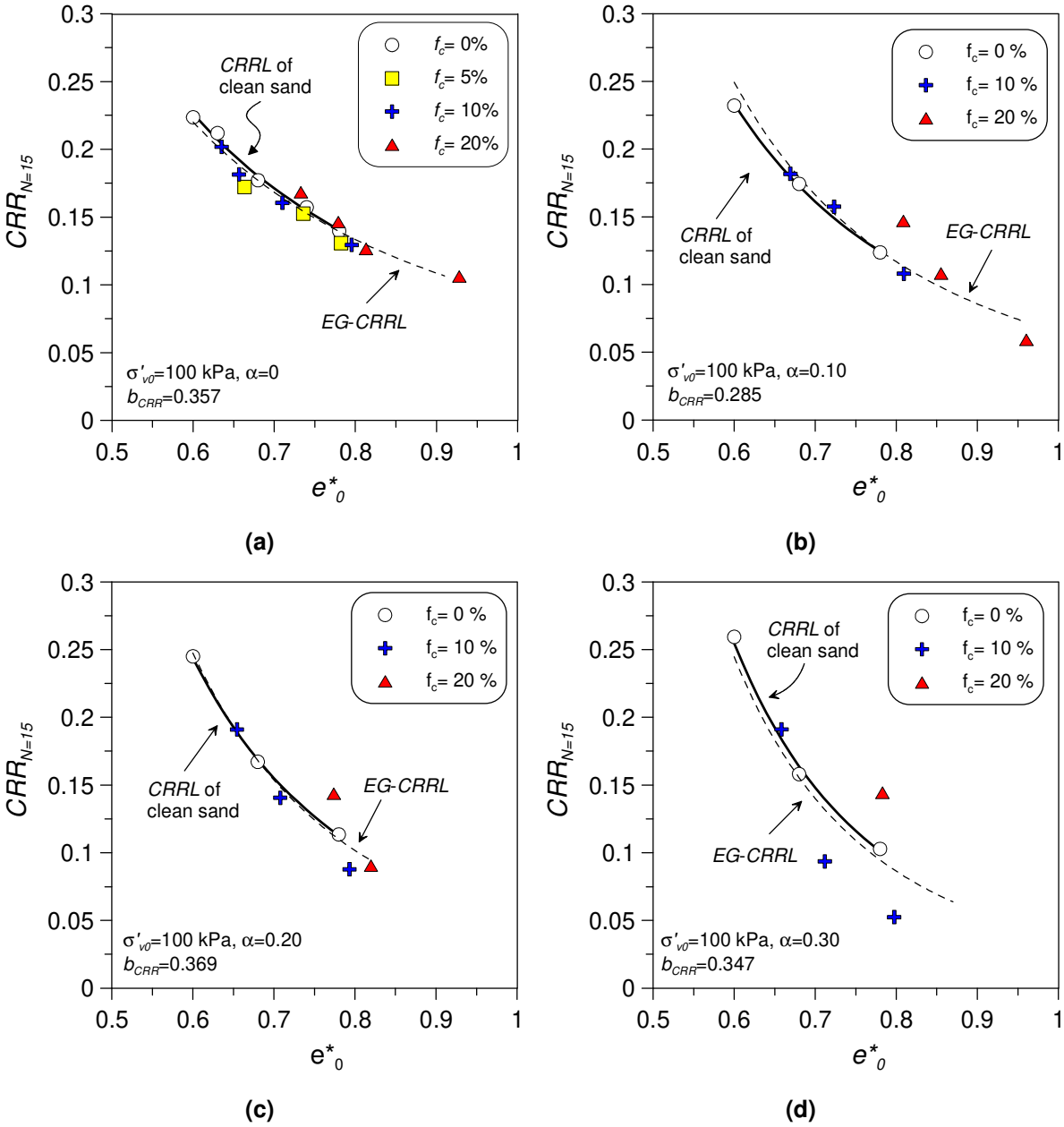

Figure 115 – Cyclic resistance ratio for N_f=15 cycles versus equivalent granular void ratio (*e) for *TS*-fines mixtures at constant initial vertical effective stress (σ'_{v0}=100 kPa) and variable void ratio (interpretation based on a constant value of b_{CRR}) for: (a) *α*=0; (b) *α*=0.10; (c) *α*=0.20 e (d) *α*=0.30.**

The relevant coefficients of determination are R^2=0.95, 0.90, 0.89, 0.65 for **Figure 115a**, **Figure 115b**, **Figure 115c** and **Figure 115d,** respectively). The curves are expressed by the following equations:

$$CRR_{N=15} = 0.090 \cdot (e^*)^{-1.740} \quad (\alpha = 0.00) \tag{34a}$$

$$CRR_{N=15} = 0.065 \cdot (e^*)^{-2.635} \quad (\alpha = 0.10) \tag{34b}$$

$$CRR_{N=15} = 0.051 \cdot (e^*)^{-3.092} \quad (\alpha = 0.20) \tag{34c}$$

$$CRR_{N=15} = 0.038 \cdot (e^*)^{-3.620} \quad (\alpha = 0.30) \tag{34d}$$

Figure 115 suggests that for a given α similar values of e^* correspond to similar cyclic resistance ratios for the *TS*-silt mixtures, regardless of fines content and global void ratio. It can be concluded that a unique correlation between $CRR_{N=15}$ and e^* can be established for the *TS*-fines mixtures reconstituted by the same method (i.e. having a given fabric). This correlation is here defined as the equivalent granular cyclic resistance ratio line, *EG-CRRL*.

Figure 116a illustrates, from data concerning moist tamped specimens reported in the literature and results obtained in the present study, that sand particle angularity has a similar effect on b_{CRR} values as previously found for b_{CSL} (**Figure 113a**).

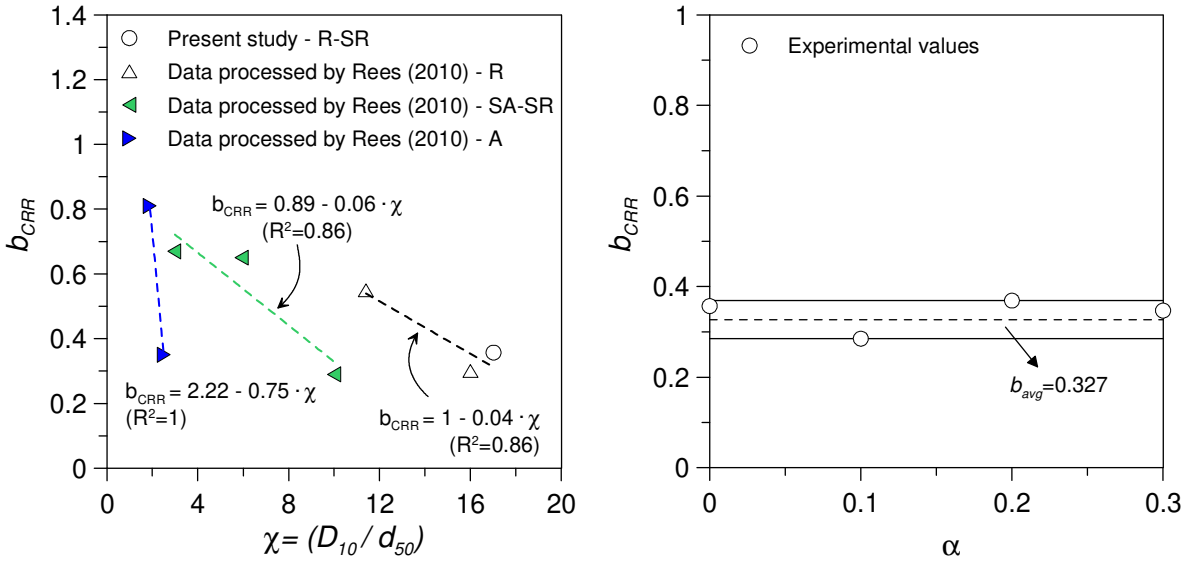

Figure 116 – Correlation of the fines influence factor values b_{CRR} with (a) particle size disparity ratio χ and angularity of the sand particles (Rees 2010) (i.e. *R-SR*=rounded to sub-rounded, *R*=rounded; *SA-SR*=sub-angular to sub-rounded, *A*=angular) for *MT* specimens tested with α=0; (b) magnitude of initial static shear stress $\alpha \neq 0$.

Sandy soils with more angular sand particles tend to have lower b_{CRR} values for a similar particle size disparity ratio χ. The effect that the presence of an initial static shear stress exerts on the factor b_{CRR} has also been studied in the present research (**Figure 116b**) and it has been observed that it is not substantially influenced by this

factor. Within the considered range of α, b_{CRR} varies between 0.285 and 0.369 with an average value of 0.327.

It is interesting to examine the difference between the fines influence factor b_{CSL} derived from undrained monotonic triaxial tests and the fines influence factor b_{CRR} calculated based on undrained cyclic simple shear tests. Their values are respectively 0.28 in the former tests and 0.36 in the latter ones, suggesting that approximately 28% of the fines participate in the soil force-chains during monotonic loading, and 36% participate during cyclic loading. Since the specimens were prepared using the same method the observed difference would suggest that the participation of the fines in the soil force-chains varies with the loading features.

The reliability of the equivalent granular void ratio approach in evaluating b_{CRR} can be improved by considering b values depending on the fines content. Thus, for a given mixture, the value of b_{CRR}, according to Eq. (18), was determined by back-analysis of the data available for each specific fines content. The evaluation was made using the same iterative procedure described in paragraph 7.1.2. The calculations were repeated for each f_c, and **Figure 117** presents the values of b_{CRR} obtained (filled circles) as a function of the fines content (normalized to the threshold value). As it can be seen b_{CRR} increases with fines content evidencing a higher contribution of the fines in the force transmission chains of the mixtures. For example, the data in **Figure 117a** would suggest that for f_c=20%, approximately 40% of the fines particles actively participate in the force transmission.

Rahman et al. (2008) developed the semi-empirical equation (20) for predicting b values where simple input parameters are required. The capability of this equation was evaluated by comparing the trend line of b_{CRR} derived from the $CRR_{N=15}$ measured in the undrained cyclic tests with the corresponding ones obtained from Eq. (20) (dashed line in **Figure 117**).

Figure 117 shows that in most cases the experimentally based b-values are higher than the corresponding ones calculated from Eq. (20) and the overestimation increases with increasing fines content. Nevertheless, when the calculations were conducted using values of the empirical parameters μ and n calibrated on the basis of the data set of the present study (solid line in **Figure 117**), the experimentally based points and the curve determined by Eq. (20) appeared to have a similar trend.

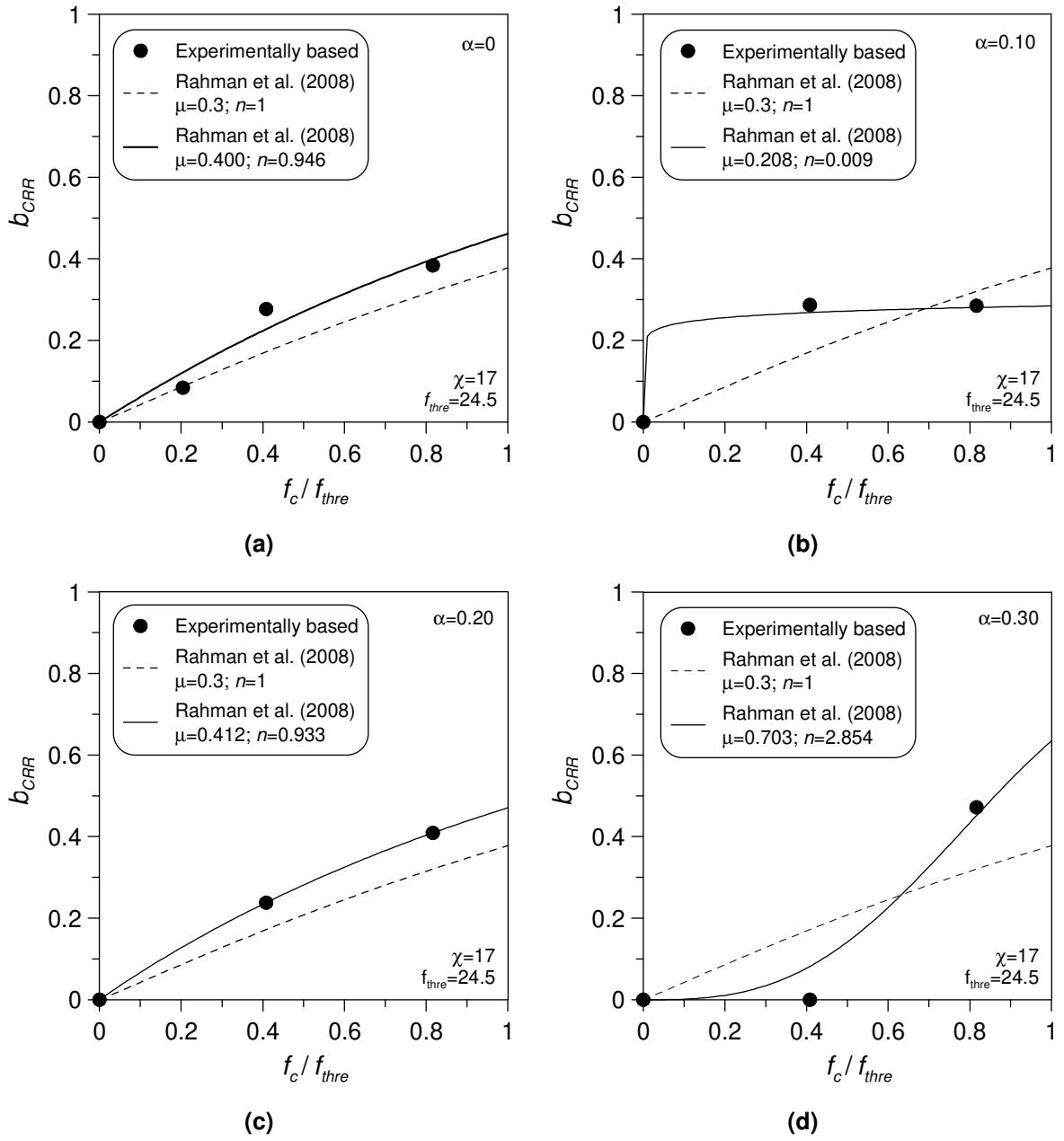

Figure 117 – Relationship between b_{CRR} and f_c/f_{thre} for: (a) α=0; (b) α=0.10; (c) α=0.20 e (d) α=0.30, and comparison with the semi-empirical correlation of Rahman et al. (2008).

The $CRR_{N=15}$ - e^* data in **Figure 118** are based on variable, f_c dependent, b_{CRR} values. The best-fit $CRR_{N=15}$ - e^* relationships for all data (dashed lines in **Figure 118**) have coefficient of determination R^2=0.98, 0.91, 0.93, 0.88 respectively for **Figure 118a**, **Figure 118b**, **Figure 118c** and **Figure 118d**). Their trends can be described by the following equations:

$$CRR_{N=15} = 0.089 \cdot (e^*)^{-1.833} \quad (\alpha = 0.00) \tag{35a}$$

$$CRR_{N=15} = 0.065 \cdot (e^*)^{-2.634} \quad (\alpha = 0.10) \tag{35b}$$

$$CRR_{N=15} = 0.049 \cdot (e^*)^{-3.296} \quad (\alpha = 0.20) \tag{35c}$$

$$CRR_{N=15} = 0.033 \cdot (e^*)^{-4.296} \quad (\alpha = 0.30) \tag{35d}$$

It is evident that the differences between the *EG-CRRL* of the sand-silt mixtures and the benchmark response of the clean sand (*CRRL*) are in general smaller in **Figure 118**, based on a variable *b* value, than in **Figure 115**, based on a constant one.

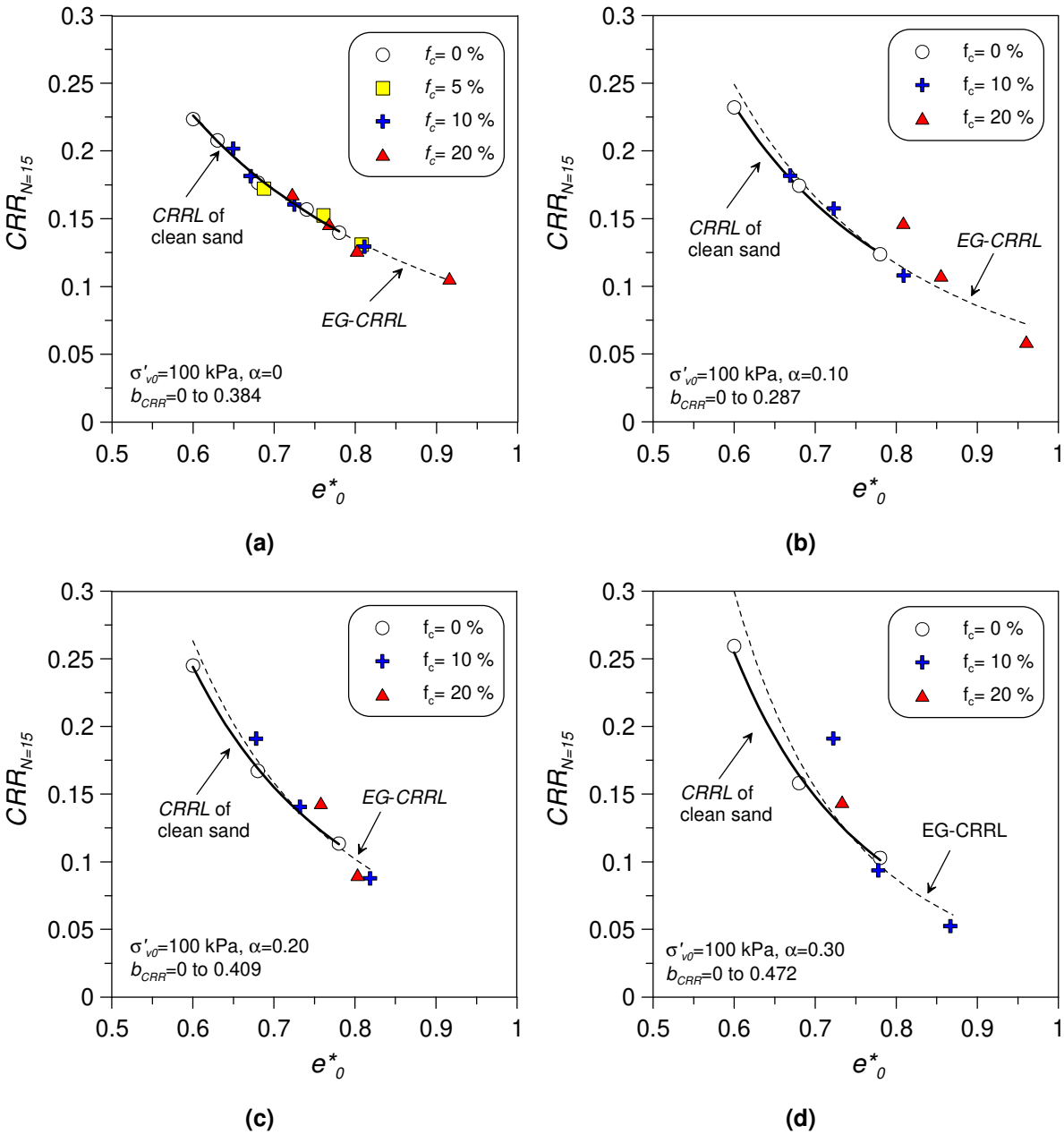

Figure 118 – Cyclic resistance ratio for N_f=15 cycles versus equivalent granular void ratio (e^*) for *TS*-fines mixtures at constant initial vertical effective stress (σ'_{v0}=100 kPa) and variable void ratio (interpretation based on b_{CRR} variable with fines content) for: (a) α=0; (b) α=0.10; (c) α=0.20 e (d) α=0.30.

The performance of the two approaches based on back-analysis, using, namely: (1) a constant *b* irrespective of fines content (**Figure 115**); and (2) *b* increasing with fines content (**Figure 118**), can be compared through the values of the determination coefficient R^2 of the best fit curves. As can be inferred from the data reported before, the smaller R^2 concerns the variable *b* approach. As conclusive remark, it can be stated that the equivalent granular void ratio concept in combination with the consideration of the undrained cyclic resistance ($CRR_{N=15}$) of the clean sand can be reliably used for predicting the liquefaction resistance of the same sand mixed with different non-plastic fines content in the range $f_c < f_{thre}$, provided that reliable values of *b* are adopted. Note that in case of clean sand (f_c = 0%), e^* is equal to *e*.

7.2 Interpretation using equivalent granular state indices

7.2.1 The concepts of equivalent granular state parameter, equivalent pressure index and equivalent modified state parameter

According to the critical state soil mechanics, sand behaviour in shearing is controlled by its corresponding position in *e-p'* space. In other words, it is the combination of stress level (*p'*) and relative density (as a function of *e*), not density alone, that determines the sand behaviour. Stress level modifies the behaviour of the material in a way that even dense samples, when consolidated under sufficiently high confining pressures, can behave similarly to loose samples tested at lower pressures (Been and Jefferies 1985). “State” is defined as the corresponding position of the soil in the *e-p'* space. In the previous chapter (chapter 6) the effectiveness of the critical state soil mechanics in interpreting the behaviour of non-plastic sand-silt mixtures was verified for fines contents lower than the threshold fines content (sand controlled behaviour). If e^* is used instead of *e*, this definition of state can be generalized to e^*-*p'* space, where in addition to the *e* and *p'*, the value of f_c controls the location of the soil state, and thus plays the role of a state variable.

Using e^* and e^*_{CS} (the void ratio related to *EG-CSL*) in lieu of *e* and e_{CS} respectively, it is possible to redefine the distance with respect to the critical state. Following this approach, a revised form of the state parameter Ψ, named equivalent granular state parameter Ψ^* was defined by Rahman (2012) as:

$$\Psi^* = e^* - e^*_{CS} \tag{36}$$

to be used for sands containing fines. Recently, various authors (Rahman et al. 2011; Huang and Chuang 2011; Rahman and Lo 2012; Rahman and Sitharam 2020; Porcino

et al. 2019b; Porcino et al. 2021) correlated the undrained monotonic and cyclic resistance of non-plastic silty sands with different fines contents below the threshold value, with Ψ^*. Baki et al. (2012) found that the results of monotonic and cyclic tests performed on samples with the same Ψ^* were well correlated to each other. Using *EG-CSL* as reference line, instead of *CSL,* for sands containing fines also the pressure index can be converted in an equivalent pressure index (revised form of the pressure index I_p defined by Klotz and Coop (2001)):

$$I_p^* = p'/p'_{CS} \tag{37}$$

where p'_{CS} is the mean effective stress on the *EG-CSL* at the current e^*. This state parameter was used recently to interpret the monotonic and cyclic triaxial test results for sand containing non-plastic silt (Qadimi and Mohammadi, 2014) but further verification is needed.

Combining Ψ^* and I_p^*, it is possible to introduce the equivalent modified state parameter Ψ^*_m (revised form of the modified state parameter Ψ_m defined by Bobei et al., 2009) as:

$$\Psi_m^* = \Psi^* \cdot \left|1 - \left(1/I_p^*\right)\right| \cdot e^* \tag{38}$$

This state parameter was also used recently to interpret the monotonic and cyclic triaxial test results for sand containing non plastic silt (Qadimi and Mohammadi 2014); once again more efforts are required to confirm the obtained results.

The state parameter Ψ, the pressure index I_p, and the modified state parameter Ψ_m are the most commonly used state indices to describe the behaviour of sandy soils (Been and Jefferies 2004; Bobet et al. 2009; Coop 2003; Coop et al. 2005; Qadimi 2005; Stamatopoulos 2010). The state indices are capable of combining the effect of fines content, density and stress level on the soils' behaviour and can be used to predict the monotonic and cyclic strength of sands with different amounts of fines (Huang and Chuang 2011; Stamatopoulos 2010). However, employing these state indices for sands with different fines contents would require a large number of triaxial tests in order to ascertain the critical state lines of all mixtures, owing to the fact that any state index, according to the original definition, should be referenced to the *CSL* of the specific material investigated. Previous studies conducted in literature have demonstrated that the state indices defined in terms of e^*, similarly to the conventionally defined state indices, are capable of predicting the soil behaviour at different fines contents, densities and stress levels. In other words, defining the state indices in terms of e^* does not meaningfully influence their effectiveness in

characterizing soil behaviour. Nevertheless using the equivalent state indices instead of the traditional ones has an important advantage from the practical point of view since they allow to minimize the required experimental work. The reference line that the equivalent indices are linked with, at every f_c, is the *EG-CSL* (**Figure 112b**). Considering the coincidence between the *EG-CSL* and the *CSL* of clean sand, the latter one can be used as reference line for the sand- silt mixtures at every f_c (lower than f_{thre}). This leads to a significant reduction in the required experimental data. The capability of Ψ^*, I_p^* and Ψ^*_m to reduce the amount of the experimental data needed for predicting the relevant parameters of sands with different fines contents will be further discussed in the following. In the next paragraphs their capability to predict the undrained monotonic and cyclic behaviour of the materials investigated in this study is presented.

7.2.2 Prediction of undrained monotonic behaviour of Ticino silty sand

The results derived from processing the data of undrained monotonic triaxial tests are illustrated in **Figure 119, Figure 120** and **Figure 121**. **Figure 119a**, **b**, **c** and **d** show the trends of the instability stress ratio, the normalized liquefaction potential, the transformation phase stress ratio, and the normalized critical state resistance against $\Psi^*_{(0)}$, respectively. The relevant values for *b* taken to calculate the initial e^* of the samples for each mixture are the same as the ones previously used to identify the *EG-CLS* in **Figure 112b**. The R^2 values given in the figures resulted from the regressions analyses conducted on all the data together. It is evident that the use of $\Psi^*_{(0)}$ instead of $\Psi_{(0)}$ doesn't meaningfully improve the scatter in the data, so that a unique correlation can be considered appropriate for both cases.

The results obtained in this section prove that the relationships between the undrained monotonic soil behaviour indices and the equivalent state parameter for clean sand can be considered representative even for mixtures with fines contents below f_{thre}, providing that the *b* value is selected correctly. The same conclusion applies to the equivalent pressure index $I^*_{p(0)}$ and to the equivalent modified state parameter $\Psi^*_{m(0)}$ as it can be inferred from the data reported in **Figure 120** and **Figure 121** respectively. If a comparison is made among the performances of the equivalent granular indexes taken into account in the analyses described above, the equivalent granular state parameter is the index that exhibits the highest values of R^2 in most of the correlations shown in the previous figures (**Figure 119** to **Figure 121**).

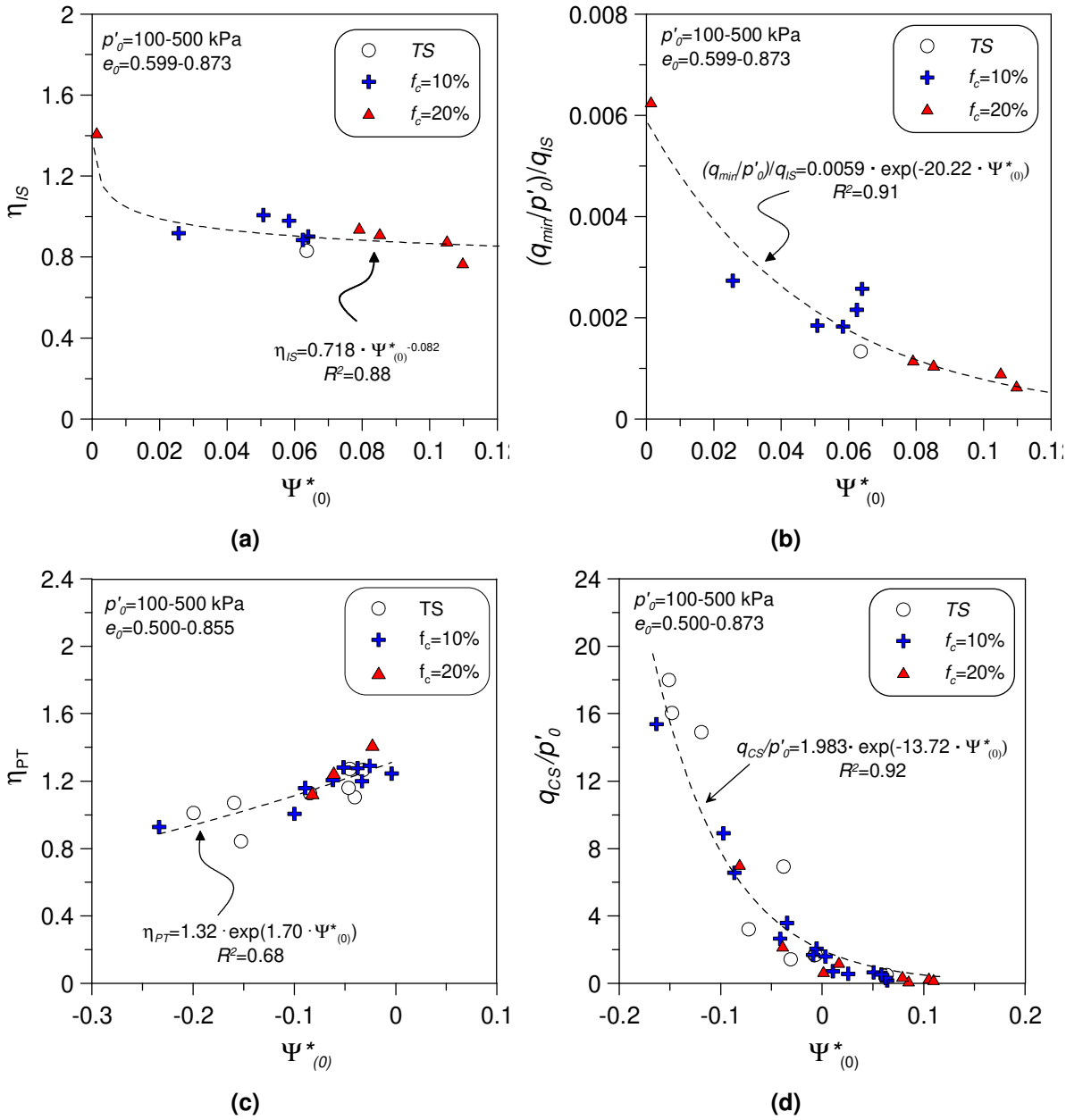

Figure 119 – Variation of (a) η_{IS}, (b) $(q_{min}/p'_0)/q_{IS}$, (c) η_{PT} and (d) q_{CS}/p'_0 for non-plastic Ticino sand–silt mixtures with equivalent granular state parameter $\Psi^*_{(0)}$.

For this reason, in the following paragraph the prediction of the undrained cyclic behaviour of the investigated *TS* with fines mixtures is based on the equivalent granular state parameter Ψ^*.

In **Figure 122** the initial states (i.e. the states just prior to shearing) of the undrained monotonic triaxial tests conducted on *TS* sand-silt mixtures were plotted in e^* - p'_0 space. As it can be seen the data points that clearly lie below the *EG-CSL* ($\Psi^*_{(0)}<0$) all correspond to non-flow (*NF*) type behaviour while those located above the *EG-CSL* ($\Psi^*_{(0)}>0$) mainly belong to limited flow (*LF*) and flow (*F*) type behaviour with the latter

ones occupying the upper part of the diagram. Some small deviations from this trend should be ascribed to the fact that differentiating flow and non-flow behaviour can be sometimes complicated.

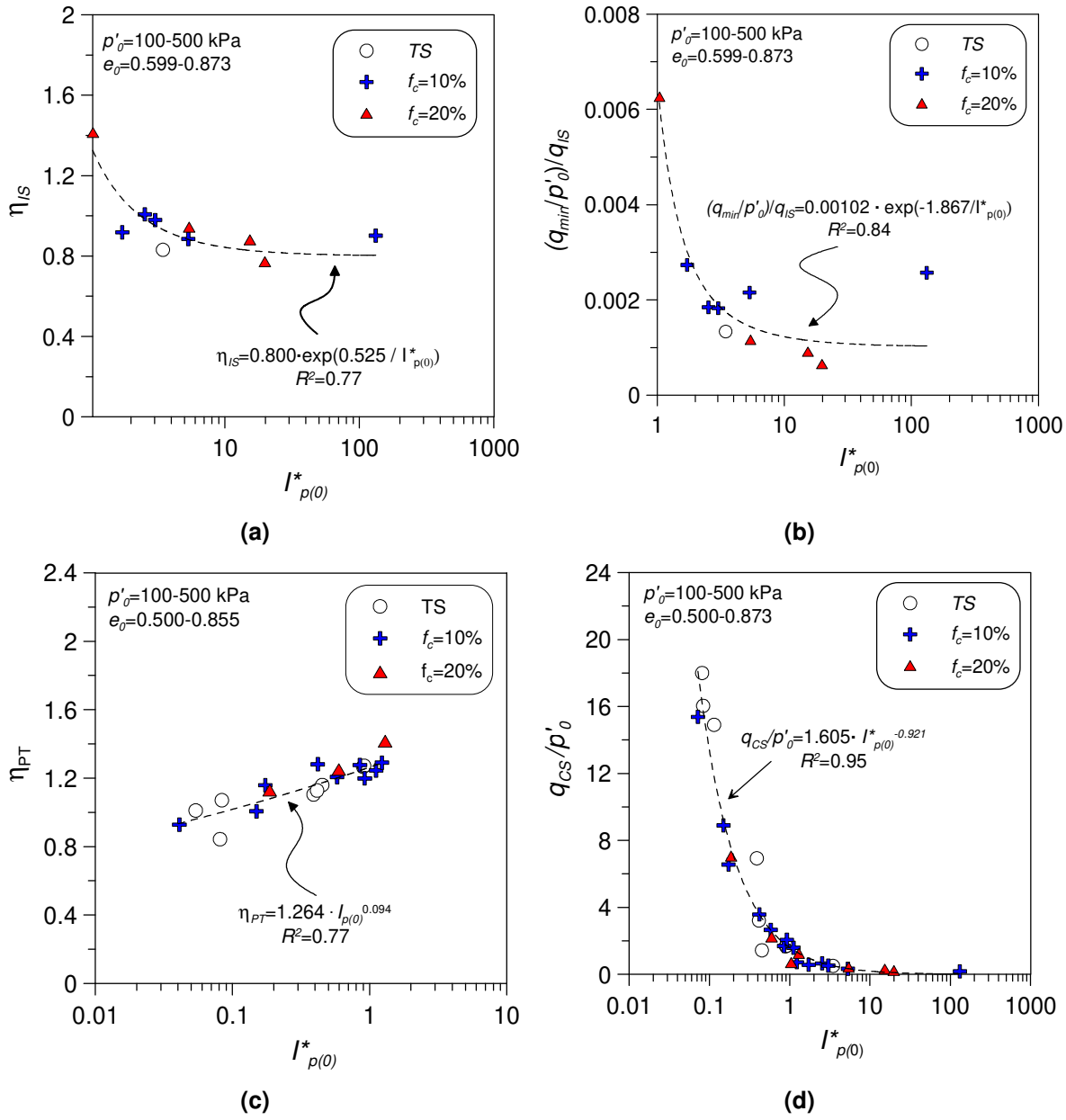

Figure 120 – Variation of (a) η_{IS}, (b) $(q_{min}/p'_0)/q_{IS}$, (c) η_{PT} and (d) q_{CS}/p'_0 for non-plastic Ticino sand-silt mixtures with equivalent pressure index $I^*_{p(0)}$.

It turns out that values of $\Psi^*_{(0)}$ tend to increase (from negative to positive) moving from specimens that exhibit non flow type behaviour to those exhibiting flow type behaviour; specimens showing limited flow behaviour have positive intermediate values. This is confirmed by the curves reported in **Figure 123**. This figure depicts the stress paths

and the stress strain curves obtained in undrained monotonic triaxial tests carried out on some specimens represented by points in **Figure 122**.

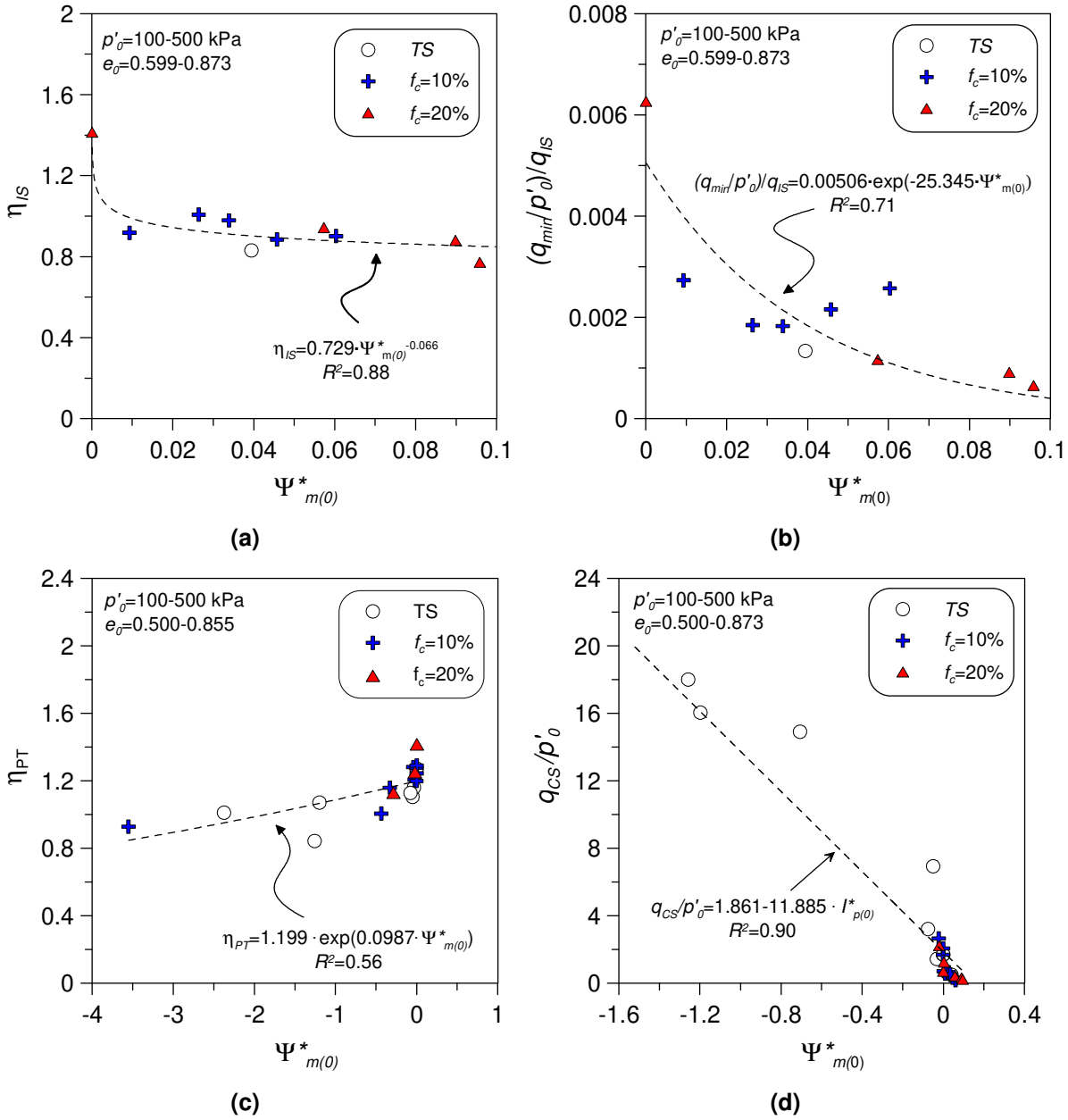

Figure 121 – Variation of (a) η_{IS}, (b) $(q_{min}/p'_0)/q_{IS}$, (c) η_{PT} and (d) q_{CS}/p'_0 for non-plastic Ticino sand- mixtures with the equivalent modified state parameter $\Psi^*_{m(0)}$.

It is interesting to note that, regardless of the initial global void ratio, initial mean effective stress and fines content, the behaviours observed are in good agreement with the critical state theory framework, namely: specimens with $\Psi^*_{(0)}$ greater that 0 exhibit flow or limited flow behaviour, and specimens with $\Psi^*_{(0)}$ less than 0 exhibit non-flow behaviour.

7.2.3 Prediction of the undrained cyclic resistance of Ticino silty sand using $\Psi^*_{(0)}$

In this section the equivalent granular state parameter $\Psi^*_{(0)}$ was used to predict the undrained cyclic resistance of Ticino silty sand. In **Figure 124**, $CRR_{N=15}$ is plotted versus $\Psi^*_{(0)}$, for different values of the initial static shear stress (α varying from 0 to 0.30).

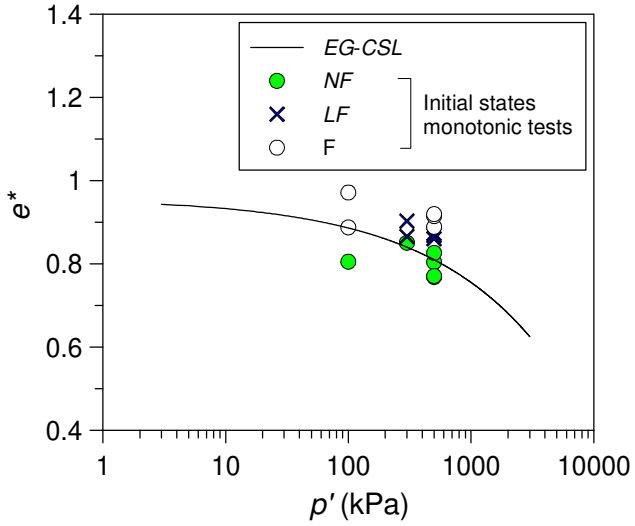

Figure 122 – *EG-CSL* for Ticino sand-silt mixtures and the initial states of the undrained monotonic tests.

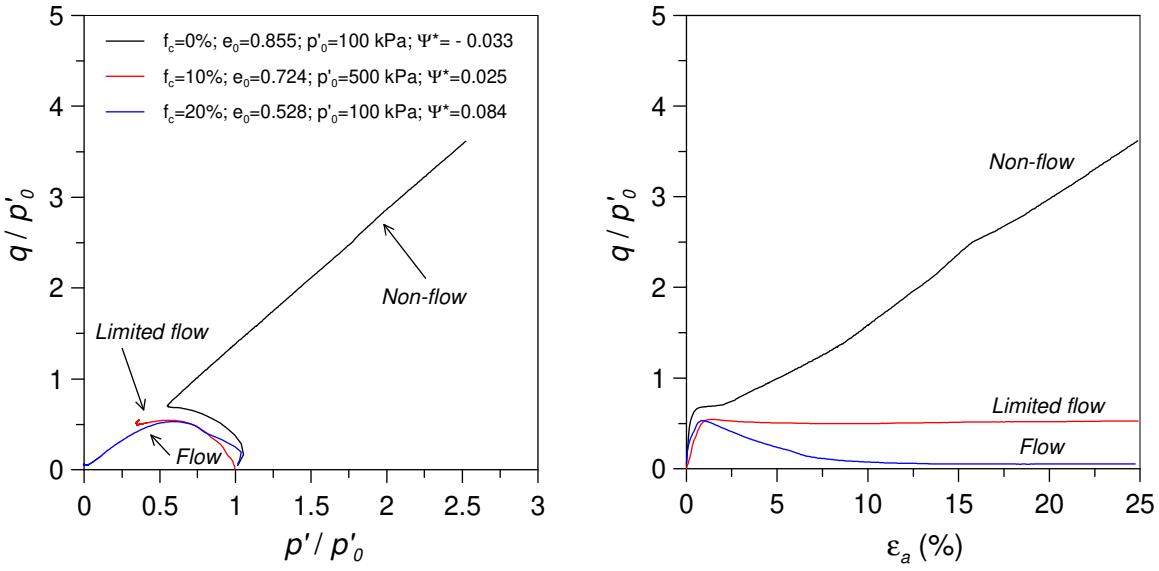

(a) **(b)**

Figure 123 – Various forms of undrained monotonic behaviour: (a) effective stress-path, and (b) stress-strain behaviour.

A clear trend between the $CRR_{N=15}$ and Ψ^*_0 is observed, with a limited scatter of the data irrespective of the fines contents around the experimental points of the clean

sand. In particular the scatter is significantly smaller than that exhibited by the $CRR_{N=15}$ – $\Psi_{(0)}$ plot in **Figure 107**. The best-fit relationships describing the experimental data in **Figure 124** are expressed by the following exponential equations:

$$CRR_{N=15} = 0.109 \cdot exp\left(-2.282 \cdot \Psi^*_{(0)}\right) \quad (\alpha = 0.00) \tag{39a}$$

$$CRR_{N=15} = 0.094 \cdot exp\left(-2.992 \cdot \Psi^*_{(0)}\right) \quad (\alpha = 0.10) \tag{39b}$$

$$CRR_{N=15} = 0.074 \cdot exp\left(-3.988 \cdot \Psi^*_{(0)}\right) \quad (\alpha = 0.20) \tag{39c}$$

$$CRR_{N=15} = 0.060 \cdot exp\left(-4.923 \cdot \Psi^*_{(0)}\right) \quad (\alpha = 0.30) \tag{39d}$$

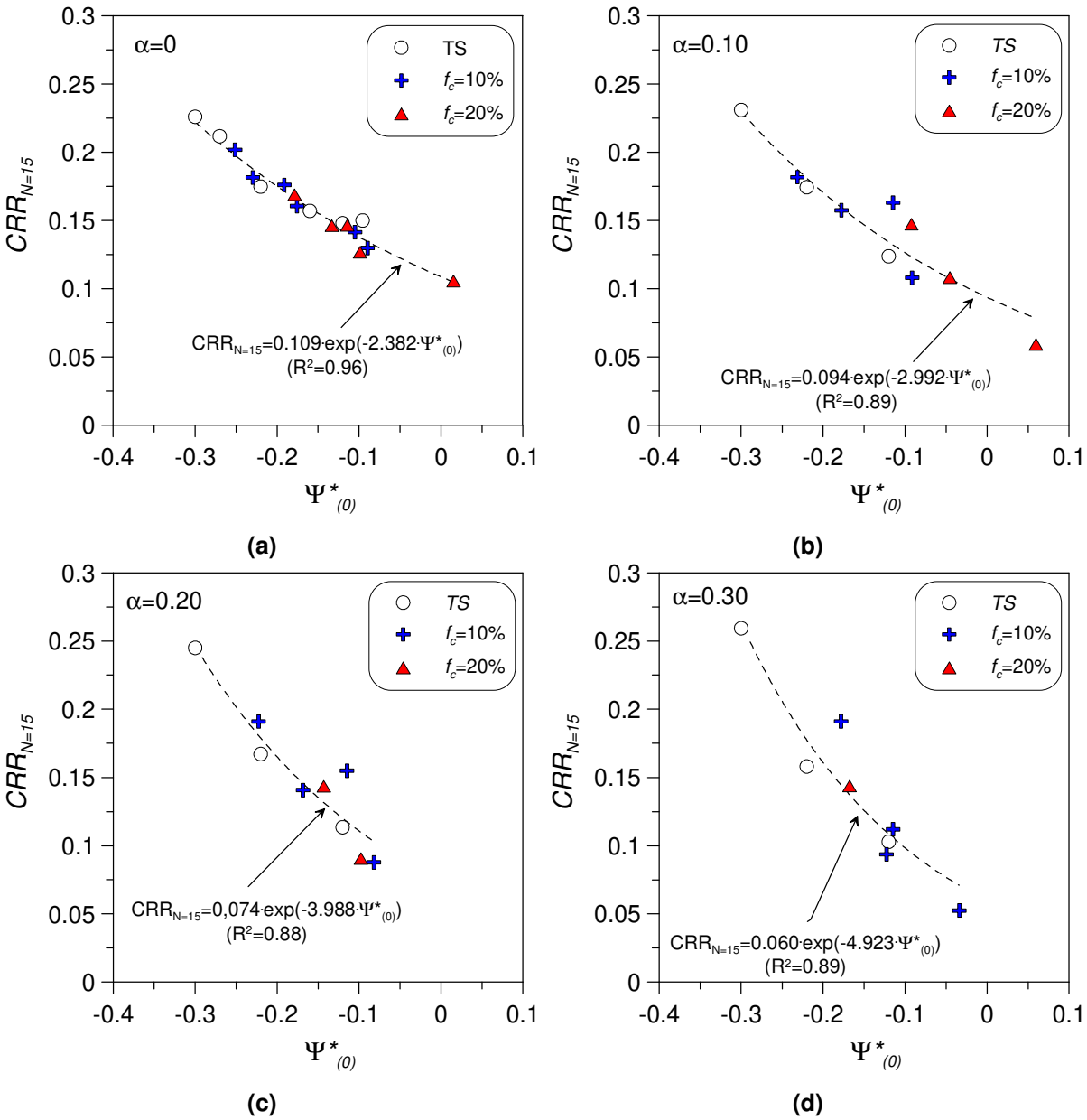

Figure 124 – Variation of undrained cyclic resistance $CRR_{N=15}$ for non-plastic Ticino sand-silt mixtures (f_c<f_{thre}) with equivalent granular state parameter Ψ^* for different initial static shear stresses: (a) α=0, (b) α=0.10, (c) α=0.20 and (d) α=0.30.

The corresponding determination coefficients R^2 are 0.96, 0.89, 0.88 and 0.89, respectively. The trends of the curves in **Figure 124** show that $CRR_{N=15}$ increases as $\Psi^*_{(0)}$ becomes more negative. This is consistent with the fact that more negative values of $\Psi^*_{(0)}$ are indicative of a more dilative soil behaviour. The slope of the curves is more pronounced as the value of the initial static shear stress ratio (α) increases. **Figure 125** summarises this feature evidencing the existence of a clockwise rotation of the best fit curves around a value of the equivalent state parameter equal to $\Psi^*_0 = -0.225$, that identifies those initial states for which the undrained cyclic resistance $CRR_{N=15}$ is unaffected by the initial static shear stress.

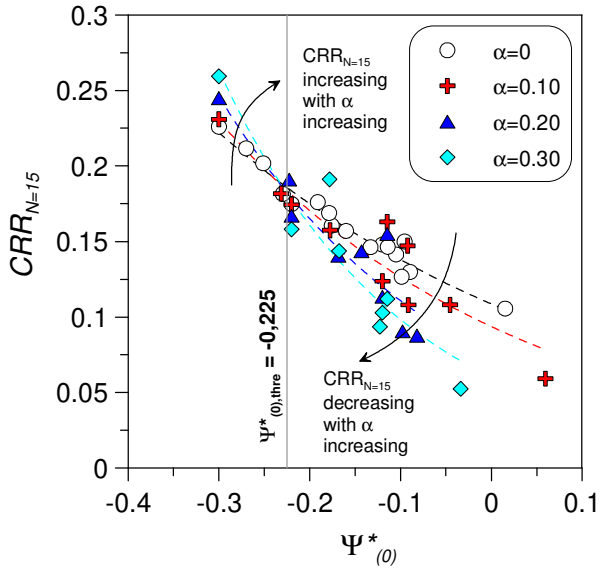

Figure 125 – Clockwise rotation of the $CRR_{N=15}$-$\Psi^*_{(0)}$ correlation of Ticino clean sand under different values of α.

In the present research the tests in which the equivalent granular state parameter took positive values ($\Psi^*_{(0)} > 0$) were relatively few and all corresponded to high fines contents. The trend of the curves in the positive range of $\Psi^*_{(0)}$ should be more precisely defined by performing more tests on specimens reconstituted at high fines contents.
Recently, a number of investigations involving cyclic triaxial tests have demonstrated the suitability of the state parameter Ψ and its revised form Ψ^*, for predicting the undrained cyclic strength of sands with different fines contents, densities, and stress levels. However, all these studies involved cyclic triaxial tests while, in the present study, the approach was for the first time investigated basing on cyclic simple shear tests which better represent the conditions in the ground before and during an

earthquake. Furthermore, this approach has been successfully applied, once again for the first time, taking into account the presence of an initial static shear stress.

The analysis of literature data, restricted to the symmetrical loading condition (i.e. α=0), along with the data gathered from the present study, evidenced that the CRR-$\Psi^*_{(0)}$ correlation is dependent on the properties of the host sand and the fines, the fabric (or sample preparation method), and the type of test or loading path. This is apparent in **Figure 126** where the CRR-$\Psi^*_{(0)}$ relationships derived from previous studies (Jefferies and Been 2006; Huang and Chuang 2011; Rahman and Sitharam 2020) are shown together with the data obtained in the present study.

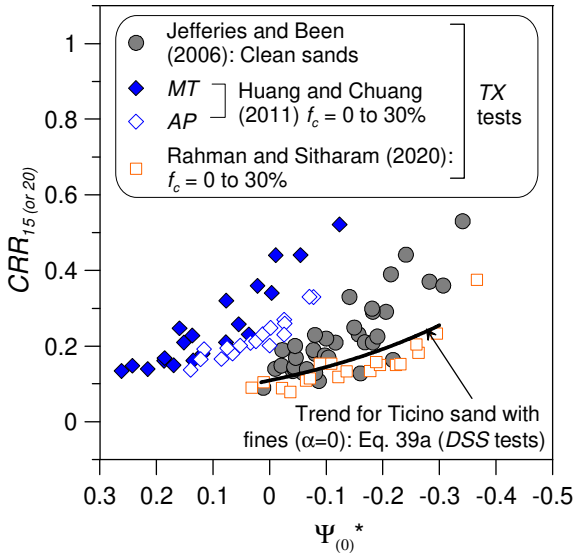

Figure 126 – Relation between CRR and $\Psi^*_{(0)}$: comparison between data from the present study (α=0) and published data from Jefferies and Been (2006), Huang and Chuang (2011), and Rahman and Sitharam (2020).

The relationships found in the literature are based on undrained cyclic triaxial tests performed on several granular soils, reconstituted by different methods, namely, (1) 13 clean sands tested with different reconstitution methods (Jefferies and Been 2006); (2) sand-fines mixtures (f_c = 0%–30%, PI < 8) prepared by moist tamping or air pluviation (Huang and Chuang 2011); and (3) sand fines mixtures (f_c=0-30%, PI=1.57) reconstituted by air pluviation (Rahman and Sitharam 2020). Superimposed in **Figure 126** is the trend for Ticino sand with non-plastic fines (Eq. 39a) determined in the present research from undrained cyclic simple shear tests. It agrees quite well with the data by Rahman and Sitharam (2020) but predicts lower $CRR_{N=15}$ values than those measured by Jefferies and Been (2006) and Huang and Chuang (2011).

In the following an attempt has been made to use the *EG-CSL* to predict the undrained cyclic failure pattern observed in *DSS* tests taking also into account the effect of an initial static shear stress. It is well known that liquefaction of clean sands under undrained cyclic loading can occur in two different patterns, cyclic mobility and cyclic instability, the latter being also termed flow liquefaction or limited flow liquefaction. When there is the presence of an initial static shear stress, plastic strain accumulation can be also observed. In silty sands, the type of behaviour can be affected by the presence of fines. The parameter Ψ^* enables an estimate of the failure type to be expected.

Firstly, the results of the undrained cyclic simple shear tests, without an applied initial static shear stress, were examined in terms of the equivalent granular state parameter Ψ^*. A cyclic mobility type behaviour is expected for the samples tested with initial conditions well below the *EG-CSL*, i.e., $\Psi^*_{(0)}<0$, whereas a cyclic instability (in this case limited flow liquefaction) type behaviour, is anticipated for initial states above the *EG-CSL*, i.e., $\Psi^*_{(0)}>0$. Further, it is hypothesized that soil specimens with an identical initial fabric, but different combinations of the initial void ratio, initial mean effective stress, and fines content, will exhibit a similar type of behaviour under undrained cyclic loading, provided that the state parameter $\Psi^*_{(0)}$ is the same. The initial conditions (e^*_0, p'_0) of all specimens with $f_c < f_{thre}$ (24.5%) tested in the present study in undrained cyclic *DSS* tests with α=0 relative to the *EG-CSL* are presented in **Figure 127**. Evidently, almost all points fall well below the *EG-CSL* ($\Psi^*_{(0)}<0$), which means that a cyclic mobility type behaviour should be expected for most of the specimens, while a limited flow liquefaction behaviour should be observed only in a few tests. **Figure 128** presents the normalized shear stress (τ/σ'_{v0}) versus shear strain (γ) response and the normalized effective stress path regarding two pairs of undrained cyclic *DSS* tests having clearly negative $\Psi^*_{(0)}$ values. In particular, the test pair with $\Psi^*_{(0)}$= - 0.168 ± 0.008 concerns clean *TS* sand and a silty sand mixture with f_c = 10% (**Figure 128a**) and the test pair with $\Psi^*_{(0)}$ = - 0.185 ± 0.006 concerns silty sand mixtures with f_c = 10% and 20% respectively (**Figure 128b**). In all cases, the observed behaviour can be categorized as cyclic mobility. Thus, the equivalent granular state parameter $\Psi^*_{(0)}$ appears to be a suitable measure for predicting the type of behaviour in undrained cyclic *DSS* tests on silty sands. It enables a unified description of the response of sand with fines within the context of the *CSSM* theory, provided that $f_c < f_{thre}$.

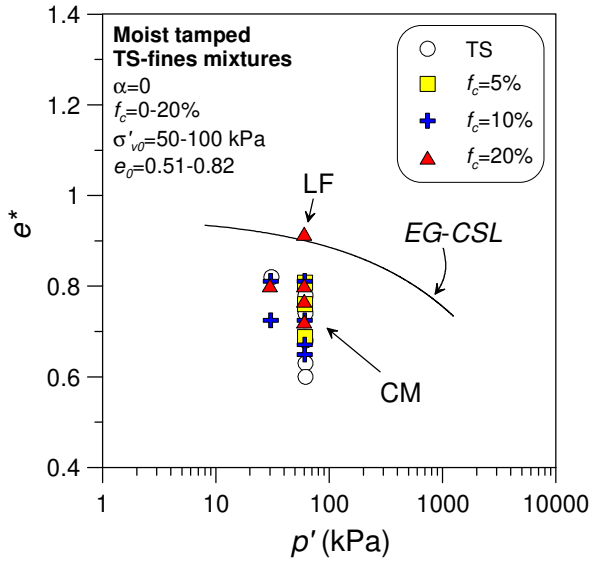

Figure 127 – Initial positions of the specimens tested in undrained cyclic simple shear tests with *α*=0, relative to *EG-CSL*.

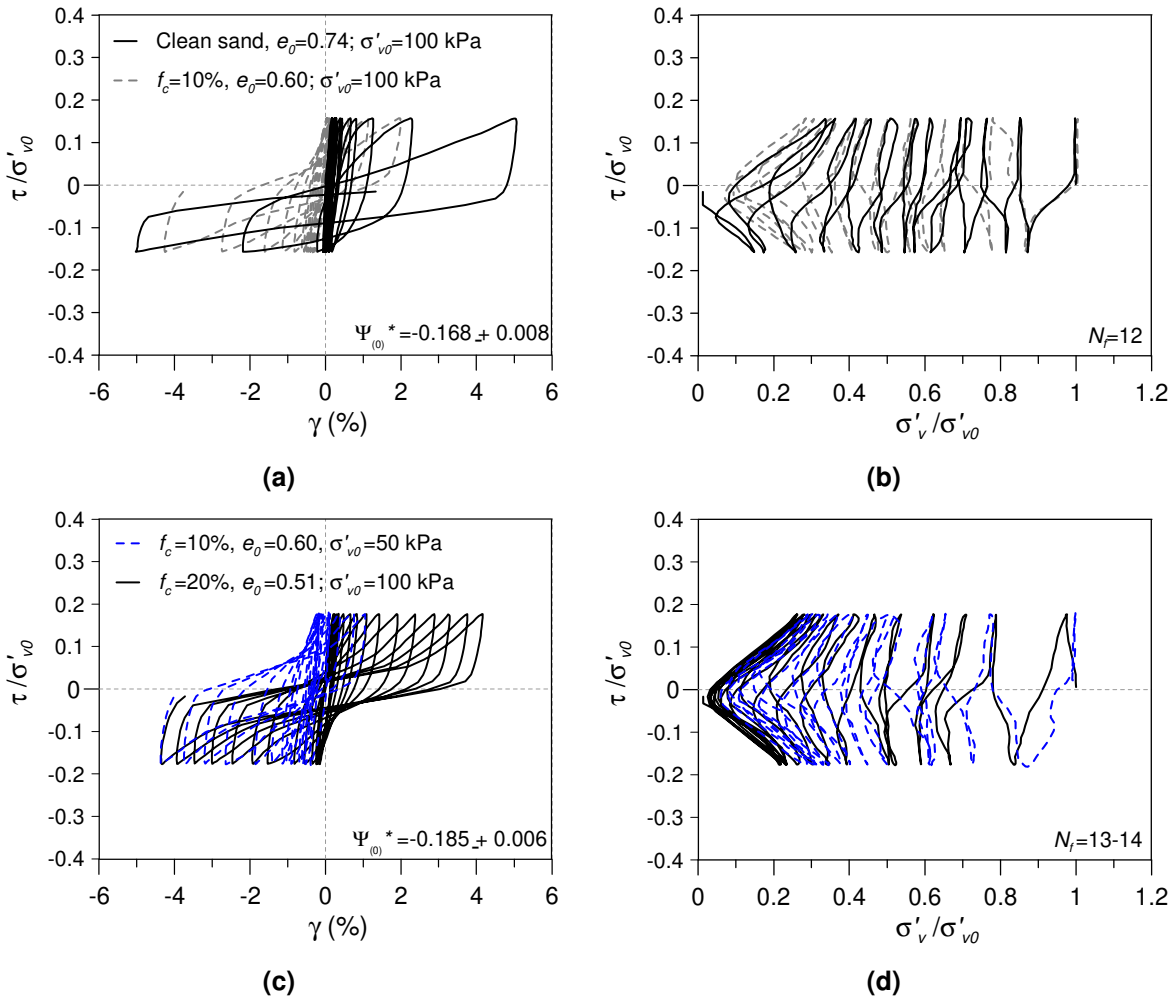

Figure 128 – Shear stress-shear strain relationship and effective stress paths from *DSS* tests on *TS*-fines mixtures with similar initial conditions (*Ψ*$_{(0)}$*<0). All tests show cyclic mobility in their final phase.

The same procedures can be applied for tests conducted in the presence of an initial static shear stress. Besides the position of the initial state with respect to the equivalent granular critical state line, an important parameter, in this case, is the ratio between the applied cyclic shear stress and the applied initial static shear stress. In **Figure 129a** the initial state conditions (e^*_0, p'_0) of all specimens with $f_c < f_{thre}$ investigated in undrained cyclic *DSS* tests with α varying between 0.05 to 0.30 are superimposed on the *EG-CSL*, while in **Figure 129b** the cyclic stress ratios *CSR* applied on specimens with $\alpha \neq 0$ are plotted as a function of α. As it can be seen from **Figure 129a** almost all points fall well below the *EG-CSL* ($\Psi^*_{(0)}<0$), but, in this case, contrary to what was observed in tests without initial static shear stress, not only cyclic mobility (*CM*) but also plastic strain accumulation (*PSA*) and an intermediate (*INT*) behaviour between cyclic mobility and plastic strain accumulation are observed. Flow liquefaction was observed only in the test with $\Psi^*_{(0)}>0$.

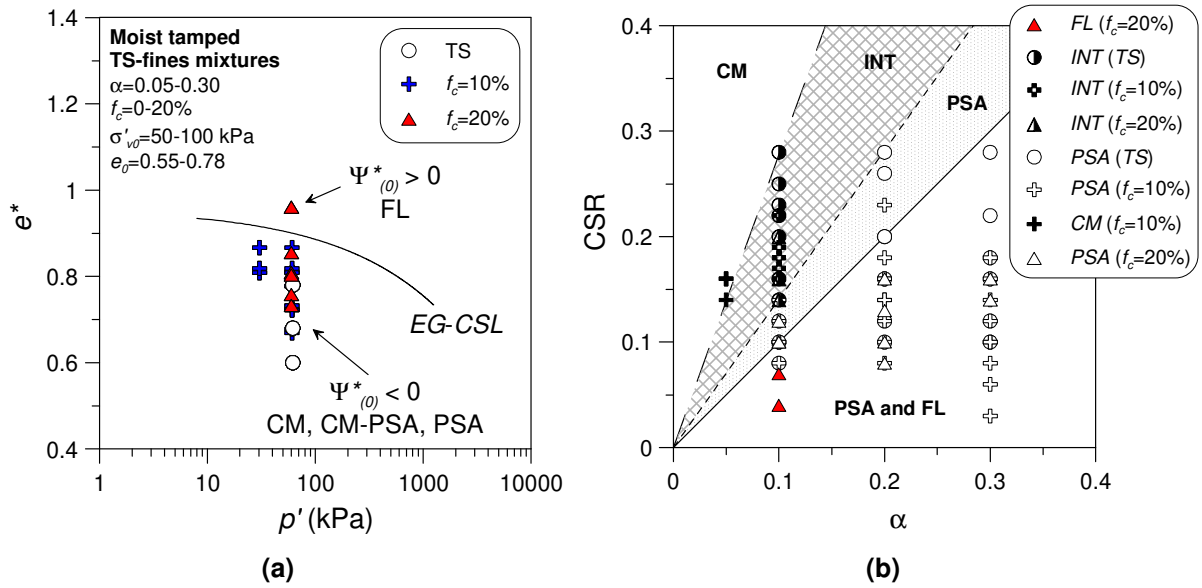

Figure 129 – (a) Initial positions of the specimens tested in undrained cyclic simple shear tests relative to *EG-CSL* with different initial static shear stresses: α=0.10, α=0.20 and α=0.30 and (b) magnitude of applied cyclic shear stress ratio against initial static shear stress with zones of observed failure patterns.

Having a closer look at **Figure 129b** one can infer that *PSA* is the most predominant failure pattern and it happens when the cyclic shear stress is relatively low compared to the static initial static shear stress. On the other hand the *CM* failure behaviour is typically observed when the ratio between the cyclic shear stress and the initial static shear stress attains the highest values. The pattern *INT* is in between them. With the

aim to establish an approximate criterion for identifying the occurrence of the various failure patterns, the internal space of **Figure 129b** has been divided in regions each one corresponding to a given behaviour. Each limiting straight line is defined by a given value of the ratio between the static and the cyclic shear stresses applied. The lowest line corresponds to a value of this ratio equal to 0.71 while the uppermost one corresponds to a value equal to 0.36. Therefore it can be concluded that if the magnitude of the initial static shear stress is higher than $0.71 \cdot CSR$ the behaviour observed is *PSA*, while if the magnitude of the initial static shear stress ratio is less than $0.36 \cdot CSR$ the observed behaviour is *CM*. An intermediate behaviour is expected for samples sheared with an initial static shear stress ratio between $0.36 \cdot CSR$ and $0.71 \cdot CSR$.

Chapter 8

Prediction of seismic pore water pressures in silty sands

The generation, dissipation, and redistribution of excess pore water pressures (*PWP*) under cyclic loading within the layers of a soil deposit can significantly influence the seismic response of that deposit. The modeling of cyclic pore water pressure generation in non-linear site response analysis has seen an extensive development based on the results of field measurements (Matasovic and Vucetic 1993) and laboratory tests (Ishihara et al. 1976), including the effects of multi-directional shaking (Seed et al. 1978).

Relevant previous studies have focused mainly on clean sand (Seed et al. 1975; Hazırbaba 2005; Polito et al. 2008) although natural soil deposits, as well as artificial soil deposits, often contain a considerable amount of fines. Although several models have been proposed in the literature to predict the development of excess pore water pressure under cyclic loading for silt (Wijewickreme and Sanin 2010; Verma and Wijewickreme 2015) and silty sand (Hazirbaba and Rathje 2009; Baziar et al. 2011; Porcino and Diano 2016; Porcino and Diano 2017), only limited studies take into account the presence of an initial static shear stress such as that acting on the horizontal plane in soil deposits under sloping ground conditions or in the near proximity of shallow foundations (Pan and Yang 2018; Pan et al. 2020). Furthermore, this limited number of studies have been conducted on clean sand or sand with a small percentage of fines in the triaxial apparatus.

For this reason, in this study a series of undrained non-symmetrical cyclic simple shear tests were performed to study the effect of the initial static shear stress acting on the horizontal plane of the specimens on pore water pressure generation of non-plastic Ticino sand-silt mixtures. In particular, this chapter analyses: a) the differences in terms of residual pore water pressure development without and in the presence of an initial static shear stress; b) the applicability of pore water pressure generation models proposed for silty sands and the accuracy of their prediction; and c) new revised models that consider the presence of initial static shear stress based on the results of the undrained cyclic simple shear tests performed in the present study.

8.1 Excess pore water pressure generation in presence of an initial static shear stress

During undrained cyclic loading, the excess *PWP* generated in the saturated soils can be divided into two components: transient and residual *PWPs* (Polito et al. 2008). The former is equal to the change in the total stress at the real-time cycling; thus it hardly affects the effective stresses acting on the soil. Conversely, the latter is the value that holds at the end of each stress cycle when the cyclic deviatoric stress comes back to its initial value and it directly alters the effective stress of the soil (Kammarer et al. 2005). **Figure 130** shows typical test results gathered from undrained cyclic *SS* tests carried out on Ticino silty sand both in the absence and in the presence of an initial static shear stress. These figures show, the excess pore pressure ratio (R_u), defined as the ratio of the excess *PWP* to the initial vertical effective stress, and the cyclic shear strain (γ) versus the number of cycles.

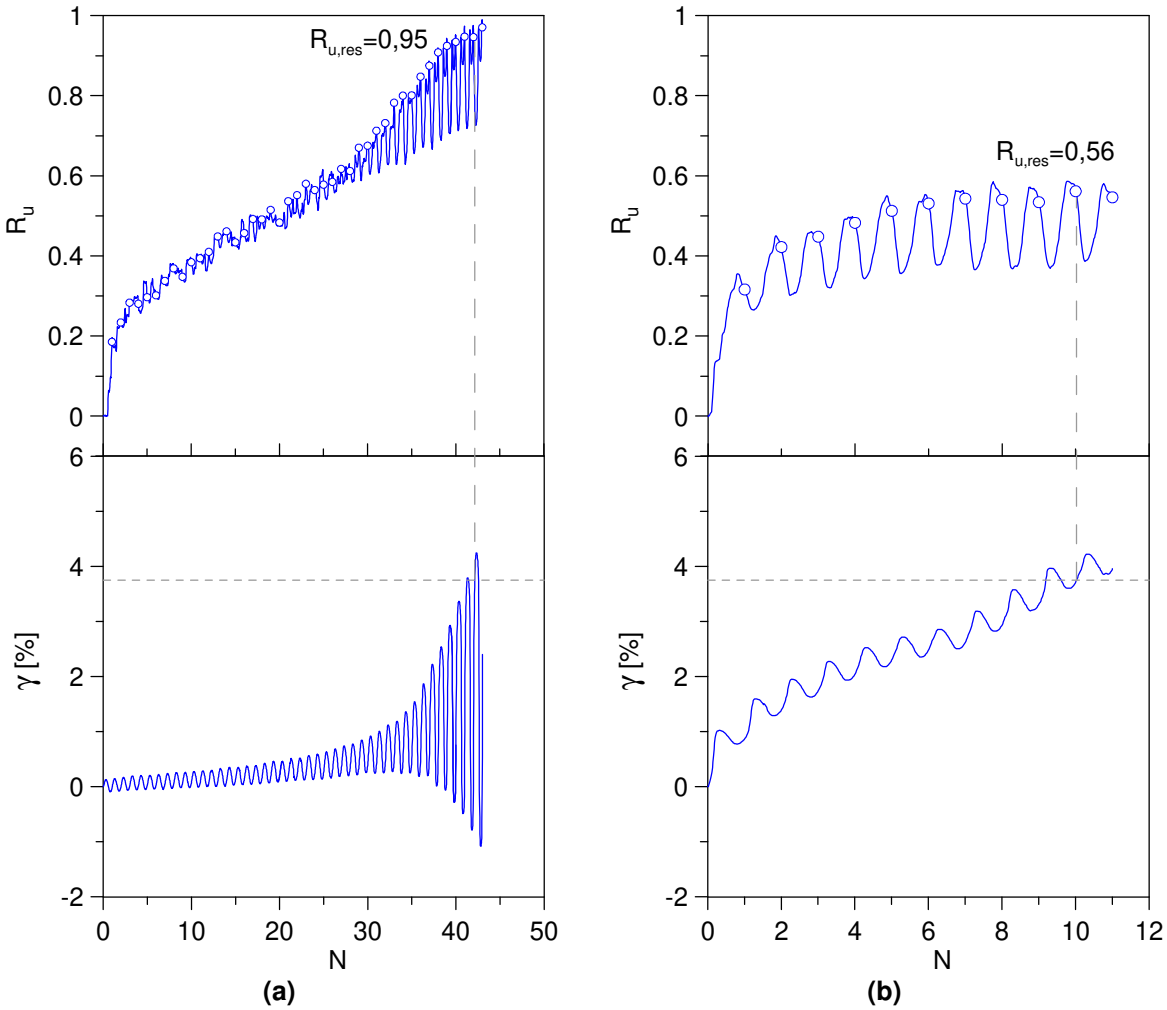

Figure 130 – Variation of excess pore water pressure ratio and shear strain of Ticino silty sand (f_c=10%, e_0=0.60) with number of cycles: (a) α=0, *CSR*=0.14; and (b) α=0.20; *CSR*=0.14.

Figure 130a presents the results for a specimen consolidated without an initial static shear stress (α=0) and subjected to a cyclic stress ratio CSR = 0.14. The residual pore pressure ratio $R_{u,res}$ increased stepwise with the number of cycles, along with the gradual increase in the cyclic shear strain. As it usually happens for symmetrical tests the pore pressure ratio reached the limiting value of $R_{u,res}$ =0.95 at N = 45, just at the end of the cyclic loading. The cyclic shear strain increased slowly in the early portion of the curve while the trend became more abrupt after a certain number of cycles reaching a final value of 3.75% in single amplitude. As shown in **Figure 130b**, for the companion sample that was subjected to an initial static shear stress (α=0.20, CSR=0.14), the residual pore pressure ratio and the cyclic shear strain increased sharply in the early cycles and more gradually at a later stage. A value of $R_{u,res}$ =0.51 was rapidly approached at N = 5 and it increased very slowly in the remaining cycles reaching a final value of 0.56. The shear strain continued to moderately increase until reaching the failure criterion of 3.75% when N = 10.

Clearly, the residual pore pressure ratio patterns observed in the presence and in the absence of an initial static shear stress were significantly different. From a general point of view, when the tests are carried out in the absence of an initial static shear stress, the pore water pressure increases up to a value very close to unity; correspondingly the vertical effective stress reaches a value near to zero causing failure. Conversely when an initial static shear stress is applied, the excess pore water pressure approaches a limiting value ($R_{u,lim}$), the magnitude of which depends on the value of the static shear stress; generally the failure is pinpointed at a conventionally assumed limiting value of the shear strain (in this study γ_{SA}=3.75%).

Figure 131 shows $R_{u,lim}$ (γ_{SA}=3.75%), i.e. the residual excess pore water pressure detected in correspondence of the assumed liquefaction criterion (γ_{SA}=3.75%), recorded during the undrained cyclic simple shear tests performed with various CSR, e_0, f_c and σ'_{v0}, plotted against α. For α varying in the range α=0-0.30 considered in this study, $R_{u,lim}$ (γ_{SA}=3.75%) decreases with the increase in α. The maximum value ($R_{u,lim}$ ≈ 1) is obtained for α = 0, i.e. when a cyclic mobility failure pattern dominates. The decreasing trend of $R_{u,lim}$ with increasing α has been consistently observed in other studies on clean sands such as the ones conducted by Vaid and Chern (1983), and Pan and Yang (2017), among others. A possible explanation can be found in the fact that the horizontal distance between the initial stress state and the CSL of the tested specimens becomes increasingly shorter with the increase in the values of α.

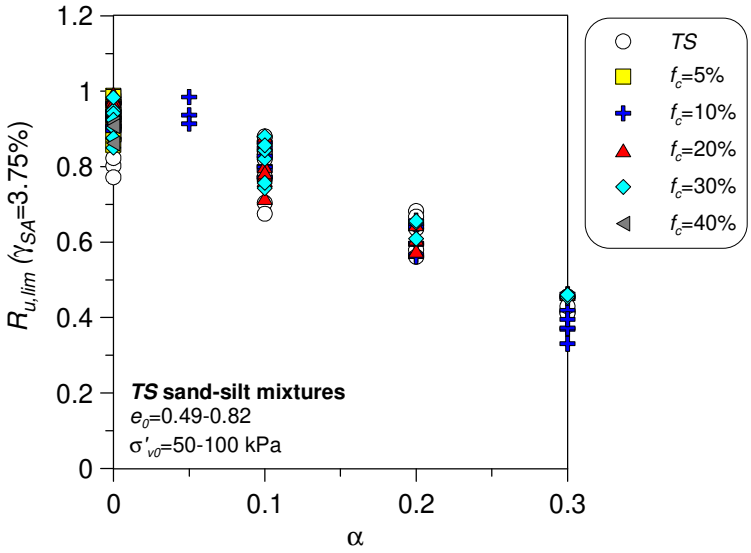

Figure 131 – Relationship between limiting pore water pressure ratio ($R_{u,lim}$) and initial static shear stress ratio (α).

8.2 Pore pressure prediction models

8.2.1 Stress-based models

In this paragraph, firstly, the development of excess pore water pressure observed in the undrained cyclic simple shear tests carried out on clean Ticino sand is analyzed considering the effect of an initial static shear stress in stress-based models.

To define the process of pore pressure development due to undrained cycling loading, the residual pore pressure ratio $R_{u,res}$, is plotted against the number of cycles N, normalized by the number of cycles required for attaining liquefaction (N_f), as shown in **Figure 132**. The test data for the symmetrically loaded (α=0) sand under various amplitudes of cyclic stresses CSR and post-consolidation void ratios e_0 are reported in **Figure 132a**. In this figure the experimental results with an initial global void ratio e_0=0.60, corresponding to a value of relative density D_R equal to 94%, were neglected since the liquefaction phenomenon in practical applications is irrelevant for specimens of such high density. As shown in **Figure 132a**, the pore pressure increases quickly in the early cycles and, subsequently, its rate becomes moderate before sharply increasing again up to the limiting value. This initial convex upward trend followed by a concave upward trend of the pore pressure generation is a common characteristic of sands.

Seed et al. (1975) proposed an empirical model to simulate the pore pressure generation of sand based on an extensive number of stress-controlled undrained cyclic tests; the model was subsequently simplified by Booker et al. (1976) as follows:

$$R_{u,res} = \frac{2}{\pi} \cdot \sin^{-1}\left(\frac{N}{N_f}^{(1/2\beta)}\right) \quad (40)$$

A value of β ranging from 0.6 to 1 was proposed by the authors and a value equal to 0.7 is traditionally assumed and recommended by Seed et al. (1975) for clean sands. **Figure 132a** shows the comparison of the test results obtained in the present work with the trend predicted by Eq. (40) considering the recommended range of β values suggested for clean sands (solid curves).

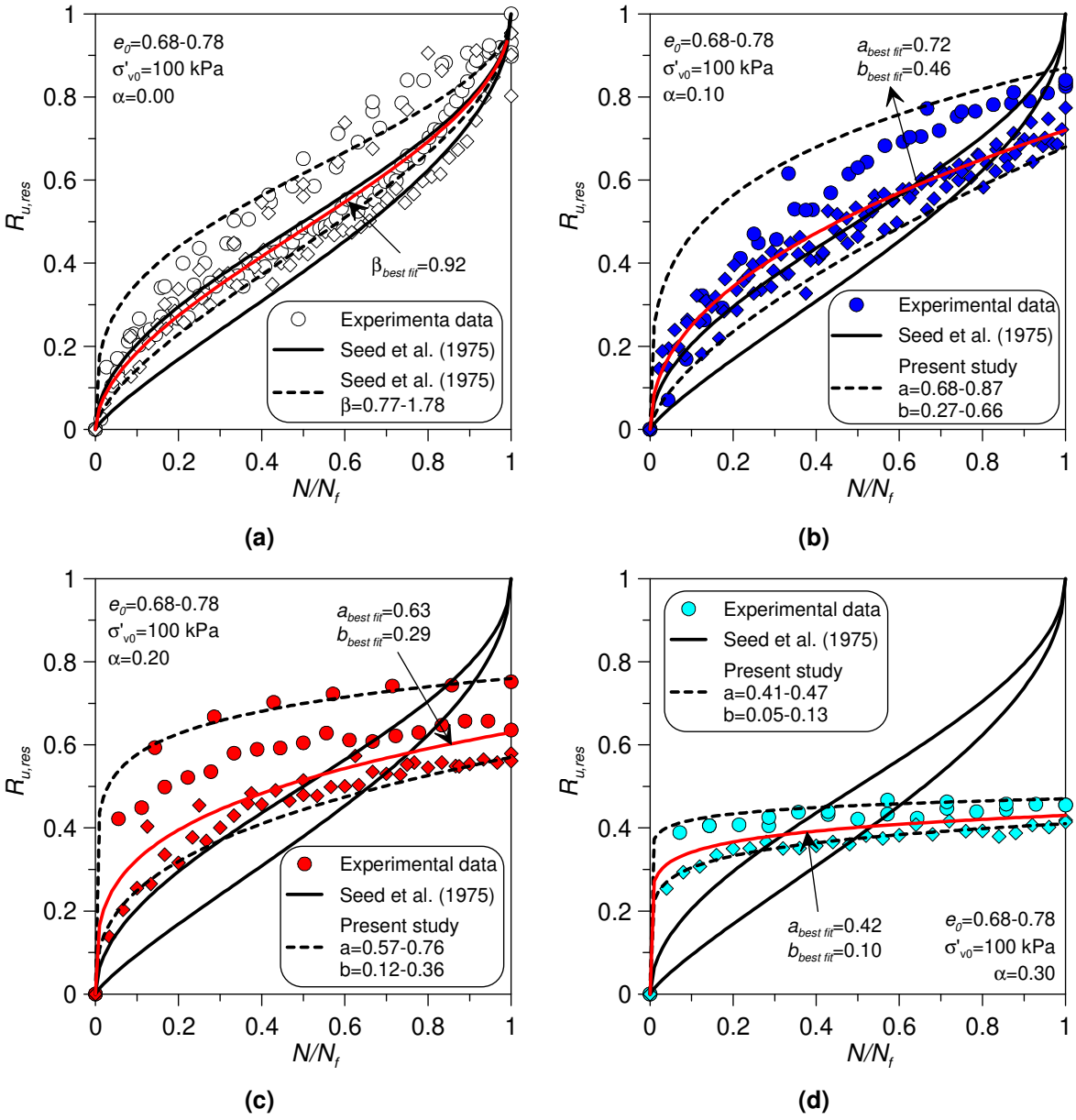

Figure 132 – Residual excess pore water pressure ratio versus normalized number of cycles for clean sand during cyclic loading: (a) α=0; (b) α=0.10; (c) α=0.20, and (d) α=0.30.

Although the model proposed by Booker et al. (1976) can be qualitatively used to obtain the general trend in the pore pressure development, the discrepancy is apparent as the predicted trend is located below most of the test data obtained in this study. For this reason, for the moist tamped Ticino sand specimens considered in this study, the following range of variation of β seems to be more appropriate: β = 0.77-1.78 (dashed curves) with a best fit value equal to 0.92 (red curve).

With the intention of verifying the applicability of stress-based models originally developed for clean sands to sands tested in presence of an initial static shear stress, plots of residual pore water pressure ratio, $R_{u,res}$, versus cycle ratio N/N_f are given in **Figure 132b, 132c** and **132d** for Ticino sand with different magnitudes of the initial static shear stress (α=0.10-0.30). While for clean sands without an applied initial static shear stress the shape of Seed's (1975) model was shown to agree well with the measured build-up of pore pressure, the performance of the model was unsatisfactory when applied to clean sand specimens tested with non-zero values of α. Thus, to better fit the test data reported in the aforementioned figures, a modified equation is proposed in this study as follows:

$$R_{u,res} = a \cdot \left(\frac{N}{N_f}\right)^b \tag{41}$$

Here, *a* and *b* are two empirical parameters that need to be determined by back analysis of undrained cyclic tests results.

An analysis of the tests data reported in **Figure 132** allows to evidence some interesting features of the excess pore pressure development of the silty sand specimens subjected to initial static shear stress ($\alpha \neq 0$). The corresponding curves do not exhibit the typical biconcave trend shape in the normalized plots: the residual pore pressure ratio increases rapidly during the early stage of the tests, and subsequently, it approaches the limiting values gradually. This trend was satisfactorily predicted using the modified model defined by Eq. (41) with the two sets of parameters *a* and *b* labeled, respectively, as lower and upper that are summarized in **Table 11**. The corresponding curves are shown in **Figure 132**.

It is interesting to analyse how the presence of the fines influences the pore water pressure generation and if the models defined for clean sands are still applicable in that case. For symmetrical loading conditions, different pore water pressure models have been proposed in the literature to consider the presence of non-plastic fines (Polito et al. 2008; Baziar et al. 2011; Porcino and Diano 2017). For Ticino sand-silt

mixtures, by analyzing the experimental data, Porcino and Diano (2017) showed that for percentages of fines lower than the threshold fines content f_{thre}, the typical inverted *S*-shape exhibited by clean sands was maintained. Referring to Seed's model, only a variation in terms of parameter β was observed; with β increasing as the percentage of fines increases. Towards higher percentages of fines, the trend of residual excess pore pressure ($R_{u,res}$) data tends to become monotonically increasing with the number of normalized cycles and this is well observed for percentages of fines greater than f_{thre} (Porcino and Diano 2017; Porcino et al. 2018b).

Table 11 – Empirical parameters of Eq. (41) used to draw the excess pore water pressure curves for clean sands reported in Figure 132.

α	$a_{lower/upper}$	$b_{lower/upper}$	$a_{best\ fit}$	$b_{best\ fit}$
0.10	0.68-0.87	0.27-0.66	0.72	0.46
0.20	0.57-0.66	0.12-0.36	0.63	0.29
0.30	0.41-0.47	0.05-0.13	0.42	0.10

In the present study the effects induced by the fines content on the excess pore water pressures developed under cyclic loading were investigated taking also into account the presence of an initial static shear stress. This will provide an advancement in the state of knowledge of these materials.

In **Figure 133** the experimental results for different magnitudes of the initial static shear stress, α, are reported. In the same figure the upper and lower bound curves obtained for clean sands were superimposed. It is possible to observe that the presence of fines does not significantly modify the trend of the data points in the $R_{u,res}$ vs. N/N_f plots drawn for the complete range of fines content investigated. The experimental data were processed through the model defined by Eq. (41) and the *a* and *b* parameters for silty sands were calculated. The majority of the calculated parameters fall inside the range proposed in **Table 11** for Ticino clean sand. As shown in **Figure 133** the calculations gave satisfactory results except for few tests with f_c=10% and α=0.30 in which the model predictions overestimated the experimental data. A further goal of the research was to define possible correlations between the empirical parameters *a* and *b* appearing in Eq. (41) and the main factors that, according to the analyses made in the previous paragraphs, could affect the development of the cyclic excess pore water pressures.

In **Figure 134**, **Figure 135**, **Figure 136**, **Figure 137** and **Figure 138** the parameters *a* and *b* adopted to process the experimental data are plotted against, respectively, the initial void ratio (e_0), the initial effective vertical stress (σ'_{v0}), the initial static shear stress (α), the fines content (f_c) and the cyclic stress ratio (*CSR*).

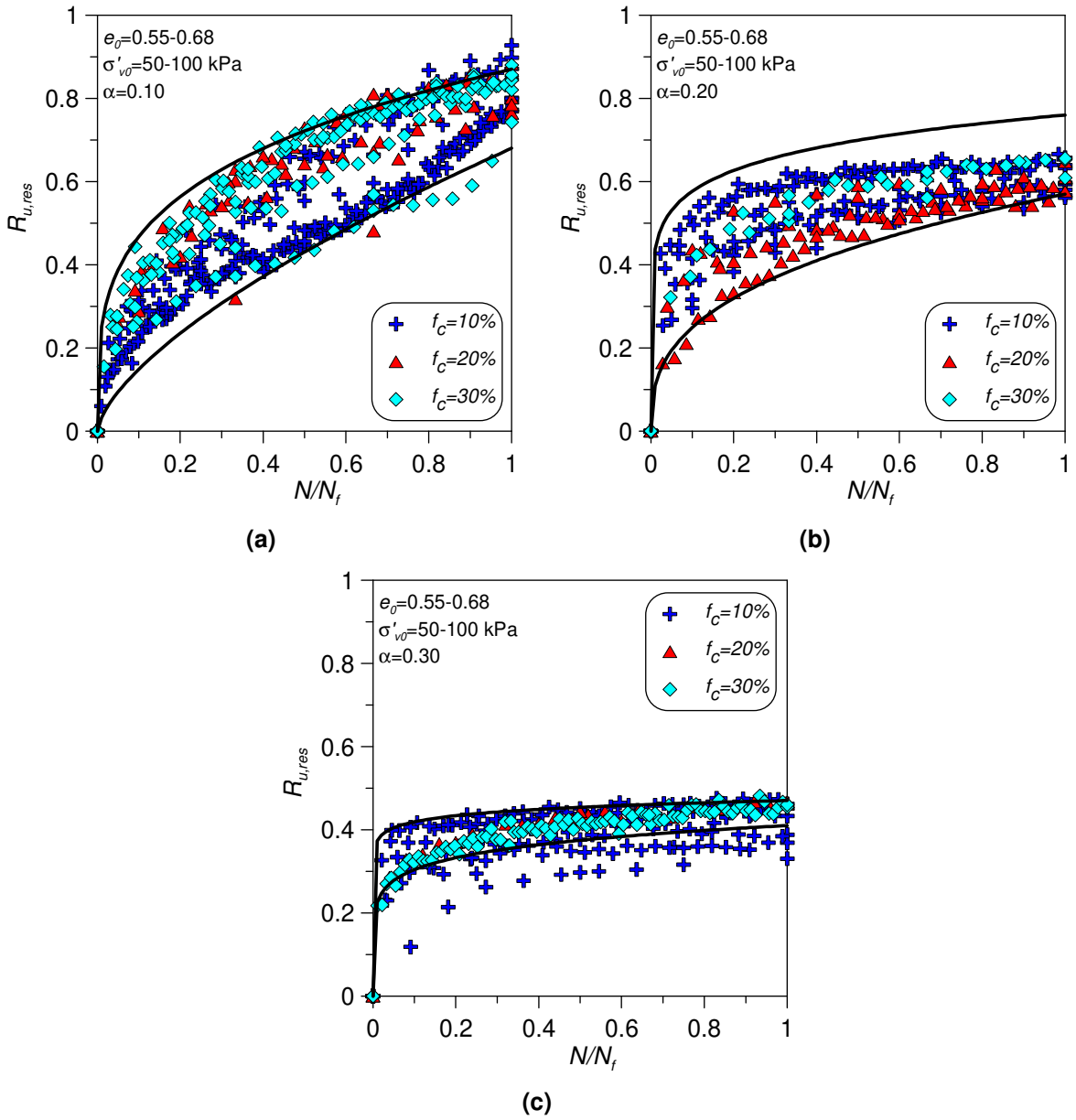

Figure 133 – Effect of fines content on excess pore water pressure ratio versus normalized number of cycles during cyclic loading: (a) α=0.10, (b) α=0.20, and (c) α=0.30. The solid curves represents the upper and the lower bounds for Ticino clean sand.

The best fit relationships obtained for the following variables: initial global void ratio e_0, initial vertical effective stress σ'_{v0}, initial static shear stress α and cyclic stress ratio *CSR* were linear, while a parabolic function proved to be adequate for the fines content

f_c. In some cases, the choice of a linear trend was a necessary option due to the limited data available, or an extrapolation of the trend observed in tests performed under similar conditions for which more data existed.

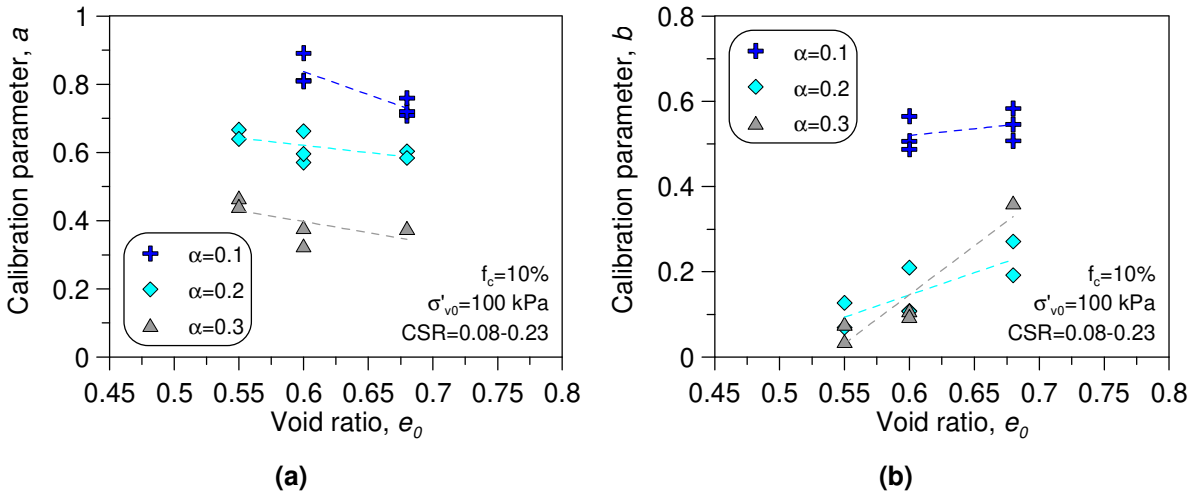

(a) **(b)**

Figure 134 – Variation of parameters *a* (a) and *b* (b) of Eq. (41) with e_0.

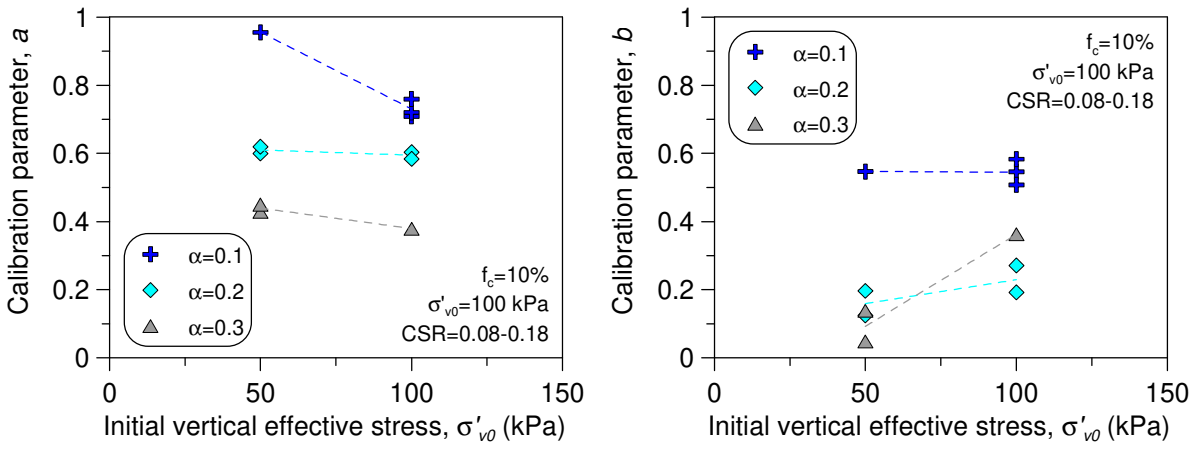

(a) **(b)**

Figure 135 – Variation of parameters *a* (a) and *b* (b) of Eq. (41) with σ'_{v0}.

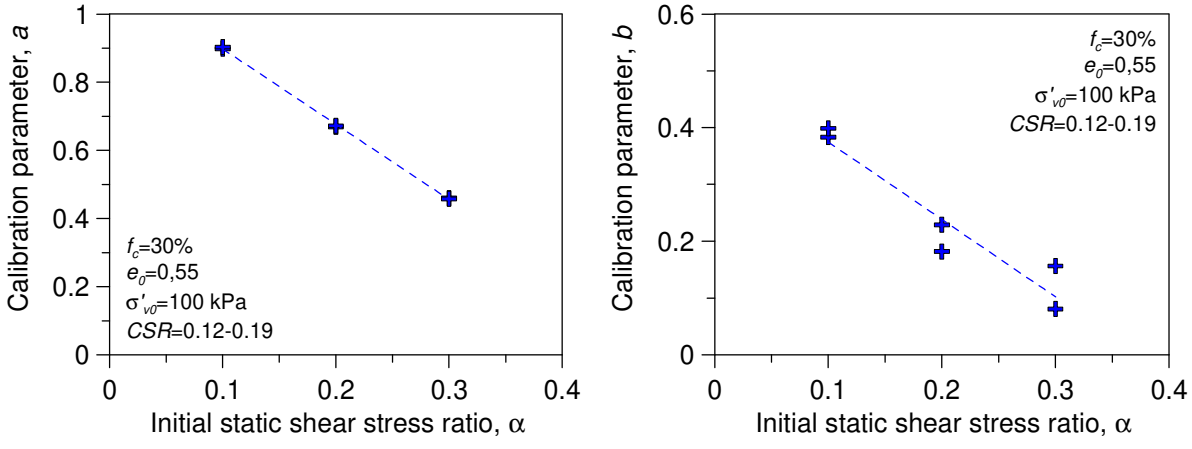

(a) **(b)**

Figure 136 – Variation of parameters *a* (a) and *b* (b) of Eq. (41) with *α*.

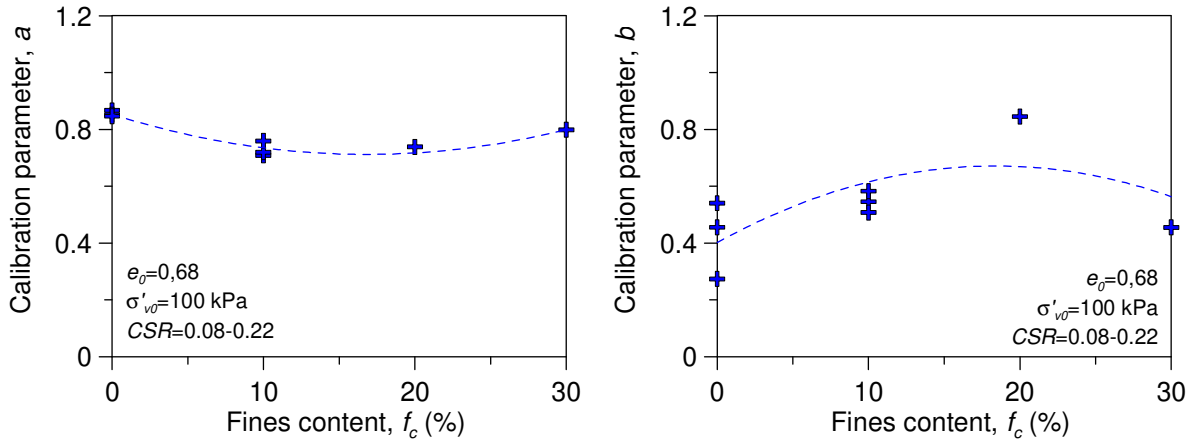

Figure 137 – Variation of parameters *a* (a) and *b* (b) of Eq. (41) with fines content f_c.

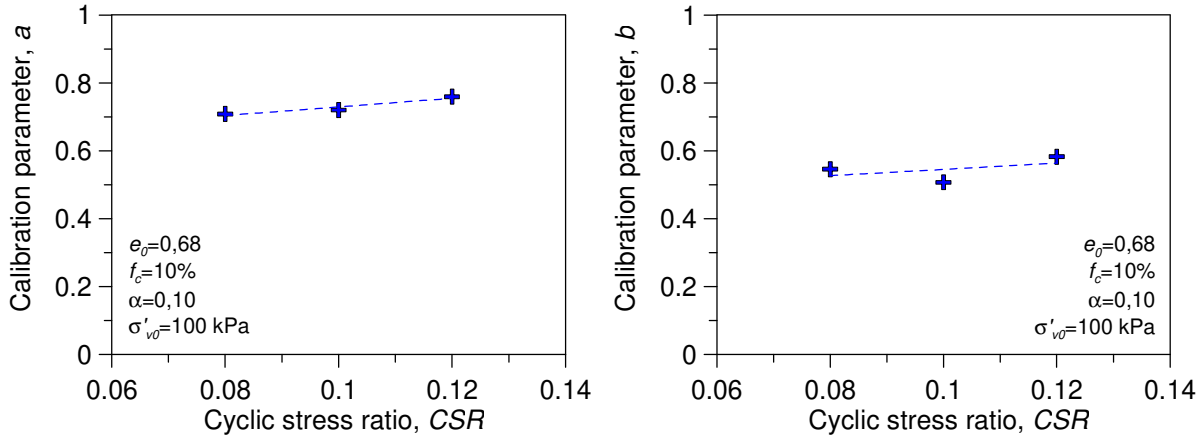

Figure 138 – Variation of the parameters *a* (a) and *b* (b) of Eq. (41) with *CSR*.

Basing on the trends of the curves observed in the previously discussed figures, a multivariable regression analysis was carried out to correlate the parameters *a* and *b* to all other factors. The relationships obtained were the following:

$$a = 1.476 - 0.565 \cdot e_0 - 0.00145 \cdot \sigma'_{v0} - 1.983 \cdot \alpha + 0.000224 \cdot f_c^2 - 0.00804 \cdot f_c + 0{,}629 \cdot CSR \quad (42a)$$

$$b = -0.543 + 1.269 \cdot e_0 + 0.00192 \cdot \sigma'_{v0} - 1.616 \cdot \alpha - 0.000462 \cdot f_c^2 + 0.0187 \cdot f_c + 0.122 \cdot CSR \quad (42b)$$

with a coefficient of determination R^2 equal to 0.94 and 0.71, respectively.

8.2.2 Strain-based models

In order to verify the applicability of strain-based models to non-plastic silty soils in the presence of an applied initial static shear stress, the approach proposed by Dobry (1985) was revisited in the present study.

Dobry (1985) proposed an upper and a lower boundary curve in the R_u versus γ domain, on the basis of the results of strain-controlled cyclic triaxial tests (solid lines in

Figure 139). Dobry's boundary curves correspond to a specific case in which only R_u values achieved after 10 shear strains cycles are considered.

More recently Cetin and Bilge (2012) observed significant differences between stress and strain controlled tests in triaxial conditions; for the sake of brevity this has not been taken into account in the following considerations. In **Figure 139a** the excess pore water pressures of the sand-silt mixtures investigated in the present research, in *SS* tests without an applied initial static shear stress, for various global void ratios and fines content (f_c<30%), are compared with the boundary curves proposed by Dobry (1985) for clean sand. As it can be seen the points inferred from the tests on silty sand carried out in the present research lie in a relatively narrow band on the right-hand side of the lower boundary curve for clean sand. In this figure (as well as in the companion ones) the symbol γ_{max} refers to the highest value of shear strain reached in a given cycle (in this case N = 10) while $R_{u,res}$ is the residual excess pore pressure ratio evaluated at the same stage of the given cycle. These findings are consistent with those reported by other researchers from undrained cyclic triaxial tests on silty sands (Cetin and Bilge 2012; Dash and Sitharam 2009).

In **Figure 139b, Figure 139c** and **Figure 139d** the same boundary lines proposed by Dobry (1985) are compared with the experimental data obtained in tests performed on the Ticino sand-silt mixtures in presence of an initial static shear stress. Once again the experimental data ly on the right-hand side of the Dobry's lower boundary curve with the distance from this latter increasing with the increase of α. It is interesting to note that the experimental data corresponding to the same value of α lie in a quite narrow band irrespective of the f_c and e_0 values of the mixtures.

In **Figure 139** with red dashed line are indicated the best fit curves of the experimental data drawn based on the results of a regression analysis conducted using the relationship proposed by Vucetic and Dobry (1986):

$$R_{u,res} = \frac{p \cdot f \cdot N \cdot F \cdot \left(\gamma - \gamma_{tvp}\right)^s}{1 + f \cdot N \cdot F \cdot \left(\gamma - \gamma_{tvp}\right)^s} \tag{43}$$

where γ is the cyclic shear strain, N is the number of loading cycles, and f is set to 1 or 2 for 1-D and 2-D cyclic loadings, respectively. p, F, and s are curve-fitting parameters. The volumetric threshold shear strain (γ_{tvp}) is defined as the shear strain below which no residual pore pressure is generated. The suggested range of values for γ_{tvp} is 0.01%–0.02% for most soils (Dobry et al. 1982). In the present study a value of γ_{tvp} equal to 0.01% has been considered. The regression analyses conducted through Eq.

(43) provided the best fit curves shown, as red dashed lines, in **Figure 139**, each one relative for a given value of α. The corresponding p, f, F parameters are given in the internal captures of the figures. The good agreement between the trend of these curves and the experimental data, suggests that Eq. (43) can be reliably adopted for the prediction of the cyclic excess pore water pressures of non-plastic silty sands in presence of an initial static shear stress.

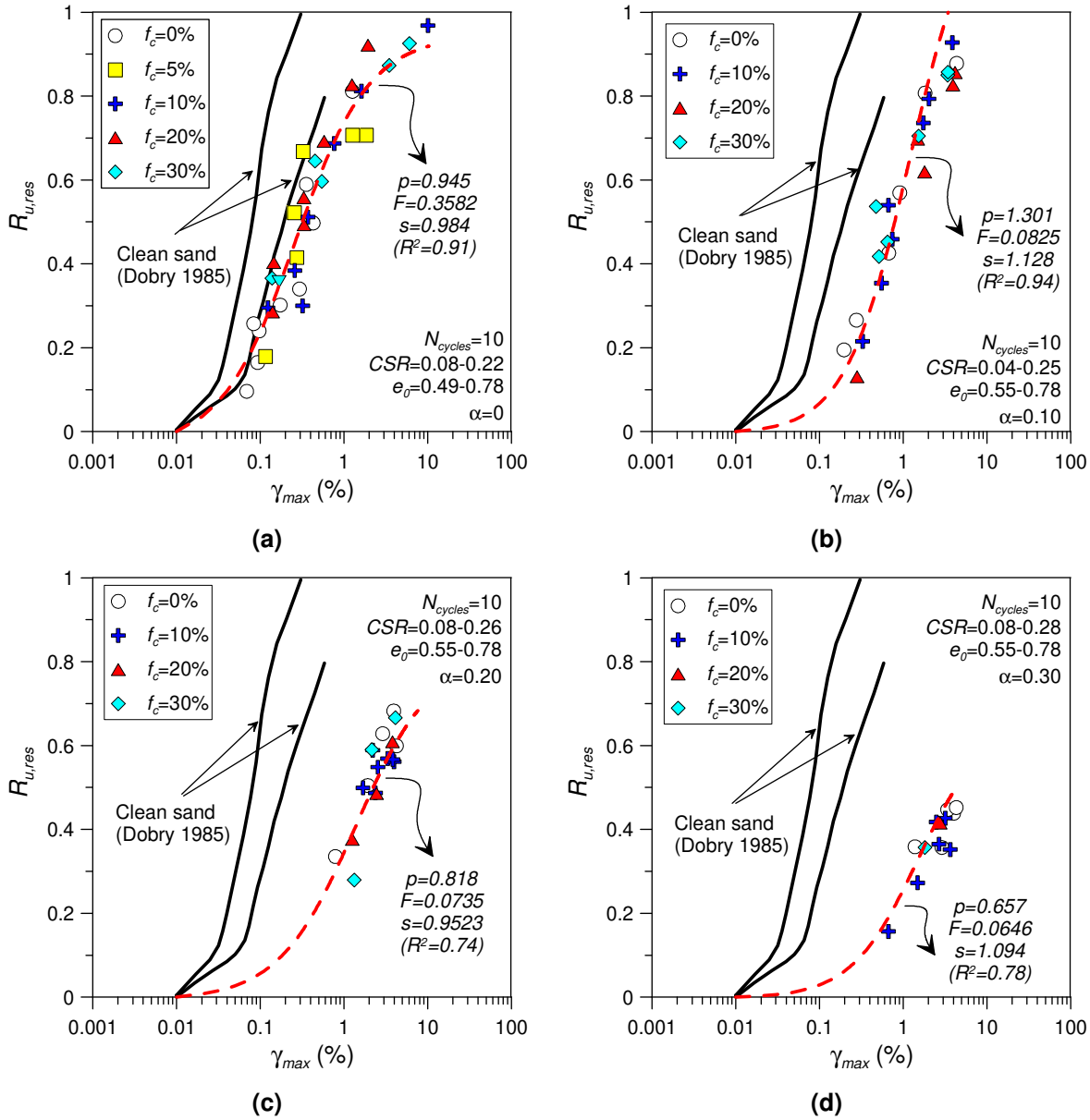

Figure 139 – Trend of residual pore water pressure ratios with maximum shear strains obtained in the present study compared with the upper and lower bound curves proposed by Dobry (1985) for clean sands: (a) α=0, (b) α=0.10, (c) α=0.20, and (d) α=0.30.

Chapter 9

Conclusion and recommended future works

A laboratory experimental research program was undertaken to improve the current knowledge on the combined effects of fines content and an applied initial static shear stress on the cyclic undrained response of non-plastic silty sands. Ticino sand (*TS*) with different percentage of non-plastic fines (up to 40%) was used as a test material for this study. The cyclic simple shear device in operation at the Geotechnical Testing Laboratory at the University Mediterranea of Reggio Calabria, Italy, was used to conduct the experimental activity of this study. Furthermore, undrained monotonic triaxial tests performed in a previously research conducted on the same material were re-analyzed.

The main results and conclusions drawn from this thesis are summarized below:

- The typical cyclic failure patterns are identified to be flow liquefaction, limited flow liquefaction, cyclic mobility, and plastic strain accumulation. There seems to be a strong state dependence of failure patterns. With increasing void ratio or increasing initial effective confining pressure, the cyclic failure patterns of the specimens may change from non-flow type (cyclic mobility or plastic strain accumulation) to flow-type (flow liquefaction or limited flow liquefaction).
- The number of cycles at failure increases with decreasing cyclic stress ratio. When the cyclic stress ratio (CRR_N) is normalized by the cyclic resistance at 15 cycles ($CRR_{N=15}$), a unified correlation exists between the normalized cyclic stress ratio, magnitude correction factor (*MSF)*, and the number of cycles to failure N_f, irrespective of initial global void ratio e_0, vertical effective stress σ'_{v0}, fines content f_c, and applied initial static shear stress (factor α).
- At the same initial void ratio e_0 and effective vertical stress σ'_{v0}, the addition of non-plastic silt reduces the cyclic resistance ($CRR_{N=15}$) of silty sands for all initial shear stress levels (i.e. α values) up to the threshold fines content f_{thre}.
- A range for the threshold fines content f_{thre} between 21% and 28% could be identified from cyclic simple shear test results at different applied initial static shear stresses with an average value equal to 24.5%; the comparison of the f_{thre} values predicted by analytical relationships (Polito 1999; Harzibaba 2005; Rahman and Lo 2008) provided inconsistent results among them with f_{thre}

values varying between 23% and 36%. f_{thre} calculated from the relationship by Hazirbaba (2005) (f_{thre} = 23%) slightly underestimates the experimental average value, while f_{thre} derived from Polito's relation (f_{thre} = 30%) tends to overestimate the experimental value. Rahman and Lo (2008) provides a value of f_{thre} = 36% being substantially higher than the experimental value.

- The effects of α on the cyclic resistance of non-plastic silty sands can be beneficial or detrimental depending on the initial global void ratio e_0, the initial vertical effective stress σ'_{v0}, and fines content f_c. The concept of threshold α was verified for Ticino sand with a fines content f_c=10% and an effective vertical stress ranging from 50 to 100 kPa. The threshold α is affected by the initial state and decreases as the initial state parameter $\Psi_{(0)}$ increases.
- The addition of fines leads to a shift of the critical state line (*CSL*) towards lower void ratios in the e - log(p') space. The direction of shift reverses at higher f_c. This reversal in the direction of shift occurs approximately at the threshold fines content, f_{thre}.
- The main features of the undrained monotonic behaviour and the undrained cyclic resistance of silty sands, at different α, can be correlated to the initial state parameter $\Psi_{(0)}$, initial pressure index $I_{p(0)}$, and initial modified state parameter $\Psi_{m(0)}$. The $CRR_{N=15}$ - $\Psi_{(0)}$ curves rotate clockwise with increasing α, as previously reported in the literature for silty sands.
- For *TS*-fines mixtures with $f_c \leq f_{thre}$, the application of the equivalent granular void ratio-based approach to undrained *DSS* and undrained monotonic triaxial tests required the assessment of the equivalent granular void ratio e^*= f(e; f_c; b) where b is the fines influence factor. Different values of b were found depending on whether they were back-calculated using as benchmark the critical state line (b_{CSL}) or the undrained cyclic resistance (b_{CRR}) of the clean sand. The adopted e^*-based approach was found to be effective in predicting the undrained monotonic and cyclic behaviour of sands with non-plastic fines.
- A unique equivalent granular critical state line (*EG-CSL*) for all *TS*-fines mixtures with $f_c \leq f_{thre}$ was identified in the e^*- log(p') plane from undrained monotonic triaxial tests results. This approach enables the behaviour at critical state of silty sands to be unified, regardless of the fines content (provided $f_c \leq f_{thre}$) and void ratio.

- *EG-CSL* was used as a reference line to define, together with using e^* instead of e, the equivalent granular state parameter, Ψ^*, the equivalent pressure index I_p^*, and the equivalent modified state parameter Ψ_m^*. Among them Ψ^* appeared to be the most effective index for predicting, in the framework of the *CSSM* theory, the undrained monotonic and cyclic failure patterns to be expected for non-plastic sand-silt mixtures with different values of fines contents (lower than f_{thre}), void ratios, vertical effective stresses, and initial static shear stress. As a matter of fact the results showed that cyclic simple shear tests characterized by different combinations of the initial void ratio, initial effective vertical stress, initial static shear stress, and fines content (lower than f_{thre}), exhibit a similar type of failure under undrained cyclic loading, provided that $\Psi^*_{(0)}$ takes the same value.
- The cyclic resistance ratio $CRR_{N=15}$ was found to be strongly correlated with both the conventional state parameter, $\Psi_{(0)}$, and the equivalent granular state parameter, $\Psi^*_{(0)}$, through simple exponential functions. The cyclic resistance ratio considerably decreased with an increase in either $\Psi_{(0)}$ or $\Psi^*_{(0)}$. When the equivalent granular state parameter, instead of the traditional one, was considered, an improved coefficient of correlation R^2 was obtained for these relationships.
- From a practical point of view, the main advantage of using a relationship between $CRR_{N=15}$ and $\Psi^*_{(0)}$ lies the fact that it allows to assess the undrained cyclic strength of a sand with a given non-plastic fines content (lower than f_{thre}) and initial static shear stress on the basis of the undrained cyclic strength of the clean sand. Furthermore the approach does'nt need to determine the *CSLs* for all the mixtures, because this information is implicitly incorporated in the fines influence factor b appearing in the equation defining e^*. Nevertheless, the incorporation of *CRR*-Ψ or *CRR*-Ψ^* relationships into the simplified procedures for predicting the liquefaction potential that are based on in situ tests results (*SPT*, *CPT*, etc.) would require to establish realiable relationships between the state variables Ψ or Ψ^* and the in situ test results.
- The residual pore pressure generated in the saturated non-plastic silty sands may reach a limiting value $R_{u,lim}$ during the undrained cyclic loading depending on the value of α. The $R_{u,lim}$ decreases when α increases, with the largest value being close to unity at $\alpha = 0$.

- The relationship between the normalized residual pore pressure ratio and the normalized number of loading cycles is not affected by the amplitude of the cyclic stress, but it is significantly influenced by the static shear stress and slightly influenced by the initial state. Thus, a modified pore pressure generation model has been proposed in this study, which can be used to appropriately quantify the pore pressure development of the non-plastic silty sands under various static shear stress conditions.

The conclusions gathered in this study are based on specific materials (Ticino sand and *TS* with non-plastic fines), sample preparation method (moist tamping), testing apparatus (constant volume *DSS*), testing procedure conditions (stress-controlled cyclic loading) and initial states (e_0, σ'_{v0}, α) of tests used for the experimental investigation.

Further research is required in order to analyze the effects of other factors not taken into account in the present study but that are known to have an influence on the undrained monotonic and cyclic behaviour of granular soils such as grains shape and angularity, particle crushability, grading characteristics, fines plasticity and soil fabric (reconstitution method). An aspect that needs to be more deeply investigated is the undrained behaviour of non-plastic silty sand with $f_c > f_{thre}$. This should be another goal of the future research.

References

1. Alarcon-Guzman A., Chameau J. L., and Leonards, G. A. (1988). Undrained monotonic and cyclic strength of sands. Journal of Geotechnical Engineering, 114(10): 1089-1109, https://doi.org/10.1061/(ASCE)0733-9410(1988)114:10(1089).
2. Amini F., and Qi G. Z. (2000). Liquefaction testing of stratified silty sands. Journal of Geotech. and Geoenviron. Eng. 126(3): 208-217.
3. Andrus R. D., and Stokoe II K. H. (2000). Liquefaction resistance of soils from shear-wave velocity. Journal of Geotechnical and Geoenvironmental Engineering, 126(11): 1015-1025.
4. Arthur J. R. F., and Menzies B. K. (1972). Inherent anisotropy in a sand. Géotechnique. 22(1):115-128.
5. ASTM D4253 (2000). Standard Test Methods for Maximum Index Density and Unit Weight of Soils Using a Vibratory Table. West Conshohocken, PA, 1-14.
6. ASTM D4254 (2000). Standard Test Methods for Minimum Index Density and Unit Weight of and Calculation of Relative Density. West Conshohocken, PA, 1-9.
7. ASTM D854 (2014). Standard Test Methods for Specific Gravity of Soil Solids by Water Pycnometer, ASTM International, West Conshohocken, PA.
8. Athanasopoulos G., and Xenaki V. C. (2008). Liquefaction resistance of sands containing varying amounts of fines. Geotechnical Earthquake Engineering and Soil Dynamics IV. https://doi.org/10.1061/40975(318)94.
9. Baki M. A. L. (2011). Cyclic liquefaction behaviour of granular materials with fines. PhD thesis, University of New South Wales at Australian Defence Force Academy.
10. Baki M. A. L., Rahman M. M., Lo S. R., and Gnanendran C. T. (2012). Linkage between static and cyclic liquefaction of loose sand with a range of fines contents. Canadian Geotechnical Journal, 49(8): 891-906.
11. Baki M. A. L., Rahman M. M., and Lo S. R. (2014). Predicting onset of cyclic instability of loose sand with fines using instability curves. Soil Dynamics and Earthquake Engineering, 61-62: 140-151.
12. Baziar M. H., and Dobry R. (1995). Residual Strength and Large-Deformation Potential of Loose Silty Sands. Journal of Geotechnical Engineering, 121(12): 896-906.
13. Baziar M. H., and Sharafi H. (2011). Assessment of silty sand liquefaction potential using hollow torsional tests – An energy approach. Soil Dyn. Earthq. Eng., 31: 857-865.
14. Baziar M.H., Shahnazari H., and Sharafi H. (2011). A laboratory study on the pore pressure generation model for Firouzkooh silty sands using hollow torsional test. Int. J. Civil Eng., 9 (2): 126-134.
15. Been K., and Jefferies M. G. (1985). A state parameter for sands. Géotechnique, 35 (2): 99–112. https://doi.org/10.1680/geot.1985.35.2.99.
16. Been K., and Jefferies M. (2004). Stress-dilatancy in very loose sand. Can. Geotech. J. 41(5): 972–989.
17. Been K., Jefferies M. G., and Hachey J. (1991). The critical state of sands. Géotechnique, 41(3): 365-381.

18. Belkhatir M., Arab A., Della N., Missoum H., and Schanz T. (2010a). Liquefaction resistance of chlef river silty sand: Effect of low plastic fines and other parameters. Acta Polytechnica Hungarica 7(2): 119-137.
19. Belkhatir M., Arab A., Della N., Missoum H., and Schanz T. (2010b). Influence of intergranular void ratio on monotonic and cyclic undrained shear response of sandy soils. C. R. Mecanique 338(5): 290-303.
20. Belkhatir M., Missoum H., Arab A., Della N., and Schanz, T. (2011). The undrained shear strength characteristics of silty sand: an experimental study of the effect of fines. Geol. Croat. 64(1): 31–39.
21. Benahmed N., Nguyen T., Hicher P., and Nicolas M. (2015). An experimental investigation into the effects of low plastic fines content on the behaviour of sand/silt mixtures. European Journal of environmental and civil engineering, 19: 109–128.
22. Berrill J.B., and Davis R.O. (1985). Energy dissipation and seismic liquefaction of sands: revised model. Soils and Foundations, 125(2): 106–18.
23. Bjerrum L., and Landva A. (1966). Direct Simple-Shear Tests on a Norwegian Quick Clay. Géotechnique, 16(1): 1-20. https://doi.org/10.1680/geot.1966.16.1.1.
24. Bobei D. C., and Lo S. R. (2005). Reverse behaviour and critical state of sand with small amount of fines. The Proceedings of the 16th International Conference on Soil Mechanics and Geotechnical Engineering (16ICSMGE), Japan, 475-478.
25. Bobei D. C., Lo S. R., Wanatowski D., Gnanendran C. T., and Rahman M. M. (2009). A modified state parameter for characterizing static liquefaction of sand with fines. Can. Geotech. J., 46(3), 281–295.
26. Booker J. R., Rahman M. S., and Seed H. B. (1976). GADFLEA—a computer program for the analysis of pore pressure generation and dissipation during cyclic or earthquake loading. EERC Report No. 76-24, Univ. of California, Berkeley, CA.
27. Bouckovalas G. D., Andrianopoulos K. I., and Papadimitriou A. G. (2003). A critical state interpretation for the cyclic liquefaction resistance of silty sands. Soil Dynamics and Earthquake Engineering, 23(2): 115-125.
28. Boulanger R. W., Seed R. B., Chan C. K., Seed H. B., and Sousa, J. (1991). Liquefaction Behavior of Saturated Sands under Uni-directional and Bi-Directional Monotonic and Cyclic Simple Shear Loading. Geotechnical Engineering Report No. UCB/GT/91-08, University of California, Berkeley.
29. Boulanger R. W. (2003a). Relating K_α to relative state parameter index. Journal of Geotechnical and Geoenvironmental Engineering. 129(8): 770-773, https://doi.org/10.1061/(ASCE)1090-0241(2003)129:8(770).
30. Boulanger R. W. (2003b). High overburden stress effects in liquefaction analyses. Journal of Geotechnical and Geoenvironmental Engineering, 129(12): 1071-1082, https://doi.org/10.1061/(ASCE)1090-0241(2003)129:12(1071).
31. Boulanger R. W., and Idriss I. M. (2004). Evaluating the potential for liquefaction or cyclic failure of silts and clays. Rep. No. UCD/CGM-04/01, Center for Geotechnical Modeling, Dept. of Civil and Environmental Engineering, Univ. of California, Davis, Calif.

32. Boulanger R. W., and Idriss I. M. (2006). Liquefaction Suspectibility Criteria for Silts and Clays. J. Geotech. Geoenviron. Eng., 132(11): 1413-1426, doi: 10.1061/(ASCE)1090-0241(2006)132:11(1413).
33. Caridi G. (2011). Comportamento non drenato statico, ciclico e post-liquefazione di sabbie carbonatiche nell'apparecchiatura di taglio semplice. PhD thesis, Mediterranean university of Reggio Calabria.
34. Carraro J., Bandini P., and Salgado R. (2003). Liquefaction resistance of clean and nonplastic silty sands based on cone penetration resistance. Journal of Geotechnical and Geoenvironmental Engineering, 129(11): 965-976.
35. Carraro J. A. H., and Salgado R. (2004). Mechanical behavior of non-textbook soils. Final Report FHWA/IN/JTRP-2004/5 (Indiana: Pardue University).
36. Carraro J. A. H., Prezzi M., and Salgado R. (2009). Shear strength and stiffness of sands containing plastic or nonplastic fines. J. Geotech. Geoenviron. Eng. 135 (9): 1167–1178. https://doi.org/10.1061/(ASCE)1090-0241(2009)135:9(1167).
37. Carrera A., Coop M., and Lancellotta R. (2011). Influence of grading on the mechanical behaviour of Stava tailings. Géotechnique, 61(11): 935–946, https://doi.org/10.1680/geot.9.P.009.
38. Casagrande A. (1936). Characteristics of cohesionless soils affecting the stability of slopes and earth fills. Journal of the Boston Society of Civil Engineers. 23: 257-276.
39. Casagrande A. (1975). Liquefaction and cyclic deformation of sands: a critical review. In Proceedings of Fifth Panamerican Conference on Soil Mechanics and Foundation Engineering. Pierce Hall.
40. Castro G. (1969). Liquefaction of Sands. PhD thesis, Harvard University.
41. Castro G. (1975). Liquefaction and cyclic mobility of saturated sands. Journal of the Geotechnical Engineering Division, 101(6): 551-569.
42. Castro G., and Poulos S. J. (1977). Factors affecting liquefaction and cyclic mobility. Journal of the Geotechnical Engineering, 103(6): 501-516.
43. Cavarretta I., Coop M., and O'sullivan, C. (2010). The influence of particle characteristics on the behaviour of coarse grained soils. Géotechnique. 60(6): 413-423, https://doi.org/10.1680/geot.2010.60.6.413.
44. Cetin K. O., and Bilge H. T. (2012). Cyclic Large Strain and Induced Pore Pressure Models for Saturated Clean Sands. Journal of Geotechnical and Geoenvironmental Engineering, 138(3): 309-323, https://doi.org/10.1061/(ASCE)GT.1943-5606.0000631.
45. Chang N.Y., Yeh S.I., and Kaufman L.P. (1982). Liquefaction potential of clean and silty sands. In Proceedings of Third International Earthquake Microzonation Conference, Seattle, Washington, Vol. II, pp. 1017–32.
46. Chang N.-Y. (1987). Liquefaction Susceptibility of Fine-Grained Soils, Preliminary Study Report. Department of Civil and Urban Engineering, University of Colorado at Denver.
47. Chang N. Y. (1990). Influence of fines content and plasticity on earthquake induced soil liquefaction. Contract No. DACW3988-C-0078, Contract Report to US Army Engineering Waterways Experiment Station, Vicksburg, MS.

48. Chang C. S., and Yin Z.-Y. (2011). Micromechanical modeling for behavior of silty sand with influence of fine content. Int. J. Solids Struct., 48: 2655-67.
49. Chien L.-K., Oh Y.-N., and Chang C.-H. (2002). Effects of fines content on liquefaction strength and dynamic settlement of reclaimed soil. Canadian Geotechnical Journal, 39(1): 254-265, doi:10.1139/T01-083.
50. Chiu C. F., and Fu X. J. (2008). Interpreting undrained instability of mixed soils by equivalent intergranular state parameter. Géotechnique 58(9): 751-755, https://doi.org/10.1680/geot.2008.58.9.751.
51. Cho G. C., Dodds J., and Santamarina C. (2006). Particle shape effects on packing density, stiffness, and strength: natural and crushed sands. Journal of Geotechnical and Geoenviromental Engineering 132: 591-602. https://doi.org/10.1061/(ASCE)1090-0241(2006)132:5(591).
52. Chu J., and Leong W. (2002). Effect of fines on instability behaviour of loose sand. Géotechnique, 52(10): 751-755, https://doi.org/10.1680/geot.2002.52.10.751.
53. Coop M. R. (2003). On the mechanics of reconstituted and natural sands. Keynote lecture, In: Proceedings of the 3rd international symposium on deformation characteristics of geomaterials, Swets and Zeitlinger, Lisse, The Netherlands, vol 2, pp 29–58.
54. Coop M.R., Klotz E.U., and Clinton, L. (2005). The influence of the in situ state of sands on the load-deflection behaviour of driven piles. Géotechnique, 55(10): 721–730.
55. Cubrinovski M., Rees S., and Bowman E. (2010). Effects of Non-Plastic fines on Liquefaction Resistance of Sandy Soils. Garevski M., Ansal A., editors. Earthquake Engineering in Europe, Geotechnical, Geological, and Earthquake Engineering 17. DOI: 10.1007/978-90-481-9544-2_6.
56. Cubrinovski M., Ntritos N., Dhakal R. and Rhodes A. (2019). Key aspects in the engineering assessment of soil liquefaction. Proceedings of 7th International Conference on Earthquake Geotechnical Engineering, ICEGE, 17-20 July 2019, Rome, Italy.
57. Dafalias Y. F., and Manzari M. T. (2004). Simple plasticity sand model accounting for fabric change effects. J. Eng. Mech. 130: 622-634, https://doi.org/10.1061/(ASCE)0733- 9399(2004)130:6(622).
58. Dafalias Y. F., and Papadimitriou A. G., Li X. S. (2004). Sand plasticity model accounting for inherent fabric anisotropy. ASCE J. Eng. Mech., 130(11): 1319-33.
59. Dafalias Y. F., and Taiebat M. (2016). SANISAND-Z: zero elastic range sand plasticity model. Géotechnique, 66: 999-1013, https://doi.org/10.1680/jgeot.15.P.271.
60. Dai B. B., Yang J., and Luo X. D. (2015). A numerical analysis of the shear behavior of granular soil with fines. Particuology, 21: 160-172, http://dx.doi.org/10.1016/j.partic.2014.08.010.
61. Dash H.K., and Sitharam T.G. (2009) Undrained cyclic pore pressure response of sand-silt mixtures: effect of nonplastic fines and other parameters. J. Geotech. Geolog. Eng., 27(4): 501-517, doi: 10.1007/s10706-009-9252-5.
62. Dash H. K., Sitharam T. G., and Baudet B. A. (2010). Influence of non-plastic fines on the response of a silty sand to cyclic loading. Soils Found., 50(5): 695–704.
63. Dash H.K., and Sitharam T.G. (2011). Undrained Cyclic and Monotonic Strength of Sand-Silt Mixtures.Geotech. Geol. Eng., 29: 555-570, doi: 10.1007/s10706-011-9403-3.

64. Davis R. O., and Berrill J. B. (2001). Pore pressure and dissipated energy in earthquakes—Field verification. J. Geotech. Geoenviron. Eng.,127(3): 269–274, https://doi.org/10.1061/(ASCE)1090-0241(2001)127:3(269).
65. De Alba P., Chan C. K., and Seed H. B. (1975). Determination of soil liquefaction characteristics by large scale laboratory tests. EERC Rep. No. 75-14, Univ. of California, Berkeley, CA.
66. Derakhshandi M., Rathje E. M., Hazirbaba K., and Mirhosseini S. M. (2008). The effect of plastic fines on the pore pressure generation characteristics of saturated sands. Soil Dyn. Earthq. Eng., 28(5): 376–386.
67. Diano V. (2017). Influence of non-plastic fines on monotonic and cyclic behaviour of silty sands. PhD thesis, Mediterranean university of Reggio Calabria.
68. Dobry R., Ladd R. S., Yokel F. Y., Chung R. M., and Powell D. (1982). Prediction of pore-water pressure buildup and liquefaction of sands during earthquakes by the cyclic strain method. NBS Building Science Series 138, National Bureau of Standards, U.S. Dept. of Commerce, Washington, D.C.
69. Dobry R. (1985). Liquefaction of soils during earthquakes. Rep. No. CETS-EE-001, National Research Council (NRC), Committee on Earthquake Engineering, Washington, DC.
70. Dobry R., Pierce W. G., Dyvik R., Thomas G. E., and Ladd R. S. (1985). Pore pressure model for cyclic straining of sand. Research Rep. 1985-06, Rensselaer Polytechnic Institute, Troy, NY.
71. Dobry R., Abdoun T., Stokoe II K. H., Moss R. E. S., Hatton M., and Gannainy H. E. (2015). Liquefaction potential of recent fills versus natural sands located in high-seismicity regions using shear-wave velocity. Journal of Geotechnical and Geoenvironmental Engineering. 141(3): 04014112.
72. Dyvik R., Berre T., Lacasse S., and Raadim B. (1987). Comparison of truly undrained and constant volume direct simple shear tests. Geotechnique, 37(1): 3-10.
73. Elgamal A., Yang Z., Parra E., and Ragheb A. (2003). Modeling of cyclic mobility in saturated cohesionless soils. Int. J. Plast., 19(6): 883–905.
74. Erten D., and Maher M. H. (1995). Cyclic undrained behavior of silty sand. Soil. Dyn. Earthquake Eng.,14(2): 115–123.
75. Finn W. D. L. (1985). Aspects of constant volume cyclic simple shear. Proc. Advances in the art of testing soils under cyclic conditions, ASCE, New York, 74–98.
76. Finn W. D. L., Ledbetter R. H., and Wu G. (1994). Liquefaction in silty soils: design and analysis. Ground failures under seismic conditions, geotechnical special publication ASCE 44: 51-74.
77. Finno R. J., and Rechenmacher A. L. (2003). Effects of consolidation history on critical state of sand. Journal of Geotechnical and Geoenvironmental Engineering, 129(4): 350-360, https://doi.org/10.1061/(ASCE)1090-0241(2003)129:4(350).
78. Fioravante V. (2000). Anisotropy of small strain stiffness of Ticino and Kenya sands for seismic wave propagation measured in triaxial testing. Soils and Foundations, 40(4): 129-142.
79. Fuggle A. R., Roozbahani M. M. and Frost J. D. (2014). Size effects on the void ratio of loosely packed binary particle mixtures. Geo-Congress 2014 Technical Papers, GSP 234 (C) ASCE 2014.
80. Gens A. (2019). Hydaulic fills with special focus on liquefaction. Proc. of the XVII ECSMGE-2019.

81. Georgiannou V. N., Burland J. B., and Hight D. W. (1990). The undrained behaviour of clayey sands in triaxial compression and extension. Geotechnique, 40(3):431–449.
82. Ghahremani M., and Ghalandarzadeh A. (2006). Effect of plastic fines on cyclic resistance of sands. Soil and Rock Behavior and Modeling (GSP 150), Shanghai, China, 406-412.
83. Ghahremani M., Ghalandarzadeh A., and Moradi M. (2006). Effect of plastic fines on the undrained behavior of sands. Soil and Rock Behavior and Modeling, ASCE GSP 150: 48-54, https://doi.org/10.1061/40862(194)5.
84. Goudarzy M., Rahman M. M., König D., and Schanz T. (2016). Influence of non-plastic fines content on maximum shear modulus of granular materials. Soils and Foundation, 56(6): 973–983, http://dx.doi.org/10.1016/j.sandf.2016.11.003.
85. Green R. A., Mitchell J. K., and Polito C. P. (2000). An energy-based excess pore-water pressure generation model for cohesionless soils. Proc., Developments in Theoretical Geomechanics-The John Booker Memorial Symposium, Sydney, New South Wales, Australia, 16-17.
86. Green R. A., Olson S. M., and Polito C. P. (2006). A comparative study of the influence of fines on the liquefaction susceptibility of sands: Field versus laboratory." Proc., 8th National Conf. on Earthquake Engineering, Earthquake Engineering Research Institute, Oakland, Ca.
87. Guo T., and Prakash S. (1999). Liquefaction of silts and silt-clay mixtures. J. Geotech. Geoenviron. Eng., 125(8), 706–710, https://doi.org/10.1061/(ASCE)1090-0241(1999)125:8(706).
88. Harder Jr L. F., and Boulanger R. (1997). Application of Kσ and Kα correction factors. In Proceedings of NCEER Workshop on Evaluation of Liquefaction Resistance of Soils. US National Center for Earthquake Engineering Research (NCEER). 129-148.
89. Hazirbaba K. (2005). Pore pressure generation characteristics of sands and silty sands: a strain approach. Dissertation presented for PhD program to the faculty of Graduate School at the University of Texas at Austin.
90. Hazirbaba K., and Rathje E. M. (2009). Pore Pressure Generation of Silty Sands due to Induced Cyclic Shear Strains. Journal of Geotechnical and Geoenvironmental Engineering, 135(12): 1892-1905, https://doi.org/10.1061/(ASCE)GT.1943-5606.0000147.
91. Hird C. C., and Hassona F. A. K. (1990). Some factors affecting the liquefaction and flow of saturated sands in laboratory tests. Engineering Geology, 28(1–2): 149-170, https://doi.org/10.1016/0013-7952(90)90039-4.
92. Hsiao D. H., and Phan V. T. A. (2016). Evaluation of static and dynamic properties of sand–fines mixtures through the state and equivalent state parameters. Soil Dynamics and Earthquake Engineering, 84: 134-144.
93. Huang Y.-T., Huang A.-B., Kuo Y.-C., and Tsai M.-D. (2004). A laboratory study on the undrained strength of a silty sand from Central Western Taiwan. Soil Dynamics and Earthquake Engineering, 24(9–10): 733-743.
94. Huang A.B. and Huang Y.T. (2007). Undisturbed sampling and laboratory shearing tests on a sand with various fines con-tents. Soils and Foundations, Vol.47, No.4, pp.771-781.
95. Huang A.-B., and Chuang S.-Y. (2011). Correlating cyclic strength with fines content through state parameters. Soils and Foundations, 51(6): 991-1001.

96. Huang A. B. (2016). The seventh James K. Mitchell lecture: characterization of silt/sand soils Geotechnical and Geophysical Site Characterisation. 5 ed Lehane et al. (Sydney: 2016 Australian Geomechanics Society) pp 3-18.
97. Idriss I. M. (1999). An update to the Seed-Idriss simplified procedure for evaluating liquefaction potential. In Proceedings of TRB Workshop on New Approaches to Liquefaction. Federal Highway Administration.
98. Idriss I. M., and Boulanger R. W. (2008). Soil Liquefaction during Earthquakes. Earthquake Engineering Research Institute.
99. Ishihara K., Lysmer J., Yasuda S., and Hirao H. (1976). Prediction of liquefaction in sand deposits during earthquakes. Soils and Foundations, 16(1), 1-16, https://doi.org/10.3208/sandf1972.16.1.
100. Ishihara K. (1993). Liquefaction and flow failure during earthquakes. Géotechnique, 43(3):351-451.
101. Jamiolkowski M., Lo Presti D. C. F., and Manassero M. (2003). Evaluation of relative density and shear strength of sands from CPT and DMT." In Proc., Symp. on Soil Behavior and Soft Ground Construction Honoring Charles C. "Chuck" Ladd, 1–37. Reston, VA: ASCE. https://doi.org/10.1061/40659(2003)7.
102. Jamiolkowski M. (2014) Soil mechanics and the observational method: challenges at the Zelazny Most copper tailings disposal facility. Géotechnique 64(8):590–619. https://doi.org/10.1680/geot.14.RL.002.
103. Jefferies M. G. (1993). Nor-Sand: a simple critical state model for sand. Géotechnique, 43:91-103, https://doi.org/10.1680/geot.1993.43.1.91.
104. Jefferies M. G., and Been K. (2006). Soil Liquefaction: A Critical State Approach. Taylor & Francis.
105. Jefferies M., and Been, K. (2016). Soil liquefaction: A critical state approach. 2nd ed. New York: Taylor & Francis.
106. Kammerer A. M., Pestana J. M., and Seed R. B. (2005). Behavior of Monterey 0/30 sand under multidirectional loading conditions. In: Geomechanics: testing, modeling, and simulation (pp 154–173). ASCE
107. Kanagalingam T., and Thevanayagam S. (2005). Discussion: Contribution of fines to the compressive strength of mixed soils. Géotechnique, 55(8): 627-628, https://doi.org/10.1680/geot.2005.55.8.627.
108. Karim M. E., and Alam M. J. (2015). Equivalent granular void ratio concept for sand-silt mixtures. IABSE-JSCE Joint Conference on Advances in Bridge Engineering-III, August 21-22, 2015, Dhaka, Bangladesh.
109. Karim M. E., and Alam M. J. (2017). Effect of nonplastic silt content on undrained shear strength of sand silt mixtures. Geo-Engineering, 8(14): 1-26. doi: 10.1186/540703-017-0051-1.
110. Kaufman L. P., and Change N. Y. (1982). Percentage silt content in sands and its effect on liquefaction potential. Proc., Int. Conf. On Computational Methods and Experimental Measurements, Whashington, D.C.
111. Klotz E. U., and Coop M. R. (2001). An investigation of the effect of soil state on the capacity of driven piles in sands. Géotechnique, 51(9): 733–751, 10.1680/geot.2001.51.9.733.

112. Koester J. P. (1994). The influence of fines type and content on cyclic strength. Ground failures under seismic conditions. Geotech. Special Pub. ASCE, 44:17–33.

113. Kokusho T., Ito F., Nagao Y., and Green A. (2012). Influence of non/low-plastic fines and associated aging effects on liquefaction resistance. Journal of Geotechnical and Geoenvironmental Engineering, 138(6): 747-756.

114. Kokusho T. (2020). Earthquake-induced flow liquefaction in fines-containing sands under initial shear stress by lab tests and its implication in case histories. Soil Dynamics and Earthquake Engineering, 130, 105984, https://doi.org/10.1016/j.soildyn.2019.105984.

115. Konrad J.-M. (1988). Interpretation of flat plate dilatomer tests in sands in terms of the state parameter. Géotechnique, 38(2): 263–277.

116. Kramer S. L. (1996). Geotechnical earthquake engineering. Prentice Hall, Upper Saddle River, N.J.

117. Kuerbis R. H. (1985). The effect of gradation and fine content on the undrained loading response of sand. PhD thesis, University of British Columbia.

118. Kuerbis R. H., Negussey D., and Vaid Y. P. (1988). Effect of gradation and fines content on the undrained response of sand. Hydraulic Fill Structures, ASCE Geotechnical Special Publication 21: 330-345.

119. Kuerbis R., and Vaid Y. P. (1988). Sand sample preparation-the slurry deposition method. Soils and Foundations. 28(4):107-118.

120. Ladd R., Dobry R., Dutko P., Yokel F., and Chung R. (1989). Pore water pressure buildup in clean sands because of cyclic straining. ASTM, Geotechnical Testing J., 12(1): 77–86.

121. Lade P. V. (1993). Initiation of static instability in the submarine Nerlerk berm. Canadian Geotechnical Journal. 30(6): 895-904.

122. Lade P. V., Liggio C. D., and Yamamuro J. A. (1998). Effects of non-plastic fines on minimum and maximum void ratios of sand. Geotechnical Testing Journal, 21(4): 336-347.

123. Lade P. V., and Yamamuro J. A. (1997). Effects of nonplastic fines on static liquefaction of sands. Canadian Geotechnical Journal, 34(6): 918–928, doi:10.1139/cgj-34-6-918.

124. Lade P. V., and Yamamuro J. A. (2011). Evaluation of static liquefaction potential of silty sand slopes. Can. Geotech. J. 48 (2), 247–264.

125. La Rochelle P., Sarrailh J., Tavenas F., Roy M., and Laroueil S. (1981). Causes of sampling disturbance and design of a new sampler for sensitive soils. Canadian Geotechnical Journal, 18(1):52-66.

126. Lashkari A. (2014). Recommendations for extension and re-calibration of an existing sand constitutive model taking in to account varying non-plastic fines content. Soil Dynamics and Earthquake Engineering, 61-62: 212-238, http://dx.doi.org/10.1016/j.soildyn.2014.02.012.

127. Lashkari A. (2016). Prediction of flow liquefaction instability of clean and silty sands. Acta Geotechnica, 11: 987-1014, doi:10.1007/s11440-015-0413-9.

128. Lee K. L., and Singh A. (1971). Relative density and relative compaction. Journal of the Soil Mechanics and Foundations Division, 97(7): 1049-1052.

129. Lee K. L., and Albaisa A. (1974). Earthquake induced settlements in saturated sands. J. Geotech. Eng. Div., 100(4): 387–405.

130. Lee W. F., Liao H. J., and Ishihara K. (2006). A study on engineering properties of Kaohsiung silty sand. (in Chinese), In-ternal Research Report, Taiwan Construction Research Insti-tute, Taipei, Taiwan, p. 204.
131. Lee W.F., Ishihara K., and Chen C-C (2012) Liquefaction of silty sand-preliminary studies from recent Taiwan, New Zealand and Japan earthquakes Proc. Int. Symp. Eng. Lessons learned from the 2011 Great East Japan Earthquake (Tokyo) pp 747-58.
132. Li X.-S., Dafalias Y.F., Wang Z.-L. (1999). State-dependant dilatancy in critical-state constitutive modelling of sand. Can. Geotech. J., 36 (4): 599–611, https://doi.org/10.1139/t99-029.
133. Li X. S., and Dafalias, Y. F. (2000). Dilatancy for cohesionless soils. Géotechnique, 50(4): 449-460, https://doi.org/10.1680/geot.2000.50.4.449.
134. Li X. S., and Dafalias Y. F. (2012). Anisotropic critical state theory: role of fabric. Journal of Engineering Mechanics, 138(3): 263-275, https://doi.org/10.1061/(ASCE)EM.1943-7889.0000324.
135. Liang L.-B. (2016). Static Liquefaction of Sand-Fines Mixtures with the Presence of Initial Shear Stress. MPhil thesis, Department of Civil Engineering, The University of Hong Kong.
136. Liu X., and Yang J. (2018). Influence of size disparity on small-strain shear modulus of sand-fines mixtures. Soil Dynamics and Earthquake Engineering 115: 217–224, https://doi.org/10.1016/j.soildyn.2018.08.011.
137. Lo Presti D., Pedroni S., and Crippa, V. (1992). Maximum dry density of cohesionless soils by pluviation and by ASTM D 4253-83: A comparative study. Geotechnical Testing Journal. 15(2): 180-189.
138. Luo X. D., and Yang, J. (2013). Effects of fines on shear behavior of sand: a DEM analysis. In Proceedings of 5th International Young Geotechnical Engineers' Conference, 2: 265-268.
139. Luo X. D. (2016). Investigation of the Mechanical Behavior of Granular Material: Effects of Particle Size Distribution and Particle Shape. PhD thesis, Department of Civil Engineering, The University of Hong Kong.
140. Manzari M.T., and Dafalias Y.F. (1997). A critical state two-surface plasticity model for sands. Géotechnique, 47: 255-272, https://doi.org/10.1680/geot.1997.47.2.255.
141. Marciano' V. (2011). Comportamento non drenato di sabbie cementate artificialmente per la mitigazione del richio di liquefazione. PhD thesis, Mediterranean university of Reggio Calabria.
142. Martin G. R., Finn W. D. L., and Seed H. B. (1975). Fundamentals of liquefaction under cyclic loading. J. Geotech. Eng. Div., 101(5): 423–438.
143. Matasovic N., and Vucetic M. (1993). Seismic response of horizontally layered soil deposits. Rep. No. ENG 93-182, School of Engineering and Applied Science,Univ. of California, Berkeley, CA.
144. McGeary R. K. (1961). Mechanical packing of spherical particles. Journal of the American Ceramic Society, 44(10): 513-522.
145. Mitchell J. K. (1976). Fundamentals of soil behaviour. Wiley, New York.
146. Miura K., Maeda K., Furukawa M., and Toki, S. (1997). Physical characteristics of sands with different primary properties. Soils and Foundations. 37(3): 53-64.

147. Mohammadi A, and Qadimi A. A. (2015). Simple critical state approach to predict the cyclic and monotonic response of sands with different fines contents using the equivalent intergranular void ratio. Acta Geotech.,10(5): 587-606, doi: 10.1007/s11440-014-0318-z.

148. Monkul M.M., and Yamamuro J. A. (2011). Influence of silt size and content on liquefaction behavior of sands. Can. Geotech. J., 48: 931–942, doi:10.1139/T11-001.

149. Montgomery J., Boulanger R. W., and Harder Jr. L. F. (2014). Examination of the Kσ overburden correction factor on liquefaction resistance. J. Geotech. Geoenviron. Eng. 140 (12): 04014066. https://doi.org/10.1061/(ASCE)GT.1943-5606.0001172.

150. Mulilis P. J., Seed B. H., Chan C. K., Mitchell J. K., and Arulanandan K. (1977). Effects of Sample Preparation on Sand Liquefaction. J. Geotech. D., 103(2): 91–108.

151. Murthy T. G., Loukidis D., Carraro J. A. H., Prezzi M., and Salgado R. (2007). Géotechnique, 57(3): 273–288.

152. Naeini S. A., and Baziar M. H. (2004). Effect of fines content on steady-state strength of mixed and layered samples of a sand. Soil Dynamics and Earthquake Engineering, 24: 181-187, doi:10.1016/j.soildyn.2003.11.003.

153. NRC (National Research Council). 1985. Liquefaction of soils during earthquakes. Washington, DC: National Academy Press.

154. Nguyen T.-K., Benahmed N., and Hicher P.-Y. (2017). Determination of the equivalent intergranular void ratio - Application to the instability and the critical state of silty sand. EPJ Web of Conferences, 140, doi: 10.1051/epjconf/201714002019.

155. Ni Q., Dasari G.R., and Tan T.S. (2006a). Equivalent granular void ratio for characterization of Singapore's old alluvium. Can. Geotech. J., 43(6): 563–573.

156. Ni Q., Tan T. S., Dasari G. R., and Hight D. W. (2004b). Contribution of fines to the compressive strength of mixed soils. Géotechnique. 54(9): 561-569, https://doi.org/10.1680/geot.2004.54.9.561.

157. Oda M. (1972). Initial fabrics and their relations to mechanical properties of granular material. Soils and Foundations. 12(1): 17-36.

158. Okashi Y. (1970). Effects of sand compaction on liquefaction during Tokachioki earthquake. Soils Found. JSSMFE, 10(2): 112–128.

159. Olson S. M. (2001). Liquefaction analysis of level and sloping ground using field case histories and penetration resistance. PhD thesis, Department of Civil Engineering, University of Illinois at Urbana Champaign.

160. Pan K., and Yang Z. X. (2017). Undrained behavior of sand under cyclic paths that match storm-wave loading conditions. Mar. Georesour. Geotechnol. https://doi.org/10.1080/1064119X.2017.1279697

161. Pan K., and Yang Z. X. (2018). Effects of intial static shear on cyclic resistance and pore pressure generation of saturated sand. Acta Geotechnica, 13:473-487. https://doi.org/10.1007/s11440-017-0614-5.

162. Pan K., Zhou G. Y., Yang Z. X., and Cai Y. Q. (2020). Comparison of cyclic liquefaction behaviour of clean and silty sands considering static shear effect. Soil Dyn. Earthq. Eng., 139:106338. https://doi.org/1016/j.soildyn.2020.106338.

163. Papadopoulou A., and Tika T. (2008). The effect of fines con critical state and liquefaction resistance characteristics of non-plastic silty sand. Soils and Foundations, 48(5): 713-725.

164. Papadopoulou A. I., and Tika T. M. (2016). The effect of fines plasticity on monotonic undrained shear strength and liquefaction resistance of sands. Soil Dynamics and Earthquake Engineering, 88: 191–206, http://dx.doi.org/10.1016/j.soildyn.2016.04.015.

165. Park T., and Ahn J.K. (2013). Accumulated stress based model for prediction of residual pore pressure. Proc. of the 18th International Conference on Soil Mechanics and Geotechnical Engineering, Paris, France.

166. Park S. S., and Kim Y. S. (2013). Liquefaction resistance of sand containing plastic fines with different plasticity. Journal of Geotechnical and Geoenvironmental Engineering, ASCE, 139(5): 825-830, https://doi.org/10.1061/(ASCE)GT.1943-5606.0000806.

167. Park T., Park D., and Ahn J. K. (2015). Pore pressure model based on accumulated stress. Bulletin of Earthquake Engineering, 13(7): 1913-1926.

168. Park S.-S., Nong Z.-Z., and Lee D.-E. (2020). Effect of vertical effective and intiial static shear stresses on the liquefaction resistance of sands in cyclic direct simple shear tests. Soils and Foundations, 60: 1588-1608. https://doi.org/10.1016/j.sandf.2020.09.007.

169. Pastor M., Zienkiewicz O.C., and Chan A.H.C. (1990). Generalized plasticity and the modelling of soil behaviour. Int. J. Numer. Anal. Methods Geomech. 14: 151–190, https://doi.org/10.1002/nag.1610140302.

170. Phan V.T.-A., Hsiao D.-H., Nguyen P. T.-L. (2016). Critical State Line and State Parameter fo Sand-Fines Mixtures. Procedia Engineering, 142(2016): 299-306.

171. Pitman T. D., Robertson P. K., and Sego D. C. (1994). Influence of fines on the collapse of loose sands. Can. Geotech. J., 31 (5): 728–739, https://doi.org/10.1139/t94-084.

172. Polito C. P. (1999). The effects of non-plastic and plastic fines on the liquefaction of sandy soils. Ph.D. thesis, Virginia Polytechnic Institute and State Univ., Blacksburg, VA.

173. Polito C. P., and Martin J. R. (2001). Effects of Nonplastic Fines on the Liquefaction Resistance of Sands. J. Geotech. Geoenviron. Eng., 127(5), 408-415.

174. Polito C. P., and Martin J. R. (2003). A reconciliation of the effects of non-plastic fines on the liquefaction resistance of sands reported in the literature. Earthq. Spectra, 19(3): 635–651.

175. Polito C. P., Green R. A., and Lee, J. (2008). Pore pressure generation models for sands and silty soils subjected to cyclic loading. J. Geotech. Geoenviron. Eng., 134(10): 1490–1500, https://doi.org/10.1061/(ASCE)1090-0241(2008)134:10(1490).

176. Polito C., Green R. A., Dillon E., and Sohn C. (2013). Effect of load shape on relationship between dissipated energy and residual excess pore pressure generation in cyclic triaxial tests. Canadian Geotechnical Journal, 50(11): 1118–1128.

177. Porcino D., Caridi G. and Ghionna V. N. (2005a). Behaviour of a carbonate sand in undrained monotonic simple shear tests. Proc.of the international conference on problematic soils (eds Bilsel and Nalbantoglu), 1, 407–414.

178. Porcino D., Caridi G., and Ghionna V. N. (2005b). Drained and undrained monotonic behaviour of sand in simple shear tests. Proc. 11th Int. Conf. Computer Methods Advances Geomech, IACMAG, Patron, Bologna, 183–190.

179. Porcino D., Caridi G., Malara M., and Morabito E. (2006). An automated control system for undrained monotonic and cyclic simple shear tests. In Proc., Geotechnical Engineering in the Information Technology Age, 1–6. Reston, VA: ASCE.

180. Porcino D., and Marcianò V. (2008). Effect of initial fabric on cyclic and monotonic undrained shear strength of Gioia Tauro sand. In: Proc. of the 2008 Seismic Engineering Conference commemorating the 1908 Messina and Reggio Calabria Earthquake – Part. I. p.448-455, Santini A. & Moraci N., Reggio Calabria, 08-11 July, doi: 10.1063/1.2963870.

181. Porcino D., and Diano V. (2016). Labouratory Study on Pore Pressure Generation and Liquefaction of Low-Plasticity Silty Sandy Soils during the 2012 Earthquake in Italy. J. of Geotechn. And Geoenviron. Eng., 142(10):0401048. DOI: 10.1061/(ASCE)GT.1943-5606.0001518.

182. Porcino D. D., and Diano V. (2017). The influence of non-plastic fines on pore water pressure generation and undrained shear strength of sand-silt mixtures. Soil Dyn. Earthquake Eng. 101: 311–321. https://doi.org/10.1016/j.soildyn.2017.07.015.

183. Porcino D. D., Diano V., and Tomasello G. (2018a). Effect of Non-plastic Fines con Cyclic Shear Strength of Sand Under Initial Static Shear Stress. In Proc. of China-Europe Conf. on Geotech. Eng., SSGG, pp. 597-601, Wu & Yu (Eds.).

184. Porcino D. D., Tomasello G., and Diano V. (2018b). Key factors affecting prediction of seismic pore water pressures in silty sands based on damage parameter. Bull. Earthquake Eng., 16: 5801–5819 (2018), https://doi.org/10.1007/s10518-018-0411-z

185. Porcino D.D., Monaco P. and Tonni L. (2019a). Evaluating seismic behavior of intermediate silty sands of low plasticity from Emilia Romagna, Italy Geo-Congress 2019 GSP 308 (ASCE) pp 341-351.

186. Porcino D.D., Diano V., Triantafyllidis T., and Wichtmann T. (2019b). Predicting undrained static response of sand with non-plastic fines in terms of equivalent granular state parameter. Acta Geotechnica, 15: 867-882, https://doi.org/10.1007/s11440-019-00770-5.

187. Porcino D. D., Witchtmann T., and Tomasello G. (2019c). An insight into the prediction of limiting fines content for mixtures of sand with nonplastic fines based on monotonic and cyclic tests." In Proc., Earthquake Geotechnical Engineering for Protection and Development of Environment and Constructions, edited by F. Silvestri and N. Moraci, 4540–4547. Rome: Associazione Geotecnica Italiana.

188. Porcino D.D. (2019). Recent advances in pore water pressure and liquefaction characteristics of low plasticity silty sands subjected to cyclic loading. ACEER 2019, 1-4 June, Kaohsiung, Taiwan.

189. Porcino D. D., Triantafyllidis T., Wichtmann T., and Tomasello G. (2021). Application of Critical State Approach to Liquefaction Resistance of Sand-Silt Mixtures under Cyclic Simple Shear Loading. Journal of Geotechnical and Geoenvironmental Engineering, 147(3): 04020177. DOI: 10.10611/(ASCE)GT.1943-5606.0002470.

190. Poulos S. J., Castro G., and France J. W. (1985). Liquefaction evaluation procedure. Journal of Geotechnical Engineering, 11(6): 772-792. https://doi.org/10.1061/(ASCE)0733-9410(1985)111:6(772)

191. Prevost J. H. (1985). A simple plasticity theory for frictional cohesionless soils. Soil Dyn. Earthquake Eng., 4(1): 9–17.

192. Qadimi A. (2005). The cyclic response of a carbonate sand through critical state soil mechanics. PhD thesis, Imperial College, London.

193. Qadimi A., and Mohammadi A. (2014). Evaluation of state indices in predicting the cyclic and monotonic strength of sands with different fines contents. Soil Dynamics and Earthquake Engineering, 66: 443–458, http://dx.doi.org/10.1016/j.soildyn.2014.08.002.

194. Rabbi A. T. M. Z., Rahman M. M., and Cameron D. A. (2019). The relation between the state indices and the characteristic features of undrained behaviour of silty sand. Soils and Foundations, 59: 801–813, https://doi.org/10.1016/j.sandf.2019.05.001.

195. Rahman, M. M., Lo, S. R. & Gnanendran, C. T. (2008). On equivalent granular void ratio and steady state behaviour of loose sand with fines. Canadian Geotechnical Journal, 45(10): 1439-1456.

196. Rahman M. M., and Lo S. R. (2008). The prediction of equivalent granular steady state line of loose sand with fines. Geomechanics and Geoengineering, 3(3): 179-190, https://doi.org/10.1080/17486020802206867.

197. Rahman M. M. (2009). Modelling the influence of fines on liquefaction behaviour. PhD thesis, School of Engineering and Information Technology, University of New South Wales at Australian Defence Force Academy.

198. Rahman M. M., Lo S. R., and Cubrinovski M. (2010). Equivalent granular void ratio and behaviour of loose sand with fines. Proc. of 5th International Conference on Recent Advances in Geotechnical Earthquake Engineering and Soil Dynamics, San Diego, California, p. 1–9.

199. Rahman M. M., Lo S. R., and Baki M. A. L. (2011). Equivalent granular state parameter and undrained behaviour of sand-fines mixtures. Acta Geotechnica, 6: 183-194.

200. Rahman M. M. (2012). Modelling the behaviour of sand with fines using equivalent granular void ratio." In Proc., AZN 2012 Conf., 656–661, St. Ives, Australia: Australian Geomechanics Society.

201. Rahman M. M., and Lo S. R. (2012). Predicting of the onset of static liquefaction of loose sand with fines. Journal of Geotechnical and Geoenvironmental Engineering, 138(8): 1037-1041.

202. Rahman M. M., and Lo S. R. (2014). Undrained Behavior of Sand-Fines Mixtures and Their State Parameter. Journal of Geotechnical and Geoenvironmental Engineering, 140(7), https://doi.org/10.1061/(ASCE)GT.1943-5606.0001115.

203. Rahman M. M., Lo S. C. R., and Dafalias Y. F. (2014). Modelling the static liquefaction of sand with low-plasticity fines. Géotechnique 64 (11): 881–894. https://doi.org/10.1680/geot.14.P.079.

204. Rahman M. M., and Sitharam T. G. (2020). Cyclic liquefaction screening of sand with non-plastic fines: Critical state approach. Geosci. Front., 11(2): 429–438. https://doi.org/10.1016/j.gsf.2018.09.009.

205. Rees S. D. (2010). Effects of fines on the undrained behaviour of Christchurch sandy soils. Ph.D. thesis, Dept. of Civil and Natural Resources Engineering, Univ. of Canterbury.

206. Riemer, M. F., Seed, R. B., Nicholson, P. G. & Jong, H. L. (1990). Steady state testing of loose sands: limiting minimum density. Journal of Geotechnical Engineering. 116(2): 332- 337.

207. Riemer M. F., and Seed R. B. (1997). Factors affecting apparent position of steady-state line. Journal of Geotechnical and Geoenvironmental Engineering, 123(3): 281-288, https://doi.org/10.1061/(ASCE)1090-0241(1997)123:3(281).

208. Robertson P. K. (1994). Design consideration for liquefaction reflections sul la conception pour liquefaction. XIII ICSMFE, New Delhi, India.

209. Robertson P. K., and Fear C. E. (1995). Liquefaction of sands and its evaluation. In Proceedings of 1st International Conference on Earthquake Geotechnical Engineering. (Ishihara, K. (ed)). Tokyo, Japan.

210. Robertson P. K., and Wride C. E. (1998). Evaluating cyclic liquefaction potential using the cone penetration test. Canadian Geotechnical Journal, 35(3): 442-459.

211. Roscoe K.H. (1970). The influence of strains in soil mechanics. Geotechnique, 20(2): 129-170.

212. Roscoe K. H., Schofield A. N., and Wroth C. P. (1958). On the yielding of soils. Géotechnique, 8(1): 22-53, http://doi.org/10.1680/geot.1958.8.1.22.

213. Roscoe K. H., Basset R. H., and Cole E. R. L. (1967). Principal axes observed during simple shear of a sand. Proceedings Geotechnical Conference, Oslo, 1, 231- 237.

214. Sadek S., and Saleh M. (2007). The effect of carbonaceous fines on cyclic resistance of poorly graded sands. Journal of Geotechnical and Geological Engineering 25: 257-264.

215. Sadrekarimi A. (2014). Effect of mode of shear on static liquefaction analysis. J. Geotech. Geoenviron. Eng., 04014069.

216. Sadrekarimi A., and Olson S. M. (2011). Yield strength ratios, critical strength ratios, and brittleness of sandy soils from laboratory tests. Can. Geotech. J. 48, 493–510.

217. Salgado R., Bandini P., and Karim A. (2000). Shear strength and stiffness of silty sand. ASCE J. Geotech. Geoenviron. Eng., 126(5): 451–62.

218. Sapporo City Office (2018): Publications for Forum to Residents on 2018 Earthquake Damage.

219. Schofield A., and Wroth P. (1968). Critical State Soil Mechanics. McGraw-Hill.

220. Shuttle D. A., and Cunning J. (2007). Liquefaction potential of silts from CPTu. Canadian Geotechnical Journal, 44 (1): 1-19. https://doi.org/10.1139/t06-086.

221. Seed H. B., Martin P. P., and Lysmer J. (1975). The generation and dissipation of pore-water pressures during soil liquefaction. Geotechnical Report No. EERC 75-26, Univ. of California, Berkeley, CA.

222. Seed H. B., Martin G. R., and Pyke R. M. (1978). Effect of multidirectional shaking on pore pressure development in sands. Journal of the Geotechnical Engineering Division, 104(1): 27-44, https://doi.org/10.1061/AJGEB6.0000575.

223. Seed H. B. (1981). Earthquake-resistant design of earth dams. In Proceedings of International Conferences on Recent Advances in Geotechnical Earthquake Engineering and Soil Dynamics (Prakash, S. (ed)). University of Missouri Rolla. 1157-1173.

224. Seed H. B., and Idriss I. M. (1982). Ground Motions and Soil Liquefaction During Earthquakes. Earthquake Engineering Research Institute.

225. Seed H. B., Tokimatsu K., Harder L. F., and Chung R. M. (1985). Influence of SPT procedures in soil liquefaction resistance evaluations. Journal of Geotechnical Engineering, 111(12): 1425-1445.

226. Seed R. B., and Harder Jr L. F. (1990). SPT-based analysis of cyclic pore pressure generation and undrained residual strength. In Proceedings of H. Bolton Seed Memorial Symposium.

227. Sharma K., Deng L., and Khadka, D. (2019). Reconnaissance of liquefaction case studies in 2015 Gorkha (Nepal) earthquake and assessment of liquefaction susceptibility. Int. J. Geotech. Eng., 13(4), 326-328.

228. Sinatra L., and Foti S. (2015). The role of aftershocks in the liquefaction phenomena caused by the Emilia 2012 seismic sequence. Soil Dyn. Earth. Eng., 75, 234-245. http://dx.doi.org/10.1016/j.soildyn.2015.03.024

229. Singh S. (1994). Liquefaction characteristics of silts. In Proceedings of Ground Failures under Seismic Conditions (Prakash, S., andDakoulas, P. (eds)). ASCE. 105-116.

230. Singh S. (1995). Re-examination of the Effects of Fine Contents on the Liquefaction Characteristics of Sands. Earthquake Geotechnical Engineering (Ishihara Edition), 829-831.

231. Sivathayalan S. (1994). Static, cyclic and post-liquefaction simple shear response of sands. Thesis (PhD), University of British Columbia.

232. Sivathayalan S., and Ha D. (2011). Effect of static shear stress on the cyclic resistance of sands in simple shear loading. Can. Geotech. J. 48: 1471–1484.

233. Sladen J. A., D'hollander R. D., Krahn J., and Mitchell, D. E. (1985). Back analysis of the Nerlerk berm liquefaction slides. Canadian Geotechnical Journal. 22(4): 579-588.

234. Sladen J. A., Krahn J., and Hollander R. D. (1986). Discussion: A state parameter for sand. Géotechnique, 36(1): 123-132.

235. Stamatopoulos C. A. (2010). An experimental study of the liquefaction strength of silty sands in terms of the state parameter. Soil Dynamics and Earthquake Engineering 30(8): 662-678, doi:10.1016/j.soildyn.2010.02.008.

236. Sze, H. Y. (2010). Initial Shear and Confining Stress Effects on Cyclic Behaviour and Liquefaction Resistance of Sands. PhD thesis, Department of Civil Engineering, The University of Hong Kong.

237. Sze H., and Yang J. (2014). Failure modes of sand in undrained cyclic loading: impact of sample preparation. Journal of Geotechnical and Geoenvironmental Engineering, 140(1): 152-169.

238. Tani K., and Kaneko S. (2006). Method of recovering undisturbed samples using water-soluble thick polymer. (in Japanese) Tsuchi-to-Kiso, Journal of Japanese Geotechnical Society54(4):145-148.

239. Tao M., Figueroa J. L., and Saada A. S. (2004). Inuence of nonplastic fines content on the liquefaction resistance of soil in terms of the unit energy. Proc., Cyclic Behaviour of Soils and Liquefaction Phenemena, A.A. Balkema Publishers Bochum, Germany, pp. 223-231.

240. Tatsuoka F., Ochi K., Fujii S., and Okamoto, M. (1986). Cyclic undrained triaxial and torsional shear strength of sands for different sample preparation methods. Soils and Foundations. 26(3): 23-41.

241. Thevanayagam S. (1998). Effect of fines and confining stress on undrained shear strength of silty sands. Journal of Geotechnical and Geoenvironmental Engineering, 124(6): 479-491, http:///dx.doi.org/10.1061/(ASCE)1090-0241(1998)124:6(479).

242. Thevanayagam S., and Mohan S. (2000). Intergranular state variables and stress±strain behaviour of silty sands. Géotechnique, 50(1): 1-23.

243. Thevanayagam S., and Martin G. R. (2002). Liquefaction in silty soils-screening and remediation issues. Soil Dynamics and Earthquake Engineering, 22: 1035–1042.

244. Thevanayagam S., Shenthan T., Mohan S., and Liang J. (2002). Undrained Fragility of Clean Sands, Silty Sands, and Sandy Silts. Journal of Geotechnical and Geoenvironmental Engineering, 128(10): 849–859.

245. Thevanayagam S., Shenthan T., and Kanagalingam T. (2003). Role of Intergranular contacts on Mechanisms causing Liquefaction and Slope Failures in Silty Sands. Buffalo, University of Buffalo.

246. Thevanayagam S., and Ecemis N. (2008). Effects of permeability on liquefaction resistance and cone resistance. In Proceedings of Geotechnical Earthquake Engineering and Soil Dynamics IV (Zeng, D., Manzari, M. T., andHiltunen, D. R. (eds)). 1-11.

247. Tokimatsu K., and Yoshimi Y. (1983). Empirical correlation of soil liquefaction based on SPT N-value and fines content. Soils and Foundations, 23(4): 56-74.

248. Tokimatsu K., Tamura S., Suzuki H., and Katsumata K. (2012). Building damage associated with geotechnical problems in the 2011 Tohoku Pacific Earthquake. Soils and Foundations, 52(5): 956-974.

249. Tonni, L. et al. (2015). Interpreting the deformation phenomena triggered by the 2012 Emilia seismic sequence on the Canale Diversivo di Burana banks (Analisi dei fenomeni defomativi indotti dalla sequenza sismica emiliana del 2012 su un tratto di argine del Canale Diversivo di Burana (FE). Ital. Geotech. J., 45(2), 28-58.

250. Troncoso J. H., and Verdugo R. (1985). Silt content and dynamic behavior of tailing sands. In Proc., 11th Int. Conf. on Soil Mechanics and Foundation Engineering, Balkema, Rotterdam, Netherlands, 1311–1314.

251. Tsai P.H., Lee D.H., Kung G. T.C., and Hsu C.H. (2010). Effect of content and plasticity of fines on liquefaction behavior of soils. Quart. J. Eng. Geol. Hydrogeol., 43(1): 95–106.

252. Tsukamoto, Y. Ishihara, K., Kokusho, T, Hara, T. and Tsutsumi, Y. (2009). Fluidisation and subsidence of gently sloped farming fields reclaimed with volcanic soils during 2003 Tokachi-oki earthquake in Japan, Geotechnical Case History Volume, Balkema, 109-118.

253. Ueng T.-S., Sun C.-W., and Chen C.-W. (2004). Definition of fines and liquefaction resistance of Mulou River soil. Soil Dyn. Earthquake Eng. 24 (9–10): 745–750. https://doi.org/10.1016/j.soildyn.2004.06.011.

254. Vaid Y. P., and Chern J. C. (1983). Effect of static shear on resistance to liquefaction. Soils and Foundations. 23(1): 47-60.

255. Vaid Y. P., Chung E. K. F., and Kuerbis R. H. (1990). Stress path and steady state. Canadian Geotechnical Journal, 27(1) :1-7, https://doi.org/10.1139/t90-001.

256. Vaid Y. P. (1994). Liquefaction of silty soils. In Proc., Ground failures under seismic conditions, Geotech. Spec. Publ., ASCE 44: 1-16.

257. Vaid Y. P., and Sivathayalan S. (2000). Fundamental factors affecting liquefaction susceptibility of sands. Canadian Geotechnical Journal, 37(3): 592-606.

258. Vaid Y.P., Stedman J.D., Sivathayalan S. (2001). Confining stress and static shear effects in cyclic liquefaction. J. Can. Geotech. 38, 580–591.

259. Verdugo R., and Ishihara K. (1996). The steady state of sandy soils. Soils and Foundations, 36(2): 81-91, https://doi.org/10.3208/sandf.36.2_81.

260. Verma P., and Wijewickreme D. (2015). Some Observation on the Effect of Initial Static Shear Stress on Cyclic Response of Natural Silt from Lower Mainland of British Columbia. 6th Int. Conf. on Eqrthquake Geotechn. Eng., Christchurch, New Zealand, 1-4 Novermber 2015.

261. Vucetic M., and Dobry R. (1986). Pore pressure build-up and liquefaction at level sandy sites during earthquakes [Research report CE-86-3]. Troy, NY: Dept. of Civil Engineering, Rensselaer Polytechnic Institute.

262. Wang Z.-L., Dafalias Y.F., Li X.-S., and Makdisi F.I. (2002). State pressure index for modelling sand behaviour. J. Geotech. Geoenviron. Eng., 128(6): 511–519, https://doi.org/10.1061/(ASCE)1090-0241(2002)128:6(511).

263. Wang G., and Xie Y. (2014). Modified bounding surface hypoplasticity model for sands under cyclic loading. J. Eng. Mech. 140, 91-101. https://doi.org/10.1061/(ASCE)EM.1943- 7889.0000654.

264. Wei L. M., and Yang J. (2014). On the role of grain shape in static liquefaction of sand–fines mixtures. Géotechnique. 64(9): 740-745, http://dx.doi.org/10.1680/geot.14.T.013.

265. Wei X., and Yang, J. (2015). The effects of initial static shear stress on liquefaction resistance of silty sand. In Proceedings of 6th International Conference on Earthquake Geotechnical Engineering. Christchurch, New Zealand.

266. Wei X. (2017). Cyclic Behaviour and Liquefaction Resistance of Silty Sands. PhD thesis, Department of Civil Engineering, The University of Hong Kong.

267. Wei X., and Yang J. (2019a). Characterizing the effects of fines on the liquefaction resistance of silty sands. Soils and Foundations, 59: 1800–1812, https://doi.org/10.1016/j.sandf.2019.08.010.

268. Wei X., and Yang J. (2019b). Cyclic behavior and liquefaction resistance of silty sands with presence of initial static shear stress. Soil Dynamics and Earthquake Engineering, 122: 274–289, https://doi.org/10.1016/j.soildyn.2018.11.029.

269. Wei X., Yang J., Zhuo Y.-G., and Chen Y. (2020). Influence of particle-size disparity on cyclic liquefaction resistance of silty sands. Géotechnique Letters 10: 155–161, https://doi.org/10.1680/jgele.19.00076.

270. Wichtmann T. (2016). Soil behaviour under cyclic loading - Experimental observations, constitutive description and applications. Habilitation thesis, Institute for Soil Mechanics and Rock Mechanics, Karlsruhe Institute of Technology.

271. Wijewickreme D., and Sanin M.V. (2007). Effect of plasticity on the laboratory cyclic shear response of fine-grained soils. Proc, 4th Int.Conf. on Earthquake Geotechnical Engineering, ISSMGE, Thessaloniki, Greece.

272. Wijewickreme D., and Sanin M. V. (2010). Post cyclic reconsolidation strains in low-plastic Fraser River silt due to dissipation of excess pore-water pressures. J. Geotech. Geoenviron. Eng., ASCE, 136(10):1347–1357.

273. Xenaki V. C., and Athanasopoulos G. (2003). Liquefaction resistance of sand-silt mixtures: an experimental investigation of the effect of fines. Soil Dynamics and Earthquake Engineering 23(3): 183-194, doi:10.1016/S0267-7261(02)00210-5.

274. Xiao Y., Liu H., Chen Y., and Jiang J. (2014). Bounding surface plasticity model incorporating the state pressure index for rockfill materials. J. Geotech. Geoenviron. Eng., 140(11): 04014087.

275. Xu L. Y., Zhang J. Z., Cai F., Chen W. Y., and Xue Y.Y. (2019). Constitutive modeling the undrained behaviors of sands with non-plastic fines under monotonic and cyclic loading. Soil Dynam. Earthq. Eng., 123: 413–24.

276. Yamamuro J.A., and Lade P.V. (1997). Static liquefaction of very loose sands. Canadian Geotechnical Journal, 34 (6), 905–917.

277. Yamamuro J. A., and Lade P. V. (1998). Steady-State Concepts and Static Liquefaction of Silty Sands. Journal of Geotechnical and Geoenvironmental Engineering, 124(9): 868–877.

278. Yamamuro J. A., and Lade P.V. (1999). Experiment sand modeling of silty sands susceptible to static liquefaction. Mech. Cohes.-Frict. Mater., 4: 545–64.

279. Yang J. (2002). Non-uniqueness of flow liquefaction line for loose sand. Géotechnique, 52(10): 757-760, https://doi.org/10.1680/geot.2002.52.10.757.

280. Yang S., Lacasse S., and Sandven R. (2006a). Determination of the Transitional Fines Content of Mixtures of Sand and Non-plastic Fines. Geotechnical Testing Journal, 29(2), Paper ID GTJ14010.

281. Yang S. L., Sandven R., and Grande L. (2006b). Steady-state Lines of Sand-silt Mixtures. Canadian Geotechnical Journal, 43(11): 1213 - 1219.

282. Yang J., and Sze H. Y. (2011a). Cyclic behaviour and resistance of saturated sand under non-symmetrical loading conditions. Géotechnique, 61(1): 59-73, https://doi.org/10.1680/geot.9.P.019.

283. Yang J., and Sze H. Y. (2011b). Cyclic strength of sand under sustained shear stress. Journal of Geotechnical and Geoenvironmental Engineering, 137(12): 1275-1285.

284. Yang J. and Wei L.M. (2012). Collaple of loose sand with the addition of fines: the role of particle shape. Géotechnique, 62(12): 1111-1125, doi: http:/dx.doi.org/10.1680/geot.11.P.062.

285. Yang J, and Luo X. D. (2015). Exploring the relationship between critical state and particle shape for granular materials. Journal of the Mechanics and Physics of Solids. 84: 196-213, http://dx.doi.org/10.1016/j.jmps.2015.08.001.

286. Yang J., Wei L.M. and Dai B.B. (2015). State variables for silty sands: Global void ratio or skeleton void ratio?. Soils and Foundations, 55(1): 99-111.

287. Yang Z. X., Xu T. T., and Li X. S. (2019). J2-deformation type model coupled with state dependent dilatancy. Comput. Geotech., 105: 129-141, https://doi.org/10.1016/j.compgeo.2018.09.018.

288. Yasuda S., Wakamatsu K., Nagase H. (1994). Liquefaction of artificially filled silty sands. Ground failures under seismic conditions. Geotech. Special. Pub. ASCE, 44: 91–104.

289. Yoshimine M., and Ishihara K. (1998). Flow potential of sand during liquefaction. Soils and Foundations, 38(3): 189-198.

290. Youd T., Idriss I., Andrus R., Arango I., Castro G., Christian J., Dobry R., Finn W., Harder L. J., Hynes M., Ishihara K., Koester J., Liao S., Marcuson W., Martin G., Mitchell J., Moriwaki Y., Power M., Robertson P., Seed R., and Stokoe II K. (2001). Liquefaction resistance of soils: summary report from the 1996 NCEER and 1998 NCEER/NSF workshops on evaluation of liquefaction resistance of soils. Journal of Geotechnical and Geoenvironmental Engineering. 127(10): 817-833.

291. Zhang J.-M., and Wang G. (2012). Large post-liquefaction deformation of sand, part I: physical mechanism, constitutive description and numerical algorithm. Acta Geotech. 7: 69-113, https://doi.org/10.1007/s11440-011-0150-7.

292. Zlatović S., and Ishihara K. (1995). On the influence of nonplastic fines on residual strength. In Proceedings of 1st International Conference on Earthquake Geotechnical Engineering (Ishihara, K. (ed)), 1: 239-244.

293. Zuo L., and Baudet B. A. (2015). Determination of the transitional fines content of sand-non plastic fines mixtures. Soils and Foundations. 55(1): 213-219, http://dx.doi.org/10.1016/j.sandf.2014.12.017.

Appendix

Undrained cyclic simple shear tests

- Ticino sand
- Sand-silt mixture (f_c=5%)
- Sand-silt mixture (f_c=10%)
- Sand-silt mixture (f_c=20%)
- Sand-silt mixture (f_c=30%)
- Sand-silt mixture (f_c=40%)

Ticino sand

Undrained Cyclic Simple Shear test: *C_SS_TS0_S50_A0_1*
Ticino sand (Reconstitution method: Moist Tamping)
e_0= 0.82 - D_R= 31% - σ'_{v0}= 50 kPa - α= 0 - *CSR* = 0.15

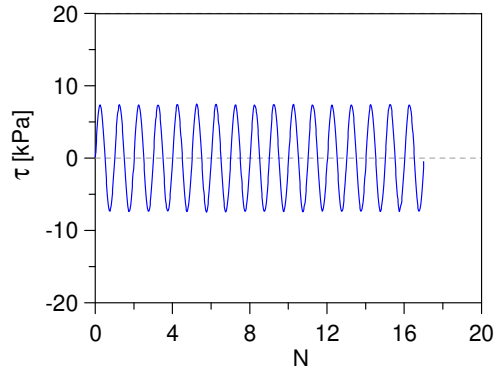

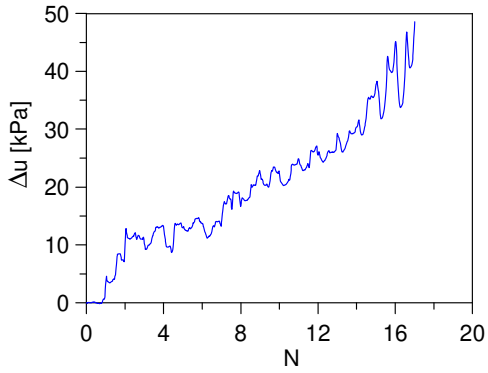

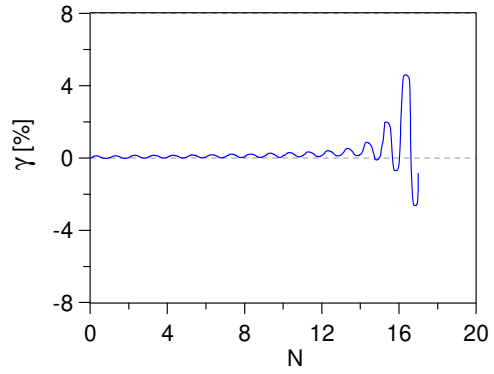

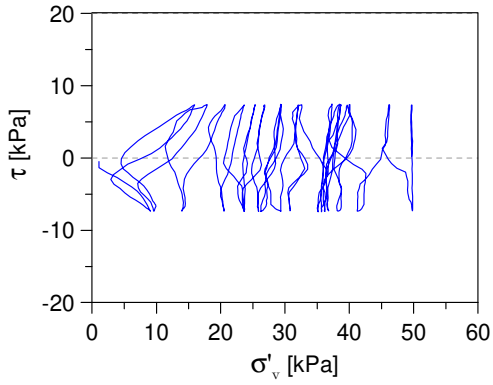

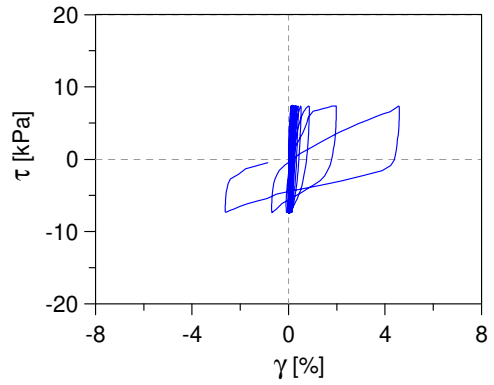

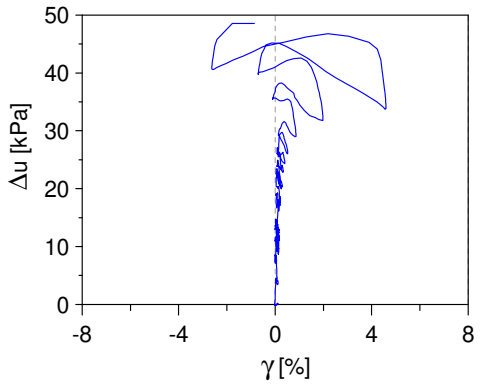

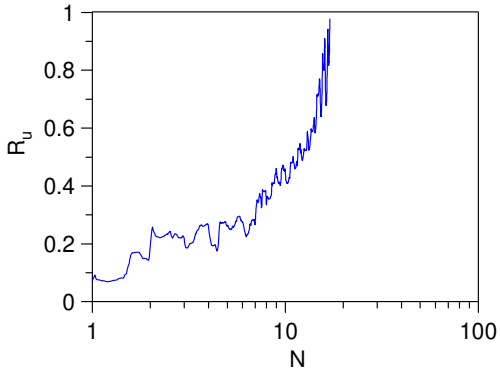

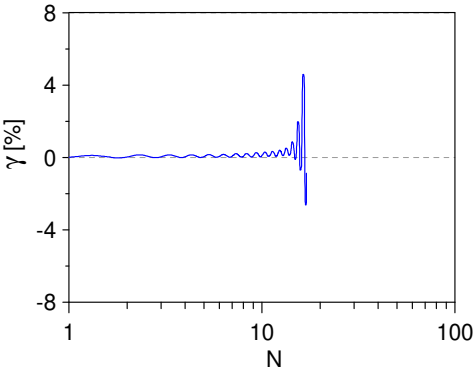

Undrained Cyclic Simple Shear test: *C_SS_TS0_S100_A0_1*
Ticino sand (Reconstitution method: Moist Tamping)
e_0= 0.78 - D_R= 43% - σ'_{v0}= 100 kPa - α=0 - *CSR* = 0.12

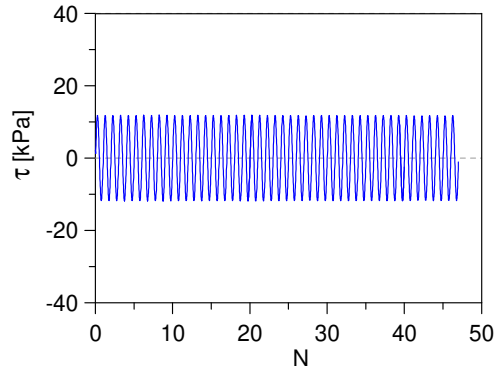

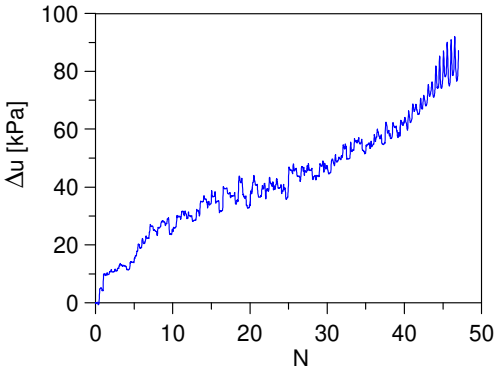

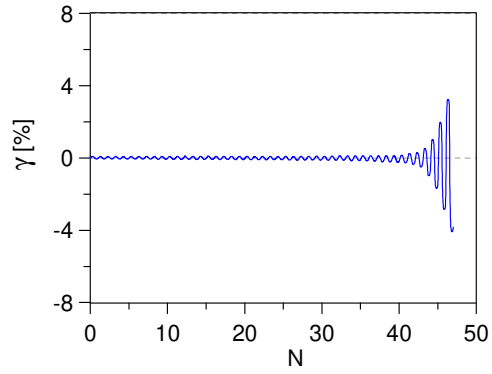

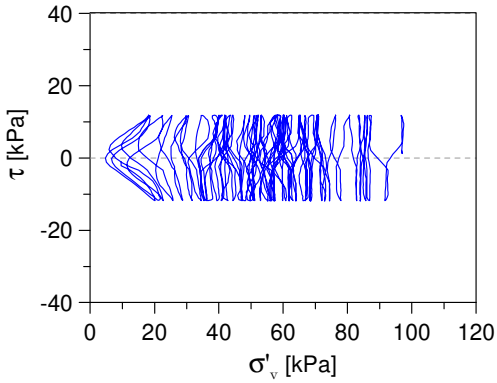

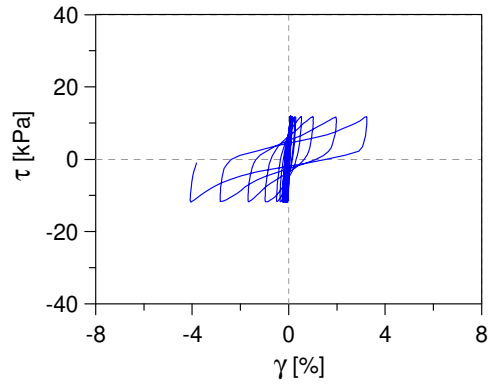

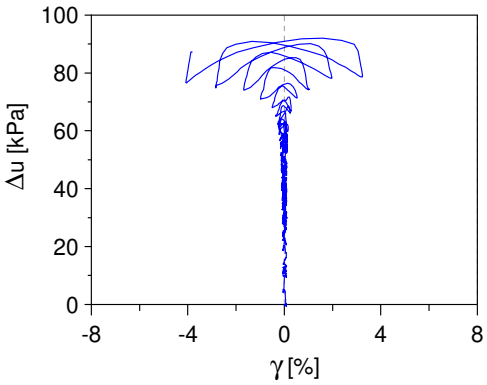

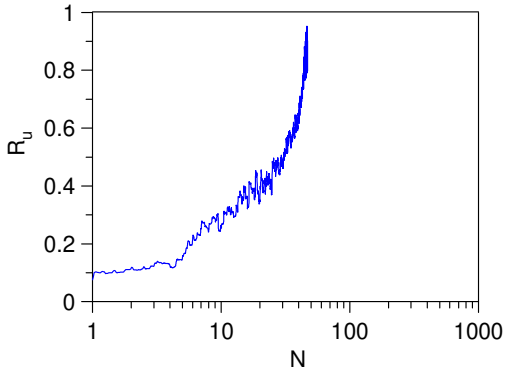

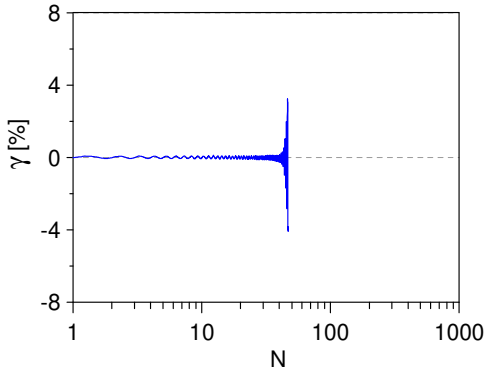

Undrained Cyclic Simple Shear test: *C_SS_TS0_S100_A0_2*
Ticino sand (Reconstitution method: Moist Tamping)
e_0= 0.78 - D_R= 43% - σ'_{v0}= 100 kPa - α=0 - *CSR* = 0.14

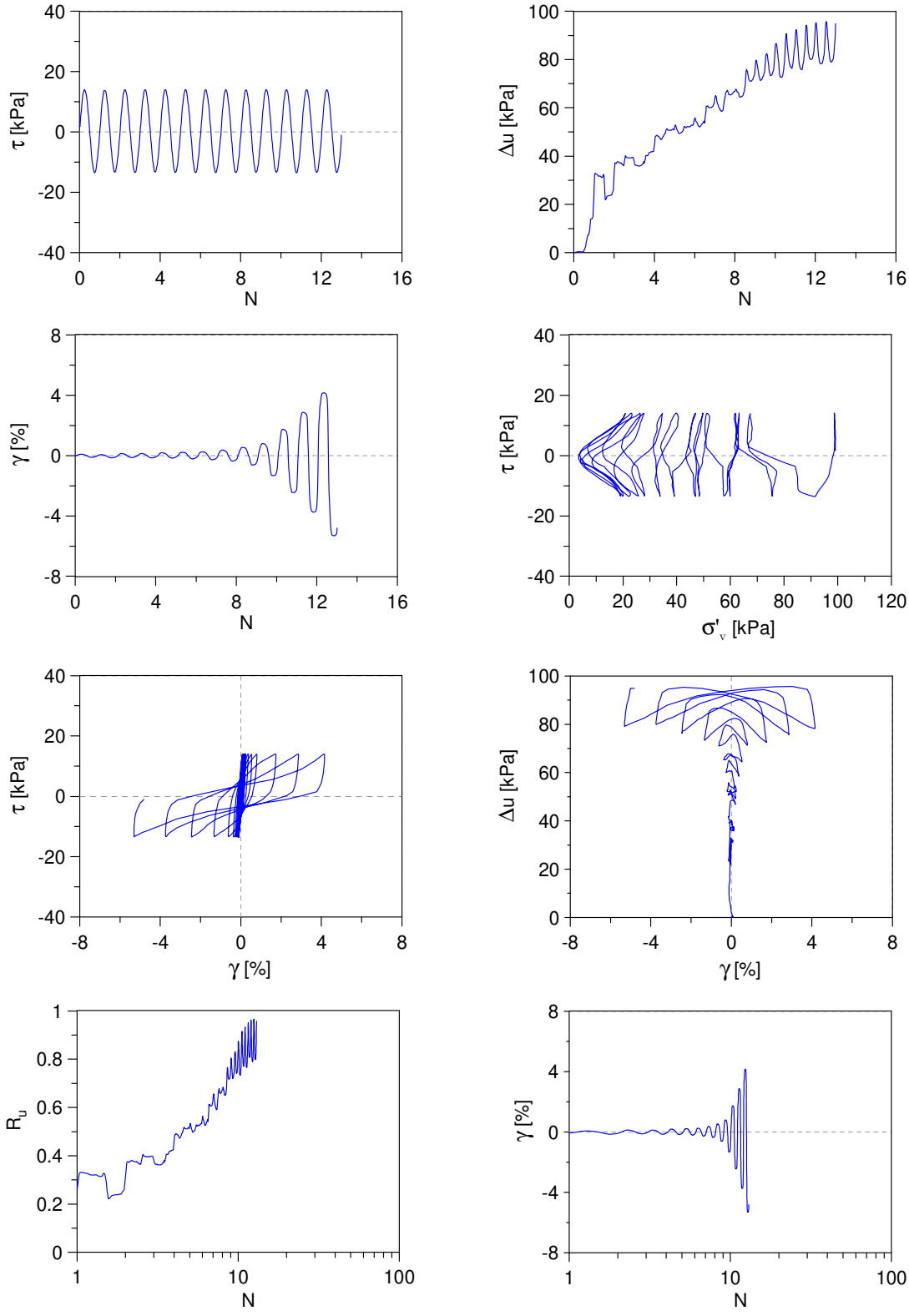

Undrained Cyclic Simple Shear test: *C_SS_TS0_S100_A0_3*
Ticino sand (Reconstitution method: Moist Tamping)
e_0= 0.78 - D_R= 43% - σ'_{v0}= 100 kPa - α= 0 - *CSR* = 0.16

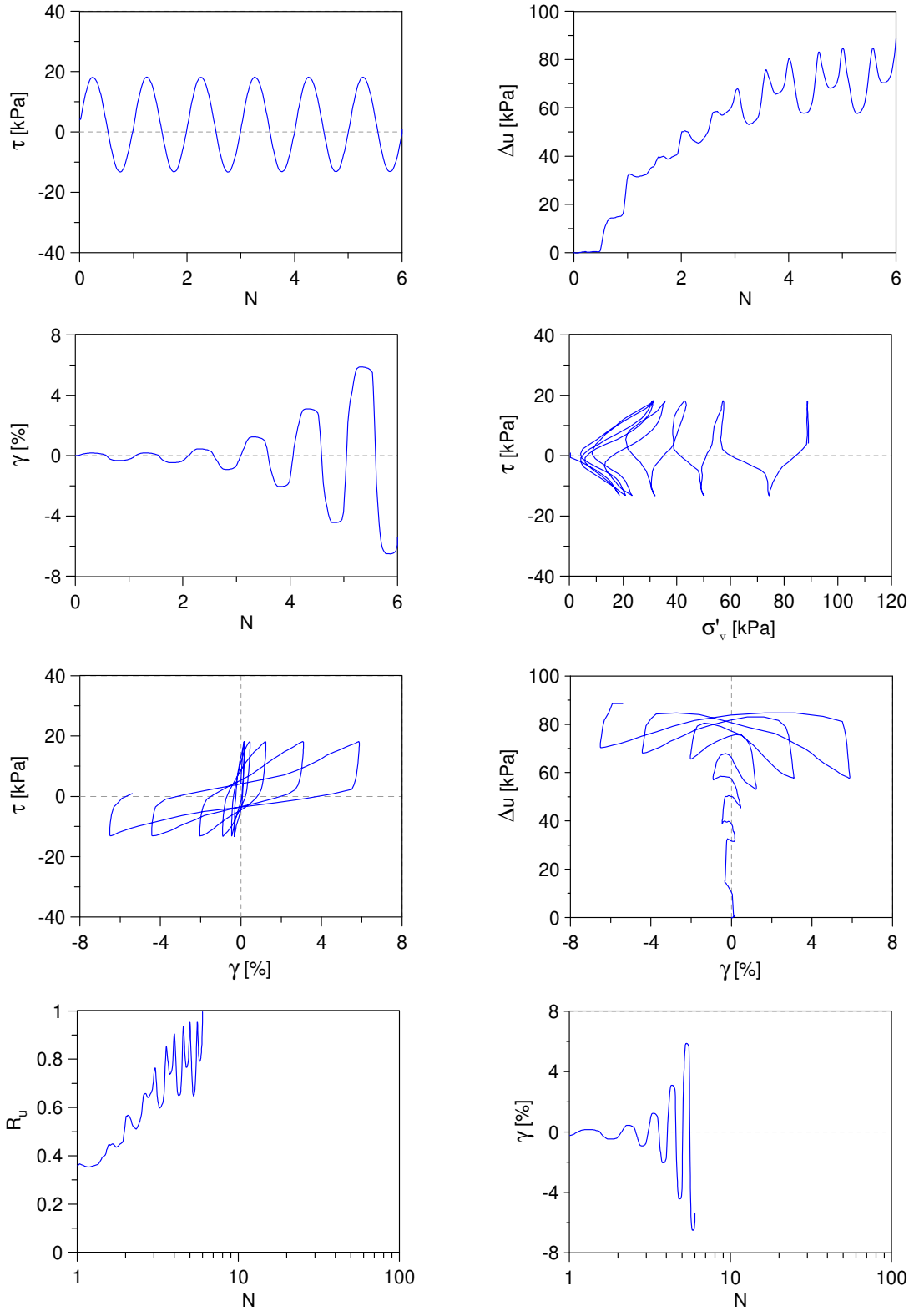

Undrained Cyclic Simple Shear test: *C_SS_TS0_S100_A0_4*
Ticino sand (Reconstitution method: Moist Tamping)
e_0= 0.78 - D_R= 43% - σ'_{v0}= 100 kPa - α= 0 - *CSR* = 0.20

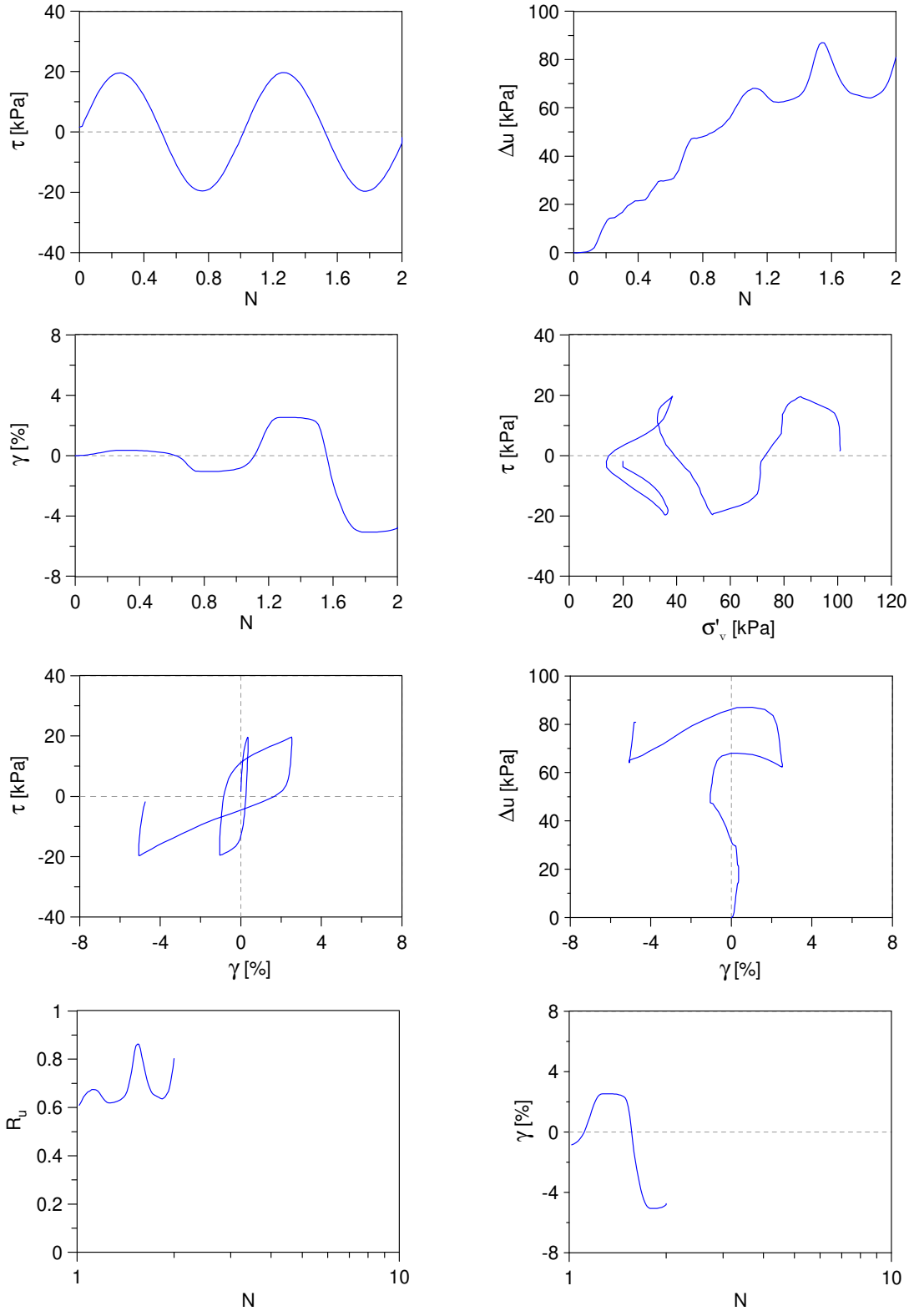

Undrained Cyclic Simple Shear test: *C_SS_TS0_S100_A0_5*
Ticino sand (Reconstitution method: Moist Tamping)
e_0= 0.74 - D_R= 54% - σ'_{v0}= 100 kPa - α=0 - *CSR* = 0.12

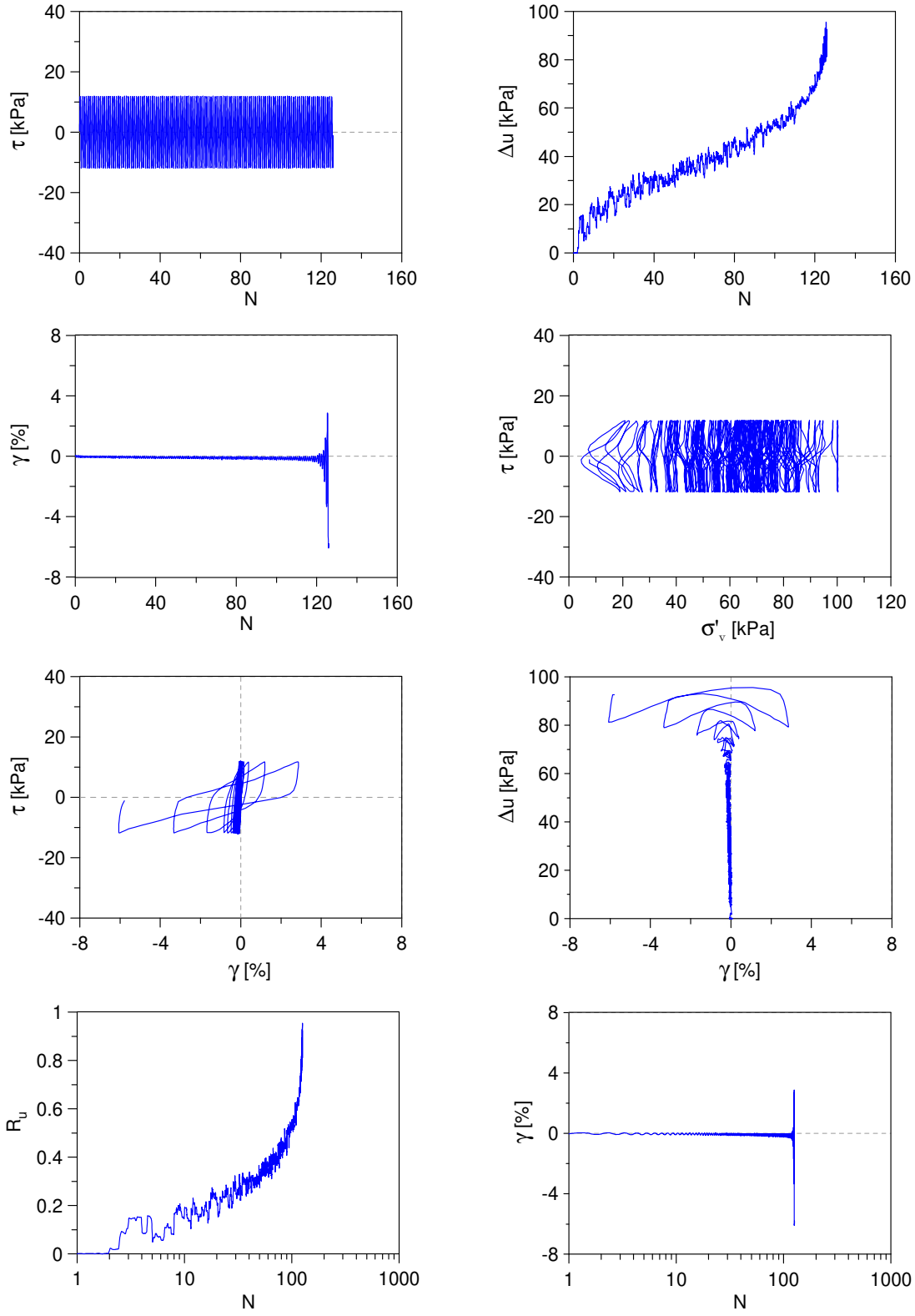

Undrained Cyclic Simple Shear test: *C_SS_TS0_S100_A0_6*
Ticino sand (Reconstitution method: Moist Tamping)
e_0= 0.74 - D_R= 54% - σ'_{v0}= 100 kPa - α=0 - *CSR* = 0.14

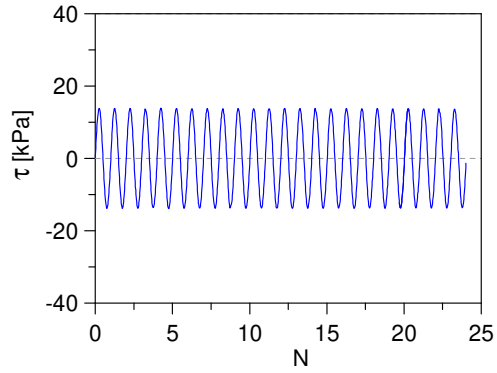

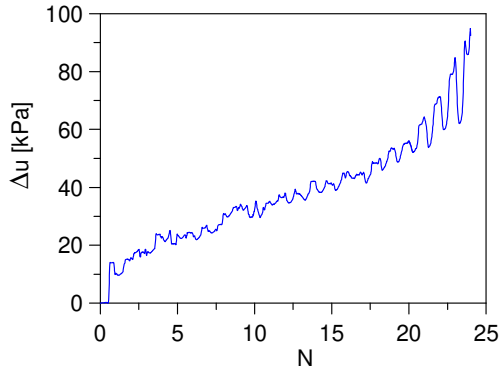

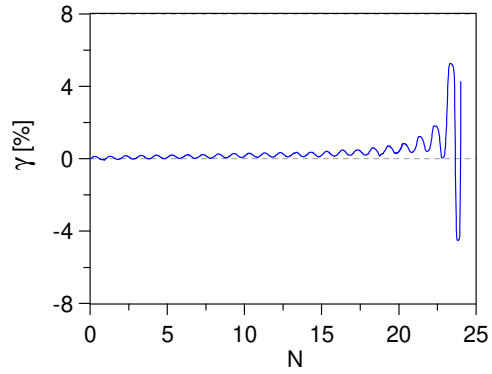

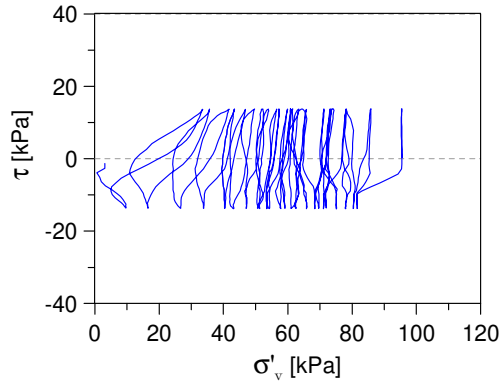

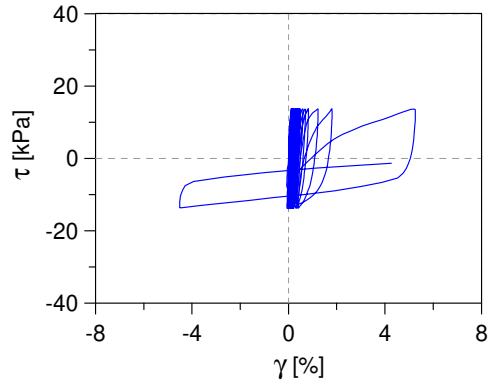

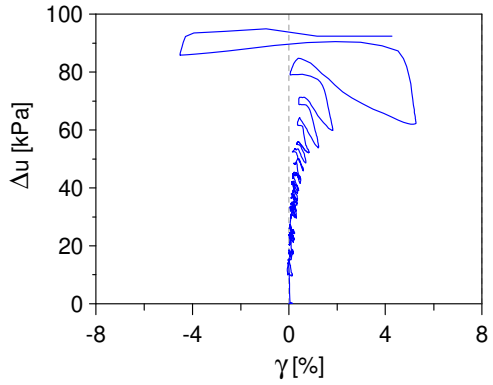

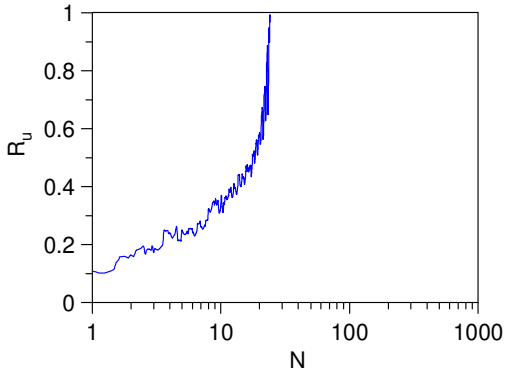

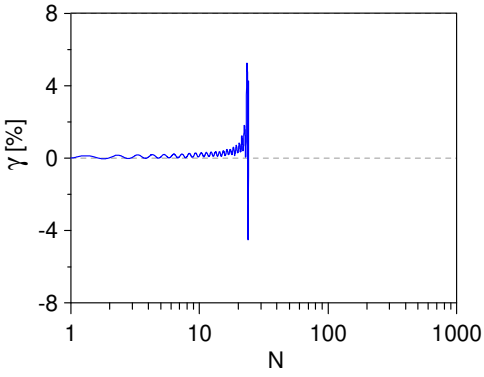

Undrained Cyclic Simple Shear test: *C_SS_TS0_S100_A0_7*
Ticino sand (Reconstitution method: Moist Tamping)
e_0= 0.74 - D_R= 54% - σ'_{v0}= 100 kPa - α=0 - *CSR* = 0.16

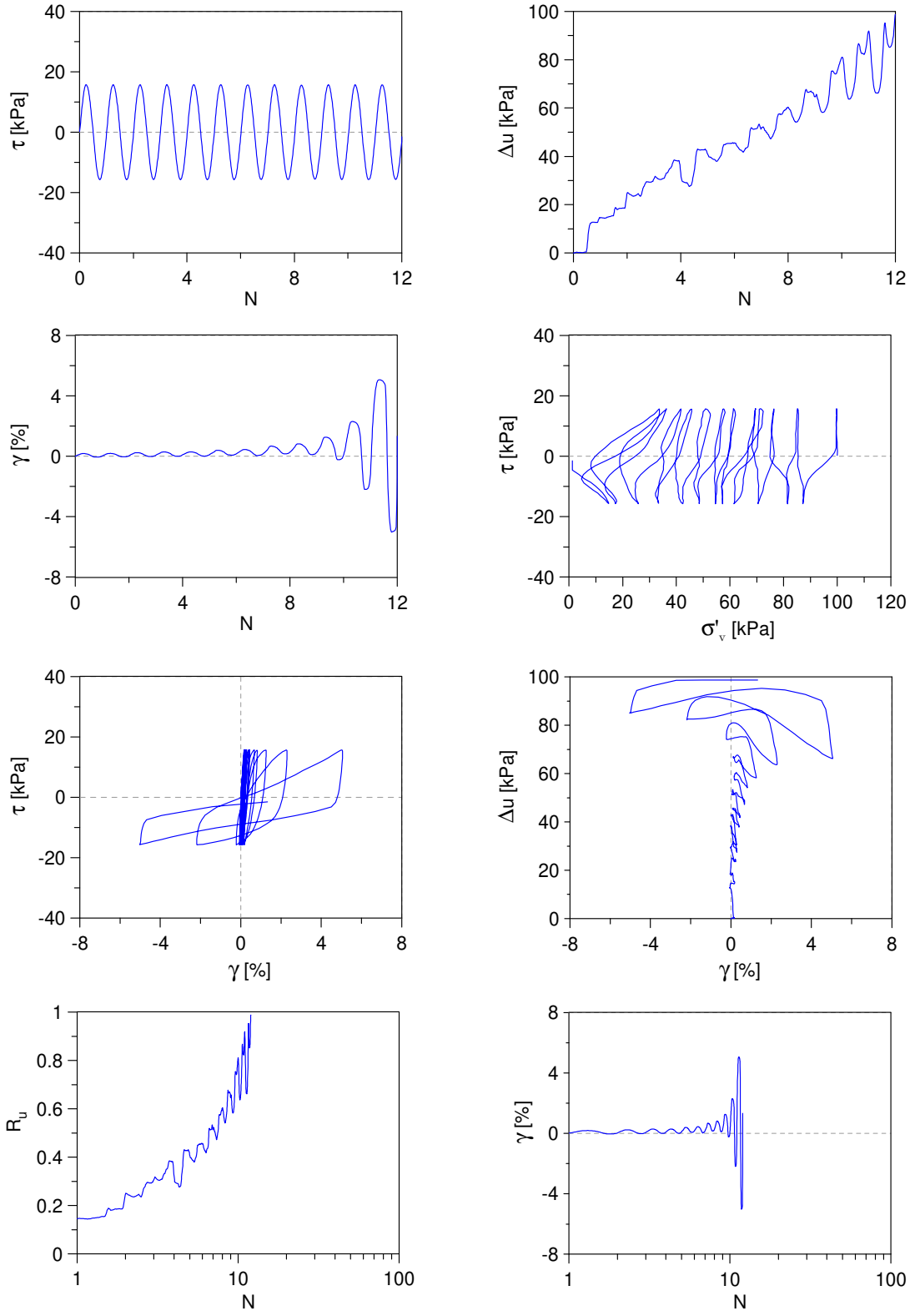

Undrained Cyclic Simple Shear test: *C_SS_TS0_S100_A0_8*
Ticino sand (Reconstitution method: Moist Tamping)
e_0= 0.74 - D_R= 54% - σ'_{v0}= 100 kPa - α=0 - *CSR* = 0.18

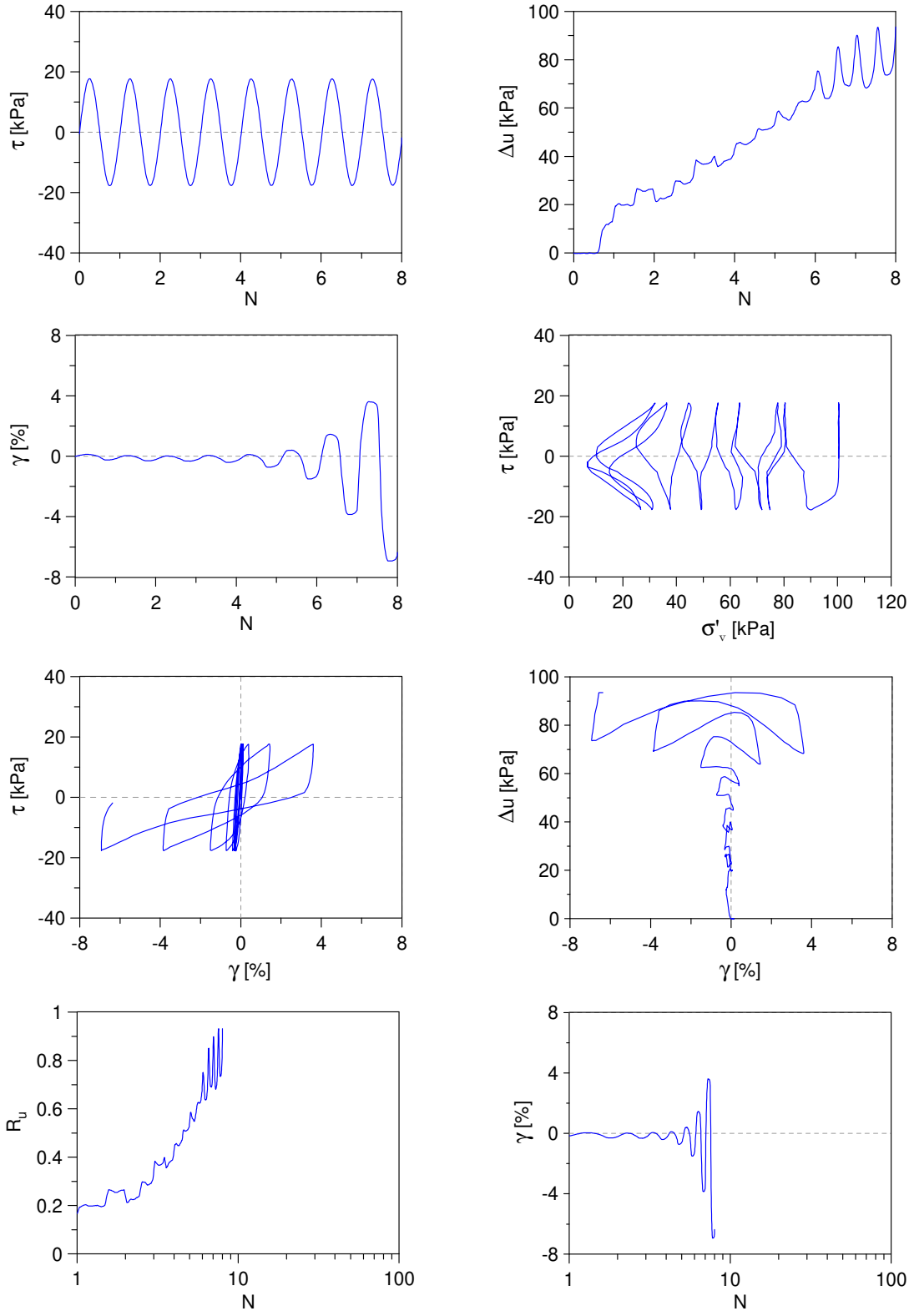

Undrained Cyclic Simple Shear test: *C_SS_TS0_S100_A0_9*
Ticino sand (Reconstitution method: Moist Tamping)
e_0= 0.68 - D_R= 71% - σ'_{v0}= 100 kPa - α= 0 - *CSR* = 0.14

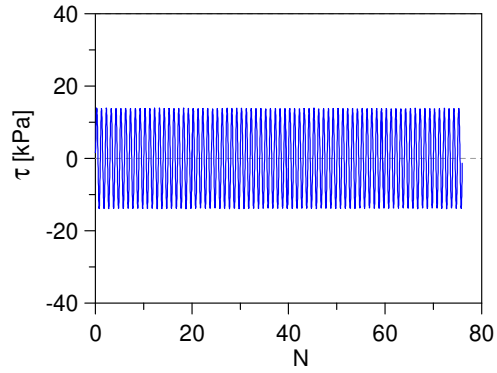

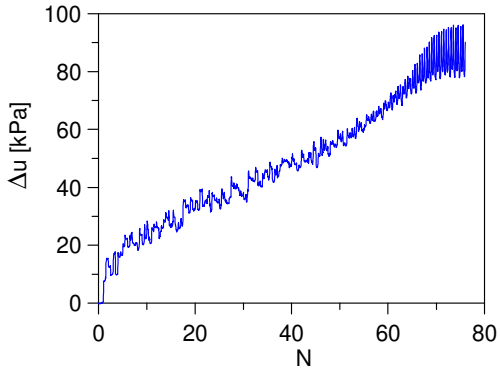

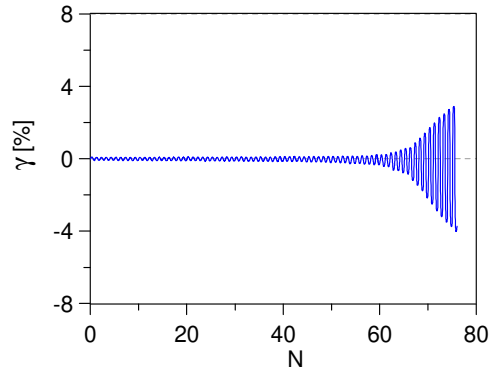

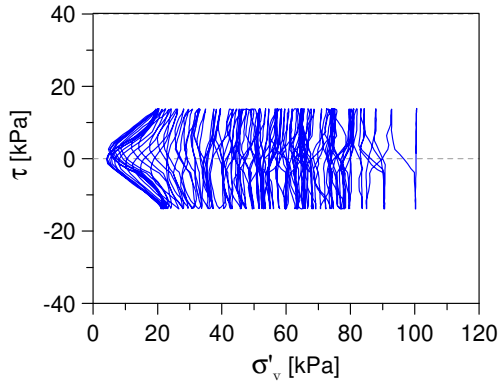

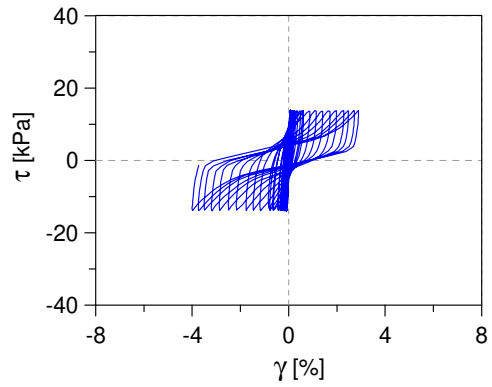

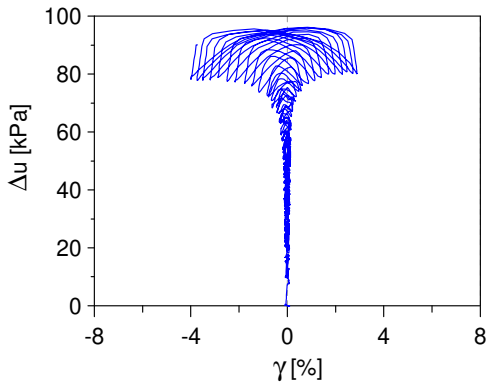

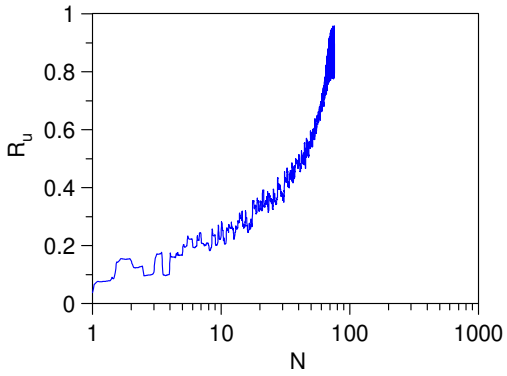

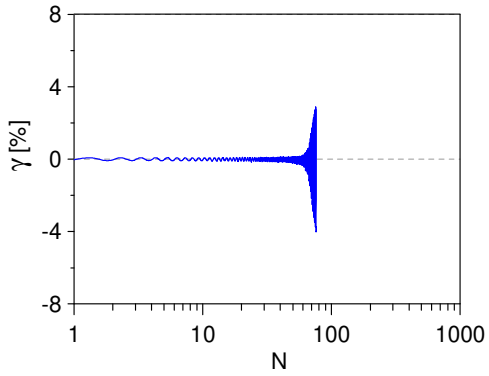

Undrained Cyclic Simple Shear test: *C_SS_TS0_S100_A0_10*
Ticino sand (Reconstitution method: Moist Tamping)
e_0= 0.68 - D_R= 71% - σ'_{v0}= 100 kPa - α= 0 - *CSR* = 0.16

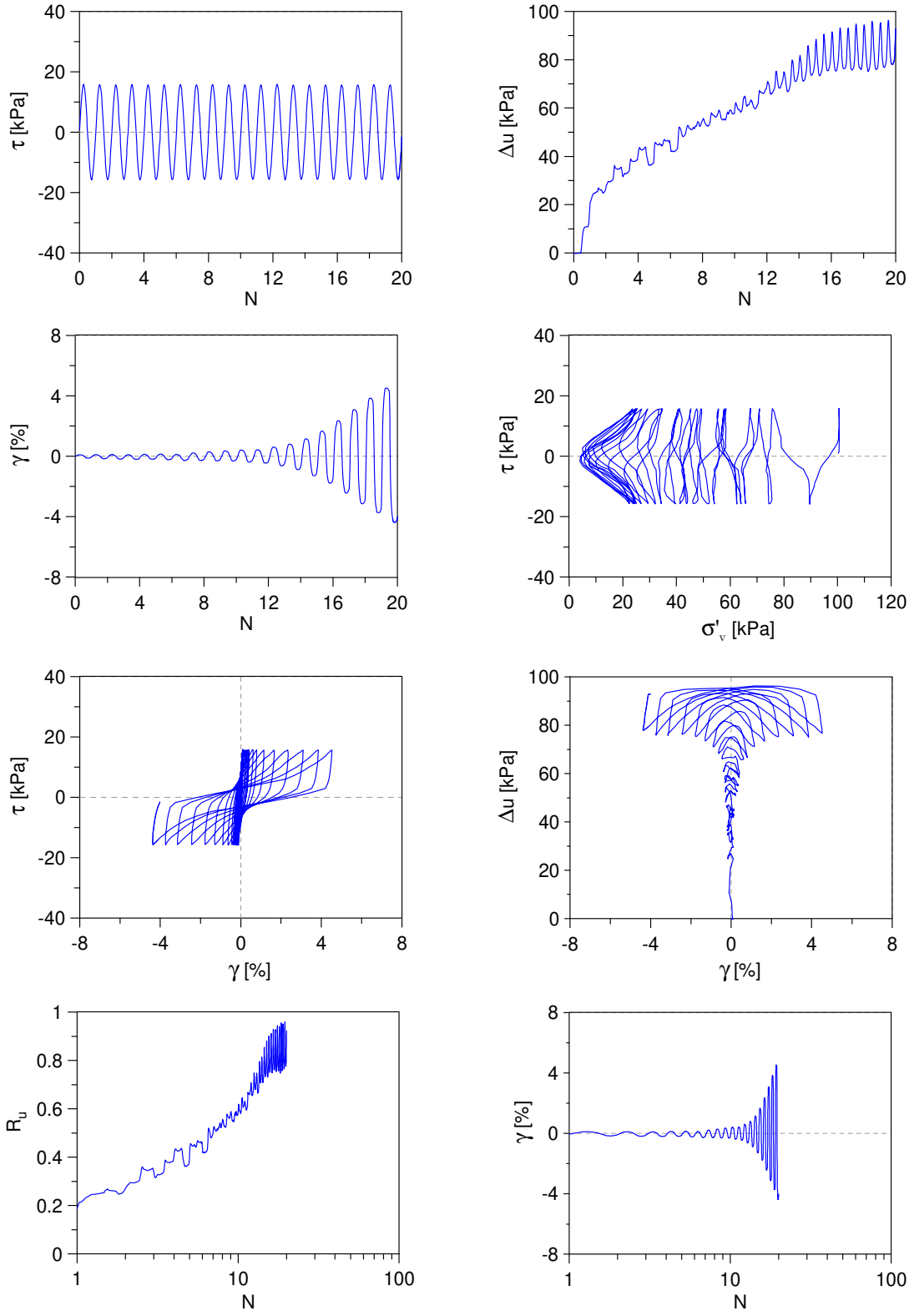

Undrained Cyclic Simple Shear test: *C_SS_TS0_S100_A0_11*
Ticino sand (Reconstitution method: Moist Tamping)
e_0= 0.68 - D_R= 71% - σ'_{v0}= 100 kPa - α= 0 - *CSR* = 0.18

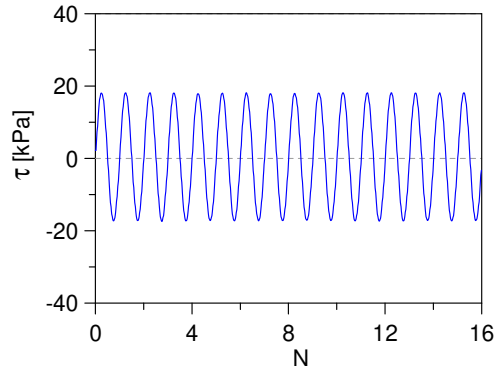

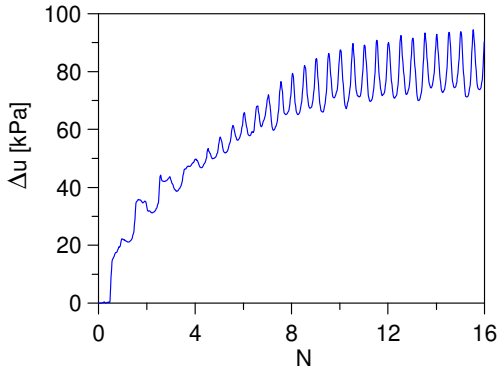

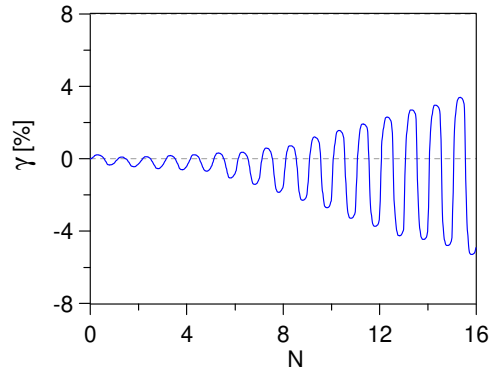

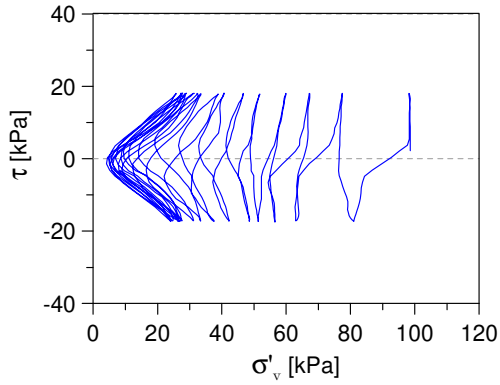

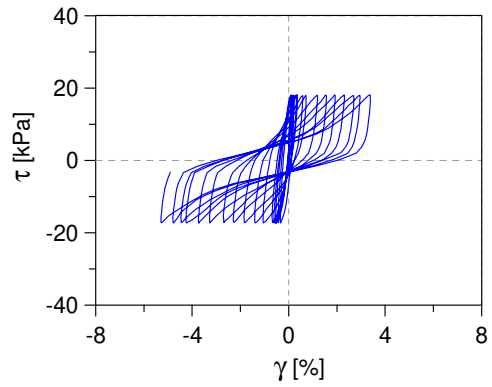

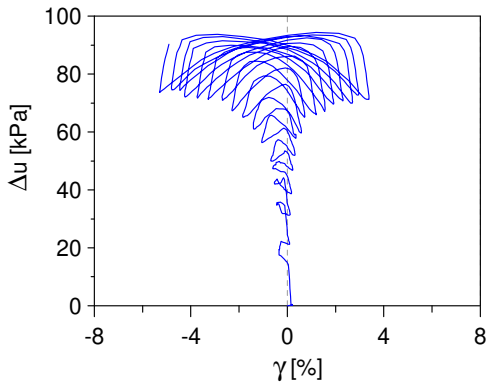

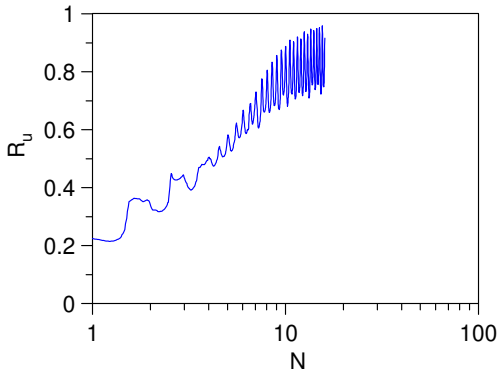

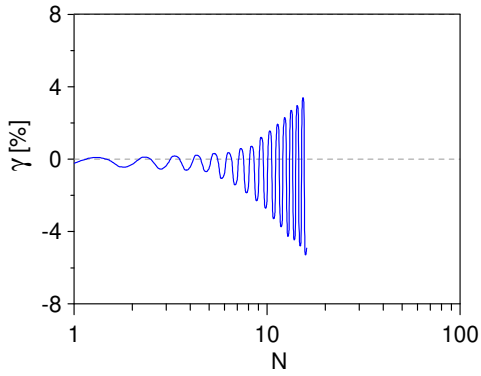

Undrained Cyclic Simple Shear test: *C_SS_TS0_S100_A0_12*
Ticino sand (Reconstitution method: Moist Tamping)
e_0= 0.68 - D_R= 71% - σ'_{v0}= 100 kPa - α= 0 - *CSR* = 0.20

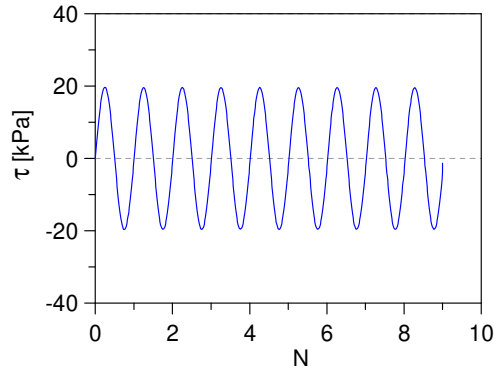

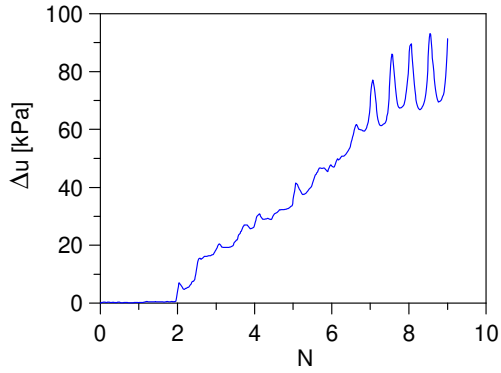

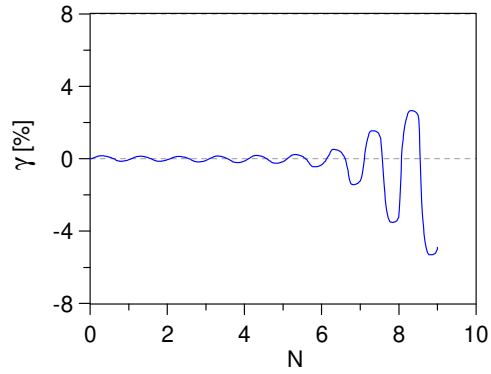

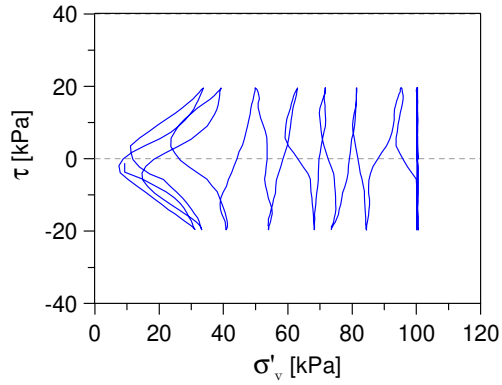

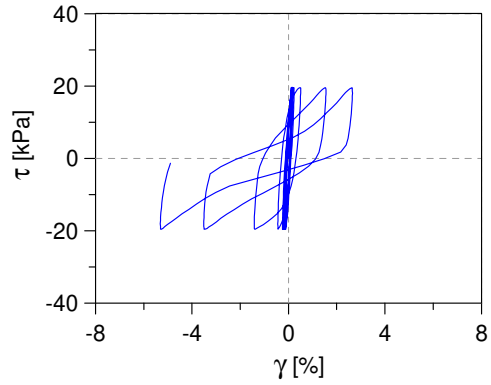

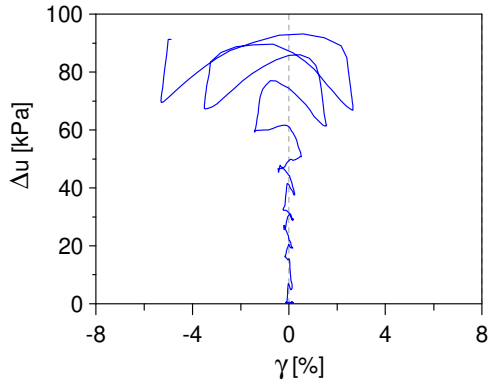

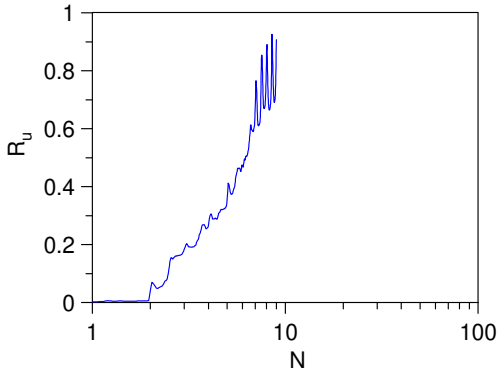

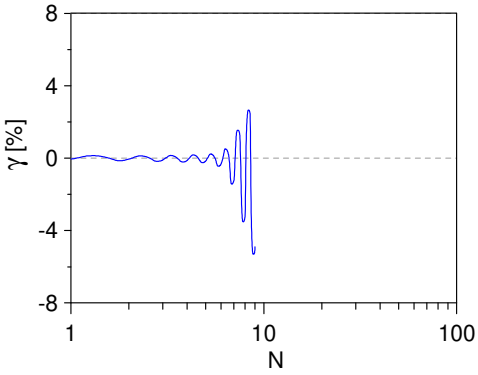

Undrained Cyclic Simple Shear test: *C_SS_TS0_S100_A0_13*
Ticino sand (Reconstitution method: Moist Tamping)
e_0= 0.68 - D_R= 71% - σ'_{v0}= 100 kPa - α= 0 - *CSR* = 0.23

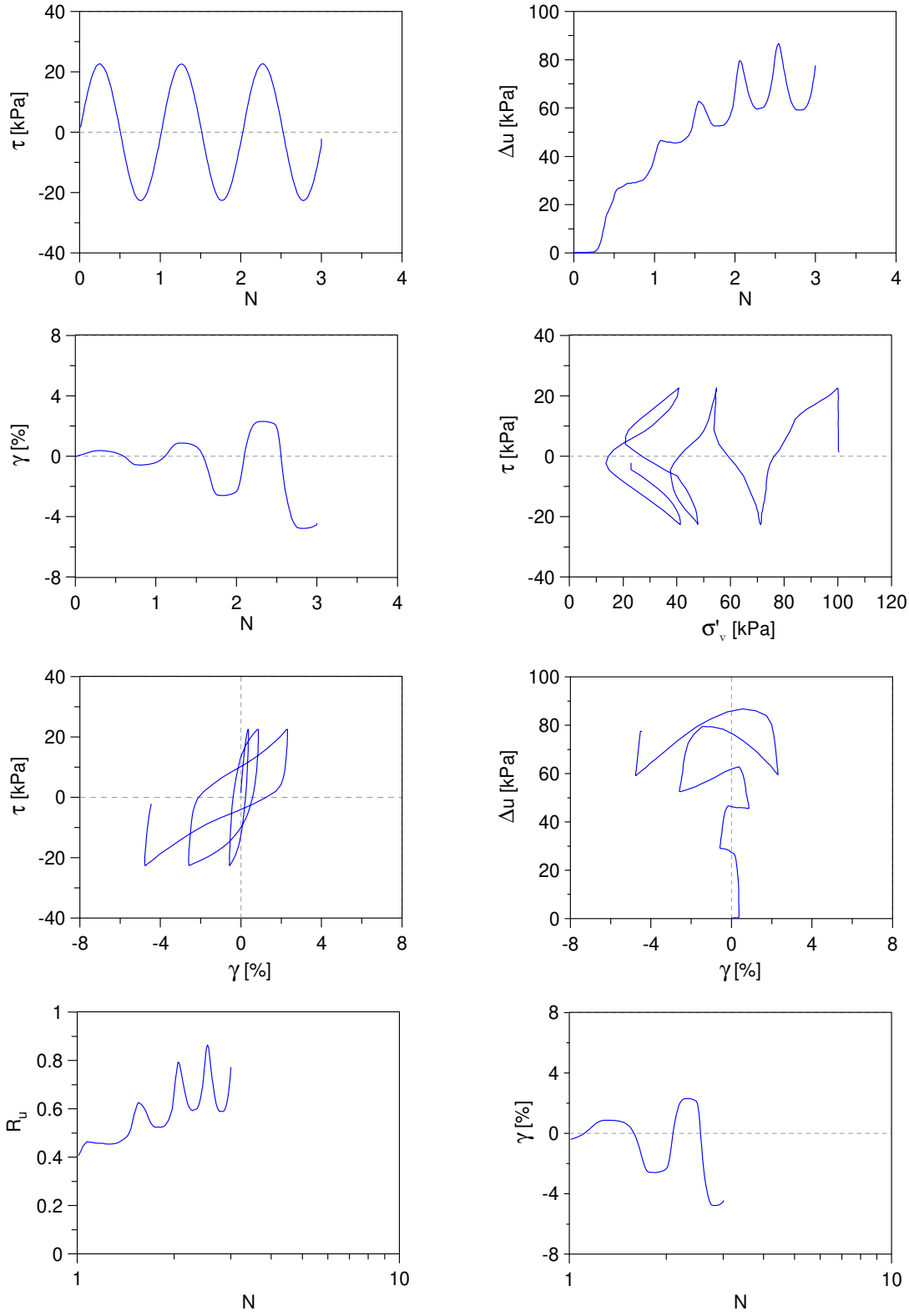

Undrained Cyclic Simple Shear test: *C_SS_TS0_S100_A0_14*
Ticino sand (Reconstitution method: Moist Tamping)
e_0= 0.63 - D_R= 86% - σ'_{v0}= 100 kPa - α= 0 - *CSR* = 0.20

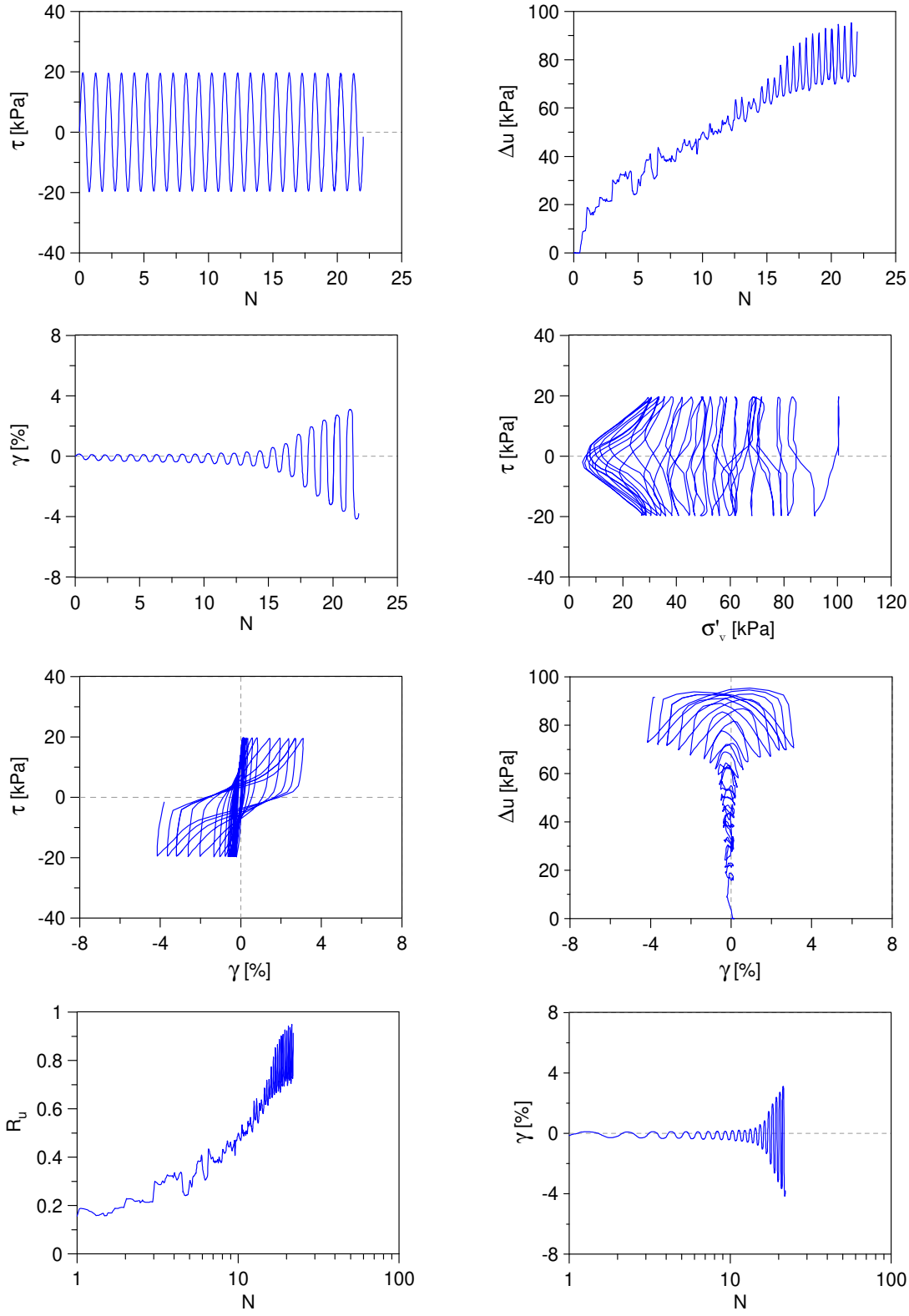

Undrained Cyclic Simple Shear test: *C_SS_TS0_S100_A0_15*
Ticino sand (Reconstitution method: Moist Tamping)
e_0= 0.63 - D_R= 86% - σ'_{v0}= 100 kPa - α= 0 - *CSR* = 0.23

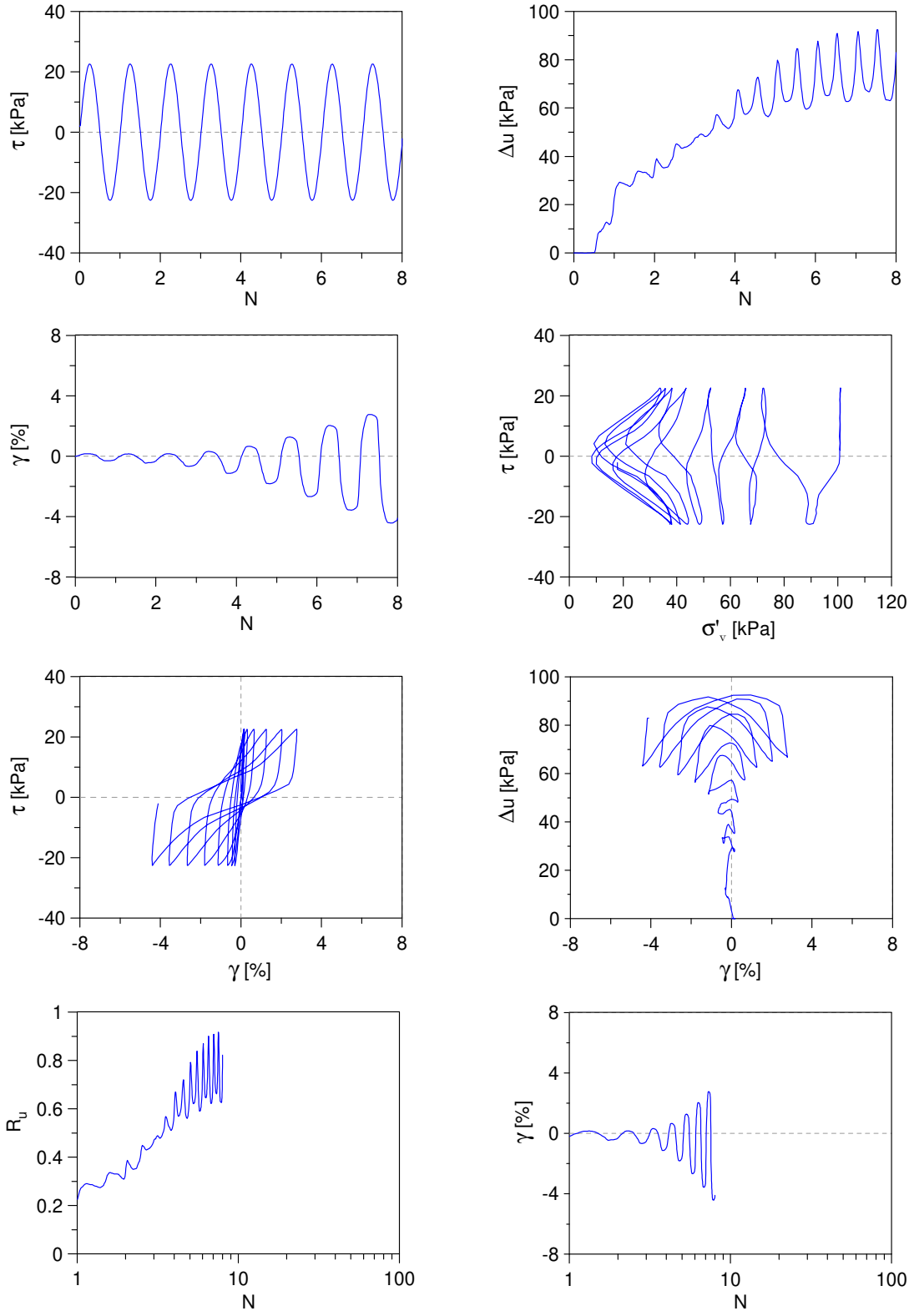

Undrained Cyclic Simple Shear test: *C_SS_TS0_S100_A0_16*
Ticino sand (Reconstitution method: Moist Tamping)
e_0= 0.63 - D_R= 86% - σ'_{v0}= 100 kPa - α= 0 - *CSR* = 0.25

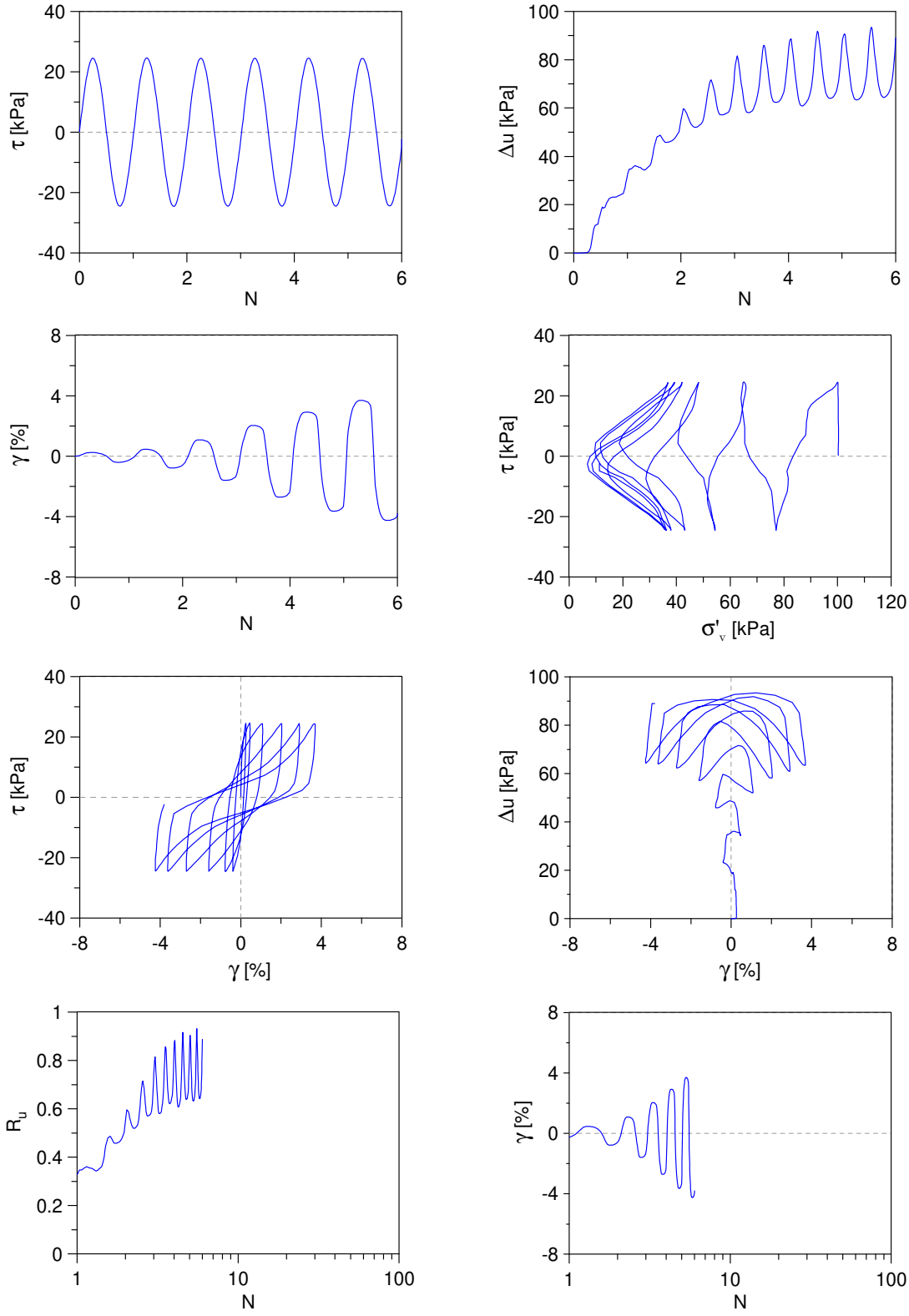

Undrained Cyclic Simple Shear test: *C_SS_TS0_S100_A0_17*
Ticino sand (Reconstitution method: Moist Tamping)
e_0= 0.60 - D_R= 94% - σ'_{v0}= 100 kPa - α= 0 - *CSR* = 0.23

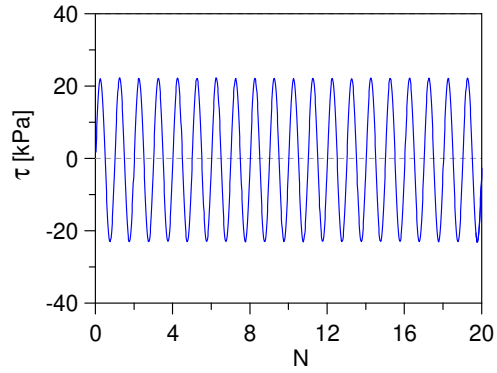

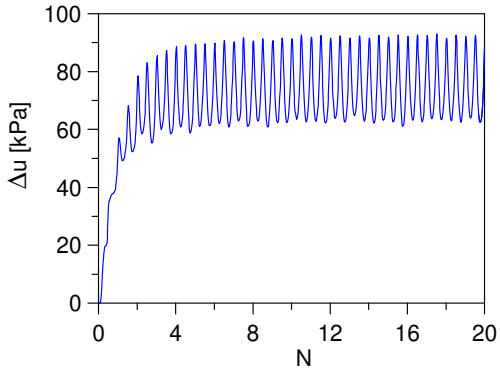

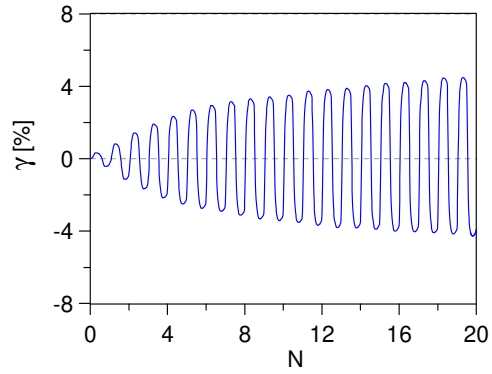

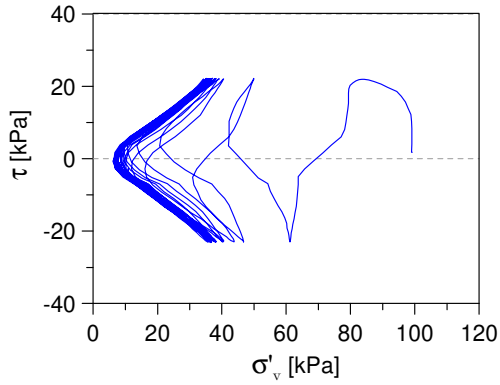

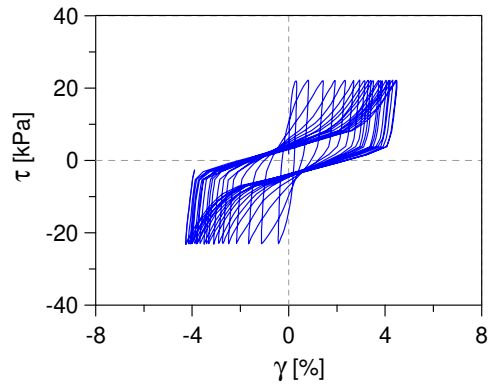

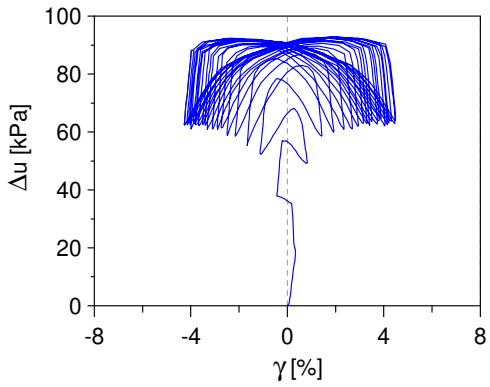

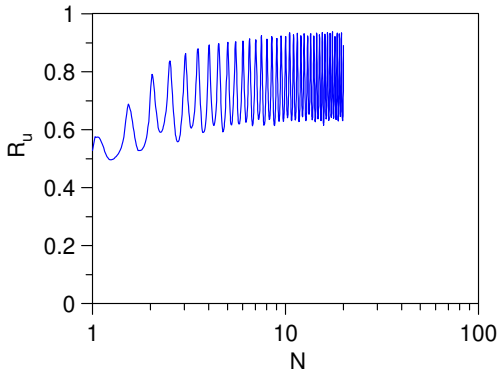

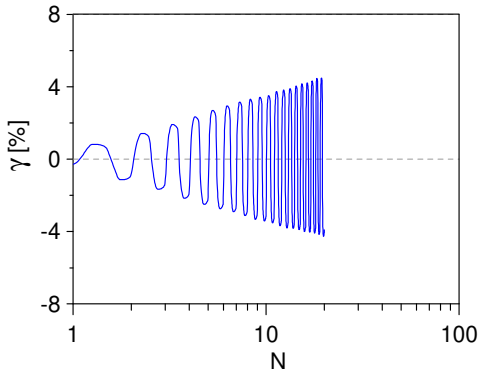

Undrained Cyclic Simple Shear test: *C_SS_TS0_S100_A0_18*
Ticino sand (Reconstitution method: Moist Tamping)
e_0= 0.60 - D_R= 94% - σ'_{v0}= 100 kPa - α= 0 - *CSR* = 0.26

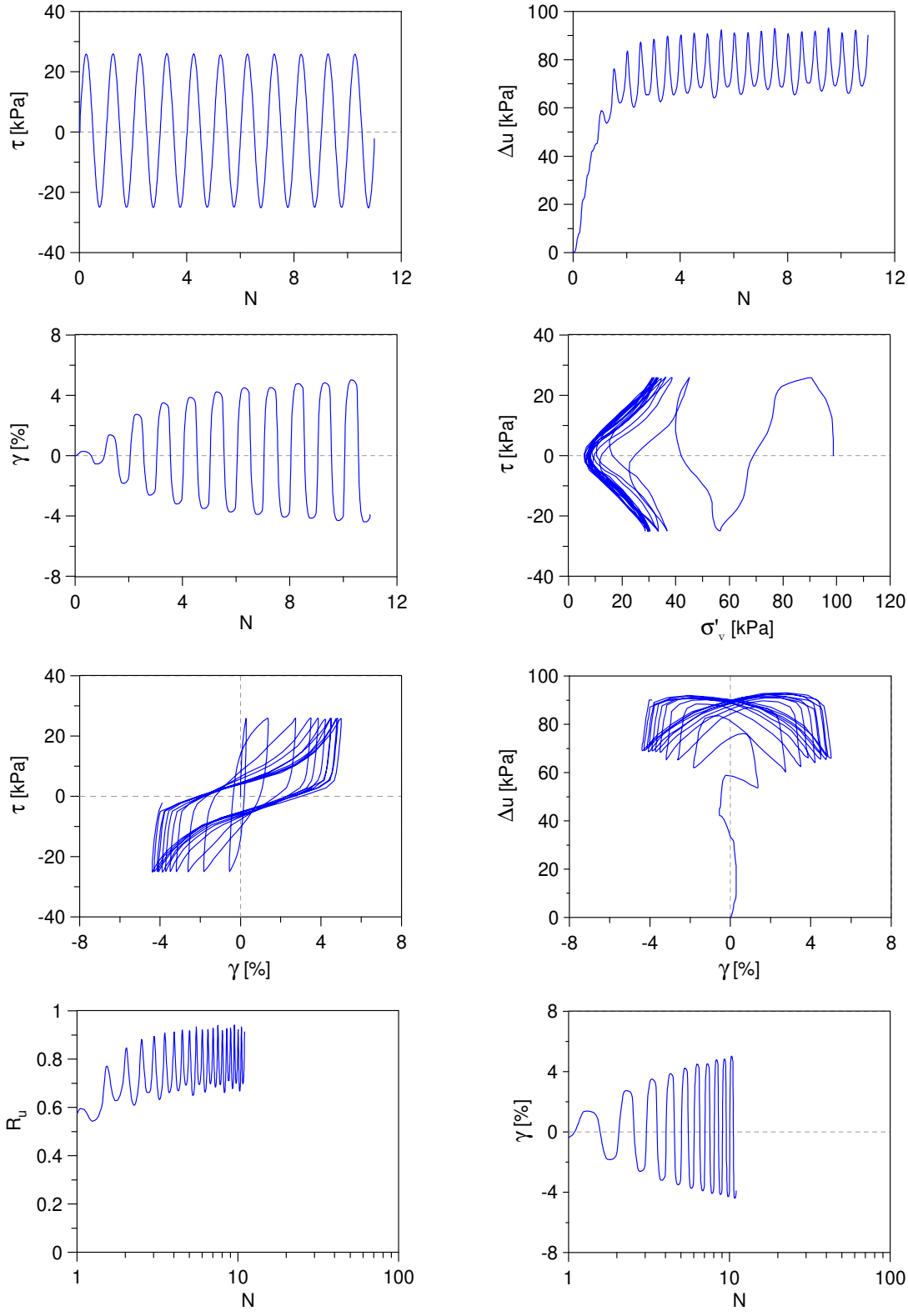

Undrained Cyclic Simple Shear test: *C_SS_TS0_S100_A1_1*
Ticino sand (Reconstitution method: Moist Tamping)
e_0= 0.78 - D_R= 43% - σ'_{v0}= 100 kPa - α= 0.1 - *CSR* = 0.08

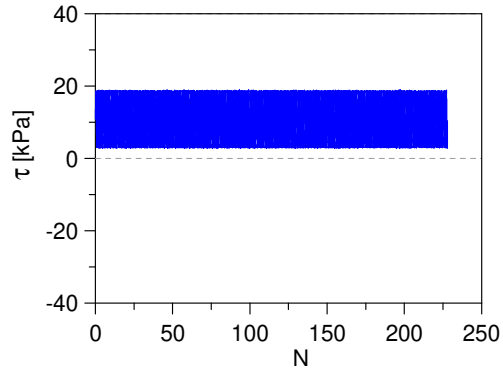

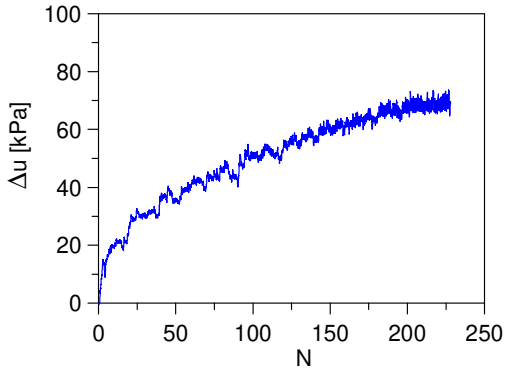

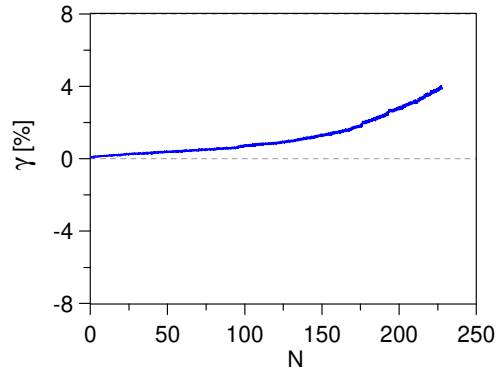

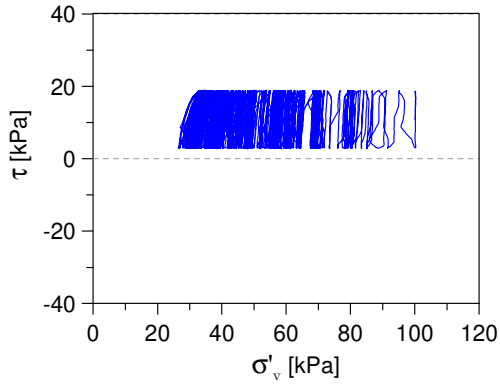

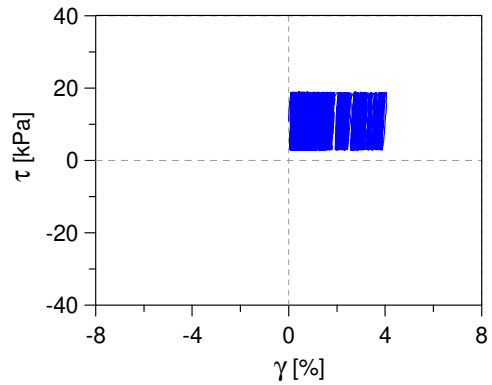

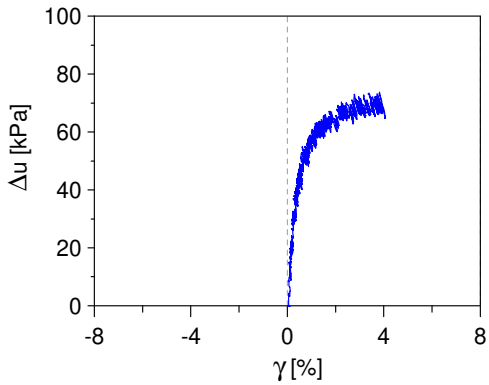

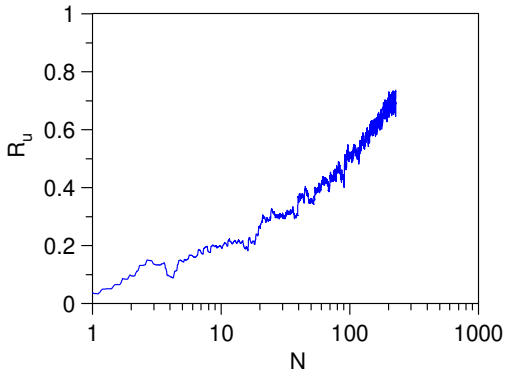

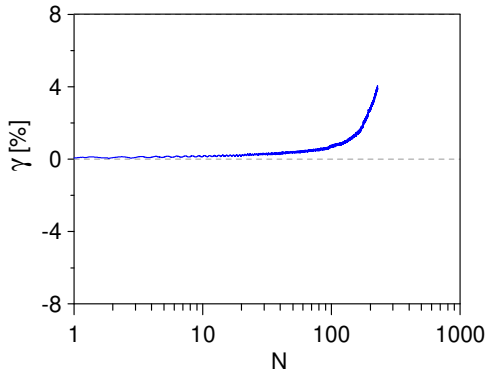

Undrained Cyclic Simple Shear test: *C_SS_TS0_S100_A1_2*
Ticino sand (Reconstitution method: Moist Tamping)
e_0= 0.78 - D_R= 43% - σ'_{v0}= 100 kPa - α= 0.1 - *CSR* = 0.10

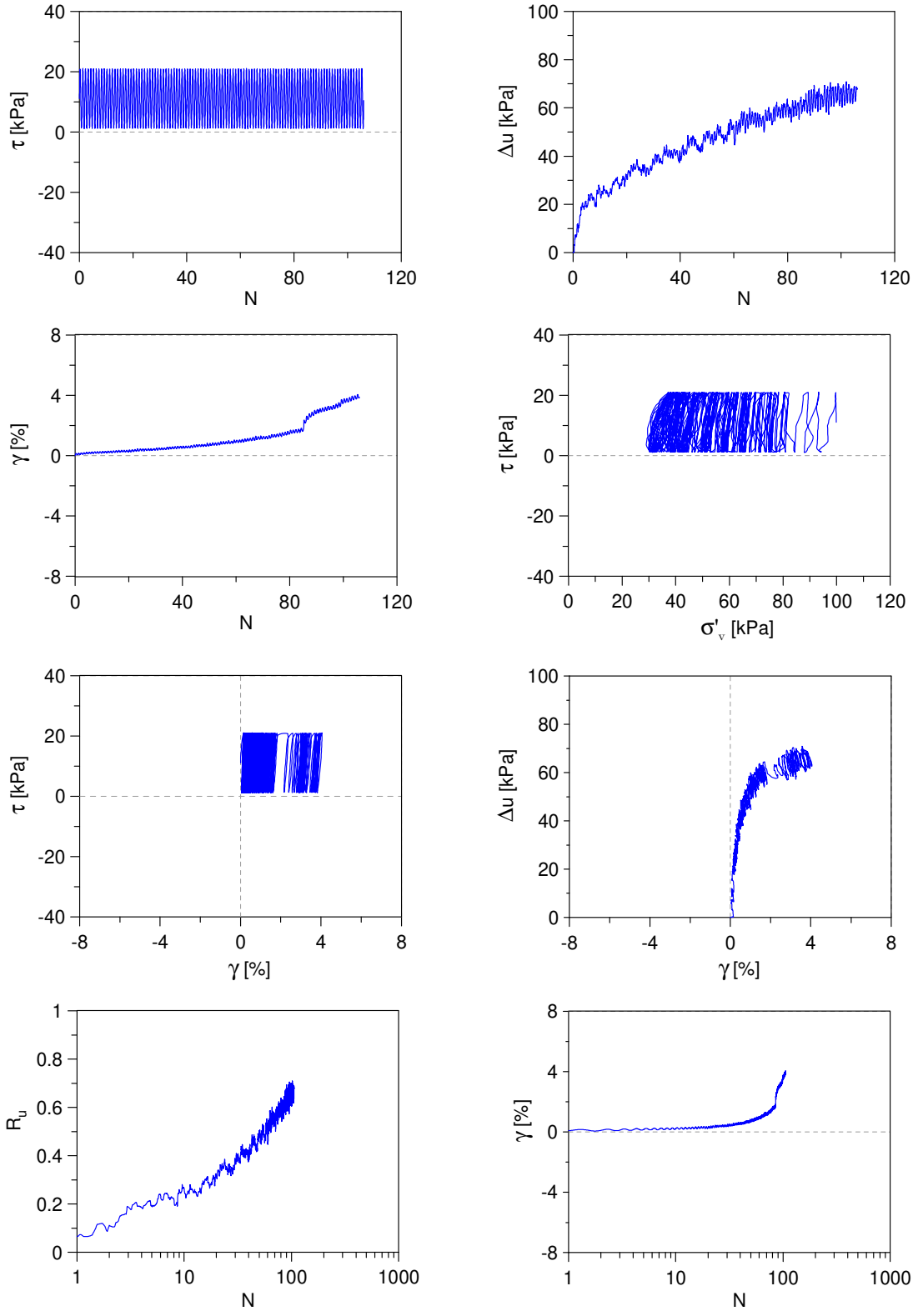

Undrained Cyclic Simple Shear test: *C_SS_TS0_S100_A1_3*
Ticino sand (Reconstitution method: Moist Tamping)
e_0= 0.78 - D_R= 43% - σ'_{v0}= 100 kPa - α= 0.1 - *CSR* = 0.12

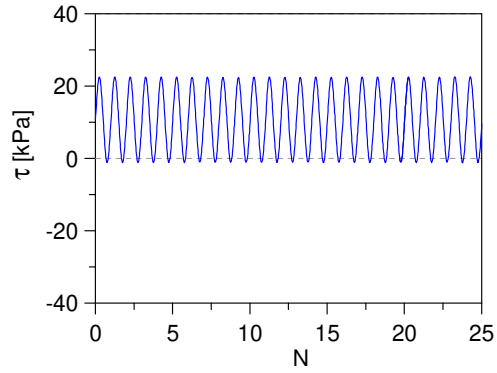

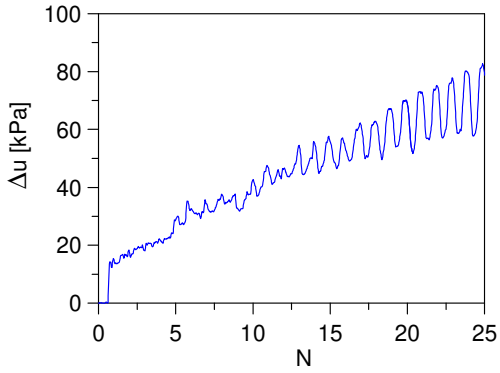

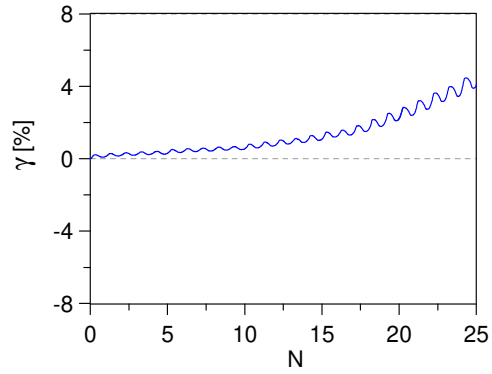

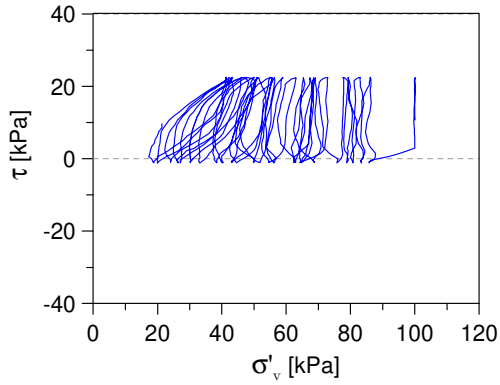

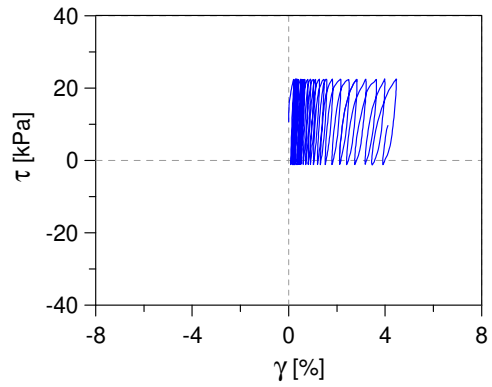

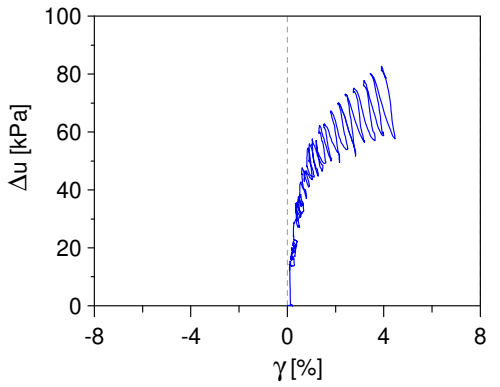

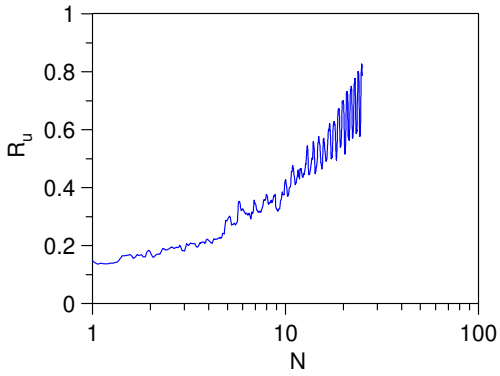

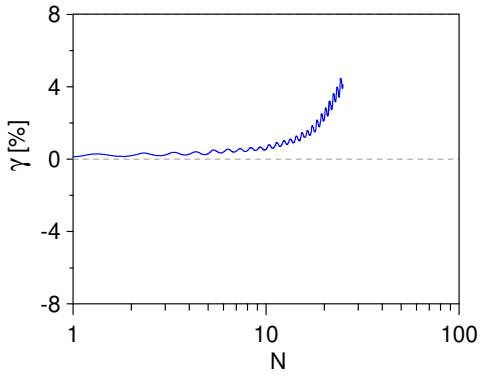

Undrained Cyclic Simple Shear test: *C_SS_TS0_S100_A1_4*
Ticino sand (Reconstitution method: Moist Tamping)
e_0= 0.78 - D_R= 43% - σ'_{v0}= 100 kPa - α= 0.1 - *CSR* = 0.14

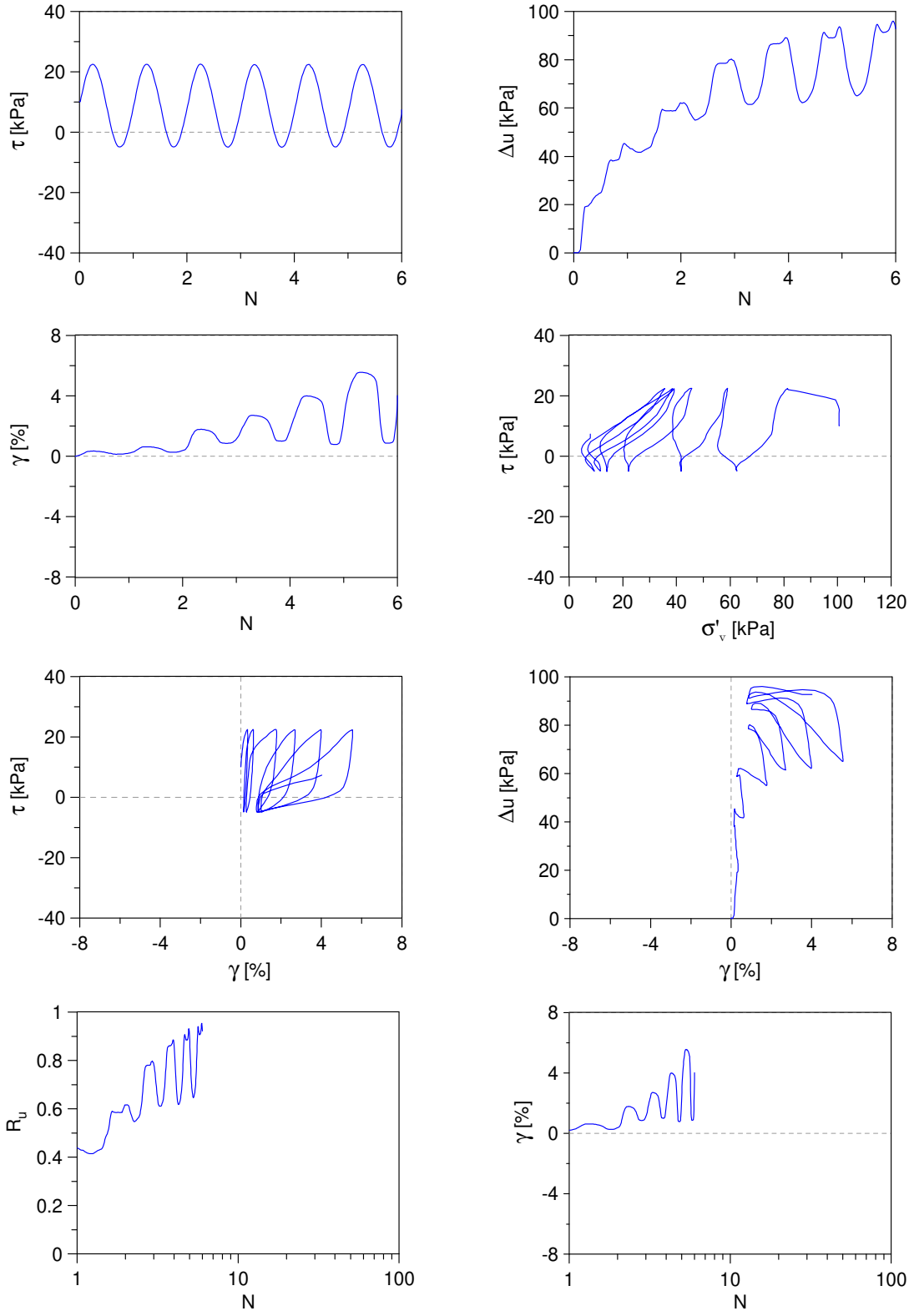

Undrained Cyclic Simple Shear test: *C_SS_TS0_S100_A1_5*
Ticino sand (Reconstitution method: Moist Tamping)
e_0= 0.68 - D_R= 71% - σ'_{v0}= 100 kPa - α= 0.1 - *CSR* = 0.16

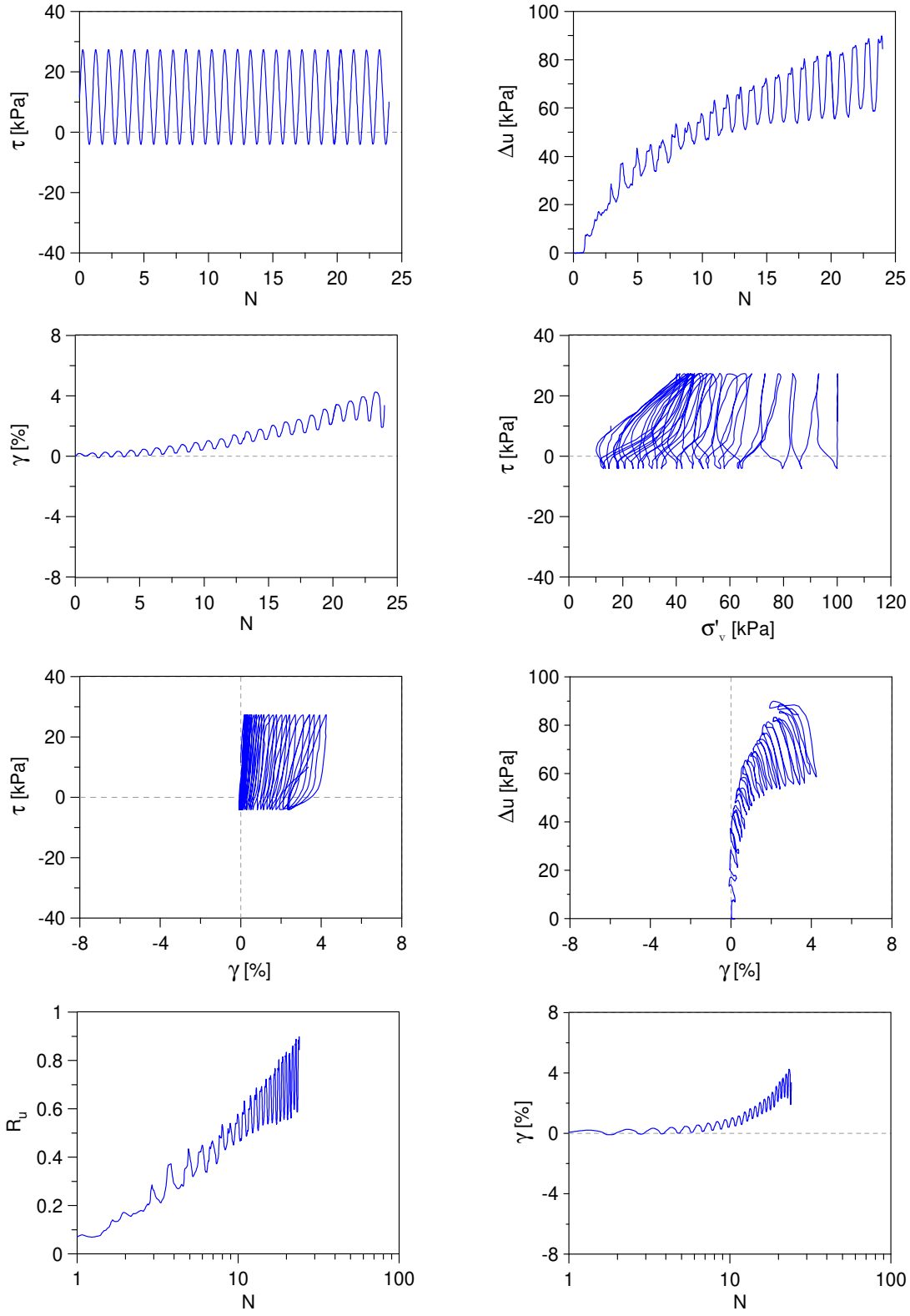

Undrained Cyclic Simple Shear test: *C_SS_TS0_S100_A1_6*
Ticino sand (Reconstitution method: Moist Tamping)
e_0= 0.68 - D_R= 71% - σ'_{v0}= 100 kPa - α= 0.1 - *CSR* = 0.20

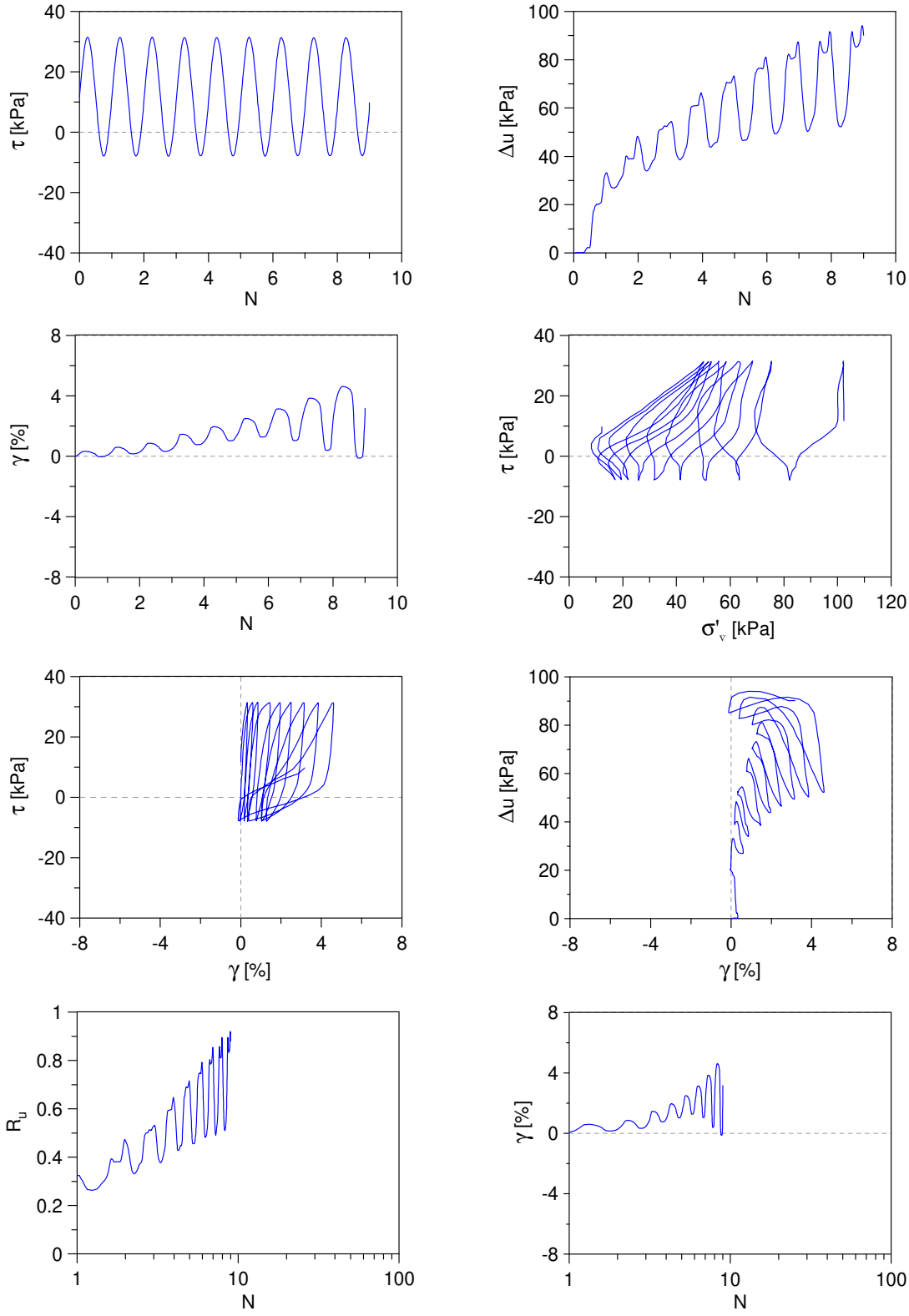

Undrained Cyclic Simple Shear test: *C_SS_TS0_S100_A1_7*
Ticino sand (Reconstitution method: Moist Tamping)
e_0= 0.68 - D_R= 71% - σ'_{v0}= 100 kPa - α= 0.1 - *CSR* = 0.22

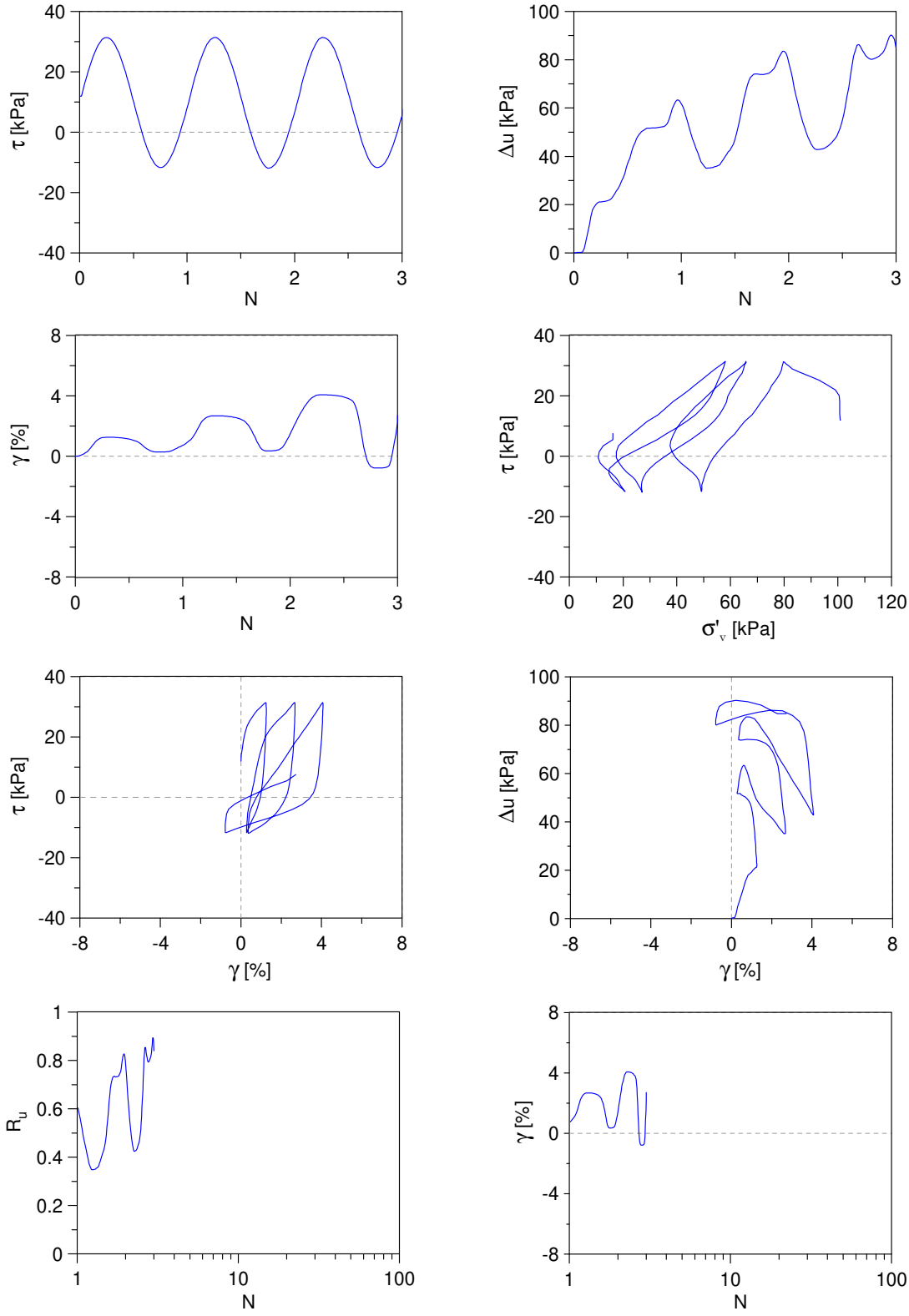

Undrained Cyclic Simple Shear test: *C_SS_TS0_S100_A1_8*
Ticino sand (Reconstitution method: Moist Tamping)
e_0= 0.60 - D_R= 94% - σ'_{v0}= 100 kPa - α= 0.1 - *CSR* = 0.23

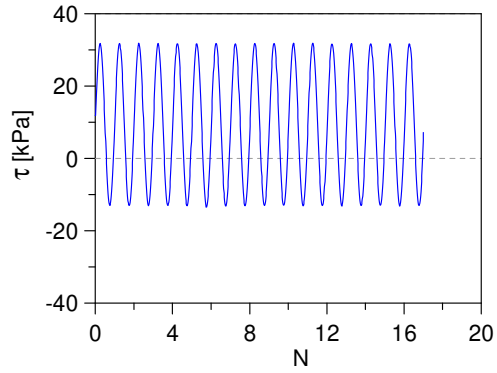

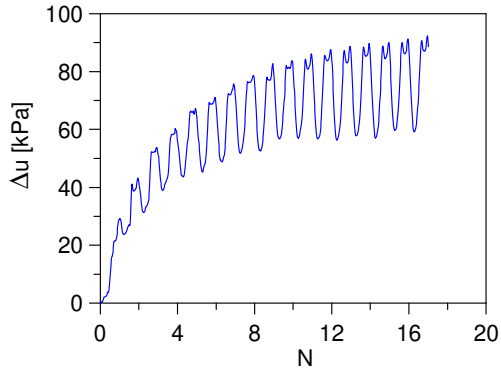

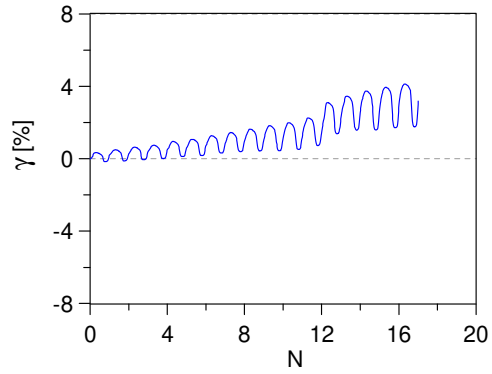

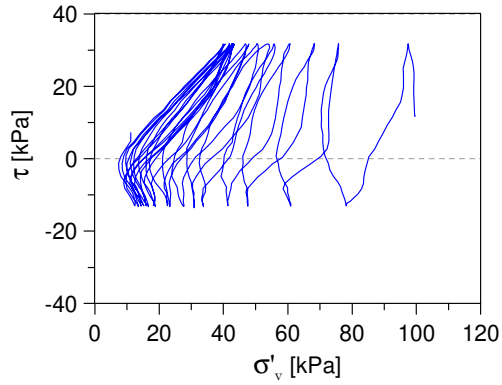

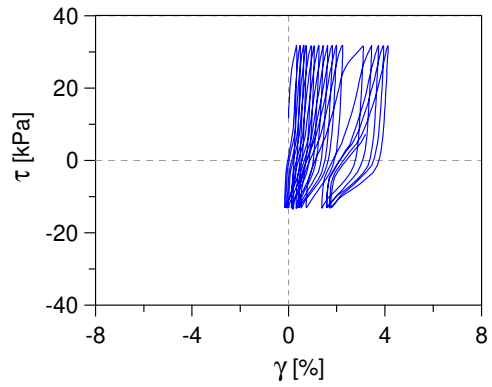

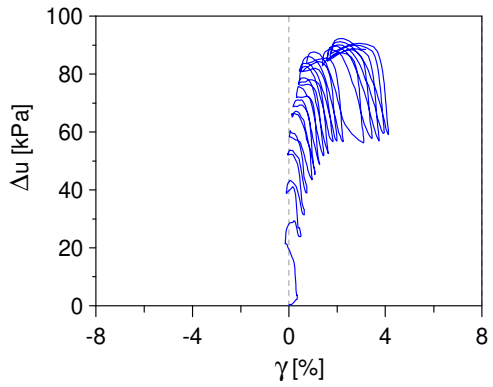

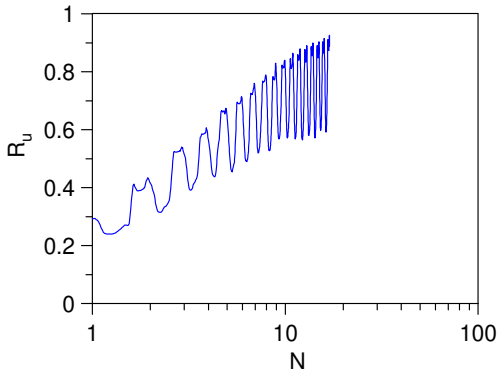

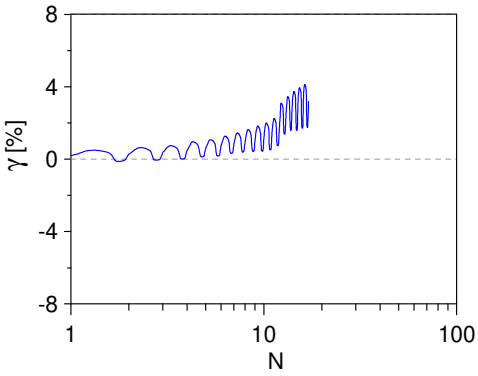

Undrained Cyclic Simple Shear test: *C_SS_TS0_S100_A1_9*
Ticino sand (Reconstitution method: Moist Tamping)
e_0= 0.60 - D_R= 94% - σ'_{v0}= 100 kPa - α= 0.1 - *CSR* = 0.25

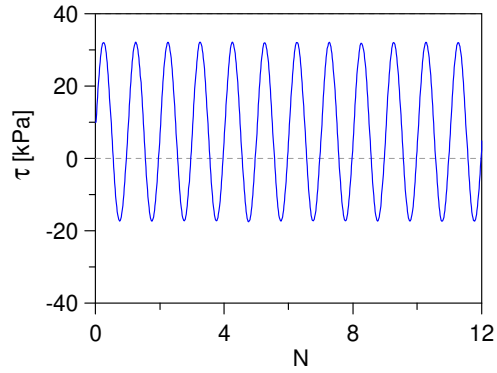

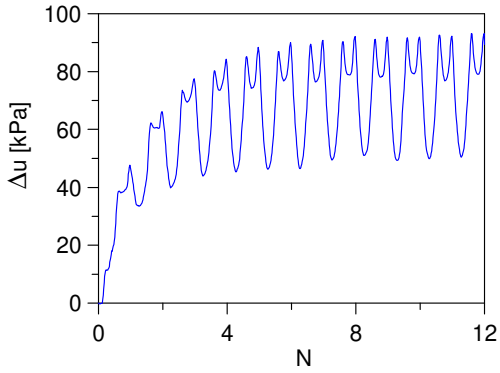

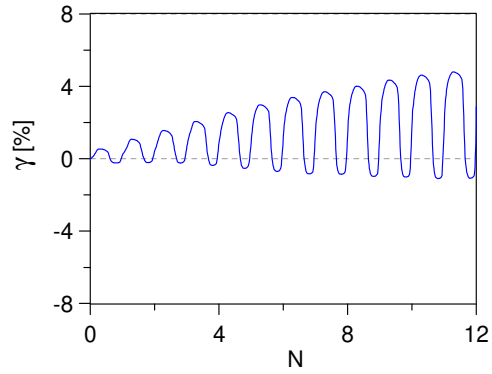

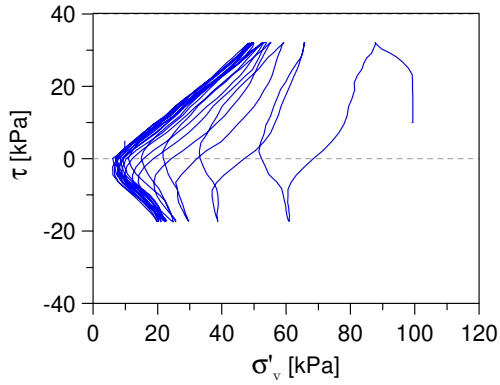

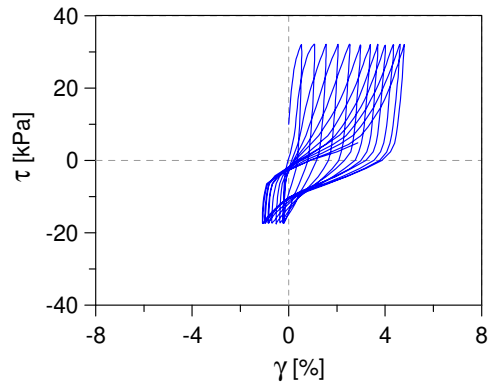

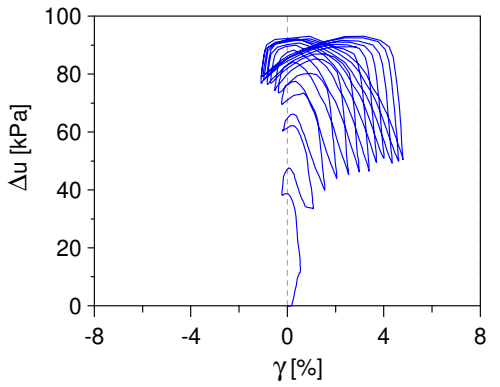

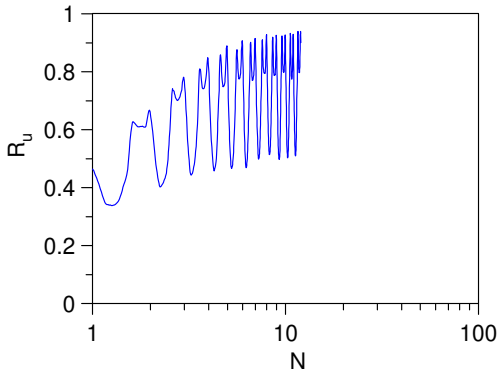

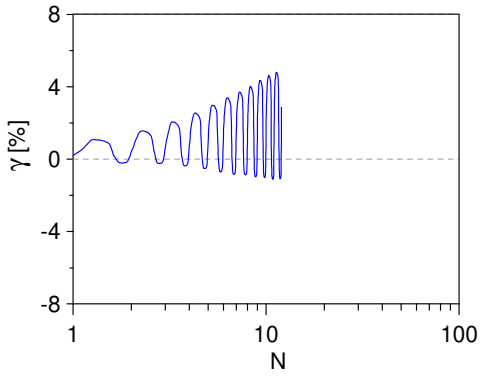

Undrained Cyclic Simple Shear test: *C_SS_TS0_S100_A1_10*
Ticino sand (Reconstitution method: Moist Tamping)
e_0= 0.60 - D_R= 94% - σ'_{v0}= 100 kPa - α= 0.1 - *CSR* = 0.28

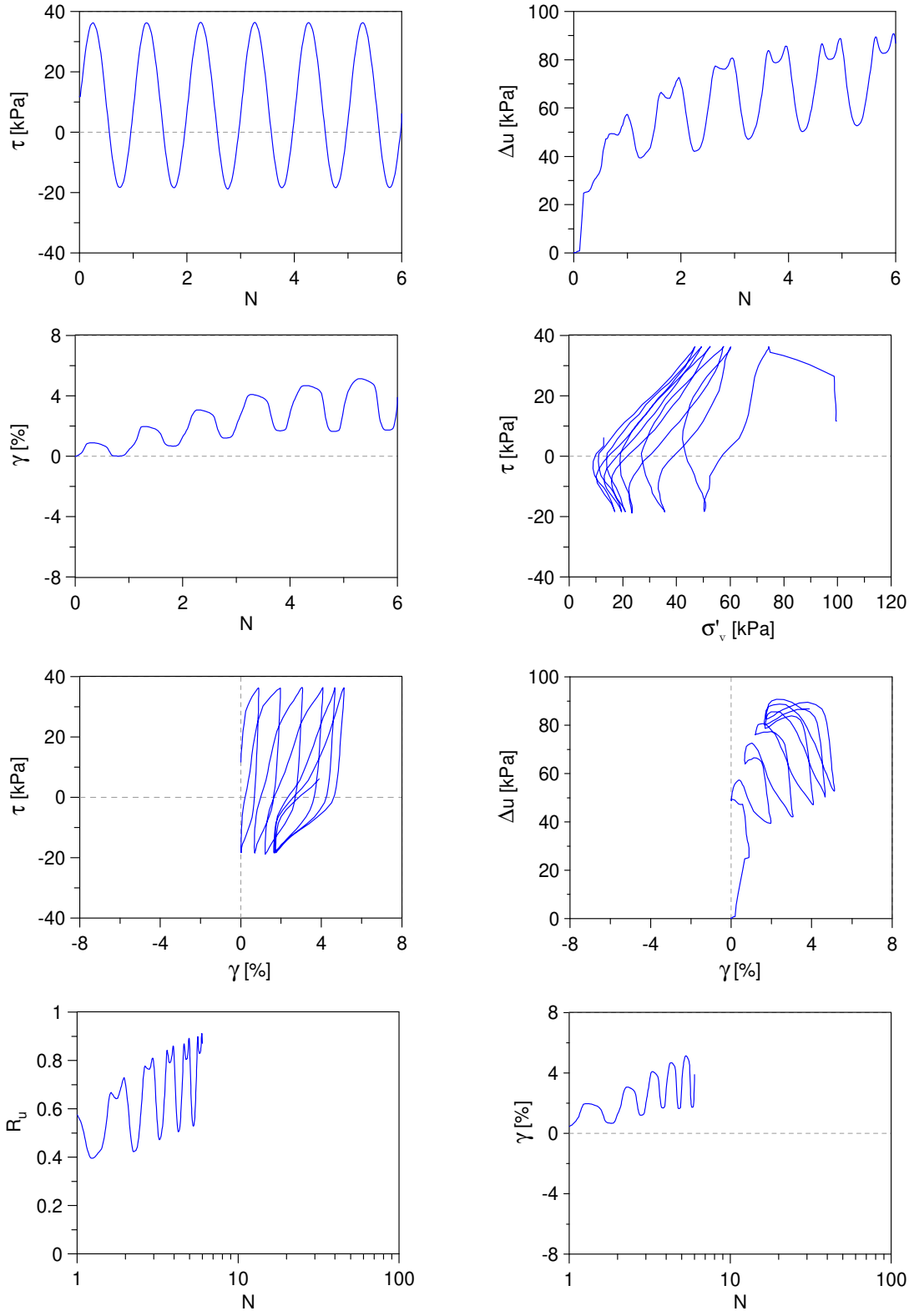

Undrained Cyclic Simple Shear test: *C_SS_TS0_S100_A2_1*
Ticino sand (Reconstitution method: Moist Tamping)
e_0= 0.78 - D_R= 43% - σ'_{v0}= 100 kPa - α= 0.2 - *CSR* = 0.10

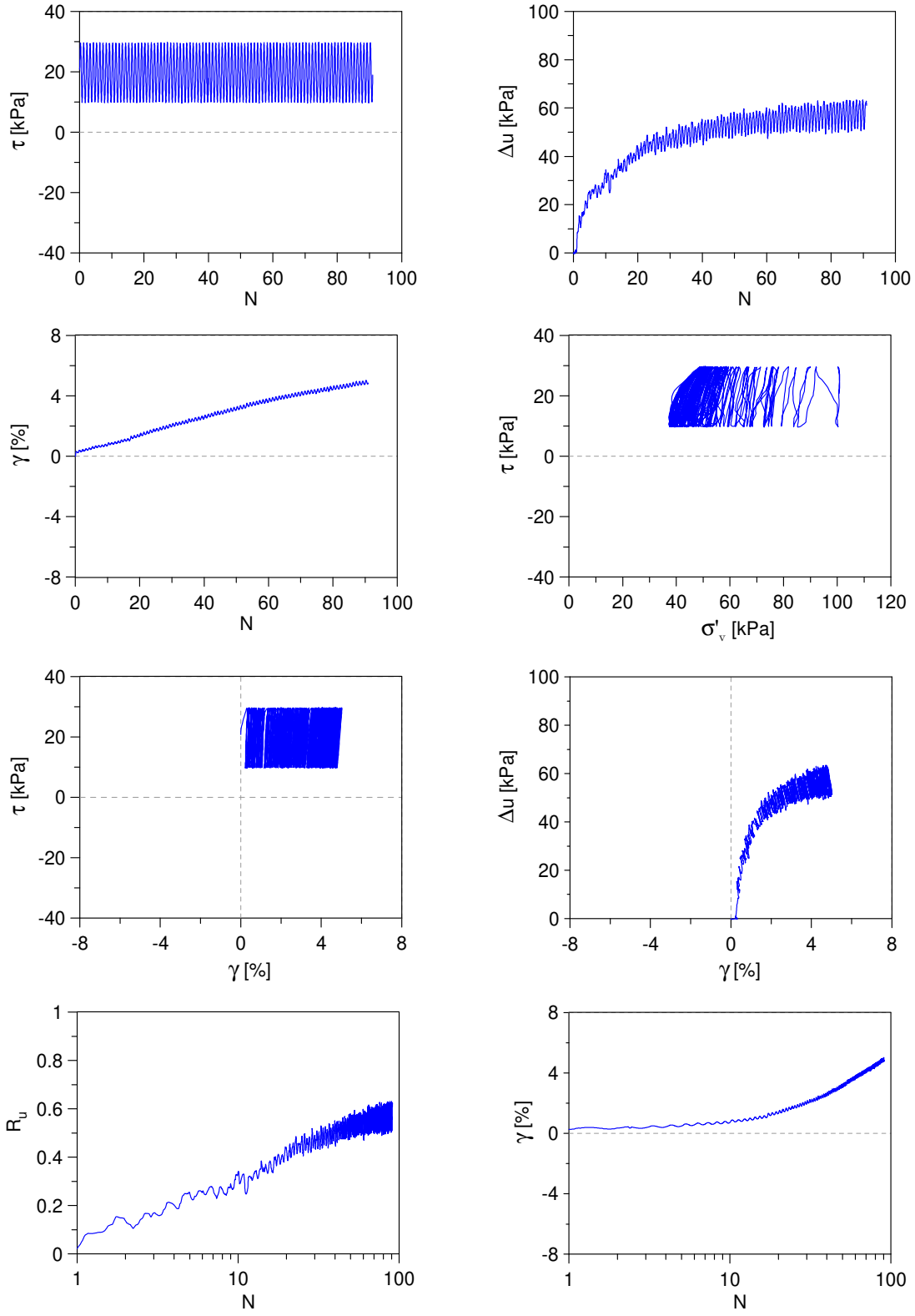

Undrained Cyclic Simple Shear test: *C_SS_TS0_S100_A2_2*
Ticino sand (Reconstitution method: Moist Tamping)
e_0= 0.78 - D_R= 43% - σ'_{v0}= 100 kPa - α= 0.2 - *CSR* = 0.12

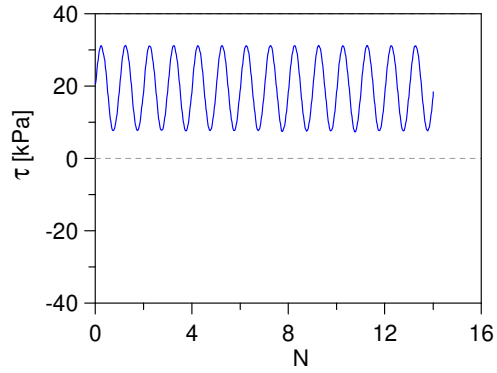

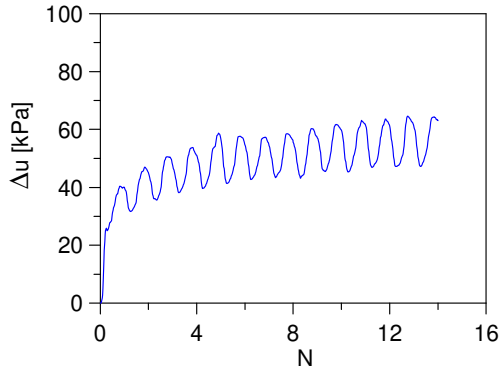

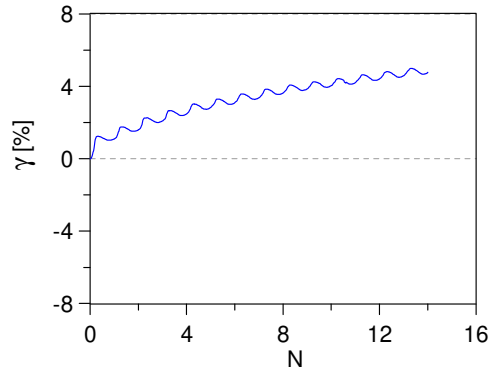

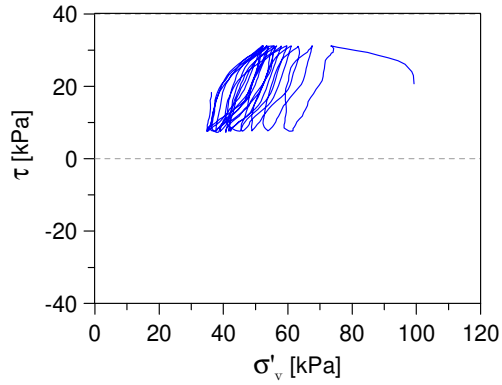

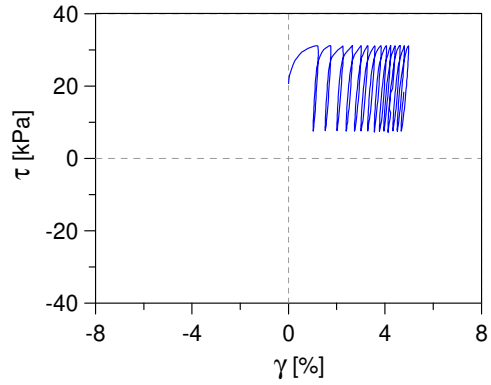

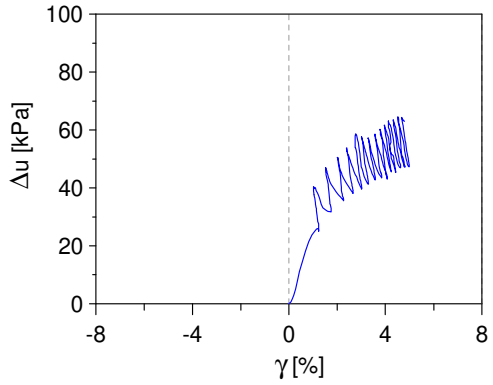

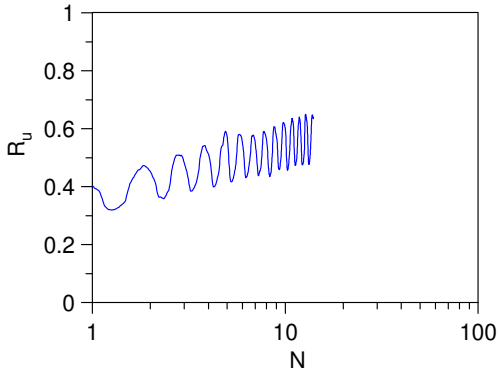

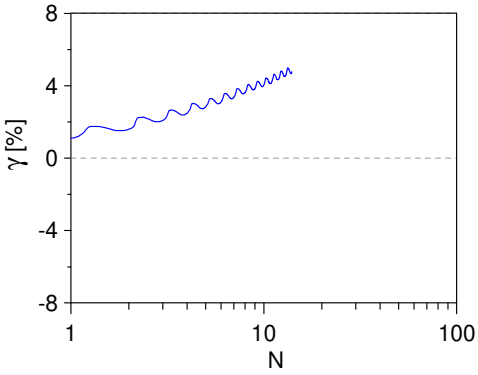

Undrained Cyclic Simple Shear test: *C_SS_TS0_S100_A2_3*
Ticino sand (Reconstitution method: Moist Tamping)
e_0= 0.68 - D_R= 71% - σ'_{v0}= 100 kPa - α= 0.2 - *CSR* = 0.16

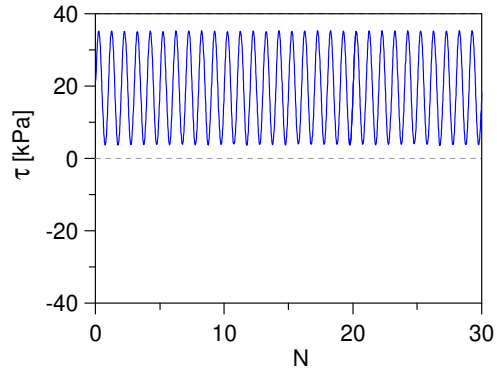

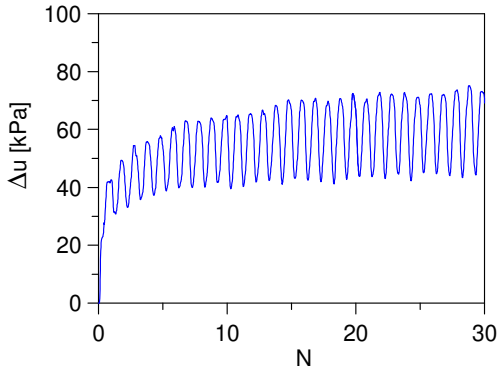

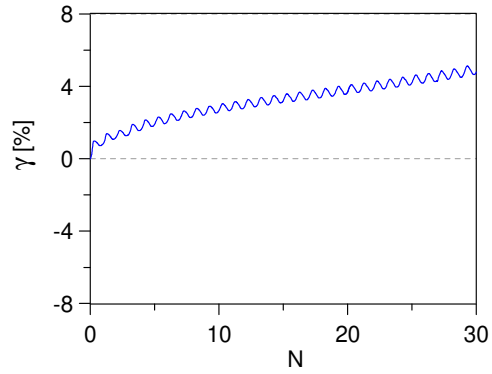

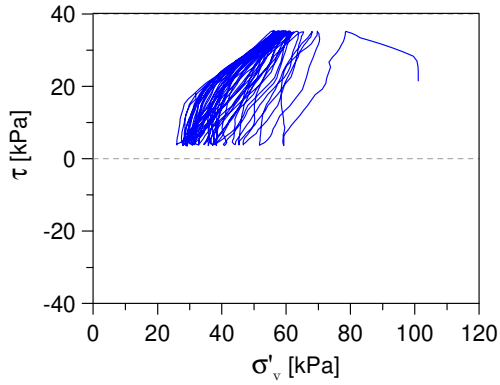

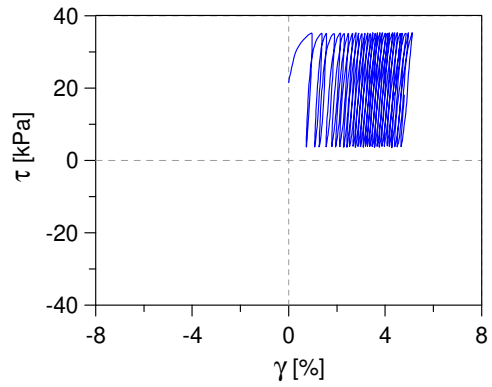

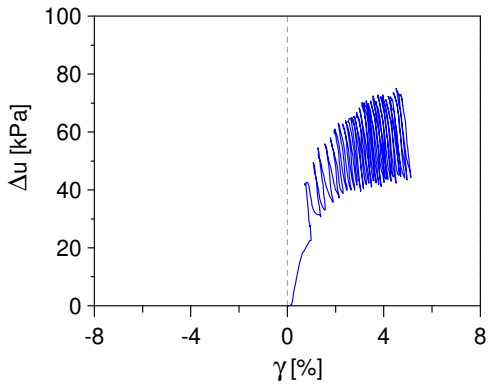

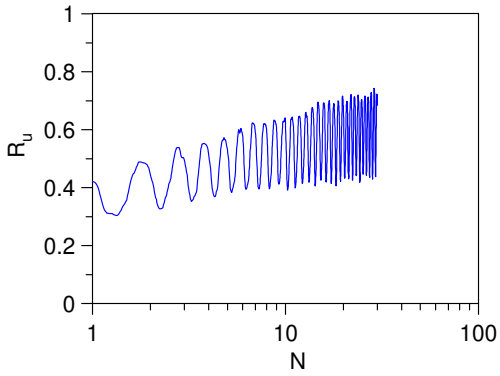

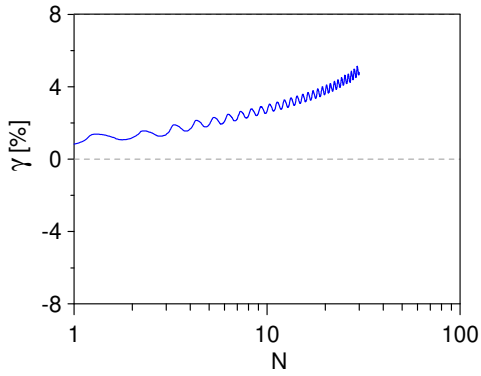

Undrained Cyclic Simple Shear test: *C_SS_TS0_S100_A2_4*
Ticino sand (Reconstitution method: Moist Tamping)
e_0= 0.68 - D_R= 71% - σ'_{v0}= 100 kPa - α= 0.2 - *CSR* = 0.20

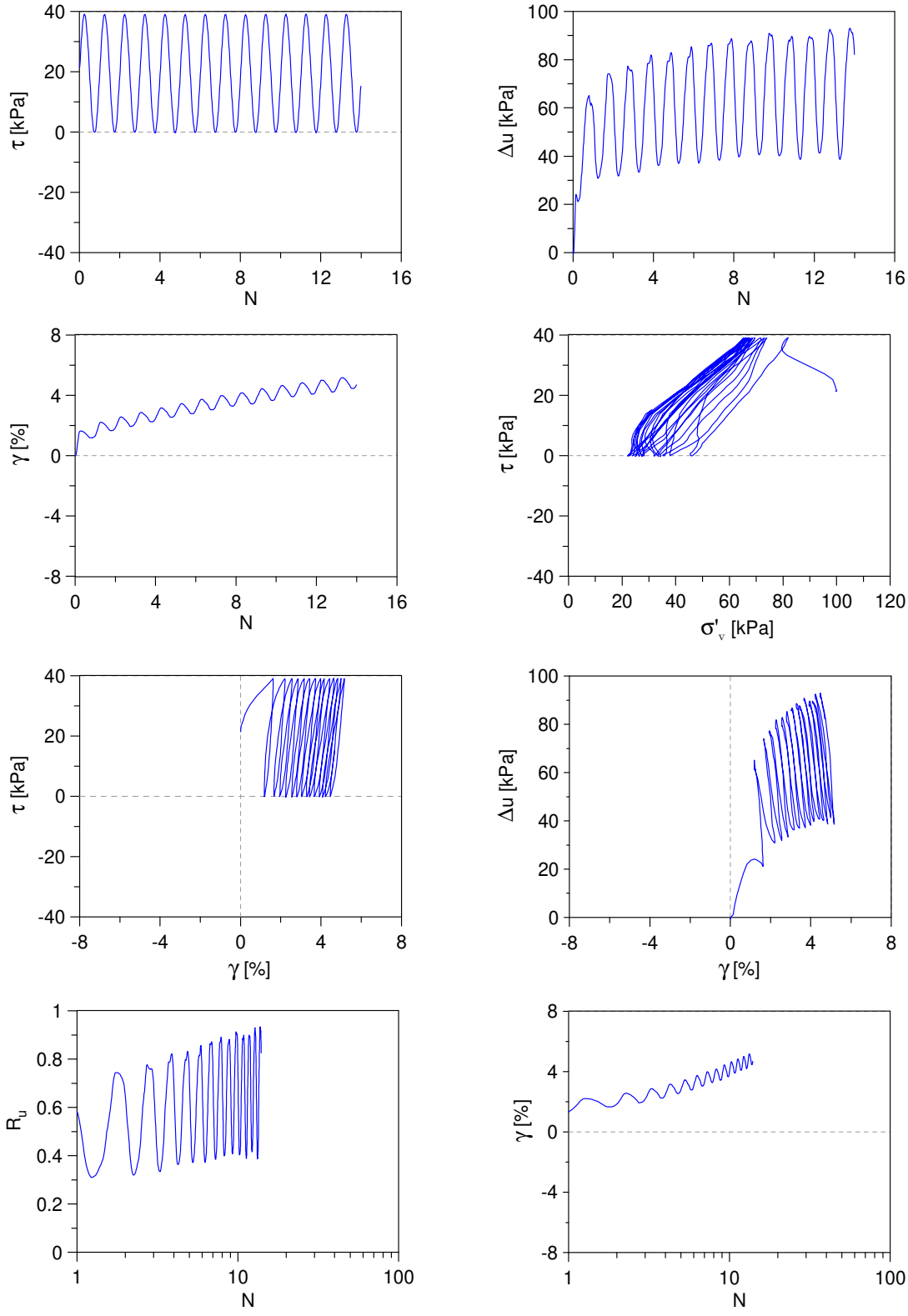

Undrained Cyclic Simple Shear test: *C_SS_TS0_S100_A2_5*
Ticino sand (Reconstitution method: Moist Tamping)
e_0= 0.60 - D_R= 94% - σ'_{v0}= 100 kPa - α= 0.2 - *CSR* = 0.20

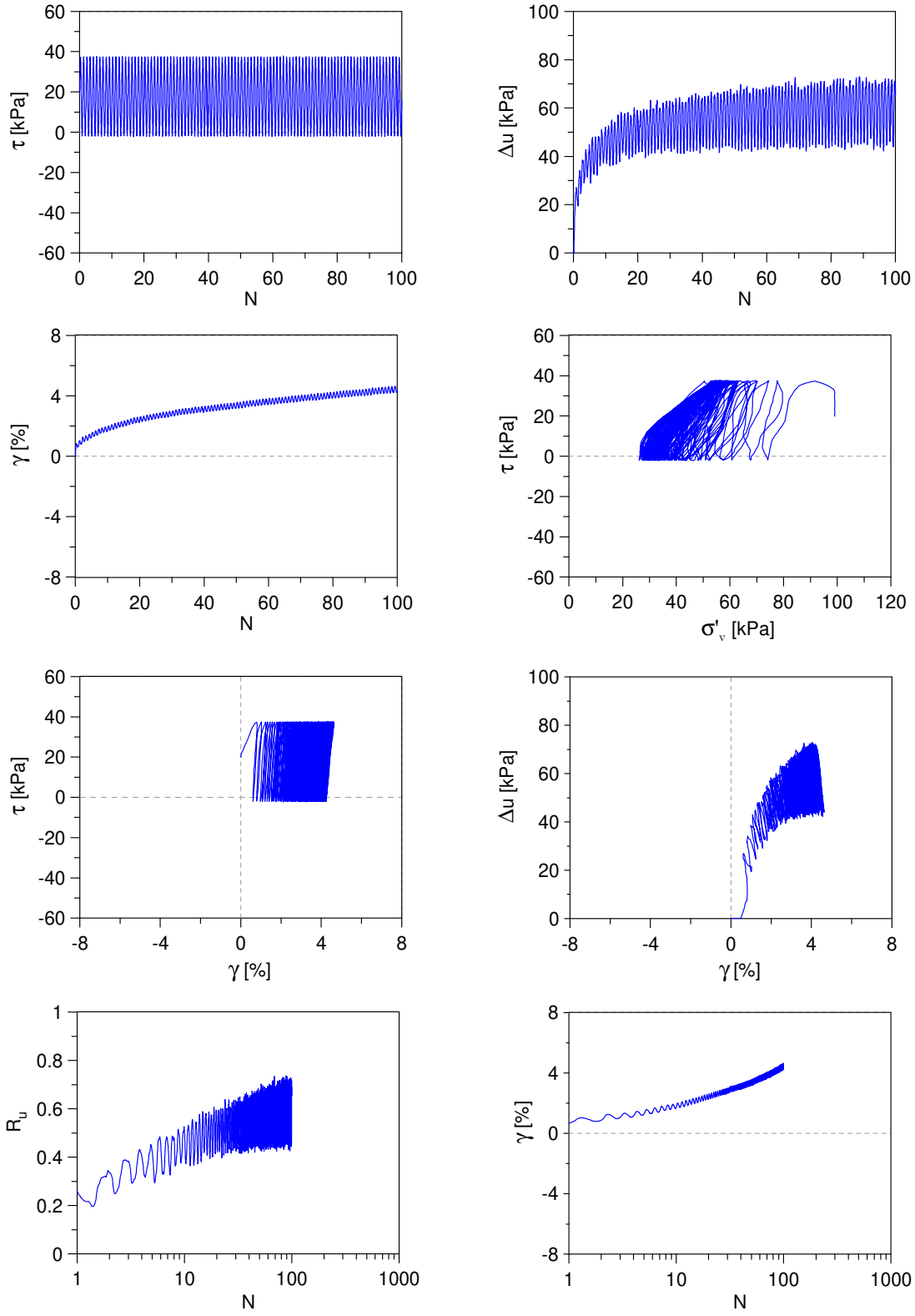

Undrained Cyclic Simple Shear test: *C_SS_TS0_S100_A2_6*
Ticino sand (Reconstitution method: Moist Tamping)
e_0= 0.60 - D_R= 94% - σ'_{v0}= 100 kPa - α= 0.2 - *CSR* = 0.26

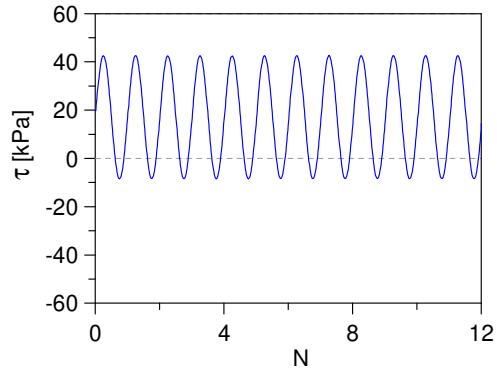

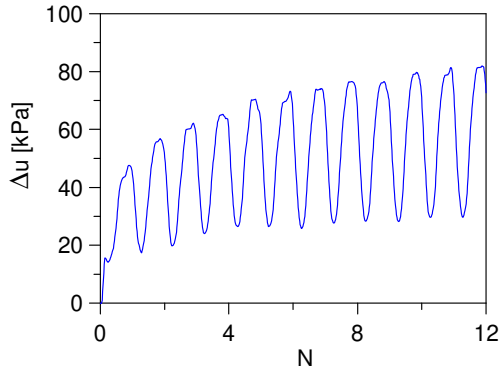

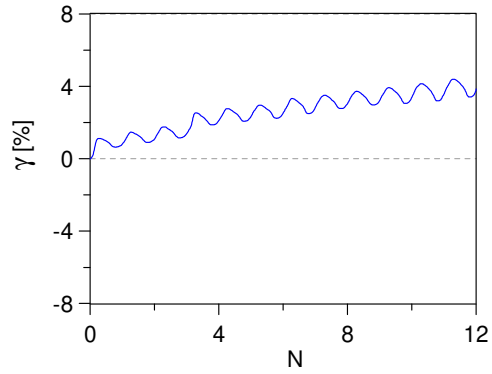

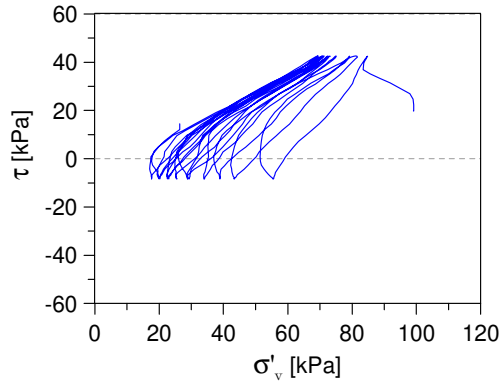

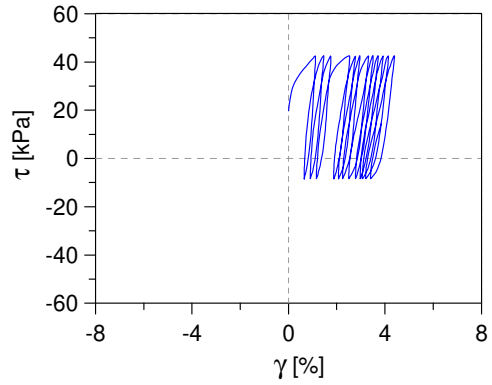

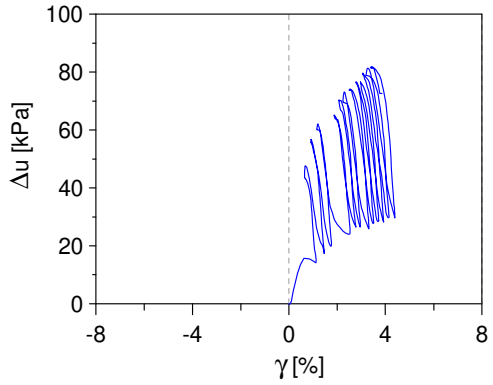

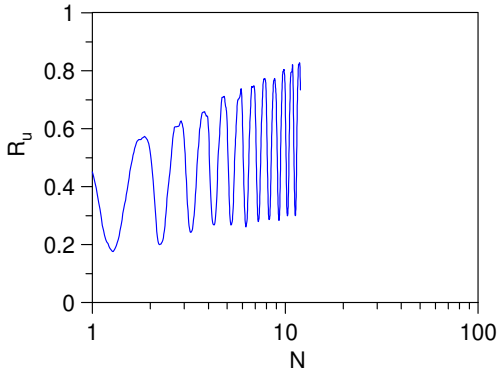

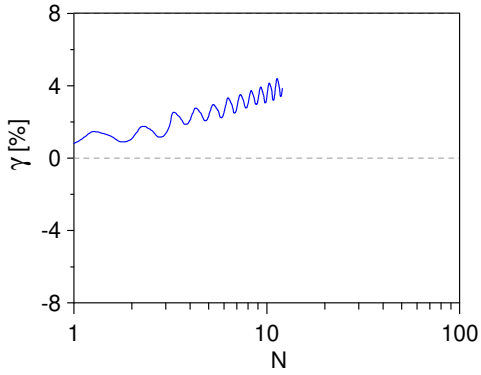

Undrained Cyclic Simple Shear test: *C_SS_TS0_S100_A2_7*
Ticino sand (Reconstitution method: Moist Tamping)
e_0= 0.60 - D_R= 94% - σ'_{v0}= 100 kPa - α= 0.2 - *CSR* = 0.28

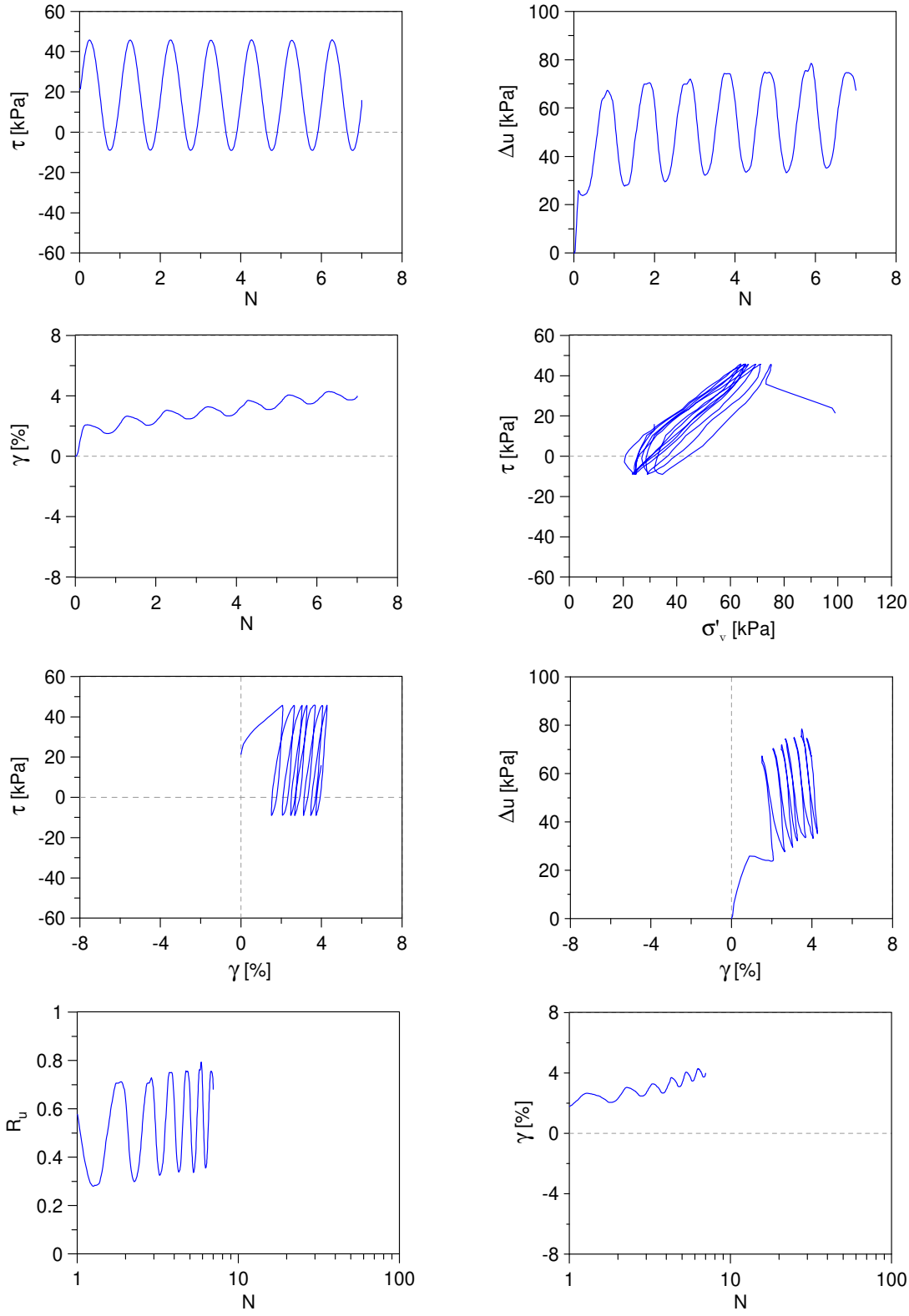

Undrained Cyclic Simple Shear test: *C_SS_TS0_S100_A3_1*
Ticino sand (Reconstitution method: Moist Tamping)
e_0= 0.78 - D_R= 43% - σ'_{v0}= 100 kPa - α= 0.3 - *CSR* = 0.10

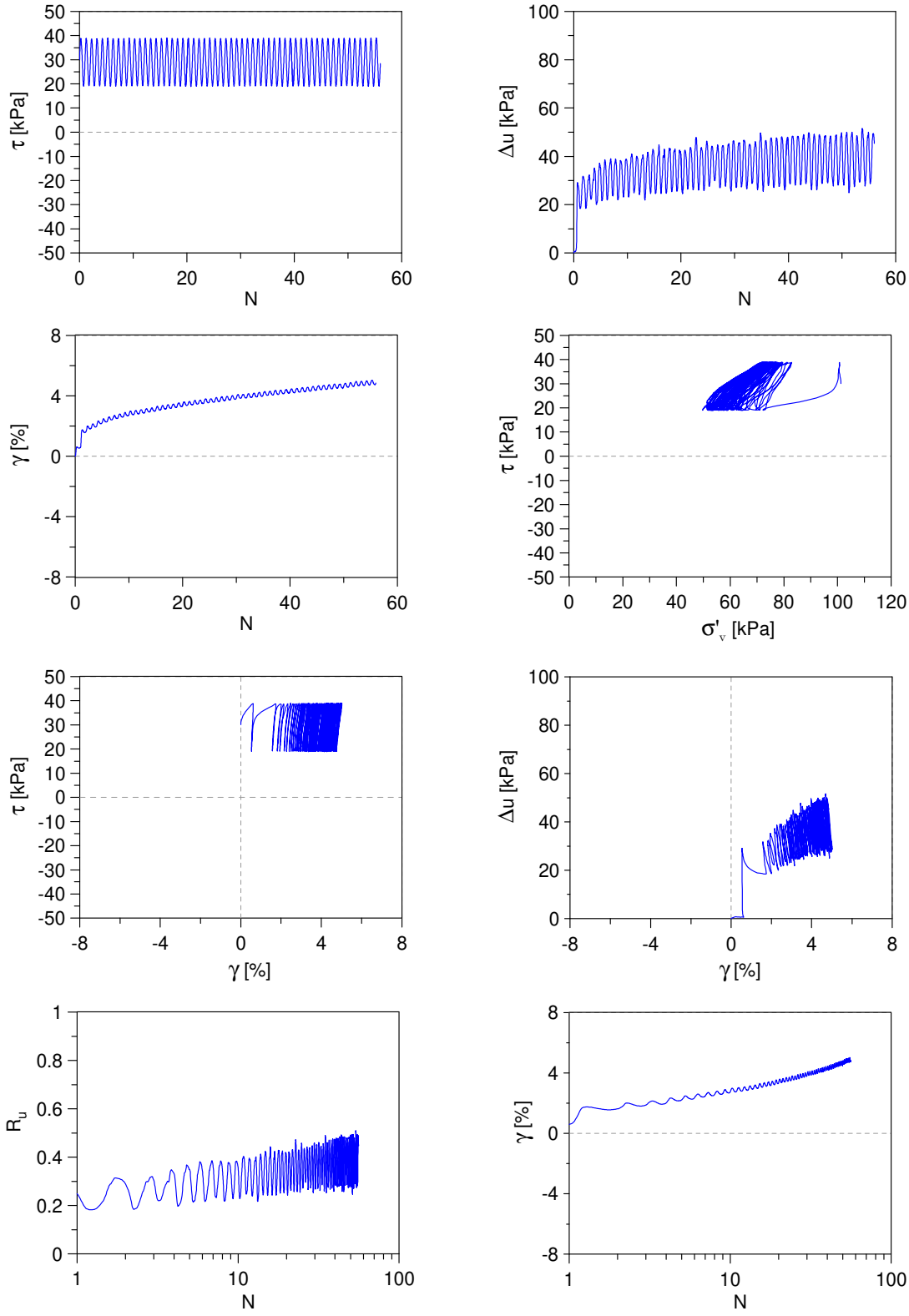

Undrained Cyclic Simple Shear test: *C_SS_TS0_S100_A3_2*
Ticino sand (Reconstitution method: Moist Tamping)
e_0= 0.78 - D_R= 43% - σ'_{v0}= 100 kPa - α= 0.3 - *CSR* = 0.12

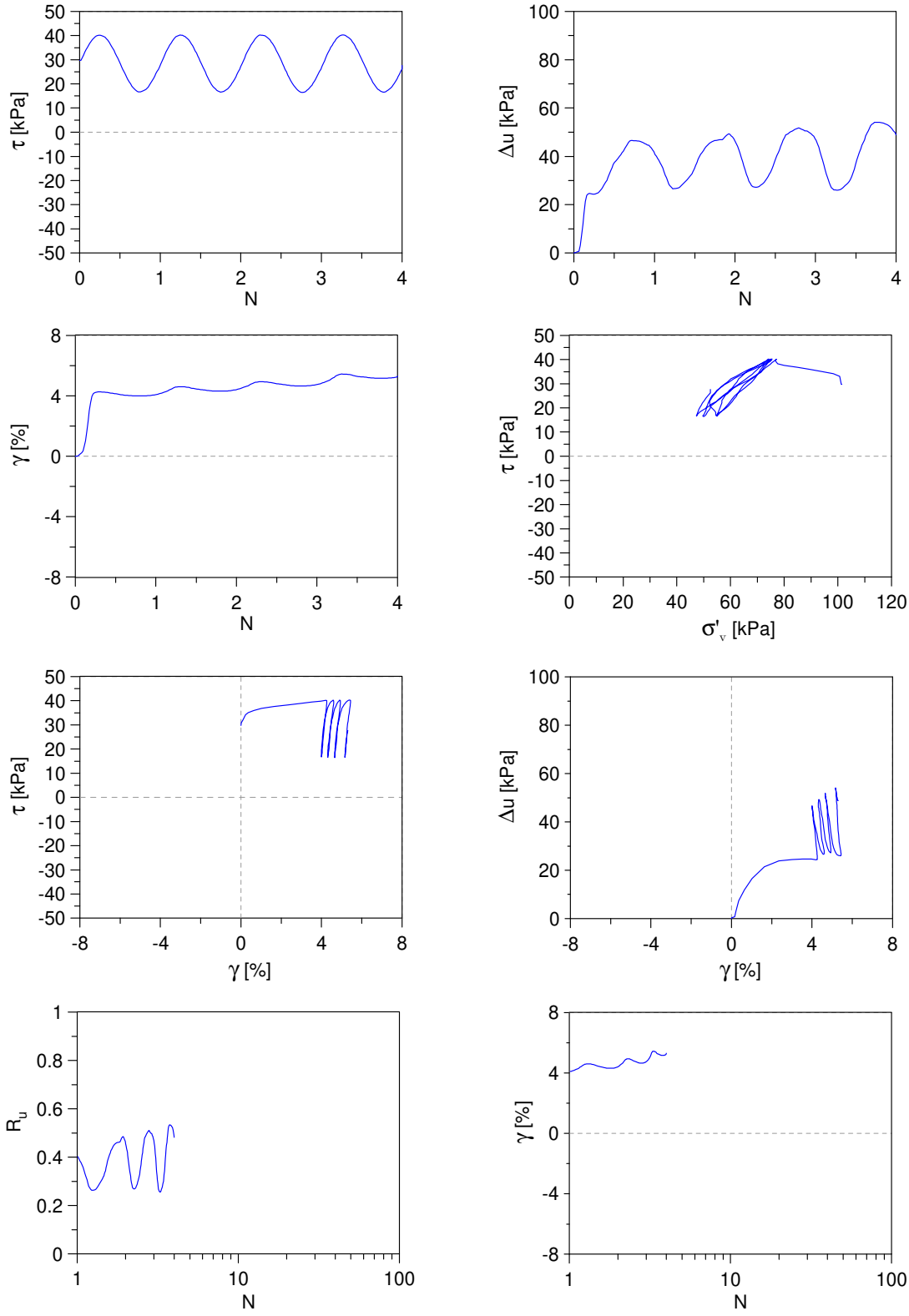

Undrained Cyclic Simple Shear test: *C_SS_TS0_S100_A3_3*
Ticino sand (Reconstitution method: Moist Tamping)
e_0= 0.68 - D_R= 71% - σ'_{v0}= 100 kPa - α= 0.3 - *CSR* = 0.16

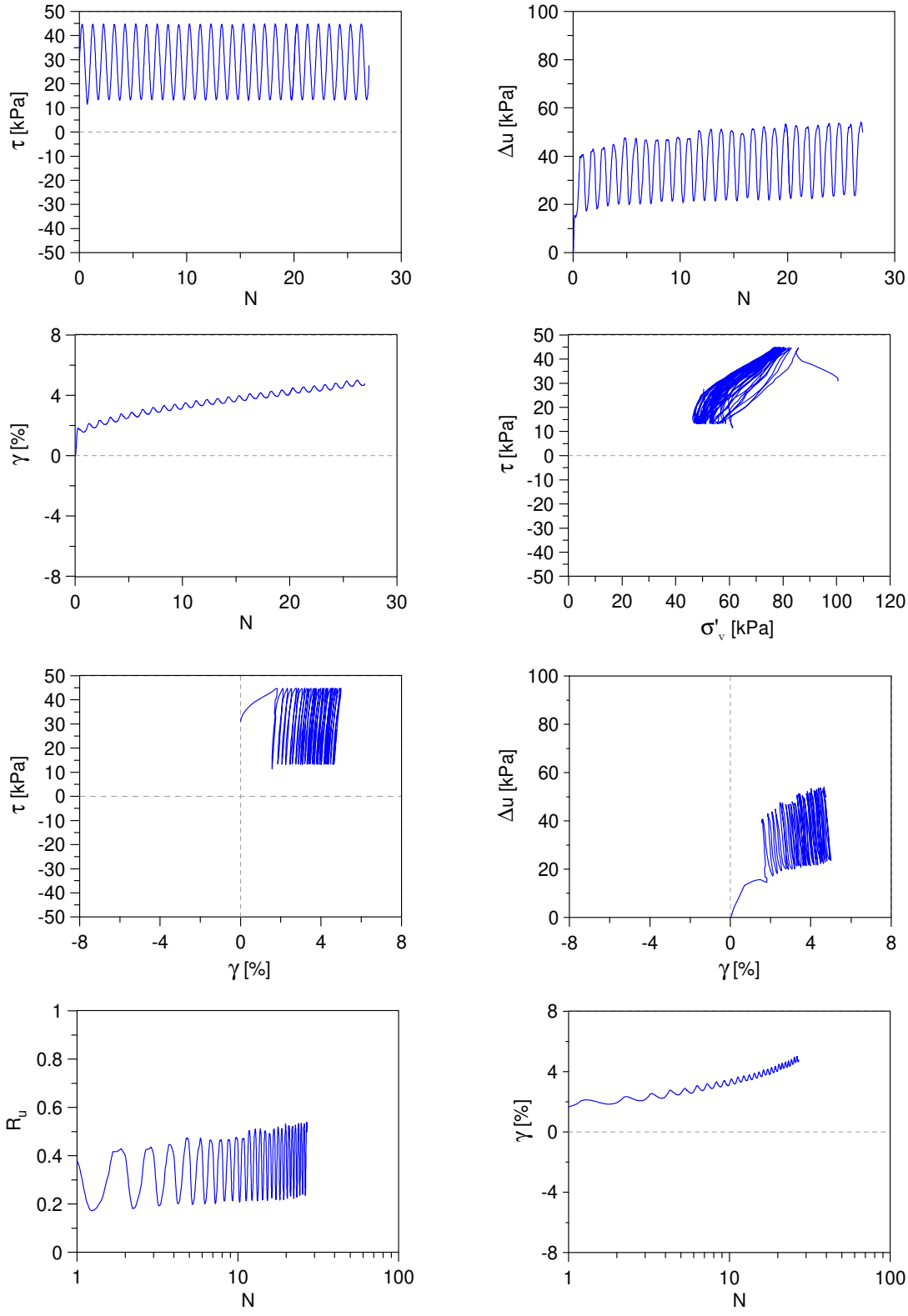

Undrained Cyclic Simple Shear test: *C_SS_TS0_S100_A3_4*
Ticino sand (Reconstitution method: Moist Tamping)
e_0= 0.68 - D_R= 71% - σ'_{v0}= 100 kPa - α= 0.3 - *CSR* = 0.18

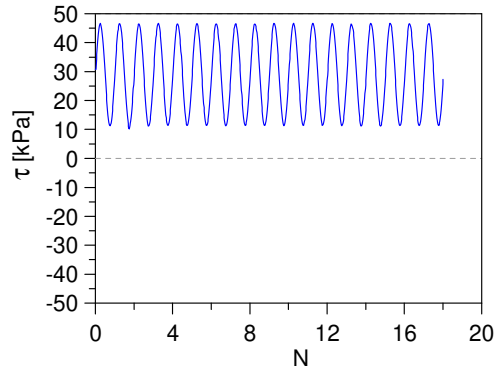

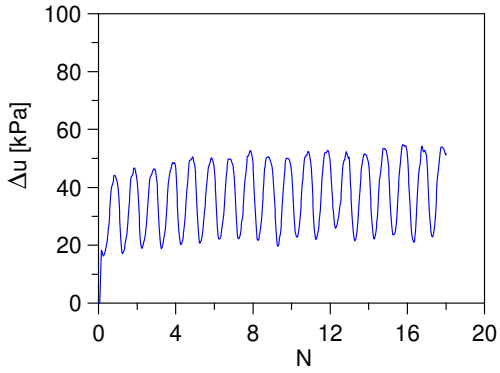

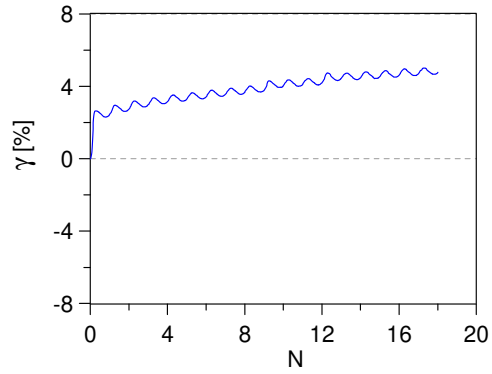

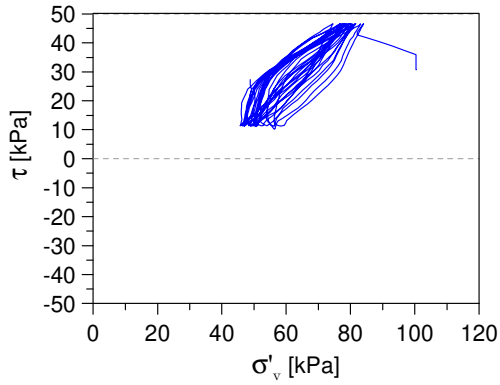

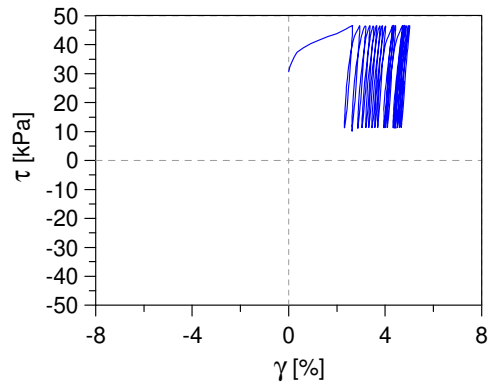

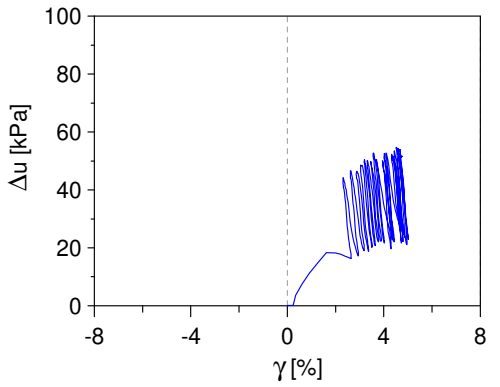

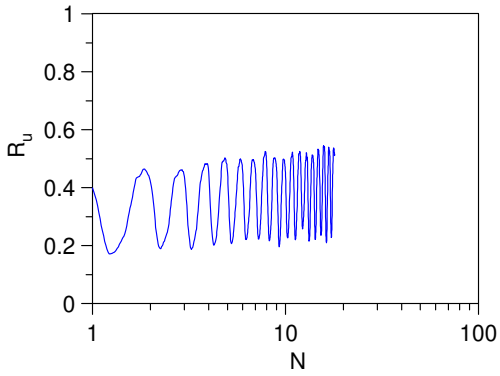

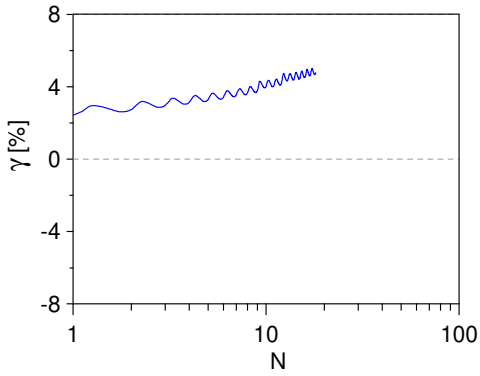

Undrained Cyclic Simple Shear test: *C_SS_TS0_S100_A3_5*
Ticino sand (Reconstitution method: Moist Tamping)
e_0= 0.60 - D_R= 94% - σ'_{v0}= 100 kPa - α= 0.3 - *CSR* = 0.22

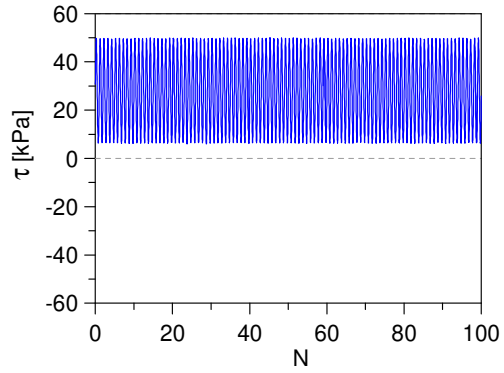

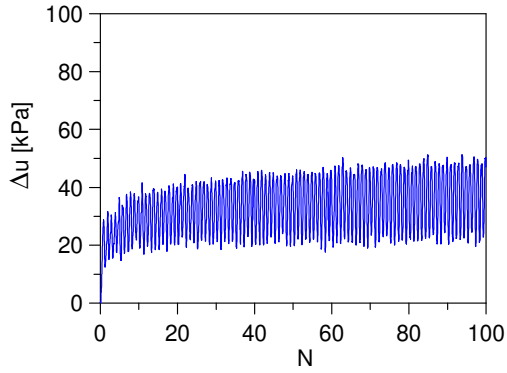

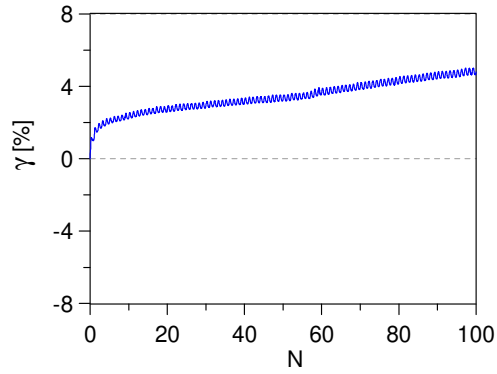

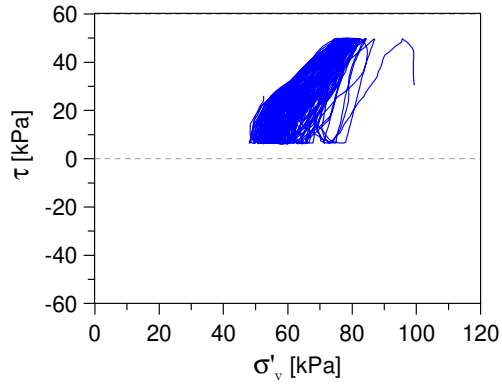

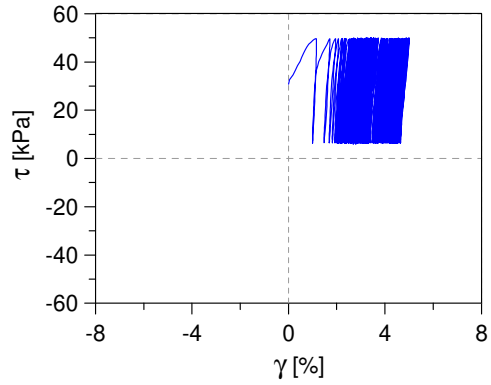

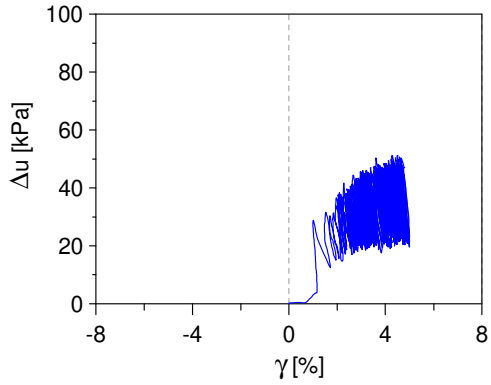

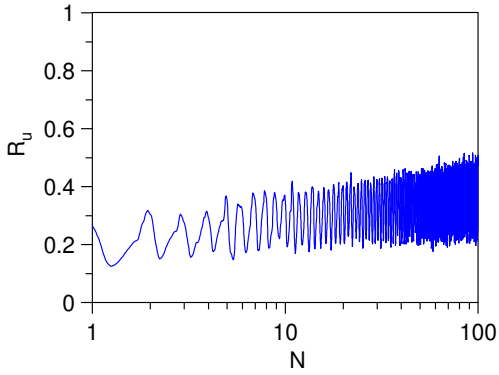

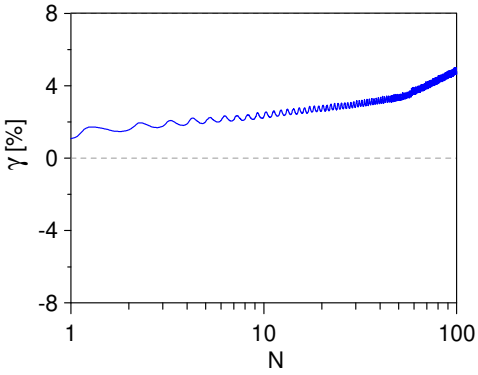

Undrained Cyclic Simple Shear test: *C_SS_TS0_S100_A3_6*
Ticino sand (Reconstitution method: Moist Tamping)
e_0= 0.60 - D_R= 94% - σ'_{v0}= 100 kPa - α= 0.3 - *CSR* = 0.28

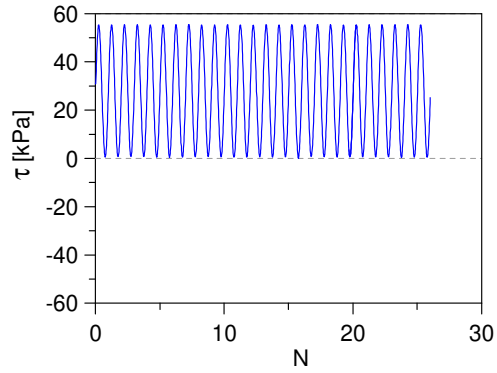

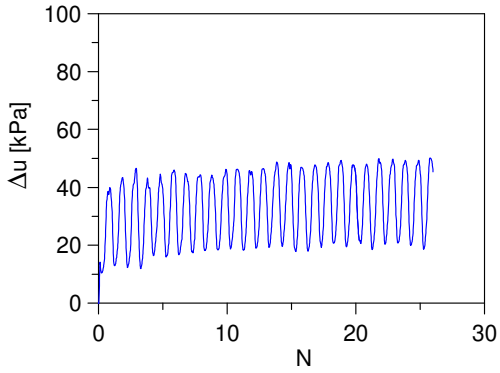

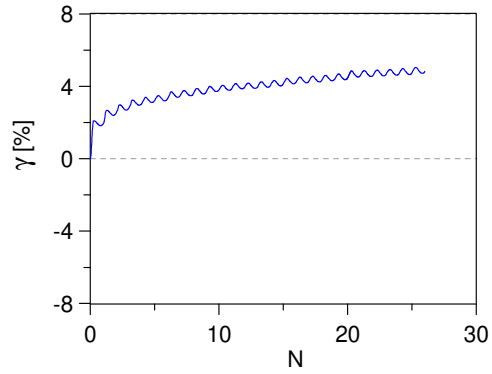

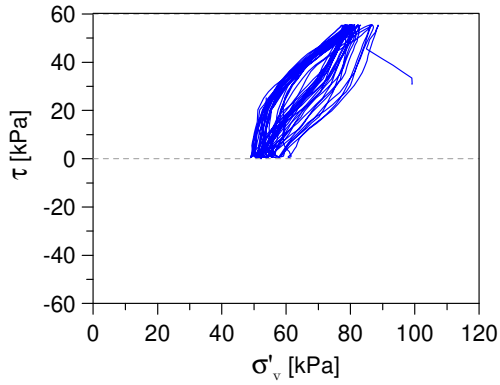

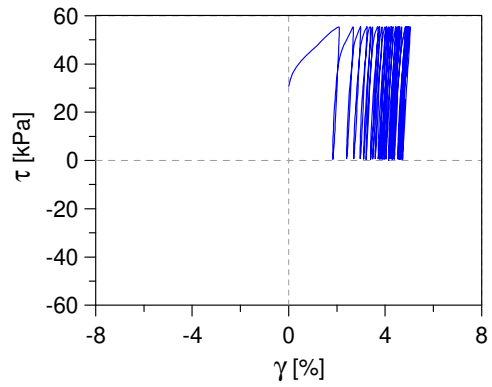

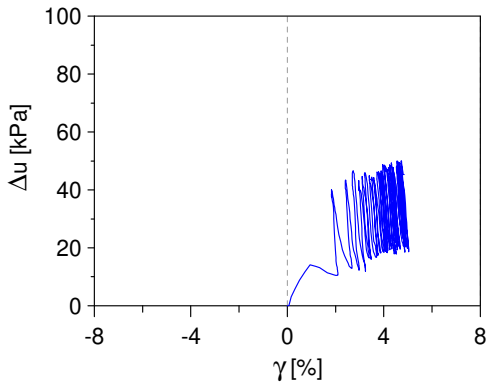

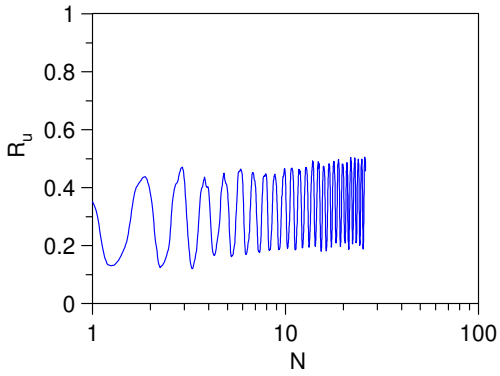

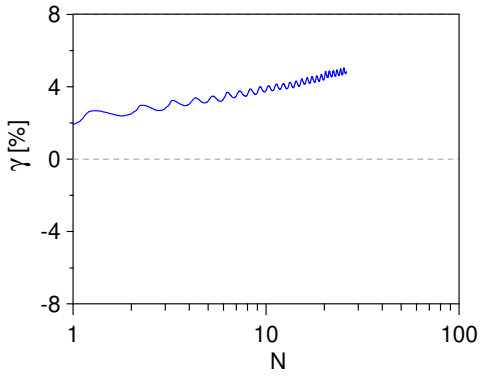

Sand-silt mixture (f_c=5%)

Undrained Cyclic Simple Shear test: *C_SS_TS05_S100_A0_1*
Ticino sand + 5% f_c (Reconstitution method: Moist Tamping)
e_0= 0.73 - D_R= 37% - σ'_{v0}= 100 kPa - α=0 - *CSR* = 0.10

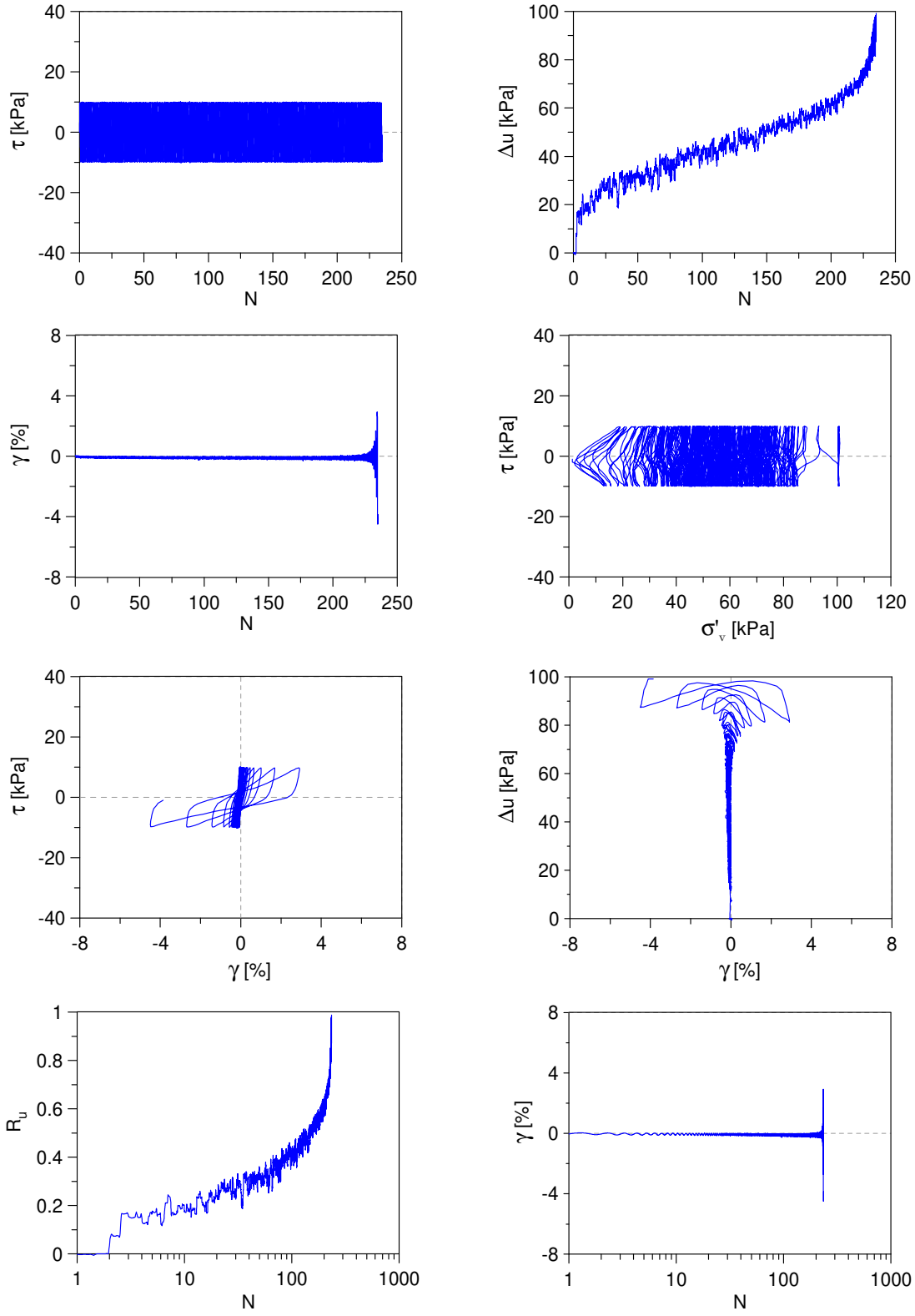

Undrained Cyclic Simple Shear test: *C_SS_TS05_S100_A0_2*
Ticino sand + 5% f_c (Reconstitution method: Moist Tamping)
e_0= 0.73 - D_R= 37% - σ'_{v0}= 100 kPa - α=0 - *CSR* = 0.12

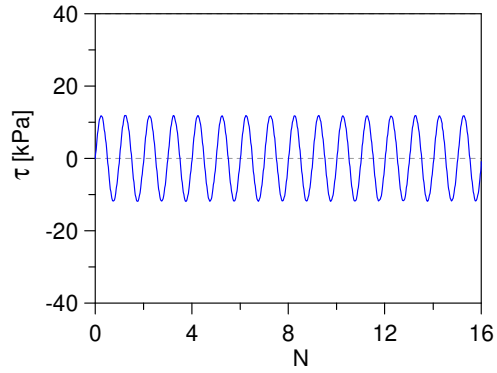

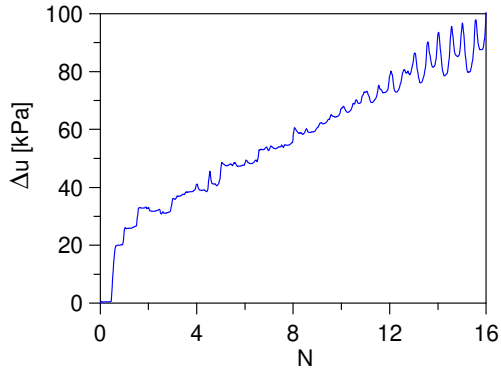

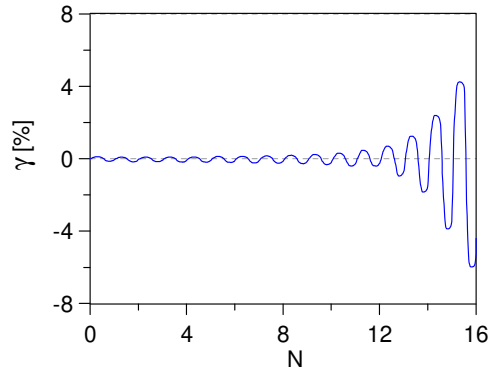

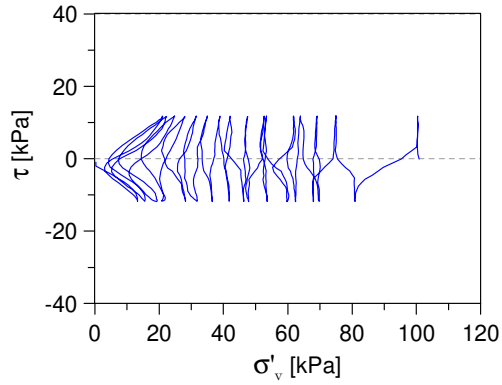

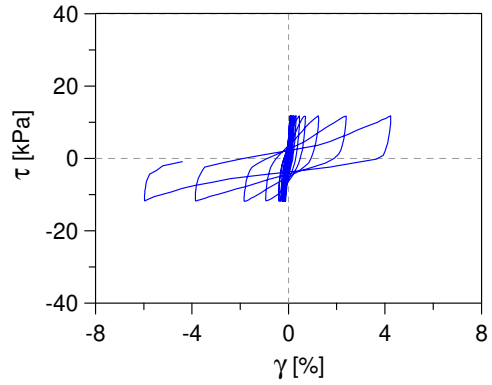

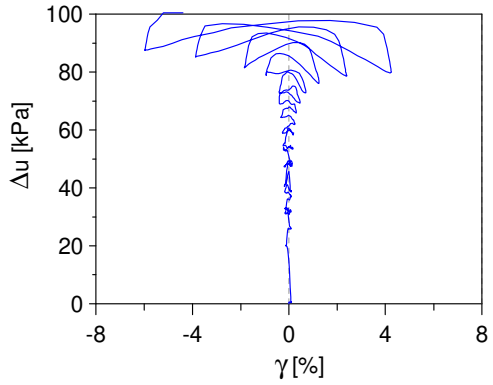

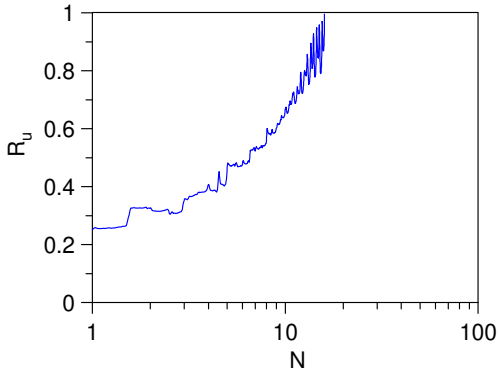

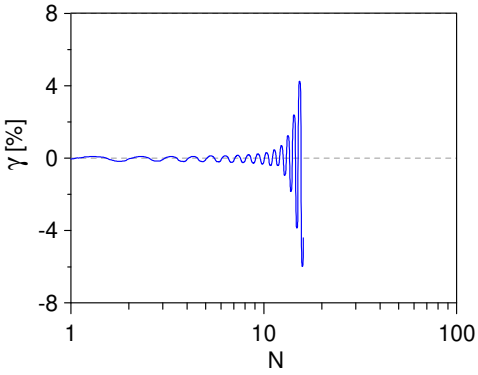

Undrained Cyclic Simple Shear test: *C_SS_TS05_S100_A0_3*
Ticino sand + 5% f_c (Reconstitution method: Moist Tamping)
e_0= 0.73 - D_R= 37% - σ'_{v0}= 100 kPa - α=0 - *CSR* = 0.16

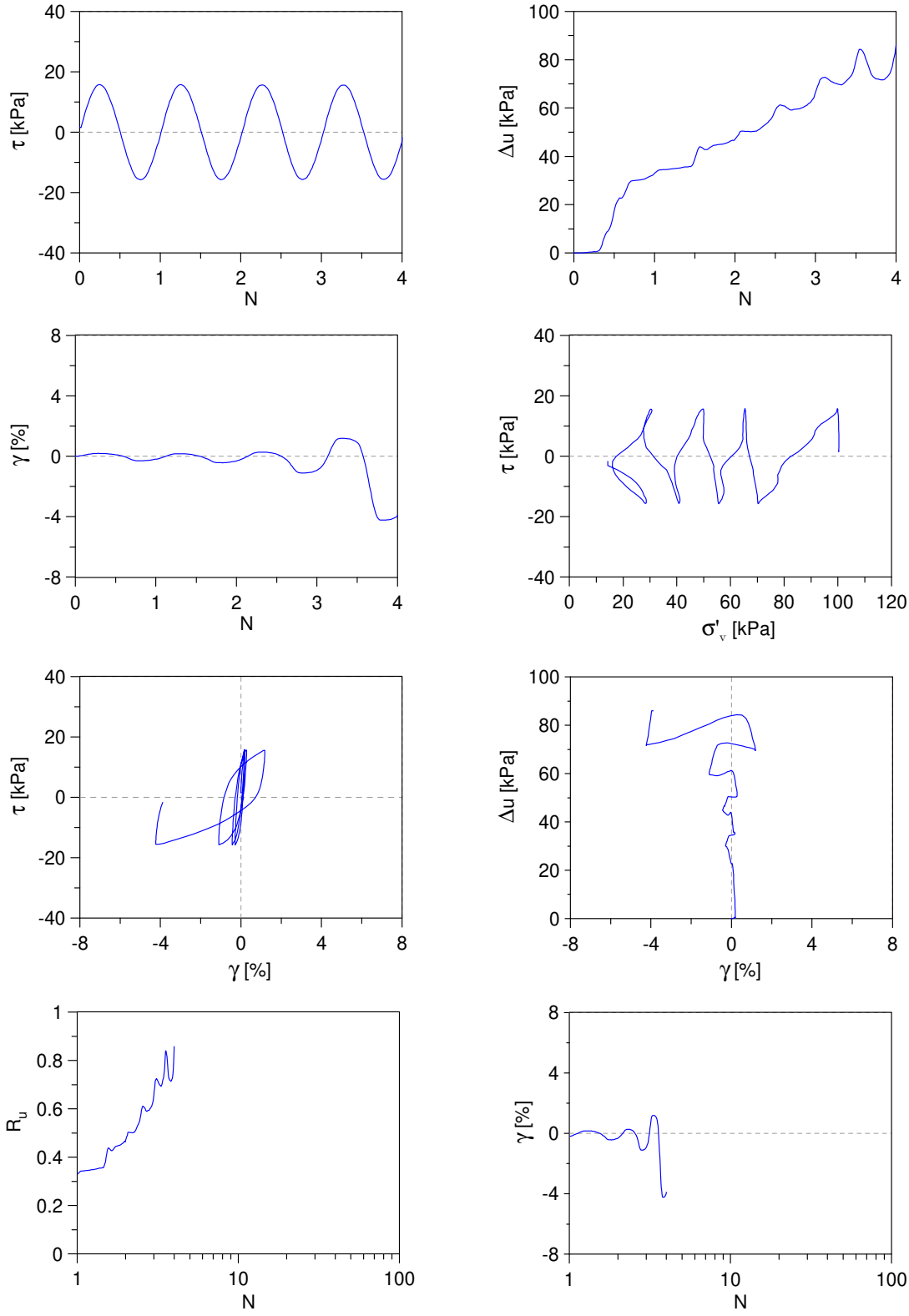

Undrained Cyclic Simple Shear test: *C_SS_TS05_S100_A0_4*
Ticino sand + 5% f_c (Reconstitution method: Moist Tamping)
e_0= 0.68 - D_R= 52% - σ'_{v0}= 100 kPa - α=0 - *CSR* = 0.14

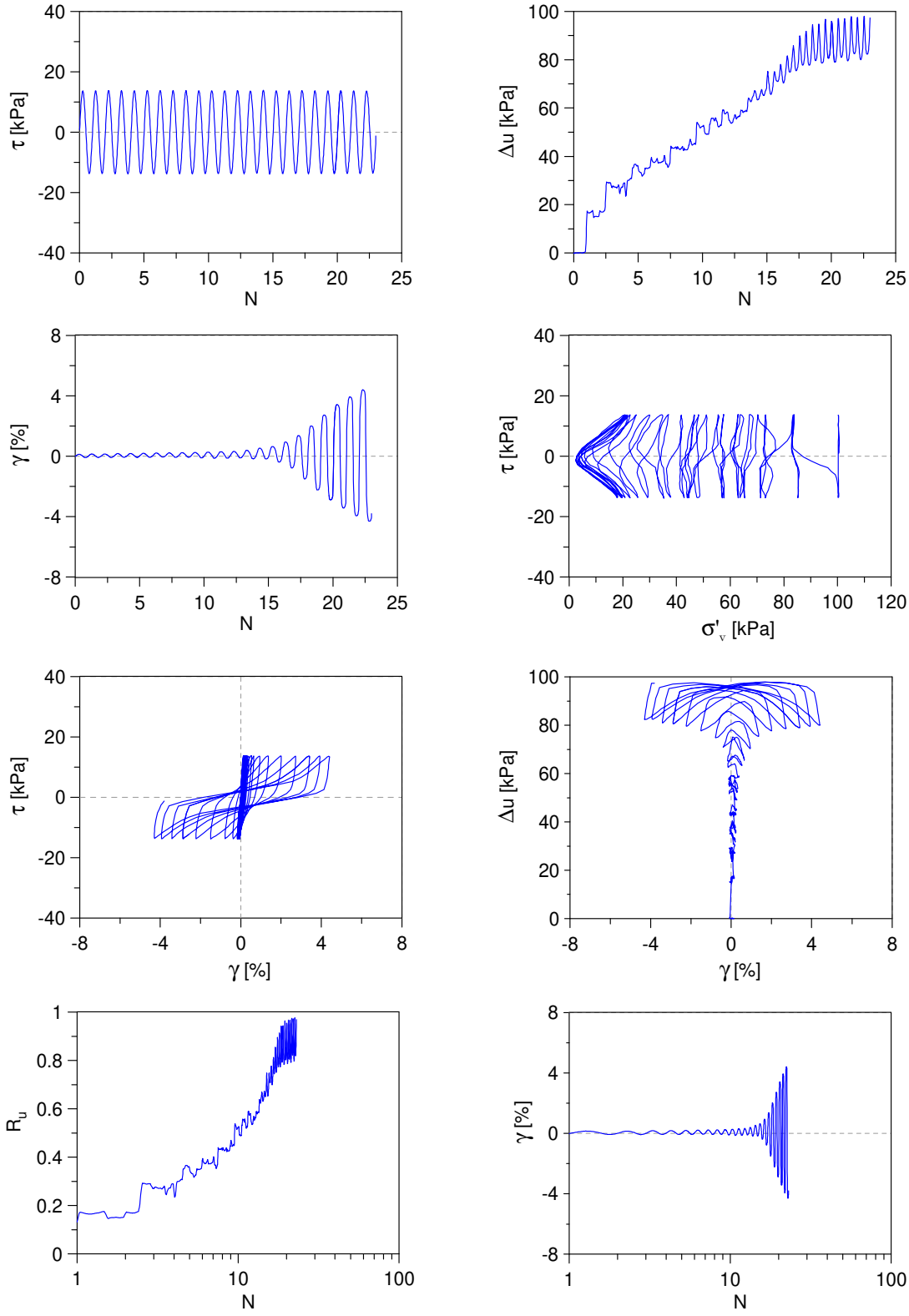

Undrained Cyclic Simple Shear test: *C_SS_TS05_S100_A0_5*
Ticino sand + 5% f_c (Reconstitution method: Moist Tamping)
e_0= 0.68 - D_R= 52% - σ'_{v0}= 100 kPa - α=0 - *CSR* = 0.16

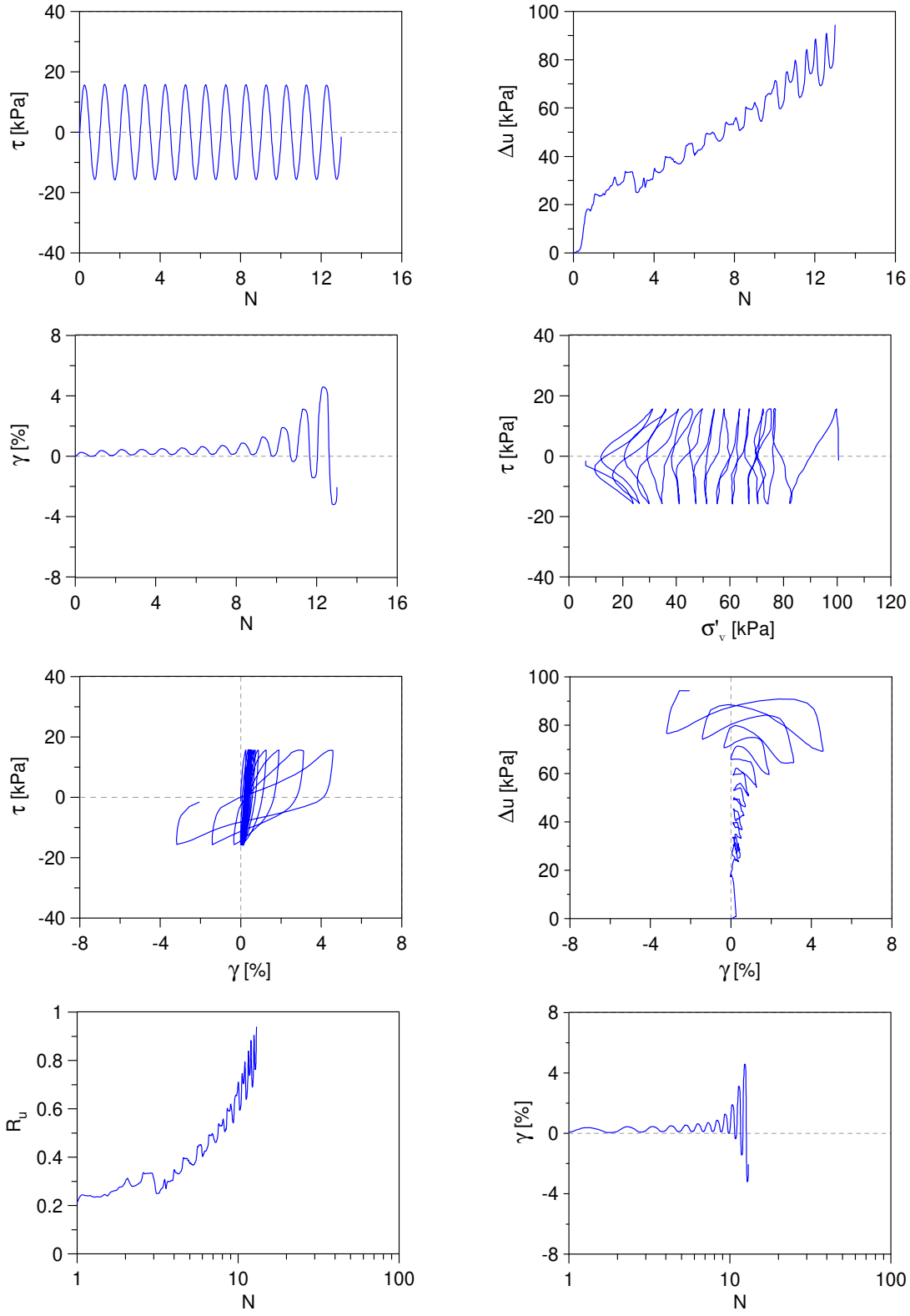

Undrained Cyclic Simple Shear test: *C_SS_TS05_S100_A0_6*
Ticino sand + 5% f_c (Reconstitution method: Moist Tamping)
e_0= 0.61 - D_R= 74% - σ'_{v0}= 100 kPa - α=0 - *CSR* = 0.14

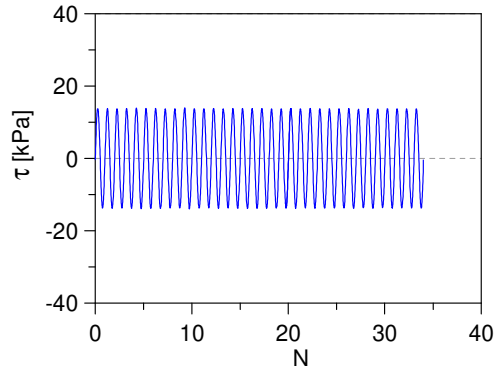

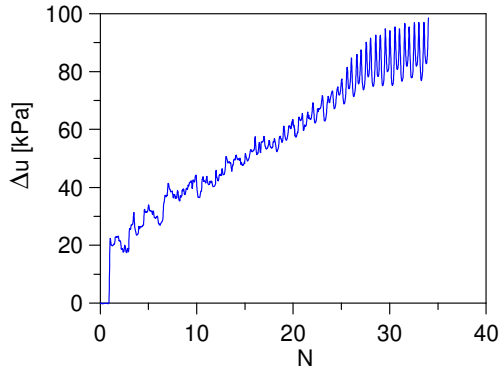

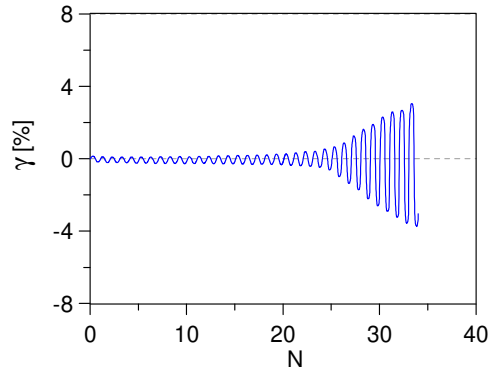

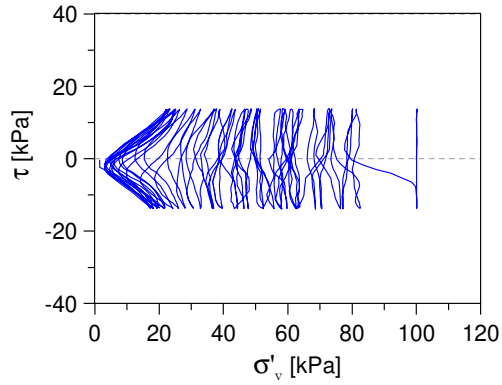

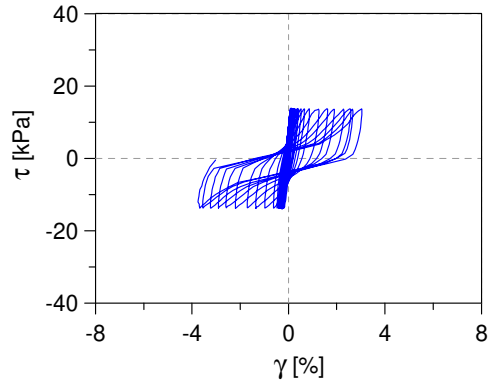

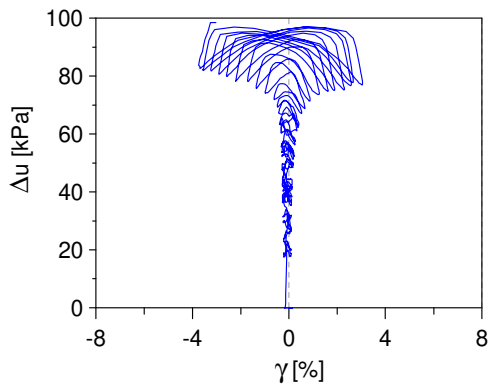

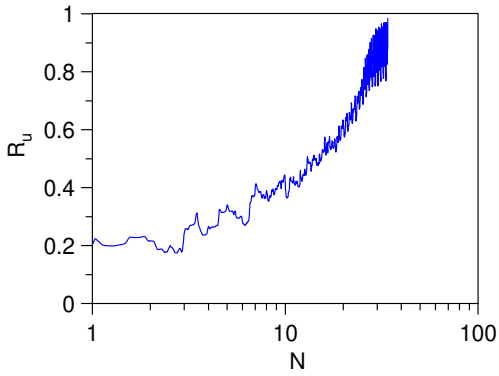

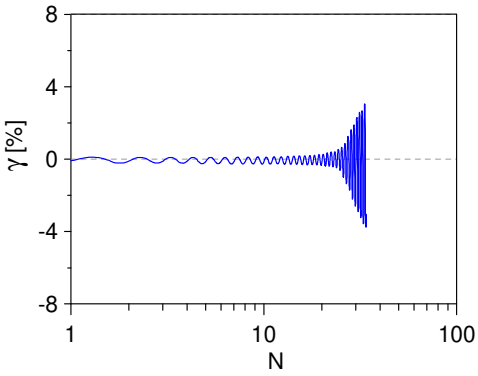

Undrained Cyclic Simple Shear test: *C_SS_TS05_S100_A0_7*
Ticino sand + 5% f_c (Reconstitution method: Moist Tamping)
e_0= 0.61 - D_R= 74% - σ'_{v0}= 100 kPa - α=0 - *CSR* = 0.20

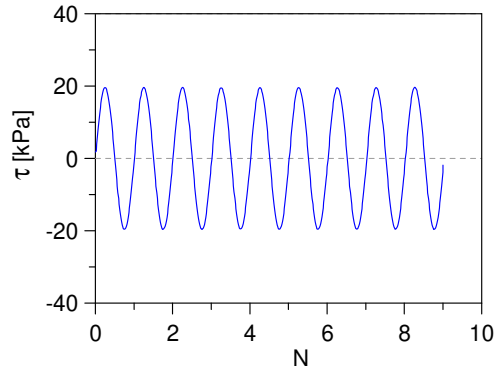

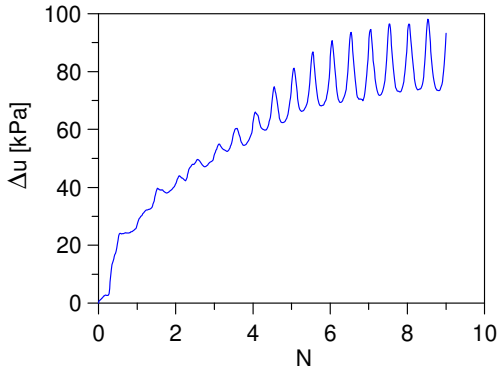

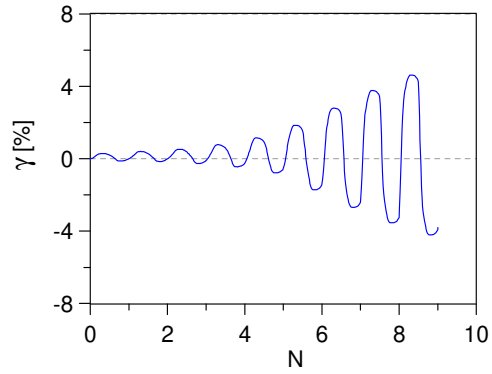

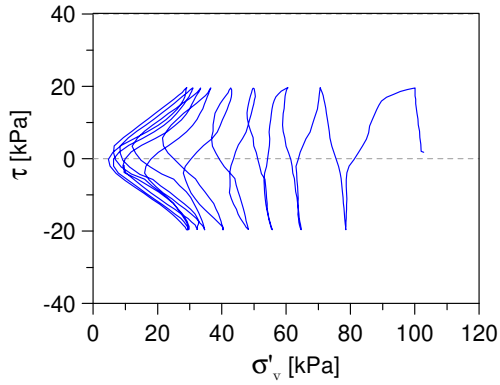

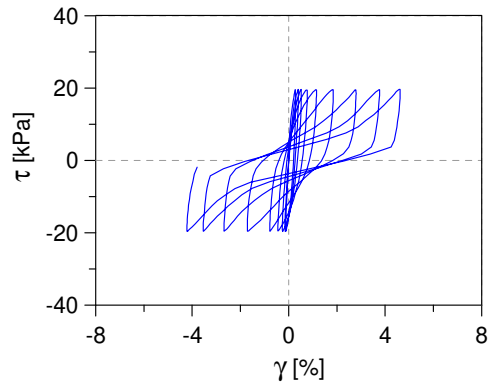

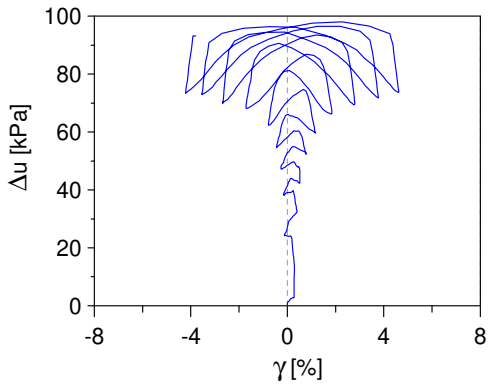

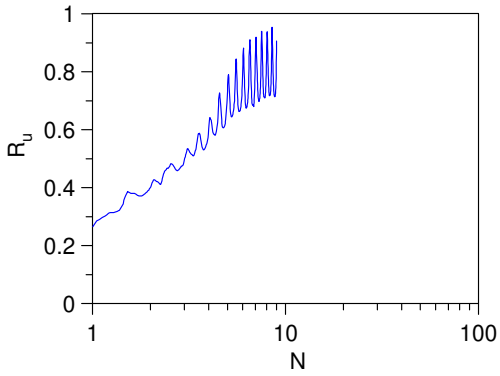

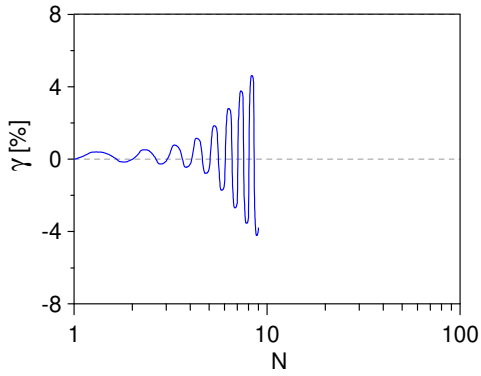

Undrained Cyclic Simple Shear test: *C_SS_TS05_S100_A0_8*
Ticino sand + 5% f_c (Reconstitution method: Moist Tamping)
e_0= 0.61 - D_R= 74% - σ'_{v0}= 100 kPa - α=0 - *CSR* = 0.22

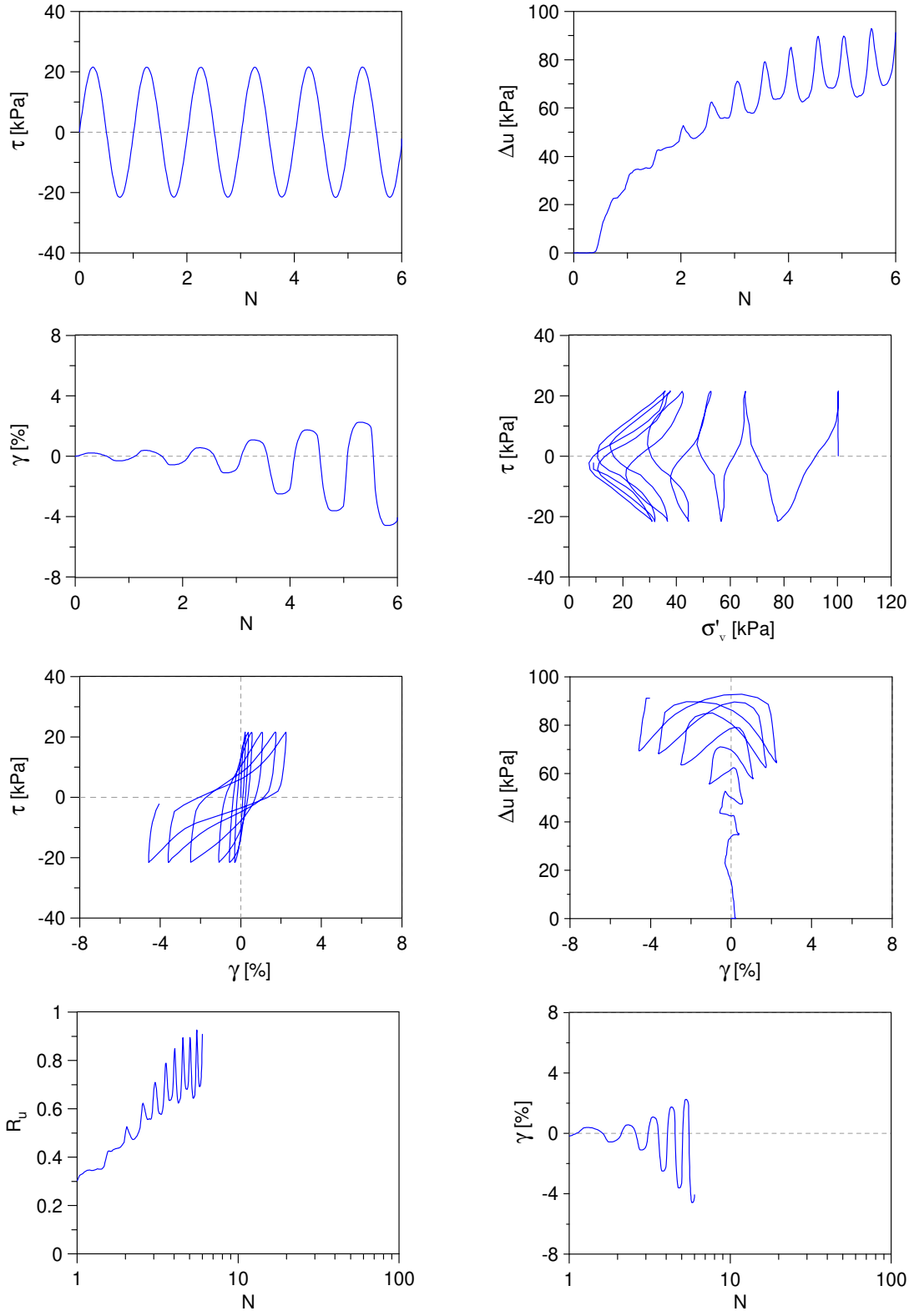

Sand-silt mixture (f_c=10%)

Undrained Cyclic Simple Shear test: *C_SS_TS10_S50_A0_1*
Ticino sand + 10% f_c (Reconstitution method: Moist Tamping)
e_0= 0.68 - D_R= 38% - σ'_{v0}= 50 kPa - α= 0 - *CSR* = 0.14

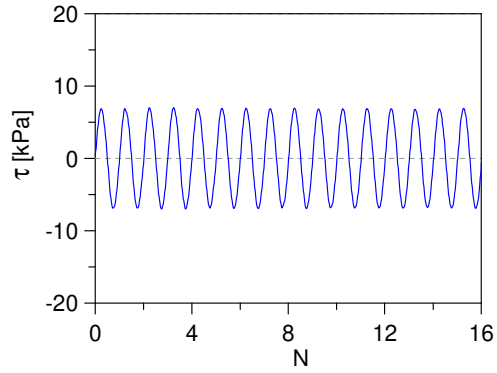

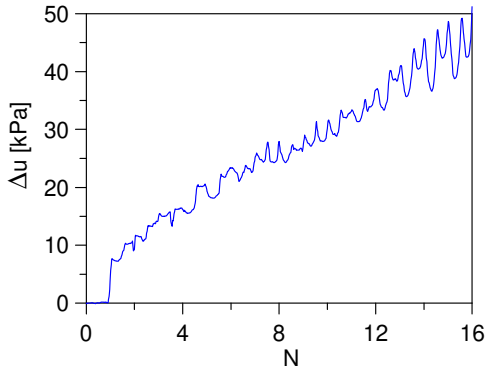

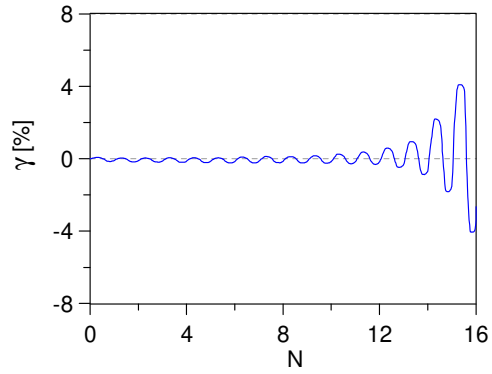

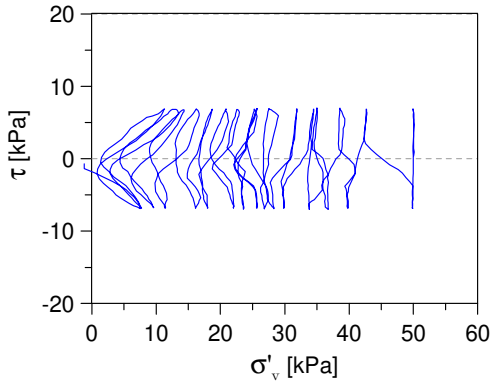

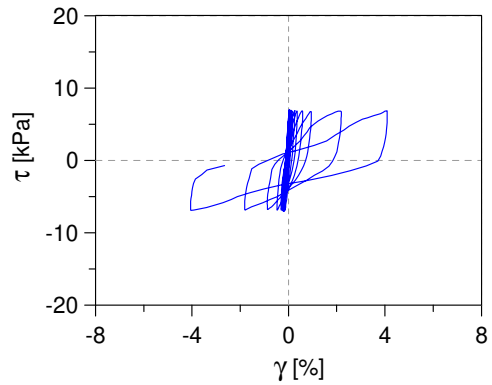

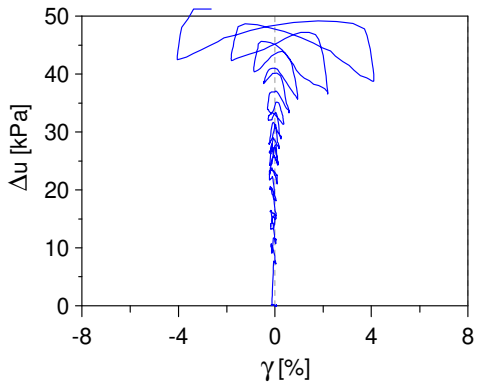

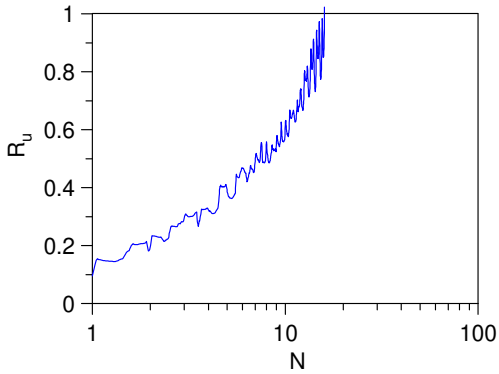

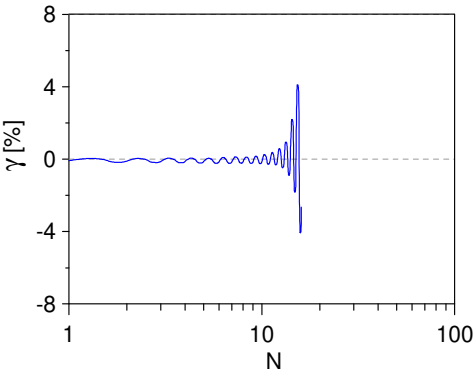

Undrained Cyclic Simple Shear test: *C_SS_TS10_S50_A0_2*
Ticino sand + 10% f_c (Reconstitution method: Moist Tamping)
e_0= 0.68 - D_R= 38% - σ'_{v0}= 50 kPa - α= 0 - *CSR* = 0.15

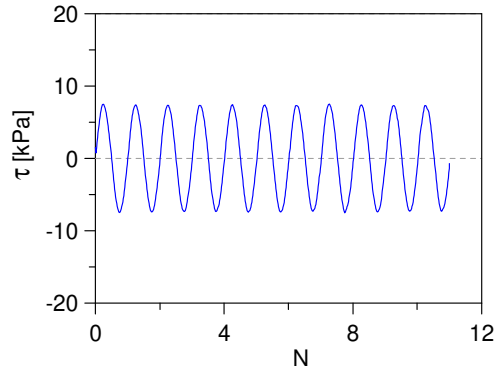

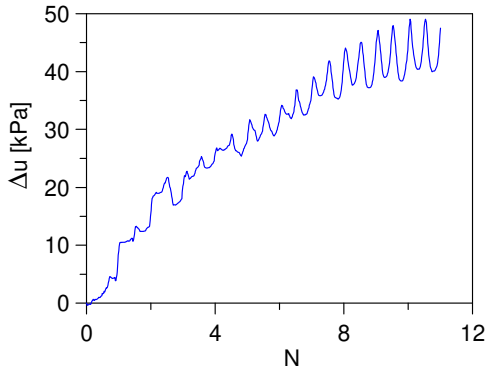

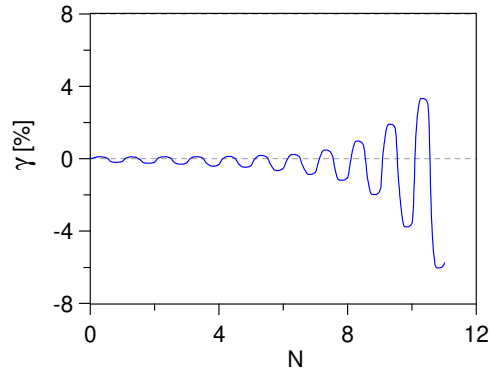

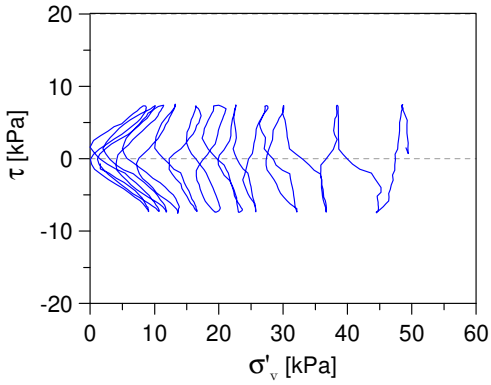

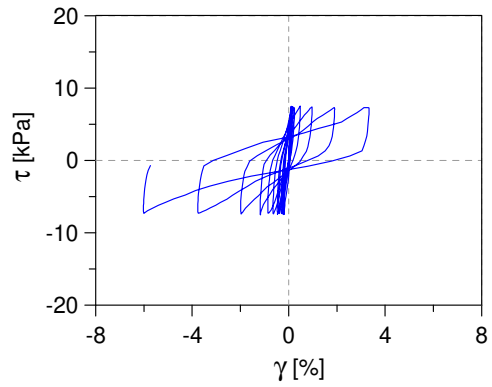

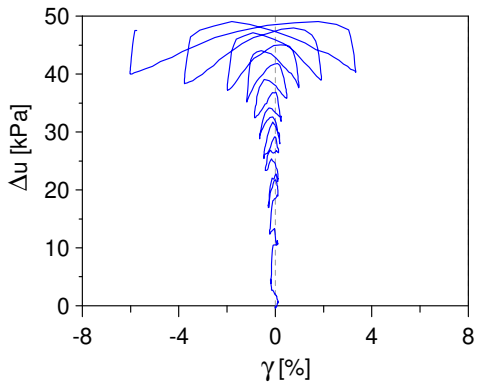

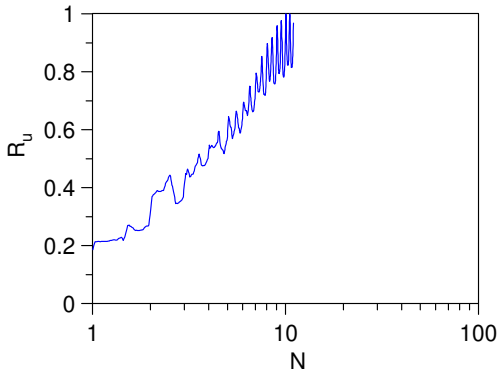

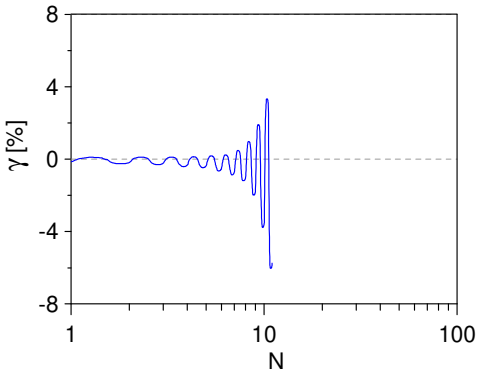

Undrained Cyclic Simple Shear test: *C_SS_TS10_S50_A0_3*
Ticino sand + 10% f_c (Reconstitution method: Moist Tamping)
e_0= 0.68 - D_R= 38% - σ'_{v0}= 50 kPa - α= 0 - *CSR* = 0.18

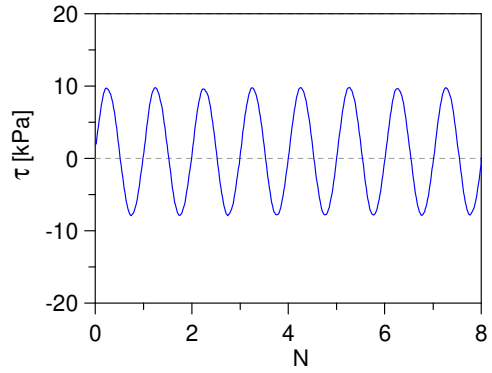

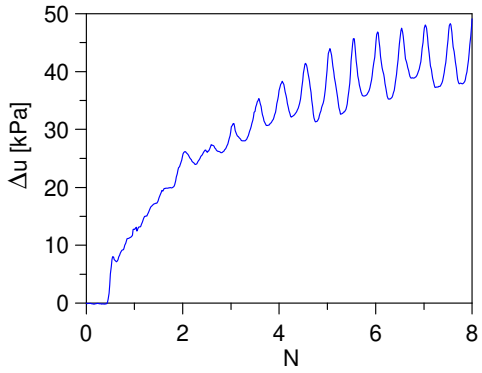

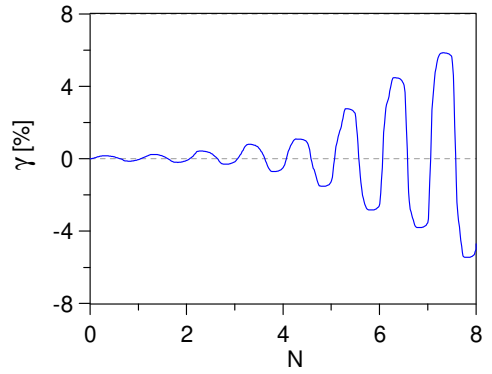

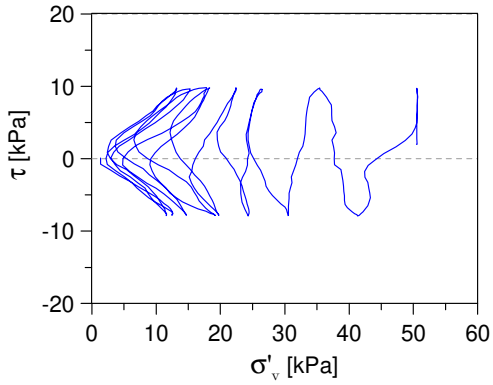

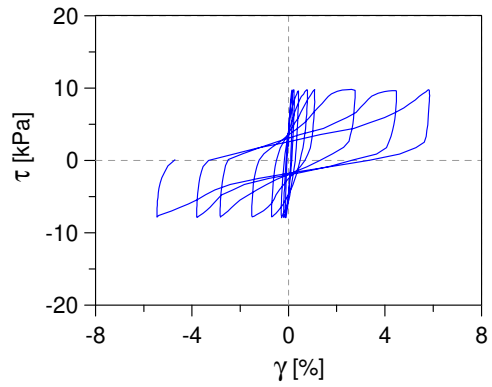

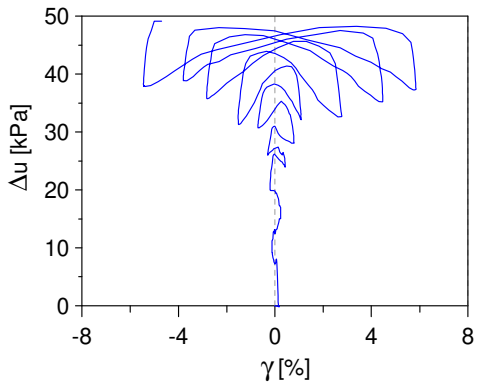

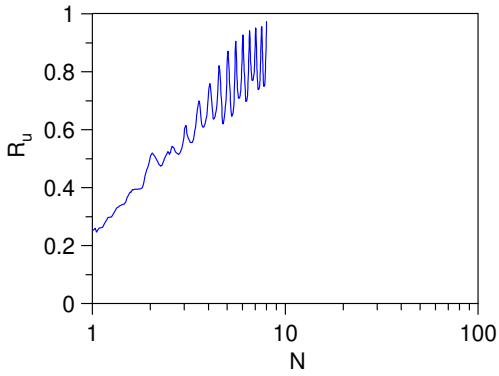

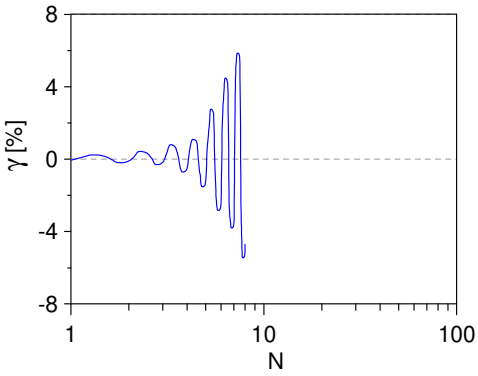

Undrained Cyclic Simple Shear test: *C_SS_TS10_S50_A0_4*
Ticino sand + 10 % f_c (Reconstitution method: Moist Tamping)
e_0= 0.60 - D_R= 62% - σ'_{v0}= 50 kPa - α= 0 - *CSR* = 0.16

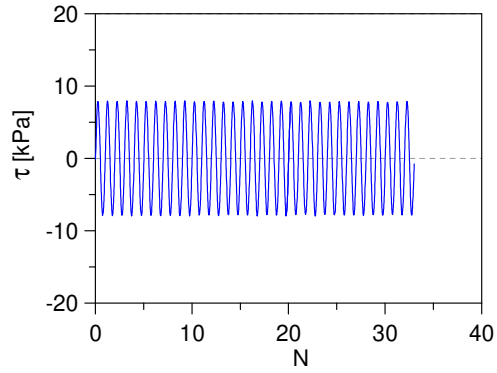

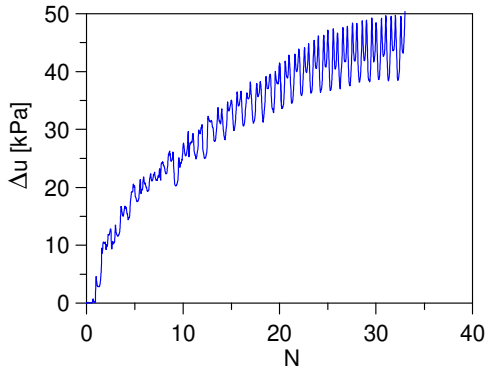

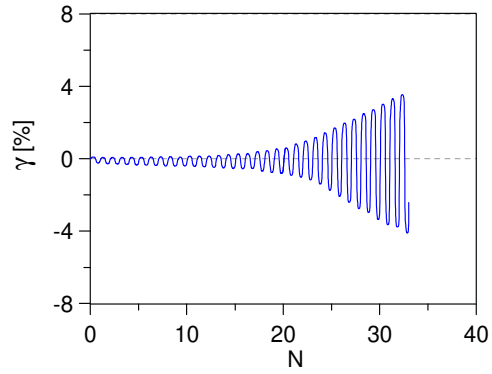

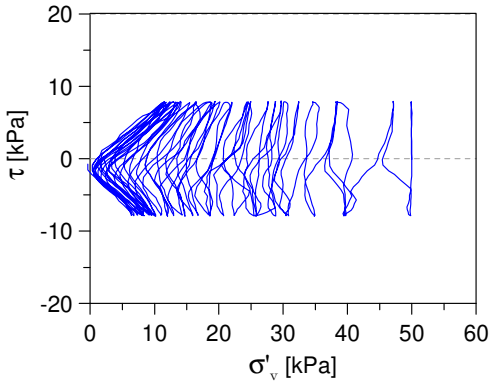

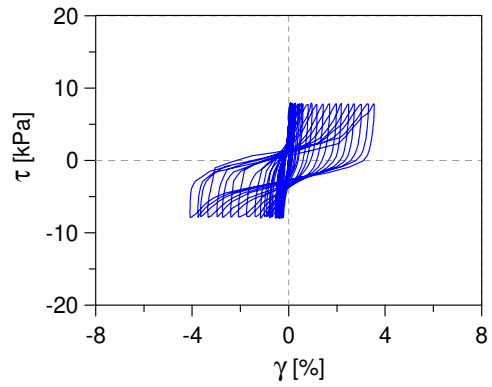

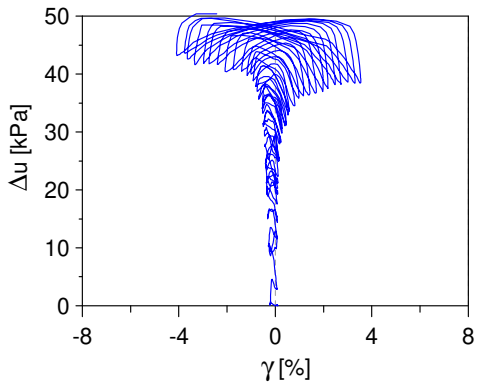

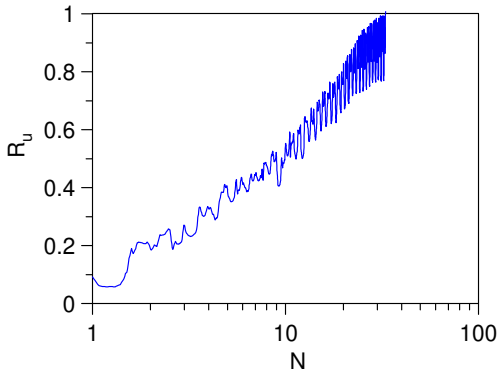

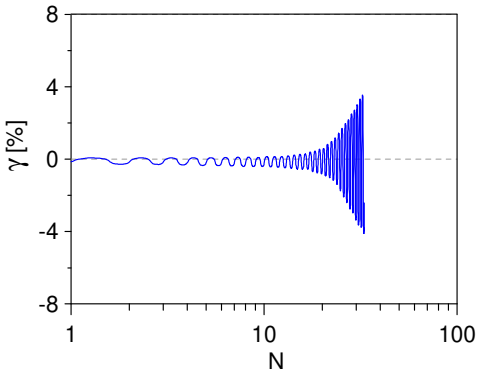

Undrained Cyclic Simple Shear test: *C_SS_TS10_S50_A0_5*
Ticino sand + 10% f_c (Reconstitution method: Moist Tamping)
e_0= 0.60 - D_R= 62% - σ'_{v0}= 50 kPa - α= 0 - *CSR* = 0.18

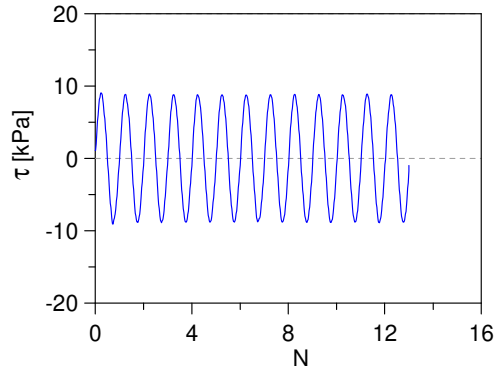

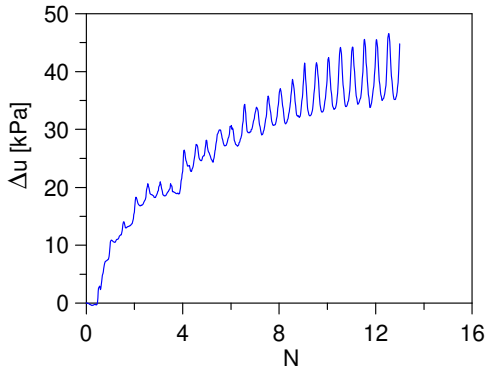

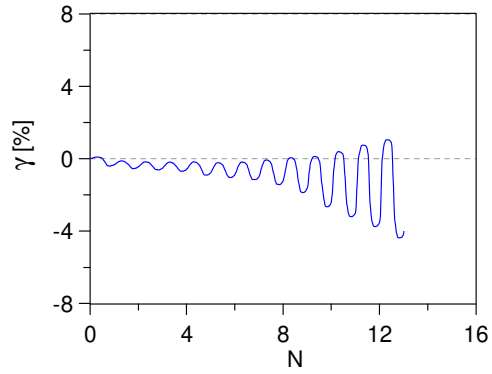

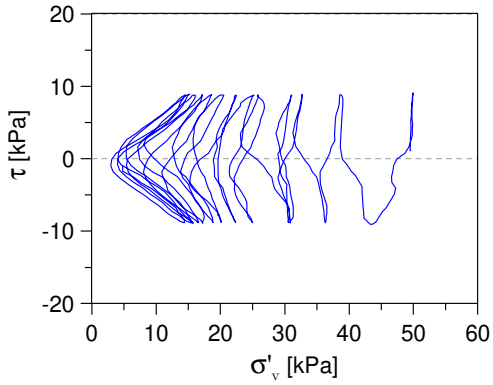

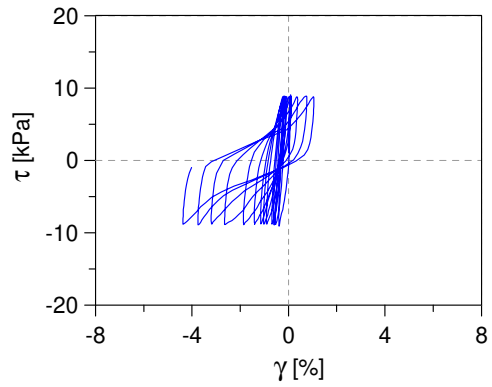

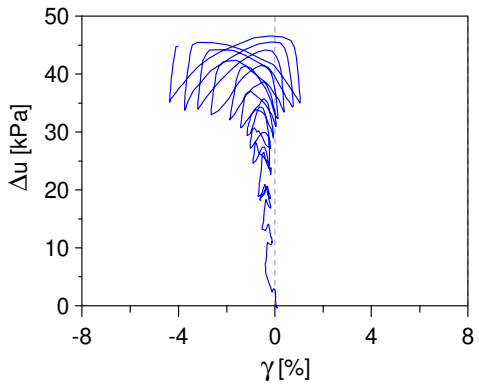

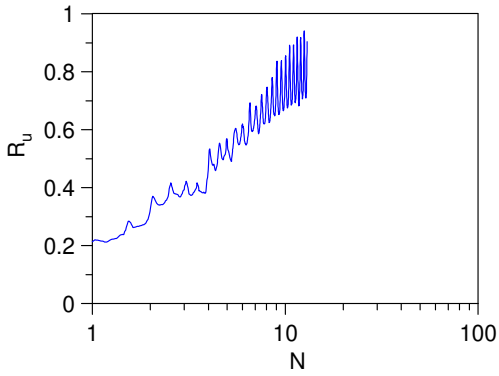

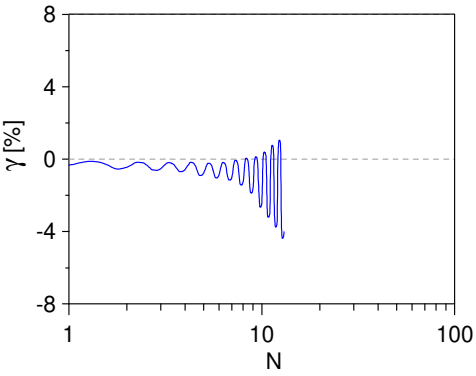

Undrained Cyclic Simple Shear test: *C_SS_TS10_S50_A1_1*
Ticino sand + 10% f_c (Reconstitution method: Moist Tamping)
e_0= 0.68 - D_R= 38% - σ'_{v0}= 50 kPa - α= 0.1 - *CSR* = 0.10

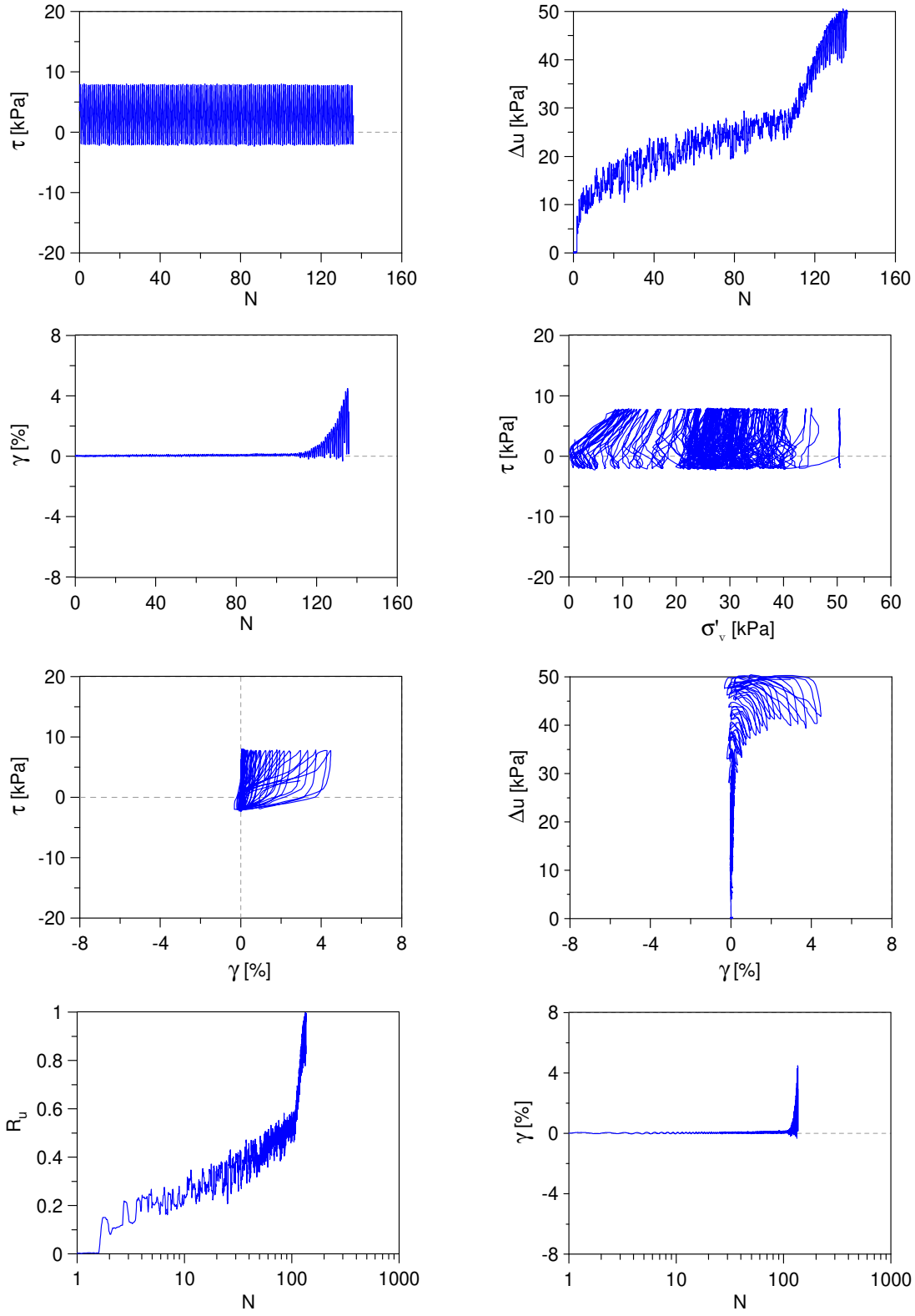

Undrained Cyclic Simple Shear test: *C_SS_TS10_S50_A1_2*
Ticino sand + 10% f_c (Reconstitution method: Moist Tamping)
e_0= 0.68 - D_R= 38% - σ'_{v0}= 50 kPa - α= 0.1 - *CSR* = 0.14

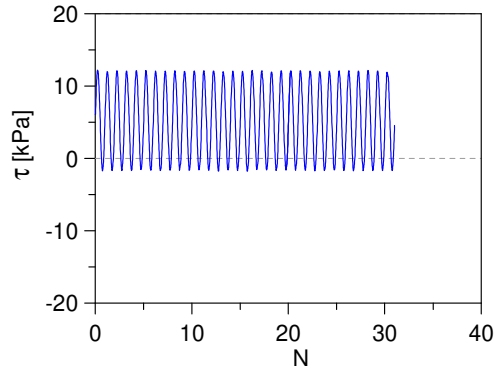

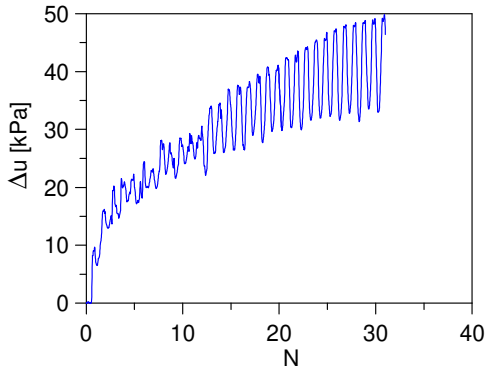

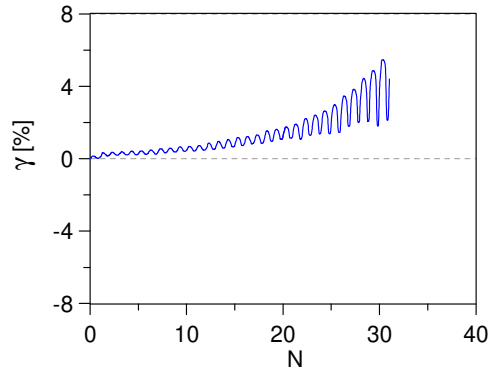

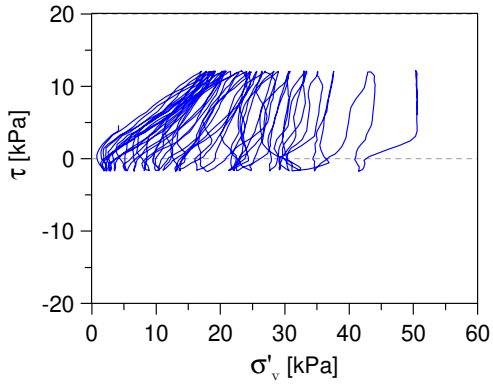

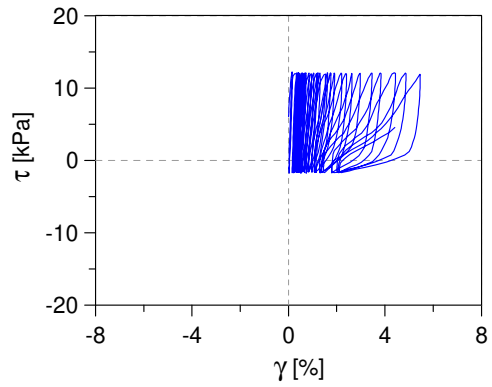

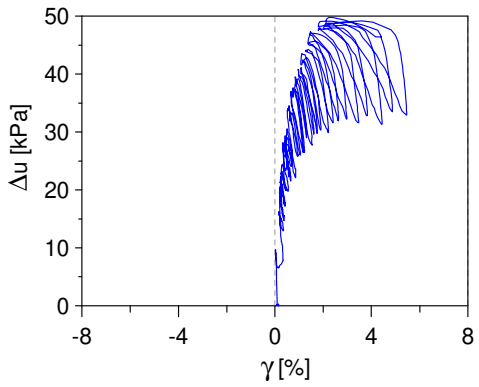

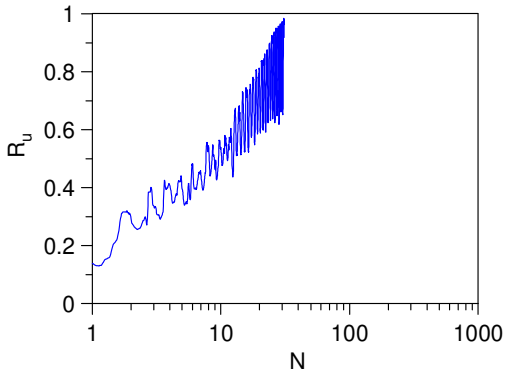

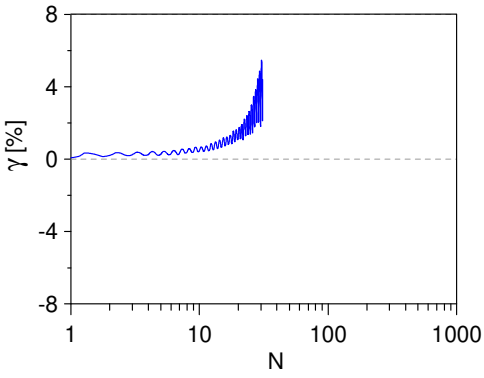

Undrained Cyclic Simple Shear test: *C_SS_TS10_S50_A01_3*
Ticino sand + 10% f_c (Reconstitution method: Moist Tamping)
e_0= 0.68 - D_R= 38% - σ'_{v0}= 50 kPa - α= 0.1 - *CSR* = 0.18

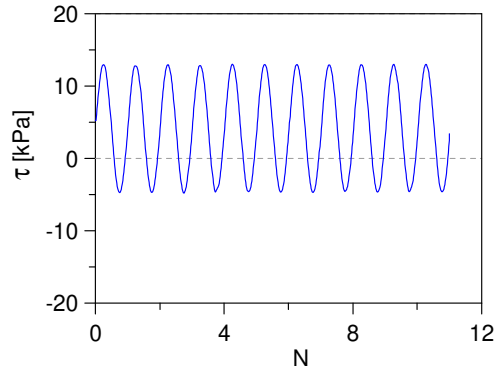

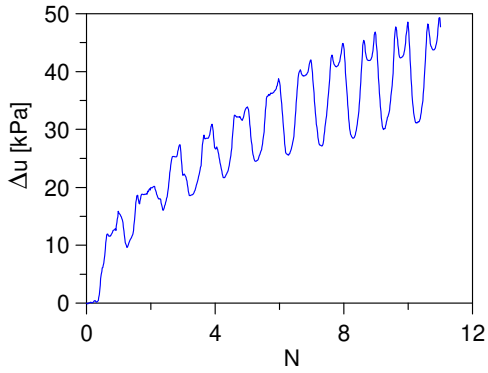

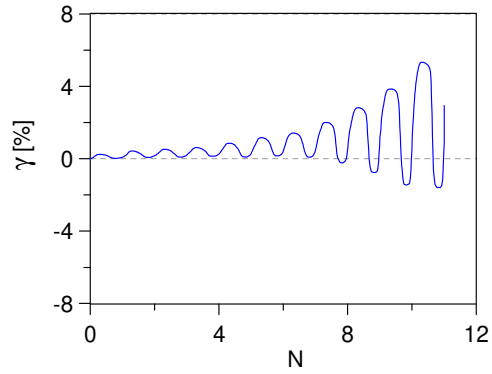

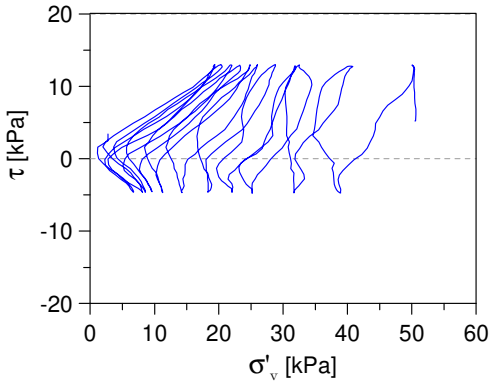

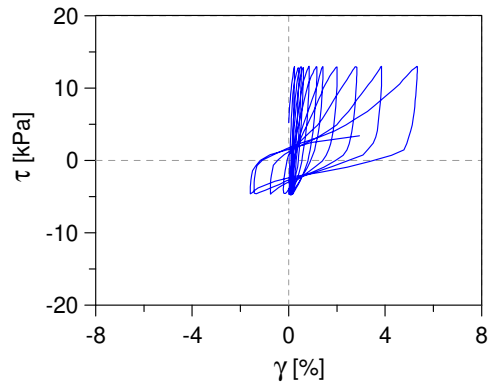

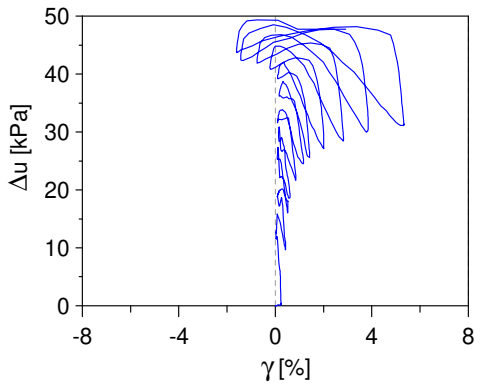

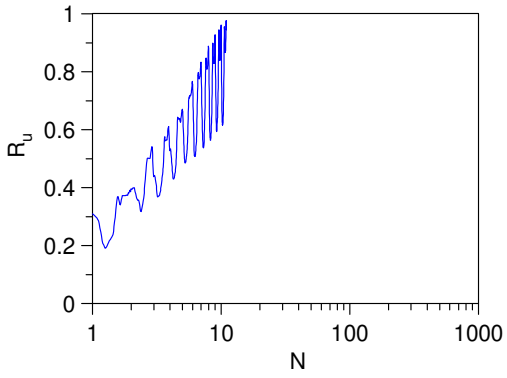

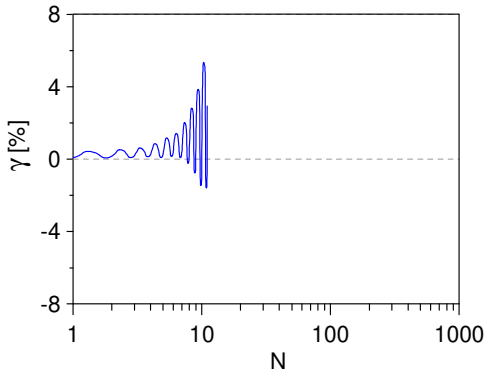

Undrained Cyclic Simple Shear test: *C_SS_TS10_S50_A2_1*
Ticino sand + 10% f_c (Reconstitution method: Moist Tamping)
e_0= 0.68 - D_R= 38% - σ'_{v0}= 50 kPa - α= 0.2 - *CSR* = 0.14

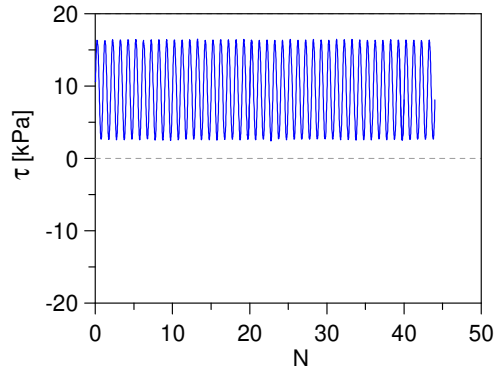

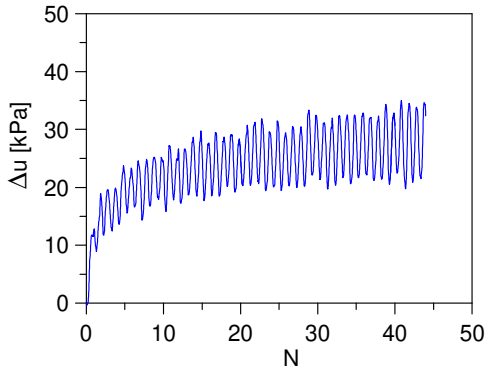

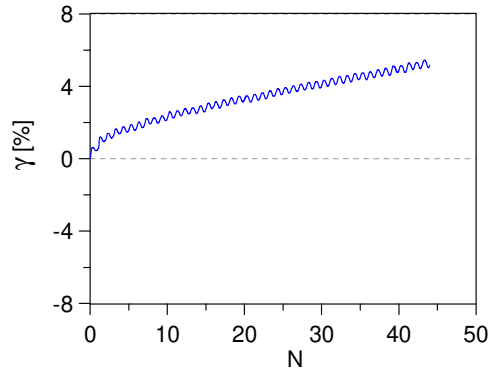

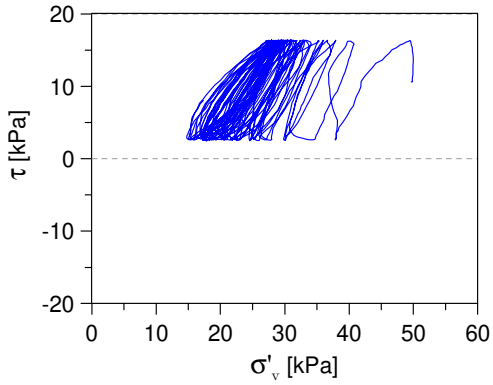

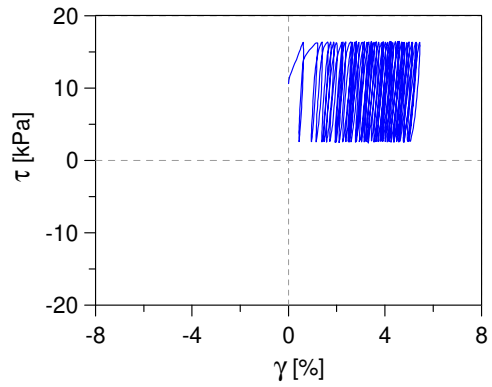

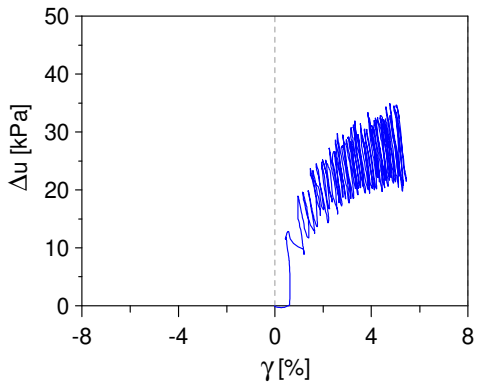

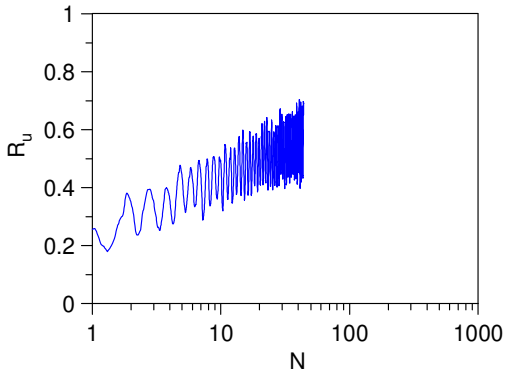

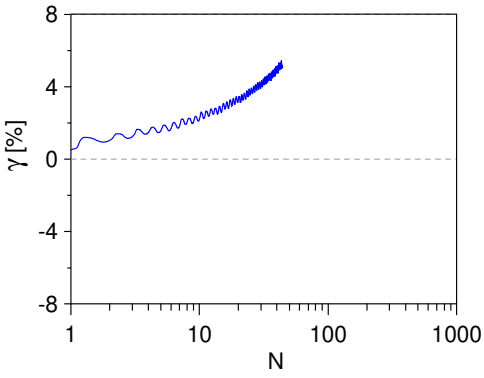

Undrained Cyclic Simple Shear test: *C_SS_TS10_S50_A2_2*
Ticino sand + 10% f_c (Reconstitution method: Moist Tamping)
e_0= 0.68 - D_R= 38% - σ'_{v0}= 50 kPa - α= 0.2 - *CSR* = 0.16

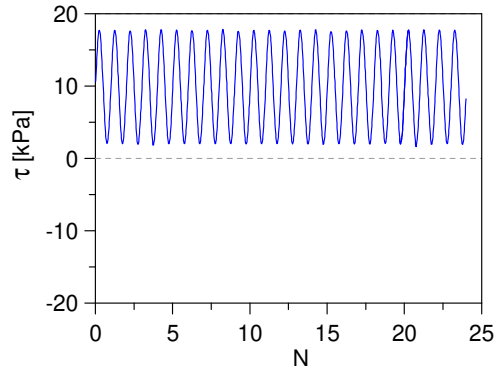

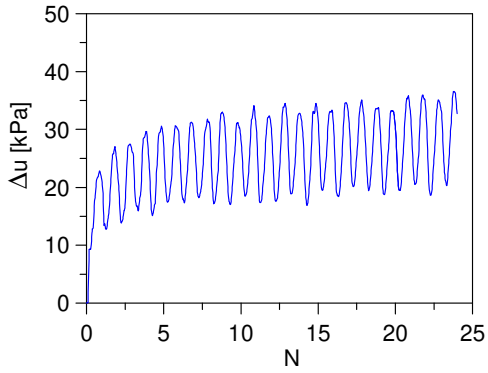

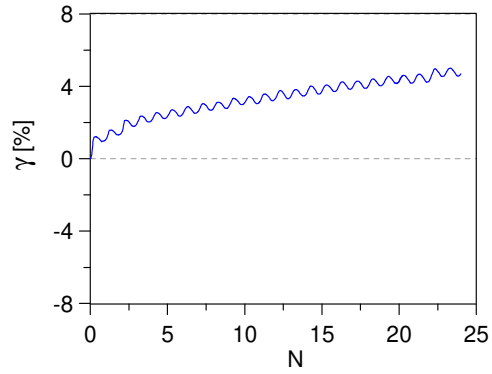

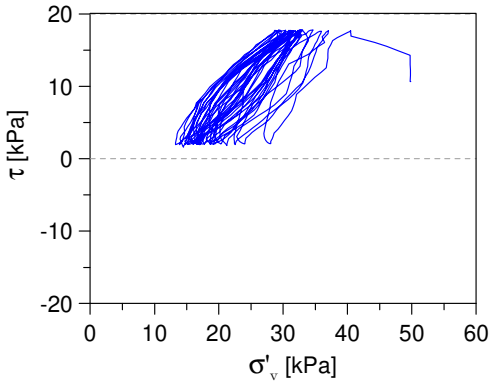

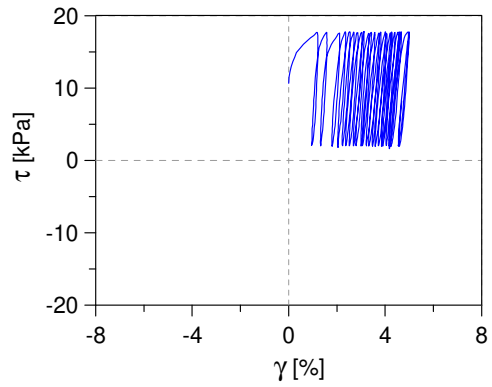

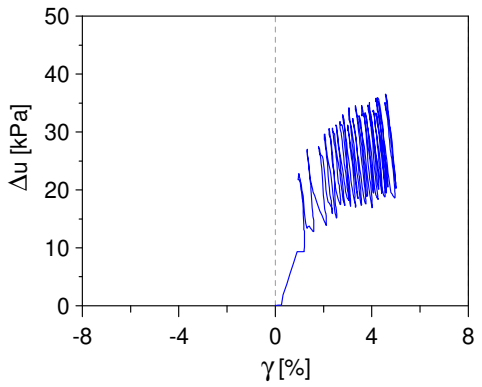

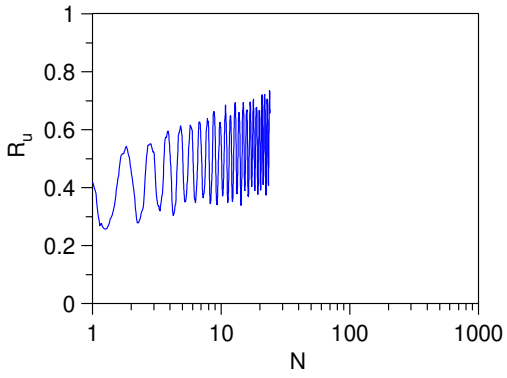

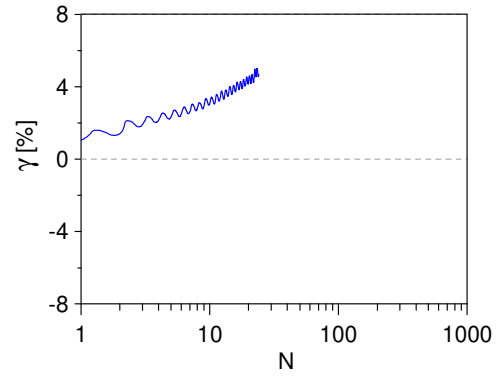

Undrained Cyclic Simple Shear test: *C_SS_TS10_S50_A3_1*
Ticino sand + 10% f_c (Reconstitution method: Moist Tamping)
e_0= 0.68 - D_R= 38% - σ'_{v0}= 50 kPa - α= 0.3 - *CSR* = 0.10

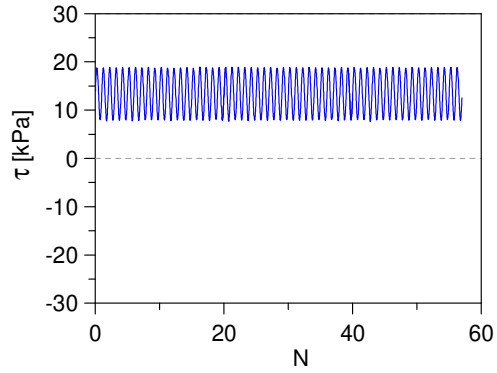

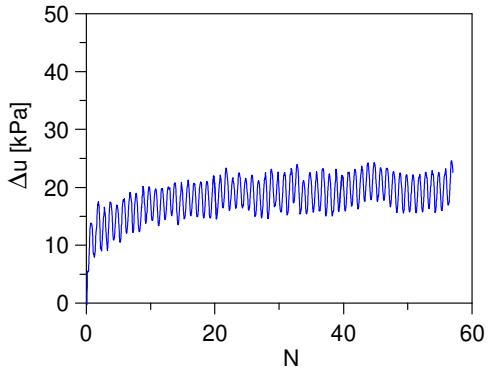

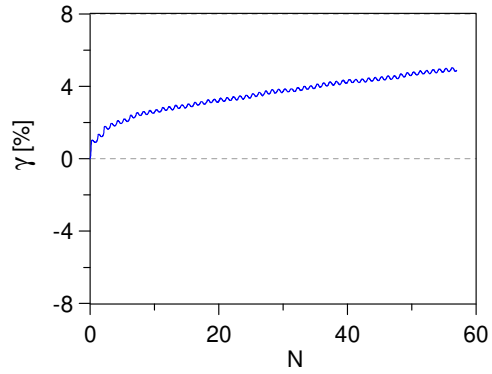

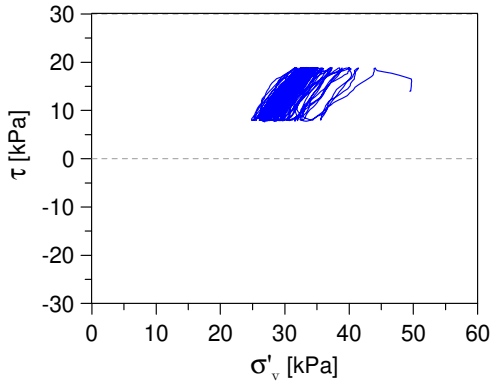

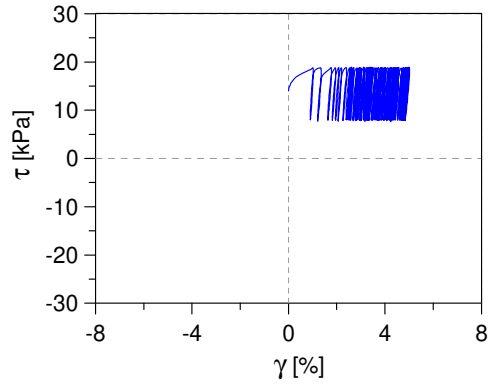

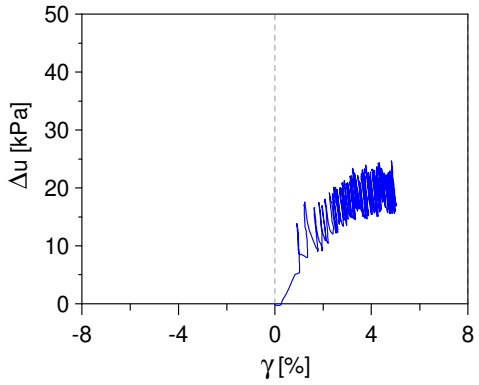

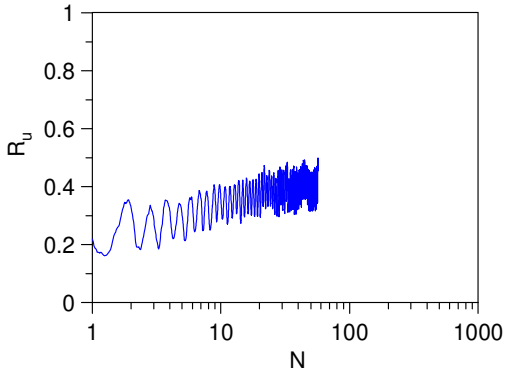

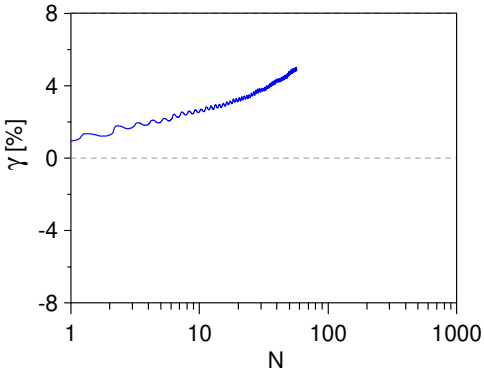

Undrained Cyclic Simple Shear test: *C_SS_TS10_S50_A3_2*
Ticino sand + 10% f_c (Reconstitution method: Moist Tamping)
e_0= 0.68 - D_R= 38% - σ'_{v0}= 50 kPa - α= 0.3 - *CSR* = 0.14

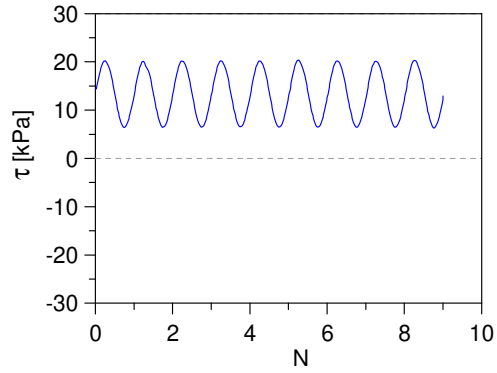

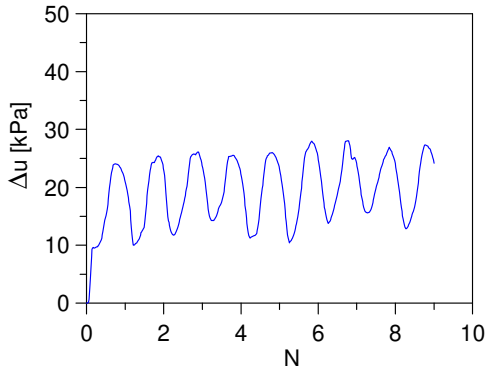

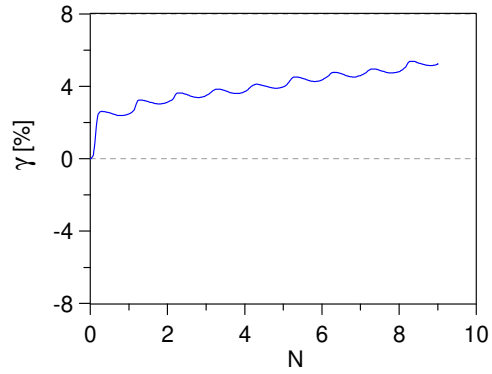

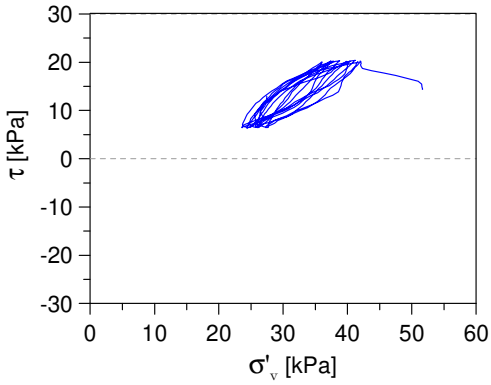

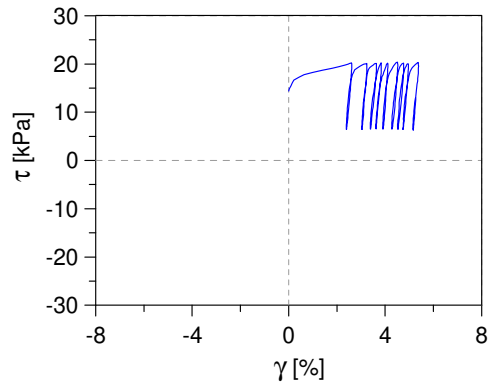

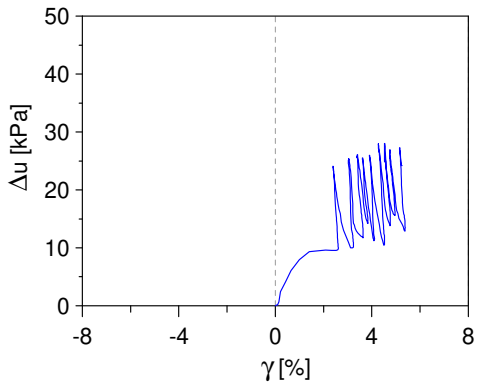

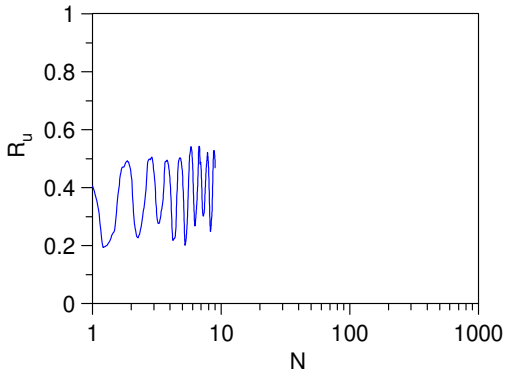

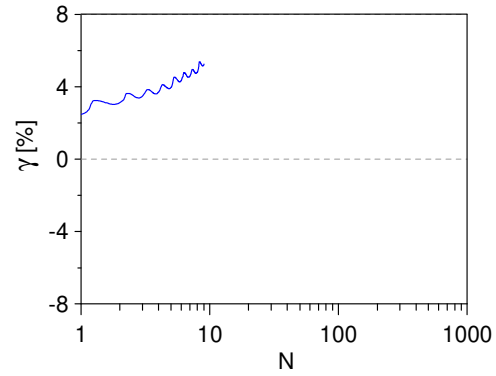

Undrained Cyclic Simple Shear test: *C_SS_TS010_S100_A0_1*
Ticino sand + 10% f_c (Reconstitution method: Moist Tamping)
e_0= 0.68 - D_R= 38% - σ'_{v0}= 100 kPa - α=0 - *CSR* = 0.10

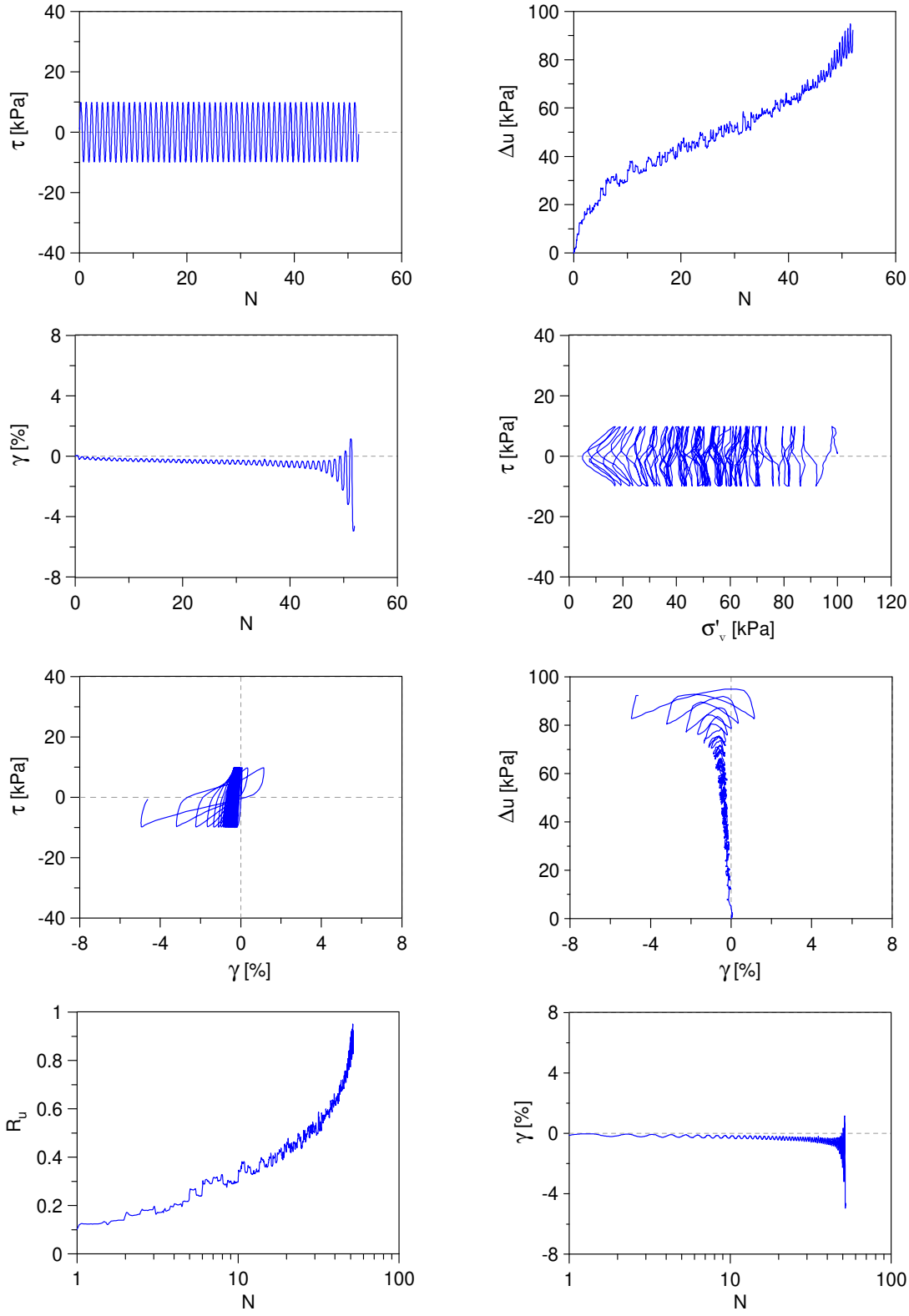

Undrained Cyclic Simple Shear test: *C_SS_TS010_S100_A0_2*
Ticino sand + 10% f_c (Reconstitution method: Moist Tamping)
e_0= 0.68 - D_R= 38% - σ'_{v0}= 100 kPa - α=0 - *CSR* = 0.12

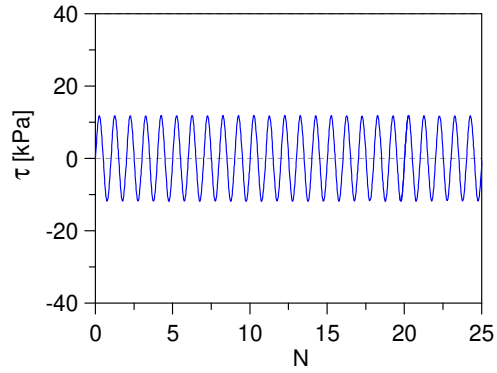

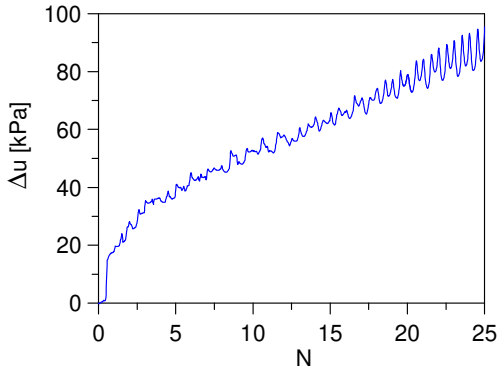

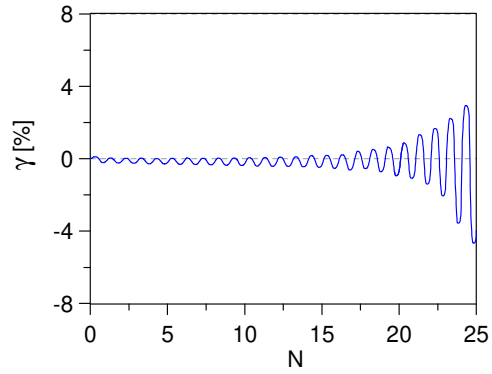

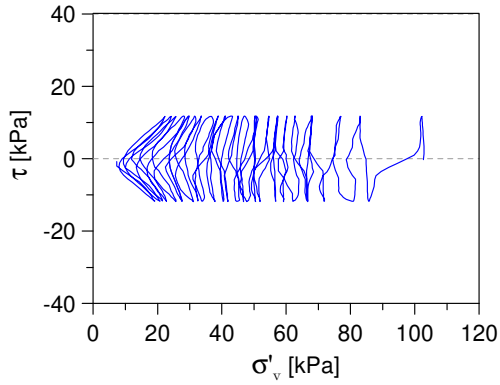

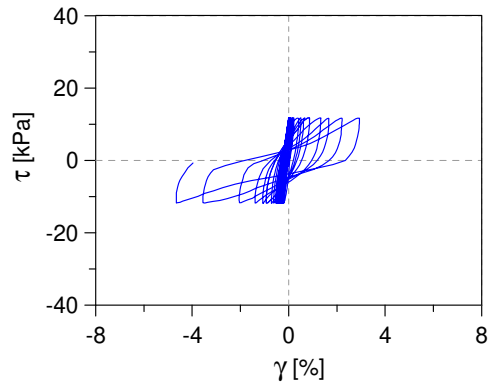

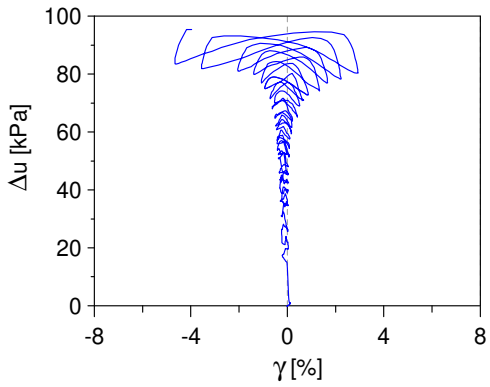

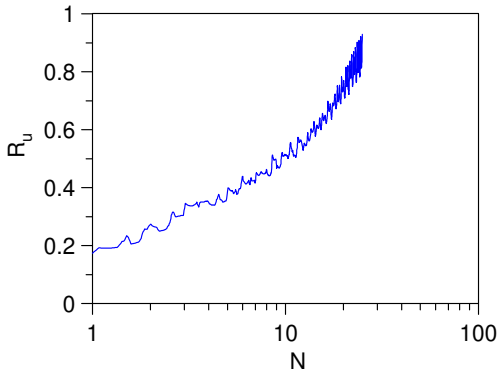

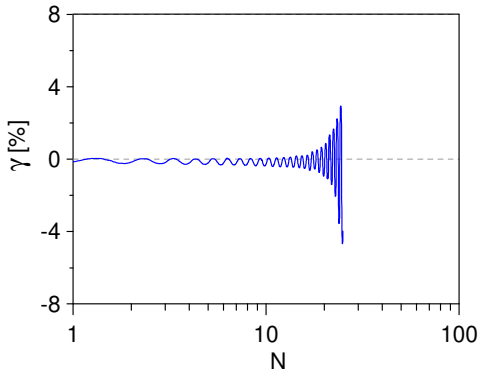

Undrained Cyclic Simple Shear test: *C_SS_TS010_S100_A0_3*
Ticino sand + 10% f_c (Reconstitution method: Moist Tamping)
e_0= 0.68 - D_R= 38% - σ'_{v0}= 100 kPa - α=0 - *CSR* = 0.14

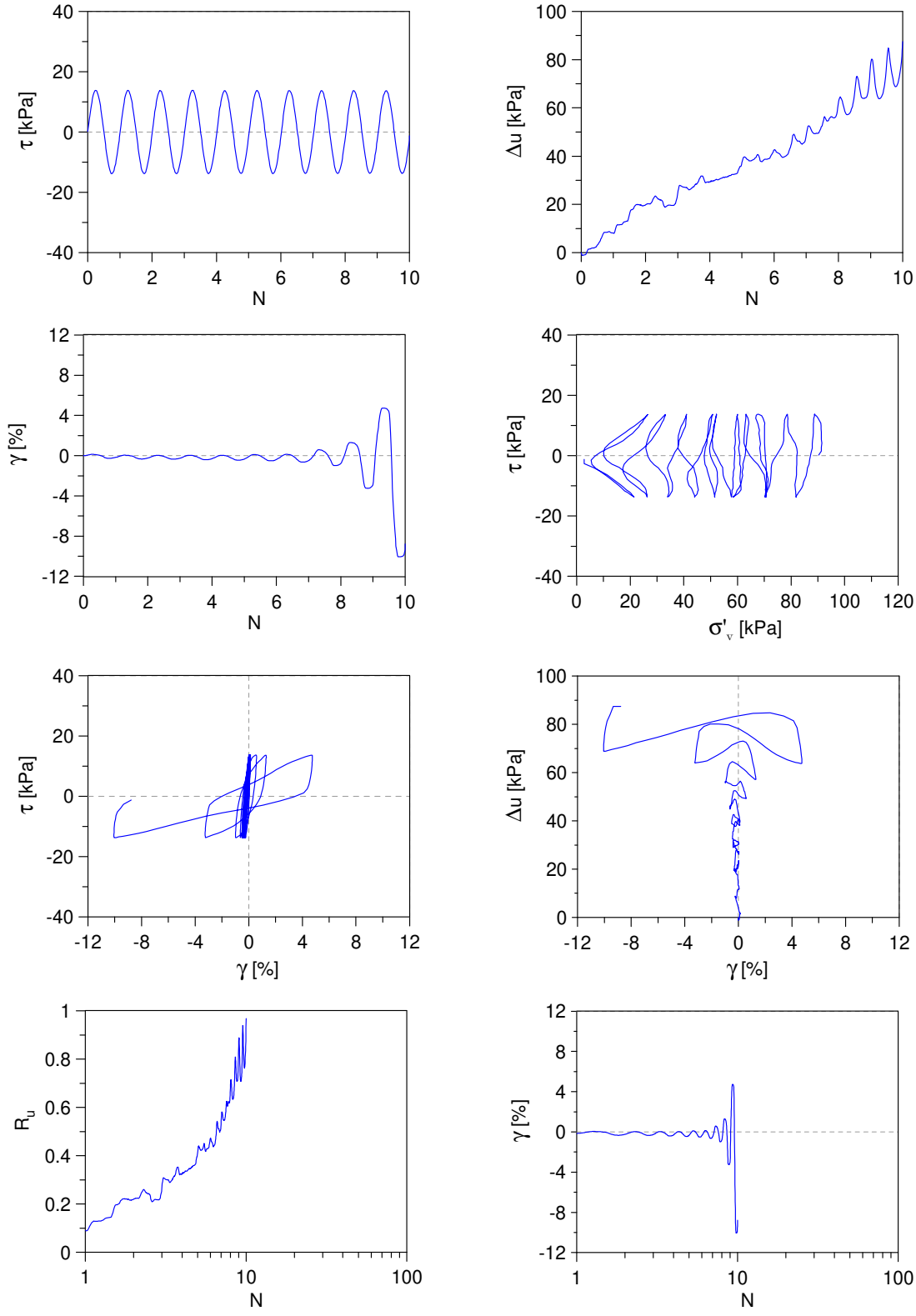

Undrained Cyclic Simple Shear test: *C_SS_TS010_S100_A0_4*
Ticino sand + 10% f_c (Reconstitution method: Moist Tamping)
e_0= 0.68 - D_R= 38% - σ'_{v0}= 100 kPa - α=0 - *CSR* = 0.16

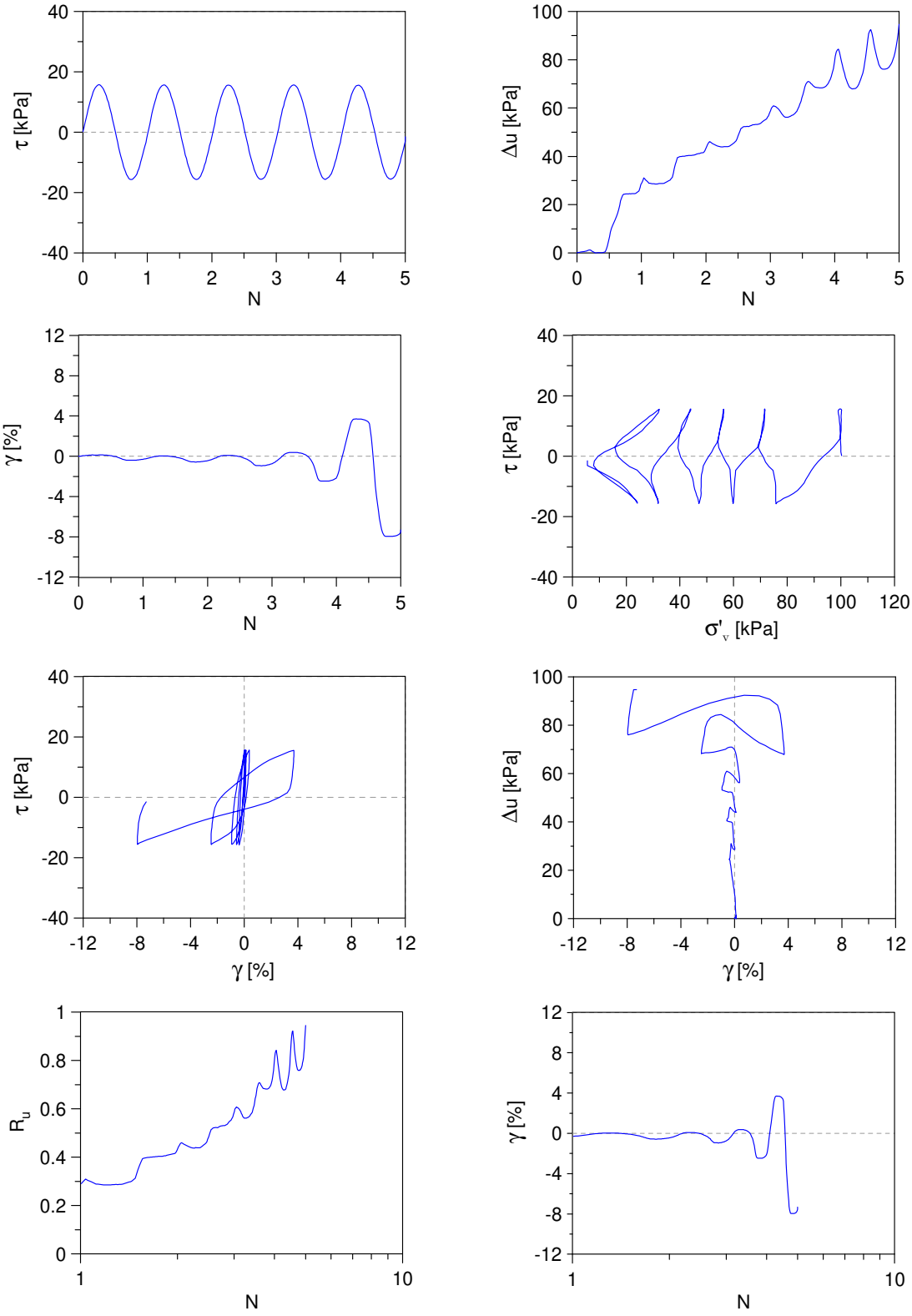

Undrained Cyclic Simple Shear test: *C_SS_TS010_S100_A0_5*
Ticino sand + 10% f_c (Reconstitution method: Moist Tamping)
e_0= 0.60 - D_R= 62% - σ'_{v0}= 100 kPa - α=0 - *CSR* = 0.14

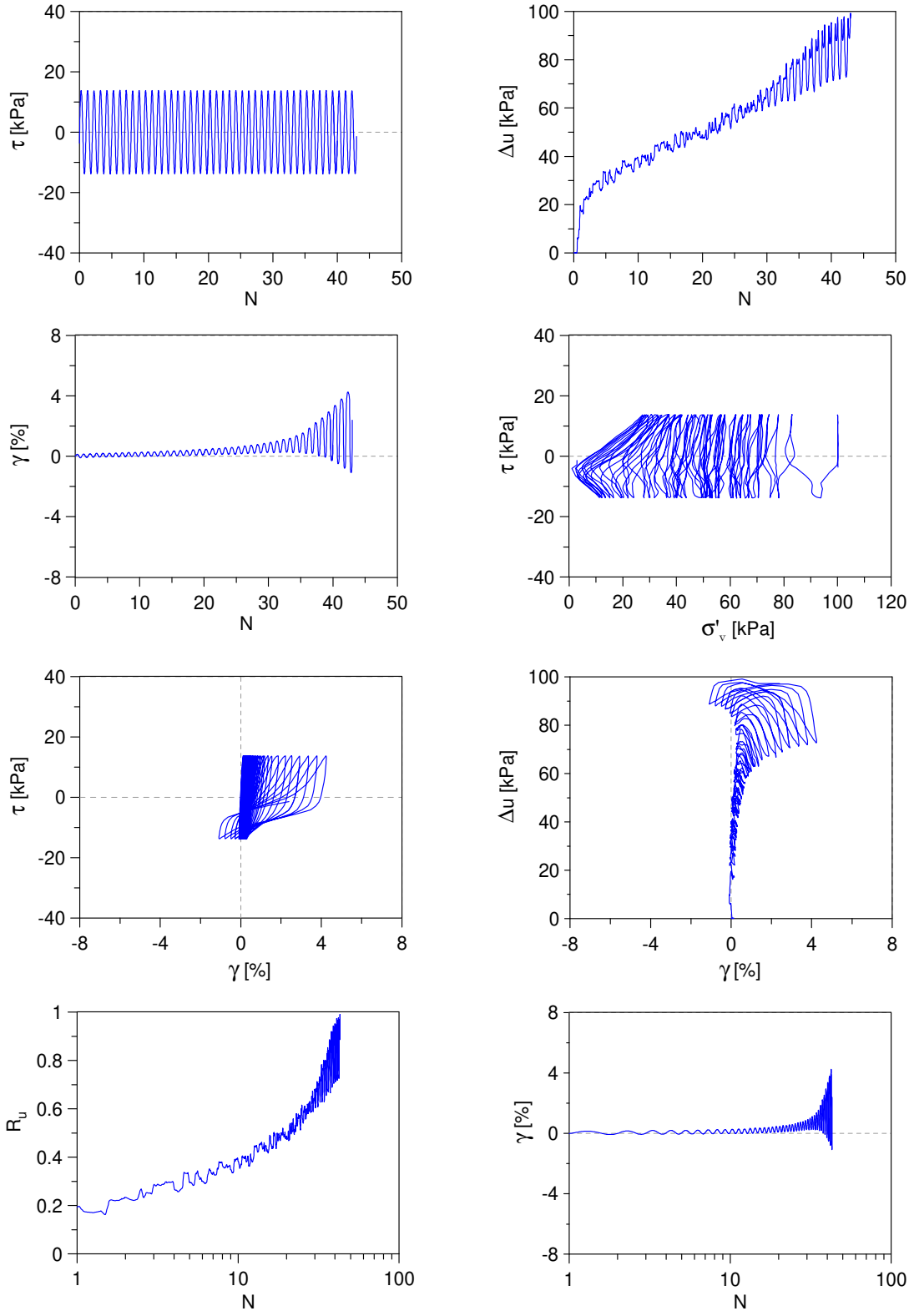

Undrained Cyclic Simple Shear test: *C_SS_TS010_S100_A0_6*
Ticino sand + 10% f_c (Reconstitution method: Moist Tamping)
e_0= 0.60 - D_R= 62% - σ'_{v0}= 100 kPa - α=0 - *CSR* = 0.16

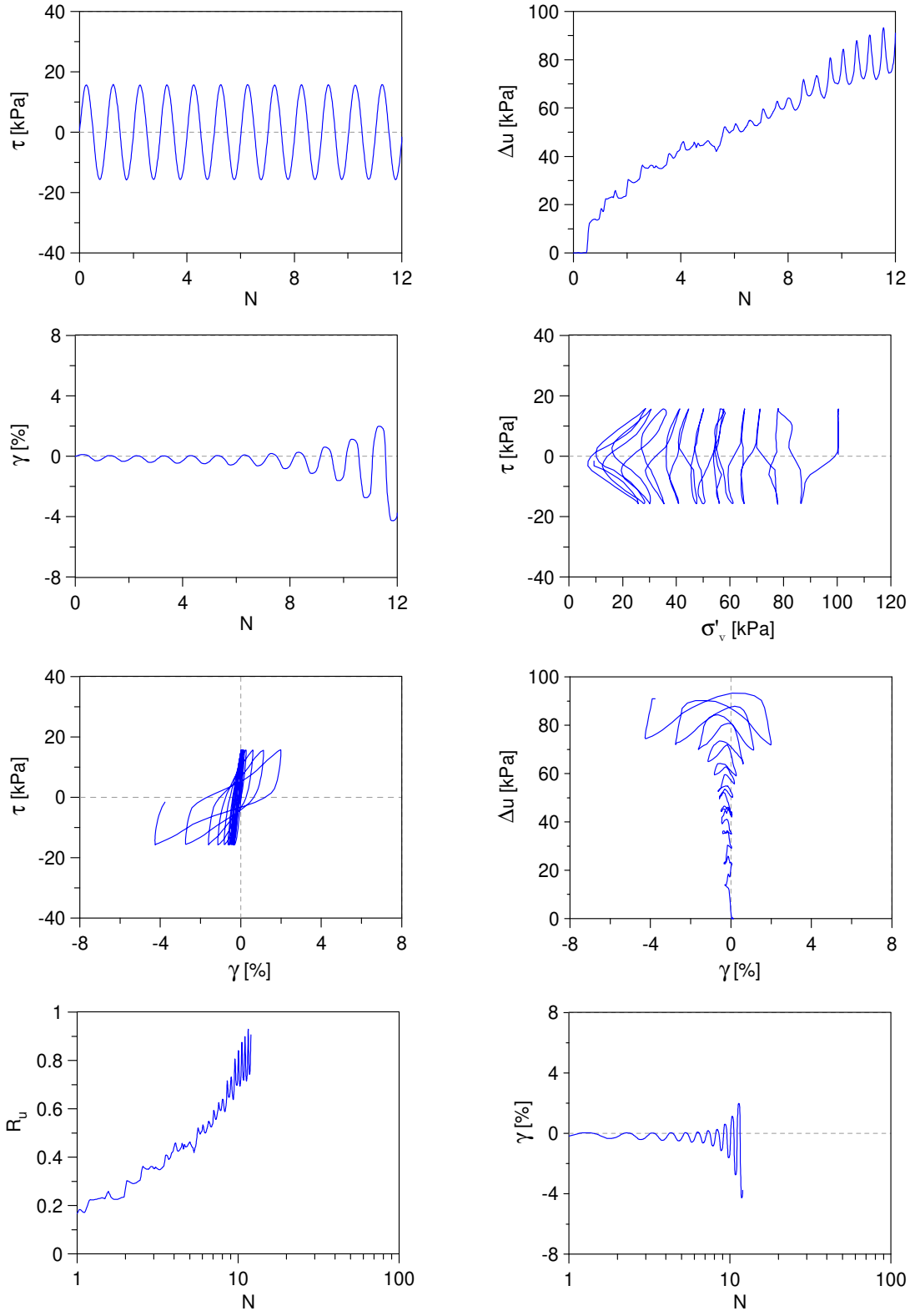

Undrained Cyclic Simple Shear test: *C_SS_TS010_S100_A0_7*
Ticino sand + 10% f_c (Reconstitution method: Moist Tamping)
e_0= 0.60 - D_R= 62% - σ'_{v0}= 100 kPa - α=0 - *CSR* = 0.20

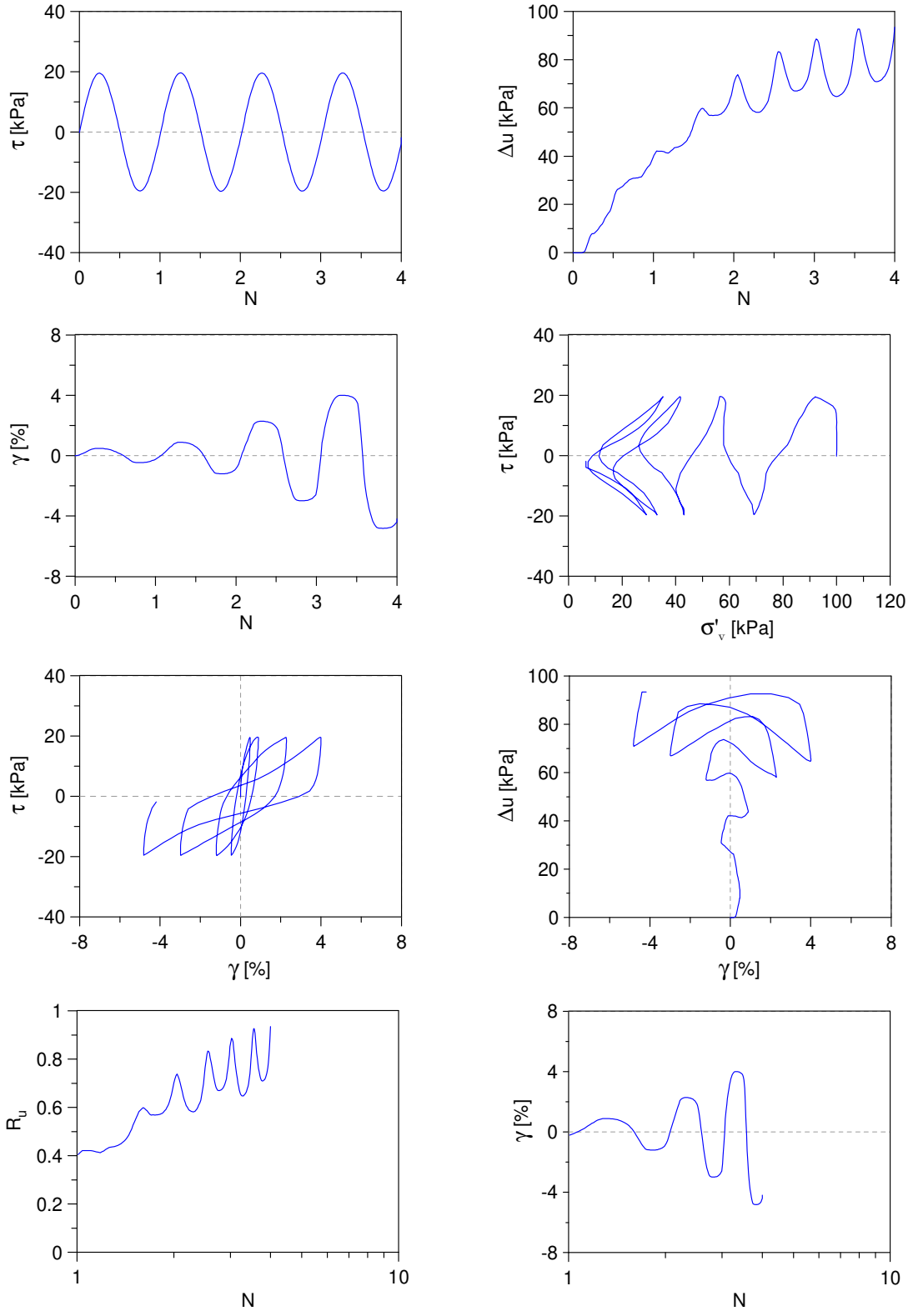

Undrained Cyclic Simple Shear test: *C_SS_TS010_S100_A0_8*
Ticino sand + 10% f_c (Reconstitution method: Moist Tamping)
e_0= 0.55 - D_R= 76% - σ'_{v0}= 100 kPa - α=0 - *CSR* = 0.14

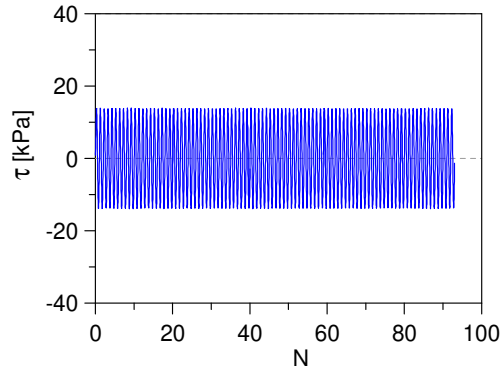

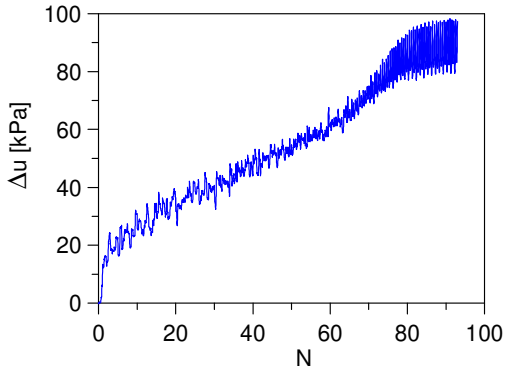

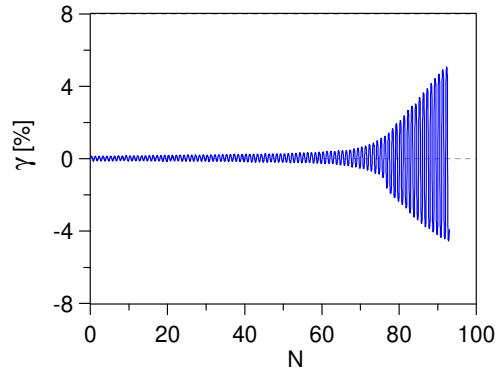

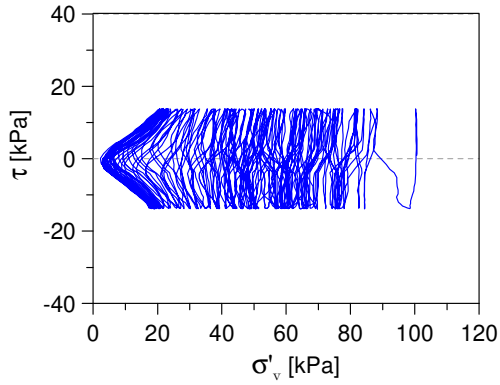

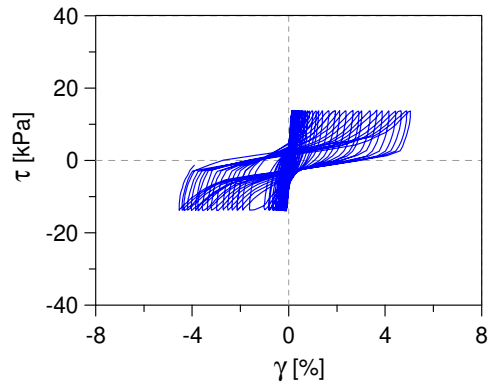

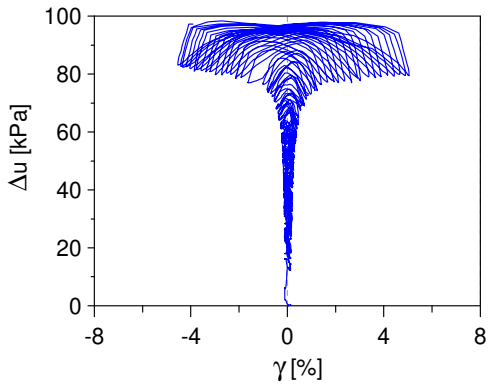

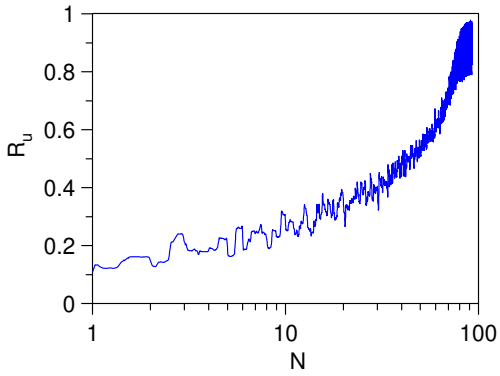

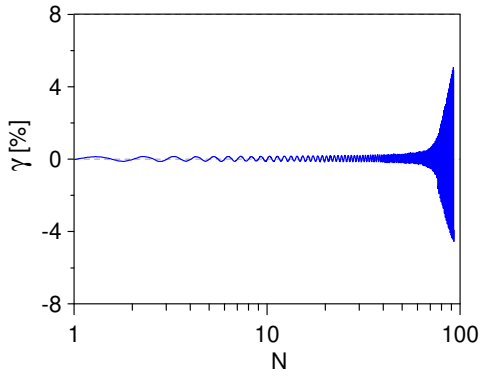

Undrained Cyclic Simple Shear test: *C_SS_TS010_S100_A0_9*
Ticino sand + 10% f_c (Reconstitution method: Moist Tamping)
e_0= 0.55 - D_R= 76% - σ'_{v0}= 100 kPa - α=0 - *CSR* = 0.18

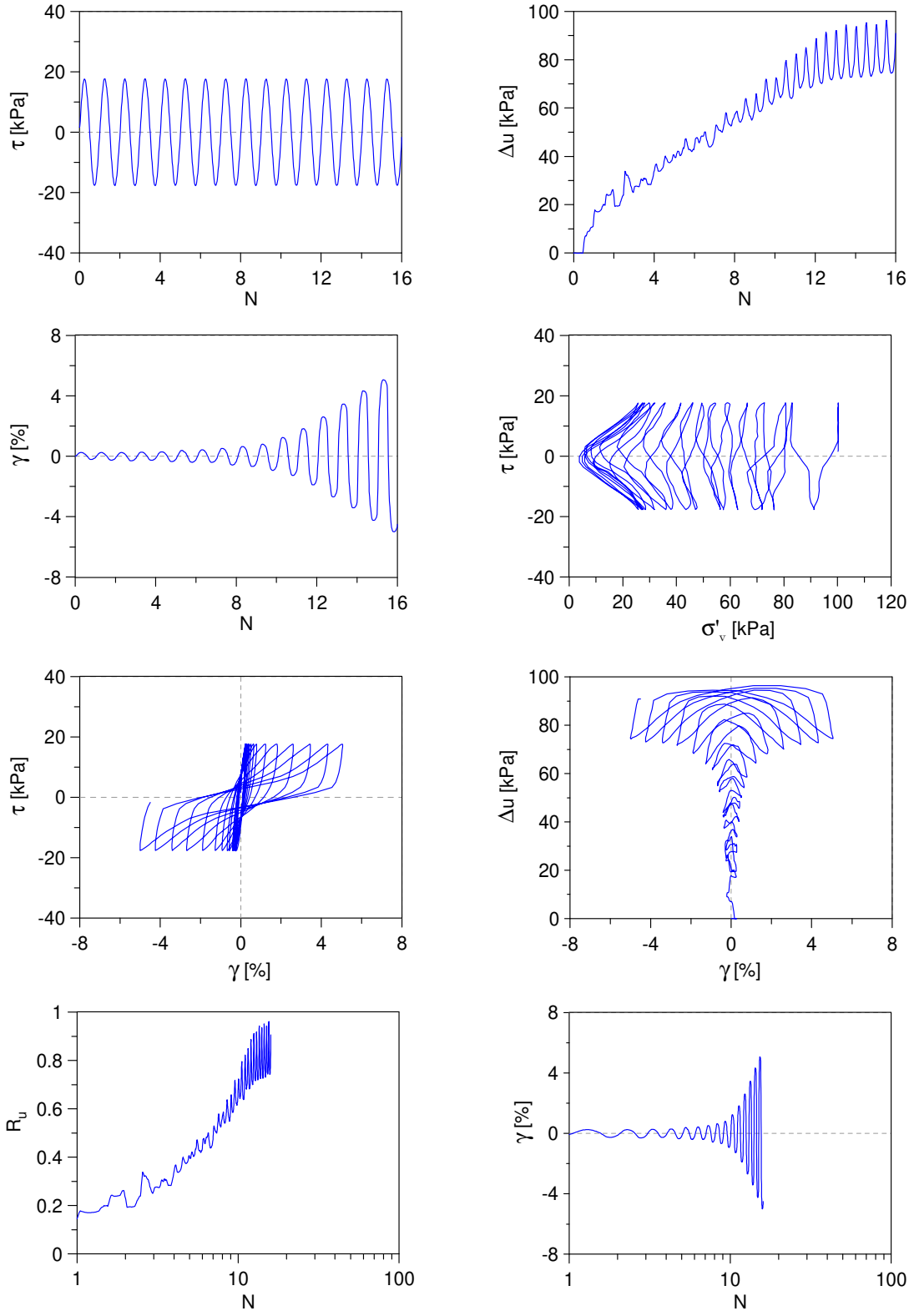

Undrained Cyclic Simple Shear test: *C_SS_TS010_S100_A0_10*
Ticino sand + 10% f_c (Reconstitution method: Moist Tamping)
e_0= 0.55 - D_R= 76% - σ'_{v0}= 100 kPa - α=0 - *CSR* = 0.20

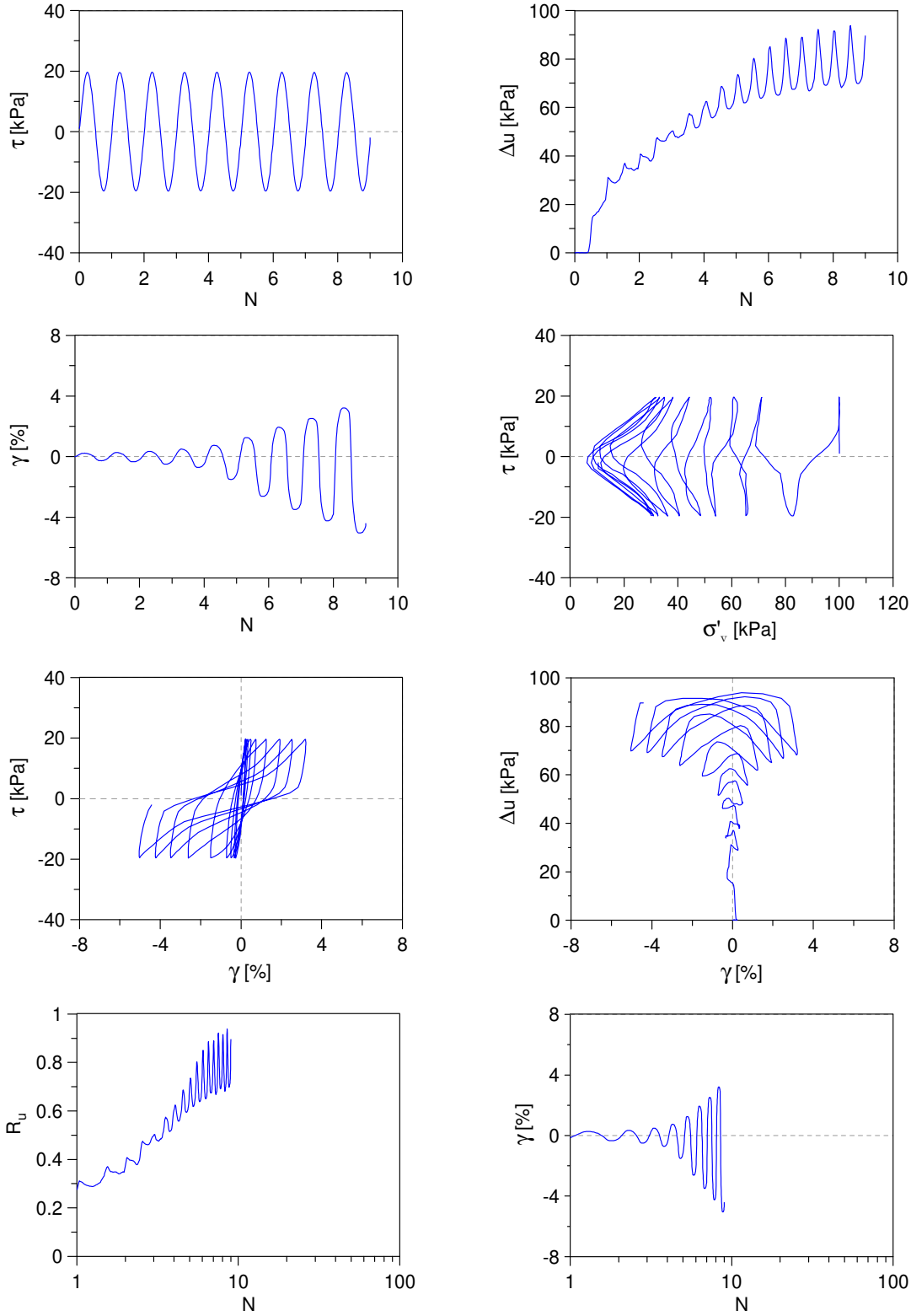

Undrained Cyclic Simple Shear test: *C_SS_TS010_S100_A0_11*
Ticino sand + 10% f_c (Reconstitution method: Moist Tamping)
e_0= 0.53 - D_R= 82% - σ'_{v0}= 100 kPa - α=0 - *CSR* = 0.16

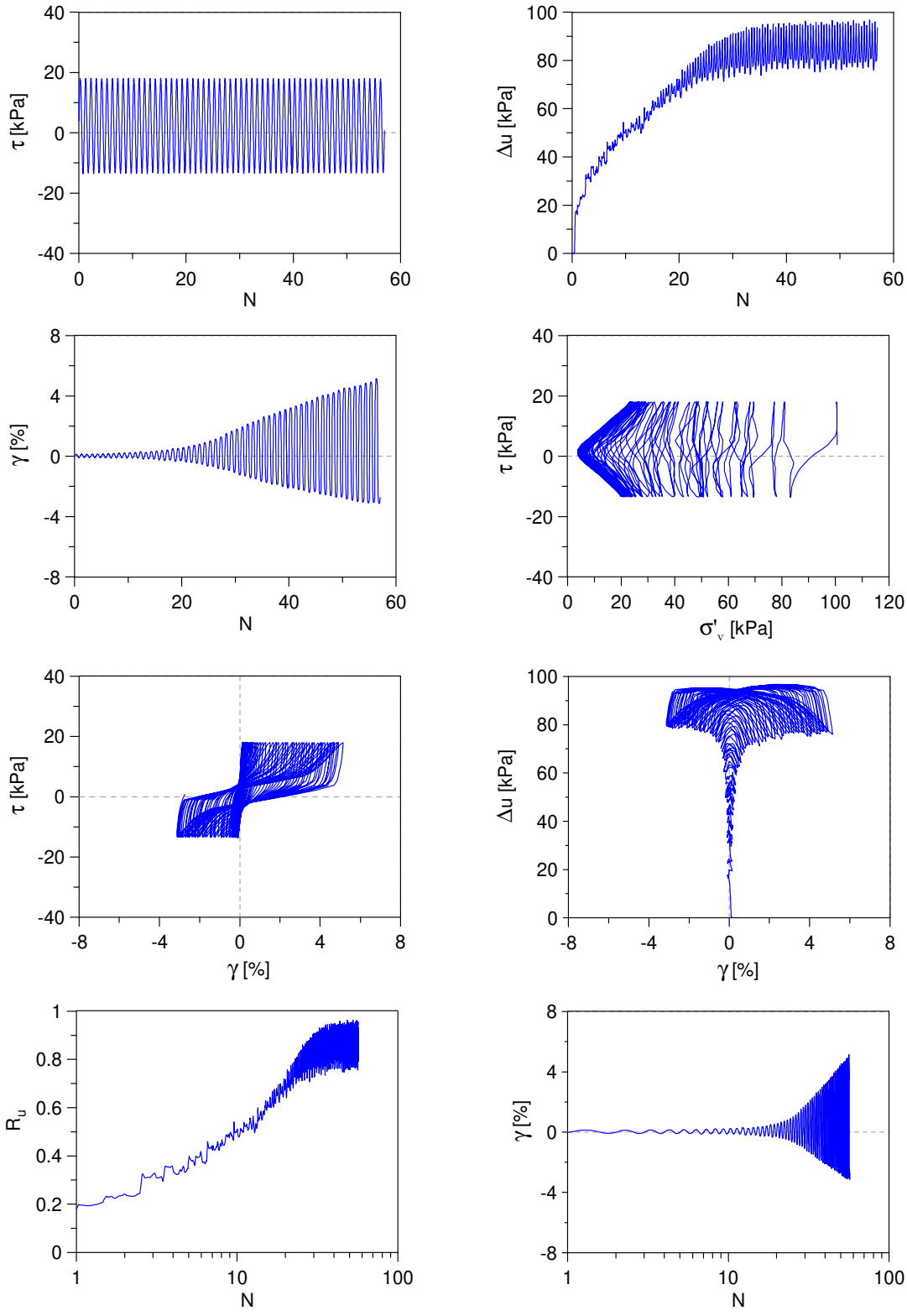

Undrained Cyclic Simple Shear test: *C_SS_TS010_S100_A0_12*
Ticino sand + 10% f_c (Reconstitution method: Moist Tamping)
e_0= 0.53 - D_R= 82% - σ'_{v0}= 100 kPa - α=0 - *CSR* = 0.19

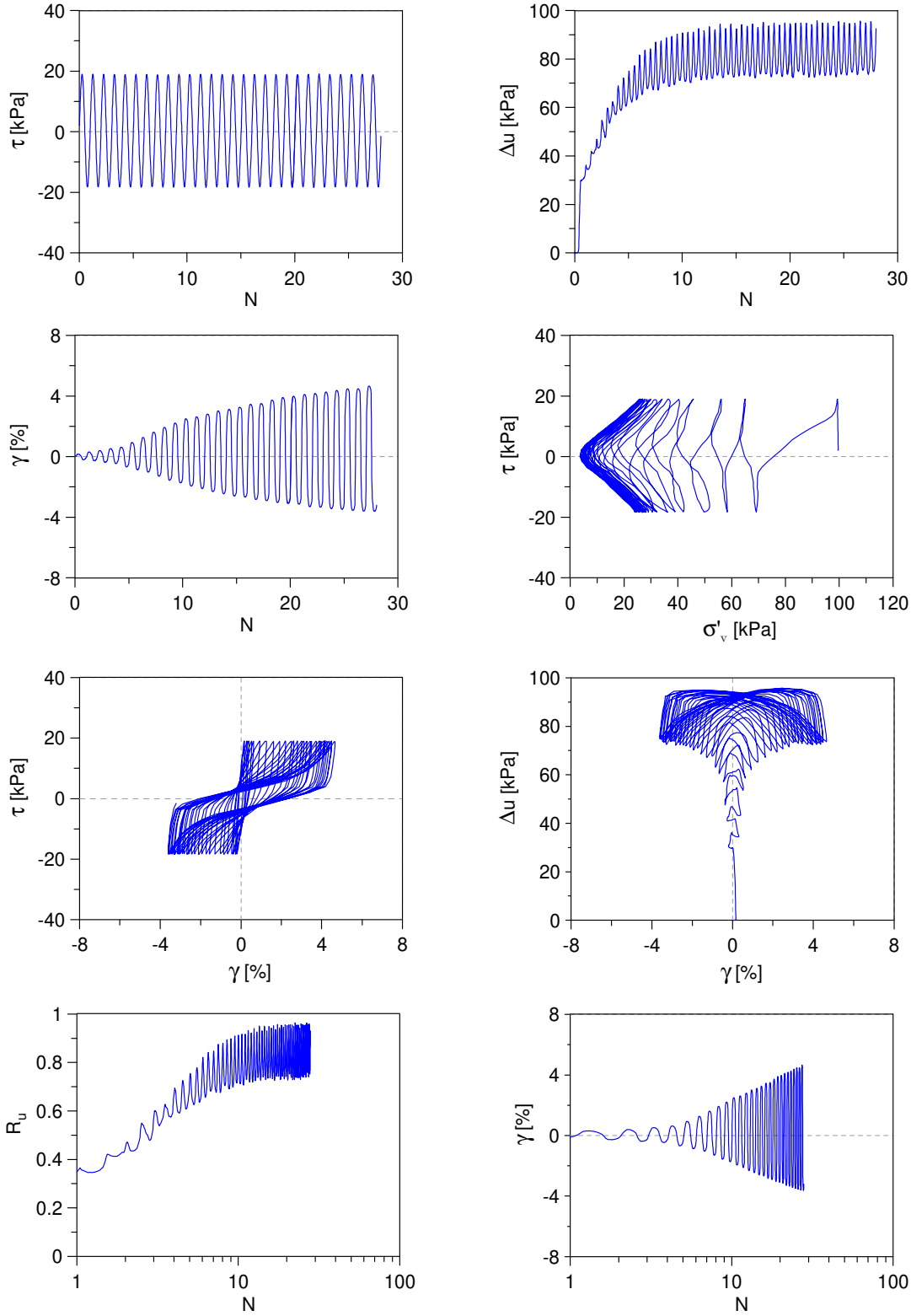

Undrained Cyclic Simple Shear test: *C_SS_TS10_S100_A05_1*
Ticino sand + 10% f_c (Reconstitution method: Moist Tamping)
e_0= 0.68 - D_R= 38% - σ'_{v0}= 100 kPa - α= 0.05 - *CSR* = 0.14

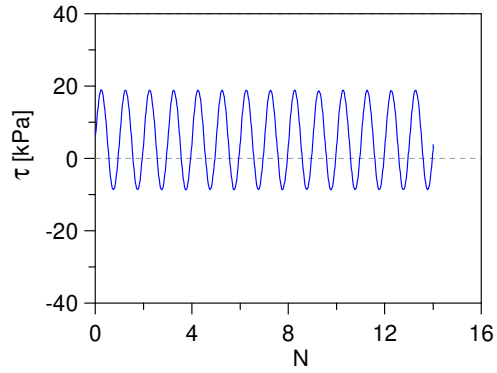

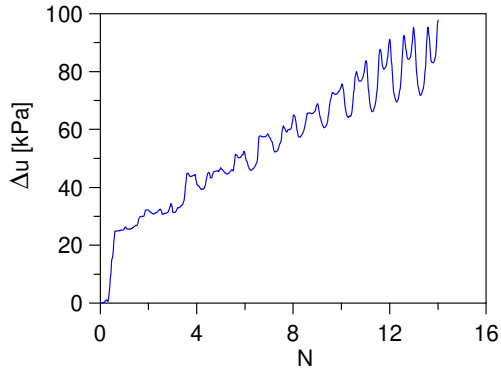

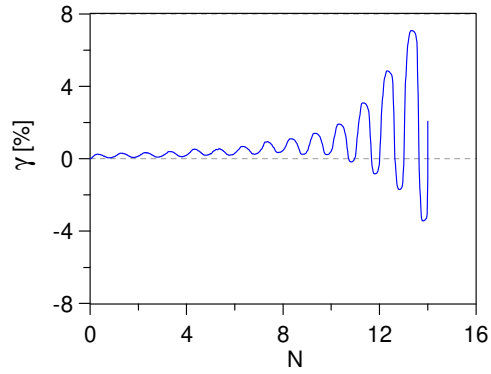

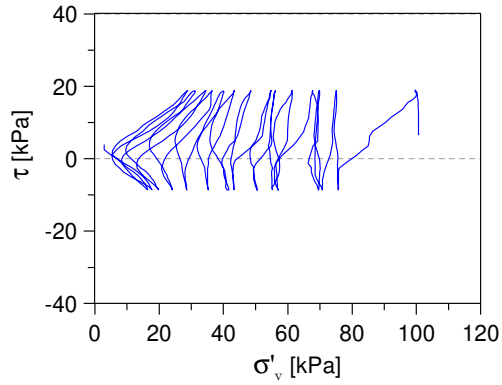

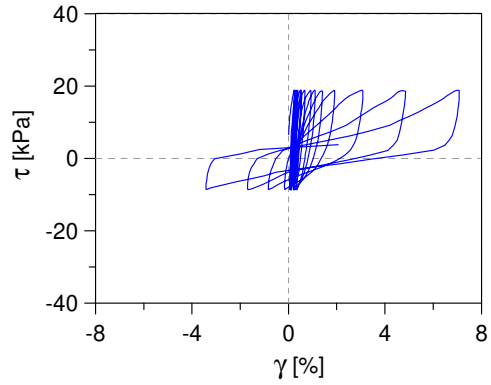

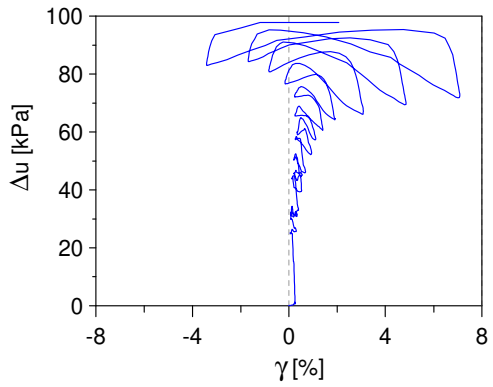

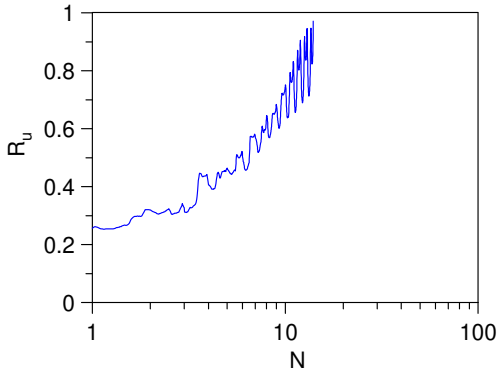

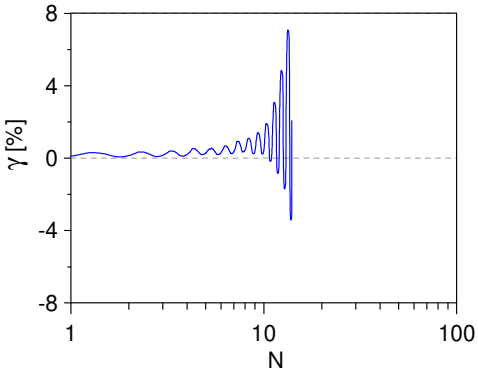

Undrained Cyclic Simple Shear test: *C_SS_TS10_S100_A05_2*
Ticino sand + 10% f_c (Reconstitution method: Moist Tamping)
e_0= 0.68 - D_R= 38% - σ'_{v0}= 100 kPa - α= 0.05 - *CSR* = 0.16

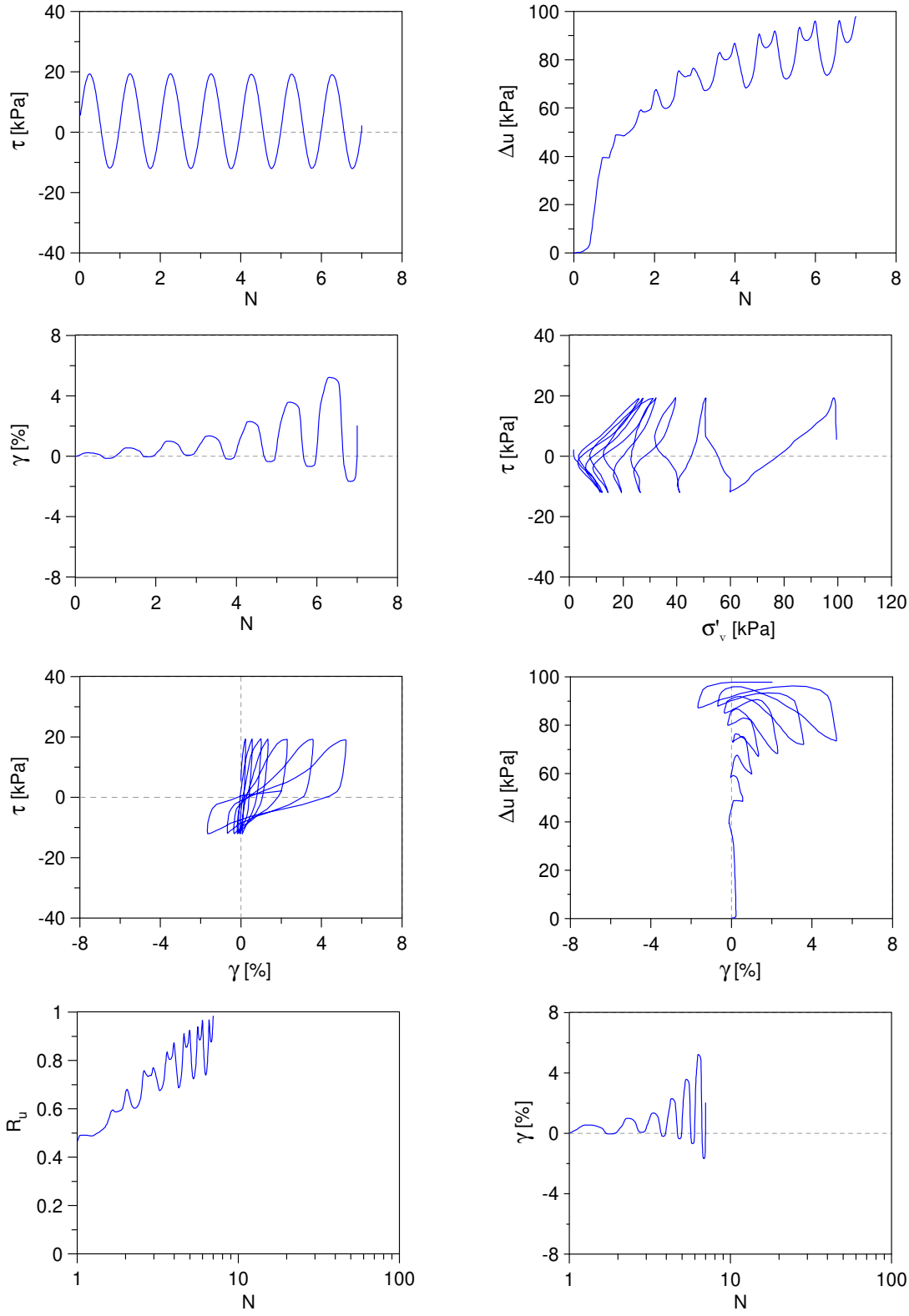

Undrained Cyclic Simple Shear test: *C_SS_TS10_S100_A05_3*
Ticino sand + 10% f_c (Reconstitution method: Moist Tamping)
e_0= 0.60 - D_R= 62% - σ'_{v0}= 100 kPa - α= 0.05 - *CSR* = 0.16

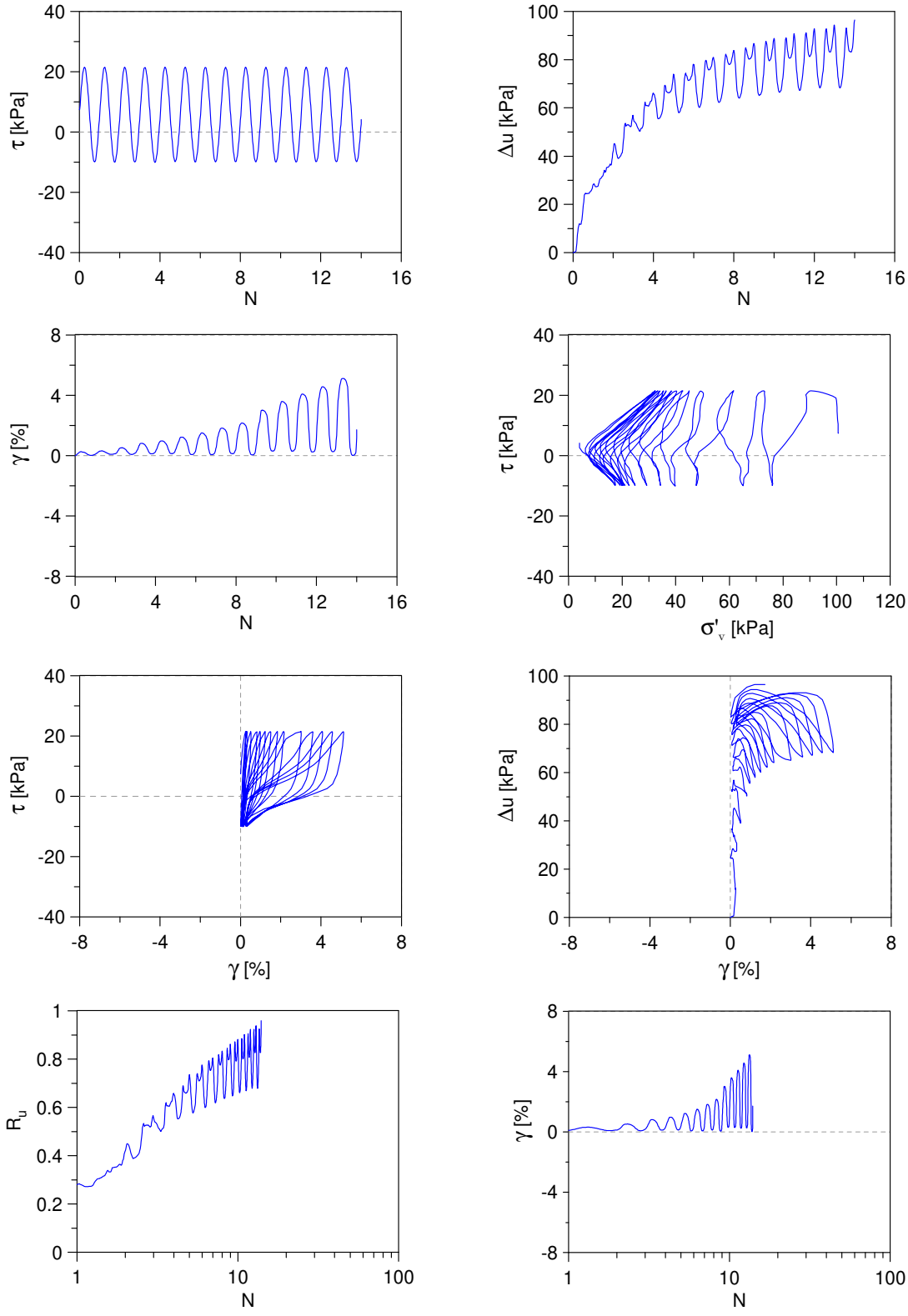

Undrained Cyclic Simple Shear test: *C_SS_TS10_S100_A1_1*
Ticino sand + 10% f_c (Reconstitution method: Moist Tamping)
e_0= 0.68 - D_R= 38% - σ'_{v0}= 100 kPa - α= 0.1 - *CSR* = 0.08

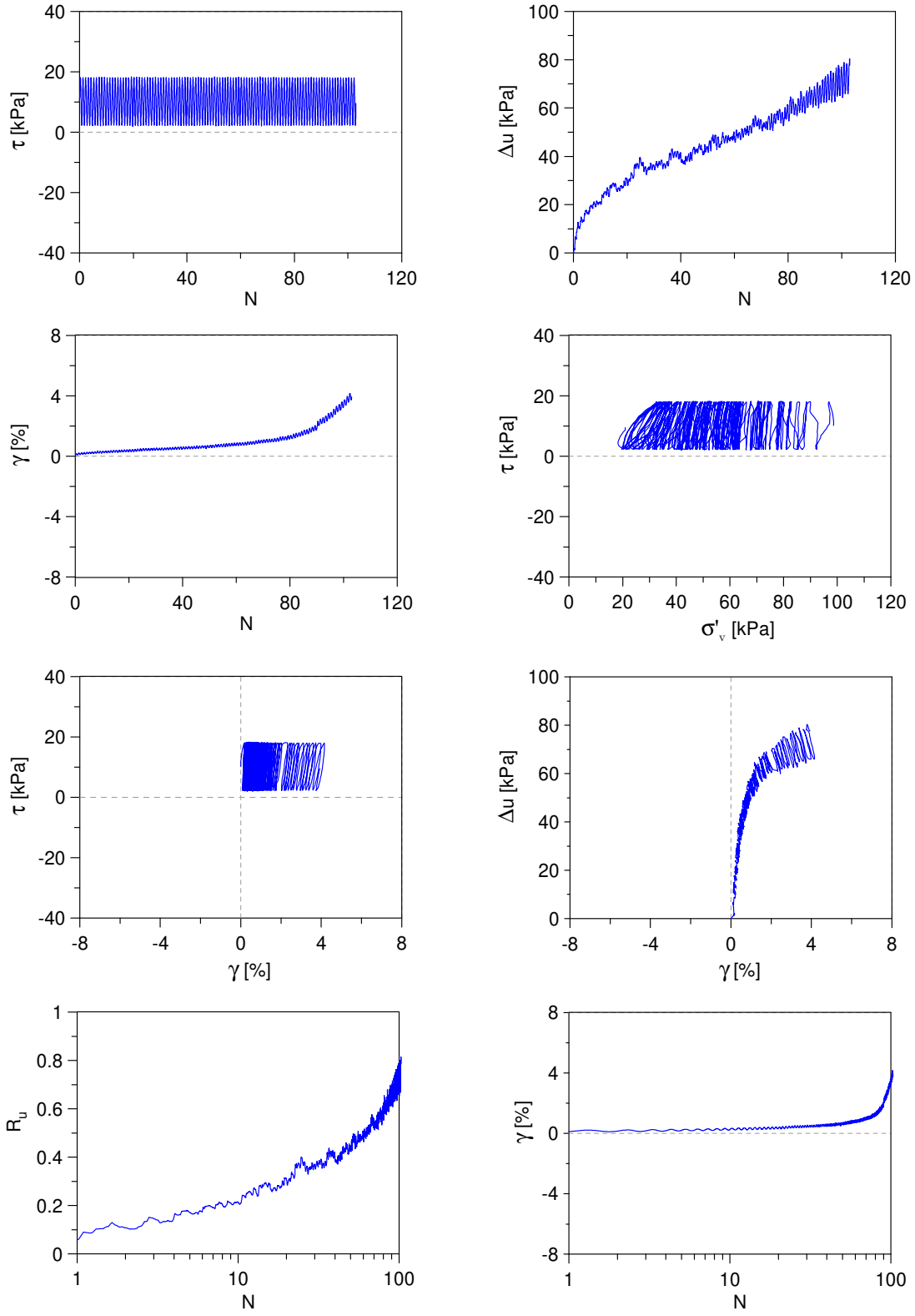

Undrained Cyclic Simple Shear test: *C_SS_TS10_S100_A1_2*
Ticino sand + 10% f_c (Reconstitution method: Moist Tamping)
e_0= 0.68 - D_R= 38% - σ'_{v0}= 100 kPa - α= 0.1 - *CSR* = 0.10

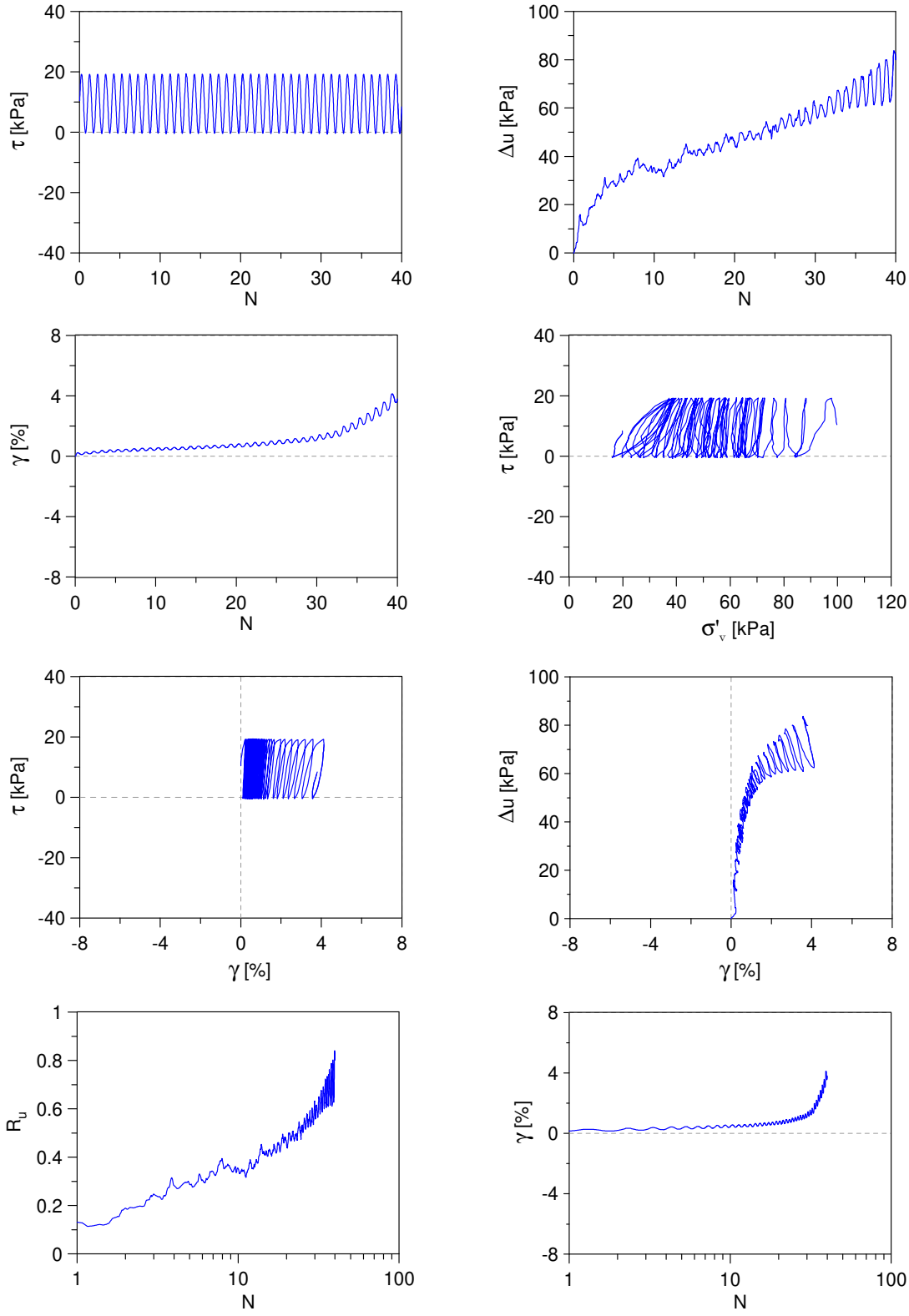

Undrained Cyclic Simple Shear test: *C_SS_TS10_S100_A1_3*
Ticino sand + 10% f_c (Reconstitution method: Moist Tamping)
e_0= 0.68 - D_R= 38% - σ'_{v0}= 100 kPa - α= 0.1 - *CSR* = 0.12

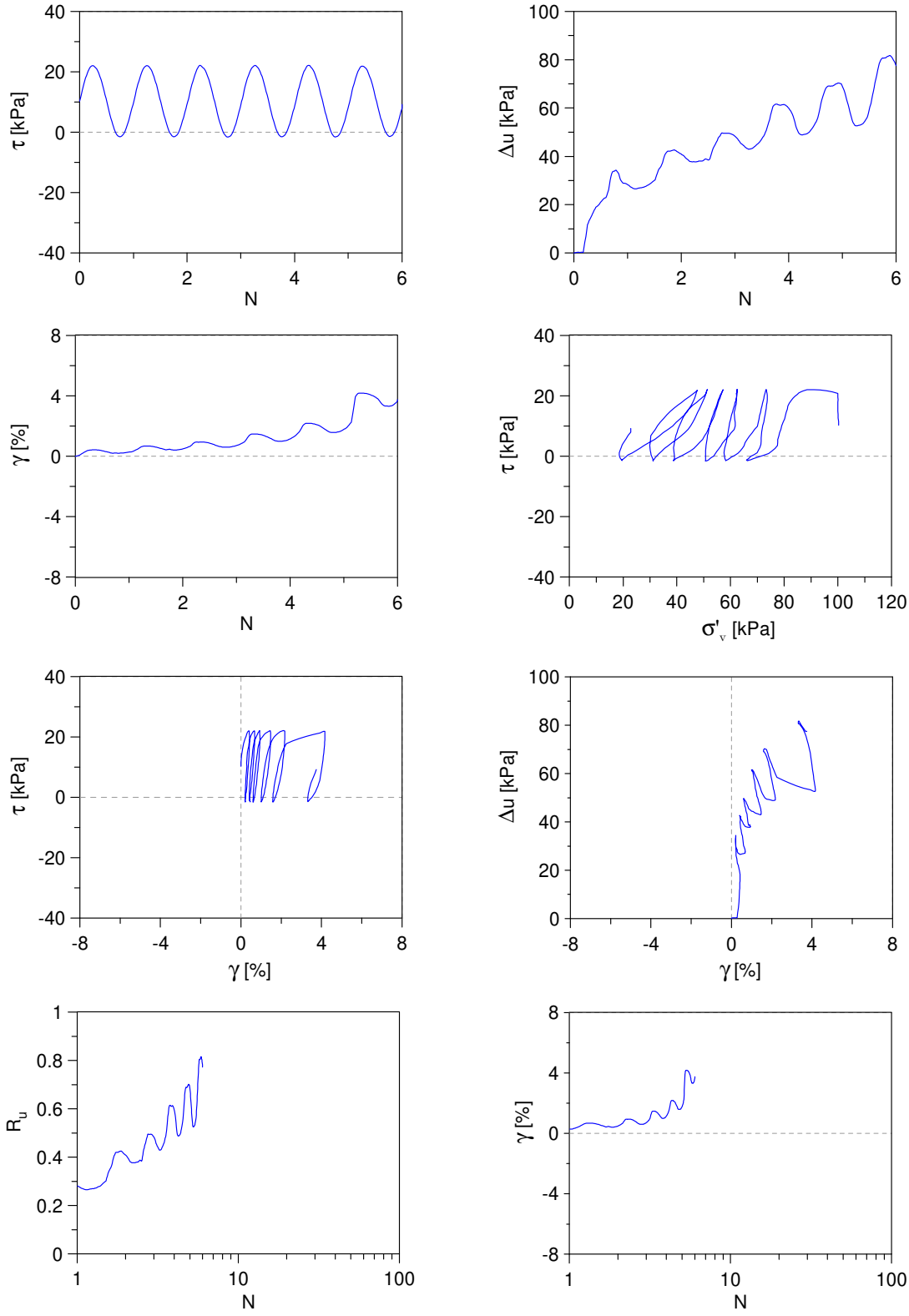

Undrained Cyclic Simple Shear test: *C_SS_TS10_S100_A1_4*
Ticino sand + 10% f_c (Reconstitution method: Moist Tamping)
e_0= 0.60 - D_R= 62% - σ'_{v0}= 100 kPa - α= 0.1 - *CSR* = 0.14

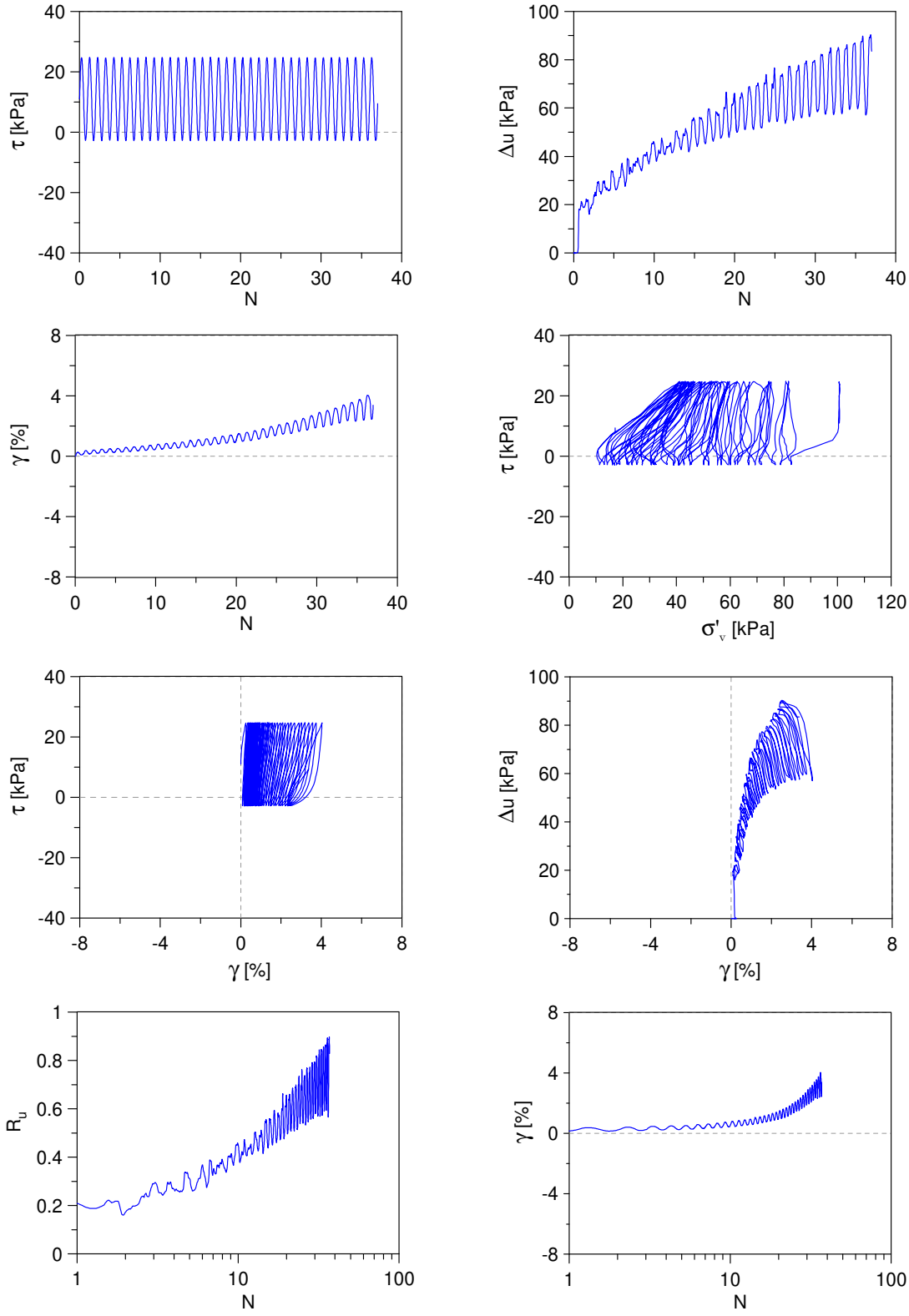

Undrained Cyclic Simple Shear test: *C_SS_TS10_S100_A1_5*
Ticino sand + 10% f_c (Reconstitution method: Moist Tamping)
e_0= 0.60 - D_R= 62% - σ'_{v0}= 100 kPa - α= 0.1 - *CSR* = 0.16

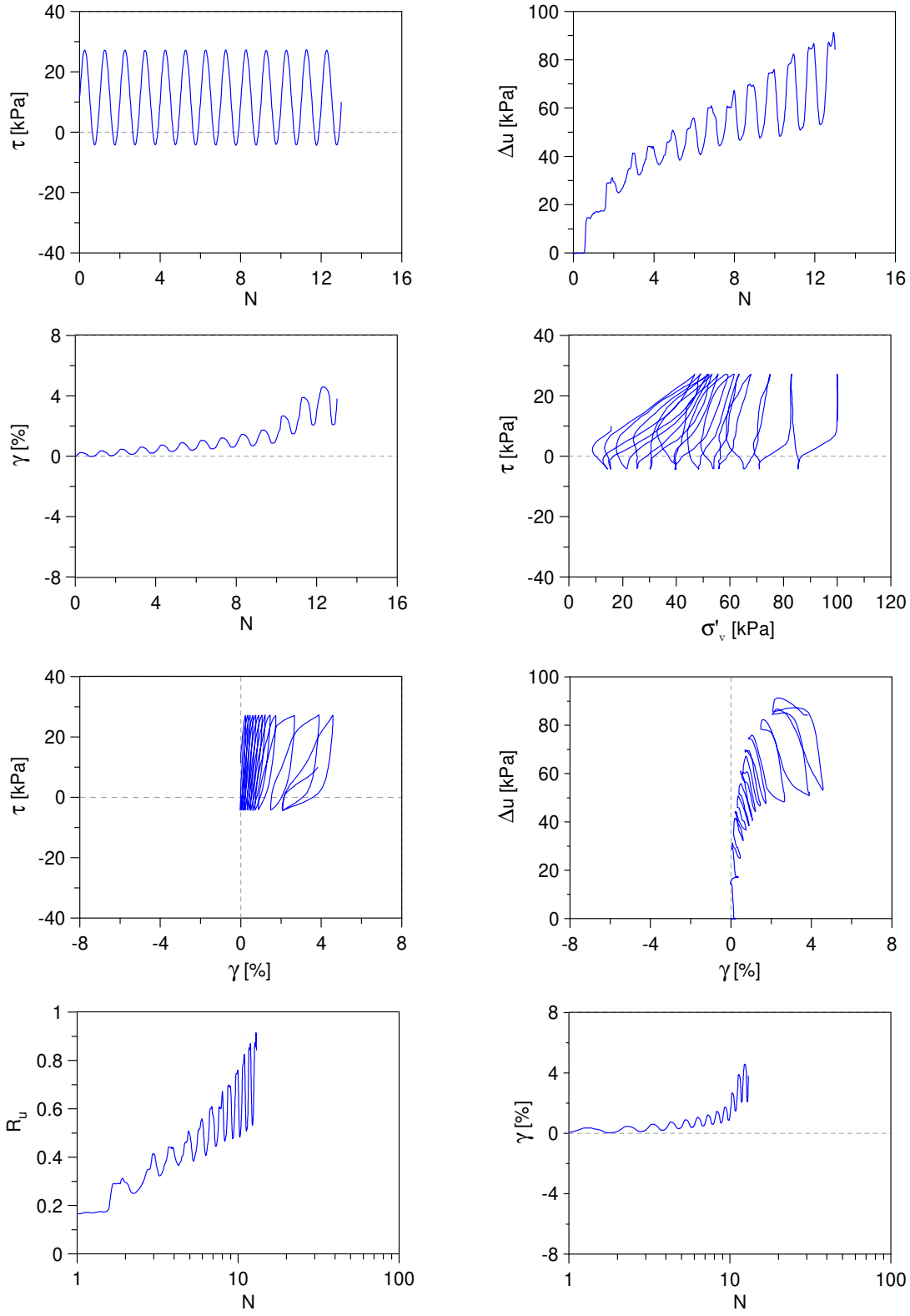

Undrained Cyclic Simple Shear test: *C_SS_TS10_S100_A1_6*
Ticino sand + 10% f_c (Reconstitution method: Moist Tamping)
e_0= 0.60 - D_R= 62% - σ'_{v0}= 100 kPa - α= 0.1 - *CSR* = 0.19

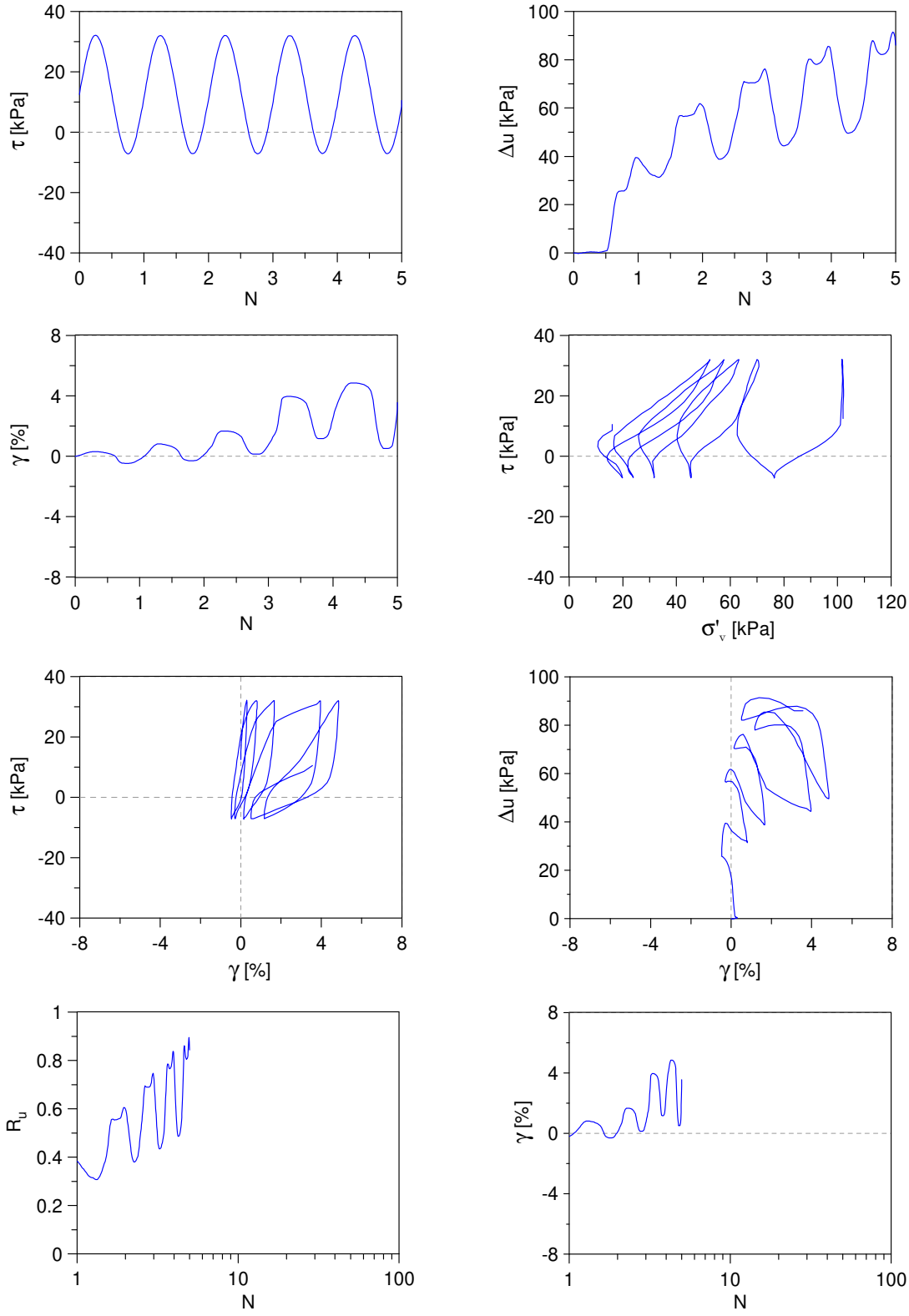

Undrained Cyclic Simple Shear test: *C_SS_TS10_S100_A1_7*
Ticino sand + 10% f_c (Reconstitution method: Moist Tamping)
e_0= 0.55 - D_R= 76% - σ'_{v0}= 100 kPa - α= 0.1 - *CSR* = 0.17

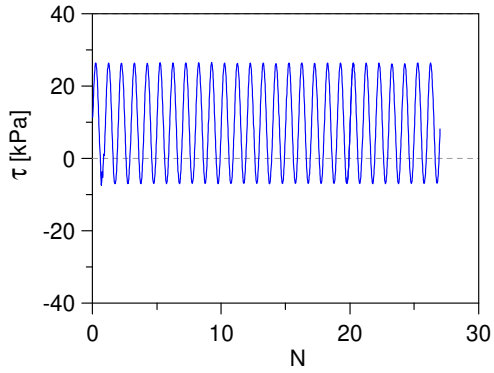

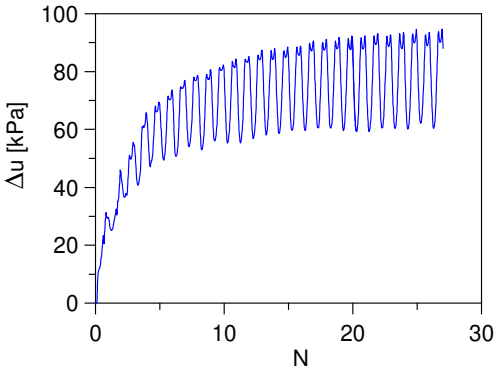

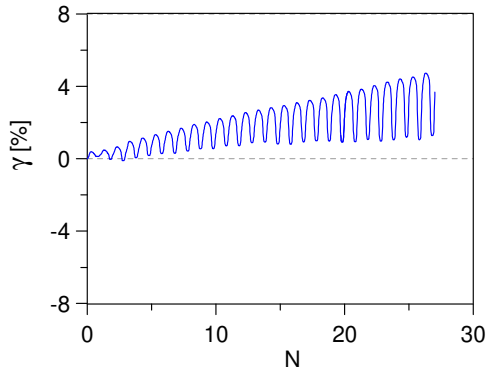

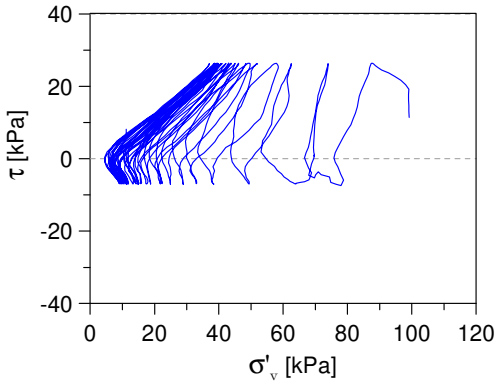

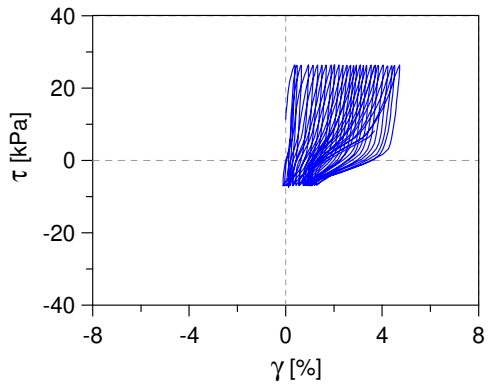

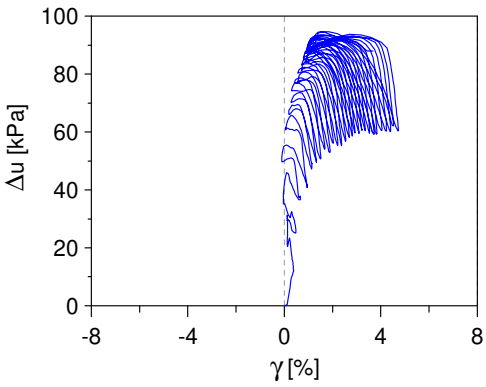

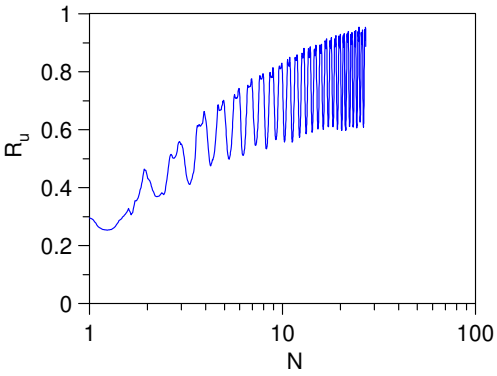

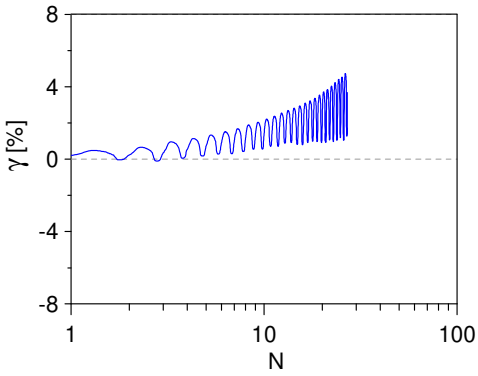

Undrained Cyclic Simple Shear test: *C_SS_TS10_S100_A1_8*
Ticino sand + 10% f_c (Reconstitution method: Moist Tamping)
e_0= 0.55 - D_R= 76% - σ'_{v0}= 100 kPa - α= 0.1 - *CSR* = 0.22

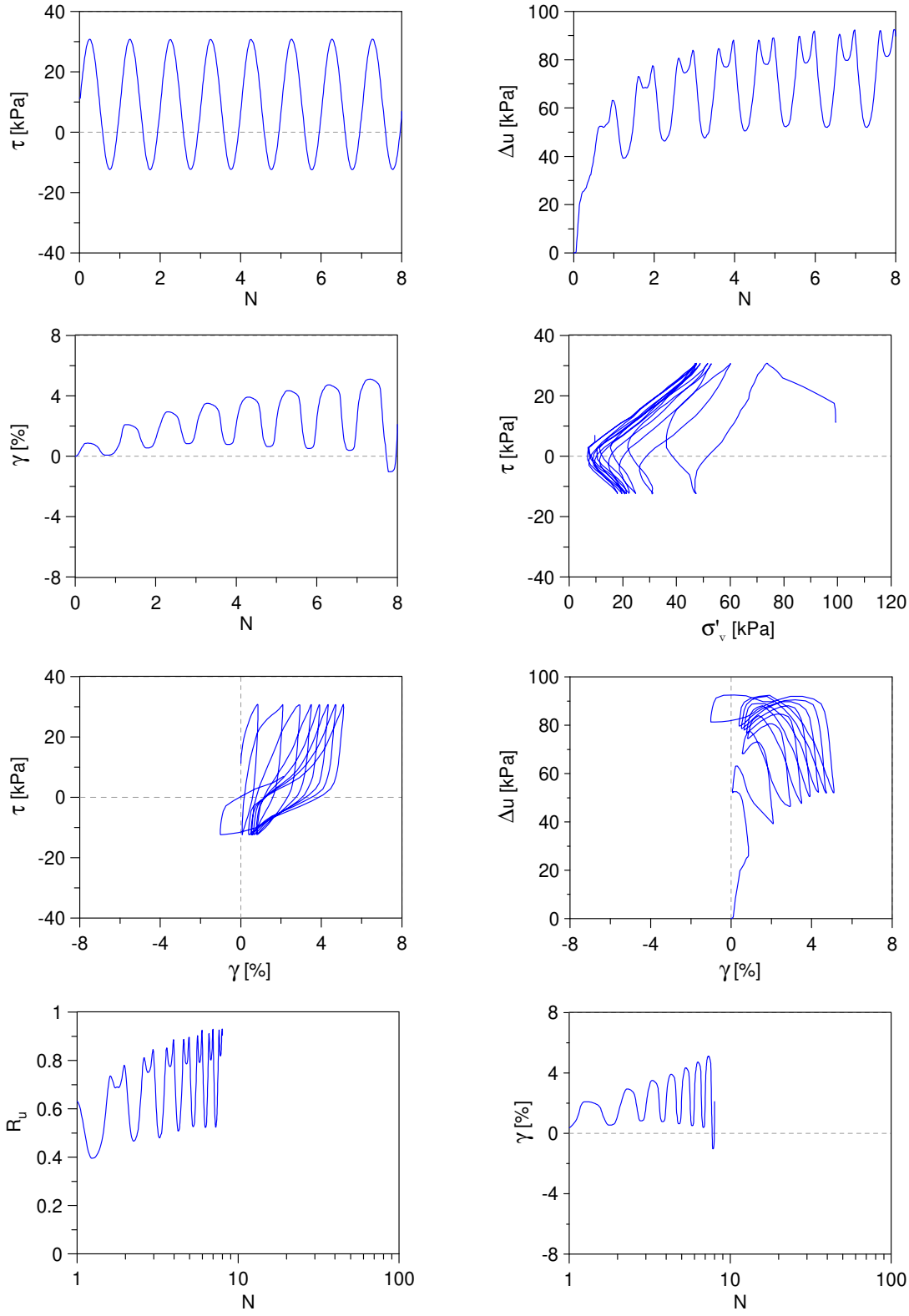

Undrained Cyclic Simple Shear test: *C_SS_TS10_S100_A2_1*
Ticino sand + 10% f_c (Reconstitution method: Moist Tamping)
e_0= 0.68 - D_R= 38% - σ'_{v0}= 100 kPa - α= 0.2 - *CSR* = 0.08

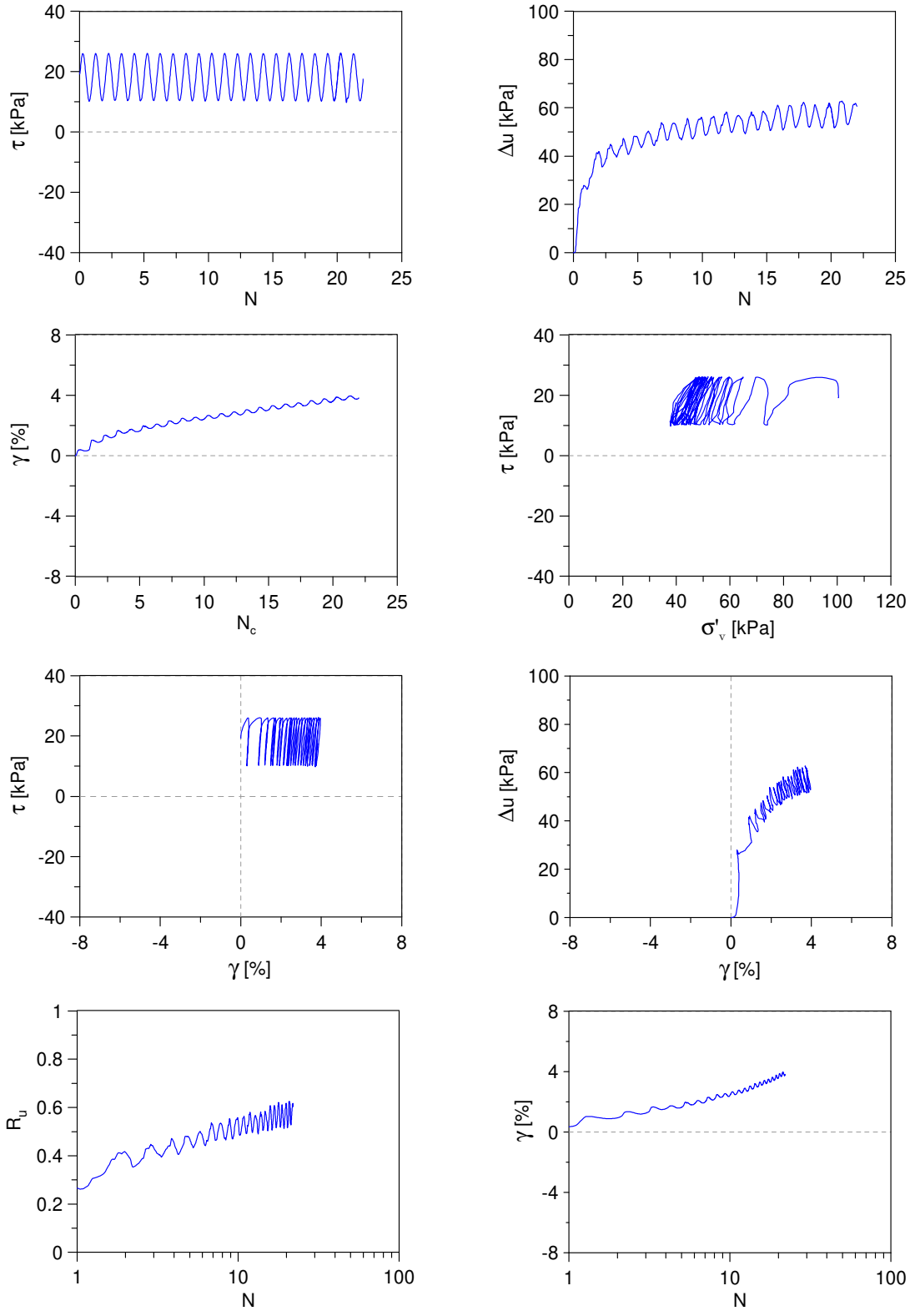

Undrained Cyclic Simple Shear test: *C_SS_TS10_S100_A2_2*
Ticino sand + 10% f_c (Reconstitution method: Moist Tamping)
e_0= 0.68 - D_R= 38% - σ'_{v0}= 100 kPa - α= 0.2 - *CSR* = 0.10

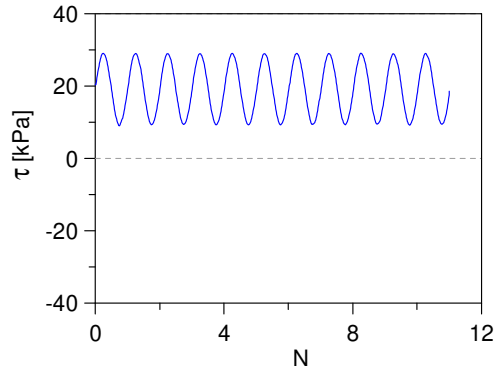

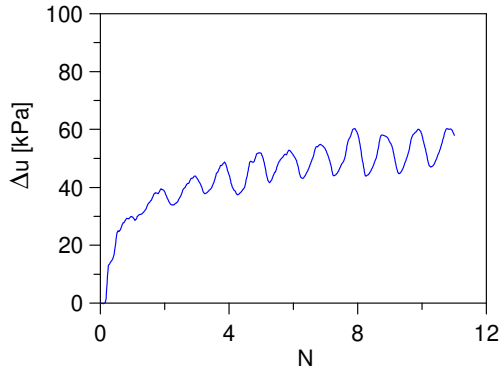

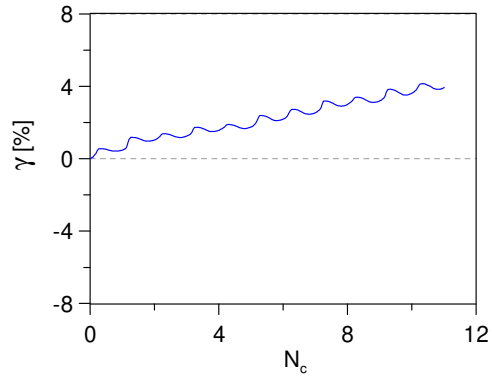

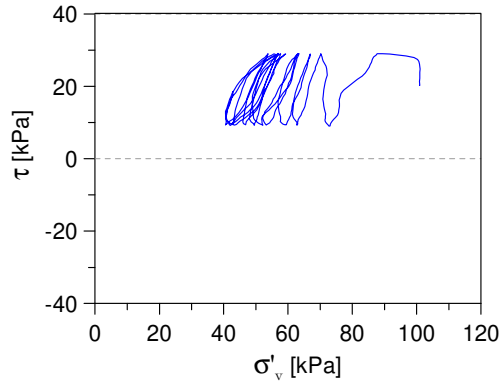

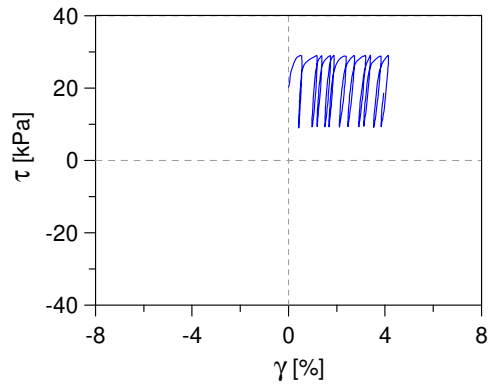

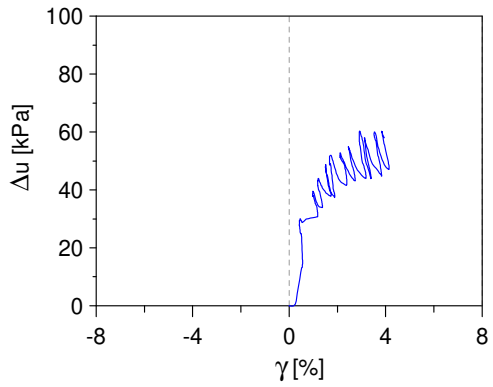

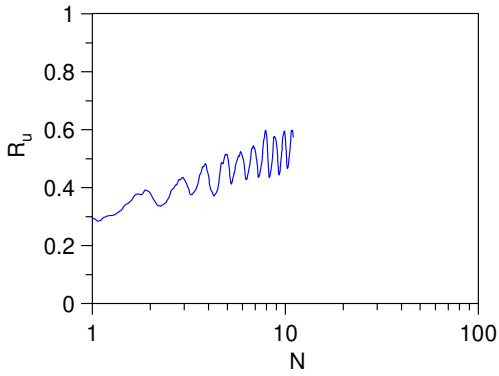

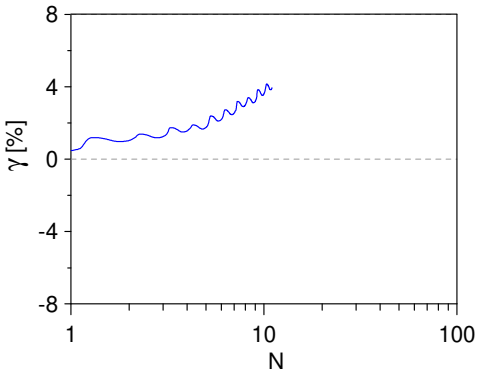

Undrained Cyclic Simple Shear test: *C_SS_TS10_S100_A2_3*
Ticino sand + 10% f_c (Reconstitution method: Moist Tamping)
e_0= 0.60 - D_R= 62% - σ'_{v0}= 100 kPa - α= 0.2 - *CSR* = 0.12

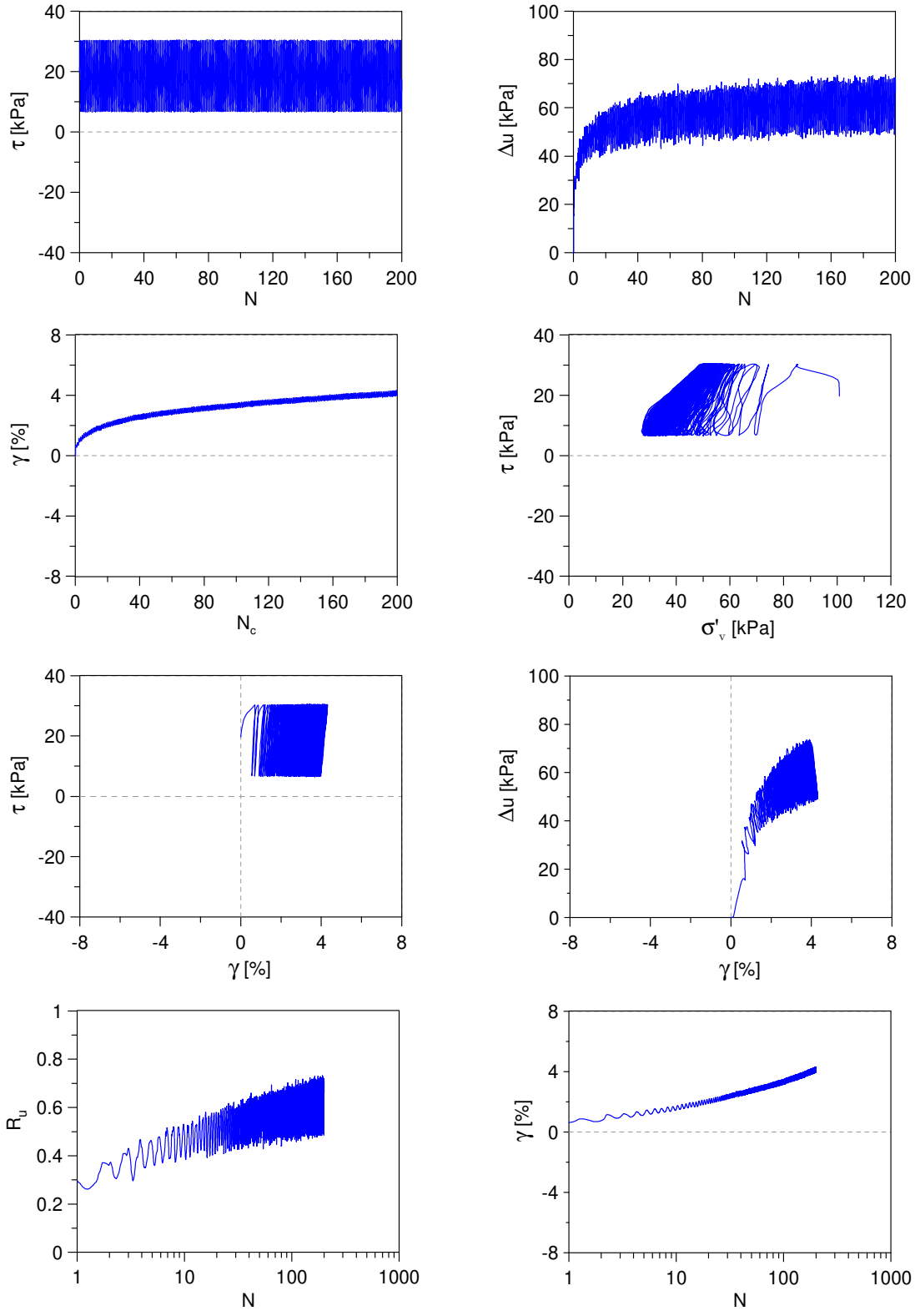

Undrained Cyclic Simple Shear test: *C_SS_TS10_S100_A2_4*
Ticino sand + 10% f_c (Reconstitution method: Moist Tamping)
e_0= 0.60 - D_R= 62% - σ'_{v0}= 100 kPa - α= 0.2 - *CSR* = 0.14

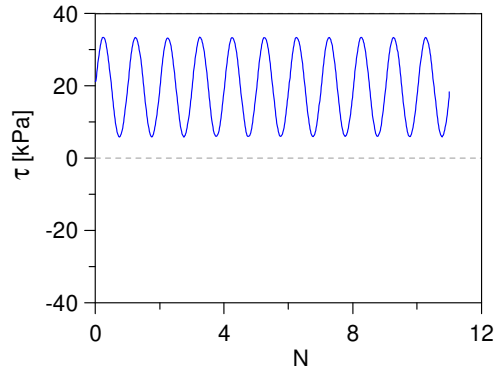

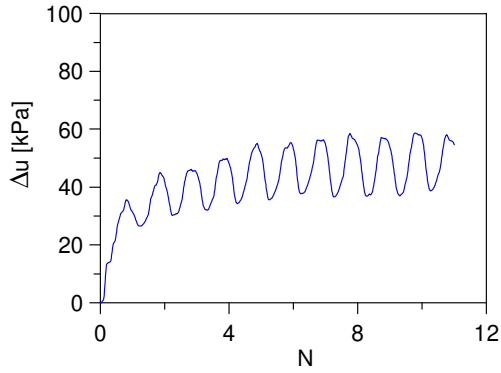

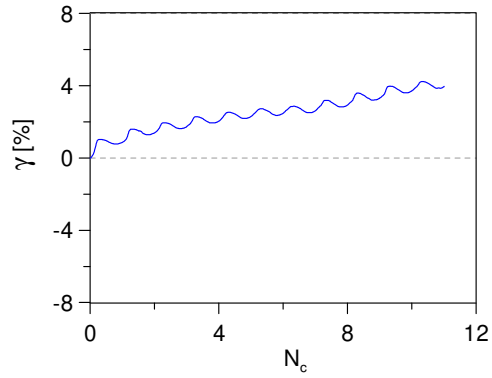

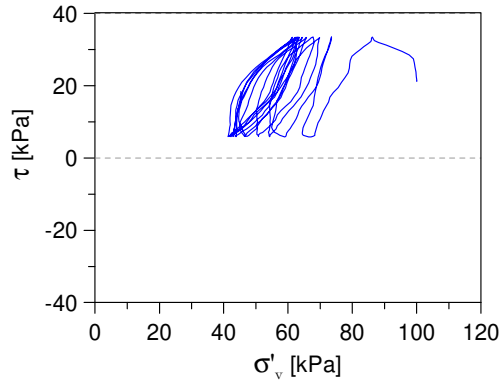

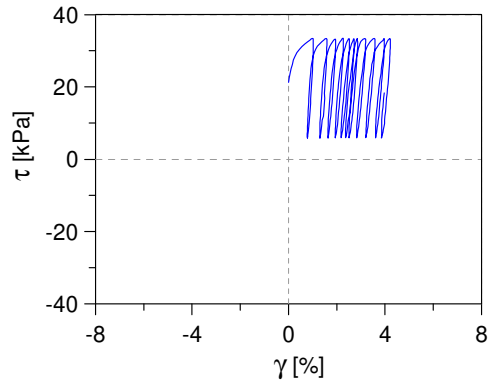

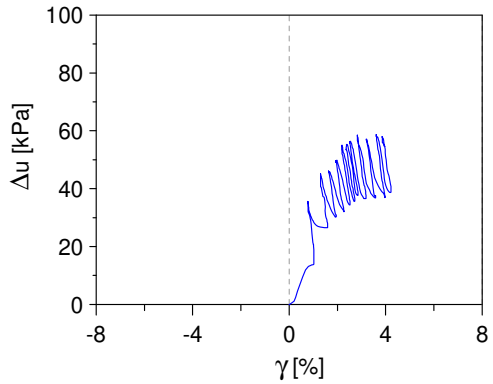

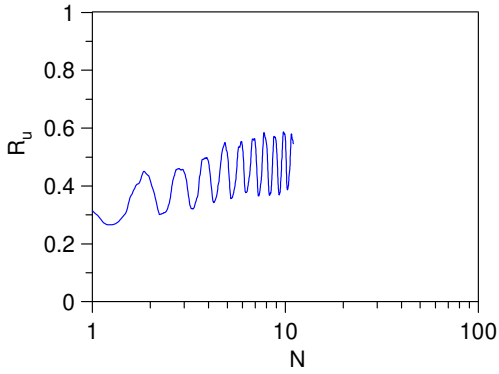

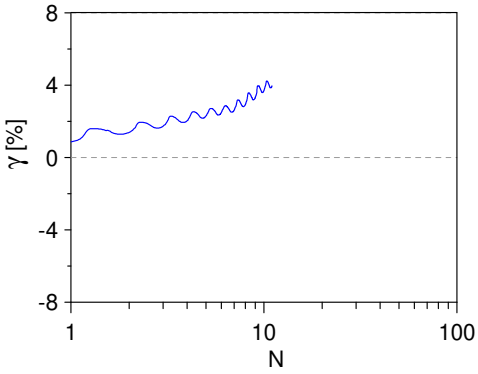

Undrained Cyclic Simple Shear test: *C_SS_TS10_S100_A2_5*
Ticino sand + 10% f_c (Reconstitution method: Moist Tamping)
e_0= 0.60 - D_R= 62% - σ'_{v0}= 100 kPa - α= 0.2 - *CSR* = 0.16

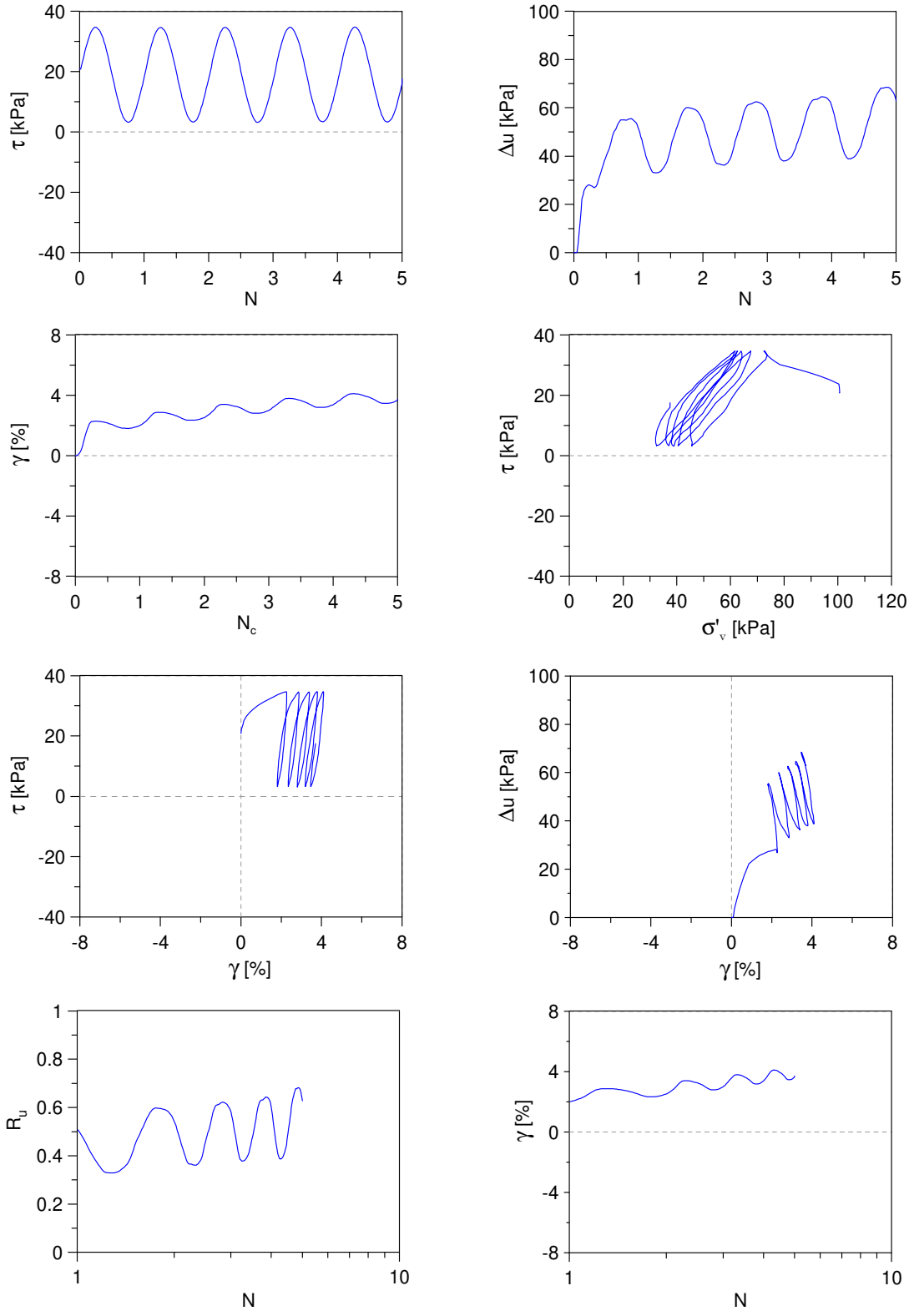

Undrained Cyclic Simple Shear test: *C_SS_TS10_S100_A2_6*
Ticino sand + 10% f_c (Reconstitution method: Moist Tamping)
e_0= 0.55 - D_R= 76% - σ'_{v0}= 100 kPa - α= 0.2 - *CSR* = 0.18

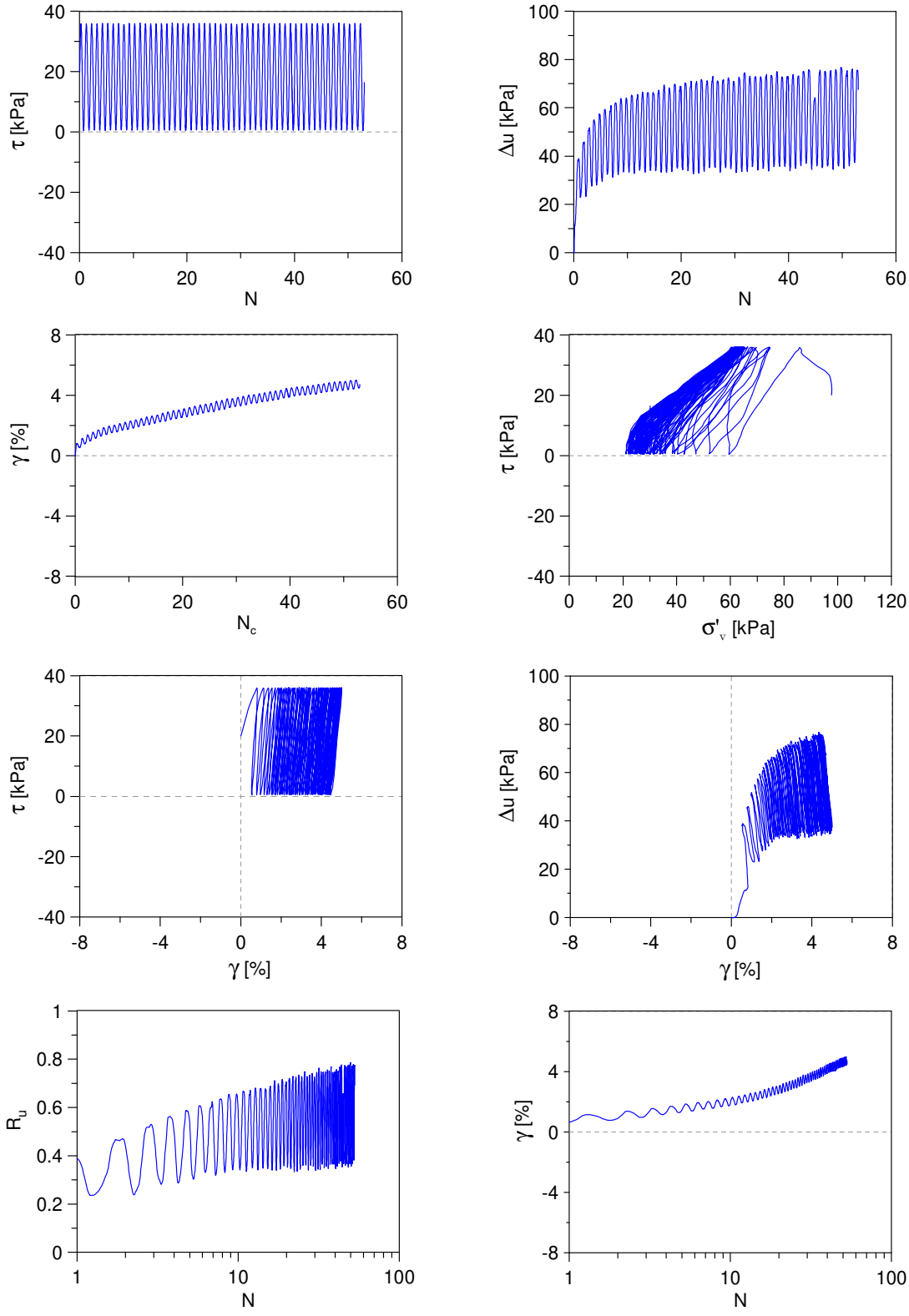

Undrained Cyclic Simple Shear test: *C_SS_TS10_S100_A2_7*
Ticino sand + 10% f_c (Reconstitution method: Moist Tamping)
e_0= 0.55 - D_R= 76% - σ'_{v0}= 100 kPa - α= 0.2 - *CSR* = 0.23

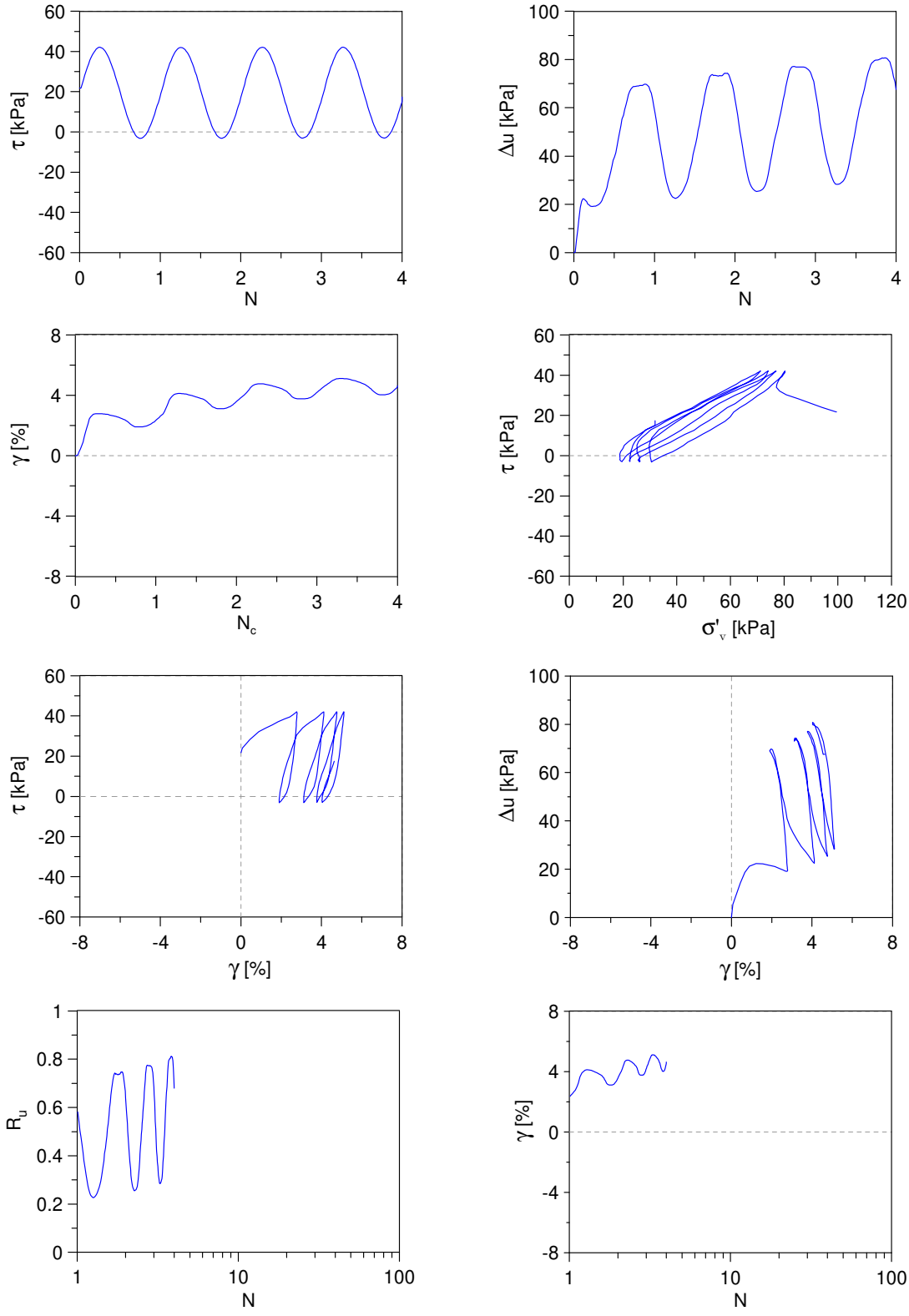

Undrained Cyclic Simple Shear test: *C_SS_TS10_S100_A3_1*
Ticino sand + 10% f_c (Reconstitution method: Moist Tamping)
e_0= 0.68 - D_R= 38% - σ'_{v0}= 100 kPa - α= 0.3 - *CSR* = 0.03

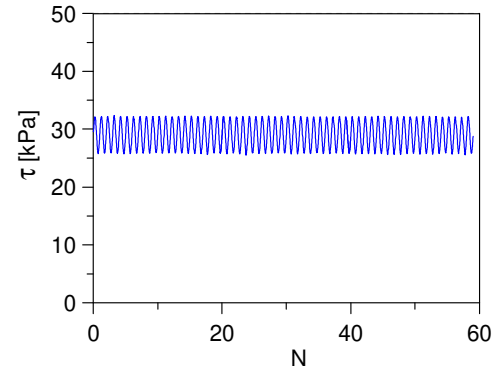

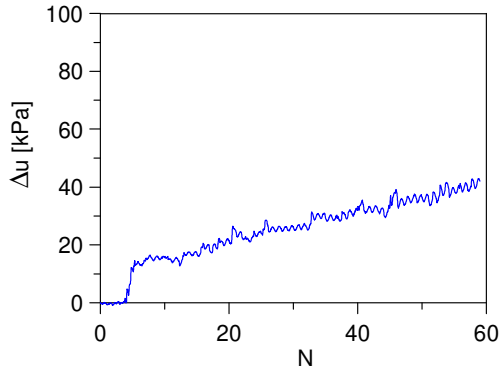

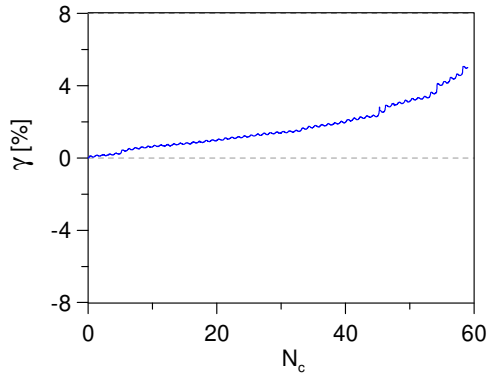

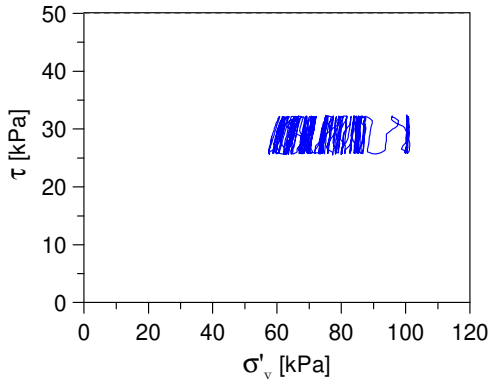

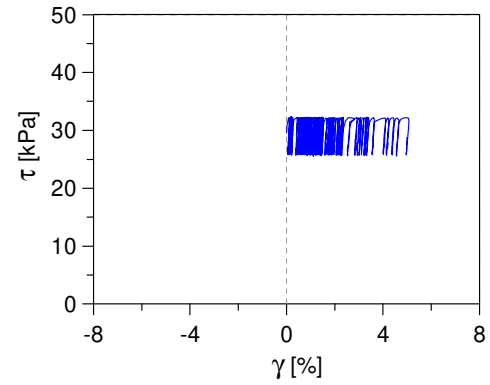

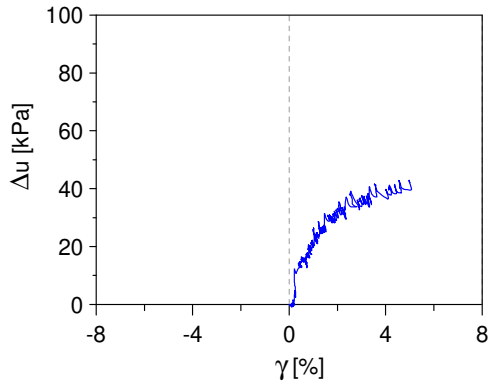

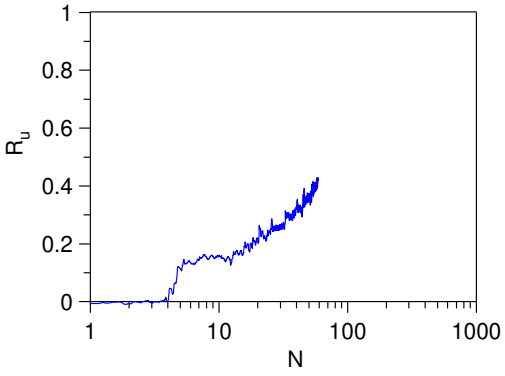

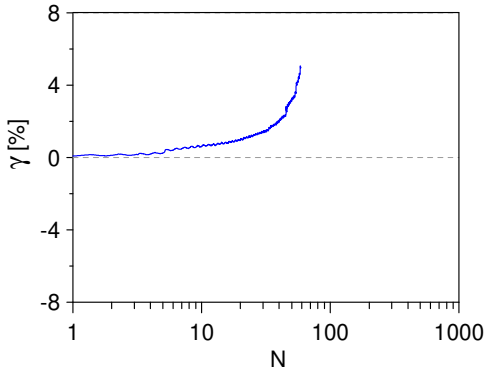

Undrained Cyclic Simple Shear test: *C_SS_TS10_S100_A3_2*
Ticino sand + 10% f_c (Reconstitution method: Moist Tamping)
e_0= 0.68 - D_R= 38% - σ'_{v0}= 100 kPa - α= 0.3 - *CSR* = 0.06

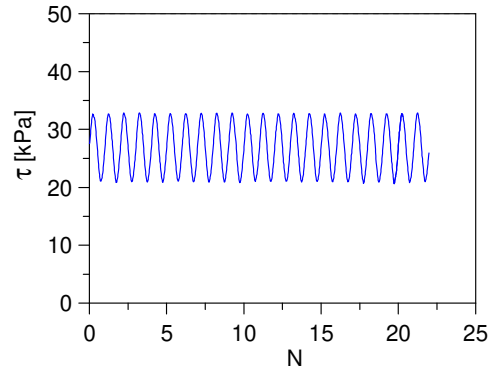

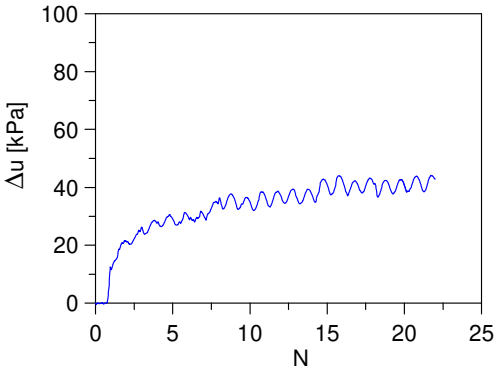

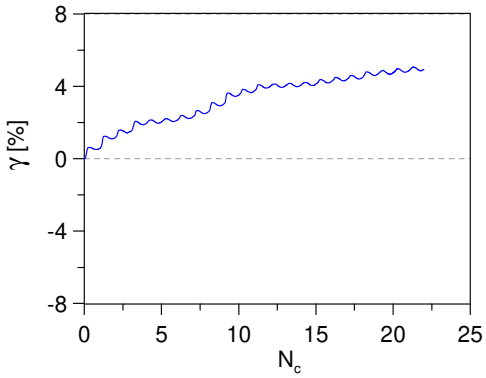

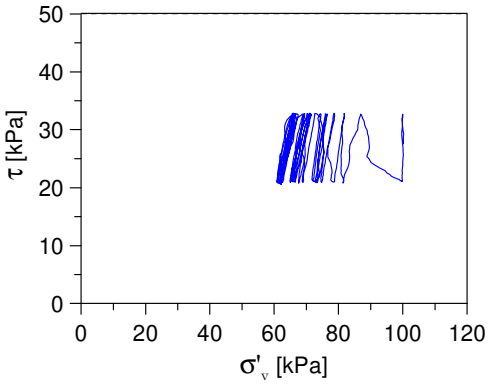

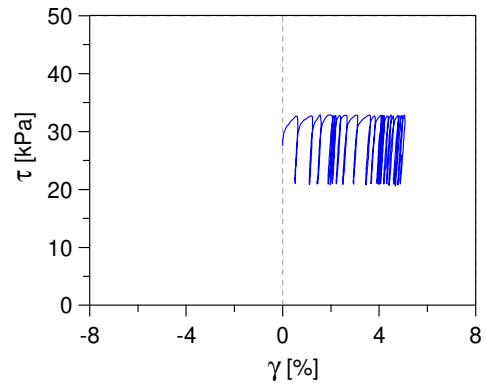

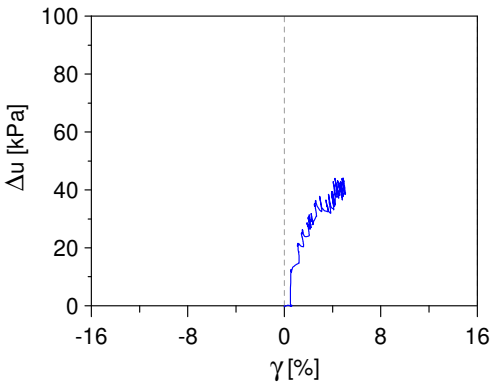

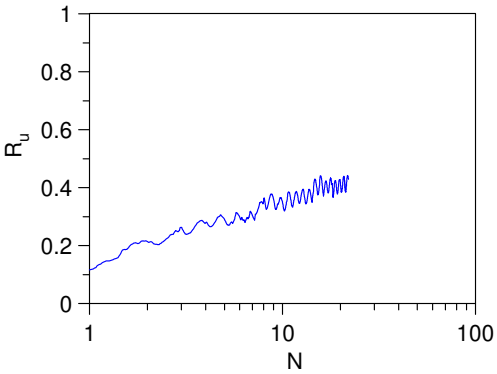

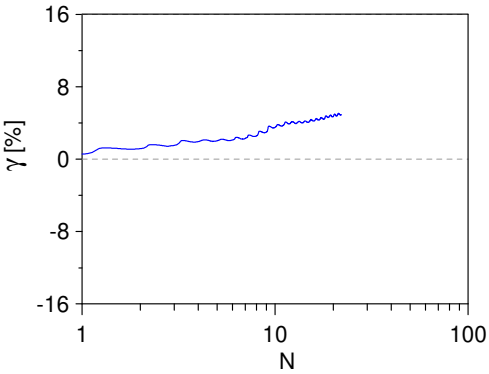

Undrained Cyclic Simple Shear test: *C_SS_TS10_S100_A3_3*
Ticino sand + 10% f_c (Reconstitution method: Moist Tamping)
e_0= 0.60 - D_R= 62% - σ'_{v0}= 100 kPa - α= 0.3 - *CSR* = 0.08

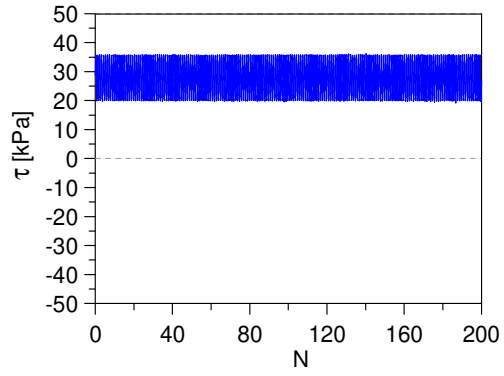

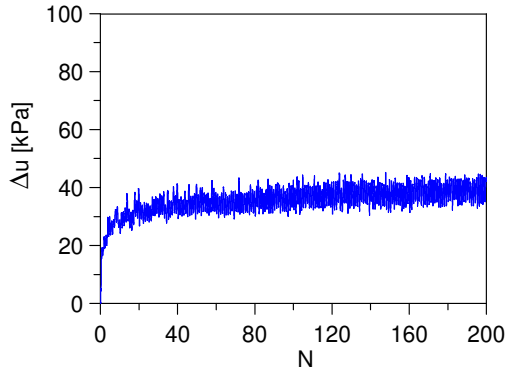

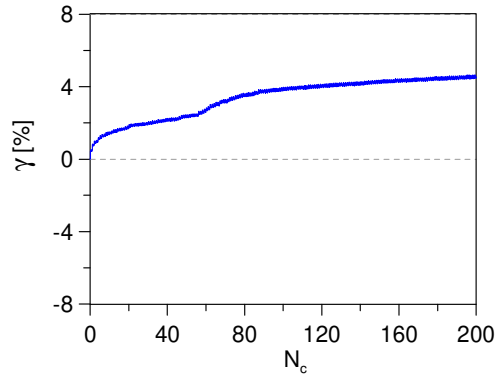

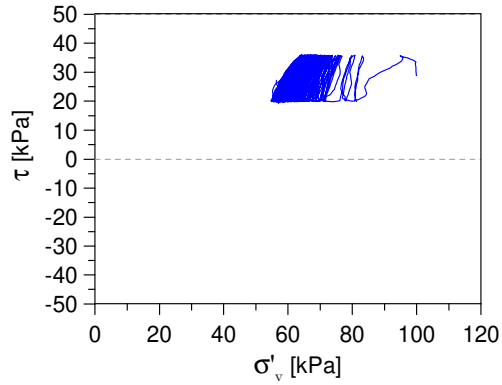

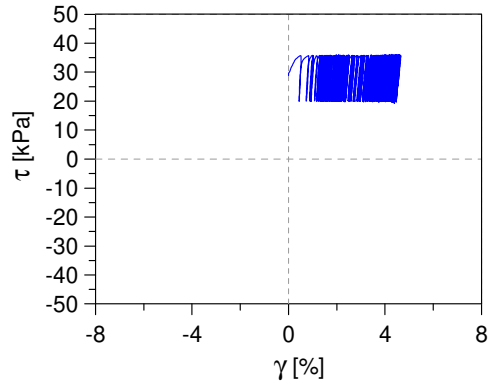

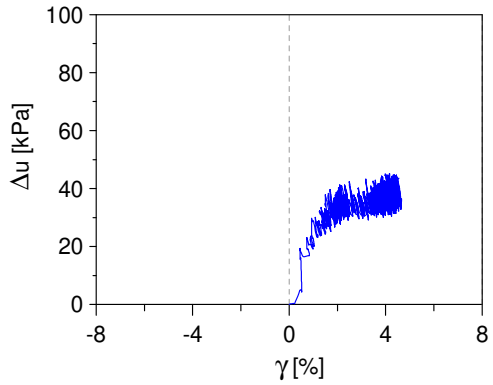

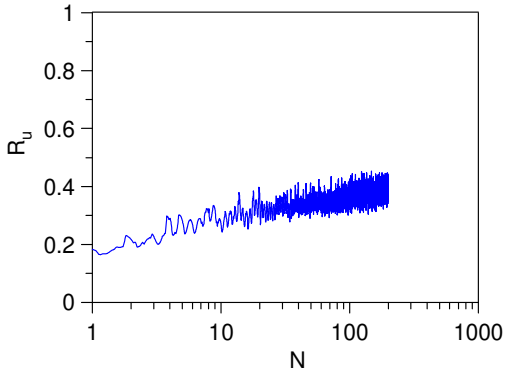

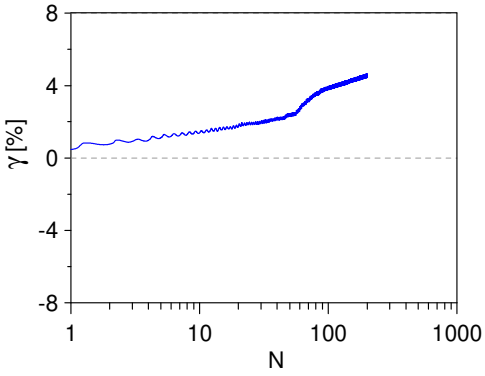

Undrained Cyclic Simple Shear test: *C_SS_TS10_S100_A3_4*
Ticino sand + 10% f_c (Reconstitution method: Moist Tamping)
e_0= 0.60 - D_R= 62% - σ'_{v0}= 100 kPa - α= 0.3 - *CSR* = 0.10

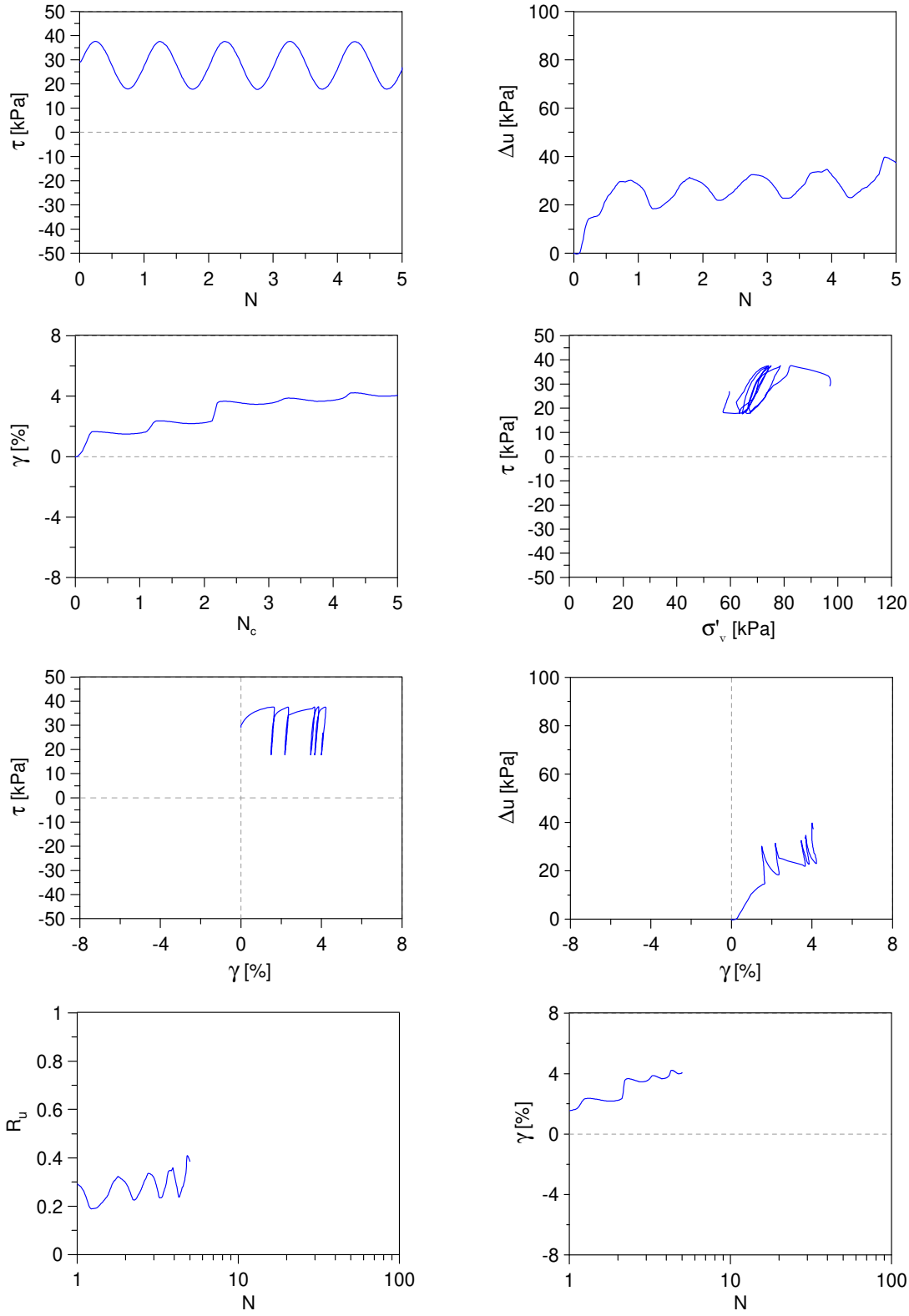

Undrained Cyclic Simple Shear test: *C_SS_TS10_S100_A3_5*
Ticino sand + 10% f_c (Reconstitution method: Moist Tamping)
e_0= 0.60 - D_R= 62% - σ'_{v0}= 100 kPa - α= 0.3 - *CSR* = 0.12

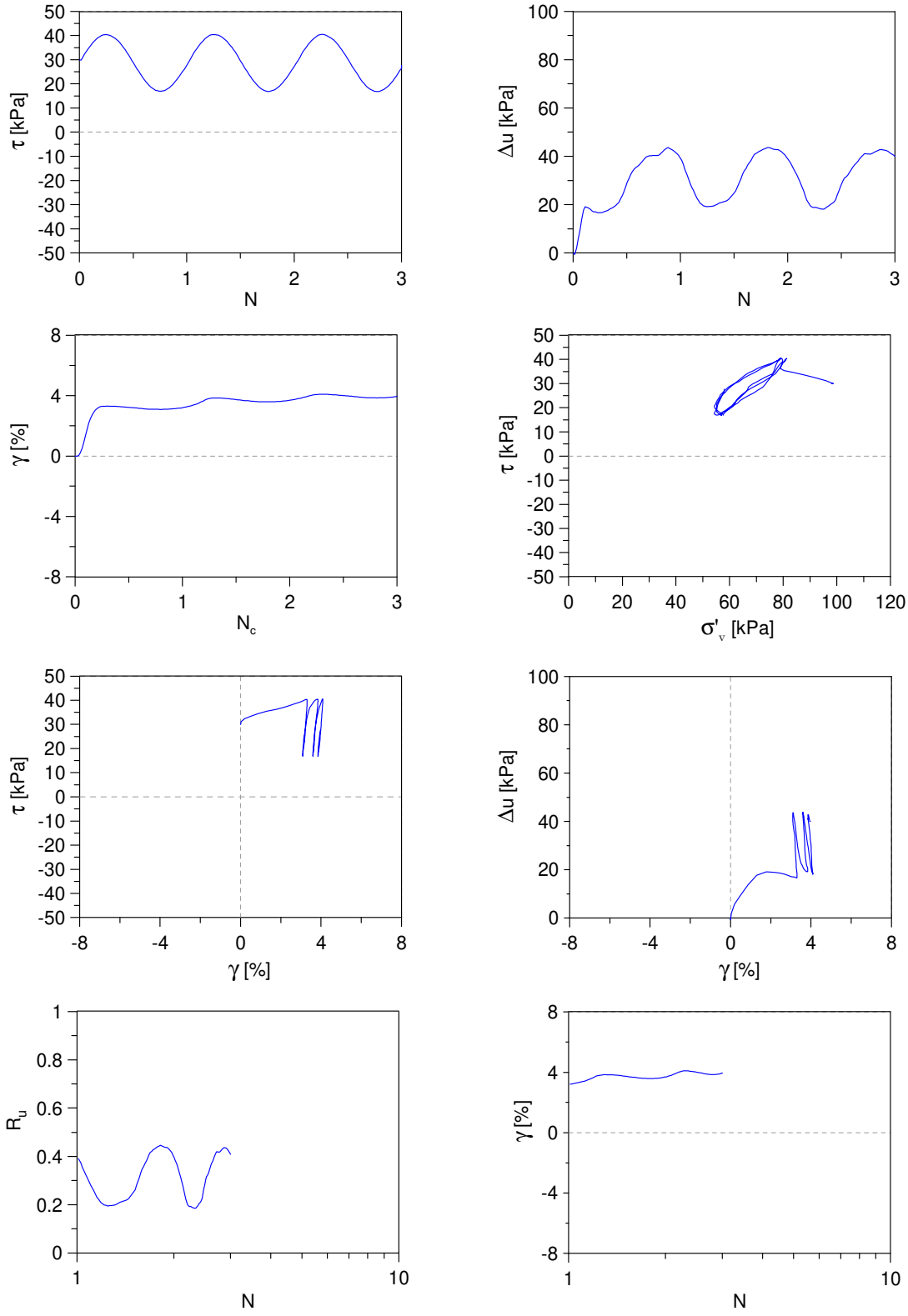

Undrained Cyclic Simple Shear test: *C_SS_TS10_S100_A3_6*
Ticino sand + 10% f_c (Reconstitution method: Moist Tamping)
e_0= 0.55 - D_R= 76% - σ'_{v0}= 100 kPa - α= 0.3 - *CSR* = 0.16

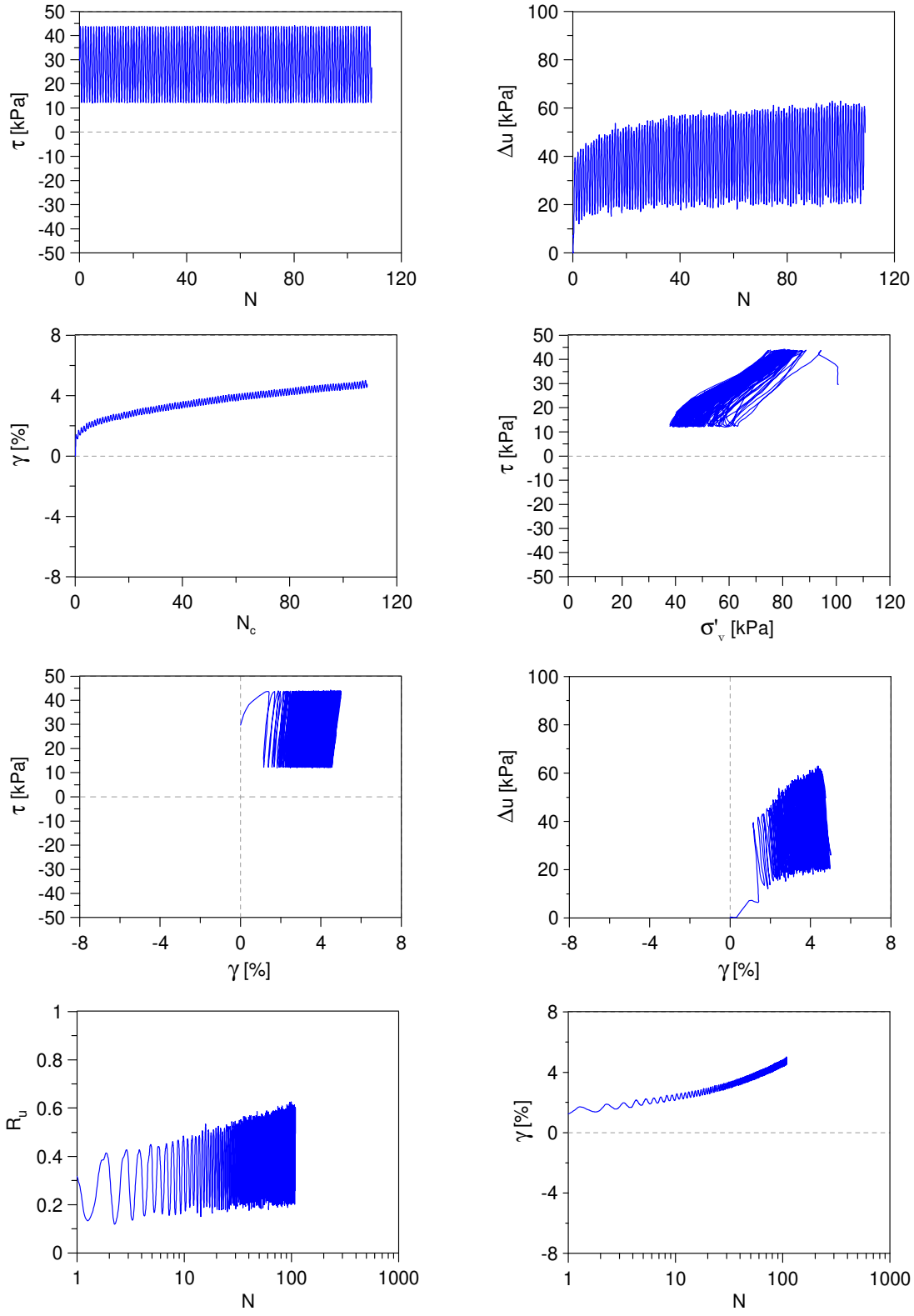

Undrained Cyclic Simple Shear test: *C_SS_TS10_S100_A3_7*
Ticino sand + 10% f_c (Reconstitution method: Moist Tamping)
e_0= 0.55 - D_R= 76% - σ'_{v0}= 100 kPa - α= 0.3 - *CSR* = 0.18

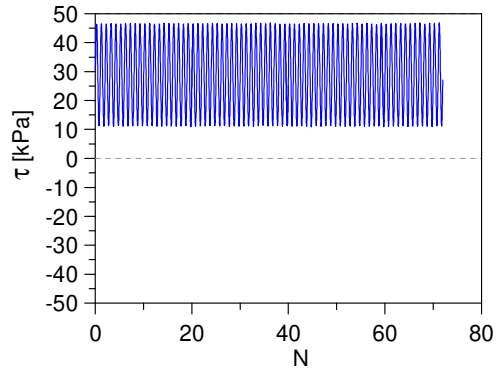

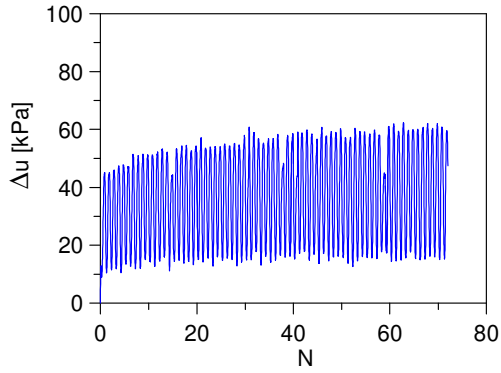

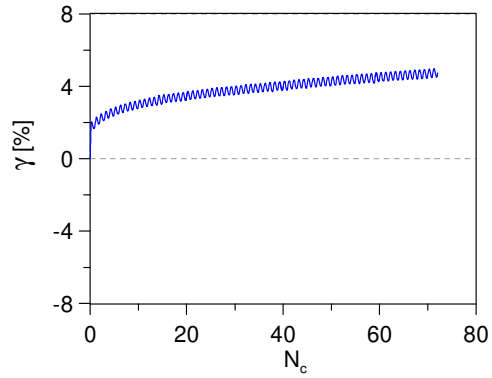

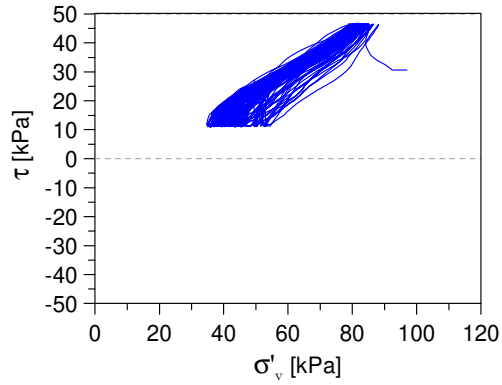

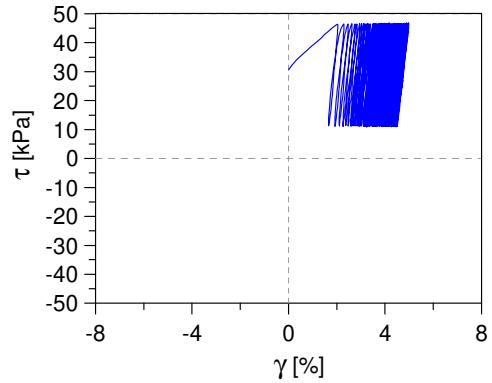

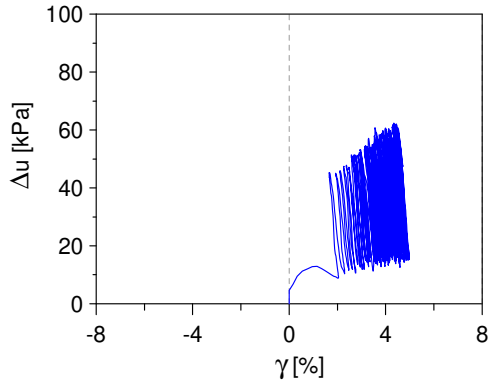

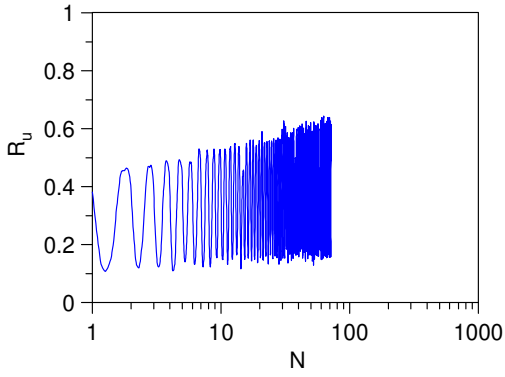

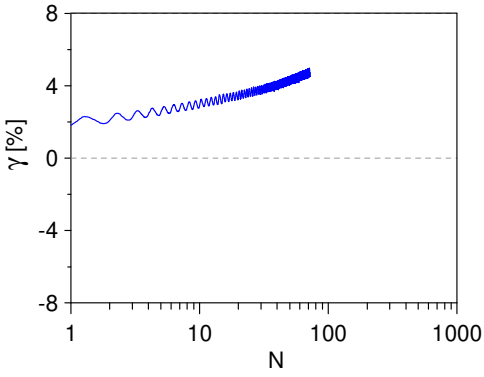

Sand-silt mixture (f_c=20%)

Undrained Cyclic Simple Shear test: *C_SS_TS20_S100_A0_1*
Ticino sand + 20% f_c (Reconstitution method: Moist Tamping)
e_0= 0.58 - D_R= 50% - σ'_{v0}= 50 kPa - α=0 - *CSR* = 0.14

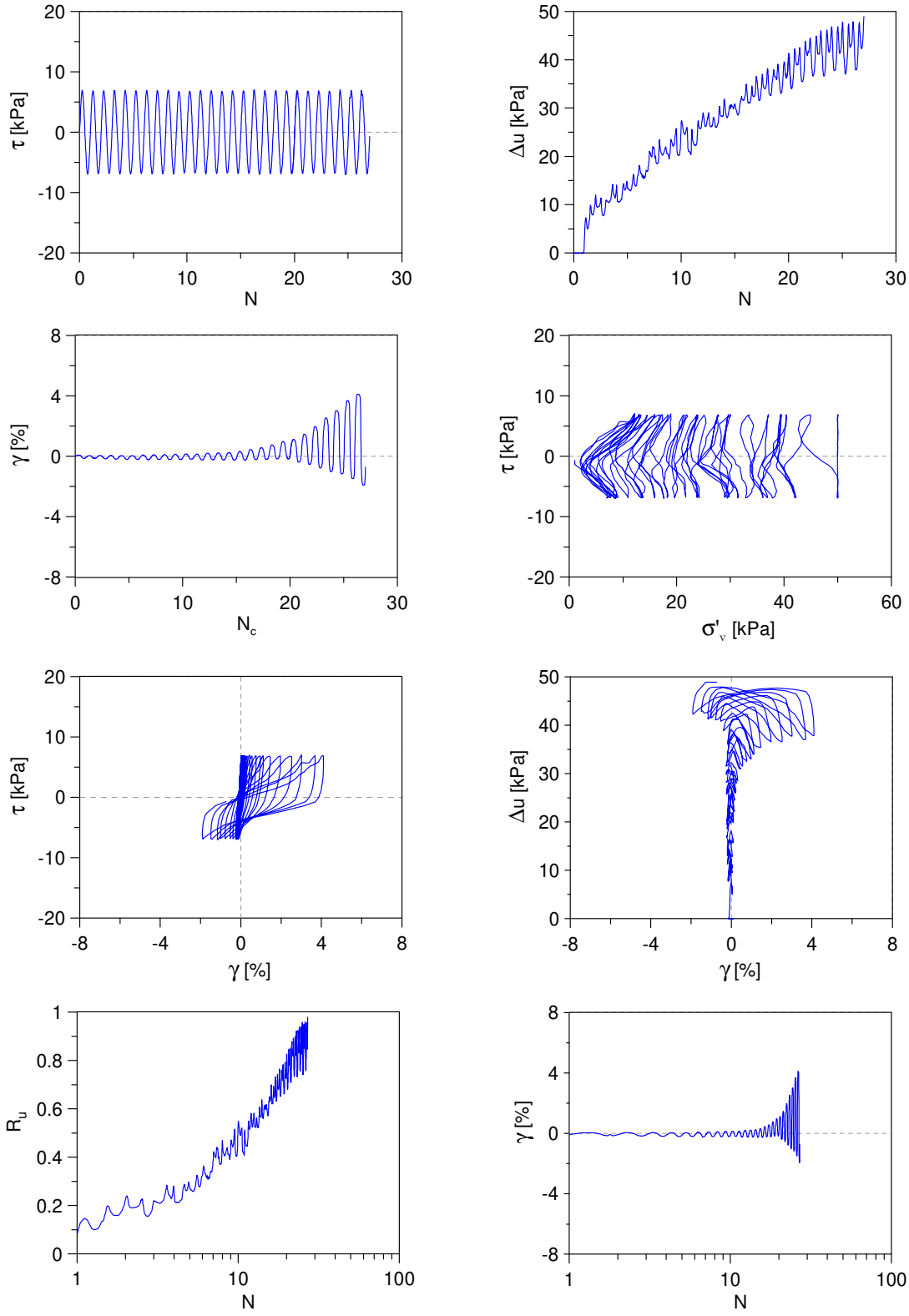

Undrained Cyclic Simple Shear test: *C_SS_TS20_S100_A0_2*
Ticino sand + 20% f_c (Reconstitution method: Moist Tamping)
e_0= 0.58 - D_R= 50% - σ'_{v0}= 50 kPa - α=0 - *CSR* = 0.15

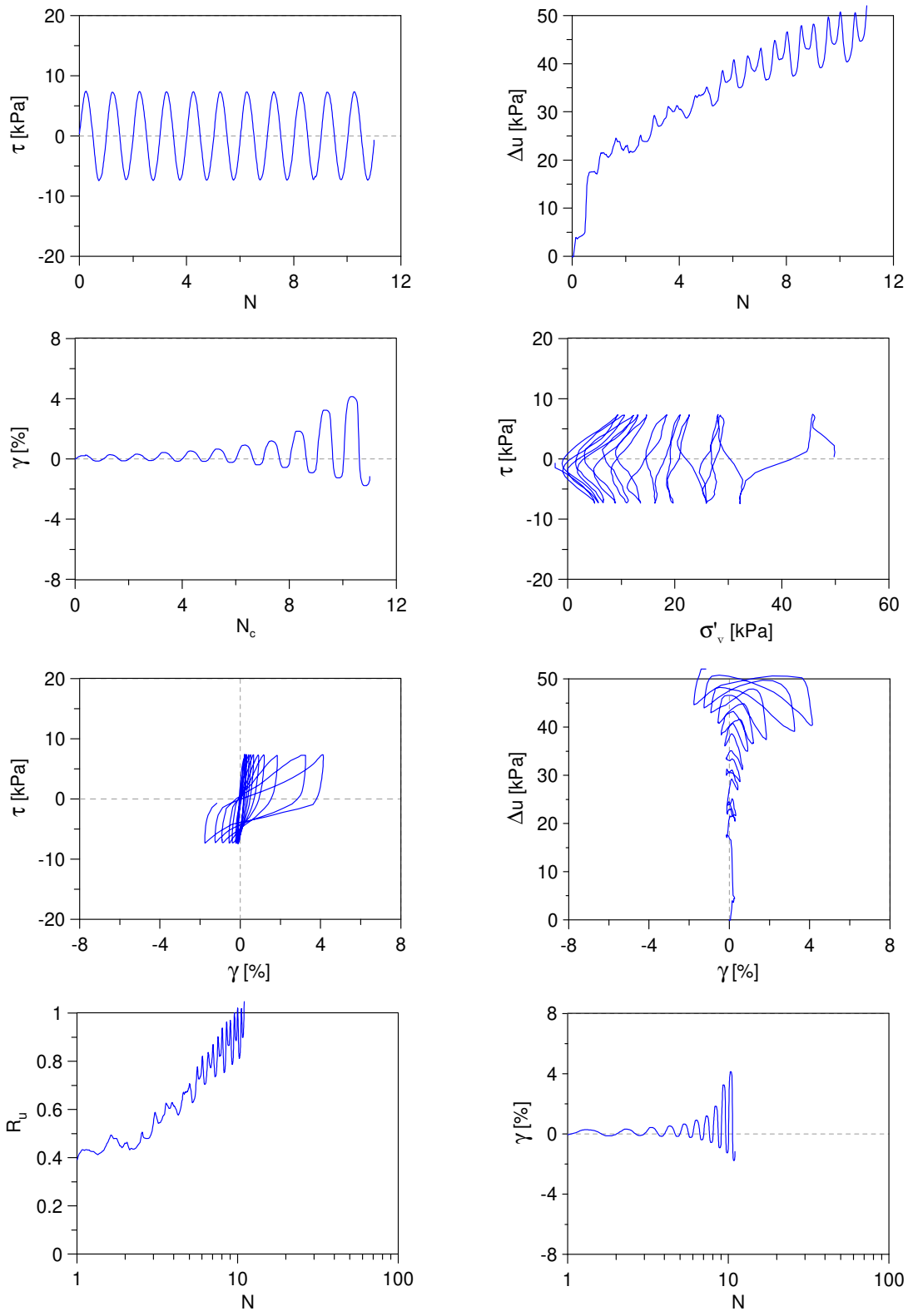

Undrained Cyclic Simple Shear test: *C_SS_TS20_S100_A0_1*
Ticino sand + 20% f_c (Reconstitution method: Moist Tamping)
e_0= 0.68 - D_R= 26% - σ'_{v0}= 100 kPa - α=0 - *CSR* = 0.08

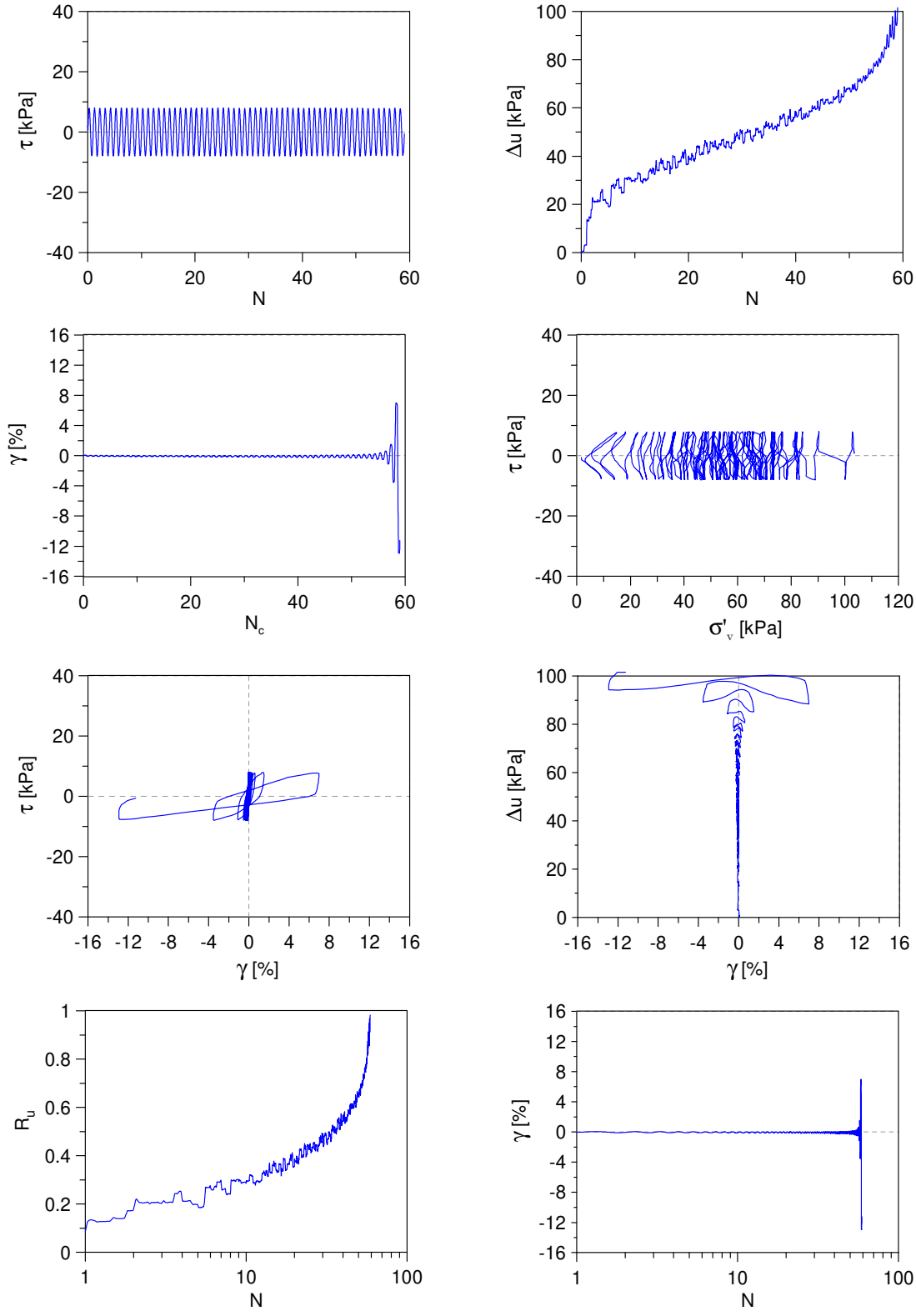

Undrained Cyclic Simple Shear test: *C_SS_TS20_S100_A0_2*
Ticino sand + 20% f_c (Reconstitution method: Moist Tamping)
e_0= 0.68 - D_R= 38% - σ'_{v0}= 100 kPa - α=0 - *CSR* = 0.10

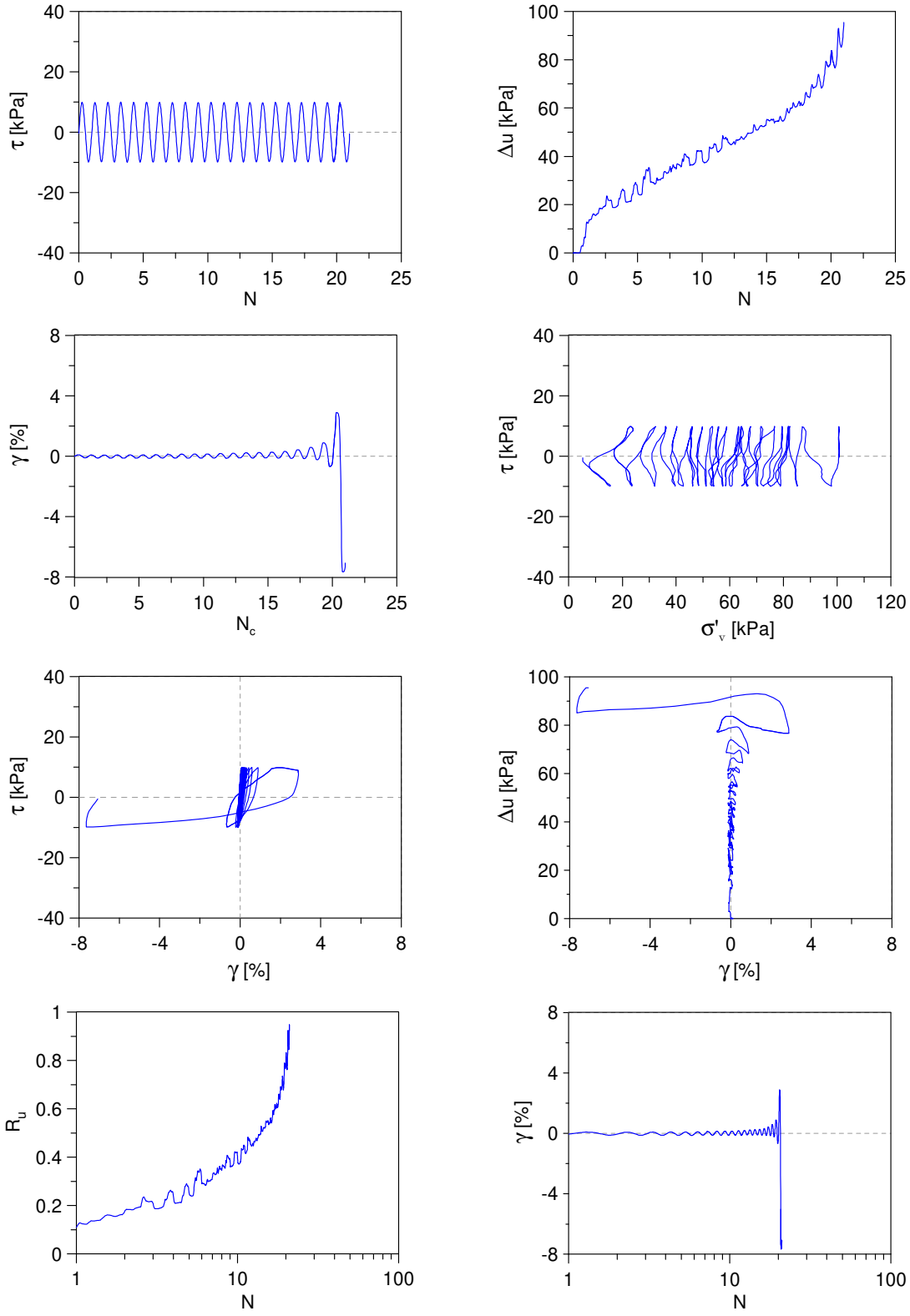

Undrained Cyclic Simple Shear test: *C_SS_TS20_S100_A0_3*
Ticino sand + 20% f_c (Reconstitution method: Moist Tamping)
e_0= 0.68 - D_R= 26% - σ'_{v0}= 100 kPa - α=0 - *CSR* = 0.12

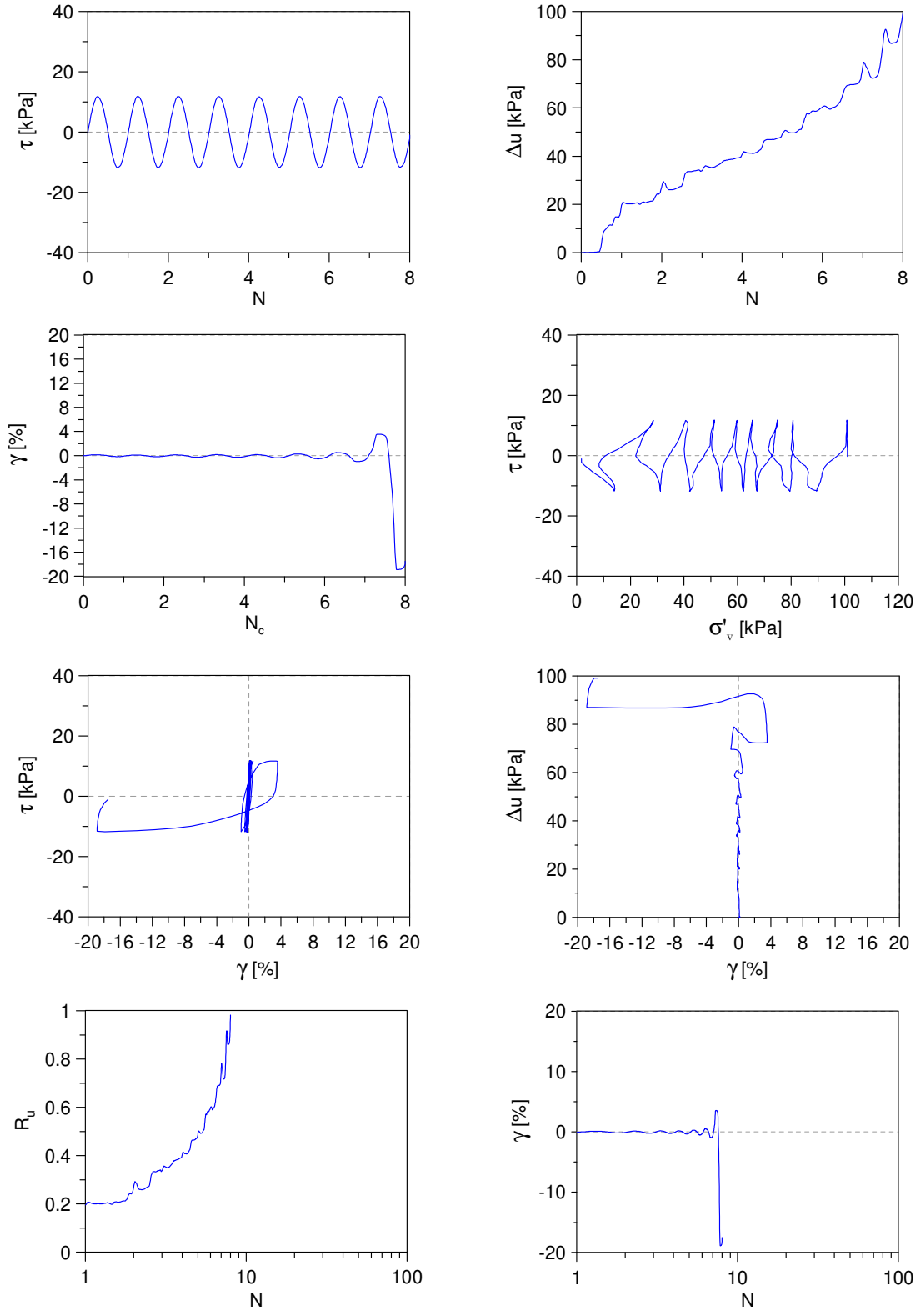

Undrained Cyclic Simple Shear test: *C_SS_TS20_S100_A0_4*
Ticino sand + 20% f_c (Reconstitution method: Moist Tamping)
e_0= 0.58 - D_R= 50% - σ'_{v0}= 100 kPa - α=0 - *CSR* = 0.12

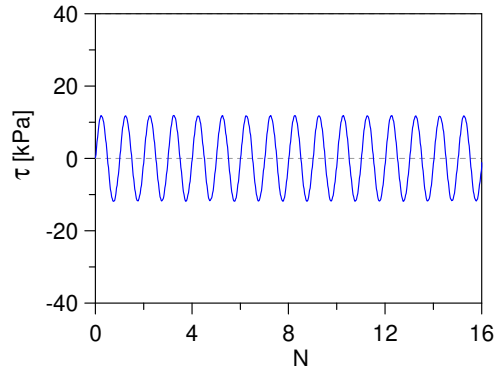

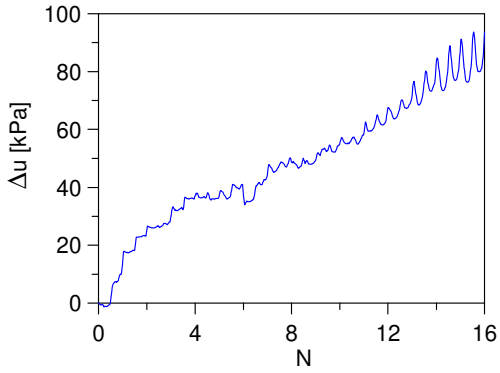

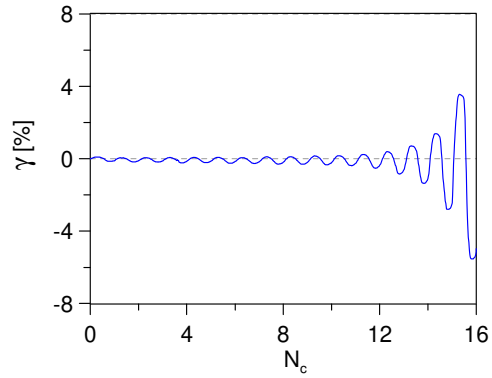

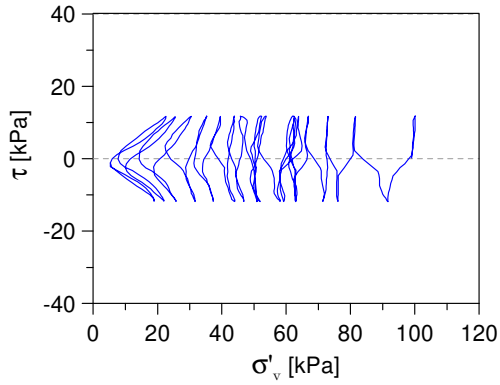

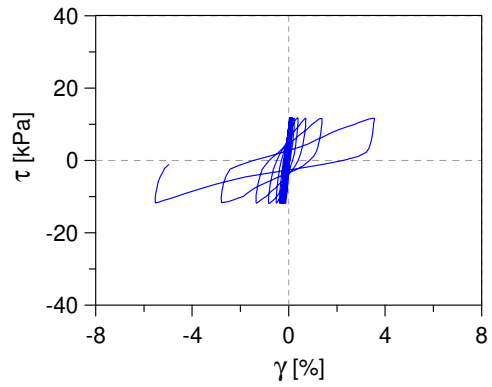

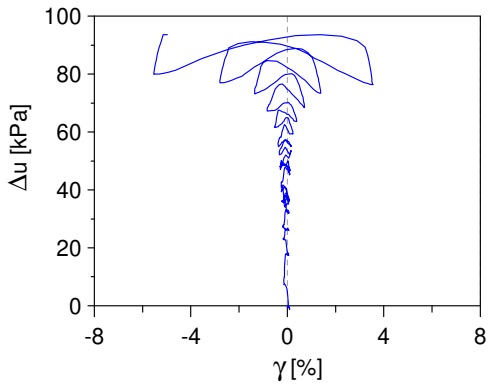

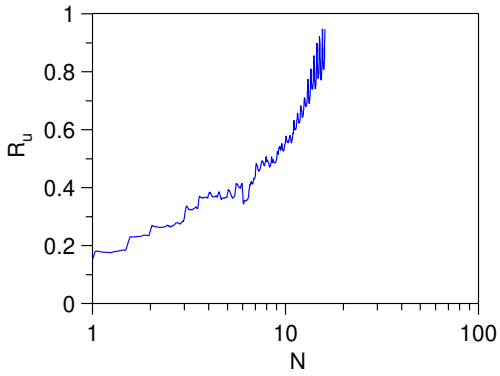

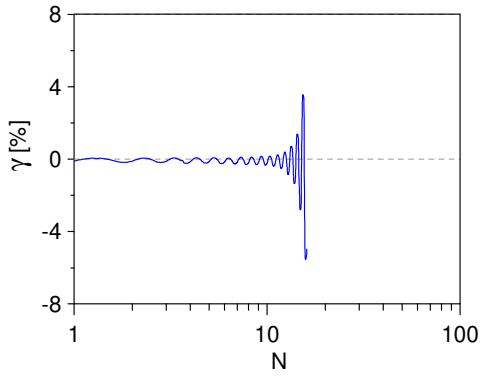

Undrained Cyclic Simple Shear test: *C_SS_TS20_S100_A0_5*
Ticino sand + 20% f_c (Reconstitution method: Moist Tamping)
e_0= 0.58 - D_R= 50% - σ'_{v0}= 100 kPa - α=0 - *CSR* = 0.14

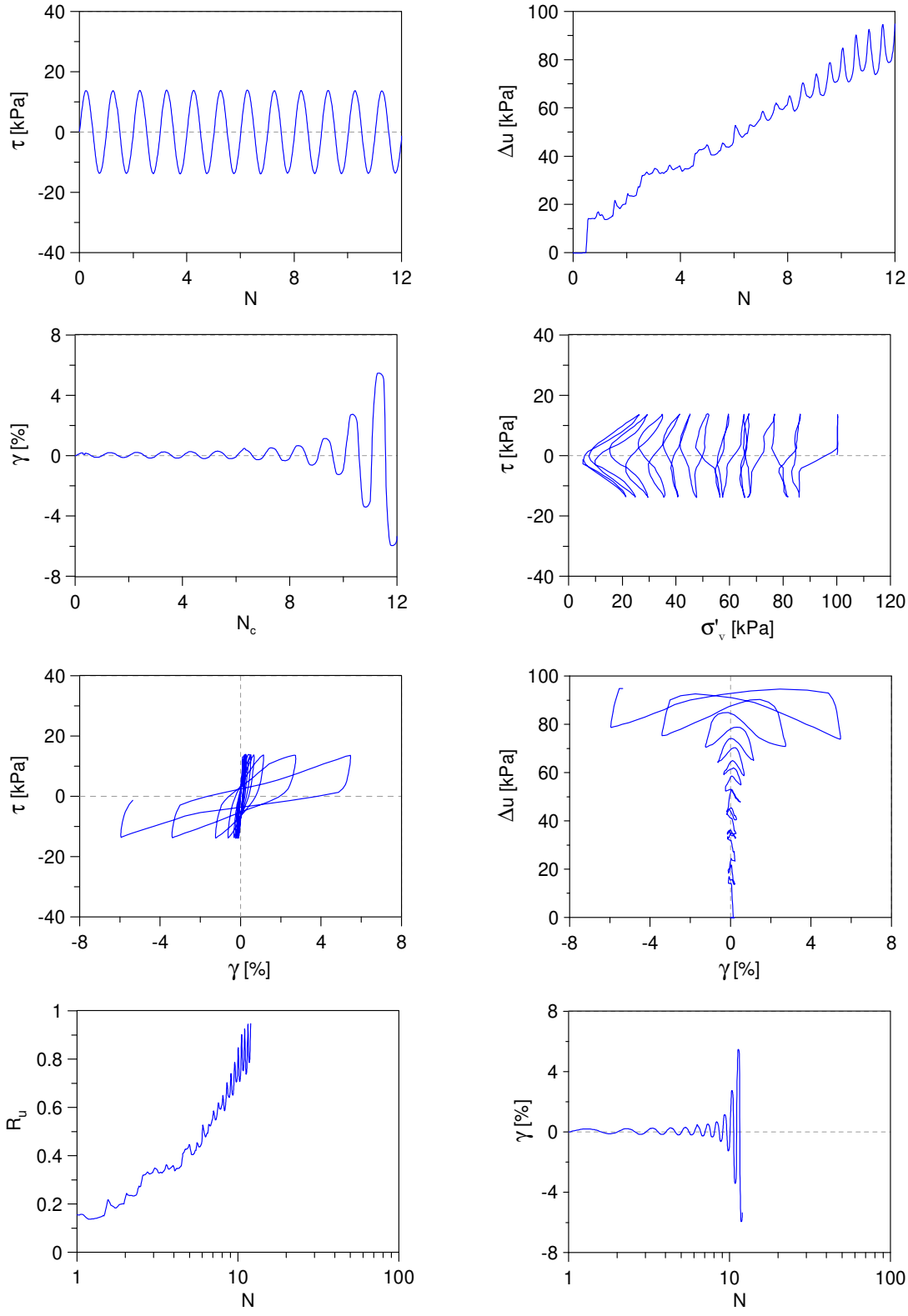

Undrained Cyclic Simple Shear test: *C_SS_TS20_S100_A0_6*
Ticino sand + 20% f_c (Reconstitution method: Moist Tamping)
e_0= 0.58 - D_R= 50% - σ'_{v0}= 100 kPa - α=0 - *CSR* = 0.16

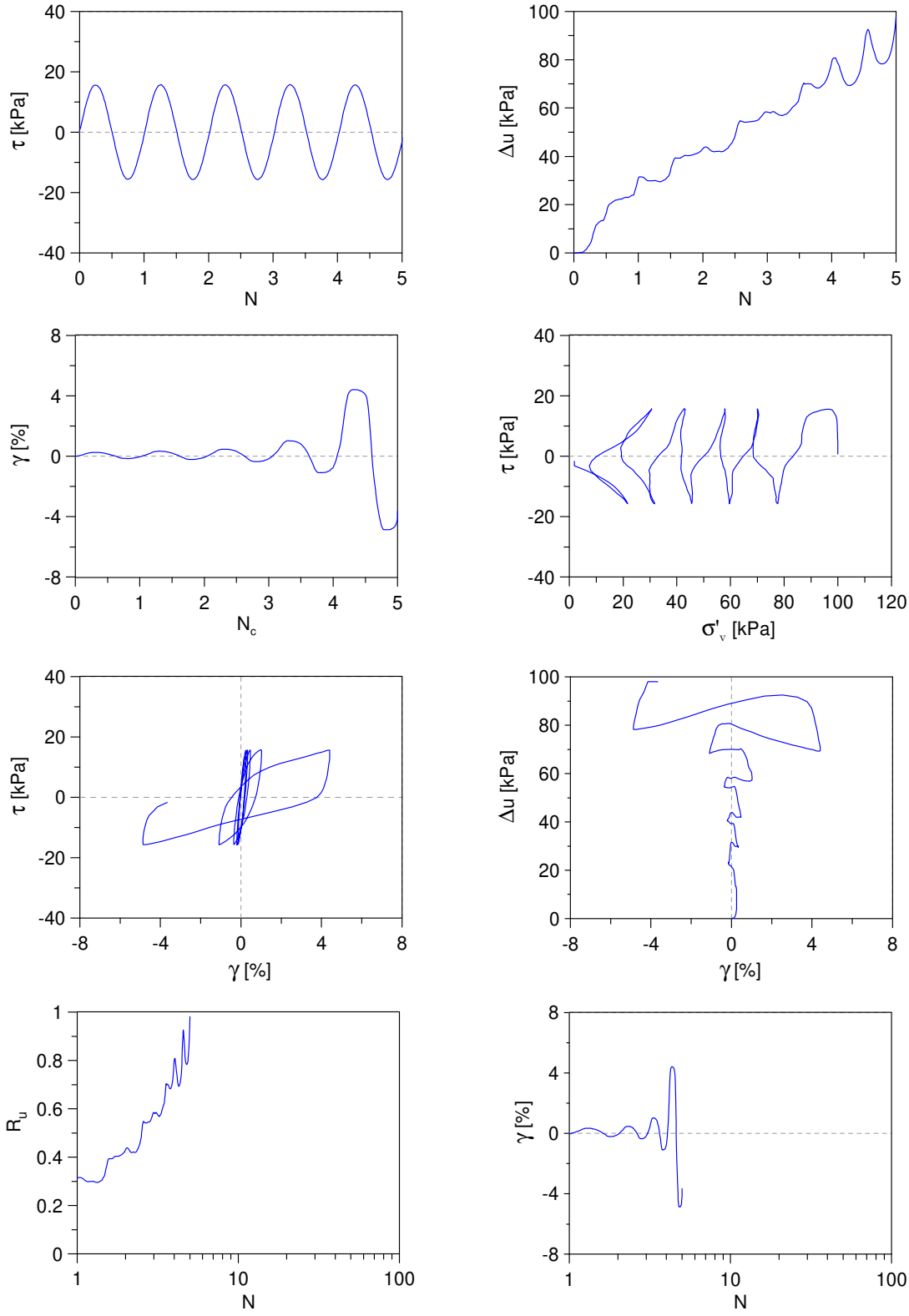

Undrained Cyclic Simple Shear test: *C_SS_TS20_S100_A0_7*
Ticino sand + 20% f_c (Reconstitution method: Moist Tamping)
e_0= 0.55 - D_R= 57% - σ'_{v0}= 100 kPa - α=0 - *CSR* = 0.14

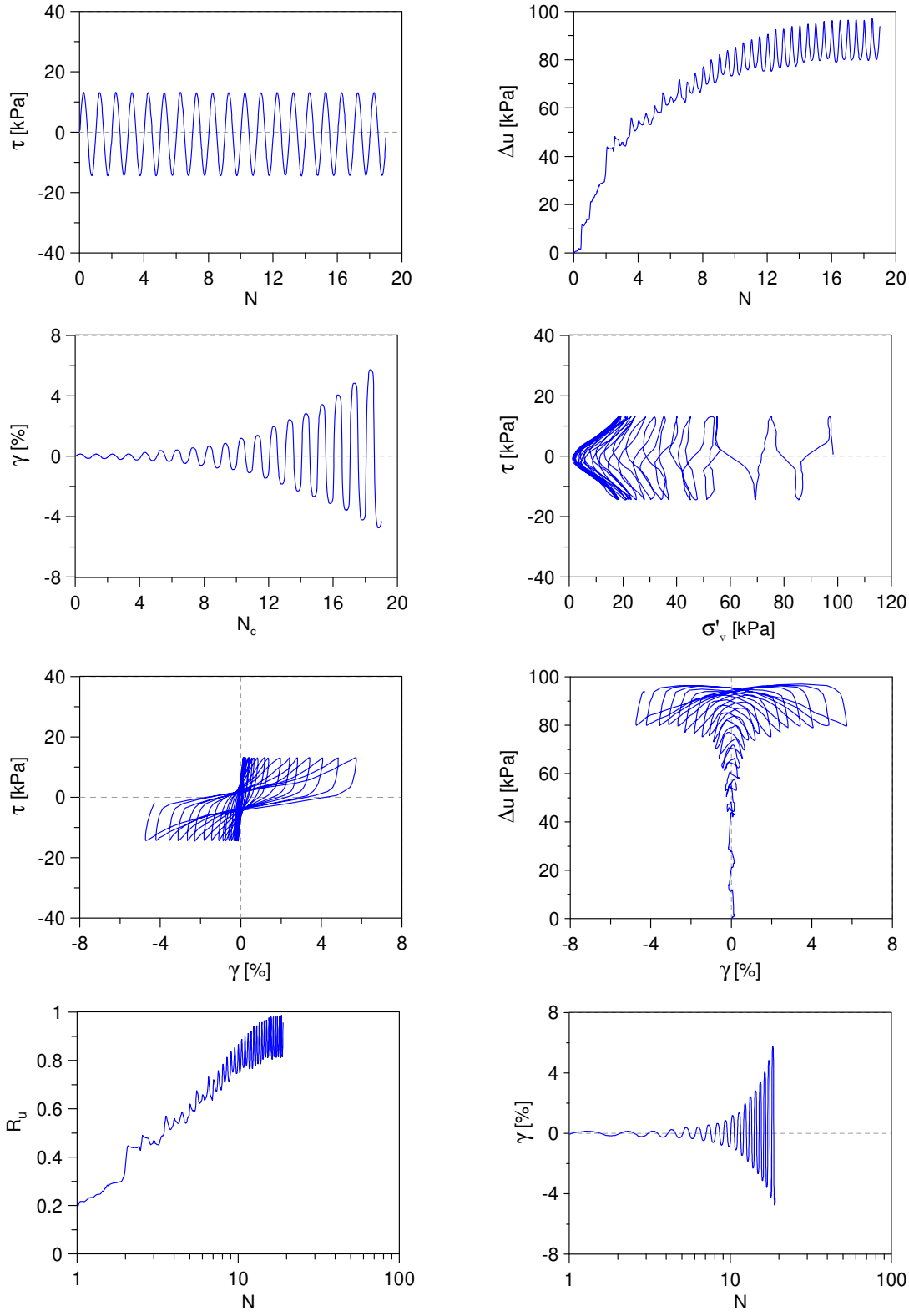

Undrained Cyclic Simple Shear test: *C_SS_TS20_S100_A0_8*
Ticino sand + 20% f_c (Reconstitution method: Moist Tamping)
e_0= 0.55 - D_R= 57% - σ'_{v0}= 100 kPa - α=0 - *CSR* = 0.16

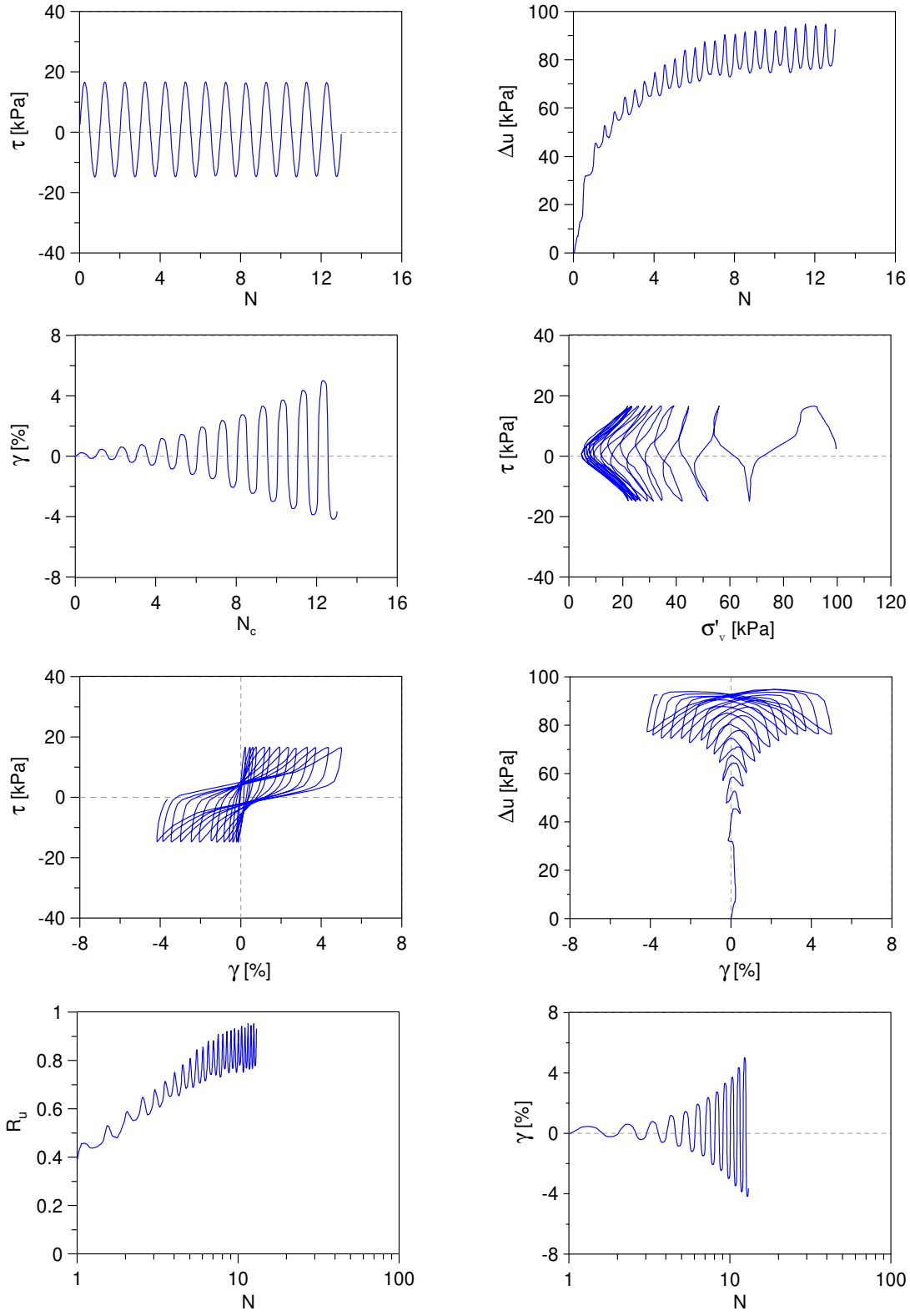

Undrained Cyclic Simple Shear test: *C_SS_TS20_S100_A0_9*
Ticino sand + 20% f_c (Reconstitution method: Moist Tamping)
e_0= 0.55 - D_R= 57% - σ'_{v0}= 100 kPa - α=0 - *CSR* = 0.20

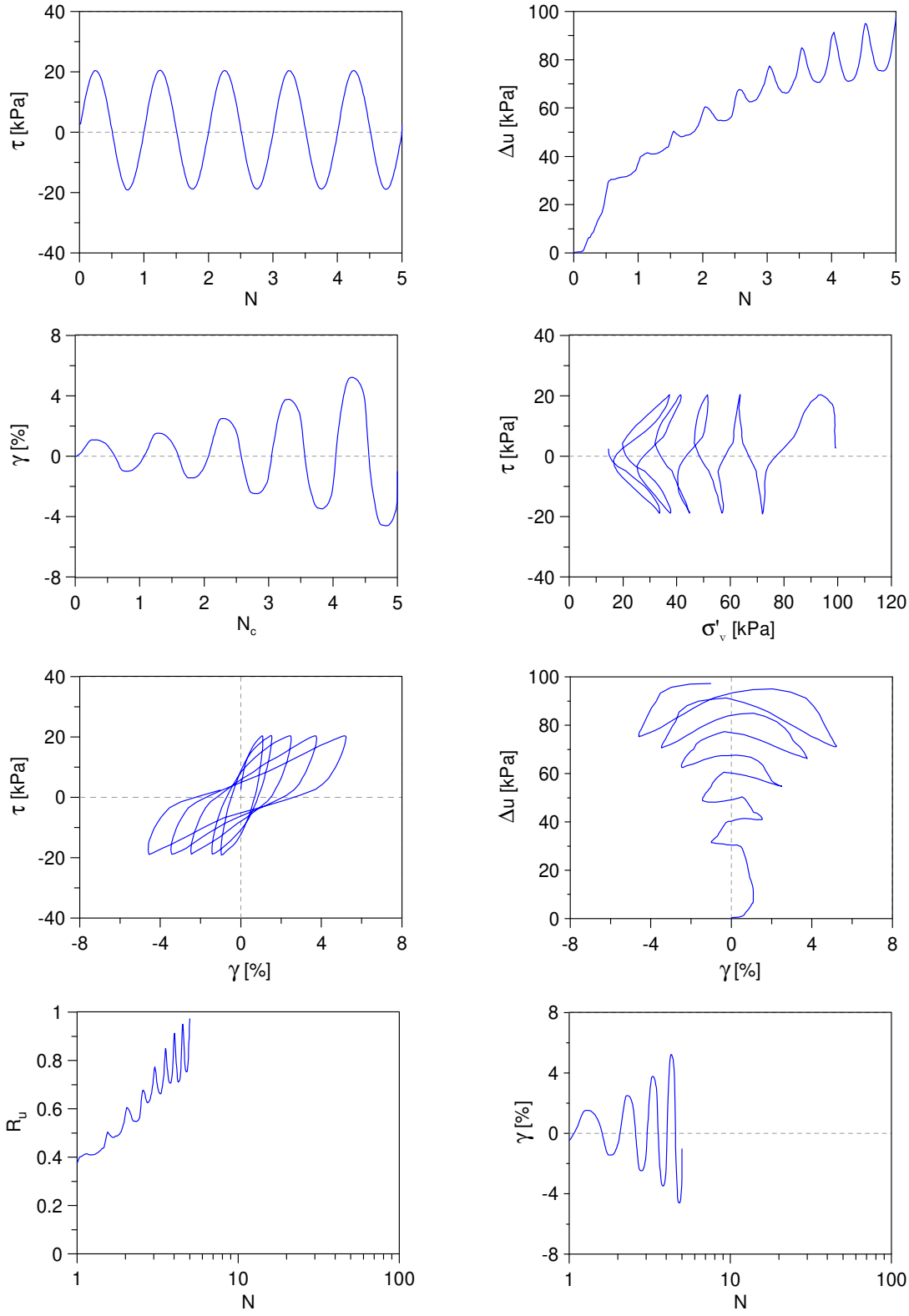

Undrained Cyclic Simple Shear test: *C_SS_TS20_S100_A0_10*
Ticino sand + 20% f_c (Reconstitution method: Moist Tamping)
e_0= 0.51 - D_R= 67% - σ'_{v0}= 100 kPa - α=0 - *CSR* = 0.14

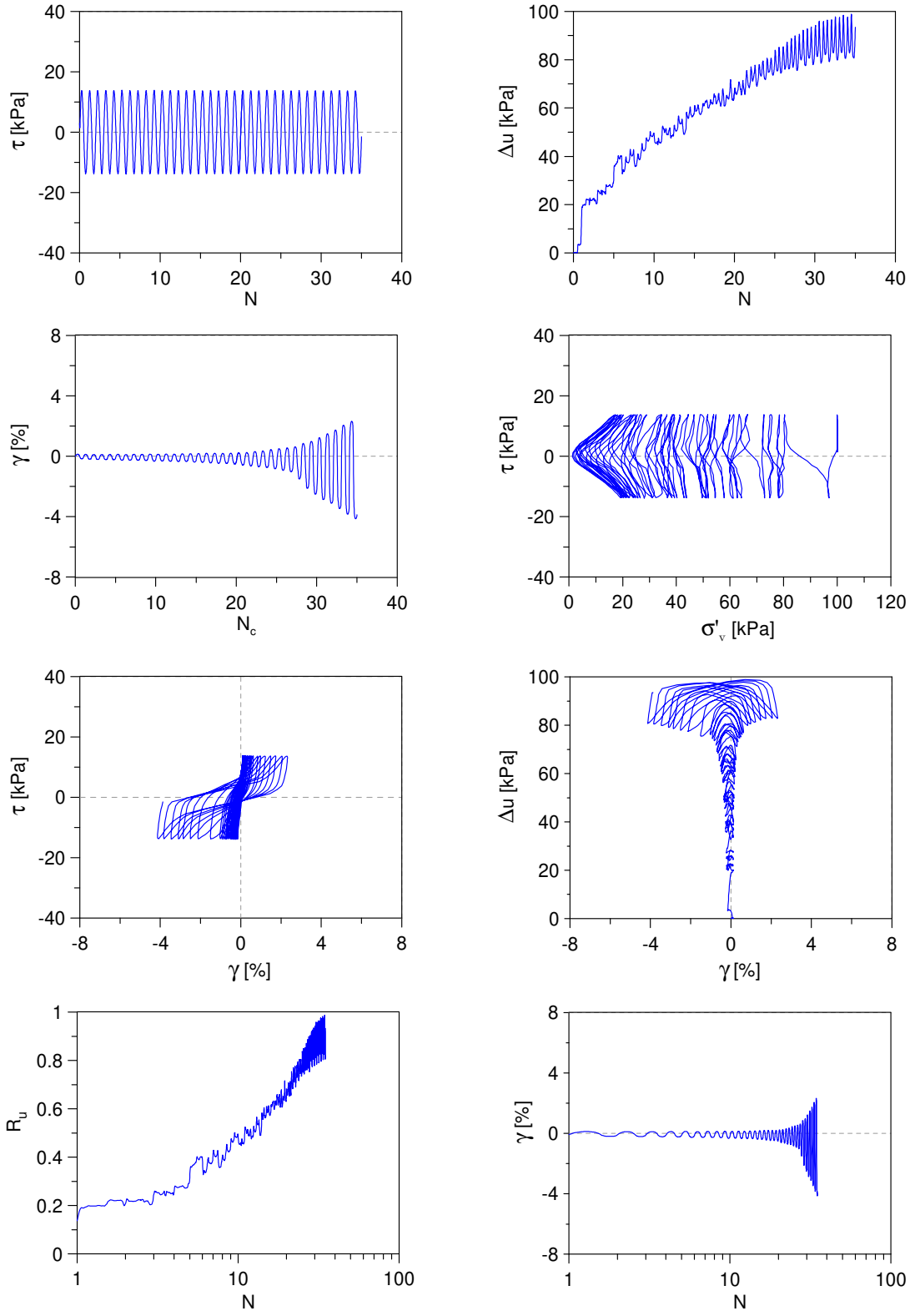

Undrained Cyclic Simple Shear test: *C_SS_TS20_S100_A0_11*
Ticino sand + 20% f_c (Reconstitution method: Moist Tamping)
e_0= 0.51 - D_R= 67% - σ'_{v0}= 100 kPa - α=0 - *CSR* = 0.16

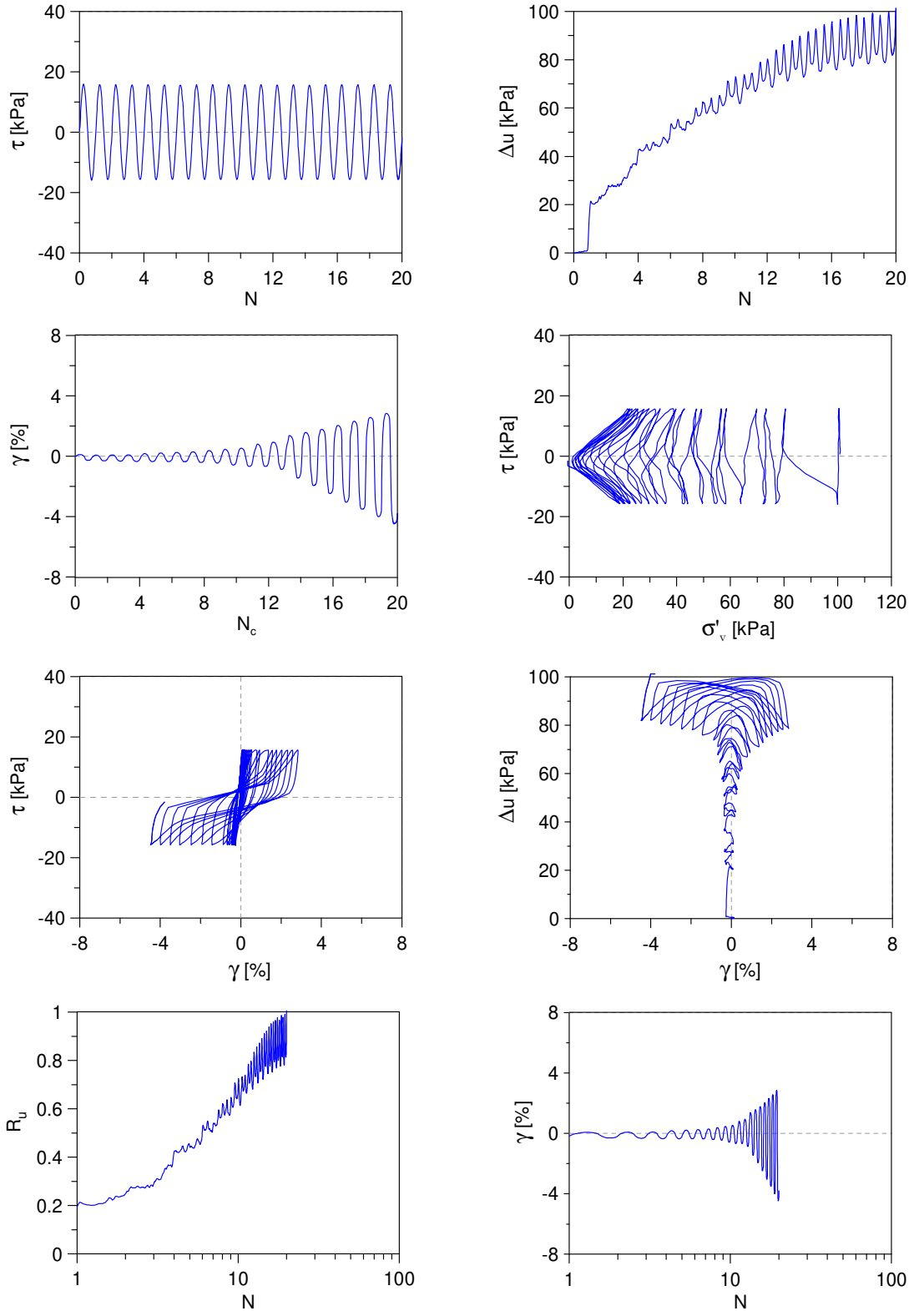

Undrained Cyclic Simple Shear test: *C_SS_TS20_S100_A0_12*
Ticino sand + 20% f_c (Reconstitution method: Moist Tamping)
e_0= 0.51 - D_R= 67% - σ'_{v0}= 100 kPa - α=0 - *CSR* = 0.18

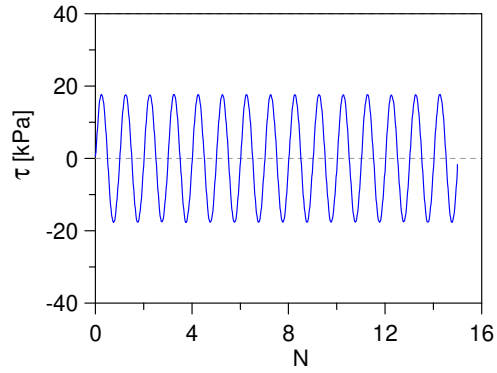

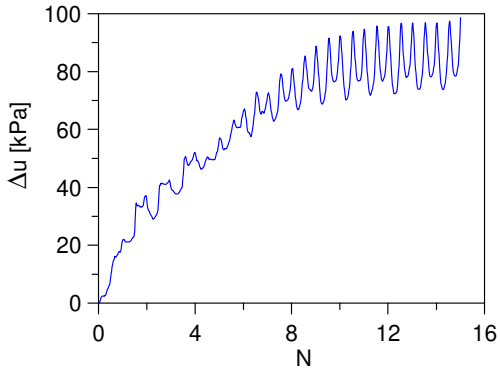

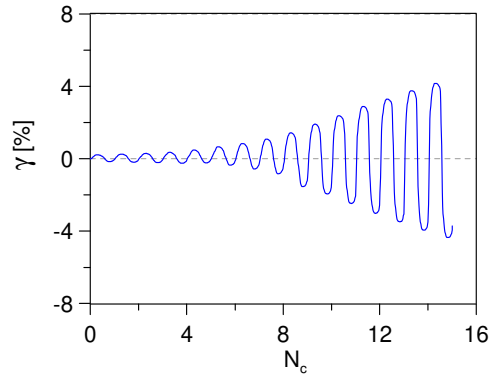

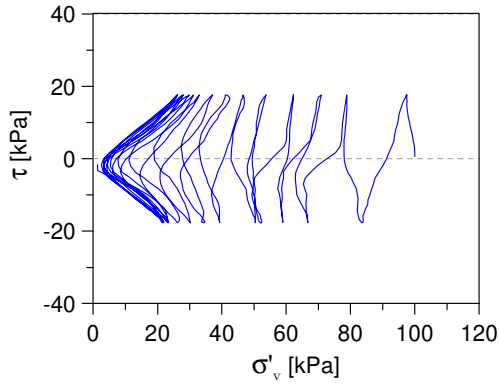

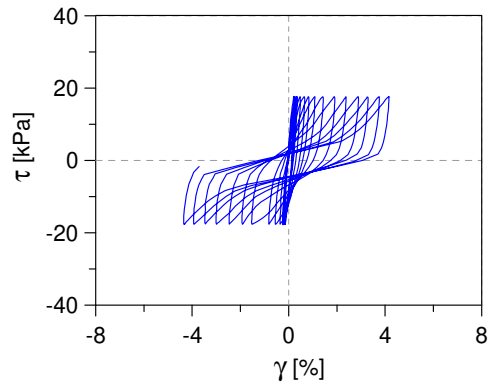

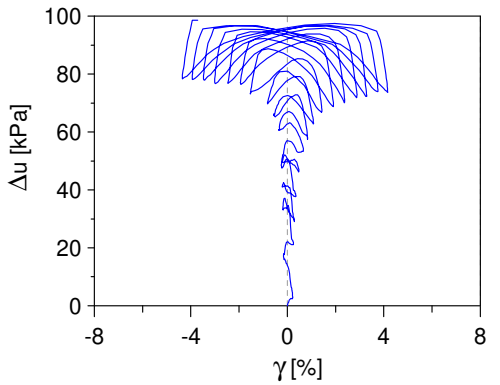

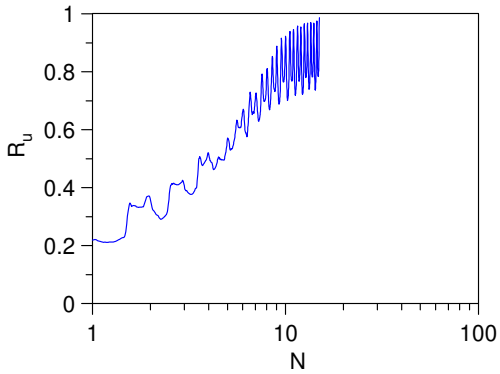

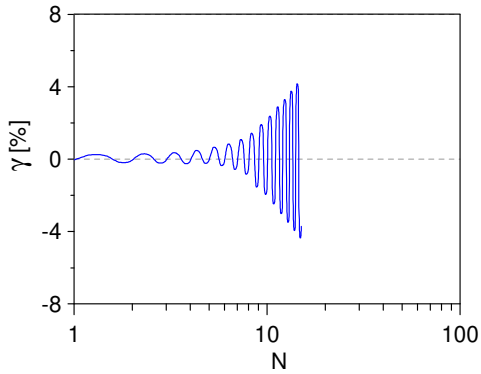

Undrained Cyclic Simple Shear test: *C_SS_TS20_S100_A0_13*
Ticino sand + 20% f_c (Reconstitution method: Moist Tamping)
e_0= 0.51 - D_R= 67% - σ'_{v0}= 100 kPa - α=0 - *CSR* = 0.19

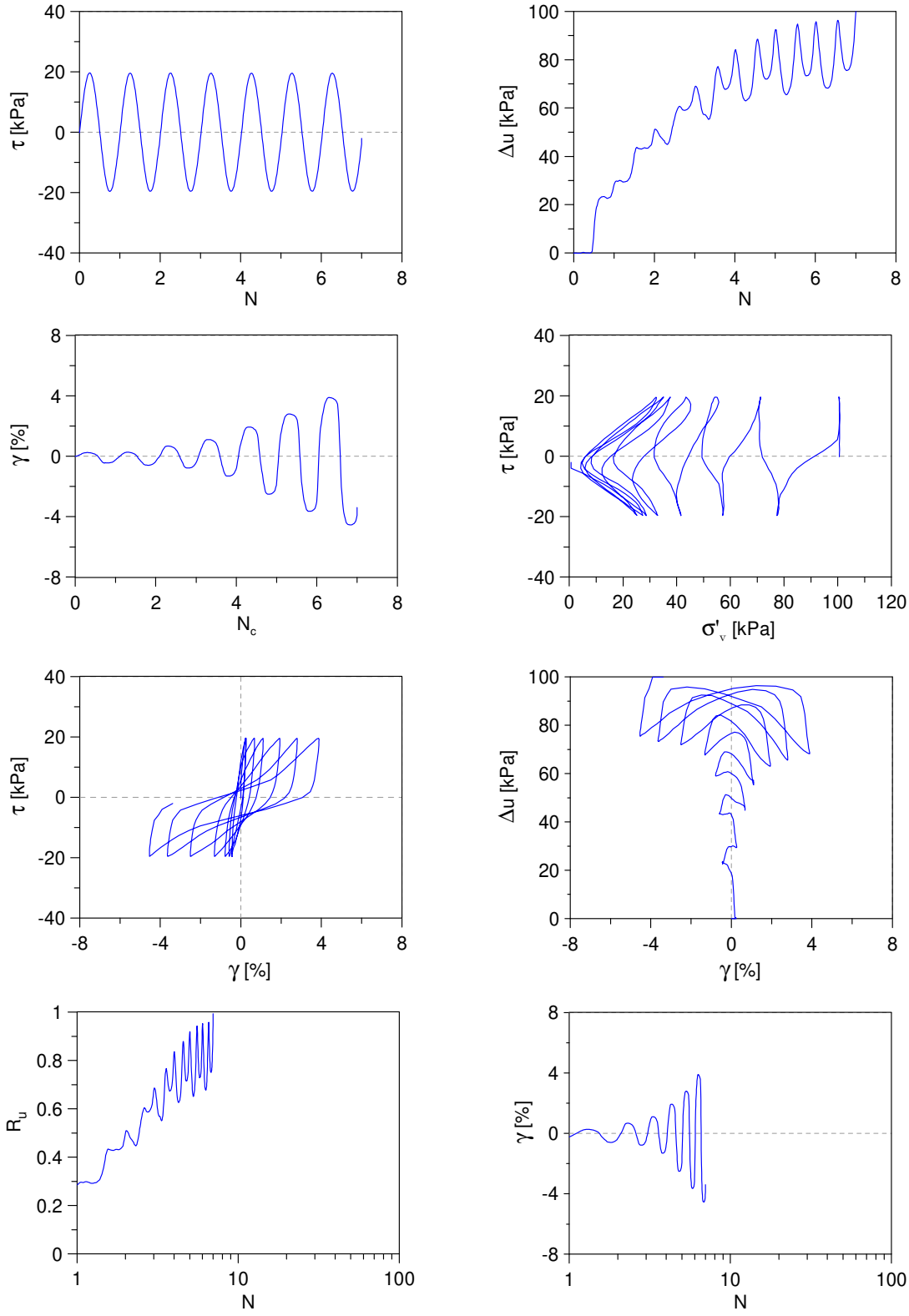

Undrained Cyclic Simple Shear test: *C_SS_TS20_S100_A1_1*
Ticino sand + 20% f_c (Reconstitution method: Moist Tamping)
e_0= 0.68 - D_R= 26% - σ'_{v0}= 100 kPa - α= 0.1 - *CSR* = 0.04

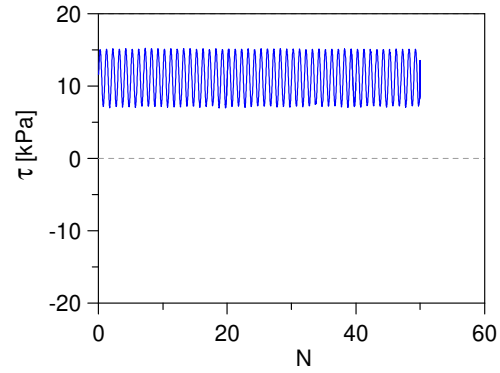

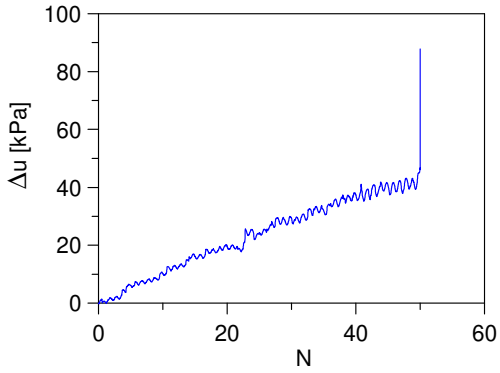

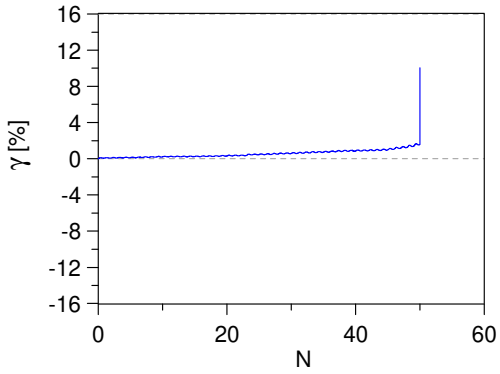

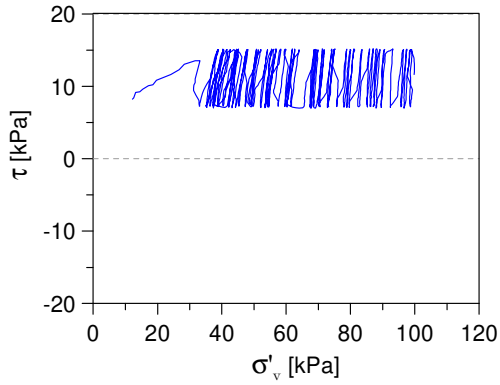

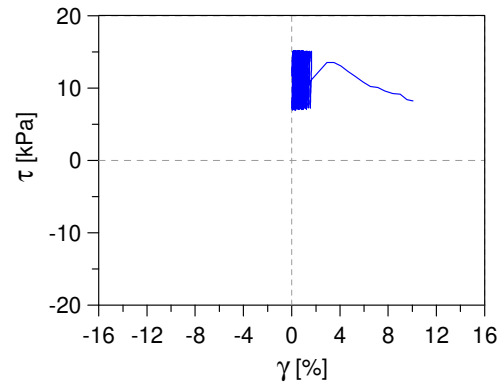

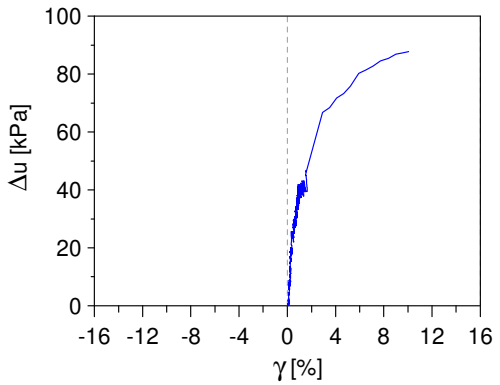

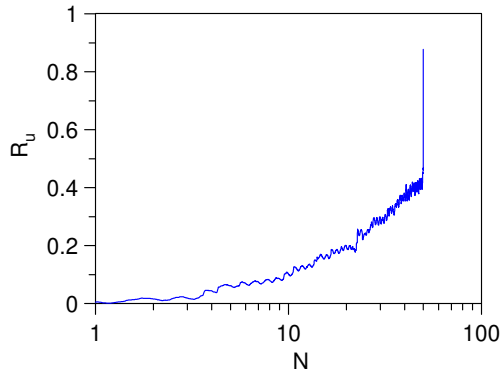

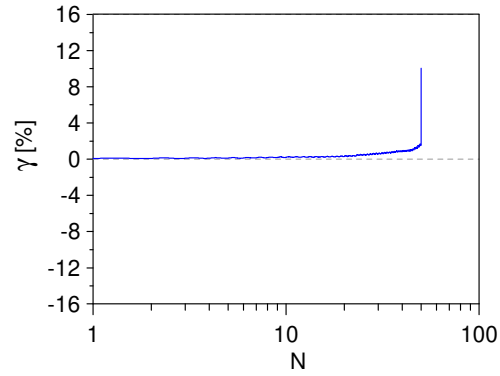

Undrained Cyclic Simple Shear test: *C_SS_TS20_S100_A1_2*
Ticino sand + 20% f_c (Reconstitution method: Moist Tamping)
e_0= 0.68 - D_R= 26% - σ'_{v0}= 100 kPa - α= 0.1 - *CSR* = 0.07

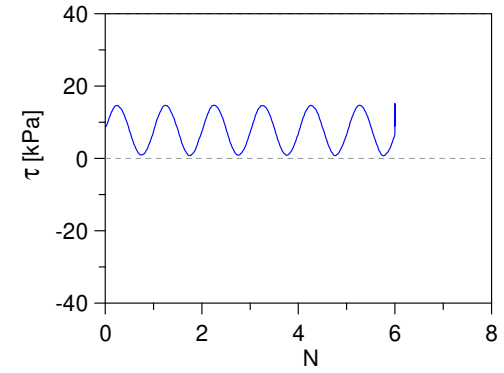

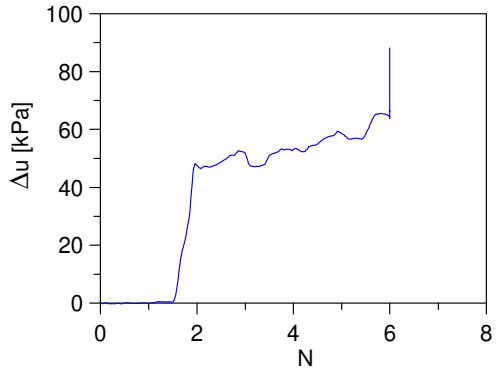

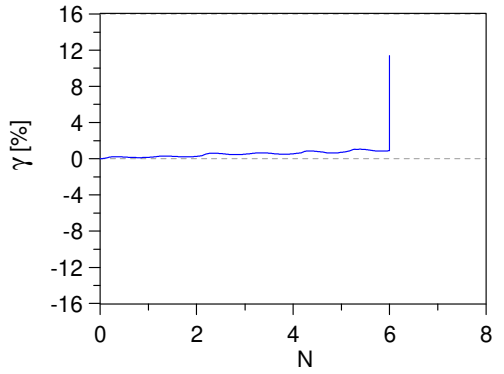

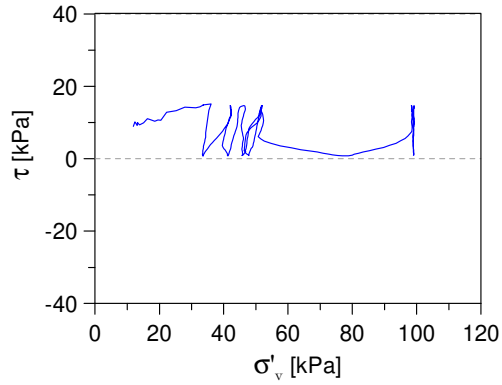

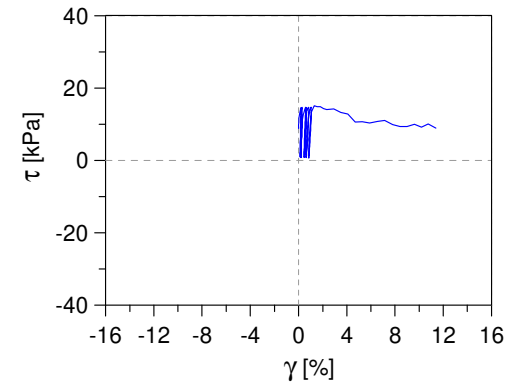

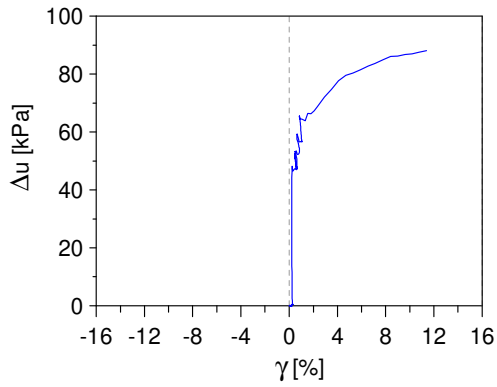

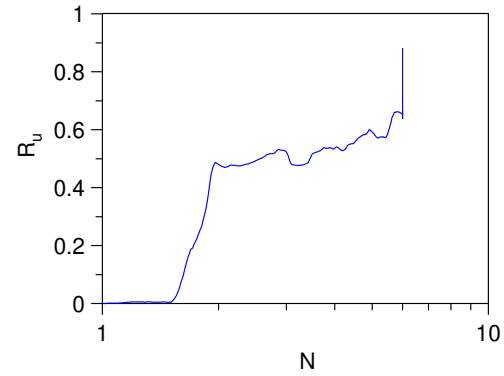

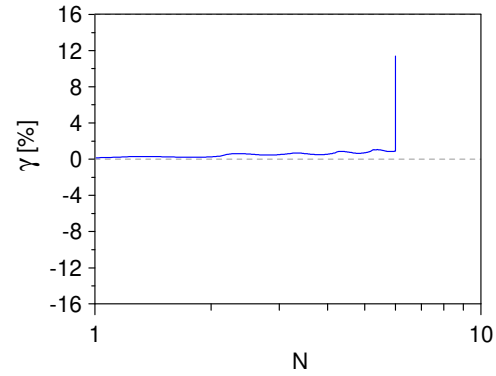

Undrained Cyclic Simple Shear test: *C_SS_TS20_S100_A1_3*
Ticino sand + 20% f_c (Reconstitution method: Moist Tamping)
e_0= 0.68 - D_R= 26% - σ'_{v0}= 100 kPa - α= 0.1 - *CSR* = 0.10

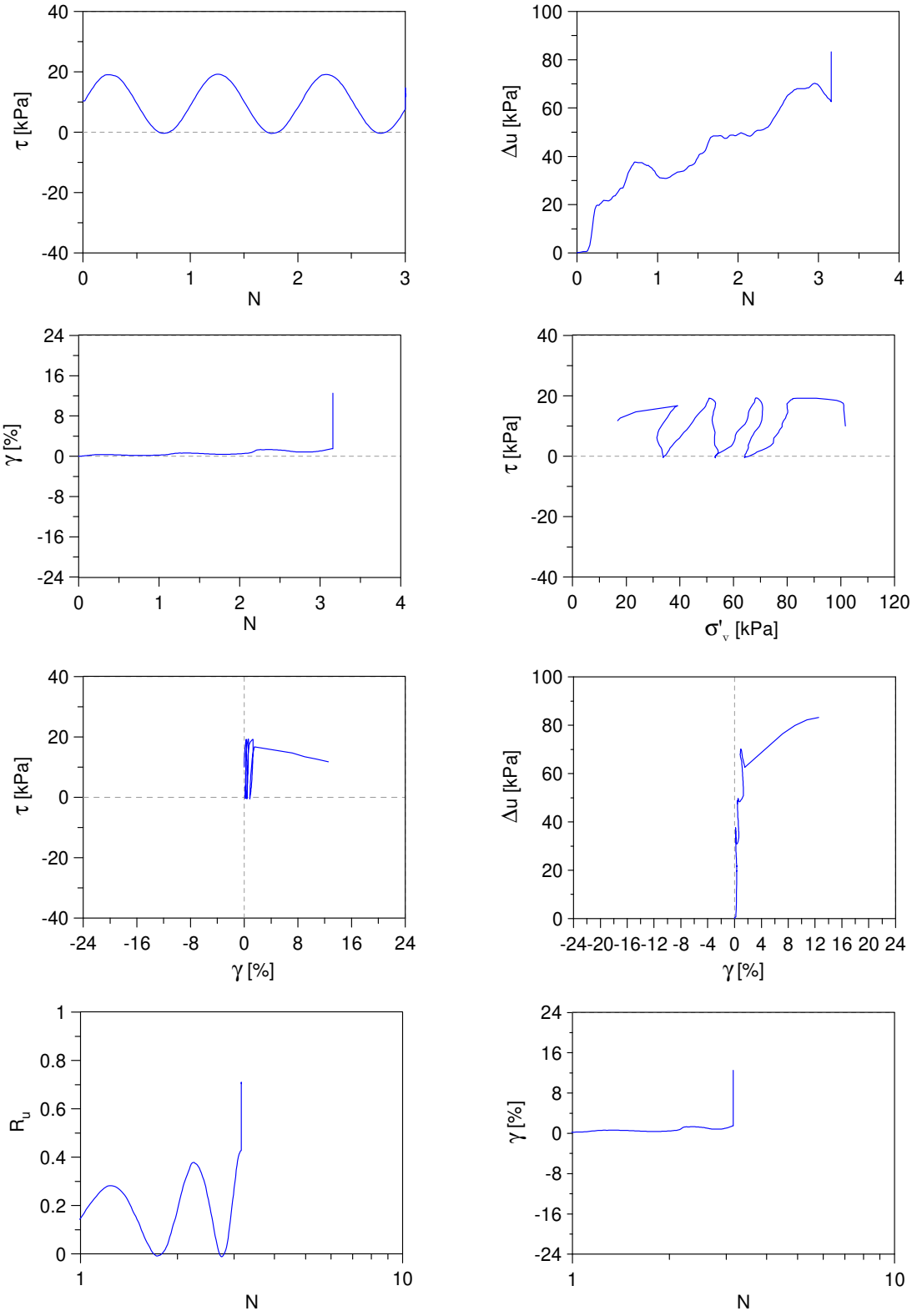

Undrained Cyclic Simple Shear test: *C_SS_TS20_S100_A1_4*
Ticino sand + 20% f_c (Reconstitution method: Moist Tamping)
e_0= 0.59 - D_R= 48% - σ'_{v0}= 100 kPa - α= 0.1 - *CSR* = 0.10

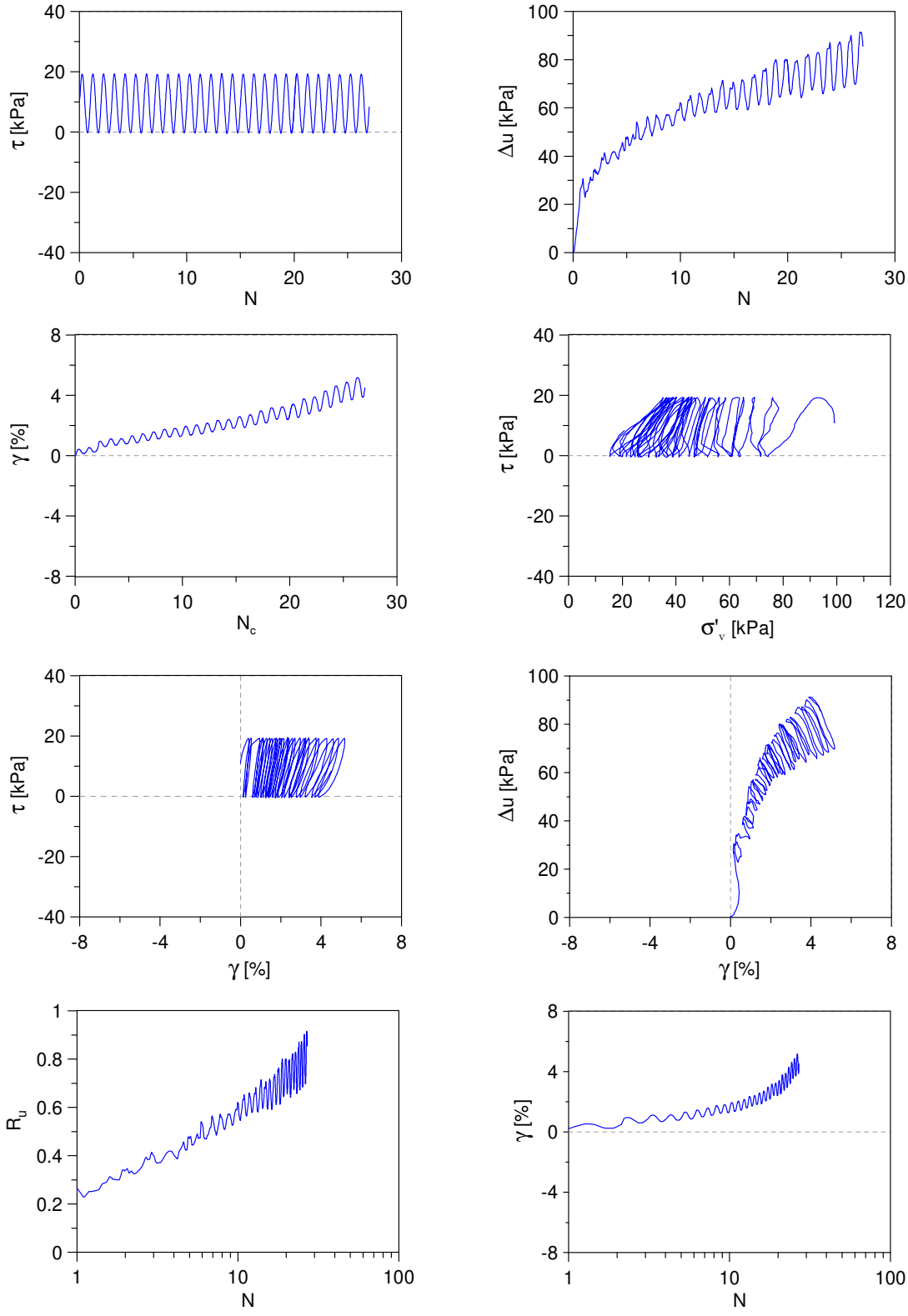

Undrained Cyclic Simple Shear test: *C_SS_TS20_S100_A1_5*
Ticino sand + 20% f_c (Reconstitution method: Moist Tamping)
e_0= 0.59 - D_R= 48% - σ'_{v0}= 100 kPa - α= 0.1 - *CSR* = 0.12

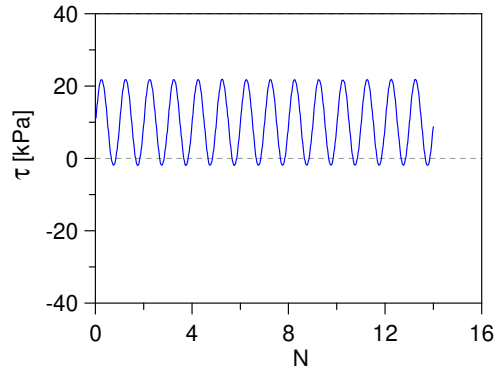

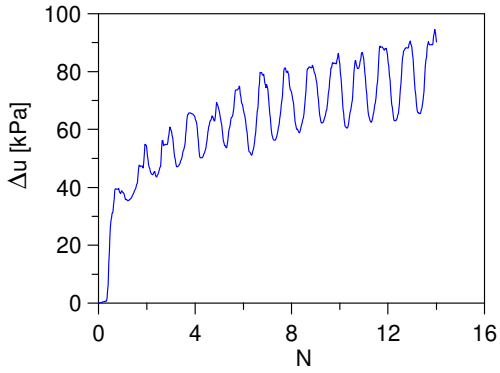

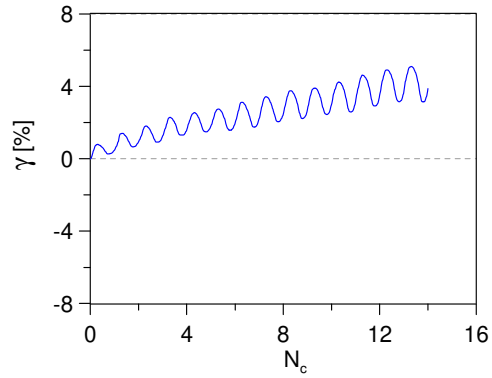

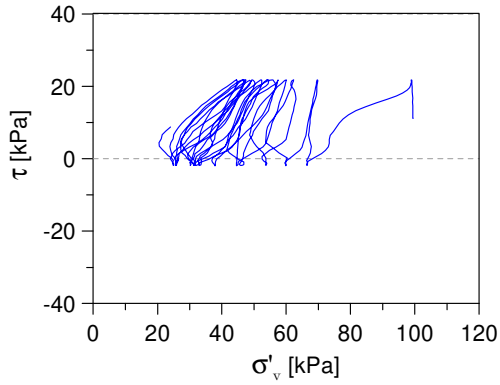

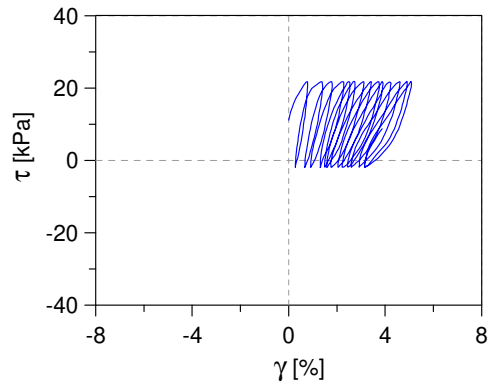

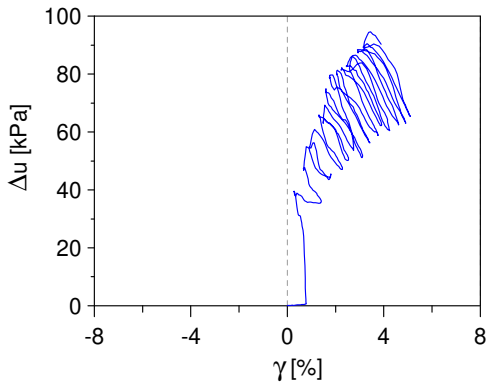

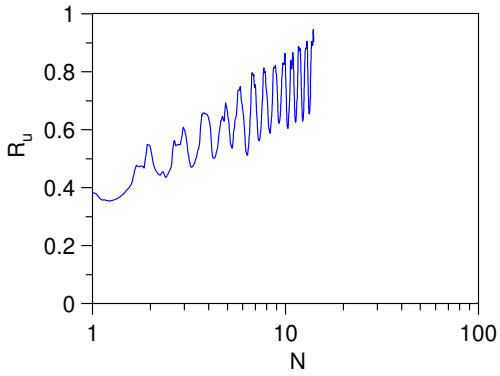

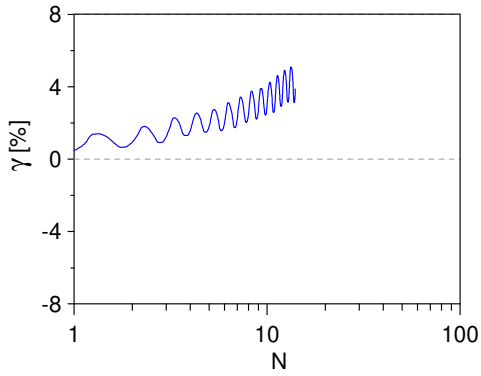

Undrained Cyclic Simple Shear test: *C_SS_TS20_S100_A1_6*
Ticino sand + 20% f_c (Reconstitution method: Moist Tamping)
e_0= 0.55 - D_R= 57% - σ'_{v0}= 100 kPa - α= 0.1 - *CSR* = 0.14

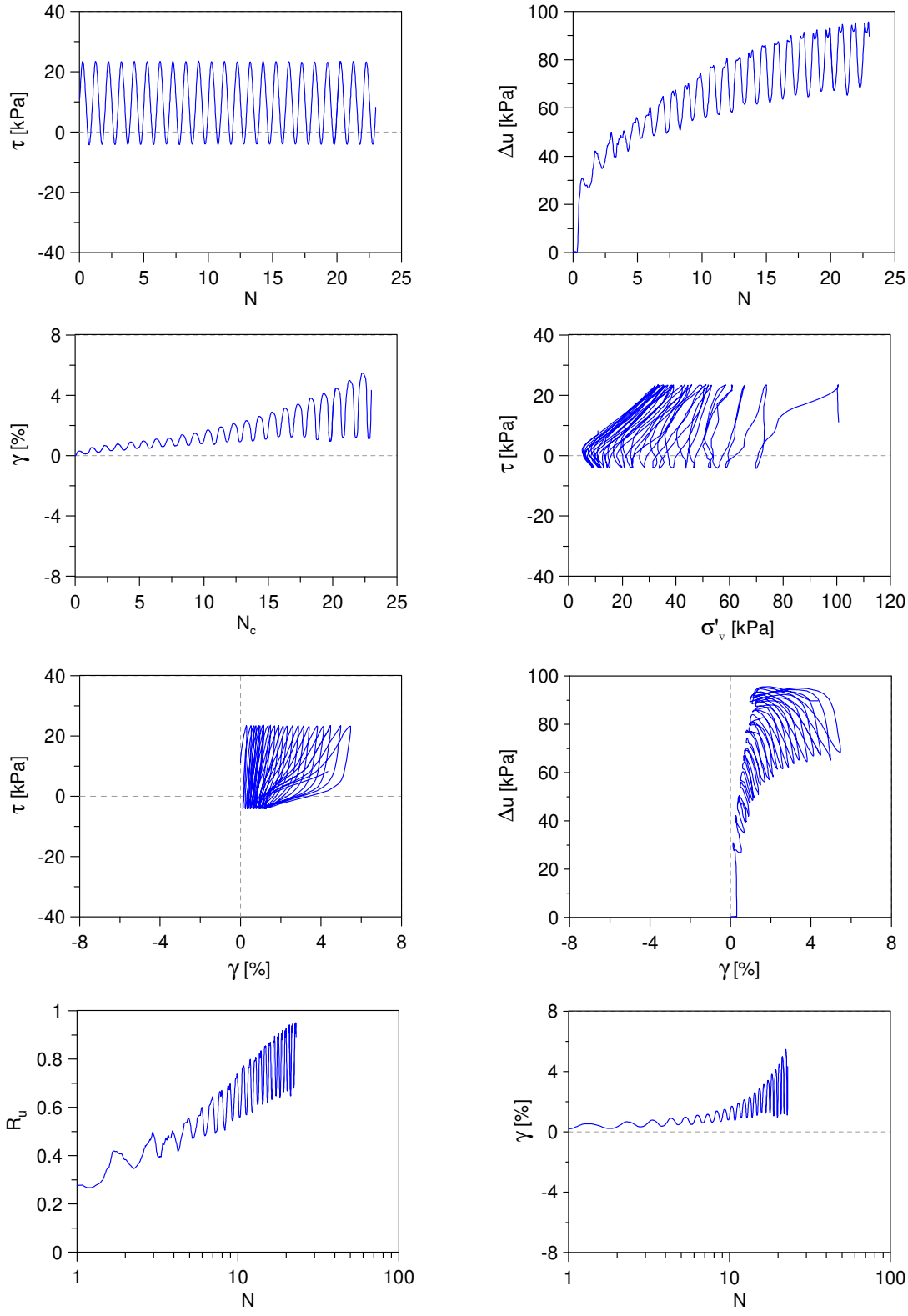

Undrained Cyclic Simple Shear test: *C_SS_TS20_S100_A1_7*
Ticino sand + 20% f_c (Reconstitution method: Moist Tamping)
e_0= 0.55 - D_R= 57% - σ'_{v0}= 100 kPa - α= 0.1 - *CSR* = 0.16

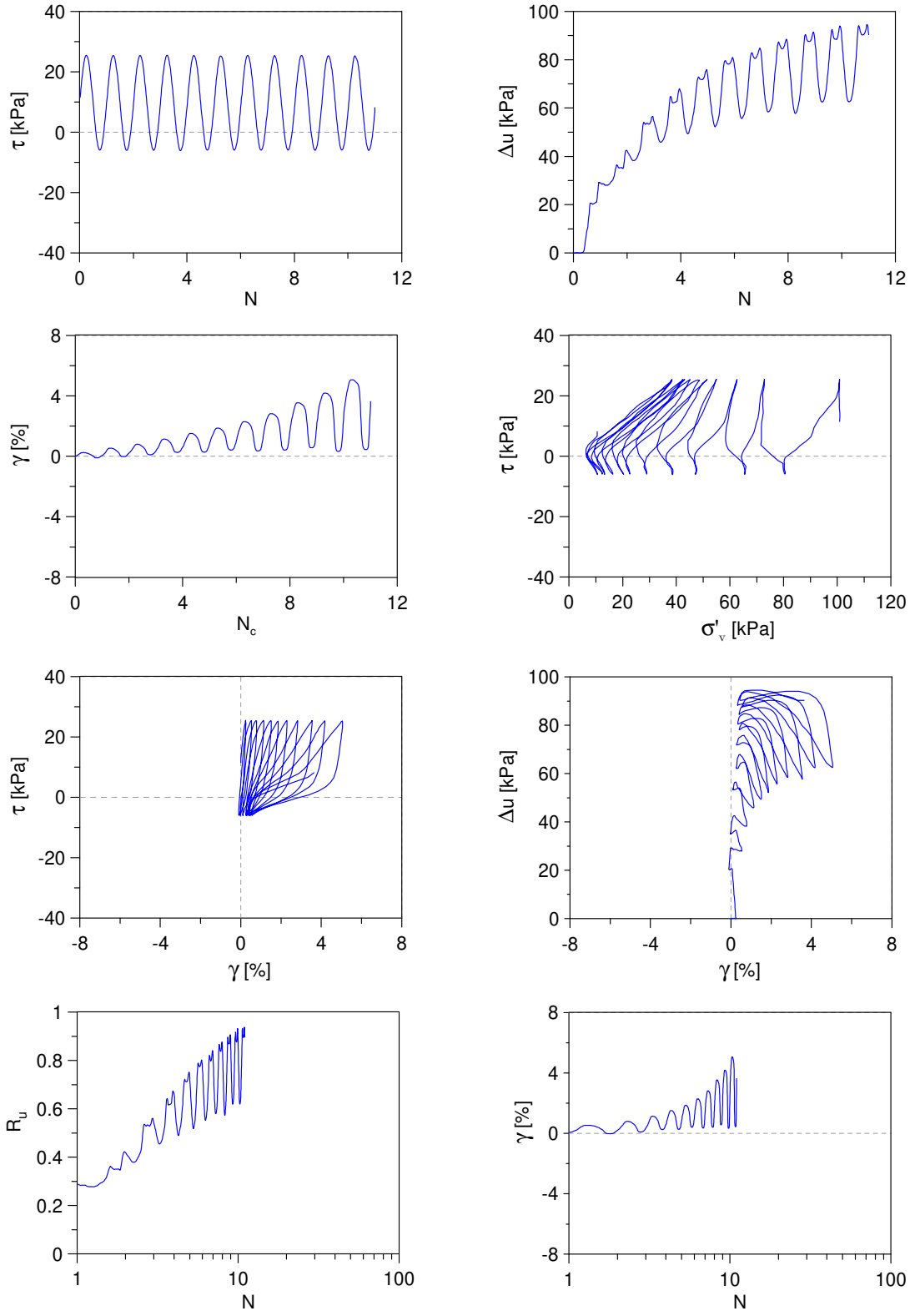

Undrained Cyclic Simple Shear test: *C_SS_TS20_S100_A1_8*
Ticino sand + 20% f_c (Reconstitution method: Moist Tamping)
e_0= 0.55 - D_R= 57% - σ'_{v0}= 100 kPa - α= 0.1 - *CSR* = 0.20

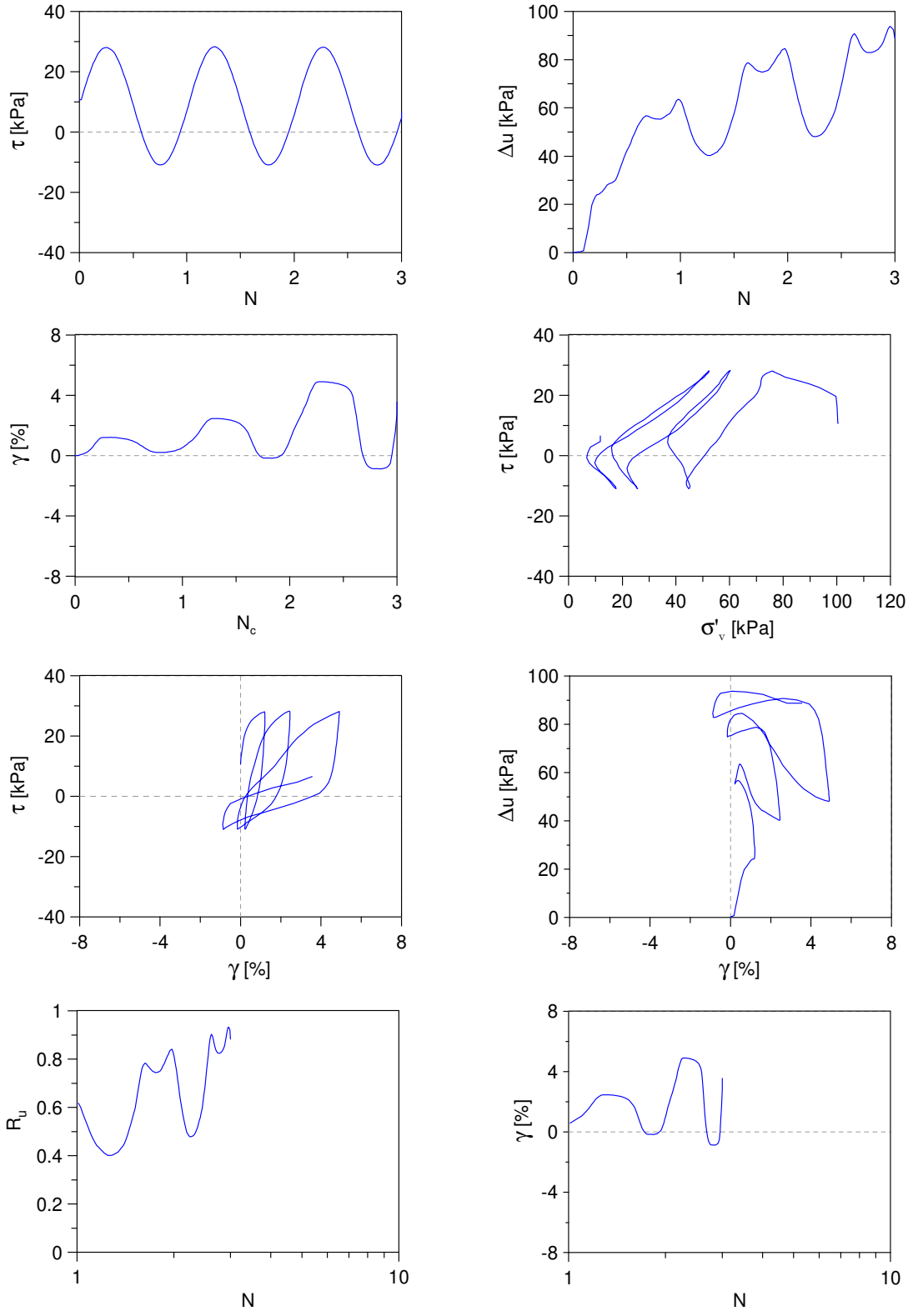

Undrained Cyclic Simple Shear test: *C_SS_TS20_S100_A2_1*
Ticino sand + 20% f_c (Reconstitution method: Moist Tamping)
e_0= 0.59 - D_R= 48% - σ'_{v0}= 100 kPa - α= 0.2 - *CSR* = 0.08

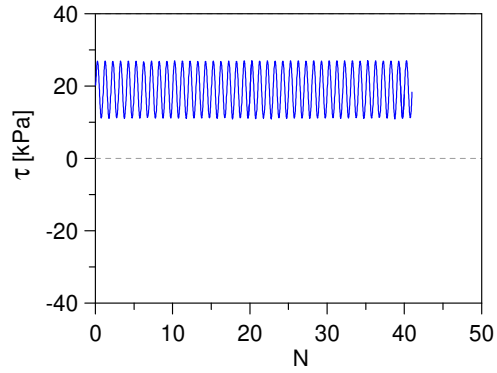

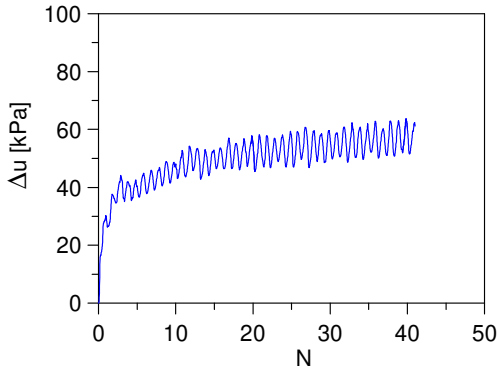

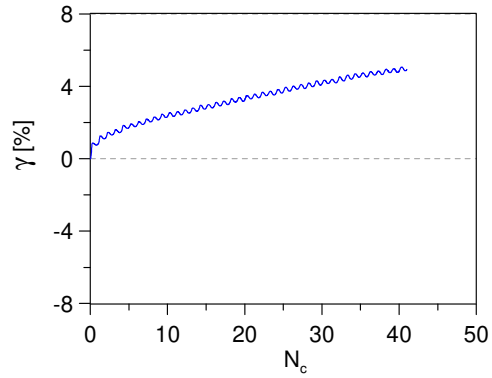

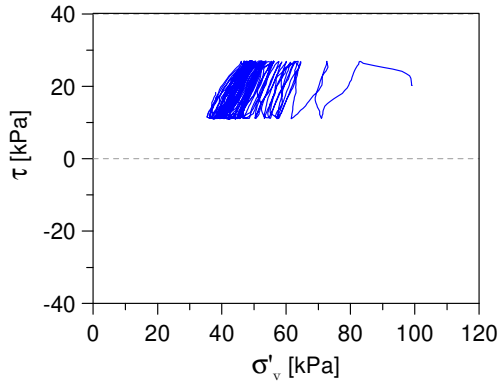

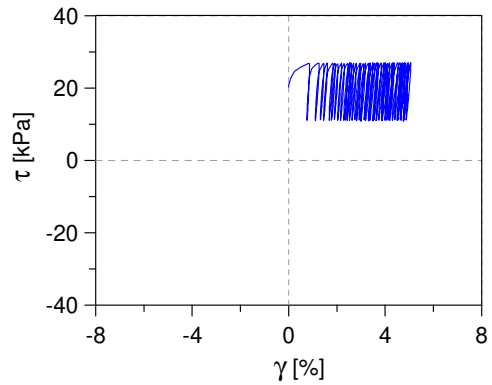

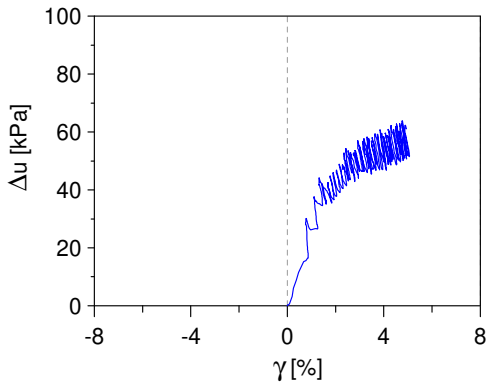

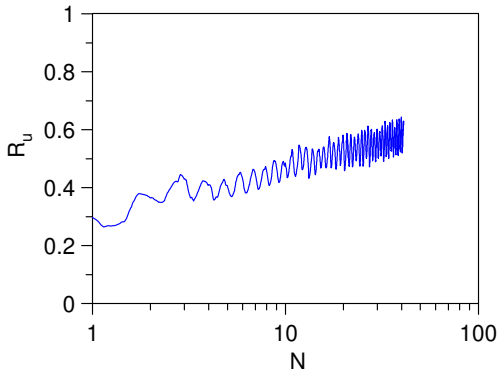

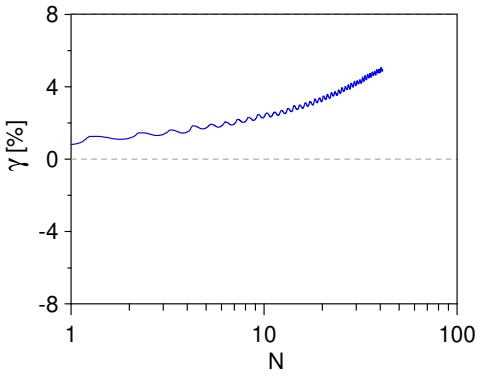

Undrained Cyclic Simple Shear test: *C_SS_TS20_S100_A2_2*
Ticino sand + 20% f_c (Reconstitution method: Moist Tamping)
e_0= 0.59 - D_R= 48% - σ'_{v0}= 100 kPa - α= 0.2 - *CSR* = 0.10

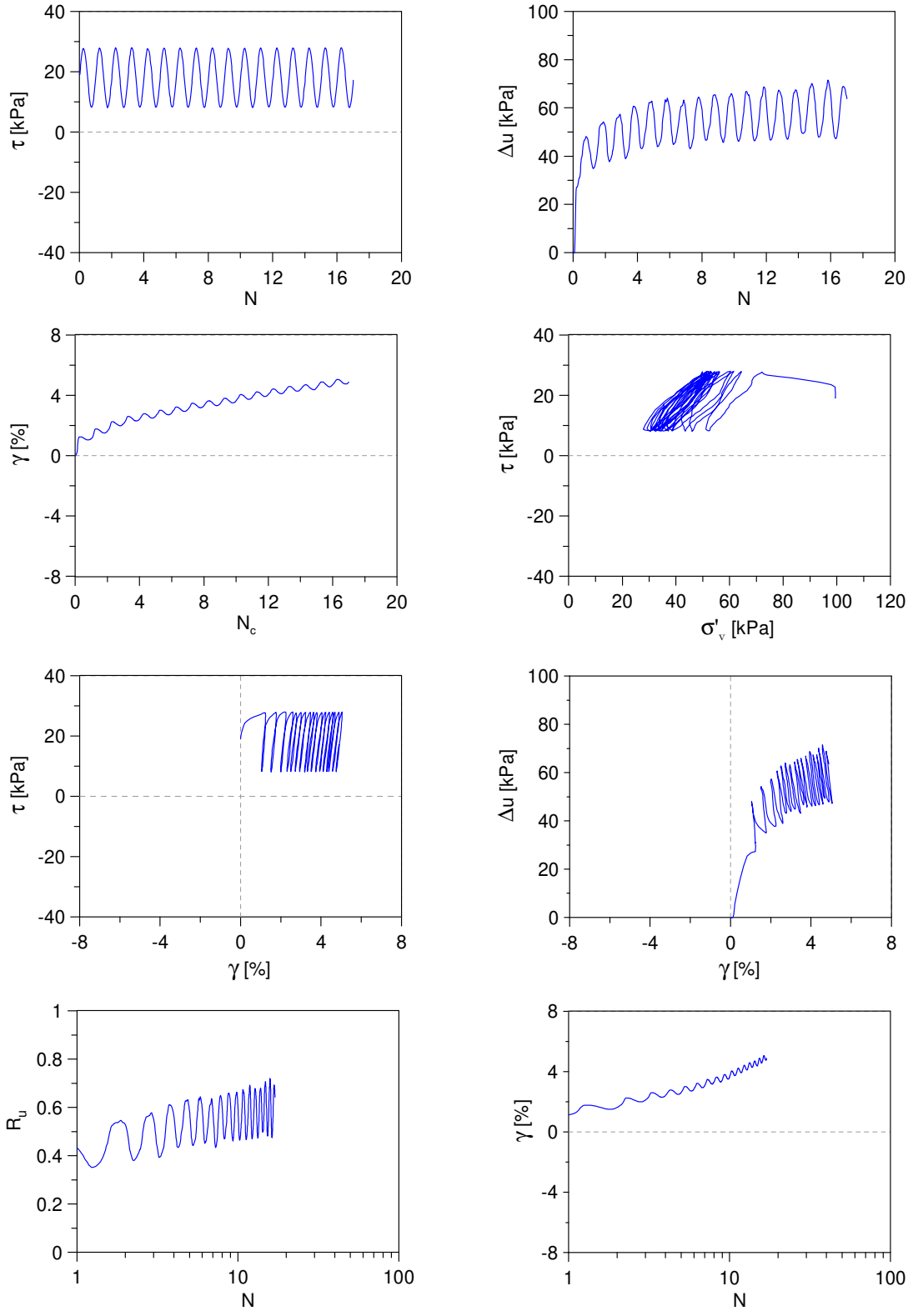

Undrained Cyclic Simple Shear test: *C_SS_TS20_S100_A2_3*
Ticino sand + 20% f_c (Reconstitution method: Moist Tamping)
e_0= 0.55 - D_R= 57% - σ'_{v0}= 100 kPa - α= 0.2 - *CSR* = 0.13

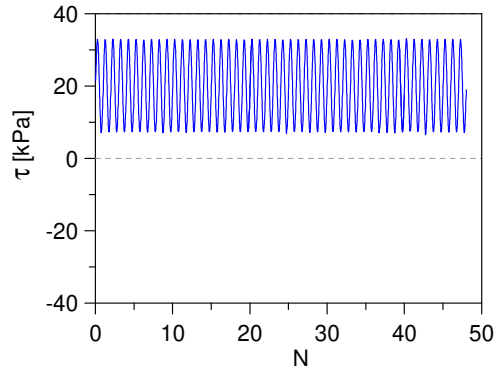

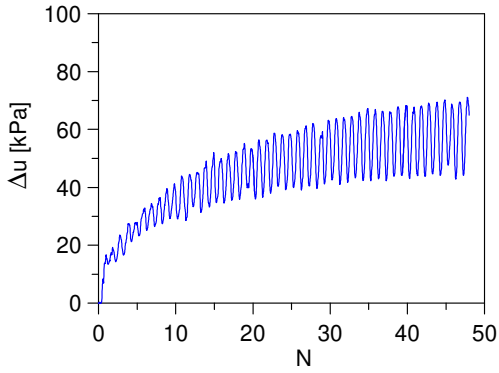

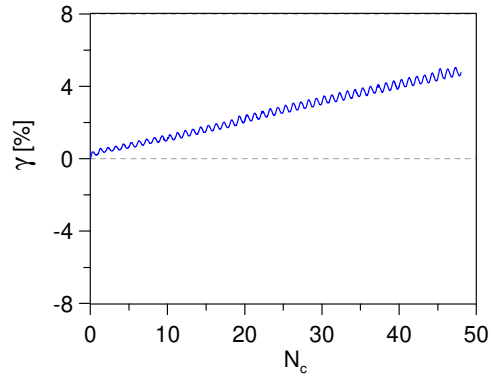

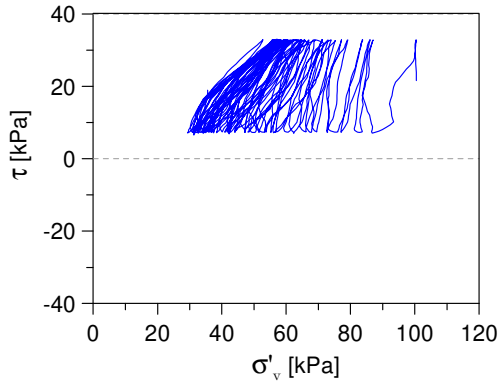

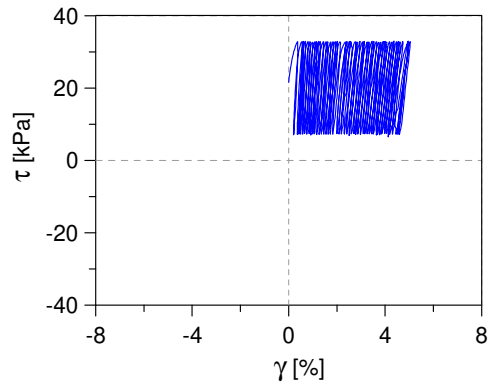

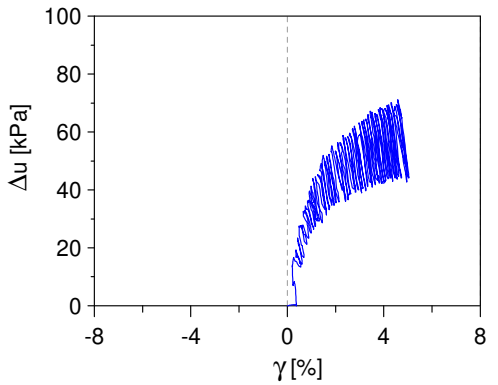

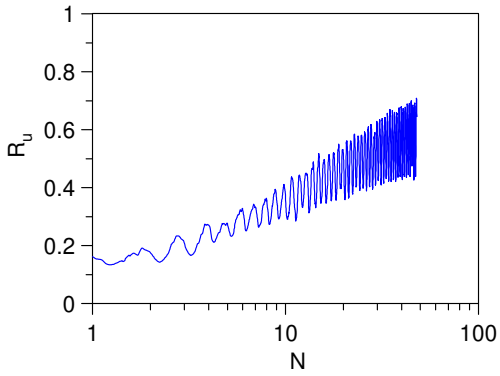

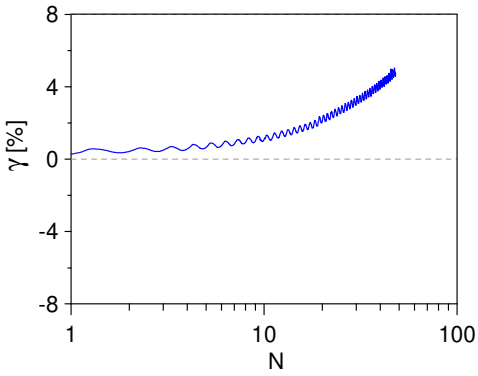

Undrained Cyclic Simple Shear test: *C_SS_TS20_S100_A2_4*
Ticino sand + 20% f_c (Reconstitution method: Moist Tamping)
e_0= 0.55 - D_R= 57% - σ'_{v0}= 100 kPa - α= 0.2 - *CSR* = 0.16

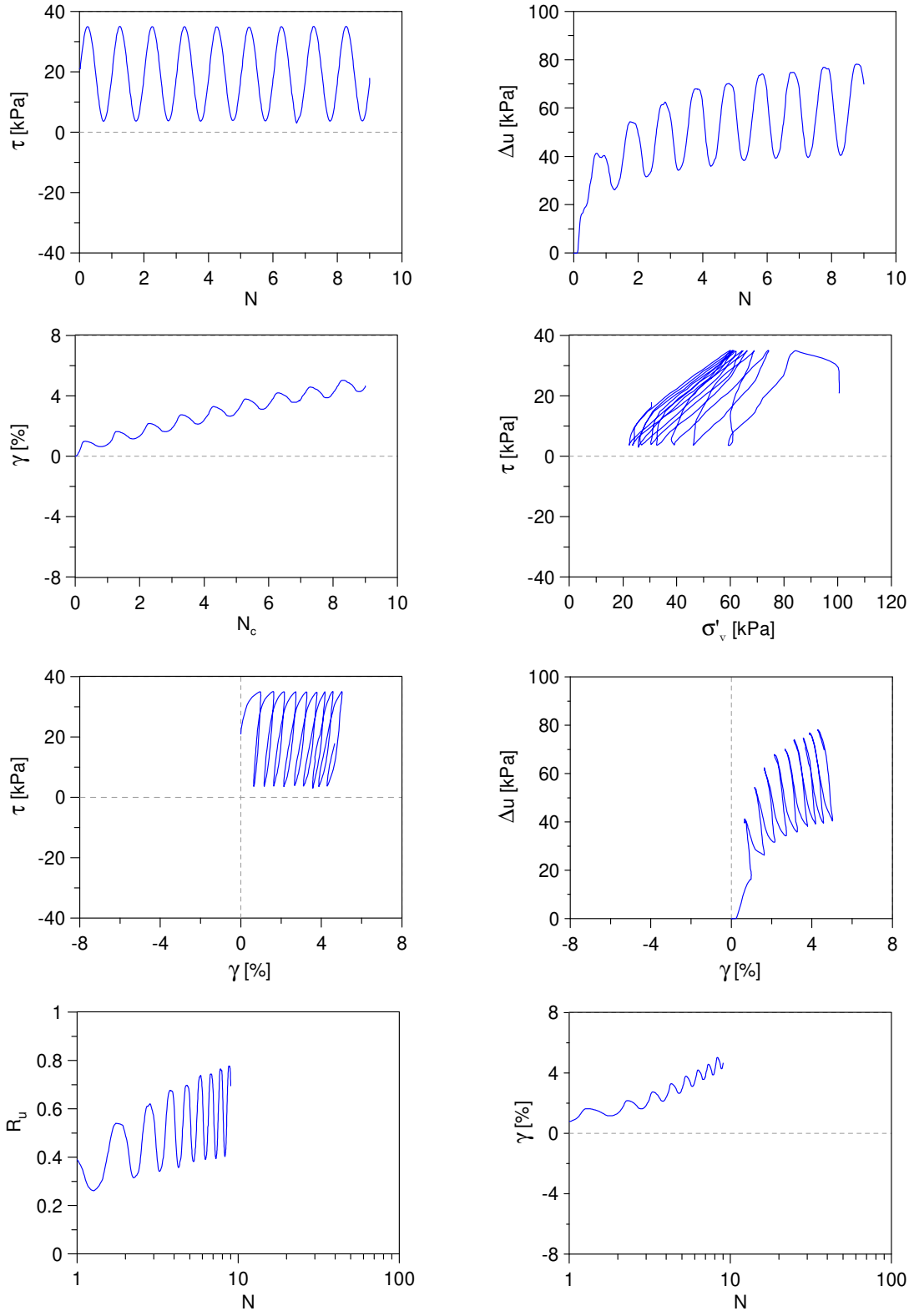

Undrained Cyclic Simple Shear test: *C_SS_TS20_S100_A3_1*
Ticino sand + 20% f_c (Reconstitution method: Moist Tamping)
e_0= 0.55 - D_R= 57% - σ'_{v0}= 100 kPa - α= 0.3 - *CSR* = 0.14

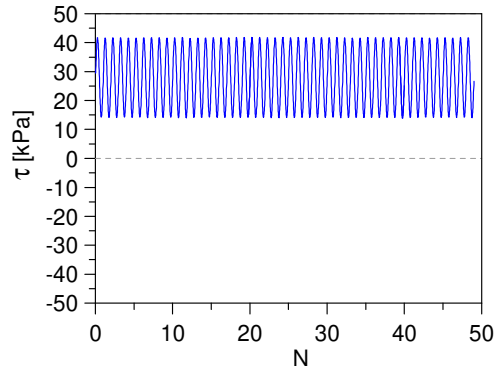

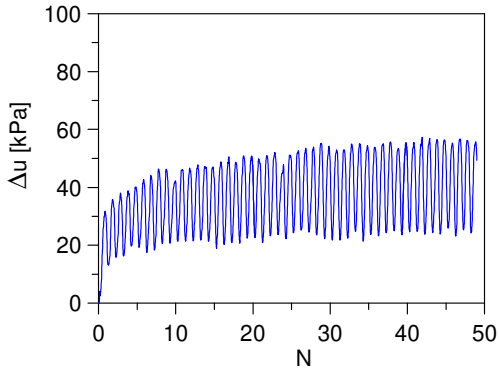

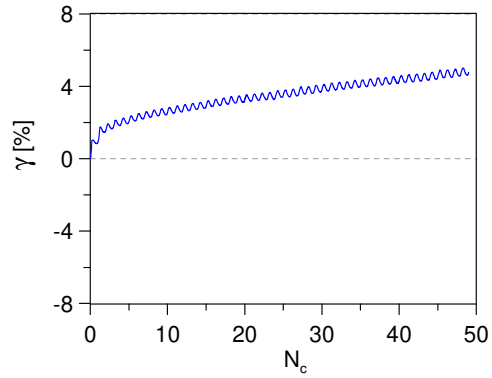

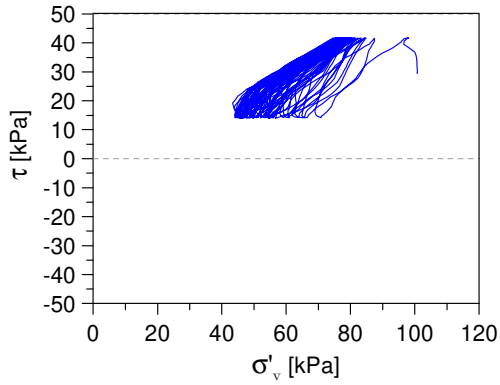

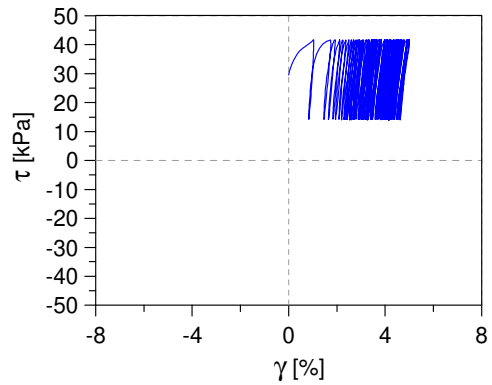

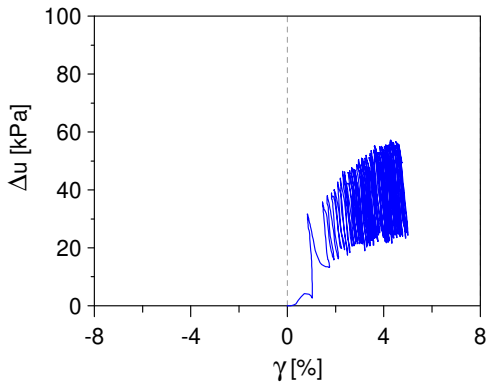

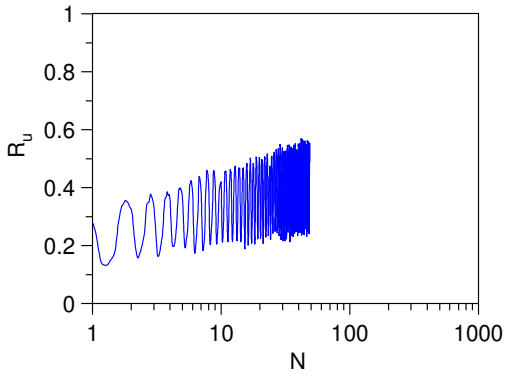

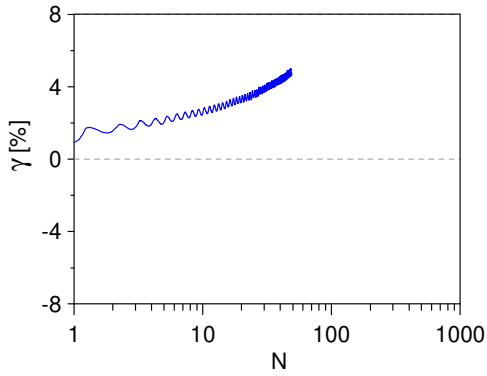

Undrained Cyclic Simple Shear test: *C_SS_TS20_S100_A3_2*
Ticino sand + 20% f_c (Reconstitution method: Moist Tamping)
e_0= 0.55 - D_R= 57% - σ'_{v0}= 100 kPa - α= 0.3 - *CSR* = 0.16

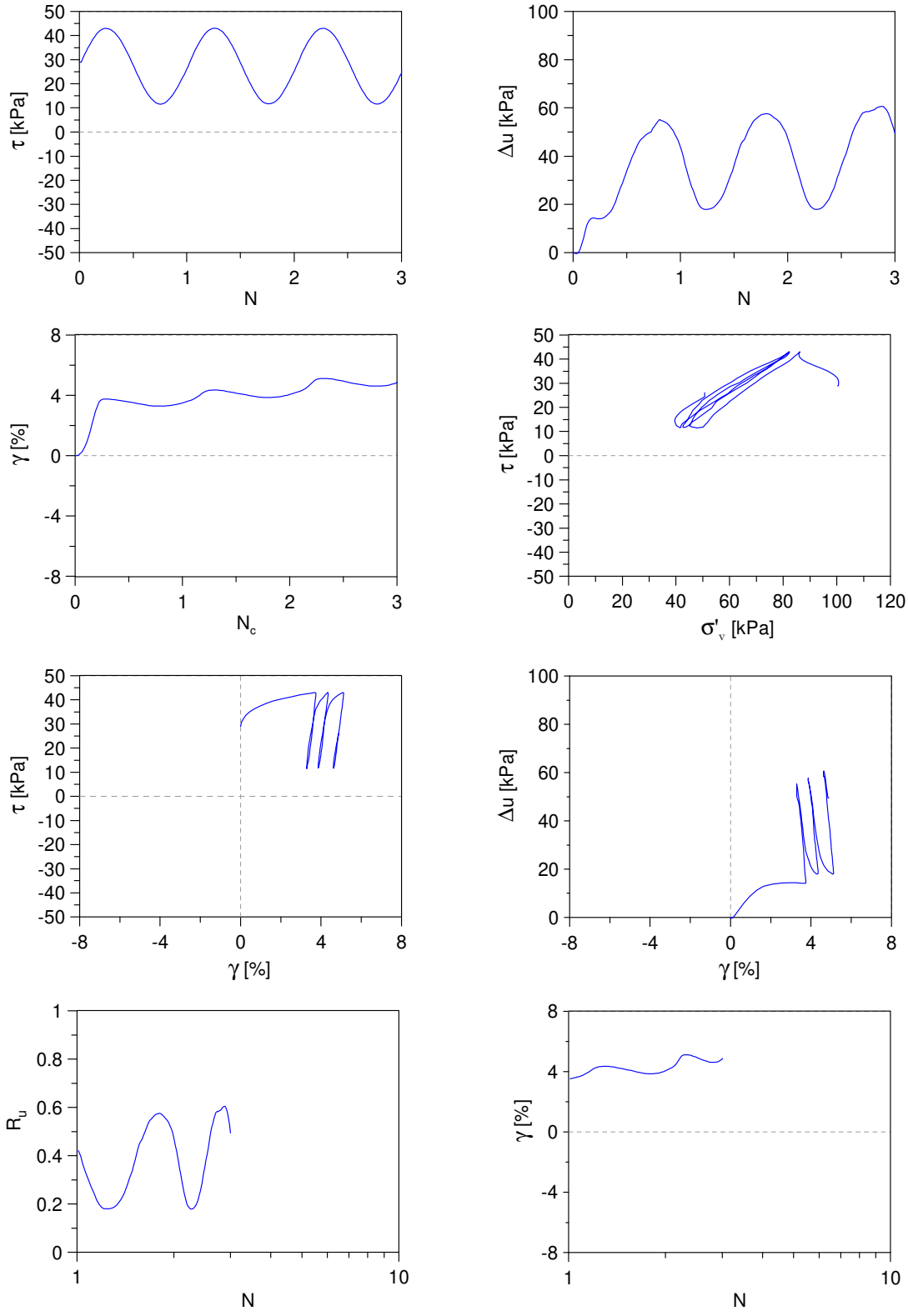

Sand-silt mixture (f_c=30%)

Undrained Cyclic Simple Shear test: *C_SS_TS30_S50_A0_1*
Ticino sand + 30% f_c (Reconstitution method: Moist Tamping)
e_0= 0.68 - D_R= 28% - σ'_{v0}= 50 kPa - α=0 - *CSR* = 0.12

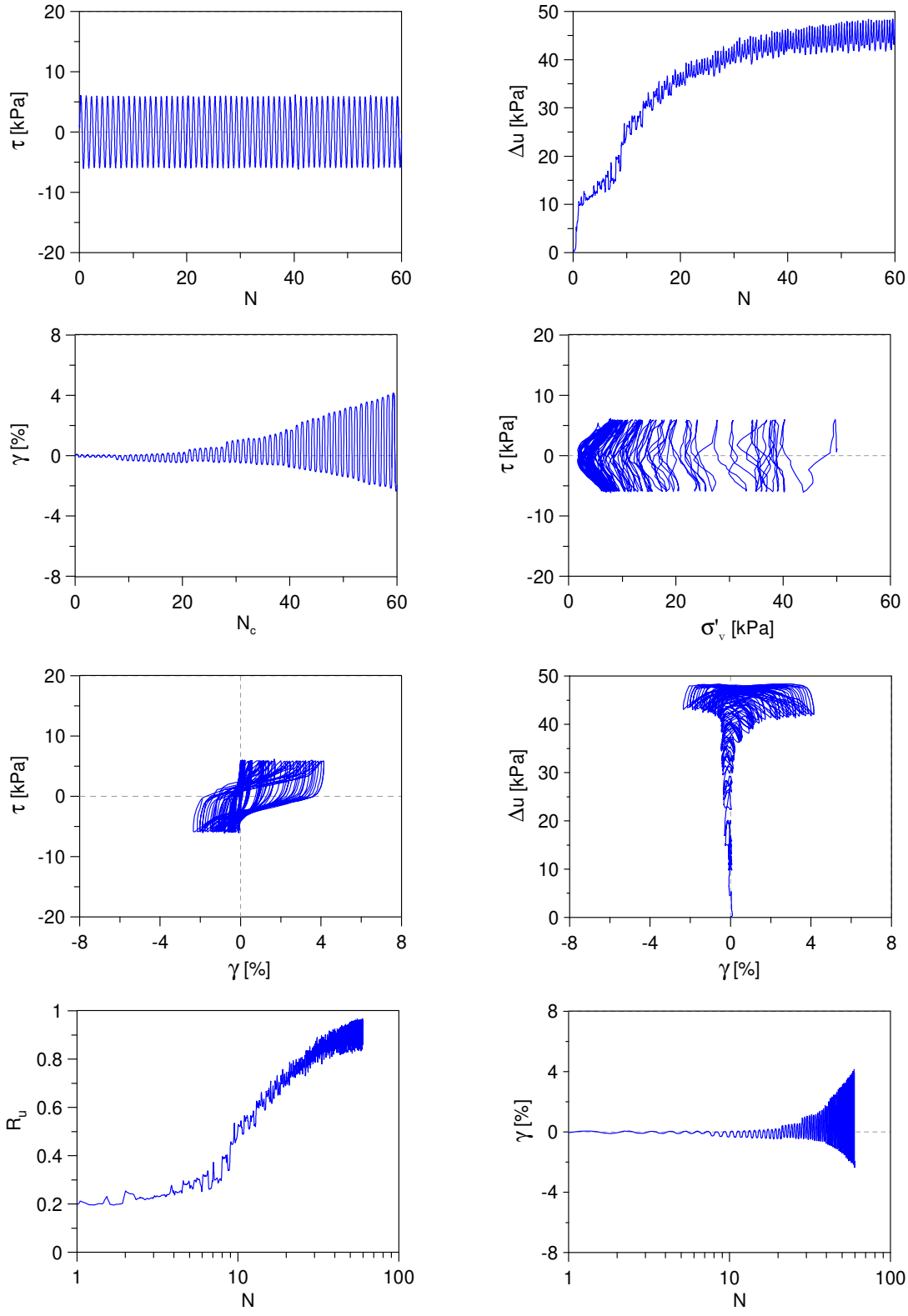

Undrained Cyclic Simple Shear test: *C_SS_TS30_S50_A0_2*
Ticino sand + 30% f_c (Reconstitution method: Moist Tamping)
e_0= 0.68 - D_R= 28% - σ'_{v0}= 50 kPa - α=0 - *CSR* = 0.14

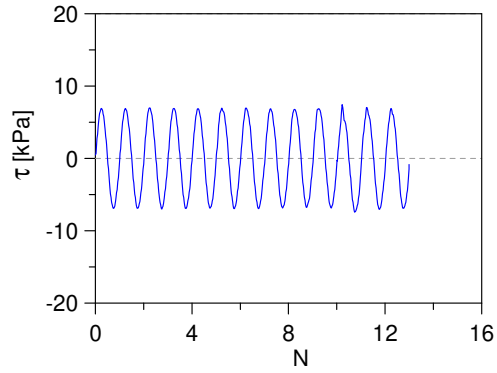

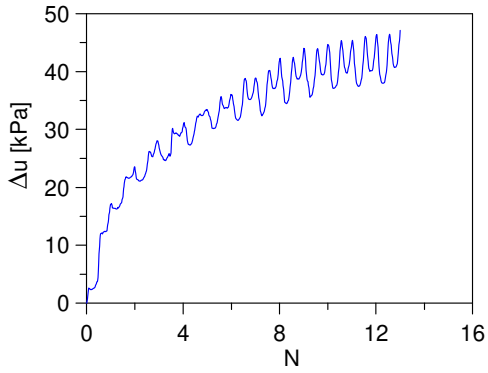

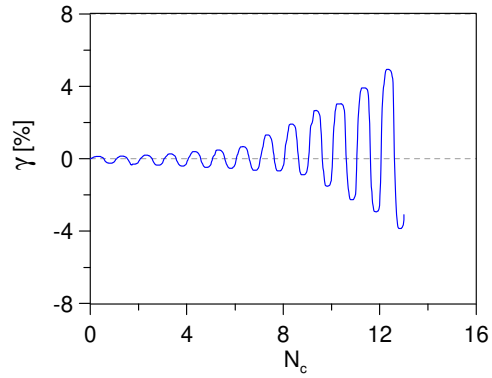

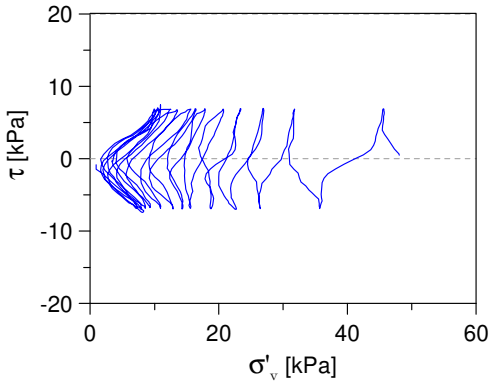

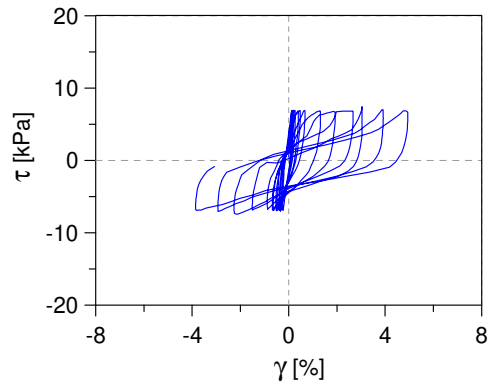

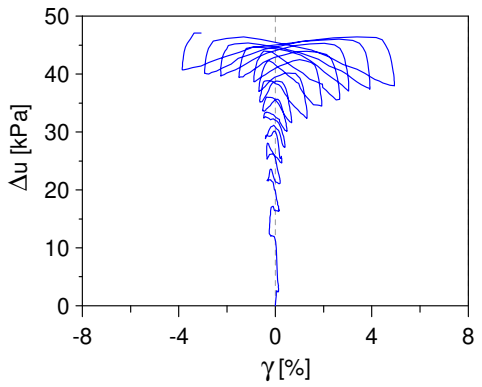

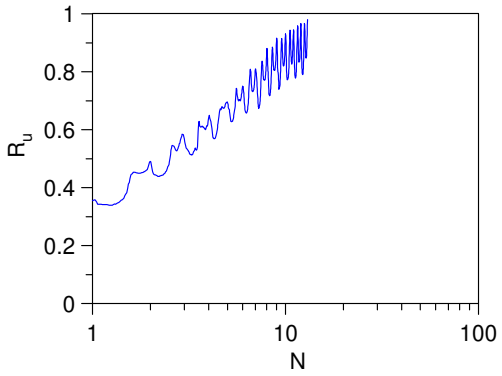

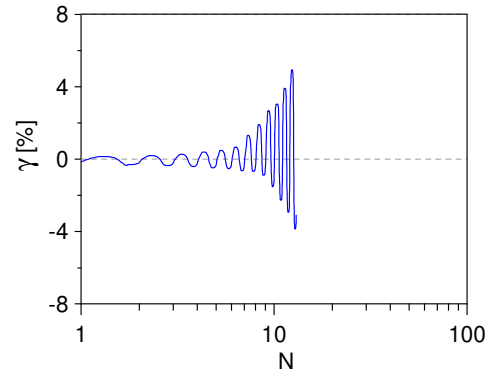

Undrained Cyclic Simple Shear test: *C_SS_TS30_S50_A0_3*
Ticino sand + 30% f_c (Reconstitution method: Moist Tamping)
e_0= 0.68 - D_R= 28% - σ'_{v0}= 50 kPa - α=0 - *CSR* = 0.18

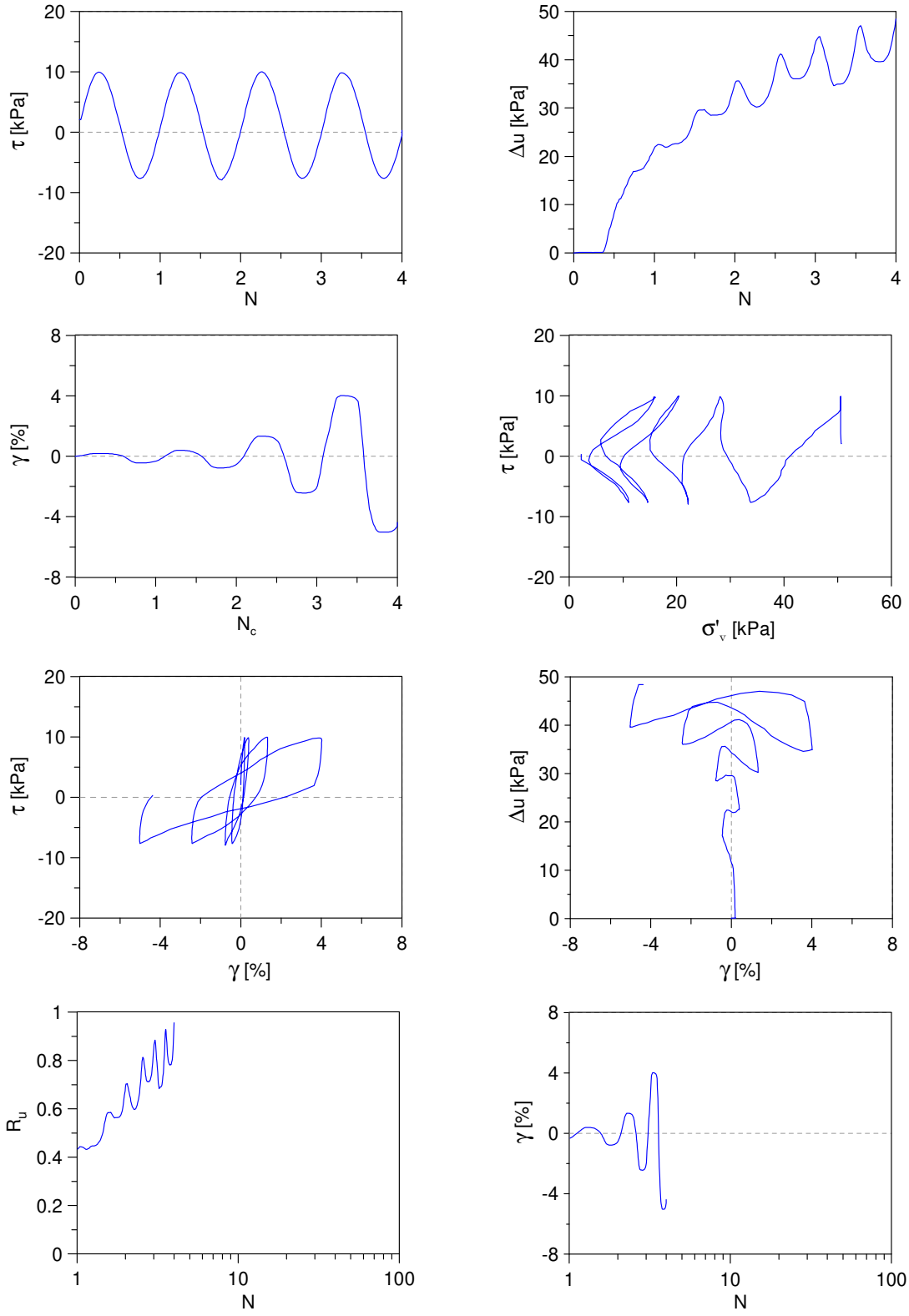

Undrained Cyclic Simple Shear test: *C_SS_TS30_S50_A1_1*
Ticino sand + 30% f_c (Reconstitution method: Moist Tamping)
e_0= 0.68 - D_R= 28% - σ'_{v0}= 50 kPa - α= 0.1 - *CSR* = 0.08

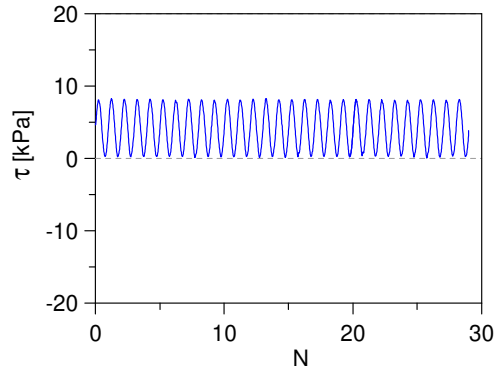

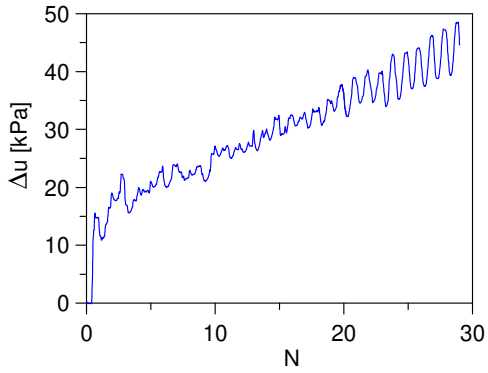

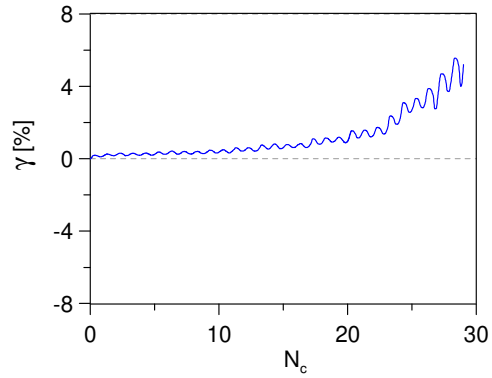

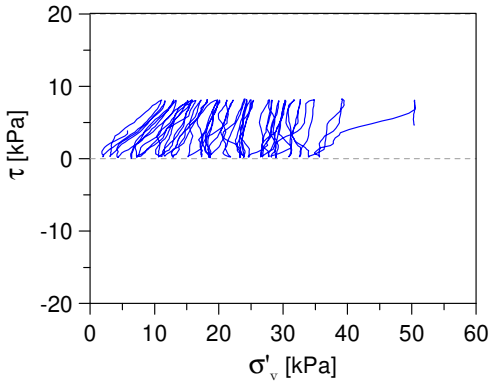

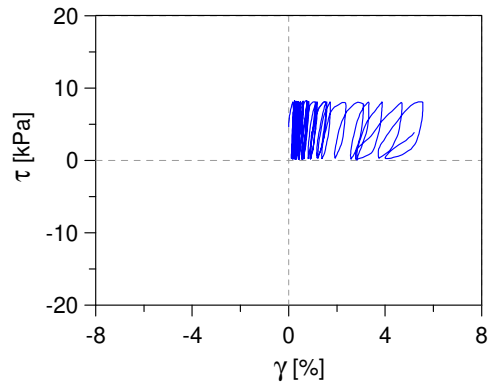

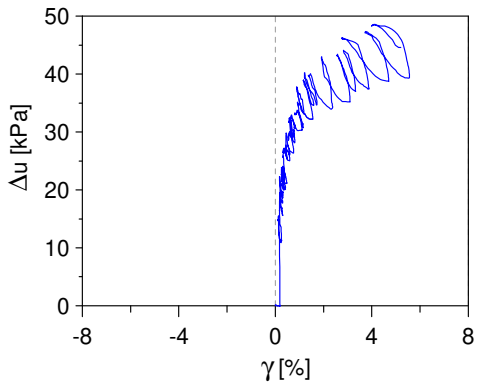

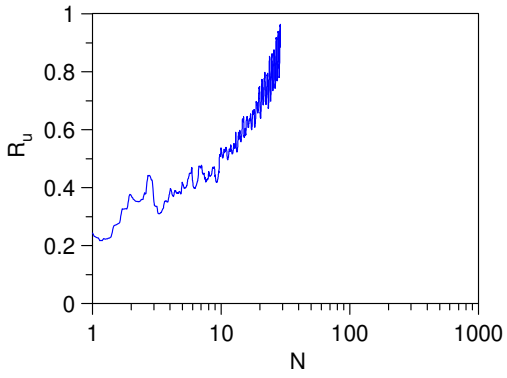

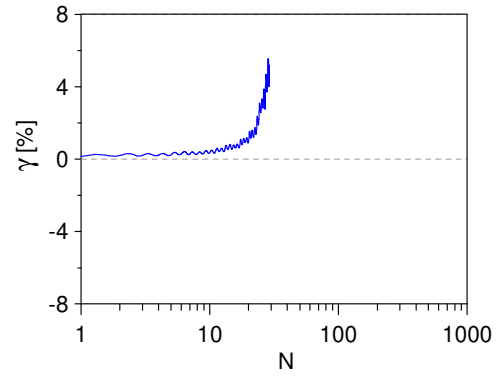

Undrained Cyclic Simple Shear test: *C_SS_TS30_S50_A1_2*
Ticino sand + 30% f_c (Reconstitution method: Moist Tamping)
e_0= 0.68 - D_R= 28% - σ'_{v0}= 50 kPa - α= 0.1 - *CSR* = 0.12

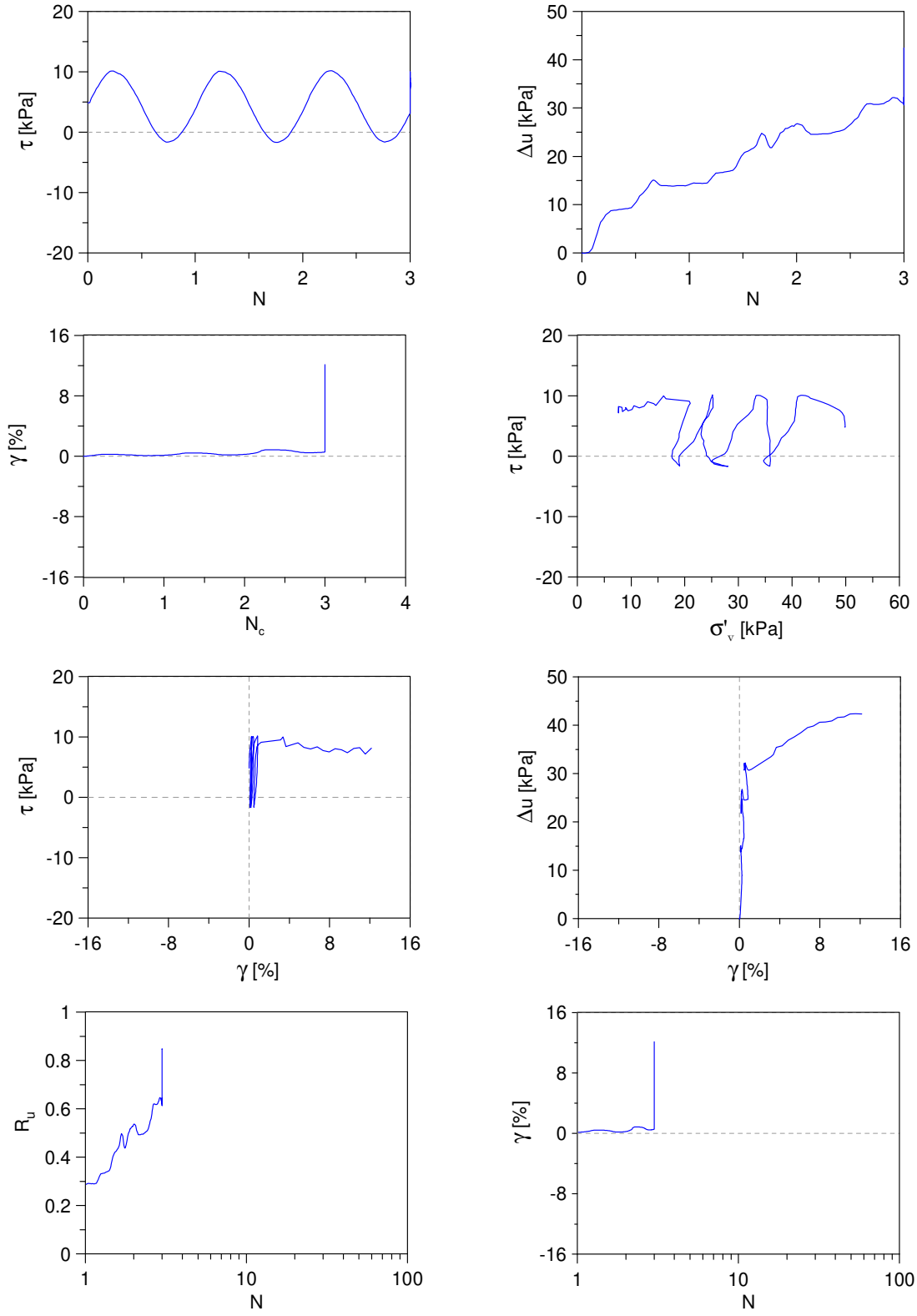

Undrained Cyclic Simple Shear test: *C_SS_TS30_S100_A0_1*
Ticino sand + 30% f_c (Reconstitution method: Moist Tamping)
e_0= 0.68 - D_R= 28% - σ'_{v0}= 100 kPa - α=0 - *CSR* = 0.08

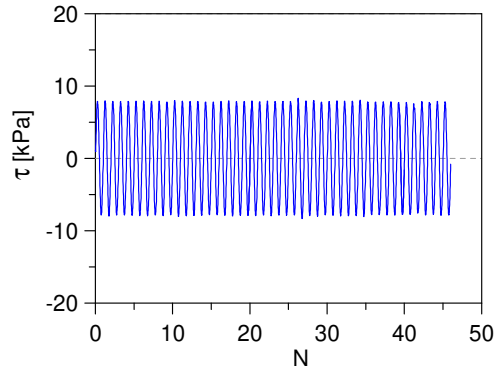

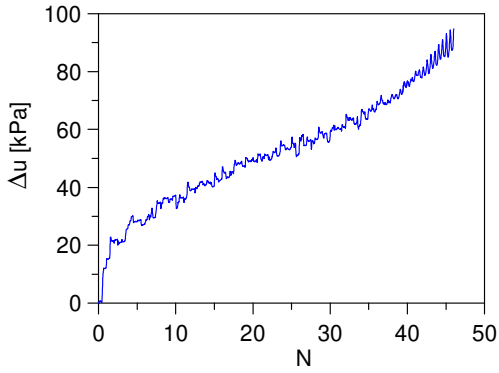

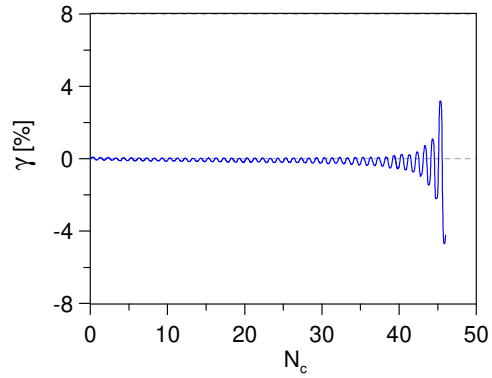

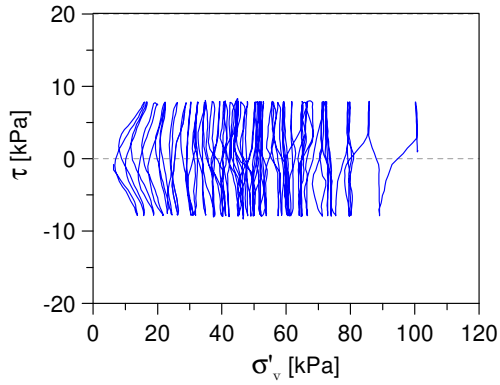

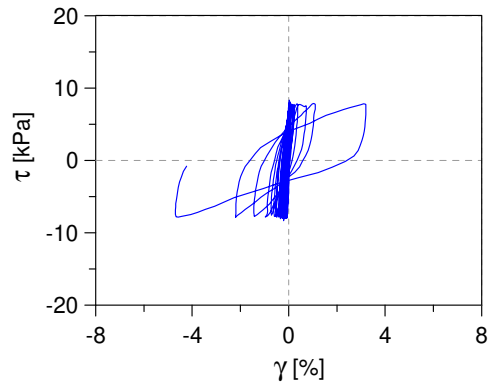

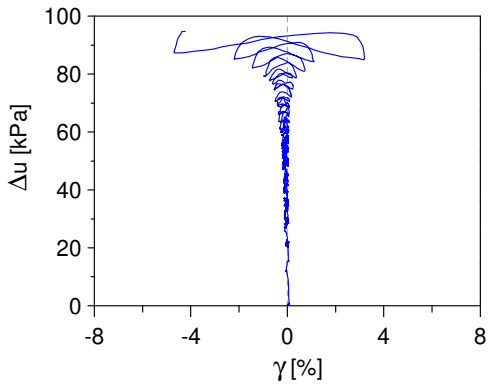

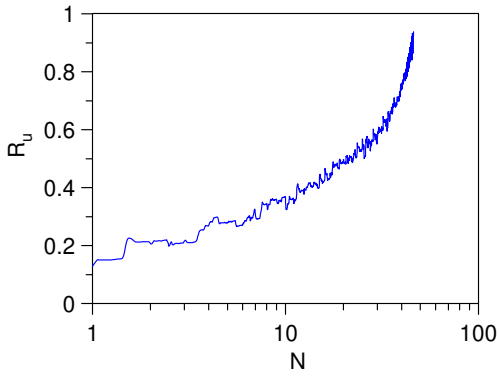

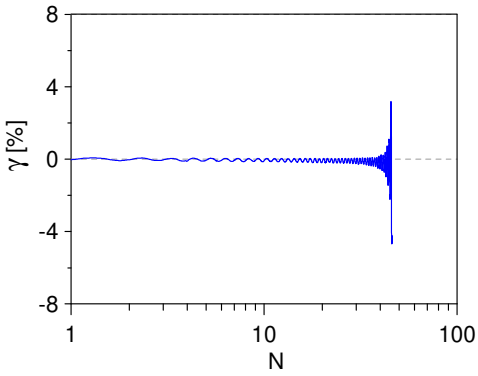

Undrained Cyclic Simple Shear test: *C_SS_TS30_S100_A0_2*
Ticino sand + 30% f_c (Reconstitution method: Moist Tamping)
e_0= 0.68 - D_R= 28% - σ'_{v0}= 100 kPa - α=0 - *CSR* = 0.10

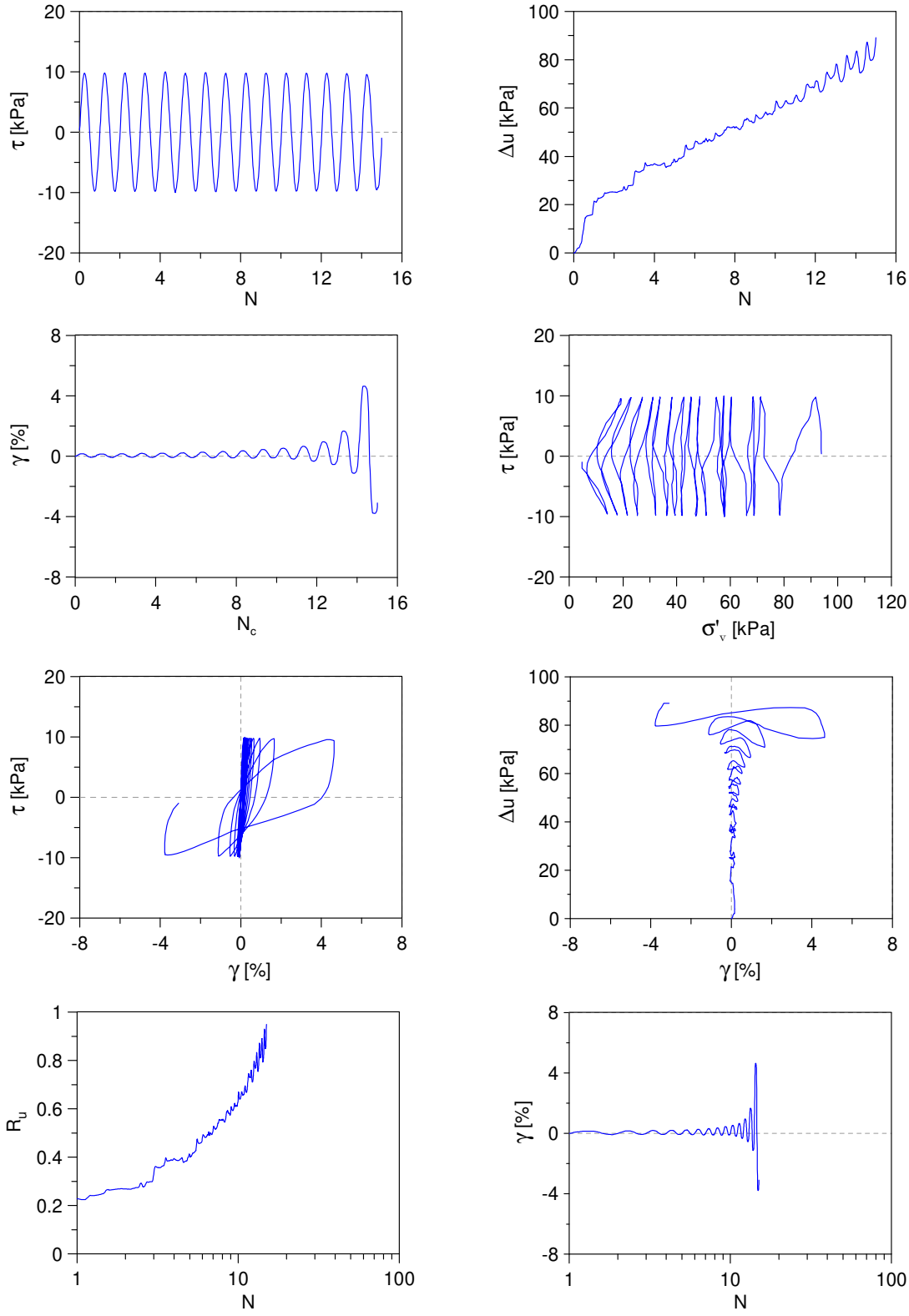

Undrained Cyclic Simple Shear test: *C_SS_TS30_S100_A0_3*
Ticino sand + 30% f_c (Reconstitution method: Moist Tamping)
e_0= 0.68 - D_R= 28% - σ'_{v0}= 100 kPa - α=0 - *CSR* = 0.12

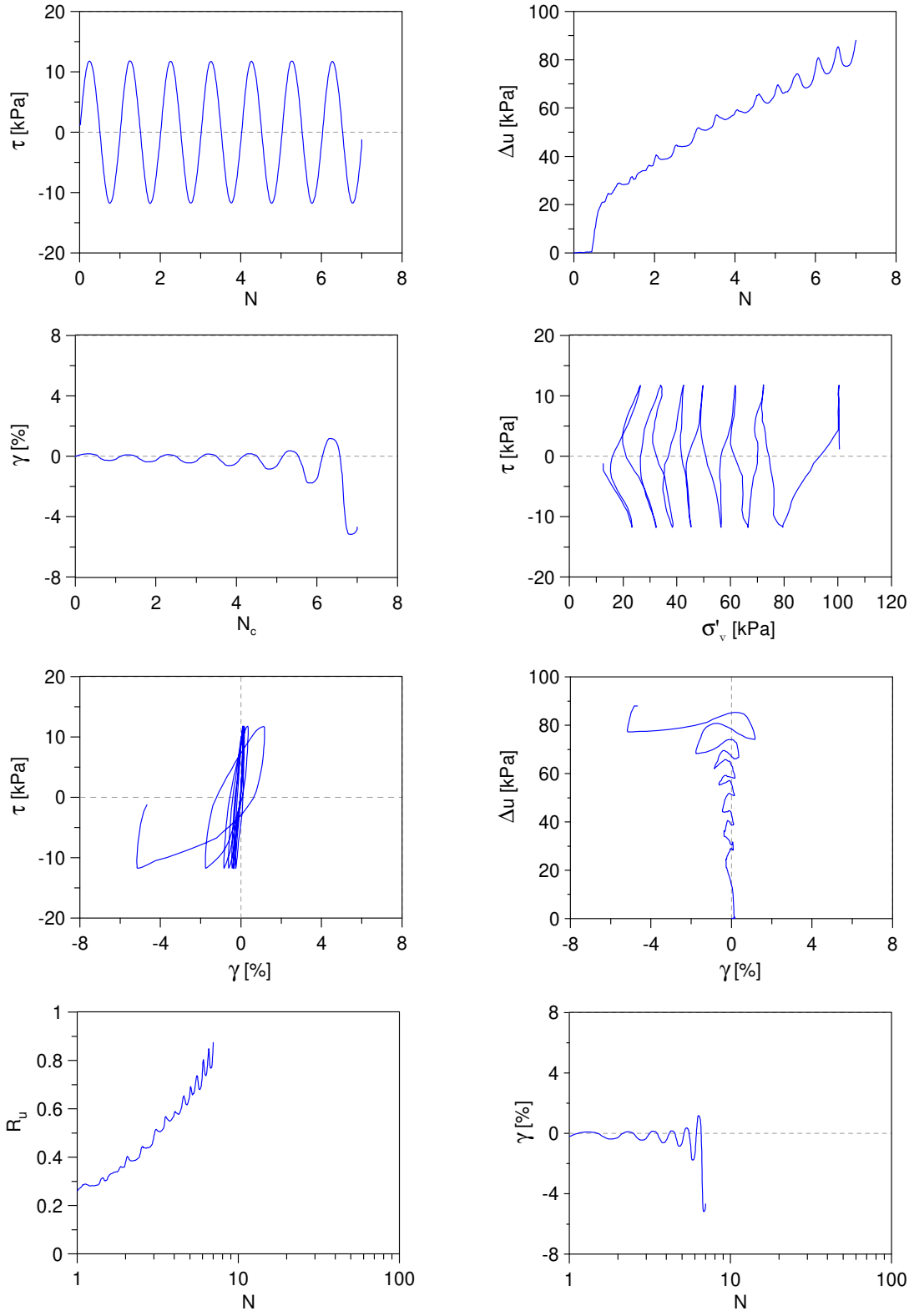

Undrained Cyclic Simple Shear test: *C_SS_TS30_S100_A0_4*
Ticino sand + 30% f_c (Reconstitution method: Moist Tamping)
e_0= 0.68 - D_R= 28% - σ'_{v0}= 100 kPa - α=0 - *CSR* = 0.14

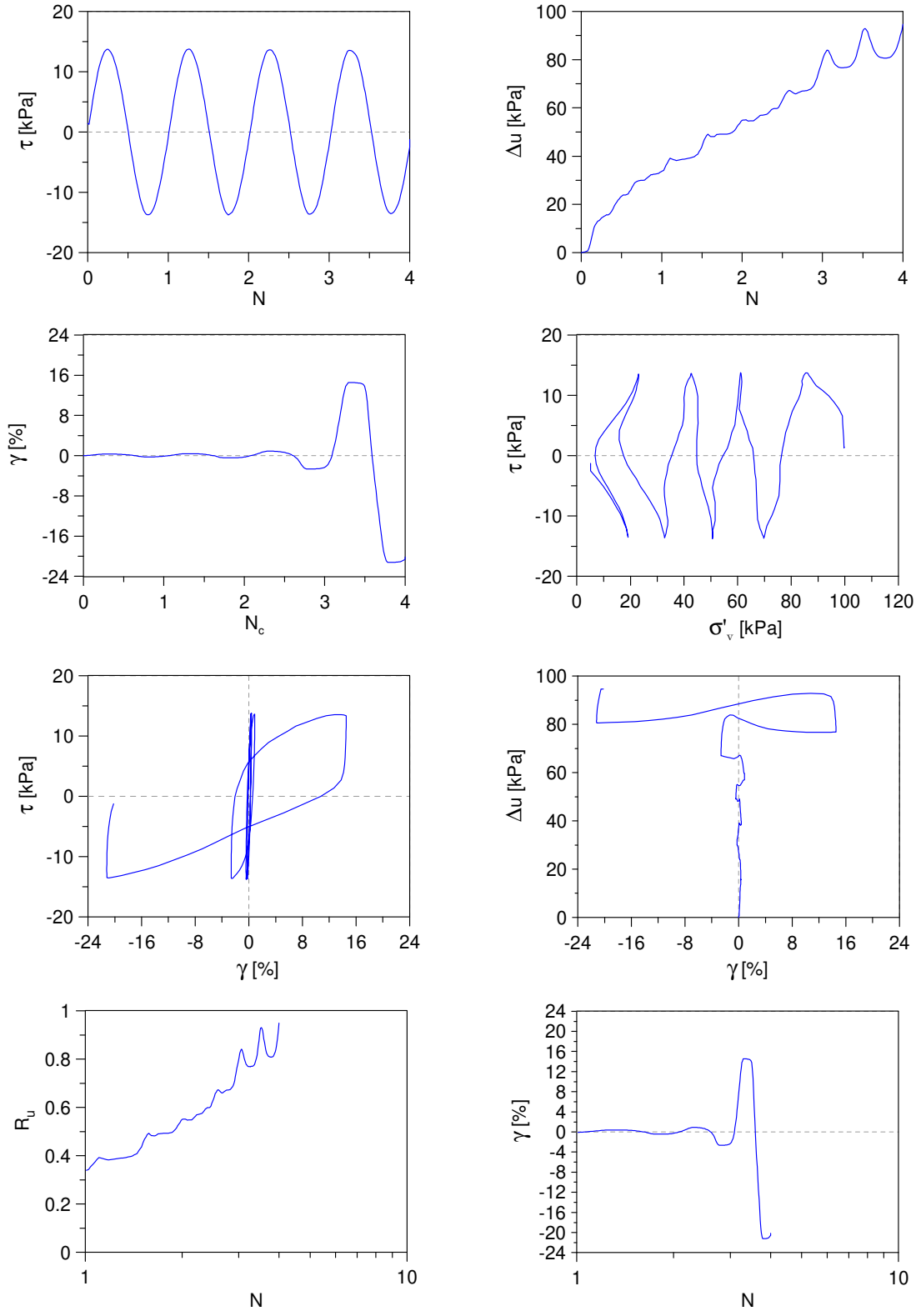

Undrained Cyclic Simple Shear test: *C_SS_TS30_S100_A0_5*
Ticino sand + 30% f_c (Reconstitution method: Moist Tamping)
e_0= 0.58 - D_R= 51% - σ'_{v0}= 100 kPa - α=0 - *CSR* = 0.12

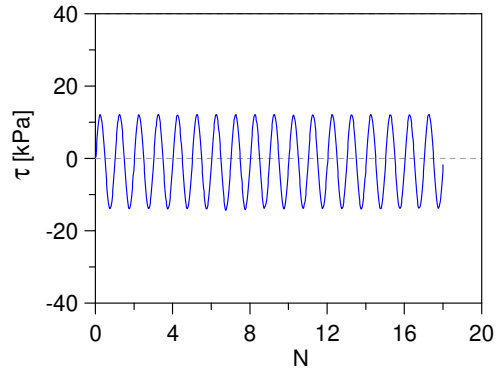

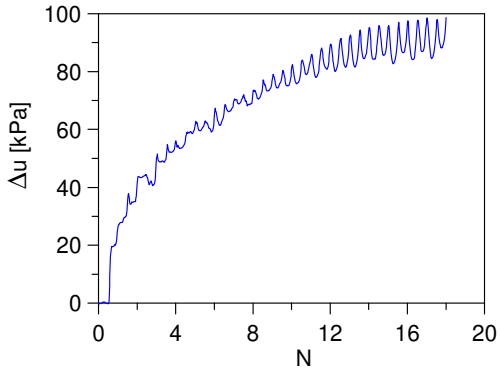

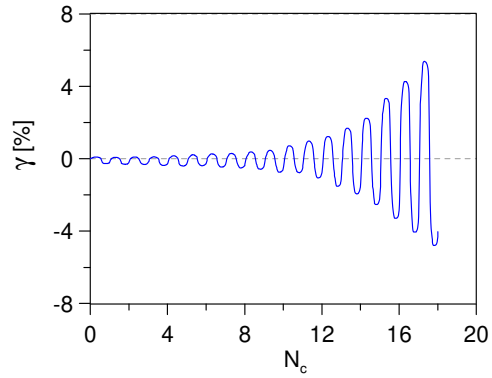

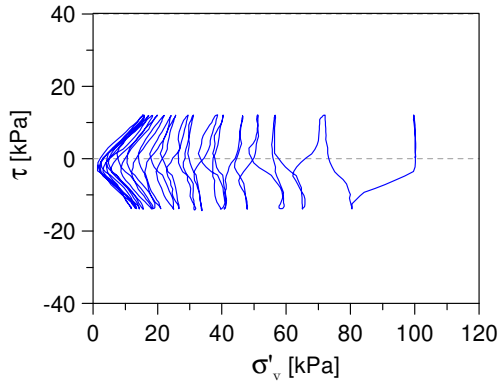

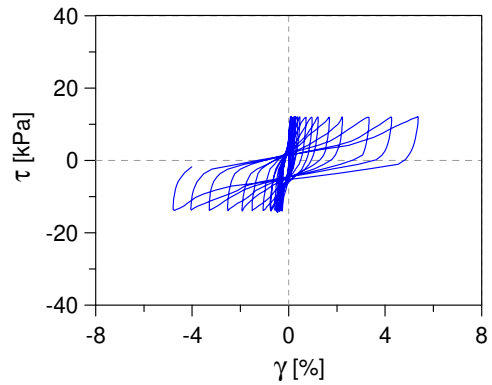

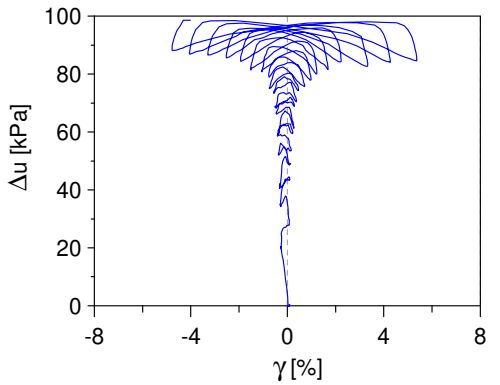

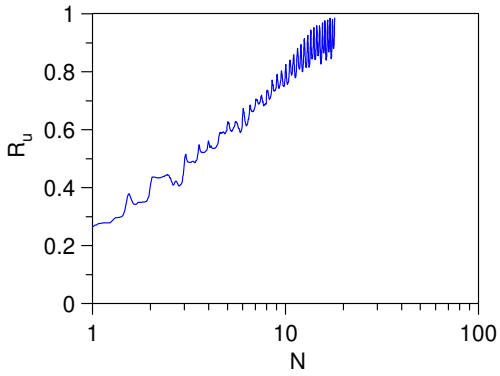

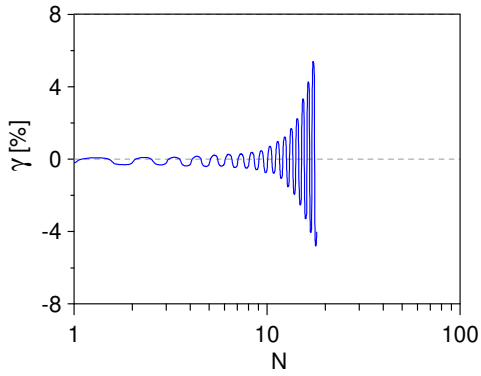

Undrained Cyclic Simple Shear test: *C_SS_TS30_S100_A0_6*
Ticino sand + 30% f_c (Reconstitution method: Moist Tamping)
e_0= 0.58 - D_R= 51% - σ'_{v0}= 100 kPa - α=0 - *CSR* = 0.14

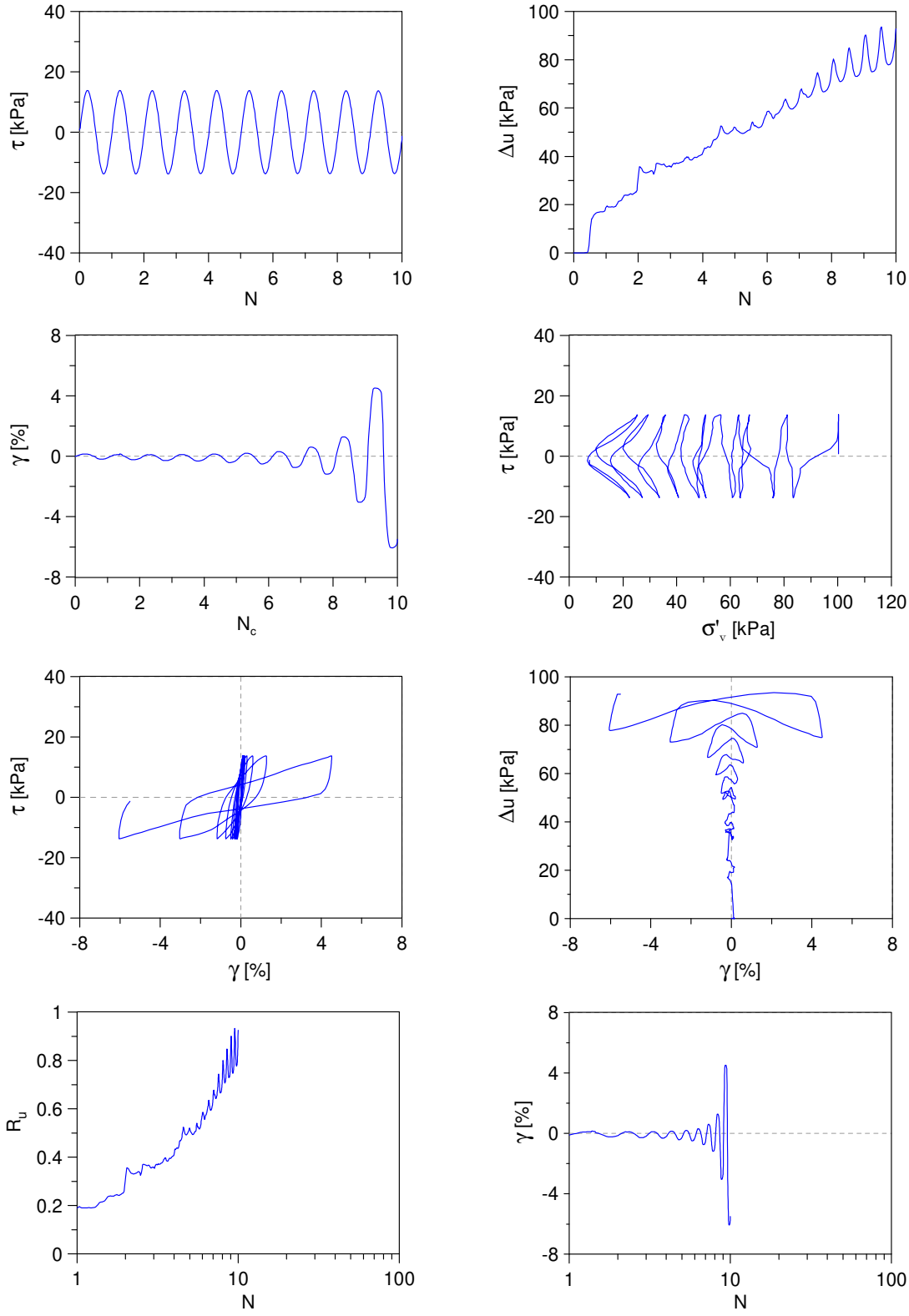

Undrained Cyclic Simple Shear test: *C_SS_TS30_S100_A0_7*
Ticino sand + 30% f_c (Reconstitution method: Moist Tamping)
e_0= 0.58 - D_R= 51% - σ'_{v0}= 100 kPa - α=0 - *CSR* = 0.18

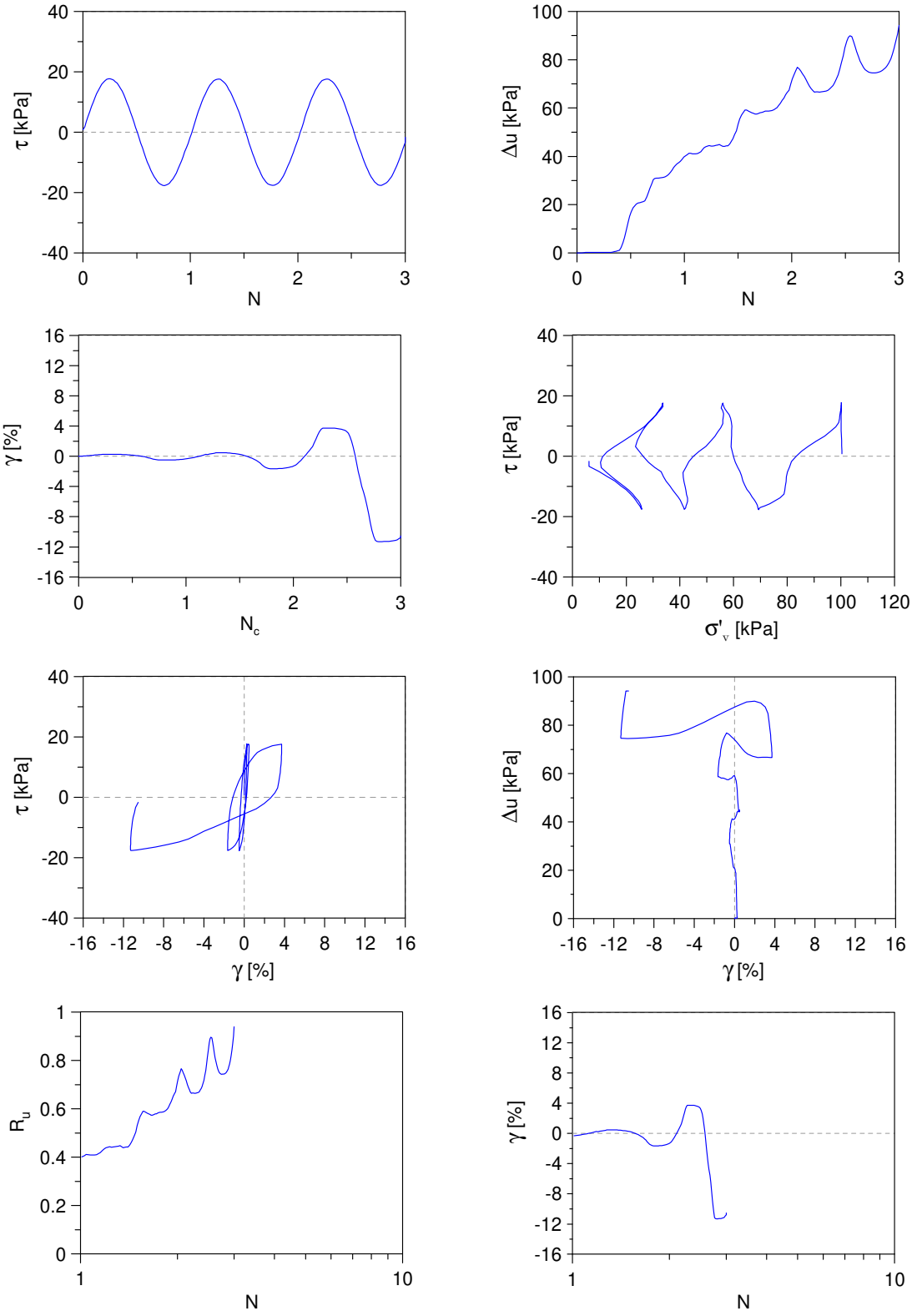

Undrained Cyclic Simple Shear test: *C_SS_TS30_S100_A0_8*
Ticino sand + 30% f_c (Reconstitution method: Moist Tamping)
e_0= 0.55 - D_R= 58% - σ'_{v0}= 100 kPa - α=0 - *CSR* = 0.16

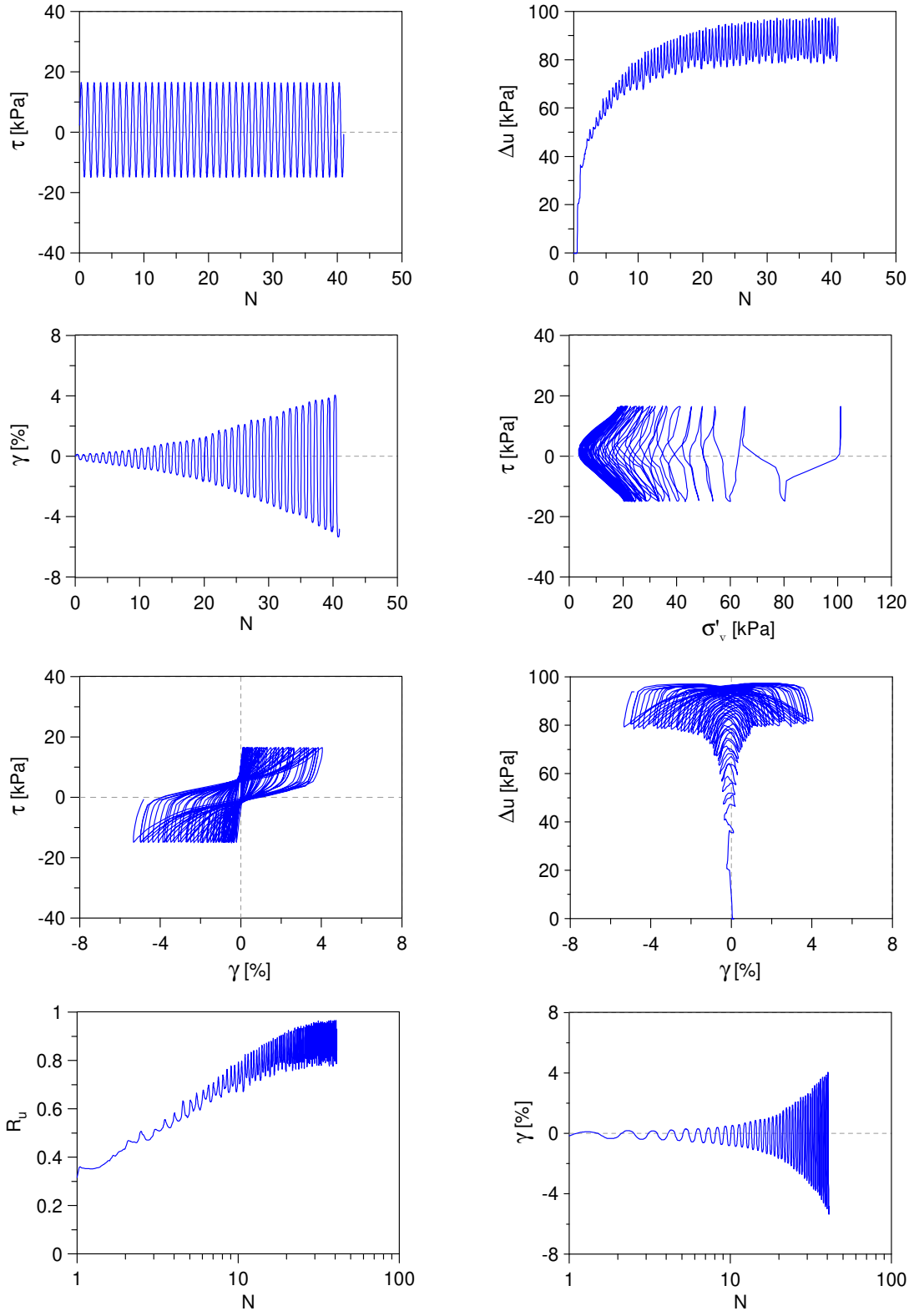

Undrained Cyclic Simple Shear test: *C_SS_TS30_S100_A0_9*
Ticino sand + 30% f_c (Reconstitution method: Moist Tamping)
e_0= 0.55 - D_R= 58% - σ'_{v0}= 100 kPa - α=0 - *CSR* = 0.20

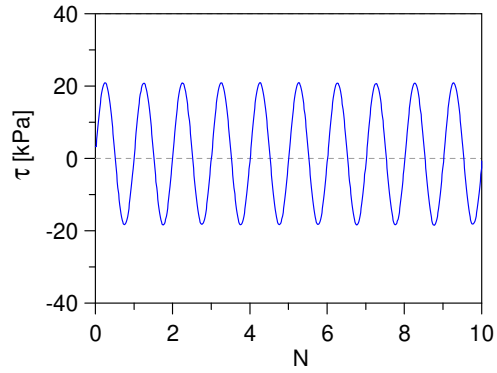

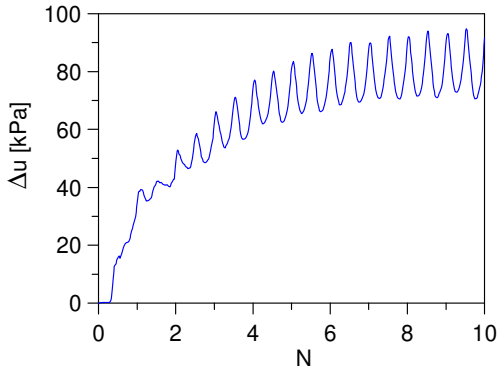

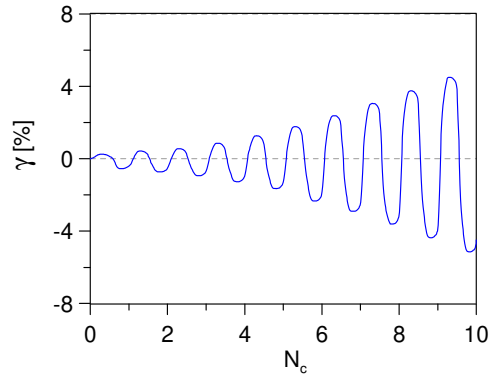

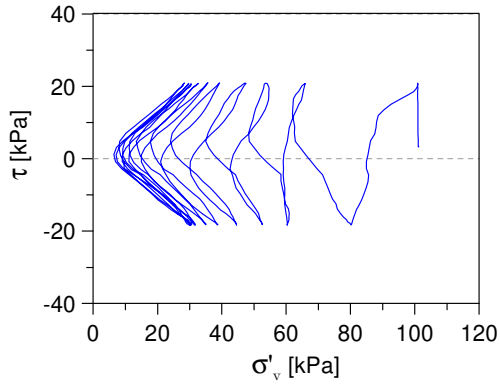

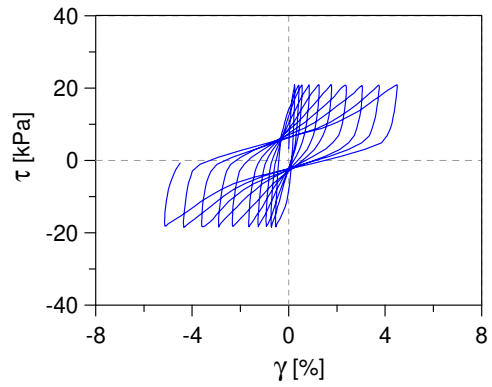

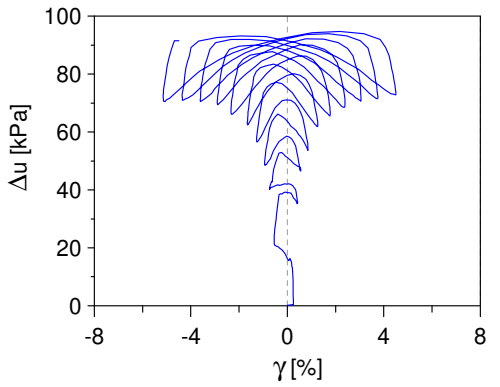

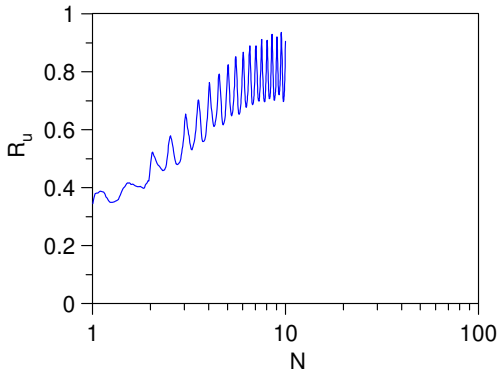

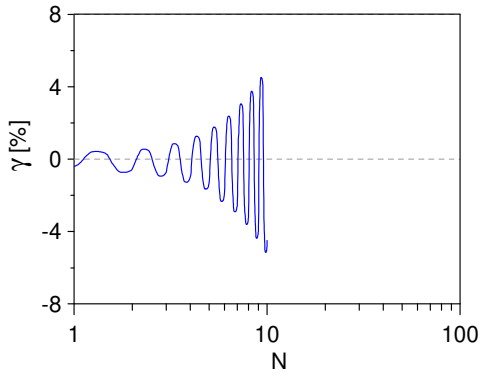

Undrained Cyclic Simple Shear test: *C_SS_TS30_S100_A0_10*
Ticino sand + 30% f_c (Reconstitution method: Moist Tamping)
e_0= 0.49 - D_R= 72% - σ'_{v0}= 100 kPa - α=0 - *CSR* = 0.20

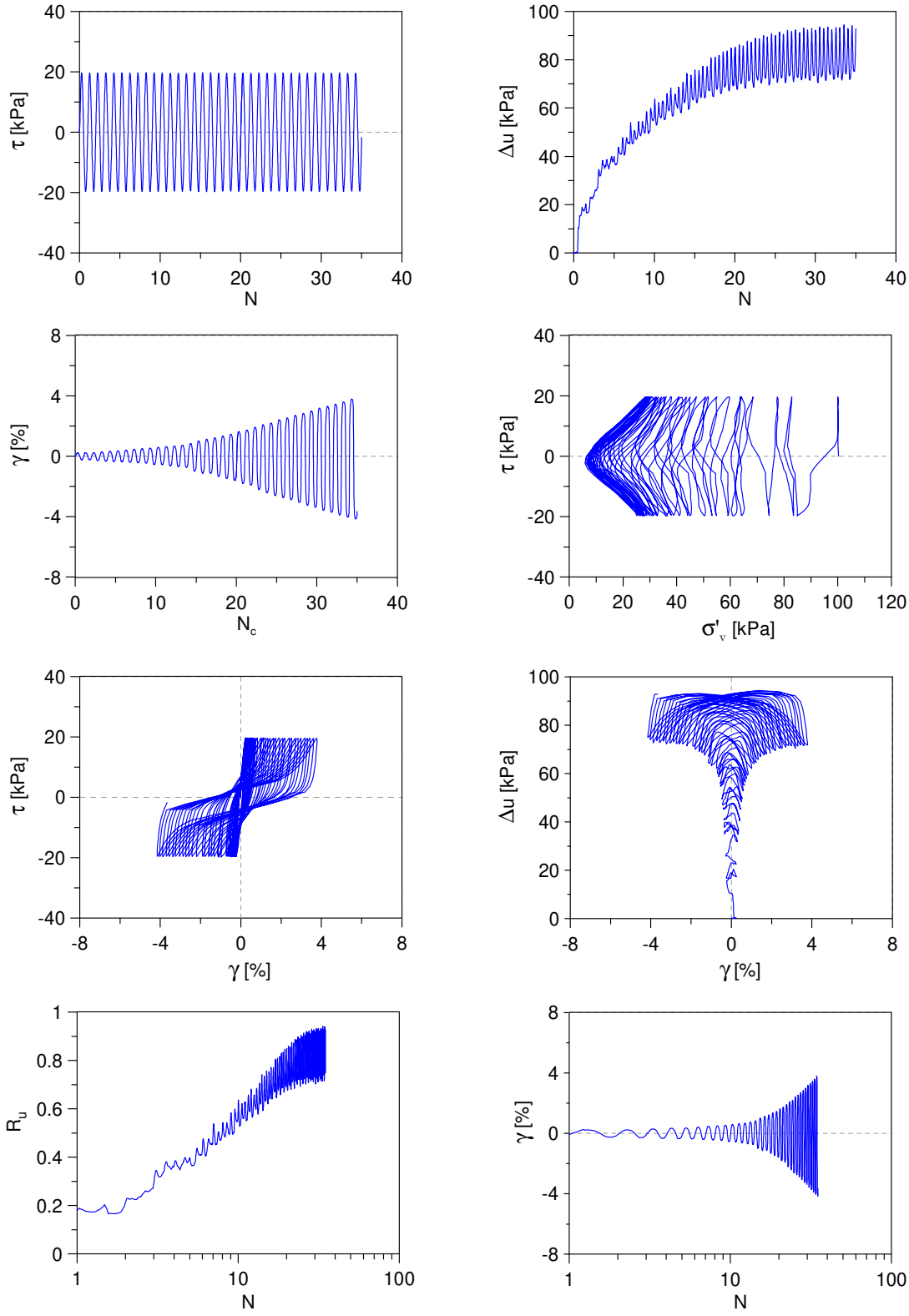

Undrained Cyclic Simple Shear test: *C_SS_TS30_S100_A0_11*
Ticino sand + 30% f_c (Reconstitution method: Moist Tamping)
e_0= 0.49 - D_R= 72% - σ'_{v0}= 100 kPa - α=0 - *CSR* = 0.22

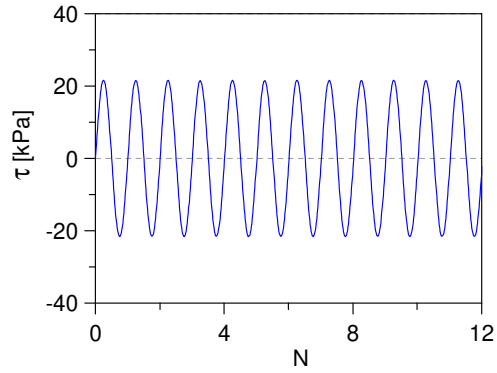

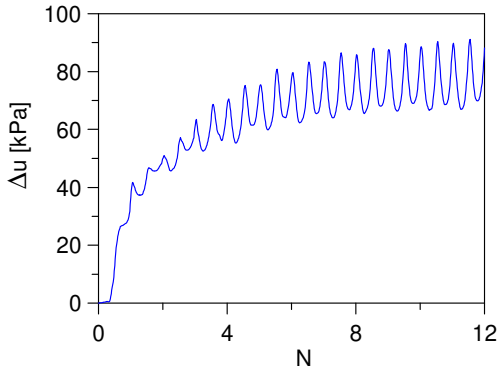

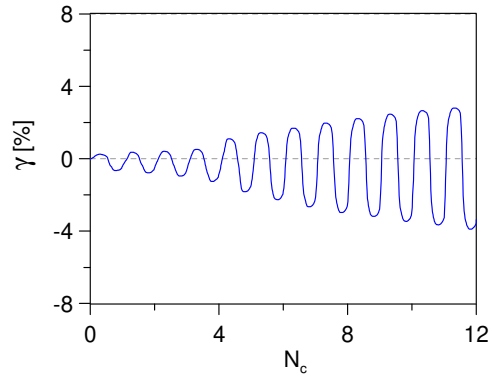

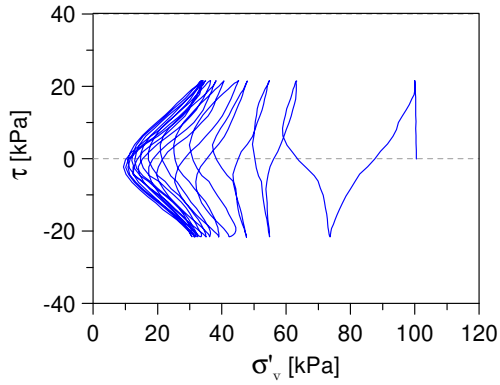

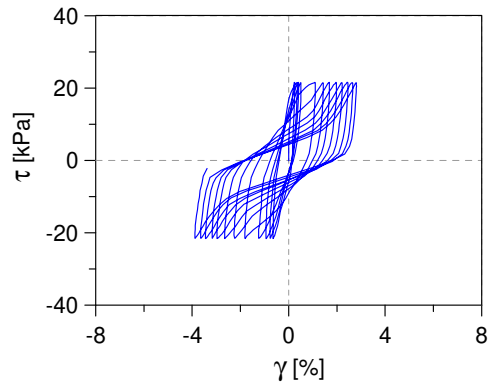

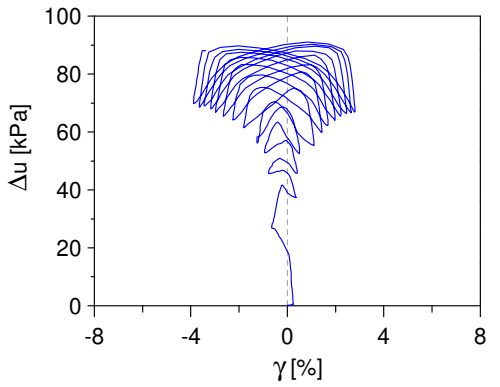

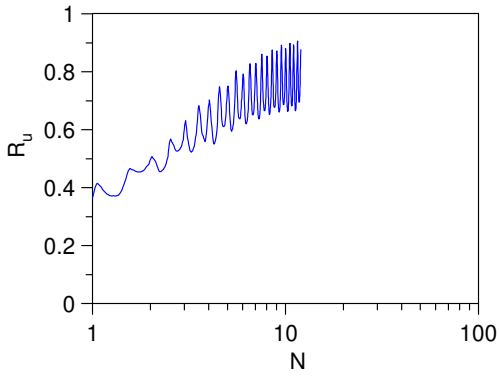

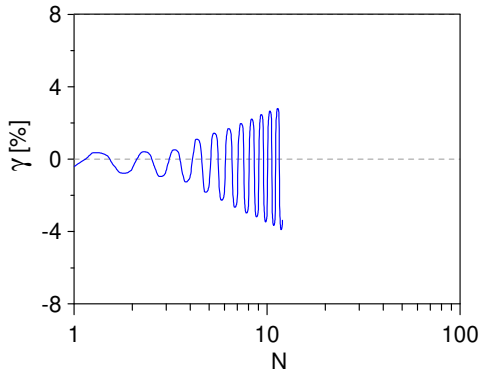

Undrained Cyclic Simple Shear test: *C_SS_TS30_S100_A0_12*
Ticino sand + 30% f_c (Reconstitution method: Moist Tamping)
e_0= 0.49 - D_R= 72% - σ'_{v0}= 100 kPa - α=0 - *CSR* = 0.24

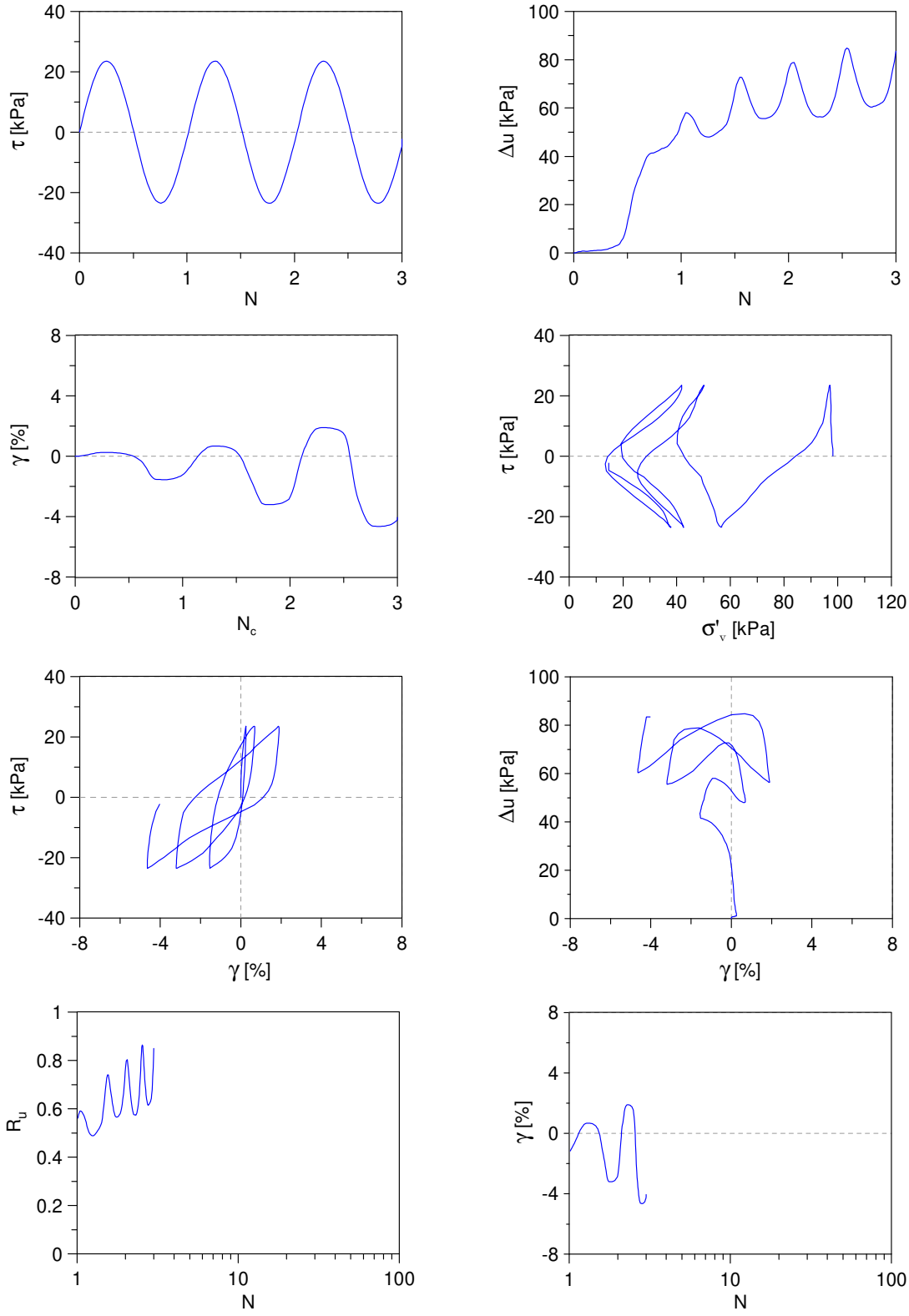

Undrained Cyclic Simple Shear test: *C_SS_TS30_S100_A1_1*
Ticino sand + 30% f_c (Reconstitution method: Moist Tamping)
e_0= 0.68 - D_R= 28% - σ'_{v0}= 100 kPa - α= 0.1 - *CSR* = 0.06

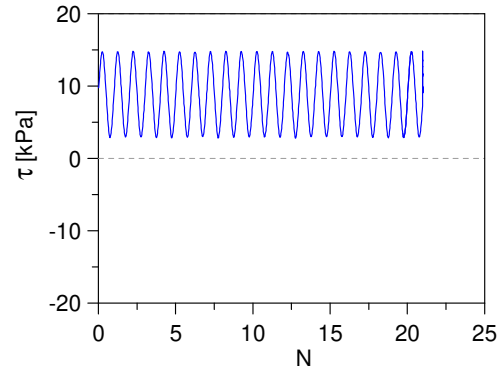

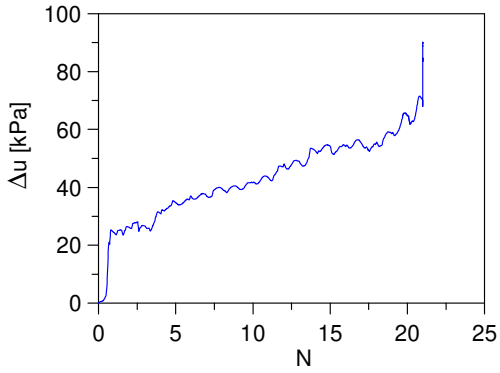

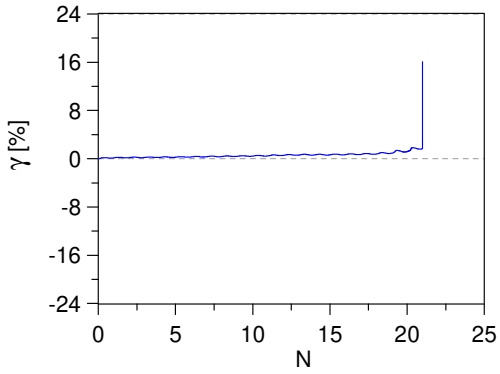

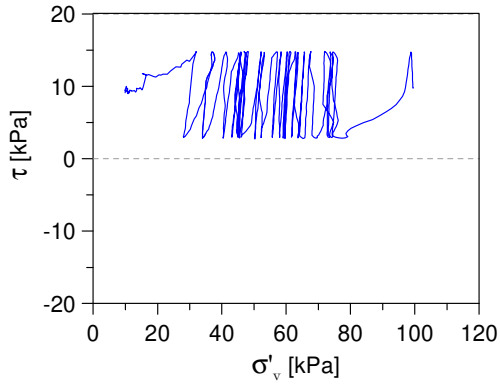

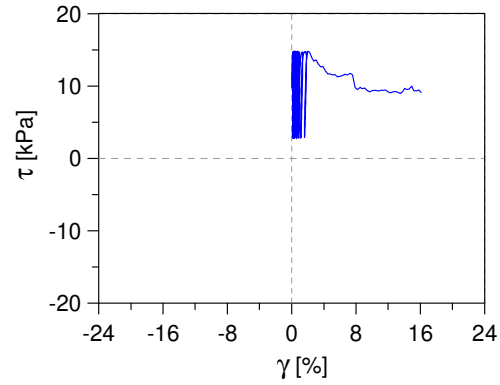

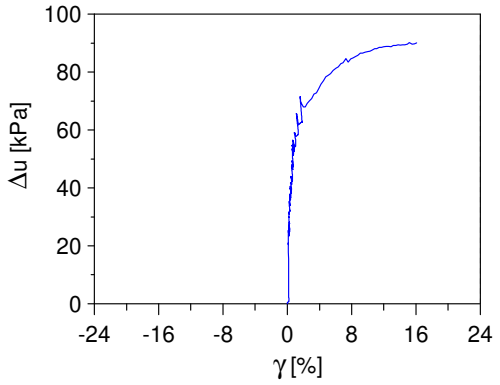

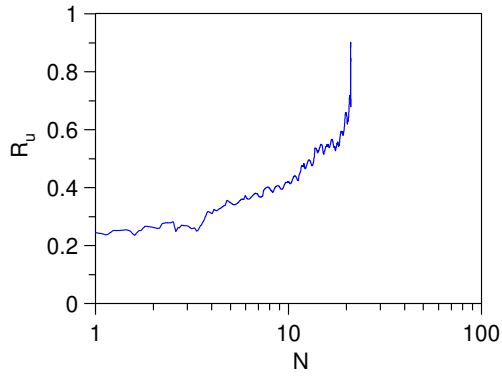

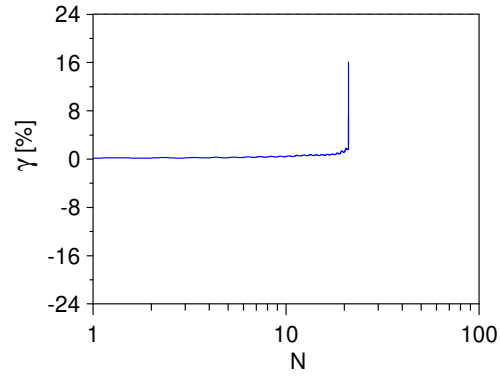

Undrained Cyclic Simple Shear test: *C_SS_TS30_S100_A1_2*
Ticino sand + 30% f_c (Reconstitution method: Moist Tamping)
e_0= 0.68 - D_R= 28% - σ'_{v0}= 100 kPa - α= 0.1 - *CSR* = 0.10

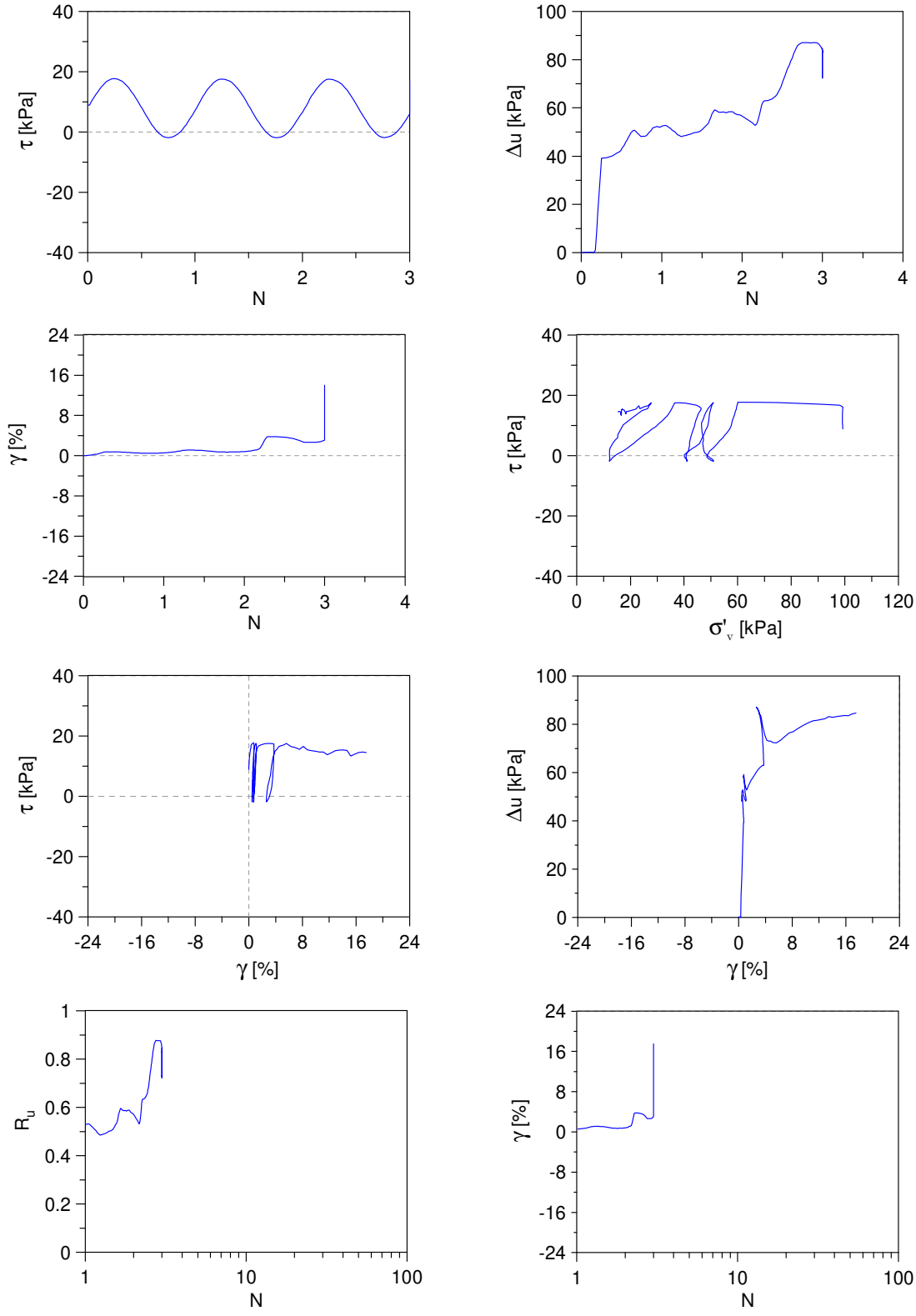

Undrained Cyclic Simple Shear test: *C_SS_TS30_S100_A1_3*
Ticino sand + 30% f_c (Reconstitution method: Moist Tamping)
e_0= 0.59 - D_R= 49% - σ'_{v0}= 100 kPa - α= 0.1 - *CSR* = 0.10

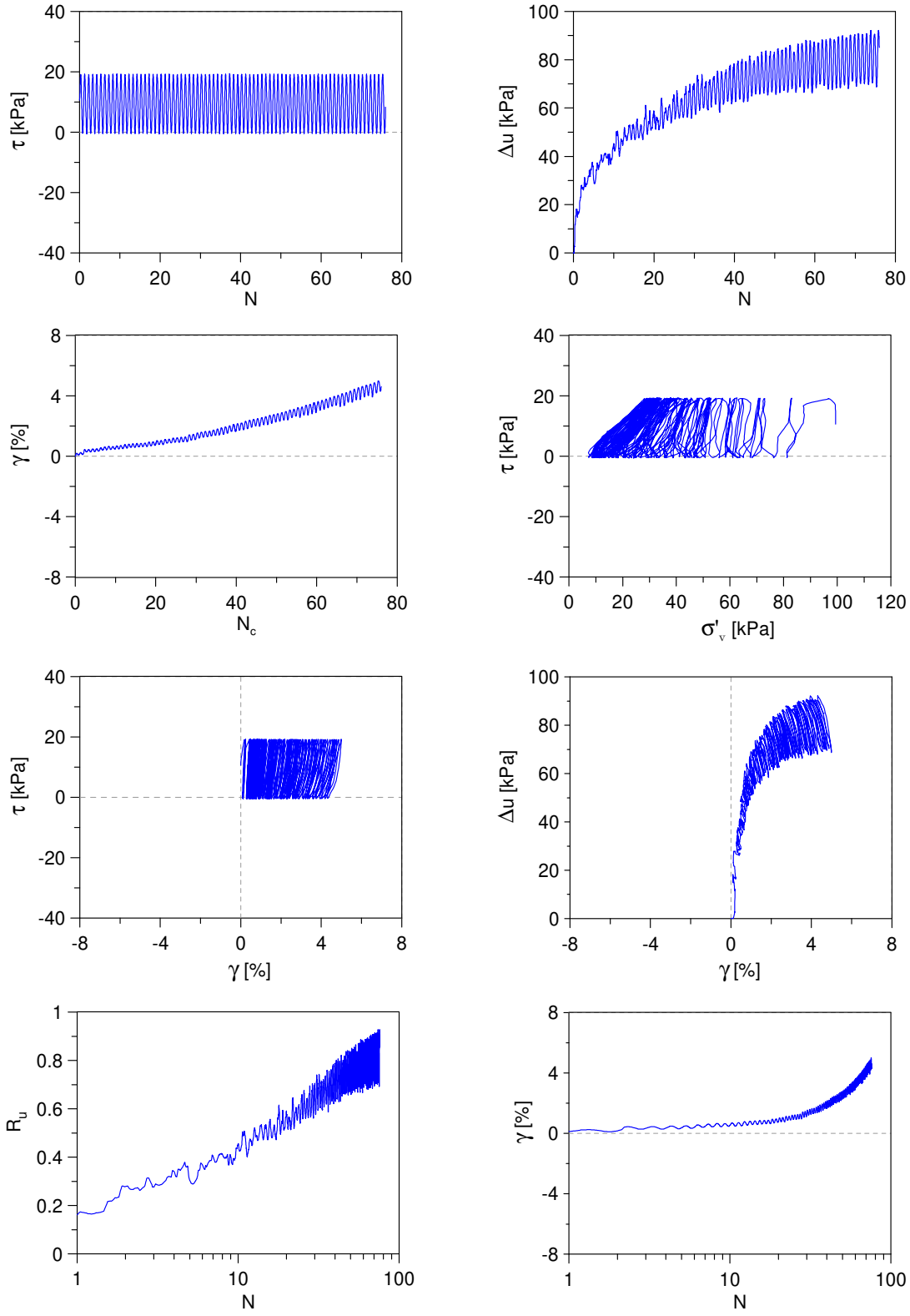

Undrained Cyclic Simple Shear test: *C_SS_TS30_S100_A1_4*
Ticino sand + 30% f_c (Reconstitution method: Moist Tamping)
e_0= 0.59 - D_R= 49% - σ'_{v0}= 100 kPa - α= 0.1 - *CSR* = 0.12

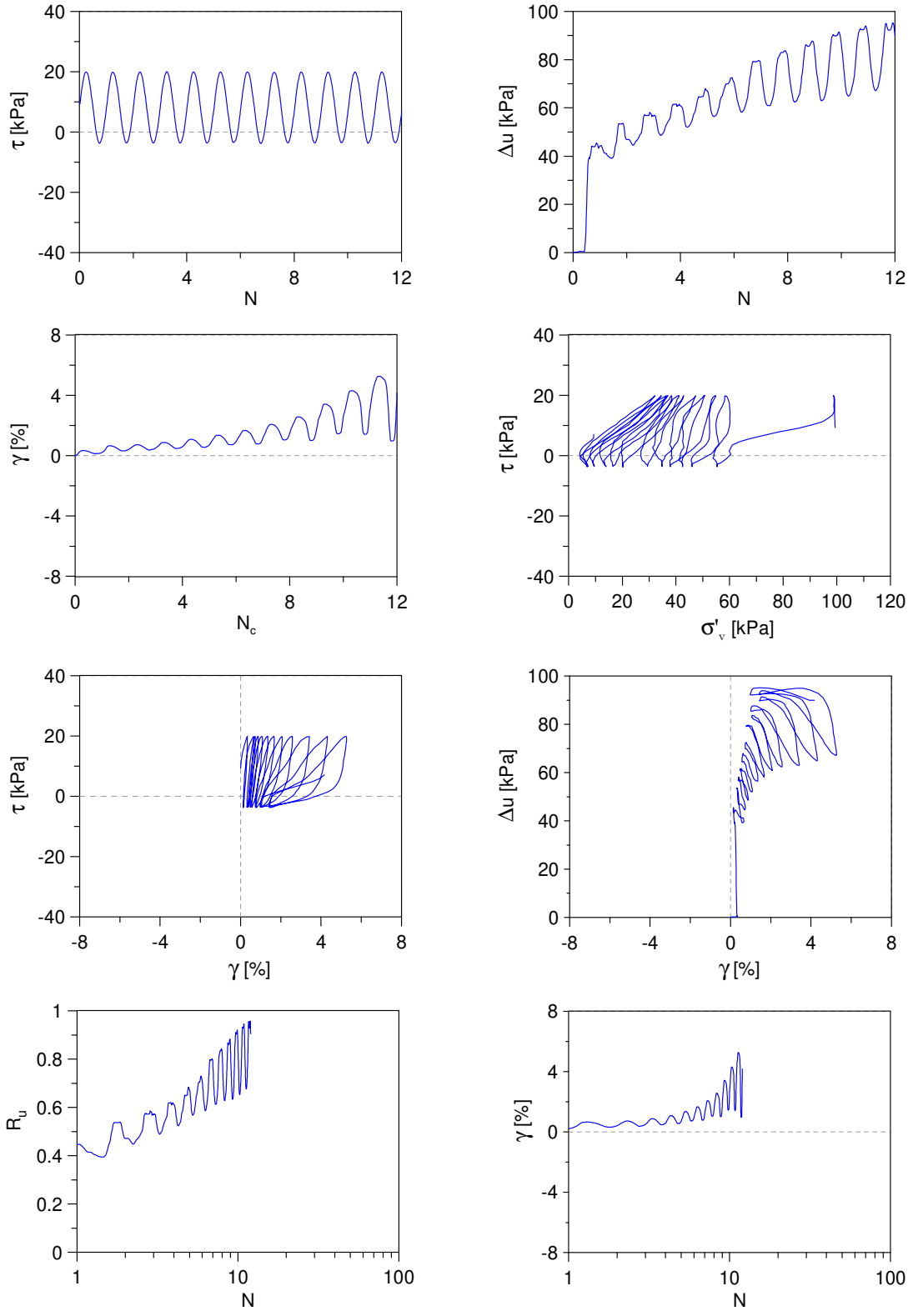

Undrained Cyclic Simple Shear test: *C_SS_TS30_S100_A1_5*
Ticino sand + 30% f_c (Reconstitution method: Moist Tamping)
e_0= 0.55 - D_R= 58% - σ'_{v0}= 100 kPa - α= 0.1 - *CSR* = 0.16

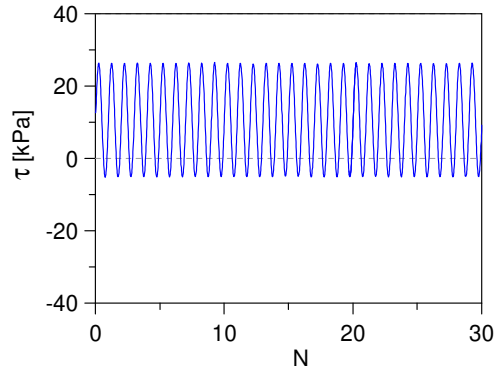

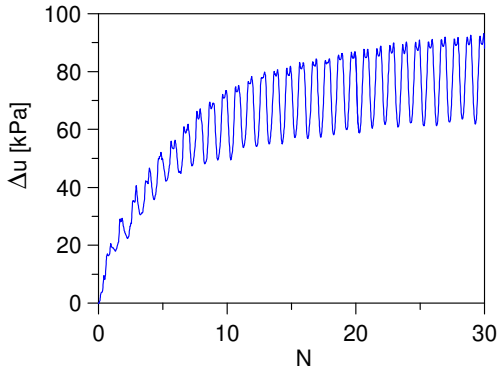

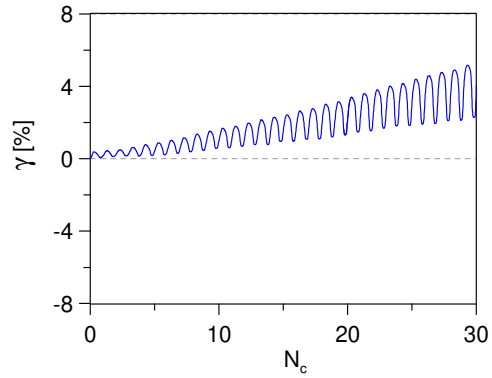

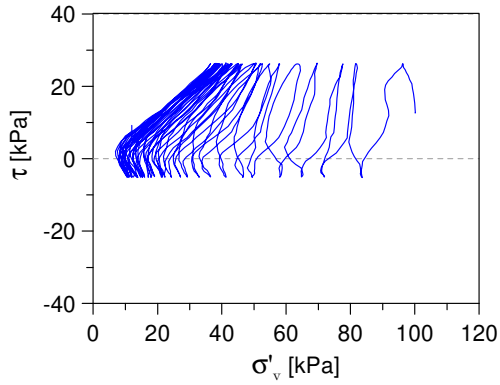

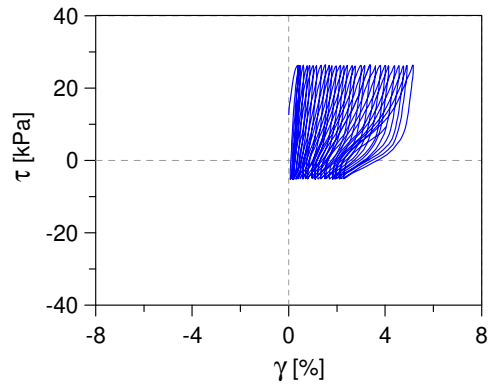

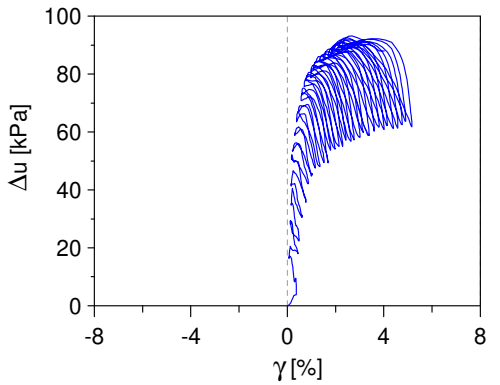

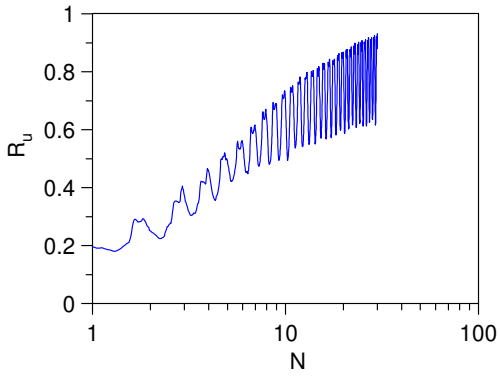

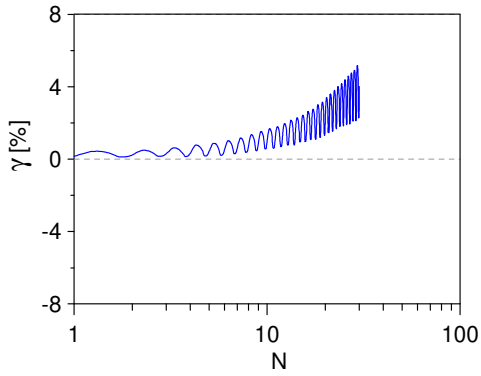

Undrained Cyclic Simple Shear test: *C_SS_TS30_S100_A1_6*
Ticino sand + 30% f_c (Reconstitution method: Moist Tamping)
e_0= 0.55 - D_R= 58% - σ'_{v0}= 100 kPa - α= 0.1 - *CSR* = 0.19

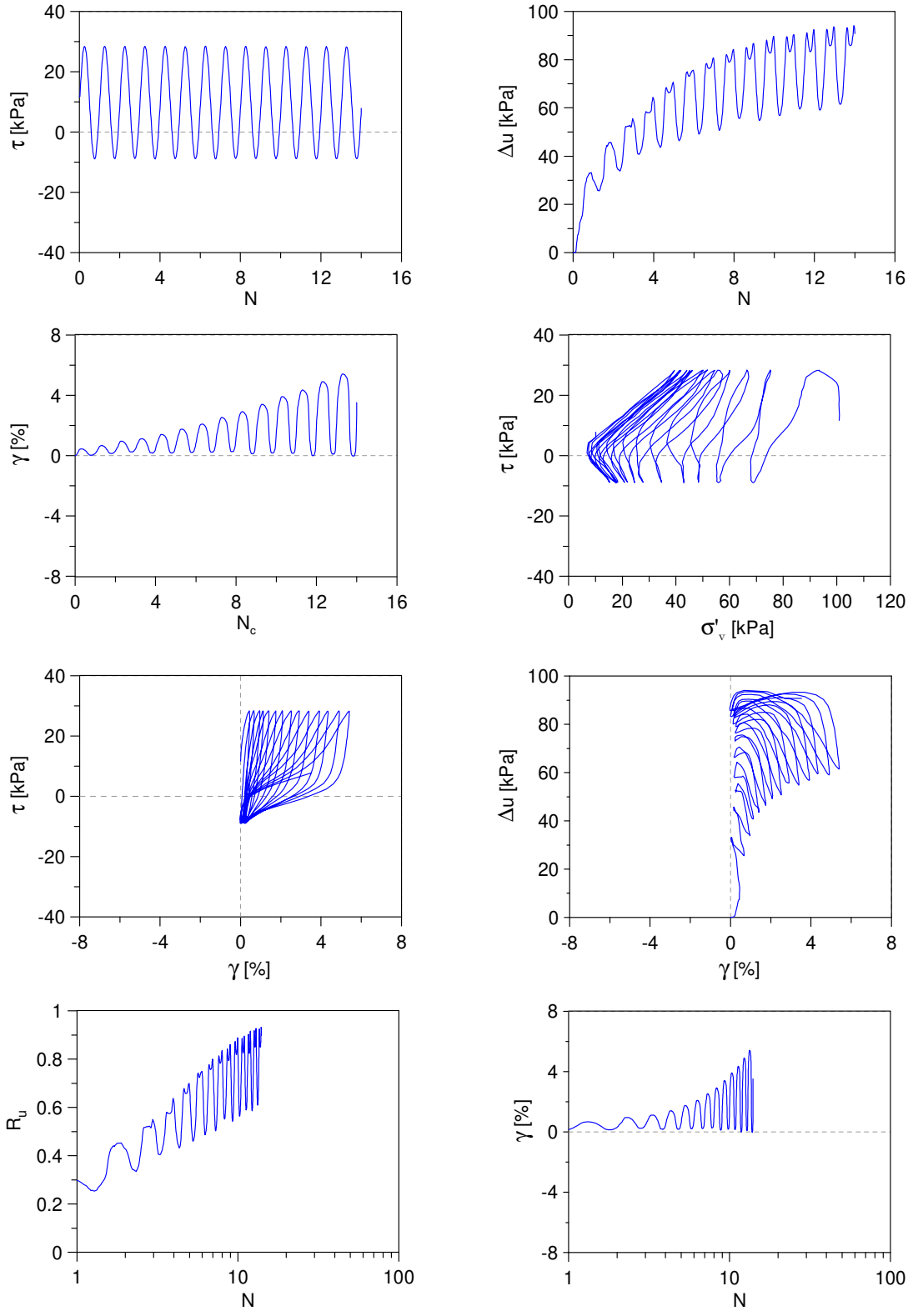

Undrained Cyclic Simple Shear test: *C_SS_TS30_S100_A2_1*
Ticino sand + 30% f_c (Reconstitution method: Moist Tamping)
e_0= 0.59 - D_R= 49% - σ'_{v0}= 100 kPa - α= 0.2 - *CSR* = 0.08

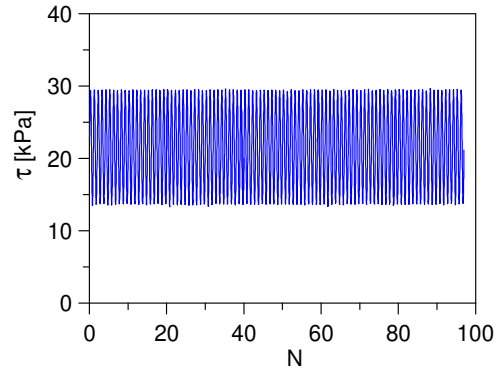

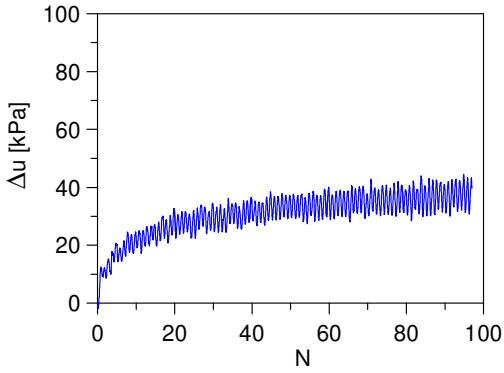

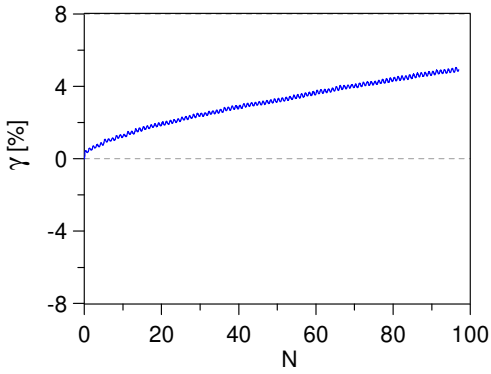

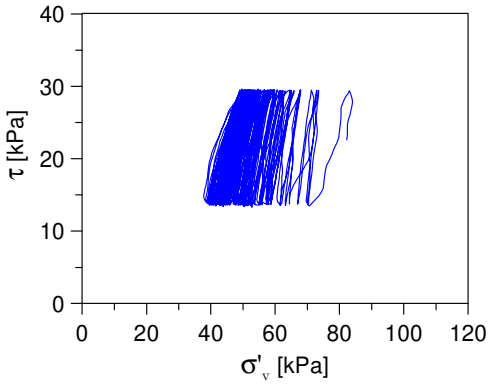

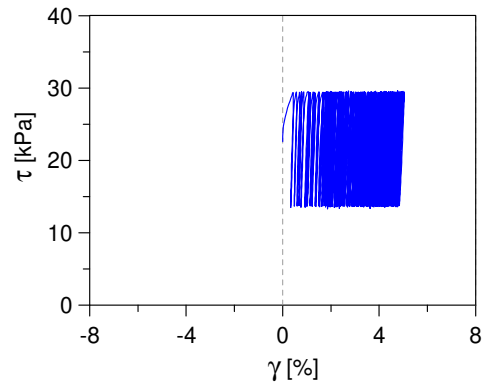

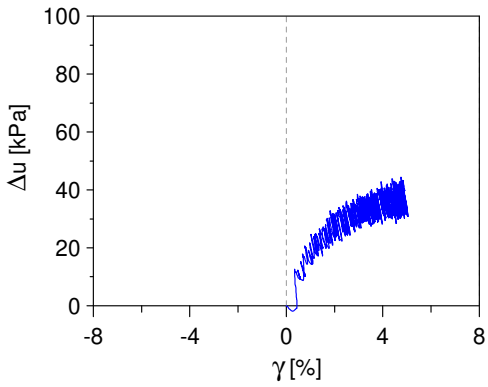

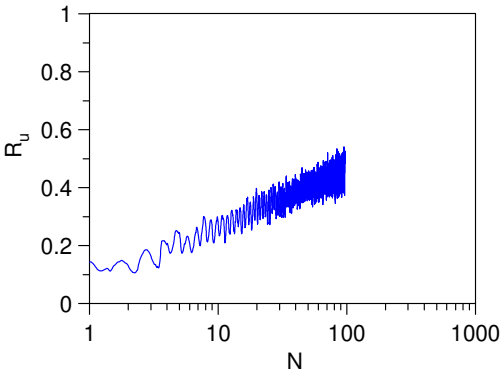

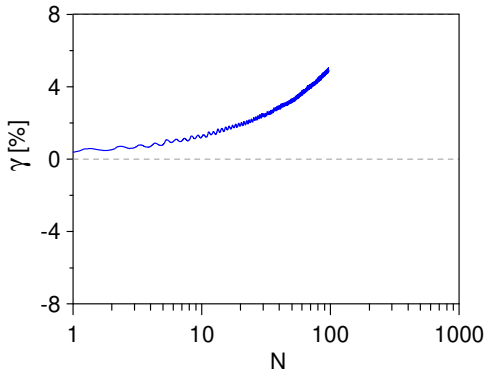

Undrained Cyclic Simple Shear test: *C_SS_TS30_S100_A2_2*
Ticino sand + 30% f_c (Reconstitution method: Moist Tamping)
e_0= 0.59 - D_R= 49% - σ'_{v0}= 100 kPa - α= 0.2 - *CSR* = 0.10

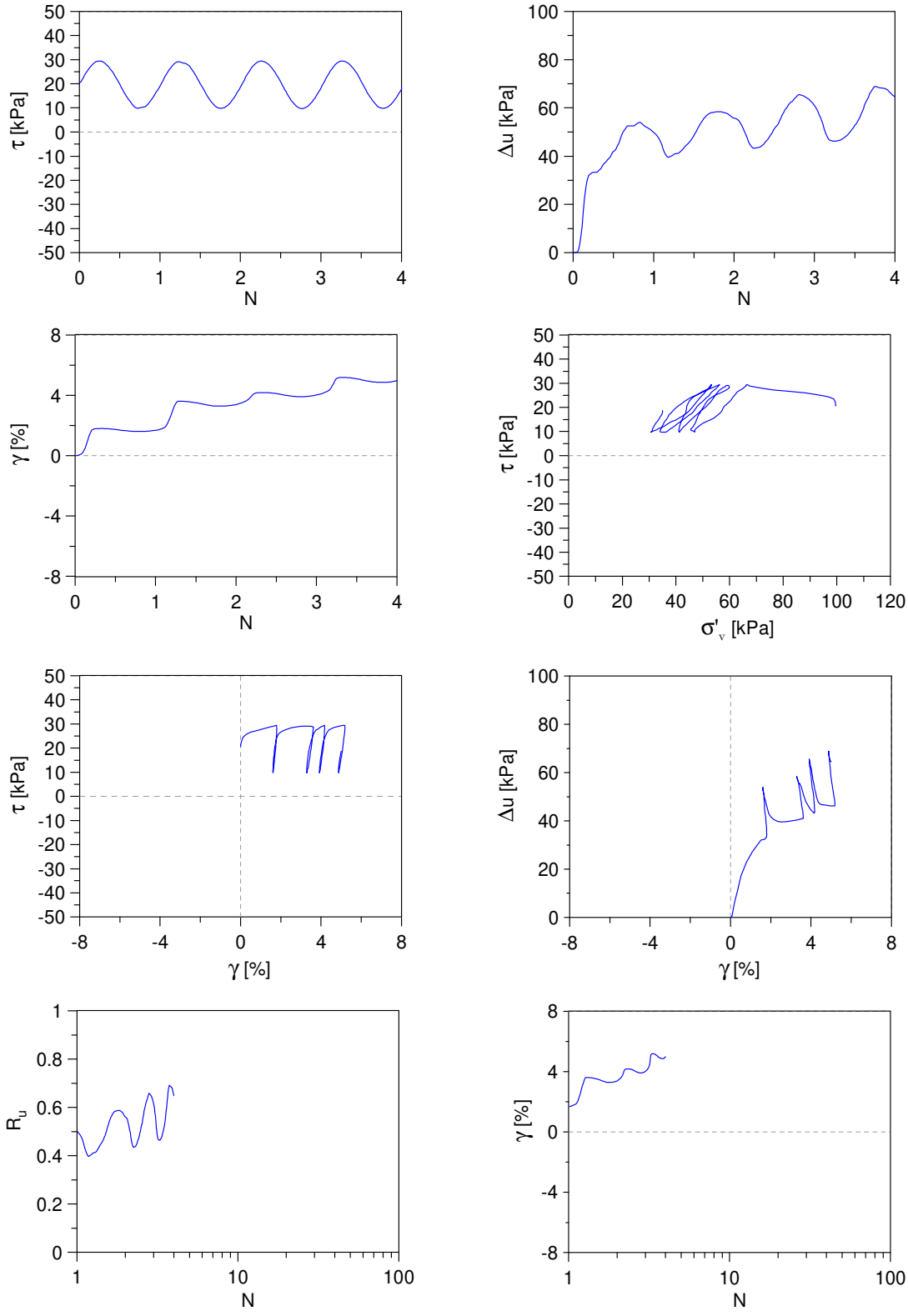

Undrained Cyclic Simple Shear test: *C_SS_TS30_S100_A2_3*
Ticino sand + 30% f_c (Reconstitution method: Moist Tamping)
e_0= 0.55 - D_R= 58% - σ'_{v0}= 100 kPa - α= 0.2 - *CSR* = 0.14

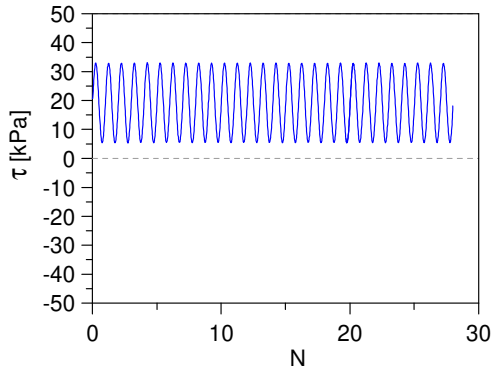

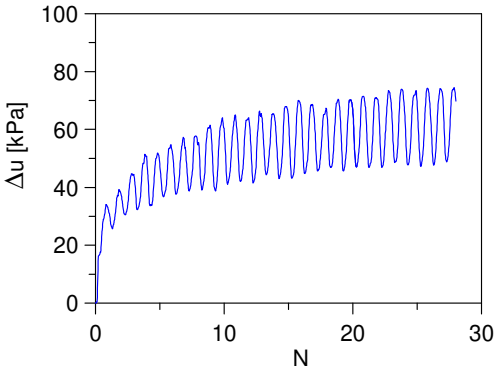

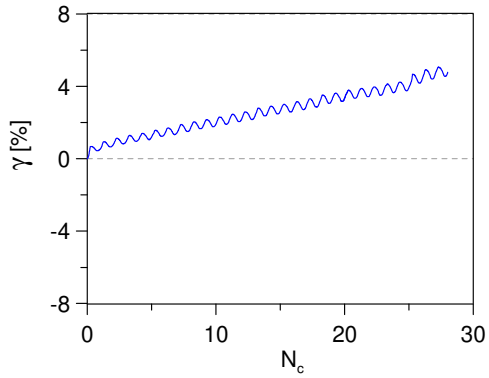

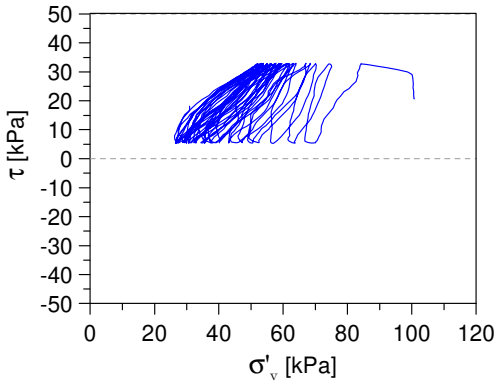

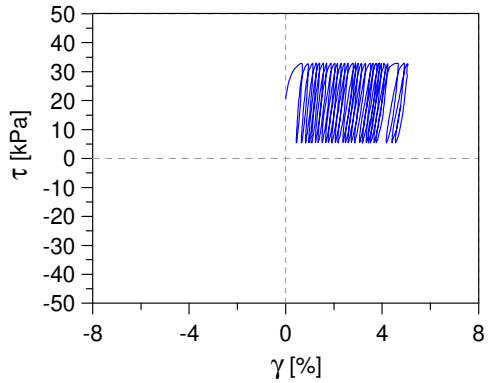

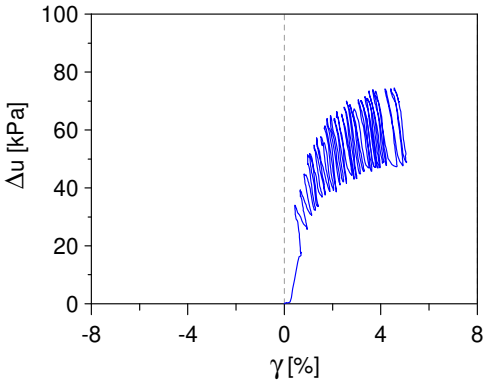

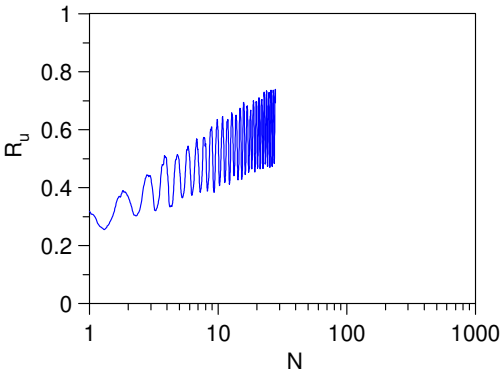

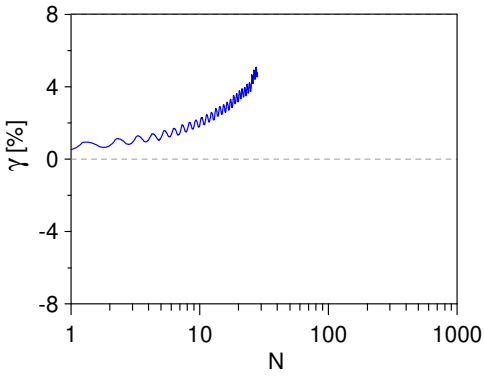

Undrained Cyclic Simple Shear test: *C_SS_TS30_S100_A2_4*
Ticino sand + 30% f_c (Reconstitution method: Moist Tamping)
e_0= 0.55 - D_R= 58% - σ'_{v0}= 100 kPa - α= 0.2 - *CSR* = 0.16

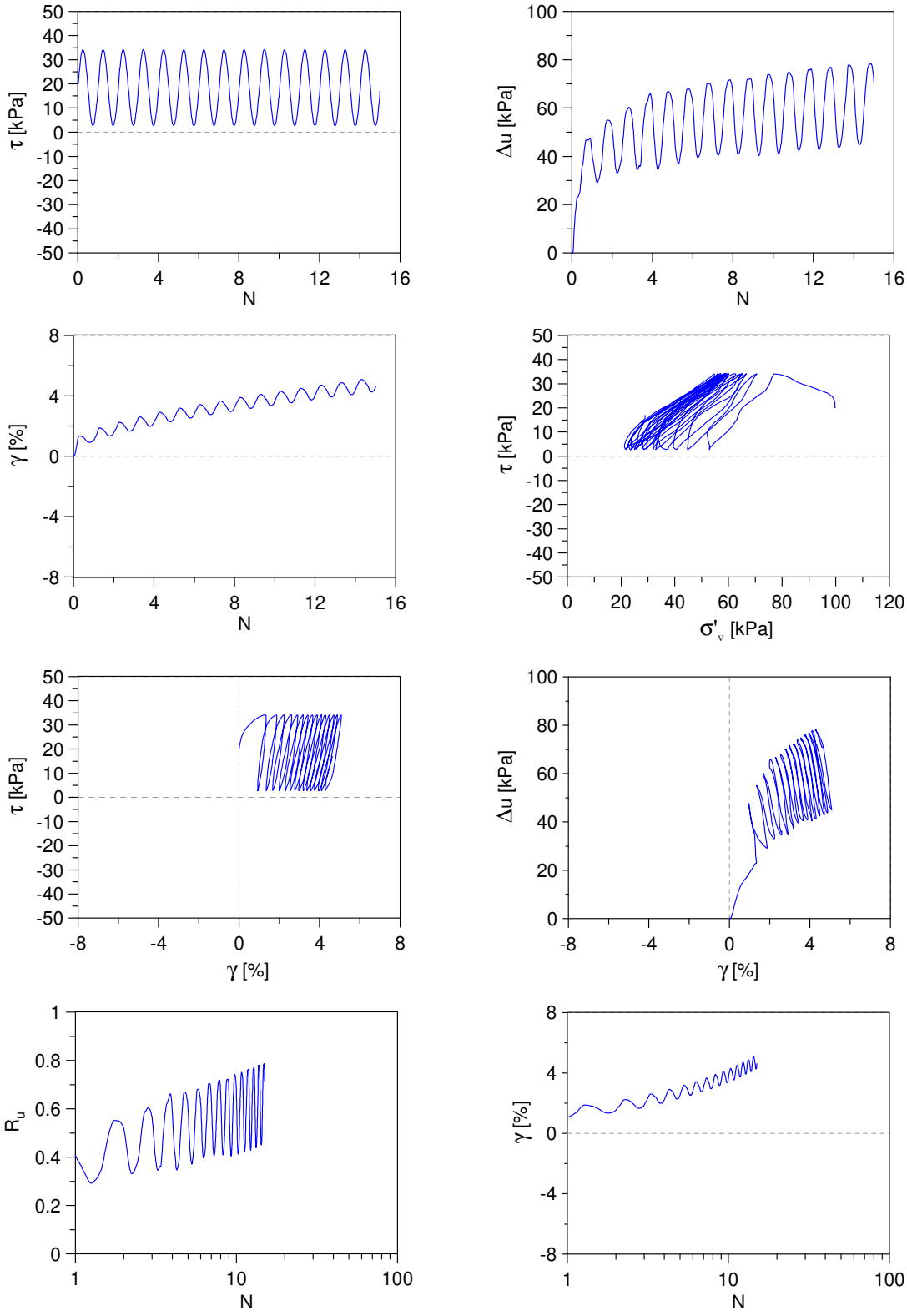

Undrained Cyclic Simple Shear test: *C_SS_TS30_S100_A3_1*
Ticino sand + 30% f_c (Reconstitution method: Moist Tamping)
e_0= 0.55 - D_R= 58% - σ'_{v0}= 100 kPa - α= 0.3 - *CSR* = 0.12

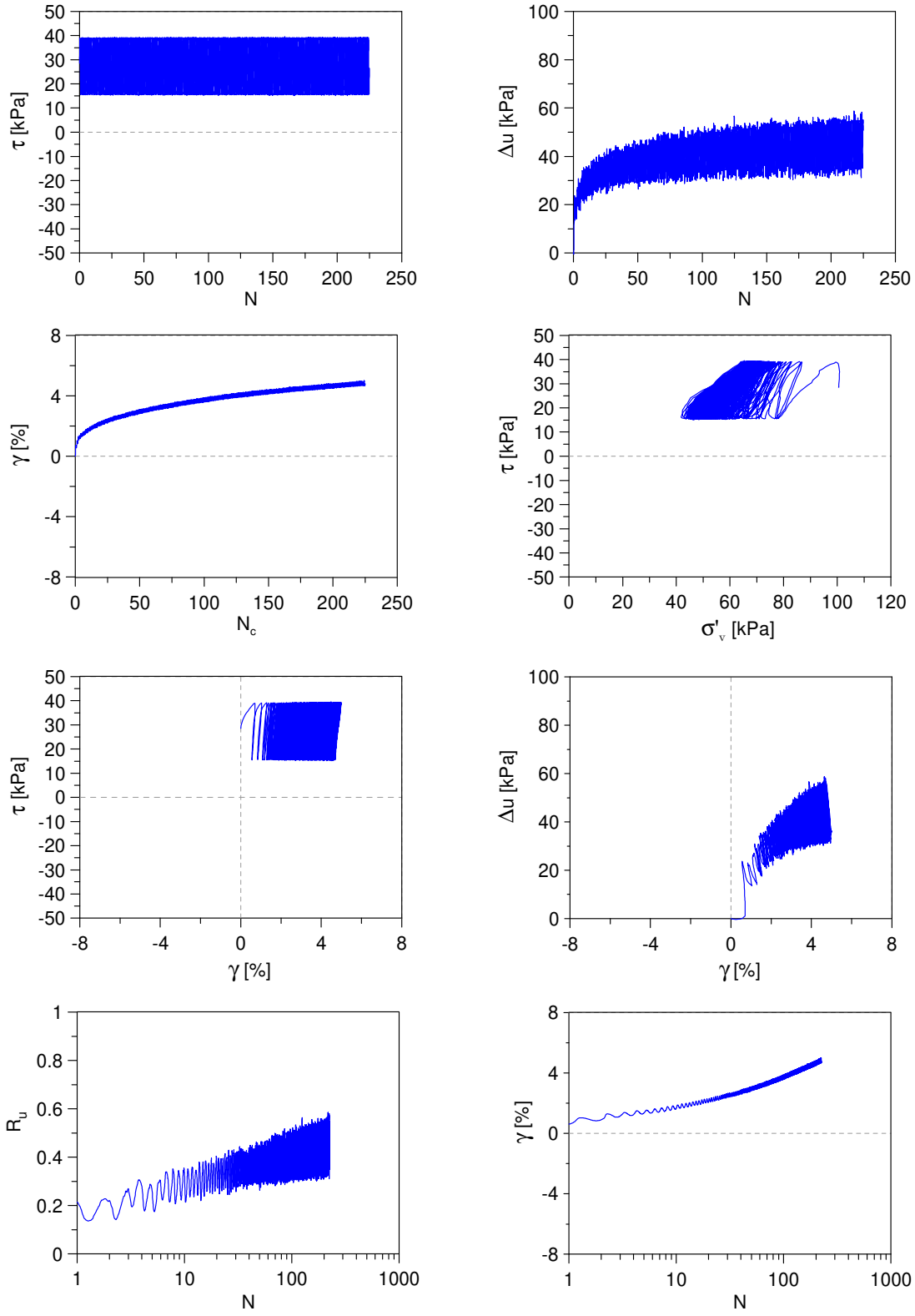

Undrained Cyclic Simple Shear test: *C_SS_TS30_A3_2*
Ticino sand + 30% f_c (Reconstitution method: Moist Tamping)
e_0= 0.55 - D_R= 58% - σ'_{v0}= 100 kPa - α= 0.3 - *CSR* = 0.14

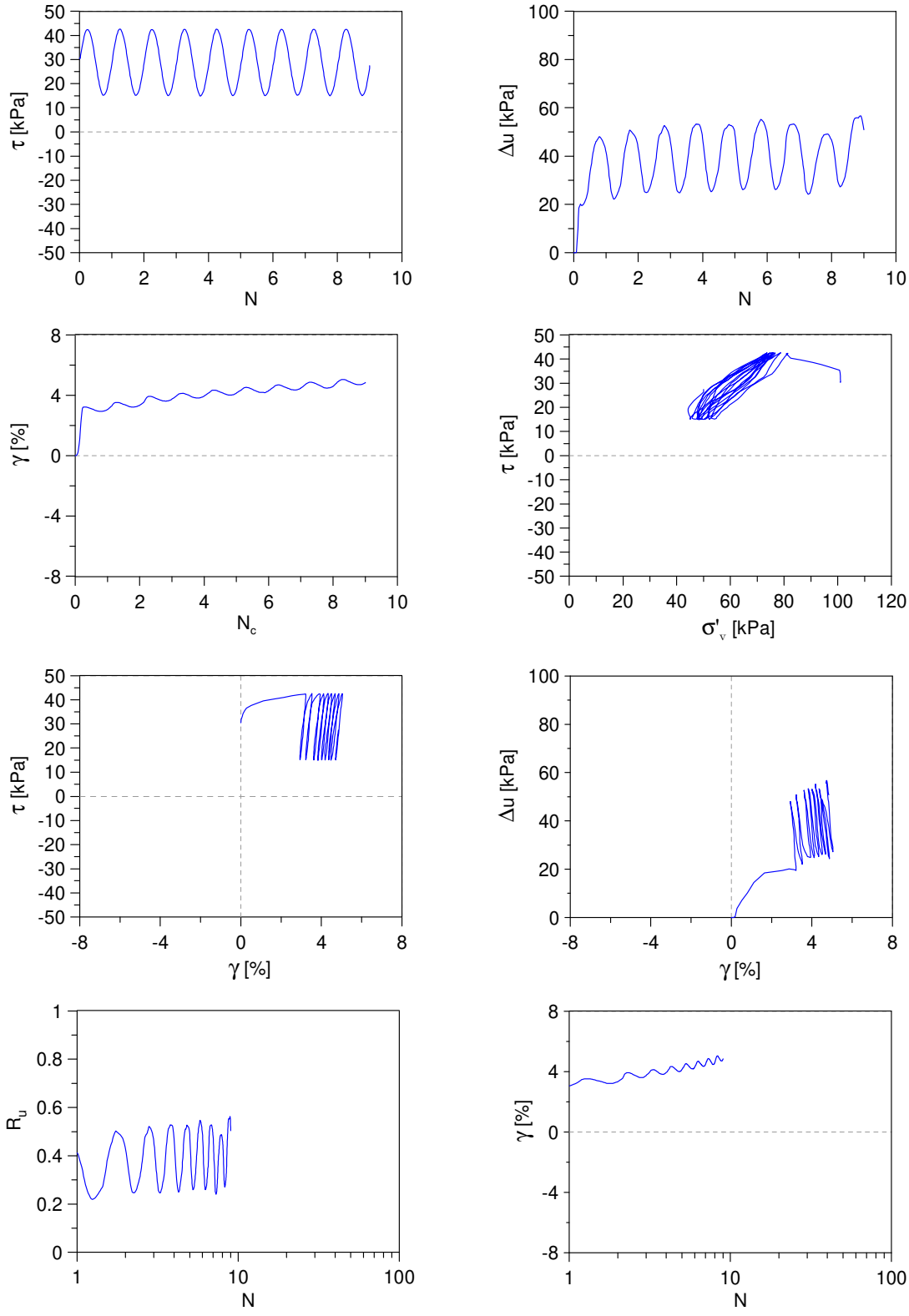

Sand-silt mixture (f_c=40%)

Undrained Cyclic Simple Shear test: *C_SS_TS40_S100_A0_1*
Ticino sand + 40% f_c (Reconstitution method: Moist Tamping)
e_0= 0.68 - D_R= 60% - σ'_{v0}= 100 kPa - α=0 - *CSR* = 0.12

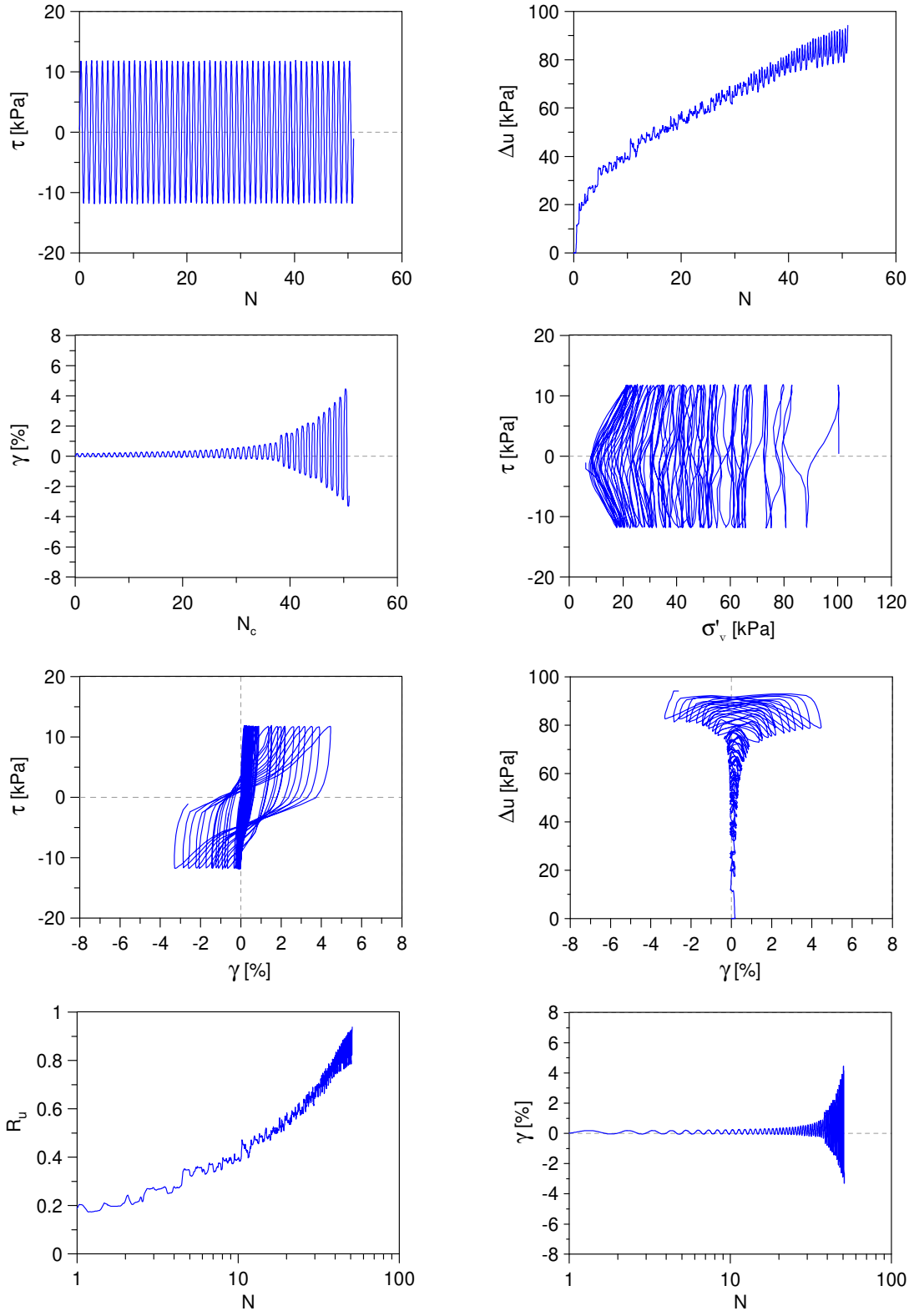

Undrained Cyclic Simple Shear test: *C_SS_TS40_S100_A0_2*
Ticino sand + 40% f_c (Reconstitution method: Moist Tamping)
e_0= 0.68 - D_R= 60% - σ'_{v0}= 100 kPa - α=0 - *CSR* = 0.14

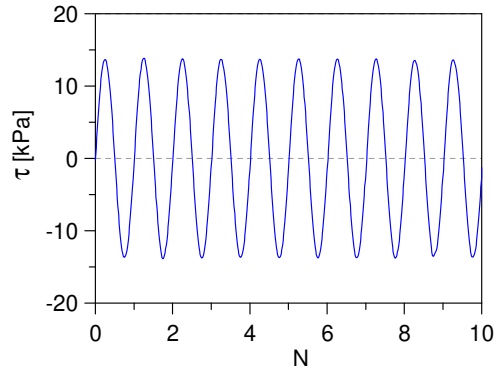

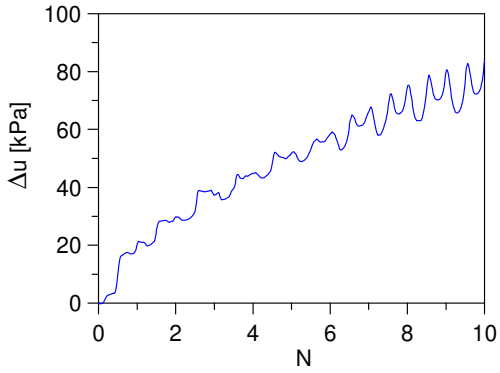

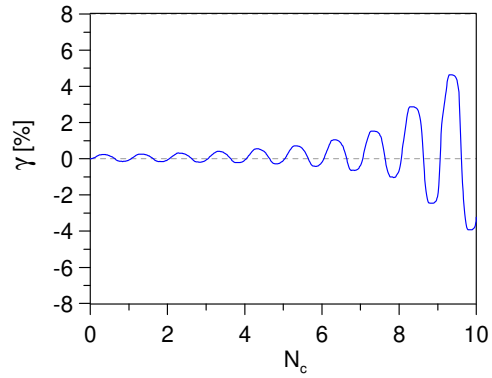

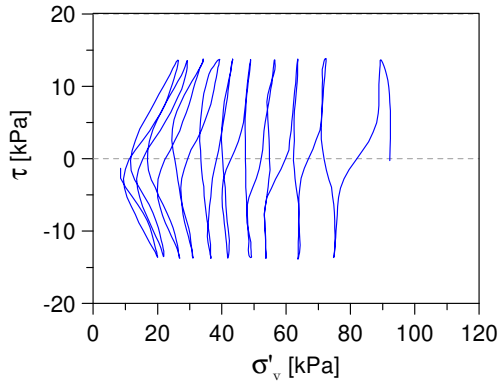

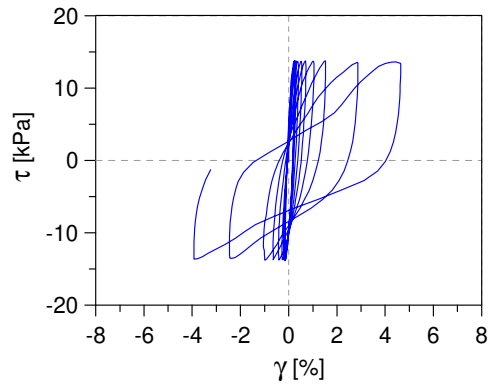

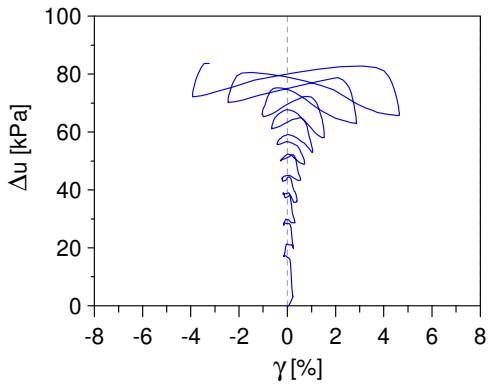

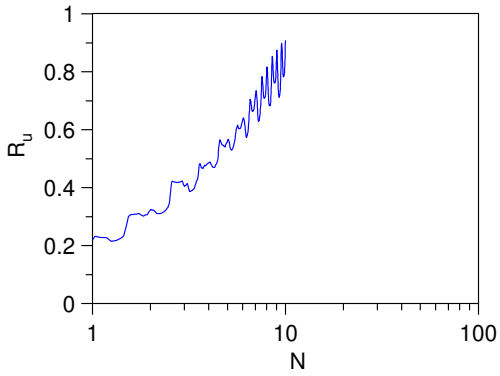

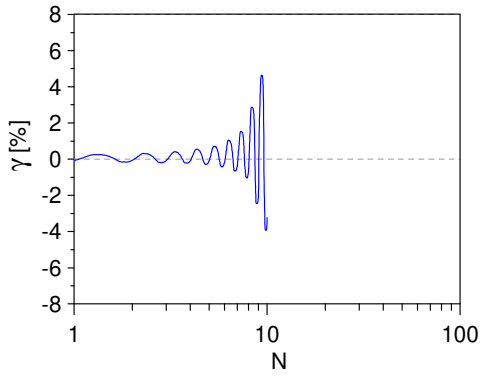

Undrained Cyclic Simple Shear test: *C_SS_TS40_S100_A0_3*
Ticino sand + 40% f_c (Reconstitution method: Moist Tamping)
e_0= 0.68 - D_R= 60% - σ'_{v0}= 100 kPa - α=0 - *CSR* = 0.16